frontiers | Research Topics

Wheat disease resistance: diagnosis, germplasm mining, and molecular breeding

Edited by
Runsheng Ren, Jing Feng, Rumiana V. Ray and Xinli Zhou

Published in
Frontiers in Plant Science

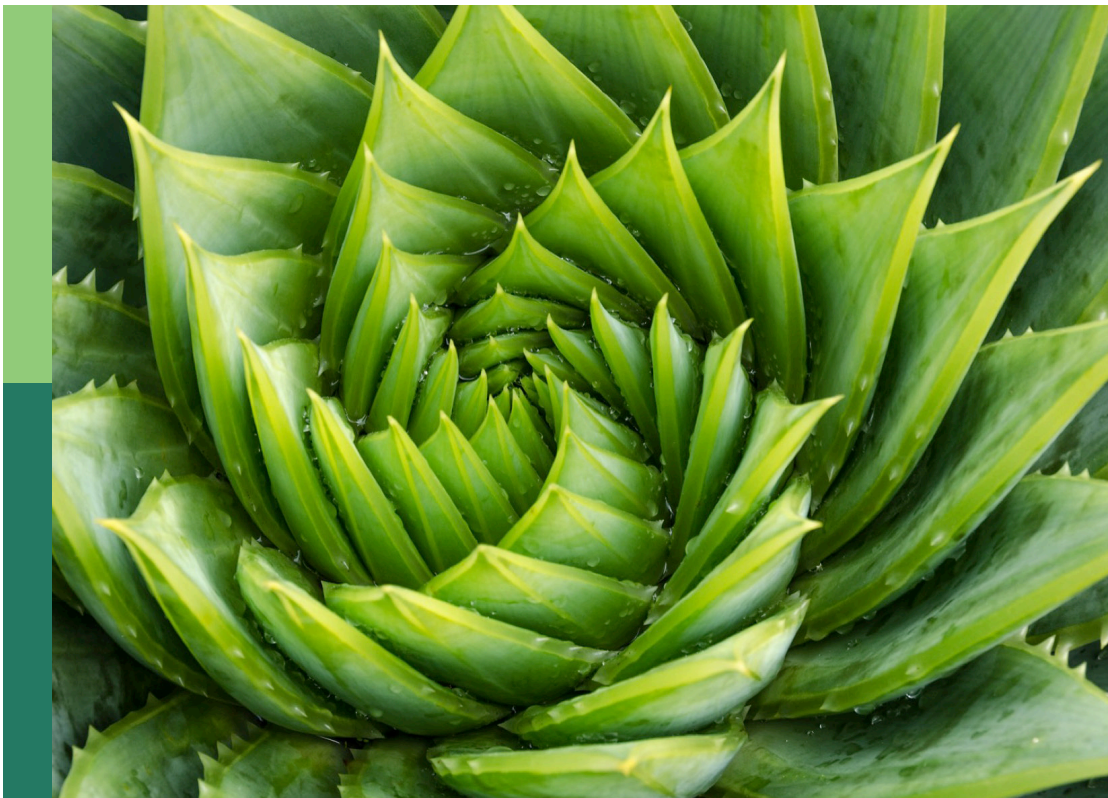

FRONTIERS EBOOK COPYRIGHT STATEMENT

The copyright in the text of individual articles in this ebook is the property of their respective authors or their respective institutions or funders. The copyright in graphics and images within each article may be subject to copyright of other parties. In both cases this is subject to a license granted to Frontiers.

The compilation of articles constituting this ebook is the property of Frontiers.

Each article within this ebook, and the ebook itself, are published under the most recent version of the Creative Commons CC-BY licence. The version current at the date of publication of this ebook is CC-BY 4.0. If the CC-BY licence is updated, the licence granted by Frontiers is automatically updated to the new version.

When exercising any right under the CC-BY licence, Frontiers must be attributed as the original publisher of the article or ebook, as applicable.

Authors have the responsibility of ensuring that any graphics or other materials which are the property of others may be included in the CC-BY licence, but this should be checked before relying on the CC-BY licence to reproduce those materials. Any copyright notices relating to those materials must be complied with.

Copyright and source acknowledgement notices may not be removed and must be displayed in any copy, derivative work or partial copy which includes the elements in question.

All copyright, and all rights therein, are protected by national and international copyright laws. The above represents a summary only. For further information please read Frontiers' Conditions for Website Use and Copyright Statement, and the applicable CC-BY licence.

ISSN 1664-8714
ISBN 978-2-8325-5811-9
DOI 10.3389/978-2-8325-5811-9

About Frontiers

Frontiers is more than just an open access publisher of scholarly articles: it is a pioneering approach to the world of academia, radically improving the way scholarly research is managed. The grand vision of Frontiers is a world where all people have an equal opportunity to seek, share and generate knowledge. Frontiers provides immediate and permanent online open access to all its publications, but this alone is not enough to realize our grand goals.

Frontiers journal series

The Frontiers journal series is a multi-tier and interdisciplinary set of open-access, online journals, promising a paradigm shift from the current review, selection and dissemination processes in academic publishing. All Frontiers journals are driven by researchers for researchers; therefore, they constitute a service to the scholarly community. At the same time, the *Frontiers journal series* operates on a revolutionary invention, the tiered publishing system, initially addressing specific communities of scholars, and gradually climbing up to broader public understanding, thus serving the interests of the lay society, too.

Dedication to quality

Each Frontiers article is a landmark of the highest quality, thanks to genuinely collaborative interactions between authors and review editors, who include some of the world's best academicians. Research must be certified by peers before entering a stream of knowledge that may eventually reach the public - and shape society; therefore, Frontiers only applies the most rigorous and unbiased reviews. Frontiers revolutionizes research publishing by freely delivering the most outstanding research, evaluated with no bias from both the academic and social point of view. By applying the most advanced information technologies, Frontiers is catapulting scholarly publishing into a new generation.

What are Frontiers Research Topics?

Frontiers Research Topics are very popular trademarks of the *Frontiers journals series*: they are collections of at least ten articles, all centered on a particular subject. With their unique mix of varied contributions from Original Research to Review Articles, Frontiers Research Topics unify the most influential researchers, the latest key findings and historical advances in a hot research area.

Find out more on how to host your own Frontiers Research Topic or contribute to one as an author by contacting the Frontiers editorial office: frontiersin.org/about/contact

Wheat disease resistance: diagnosis, germplasm mining, and molecular breeding

Topic editors

Runsheng Ren — Jiangsu Academy of Agricultural Sciences (JAAS), China
Jing Feng — Institute of Plant Protection, Chinese Academy of Agricultural Sciences, China
Rumiana V. Ray — University of Nottingham, United Kingdom
Xinli Zhou — Southwest University of Science and Technology, China

Citation

Ren, R., Feng, J., Ray, R. V., Zhou, X., eds. (2024). *Wheat disease resistance: diagnosis, germplasm mining, and molecular breeding*. Lausanne: Frontiers Media SA. doi: 10.3389/978-2-8325-5811-9

Table of contents

frontiers | Frontiers in Plant Science

TYPE Editorial
PUBLISHED 09 December 2024
DOI 10.3389/fpls.2024.1500414

Check for updates

OPEN ACCESS

EDITED BY
Huihui Li,
Chinese Academy of Agricultural Sciences, China

REVIEWED BY
Awais Rasheed,
Quaid-i-Azam University, Pakistan

*CORRESPONDENCE
Runsheng Ren
runshengren@163.com
Xinli Zhou
eli6951@sina.com
Jing Feng
jingfeng@ippcaas.cn

RECEIVED 23 September 2024
ACCEPTED 28 November 2024
PUBLISHED 09 December 2024

CITATION
Ren R, Zhou X and Feng J (2024) Editorial: Wheat disease resistance: diagnosis, germplasm mining, and molecular breeding. *Front. Plant Sci.* 15:1500414. doi: 10.3389/fpls.2024.1500414

COPYRIGHT
© 2024 Ren, Zhou and Feng. This is an open-access article distributed under the terms of the Creative Commons Attribution License (CC BY). The use, distribution or reproduction in other forums is permitted, provided the original author(s) and the copyright owner(s) are credited and that the original publication in this journal is cited, in accordance with accepted academic practice. No use, distribution or reproduction is permitted which does not comply with these terms.

Editorial: Wheat disease resistance: diagnosis, germplasm mining, and molecular breeding

Runsheng Ren[1]*, Xinli Zhou[2]* and Jing Feng[3]*

[1]Institute of Germplasm Resources and Biotechnology/Jiangsu Provincial Key Laboratory of Agrobiology, Zhongshan Biological Breeding Laboratory, Jiangsu Academy of Agricultural Sciences, Nanjing, China, [2]Wheat Research Institute, School of Life Sciences and Engineering, Southwest University of Science and Technology, Mianyang, Sichuan, China, [3]Institute of Plant Protection, Chinese Academy of Agricultural Sciences, Beijing, China

KEYWORDS

diagnosis, germplasm mining, wheat, disease resistance, molecular breeding

Editorial on the Research Topic
Wheat disease resistance: diagnosis, germplasm mining, and molecular breeding

As one of the most important food crops in the world, disease resistance in wheat is directly related to global food security and agricultural production efficiency. Breeding wheat for disease resistance combined with good agronomy can potentially improve wheat productivity to meet the future demands. To shed light on the latest breakthroughs and cutting-edge research, Frontiers in Plant Sciences presents this Research Topic: *Wheat Disease Resistance: Diagnosis, Germplasm Mining, and Molecular Breeding*, dedicated to exploring new developments, current challenges, latest discoveries, and future prospects in these fields.

Diagnosis and genetic basis of wheat disease resistance

Wheat may encounter various diseases during its growth process, such as yellow rust, leaf rust, stem rust, powdery mildew, Fusarium head blight, etc. These diseases not only affect the yield of wheat, but also have a serious impact on its quality (Stukenbrock and Gurr, 2023). Therefore, timely and accurate disease diagnosis is a prerequisite for developing effective prevention and control strategies. The diagnosis of wheat disease resistance mainly includes field natural disease identification, which is the most direct and authentic method to reflect the disease resistance of wheat varieties (Laidig et al., 2021). The evaluation index data can intuitively reflect the resistance ability of wheat varieties to specific diseases. However, this method is greatly influenced by environmental factors such as climate, soil, and cultivation management, and may require years of data accumulation to draw accurate conclusions (Kumar et al., 2019). The diagnosis of wheat disease resistance is still a complex and systematic process. The study conducted by Jevtić and Župunski presented experimental evidence for the case. They conducted a comprehensive analysis of 2715 wheat and wheat related species over a period of 8 years, including phenotypic

screening of various diseases including powdery mildew, stripe rust, leaf rust, and stem rust. The findings reveal that the plant reactions to leaf rust and stripe rust infections may be misleading. Because these are heavily influenced not only by prevalent rust races and climatic factors that impact pathogen life cycles but also by variations in the susceptibility reactions of wheat genotypes to the broader agro-ecological conditions.

In order to accurately evaluate the disease resistance of wheat varieties, artificial inoculation is a commonly used method (Francesconi, 2022). Secondly to observe and record the incidence of wheat varieties by controlling the inoculation amount of pathogenic organisms and environmental conditions under laboratory or greenhouse conditions. This method can eliminate the interference of environmental factors and more accurately portray the disease resistance of wheat varieties (Ren et al., 2015; Šarčević et al., 2023). With the development of molecular biology technology, the use of molecular markers and gene detection techniques for diagnosing wheat disease resistance is becoming increasingly important (Jabran et al., 2023; Luo et al., 2023). For example, by detecting the presence of specific disease resistance genes in wheat varieties, and their resistance to a certain disease can be predicted. This method has the advantages of being fast, accurate, and not affected by the environment. In the present Research Topic, Yan et al. identified nine quantitative trait loci (QTLs) and their linked SNP markers for stripe rust resistance. Haile et al. consistently detected six FHB- associated QTL and developed their linked KASP markers in durum wheat. Navathe et al. identified six QTLs conferring resistance to Septoria nodorum blotch and tan spot in wheat. In short, the diagnosis of wheat disease resistance is a complex and systematic process that requires the comprehensive use of multiple technical means and methods. Through accurate disease resistance diagnosis, germplasm resources with excellent disease resistance traits can be screened, providing strong support for disease resistant breeding and ensuring stable and high-yield wheat.

Exploration of wheat disease resistant germplasm

Exploring the wheat disease resistant germplasm is an important part of wheat breeding work. The materials were widely collected from local wheat varieties, agricultural varieties, wild relatives, and imported germplasm resources from other countries. Methods such as field natural disease identification and artificial inoculation identification were used to identify the disease resistance of germplasm resources and screen out germplasm resources with excellent disease resistance traits. In addition, by utilizing modern biotechnologies such as genomics, transcriptomics, and proteomics, we aim to identify disease resistance genes in wheat and provide genetic resources for disease resistance breeding. In the present Research Topics, Qian et al. screened out nine disease-related genes that show distinctive expression profile after *Bgt* invasion and might serve as potential targets to regulate the resistance against powdery mildew in a resistant durum wheat accession W762. Zhou et al. identified twenty-five candidate genes for *QYrsv.swut-1BL* within the 1.066 Mb region in the resistant cultivar. The discovered disease resistance genes will be utilized through modern biological breeding techniques such as molecular marker assisted selection, genetic modification, gene editing, as well as traditional hybrid breeding, mutagenesis breeding, etc., to create new germplasm with excellent disease resistance traits. Through field experiments and demonstration promotion on the created disease resistant germplasm, their disease resistance effect, yield performance, and quality characteristics in actual production were evaluated. Promote the application of wheat germplasm resources that have been evaluated and confirmed to have excellent disease resistance traits and wide adaptability in production, improve wheat yield and quality, and ensure food security. With the continuous development of biotechnology and innovation in breeding technology, as well as the precision and scale of phenotype identification, the exploration and utilization of wheat disease resistant germplasm will generate more significant results. In the future, it is necessary to continuously strengthen the Research Topic and identification of germplasm resources, and deeply explore and utilize the disease resistance gene resources in wheat. At the same time, we will enhance the research and application of disease resistance breeding technologies to promote the rapid development of wheat disease resistance breeding work.

Molecular breeding of wheat for disease resistance

Traditional breeding has made significant contributions to the cultivation of wheat varieties and food security worldwide. With the continuous development and innovation of biotechnology, molecular breeding for wheat disease resistance will usher in even broader development prospects. The technical means of molecular breeding for disease resistance mainly include molecular marker assisted selection, transgenic technology, gene editing technology, distant hybridization, and chromosome engineering technology, that can broaden the genetic basis of wheat and increase the level of disease resistance (Wulff and Krattinger, 2022).

Final considerations

The improvement of wheat disease resistance is a complex and systematic project that requires the comprehensive use of various technical means such as disease diagnosis, germplasm resource exploration and molecular breeding. By strengthening disease monitoring and early warning, deepening the exploration of disease resistant germplasm resources, and actively promoting molecular breeding techniques, it is believed that more significant progress will be made in wheat disease resistance breeding in the future, guaranteeing higher wheat production for needs of the rapidly increasing populations.

Author contributions

RR: Writing – original draft, Writing – review & editing. XZ: Writing – original draft, Writing – review & editing. JF: Writing – original draft, Writing – review & editing.

Conflict of interest

The authors declare that the research was conducted in the absence of any commercial or financial relationships that could be construed as a potential conflict of interest.

The author(s) declared that they were an editorial board member of Frontiers, at the time of submission. This had no impact on the peer review process and the final decision.

Publisher's note

All claims expressed in this article are solely those of the authors and do not necessarily represent those of their affiliated organizations, or those of the publisher, the editors and the reviewers. Any product that may be evaluated in this article, or claim that may be made by its manufacturer, is not guaranteed or endorsed by the publisher.

References

Francesconi, S. (2022). High-throughput and point-of-care detection of wheat fungal diseases: Potentialities of molecular and phenomics techniques toward in-field applicability. *Front. Agron.* 4, 980083. doi: 10.3389/fagro.2022.980083

Jabran, M., Ali, M. A., Zahoor, A., Muhae-Ud-Din, G., Liu, T., Chen, W., et al. (2023). Intelligent reprogramming of wheat for enhancement of fungal and nematode disease resistance using advanced molecular techniques. *Front. Plant Sci.* 14. doi: 10.3389/fpls.2023.1132699

Kumar, S., Singroha, G., Bhardwaj, S. C., Bala, R., Saharan, M. S., Gupta, V., et al. (2019). Multienvironmental evaluation of wheat (*Triticum aestivum* L.) germplasm identifies donors with multiple fungal disease resistance. *Genet. Resour. Crop Evol.* 66, 797–808. doi: 10.1007/s10722-019-00751-3

Laidig, F., Feike, T., Hadasch, S., Rentel, D., Klocke, B., Miedaner, T., et al. (2021). Breeding progress of disease resistance and impact of disease severity under natural infections in winter wheat variety trials. *Theor. Appl. Genet.* 134, 1281–1302. doi: 10.1007/s00122-020-03728-4

Luo, K., He, D., Guo, J., Li, G., Li, B., and Chen, X. (2023). Molecular advances in breeding for durable resistance against pests and diseases in wheat: opportunities and challenges. *Agronomy* 13, 628. doi: 10.3390/agronomy13030628

Ren, R., Yang, X., and Ray, R. V. (2015). Comparative aggressiveness of *Microdochium nivale* and *M. majus* and evaluation of screening methods for Fusarium seedling blight resistance in wheat cultivars. *Eur. J. Plant Pathol.* 141, 281–294. doi: 10.1007/s10658-014-0541-3

Šarčević, H., Bukan, M., Lovrić, A., and Maričević, M. (2023). Evaluation of inoculation methods for determination of winter wheat resistance to Fusarium head blight. *Agronomy* 13, 1175. doi: 10.3390/agronomy13041175

Stukenbrock, E., and Gurr, S. (2023). Address the growing urgency of fungal disease in crops. *Nature* 617, 31–34. doi: 10.1038/d41586-023-01465-4

Wulff, B. B., and Krattinger, S. G. (2022). The long road to engineering durable disease resistance in wheat. *Curr. Opin. Biotechnol.* 73, 270–275. doi: 10.1016/j.copbio.2021.09.002

frontiers | Frontiers in Plant Science

TYPE Original Research
PUBLISHED 05 July 2023
DOI 10.3389/fpls.2023.1210632

Check for updates

OPEN ACCESS

EDITED BY
Xinli Zhou,
Southwest University of Science and Technology, China

REVIEWED BY
Haifeng Liu,
Chonnam National University, Republic of Korea
Xiaojun Nie,
Northwest A&F University, China
Xiaodong Wang,
Hebei Agricultural University, China
Huan Luo,
Chungnam National University, Republic of Korea

*CORRESPONDENCE
Wang Chen
chenwangchw@163.com
Zhengwu Fang
fangzhengwu88@163.com
Wenli Wang
wliw@163.com

†These authors have contributed equally to this work

RECEIVED 23 April 2023
ACCEPTED 09 June 2023
PUBLISHED 05 July 2023

CITATION
Feng Y, Tang M, Xiang J, Liu P, Wang Y, Chen W, Fang Z and Wang W (2023) Genome-wide characterization of L-aspartate oxidase genes in wheat and their potential roles in the responses to wheat disease and abiotic stresses. *Front. Plant Sci.* 14:1210632. doi: 10.3389/fpls.2023.1210632

COPYRIGHT
© 2023 Feng, Tang, Xiang, Liu, Wang, Chen, Fang and Wang. This is an open-access article distributed under the terms of the Creative Commons Attribution License (CC BY). The use, distribution or reproduction in other forums is permitted, provided the original author(s) and the copyright owner(s) are credited and that the original publication in this journal is cited, in accordance with accepted academic practice. No use, distribution or reproduction is permitted which does not comply with these terms.

Genome-wide characterization of L-aspartate oxidase genes in wheat and their potential roles in the responses to wheat disease and abiotic stresses

Yanqun Feng[1†], Mingshuang Tang[2†], Junhui Xiang[1], Pingu Liu[1], Youning Wang[3], Wang Chen[1*], Zhengwu Fang[1*] and Wenli Wang[4*]

[1]Ministry of Agriculture and Rural Affairs (MARA) Key Laboratory of Sustainable Crop Production in the Middle Reaches of the Yangtze River (Co-Construction by Ministry and Province)/Engineering Research Center of Ecology and Agricultural Use of Wetland, Ministry of Education, Hubei Collaborative Innovation Center for Grain Industry, College of Agriculture, Yangtze University, Jingzhou, China, [2]Nanchong Academy of Agriculture Sciences, Nanchong, Sichuan, China, [3]Hubei Key Laboratory of Quality Control of Characteristic Fruits and Vegetables, Hubei Engineering University, Xiaogan, Hubei, China, [4]College of Plant Protection, Northwest A&F University, Yangling, Shaanxi, China

L-aspartate oxidase (AO) is the first enzyme in NAD^+ biosynthesis and is widely distributed in plants, animals, and microorganisms. Recently, AO family members have been reported in several plants, including *Arabidopsis thaliana* and *Zea mays*. Research on AO in these plants has revealed that AO plays important roles in plant growth, development, and biotic stresses; however, the nature and functions of AO proteins in wheat are still unclear. In this study, nine *AO* genes were identified in the wheat genome *via* sequence alignment and conserved protein domain analysis. These nine wheat *AO* genes (*TaAOs*) were distributed on chromosomes 2, 5, and 6 of sub-genomes A, B, and D. Analysis of the phylogenetic relationships, conserved motifs, and gene structure showed that the nine *TaAOs* were clustered into three groups, and the *TaAOs* in each group had similar conserved motifs and gene structure. Meanwhile, the subcellular localization analysis of transient expression mediated by Agrobacterium tumetioniens indicated that TaAO3-6D was localized to chloroplasts. Prediction of cis-elements indicated that a large number of cis-elements involved in responses to ABA, SA, and antioxidants/electrophiles, as well as photoregulatory responses, were found in *TaAO* promoters, which suggests that the expression of *TaAOs* may be regulated by these factors. Finally, transcriptome and real-time PCR analysis showed that the expression of *TaAOs* belonging to Group III was strongly induced in wheat infected by

F. graminearum during anthesis, while the expression of *TaAOs* belonging to Group I was heavily suppressed. Additionally, the inducible expression of *TaAOs* belonging to Group III during anthesis in wheat spikelets infected by *F. graminearum* was repressed by ABA. Finally, expression of almost all *TaAOs* was induced by exposure to cold treatment. These results indicate that TaAOs may participate in the response of wheat to *F. graminearum* infection and cold stress, and ABA may play a negative role in this process. This study lays a foundation for further investigation of *TaAO* genes and provides novel insights into their biological functions.

KEYWORDS

TaAO, gene structure, abiotic stresses, gene expression, quantitative PCR, biological functions

1 Introduction

L-aspartate oxidase (AO), a kind of flavin oxidase, converts aspartate to iminoaspartic acid using either molecular oxygen or fumarate as electron acceptors. It plays an indispensable role in the biosynthesis of nicotinamide adenine dinucleotide (NAD^+) (Mattevi et al., 1999). NAD^+ biosynthesis consists of five steps, of which the first is oxidation of L-aspartate into iminoaspartate catalyzed by L-aspartate oxidase (Katoh et al., 2006). NAD^+ is an important component of the respiratory chain, so it plays an important role in biological energy metabolism. It additionally participates in reduction–oxidation reactions, DNA repair, ADP-ribosylation, and a series of metabolic processes (Gakiere et al., 2018). L-aspartate oxidase, as the enzyme of the first reaction in *de novo* synthesis of NAD^+, is also thought to play an important role in the energy metabolism system and other metabolic pathways in organisms. Therefore, AO has been researched extensively over the years.

AO was initially reported in *Escherichia coli*, where the B protein of quinolinic synthase was identified as a L-aspartate oxidase (Nasu et al., 1982). Later, two conserved domains, the FAD binding domain and Succ_DH_flav_C, were found in AO proteins (Mattevi et al., 1999). Subsequently, AO was identified in *Pyrococcu shorikishii* OT-3 (Sakuraba et al., 2002), *Sulfolobus tokodaii* (Sakuraba et al., 2008), *Bacillus subtilis* (Marinoni et al., 2008), and *Pseudomonas putida* (Leese et al., 2013). Since then, the physiological and biochemical properties of AO have been extensively investigated in bacteria (Mortarino et al., 1996; Bifulco et al., 2013; Armenia et al., 2017; Chow et al., 2017). AO has the following two features: (a) *in vitro*, it is able to use different electron acceptors, such as oxygen, fumarate, cytochrome c, and quinones, suggesting that it is involved in NAD biosynthesis in anaerobic as well as aerobic conditions (Tedeschi et al., 1996); and (b) the primary and tertiary structures are not similar to those of other flavo-oxidases, but rather are similar to those of the flavoprotein subunit of the succinate dehydrogenase/fumarate reductase class of enzymes. AO can reduce fumarate and oxidize L-aspartate, but cannot oxidize succinate (Bacchella et al., 1999; Tedeschi et al., 2010). It has been reported that *Shigella*, a nicotinic acid auxotroph, is unable to synthesize NAD *via* the *de novo* pathway due to *AO* gene mutations. When AO function is restored in *Shigella*, sustained loss of virulence and inability to invade host cells are observed, which points toward AO as a locus of antivirulence (Prunier et al., 2007).

Compared with microorganisms, little is still known about AO in plants. Up to this point, AO proteins have been reported only in maize and *A. thaliana*. In maize, a gene *GRMZM2G139689* has been reported to encode AO protein. At the mononuclear stage of microspore development, the expression level of this gene was found to be greatly downregulated in male sterile line C48-2 compared with maintainer line 48-2 (Dong, 2019). This suggests that AO protein may be involved in pollen abortion in maize. In *A. thaliana*, *At5g14760* has been identified as an *AO* (Macho et al., 2012). Overexpression of *AtAO* increases NAD^+ content, and loss of AtAO activity results in a decrease in NAD^+ levels (Hao et al., 2018). It is worth noting that the expression of *AOs* is upregulated in *A. thaliana* leaves infected by avirulent *Pseudomonas syringae* pv. *tomato* strain (Petriacq et al., 2012). Furthermore, research with an *AO A. thaliana* mutant has shown that AO is required for reactive oxygen species (ROS) bursts triggered by pathogen-associated molecular patterns and for stomatal immunity (Macho et al., 2012). These studies indicate that *AO* genes play important roles in regulating plant development and response to biotic stresses.

Wheat is one of the top three crops worldwide (Guo et al., 2018). Almost 60% of the wheat produced globally is consumed as food (Sobolewska et al., 2020), and global demand for wheat is expected to grow by approximately 70% over the next 30 years with growing populations, rising income levels, and increasing household consumption (Abedi and Mojiri, 2020). Wheat often suffers from exposure to biotic and abiotic stresses during growth; it is unclear whether wheat AO participates in the plant's response to biotic/abiotic stresses, and the molecular characteristics of wheat AO are also unclear. In this study, TaAO genes were identified *via* sequence alignment and protein domain analysis, and the gene structure, phylogenetic relationships, and chromosome distribution of *TaAO* family genes were subsequently analyzed systematically

using bioinformatics methods. Finally, the expression patterns of *TaAO* family genes were quantified *via* transcriptome analysis and qRT-PCR. This study lays a foundation for further analysis of *AO* genes in wheat.

2 Materials and methods

2.1 Genome-wide identification of *AO* genes in *T. aestivum*, *Ae. tauschii*, *T. urartu*, and *T. dicoccoides*

Genome data for *T. aestivum* (IWGSCv2.1), *Ae. tauschii* (v4.0.43), *T. urartu* (v1.43), and *T. dicoccum* (v1.0.43) were downloaded from Ensembl Plants database (http://plants.ensembl:index.html). Hidden Markov models (HMMs) for the FAD binding domain (PF00890.27) and the Succ_DH_flav_C domain (PF02910.23), obtained from the Pfam database (http://pfam.xfam), were used as queries to identify wheat AOs using HMMER3.0 (http://hmmer:download.html) with hit sequences specified as those with an e-value below $1e^{-5}$. Three *Arabidopsis* AOs (AtAOs), three maize AOs (ZmAOs), and two rice AOs (OsAOs), where the identification method was similar to that of *TaAOs*, were retrieved from genome databases for *Arabidopsis* (http://www.arabidopsis:index.jsp), maize (https://www.maizegdb.org), and rice (http://rice.plantbiology.msu.edu), respectively (Table S1). These AO proteins were used as queries to search for AO proteins in the genomes of *T. aestivum, Ae. tauschii, T. urartu*, and *T. dicoccoides via* BLASTp. Hit sequences with an e-value below $1e^{-5}$ were retained. The wheat AO candidates obtained using the above two methods were combined, and the non-redundant proteins were further analyzed using Pfam (v31.05) (http://pfam.sanger.ac.uk/search) and SMART (http://smart.embl-heidelberg.de/) (Letunic and Bork, 2018). Only these proteins that contained both the FAD binding domain and the Succ_DH_flav_C domain were considered to be wheat AOs. The *AO* genes were named according to their distribution on the chromosomes.

2.2 Characteristics of TaAO proteins

The protein sequence length, isoelectric point (pI), molecular weight (MW), instability index, and grand average of hydropathicity (GRAVY) of TaAOs were predicted using the ExPASy online tool (https://www.expasy.org/) (Gasteiger et al., 2003). Subcellular localization of TaAOs was predicted using the WoLF PSORT online tool (https://wolfpsort.hgc.jp/) (Chou and Shen, 2010).

2.3 Phylogenetic analysis of TaAOs

The sequences of AO proteins from *A. thaliana*, rice, maize, *T. aestivum*, *Ae. tauschii*, *T. urartu*, and *T. dicoccoides* were aligned using the ClustalW2 software package (Thompson et al., 1994). A neighbor-joining (NJ) phylogenetic tree was constructed using the MEGA X software package (Mega Limited, Auckland, New Zealand) (Kumar et al., 2018) with 1000 bootstrap repetitions. Finally, the tree was modified using the Interactive Tree of Life tool (iTOL, v6, http://itol.embl.de) (Letunic and Bork, 2021).

2.4 Genomic organization of TaAOs in wheat

Information on the position of TaAOs in wheat chromosomes was extracted from annotated information on the wheat genome. The physical map was drawn using the MapInspect software package. Information on the exon–intron structure of *TaAO* genes was visualized using the TBtools software package (Chen et al., 2020). Conserved motifs of TaAOs were identified using the MEME suite, with the following parameter settings: number of motifs, up to 15; width range, from 6 to 50 amino acids. The outputs on the motif structures of TaAO proteins were displayed using TBtools. Gene duplication events were analyzed according to the method described by Panchy et al. (2016) and illustrated using the Circos package in TBtools. For further examination of the footprints of selection during the processes of domestication (wild emmer and *Ae. tauschii* versus landraces) and improvement (landraces versus varieties), we overlapped the identified *AO* genes with the sweep region identified by Cheng et al. (2019) to check whether they were selected. The Ka and Ks values and the Ka/Ks ratio were calculated using TBtools. A Ka/Ks value of 1 indicates a neutral selection effect; a Ka/Ks value >1 indicates positive selection for evolutionary acceleration; and Ka/Ks <1 indicates purifying selection under function constraints.

2.5 RNA isolation and cDNA first-strand synthesis

Total RNA was extracted using TRIzol reagent (Invitrogen, USA) according to the manufacturer's instructions. Subsequently, 1 µg RNA was used for cDNA first-strand synthesis using a PrimeScript RT reagent kit with gDNA Eraser (Takara, China) according to the manufacturer's instruction.

2.6 Subcellular localization analysis of TaAO3-6D protein

Subcellular localization analysis of a TaAO protein was performed using an *Agrobacterium tumefaciens* mediated transient expression system in leaves of *Nicotiana benthamiana*. First, the coding sequence of a TaAO, *TaAO3-6D*, was amplified (the primers are listed in Table S2) and cloned into a GFP fusion protein expression vector pCAMBIA1300-GFP. Next, the recombinant vector was transformed into an *Agrobacterium tumefaciens* GV3101 strain. Positive clones were cultured and injected into the leaves of 5- to 6-week-old *Nicotiana benthamiana*. These were observed using a fluorescence microscope (Olympus FV3000, Tokyo, Japan) 48 h after injection.

2.7 Cis-acting element and protein interaction network analyses of TaAOs

The 1.5 kb sequence upstream of the start codon of each of the *TaAO* genes was obtained, and these sequences were used for the prediction of cis-acting elements *via* the PlantCARE website (http://bioinformatics.psb.ugent.be/webto-ols/plantcare/html/). The cis-acting elements were arranged and displayed using the R software package "pheatmap" (Rombauts et al., 1999). To study the protein–protein interactions (PPIs) between TaAOs and other proteins, a protein network was generated using the STRING v11.5 webserver (https://cn.string-db.org/).

2.8 Expression profiling of *TaAO* genes *via* transcriptome analysis

Transcriptome data on sequences involved in wheat growth and wheat responses to biotic stresses (*Fusarium graminearum*, stripe rust, and wheat powdery mildew) and abiotic stresses (phosphorous starvation, cold, heat, and drought) were downloaded from the NCBI database (Table S3) and mapped to the wheat reference genome *via* Hisat2 (Fang et al., 2020). The expression levels of *TaAOs* were calculated using Cufflinks (Trapnell et al., 2012). All transcript values were standardized by log2 (TPM + 1) transformation, and the expression profiles of *TaAOs* were generated using the R package "pheatmap".

2.9 Growth and stress treatments of wheat seedlings

Jingshuang 16, a wheat cultivar moderately susceptible to powdery mildew and rust (Ren et al., 2015), was used in this study. The wheat seeds were disinfected with 1% hydrogen peroxide; subsequently, after washing with distilled water, the seeds were kept at 25°C for 2 days for germination. The seedlings were cultured in quarter-strength Hoagland nutrient solution for 3 days, and then transferred to one-half Hoagland nutrient solution (pH=6.0) (Bishop and Bugbee, 1998). To examine the differential expression of *TaAOs* in response to drought and abscisic acid (ABA) treatment, seedlings were cultured in a greenhouse at 25/20°C under a 16 h light/8 h dark cycle. The seedlings were treated with 20% PEG6000, once at the heart stage and once at the leaf stage. Wheat leaves were sampled at 0, 2, 12, 24, 36, and 48 h after treatment. For the ABA treatment, ABA was added to one-half strength Hoagland nutrient solution at a final concentration of 100 μM. After 0, 2, 6, 12, 24, and 48 h of treatment, leaves were harvested for further research. Finally, for the stripe rust infection treatment, seedlings were cultured in a plant growth chamber under a 16 h light/8 h dark cycle at 16°C. Wheat leaves were inoculated with fresh uredospores of stripe rust CYR32 using the smearing method and kept in dark, moist conditions for 24 hours to promote infection (Santra et al., 2008). Leaves were collected at 0, 6, 12, 24, and 48 h. All samples were immediately frozen in liquid nitrogen and stored at -80°C for future use.

2.10 qRT-PCR analysis

Real-time PCR reaction systems were used to carry out reaction schemes following the manufacturer's instruction (Vazyme, China). Gene-specific primers (Table S4) were designed using the Primer 5.0 software package. The ADP-ribosylation factor *Ta2291* was used as the internal reference gene for qRT-PCR analysis. Each experiment was carried out with three biological replicates, and three technical repeats were performed for each replicate.

3 Results

3.1 Identification and classification of *AO* genes in wheat

Ten AO candidates were obtained from the wheat genome *via* HMM search. Meanwhile, the same ten AO candidates were retrieved from the wheat genome *via* BLASTp. Of these, one gene without the Succ_DH_flav_C domain was excluded, and the remaining nine candidate genes containing both of the FAD binding domain and the Succ_DH_flav_C domain were identified as *TaAOs* (Table 1; Table S5). Using the same procedure, four, three, and six *AOs* were identified for *T. urartu*, *Ae. Tauschii*, and *T. dicoccoides*, respectively (Table S4). The locations of *AO* genes on the wheat chromosomes were determined and analyzed for genomic homology; this analysis indicated that nine *TaAO* genes were distributed evenly on chromosomes 2, 5, and 6 of sub-genomes A, B, and D, while no tandem duplication or segmental duplication events were found (Figure 1).

3.2 Analysis of TaAO protein characteristics

To further understand the characteristics of the TaAO proteins, protein length, molecular weight, instability index, isoelectric points, average hydrophilicity coefficients, and predicted subcellular localization were analyzed. As shown in Table 1, the protein length of the TaAOs ranged from 571 to 641 aa, and molecular weight ranged from 62.5 to 70.7 kDa. Instability index ranged from 30.66 to 39.48, indicating that these TaAOs were all stable proteins (instability index < 40). The isoelectric points of these TaAOs fell between 5.98 and 6.94, which showed that they were acidic proteins. Their average hydrophilicity coefficients ranged from 0.186 to 0.393, indicating that they were hydrophilic proteins. Subcellular localization prediction *via* the WoLF PSORT software package indicated that TaAO3-6A, TaAO3-6B, and TaAO3-6D were localized to chloroplasts, while TaAO1-2A, TaAO1-2B, TaAO3-3D, TaAO2-5A, TaAO2-5B, and TaAO2-5D were localized to mitochondria. The results of TaAO3-6D-GFP fusion protein expression assays showed that TaAO3-6D was localized to chloroplasts (Figure 2), which was consistent with the predicted results.

3.3 Conserved motifs and gene structures of *TaAOs*

To understand the evolutionary relationships between TaAOs, a phylogenetic tree was constructed. As shown in Figure 3A, three *TaAOs* located on chromosome 2 were grouped into Group I, three

10.3389/fpls.2023.1210632

TABLE 1 Protein features of AOs in *Triticum aestivum*.

Name	Locus ID	Len	MW	pI	II	Stability	GRAVY	Sub
TaAO1-2A	TraesCS2A03G0615500.1	619	68045.78	6.22	34.07	stable	-0.348	mitochondrion
TaAO1-2B	TraesCS2B03G0694000.1	571	62522.66	6.3	30.66	stable	-0.295	mitochondrion
TaAO1-2D	TraesCS2D03G0589200.1	619	67956.76	6.3	32.97	stable	-0.347	mitochondrion
TaAO2-5A	TraesCS5A03G0972600.1	621	68317.15	6.11	33.17	stable	-0.361	mitochondrion
TaAO2-5B	TraesCS5B03G1021700.1	621	68289.1	6.11	33.31	stable	-0.362	mitochondrion
TaAO2-5D	TraesCS5D03G0925000.1	591	65208.54	5.98	33.98	stable	-0.393	mitochondrion
TaAO3-6A	TraesCS6A03G0227300.1	641	70704.89	6.79	39.48	stable	-0.186	chloroplast
TaAO3-6B	TraesCS6B03G0316000.1	641	70780.01	6.94	38.80	stable	-0.206	chloroplast
TaAO3-6D	TraesCS6D03G0185200.1	641	70639.88	6.94	39.10	stable	-0.194	chloroplast

Len, amino acid length (aa); MW, molecular weight (KDa); pI, isoelectric point; II, instability index; GRAVY, grand average of hydropathy; Sub, subcellular localization.

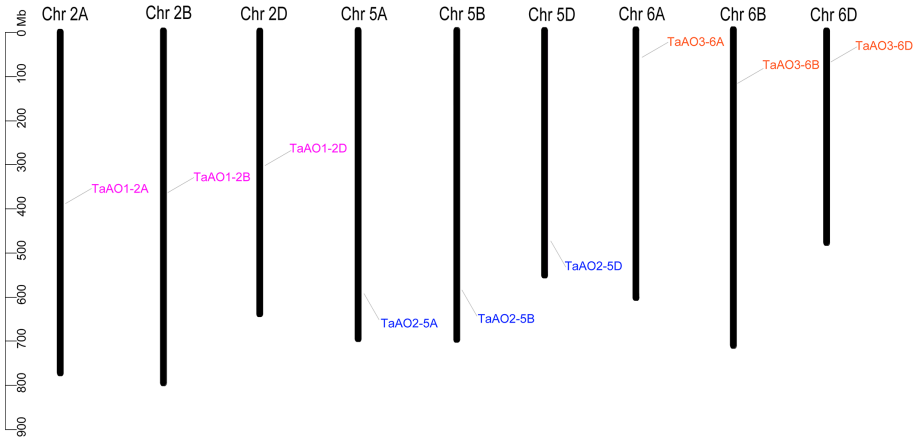

FIGURE 1
Chromosome locations of the nine TaAOs in wheat. The ruler on the left represents the physical distance between genes (Mbp).

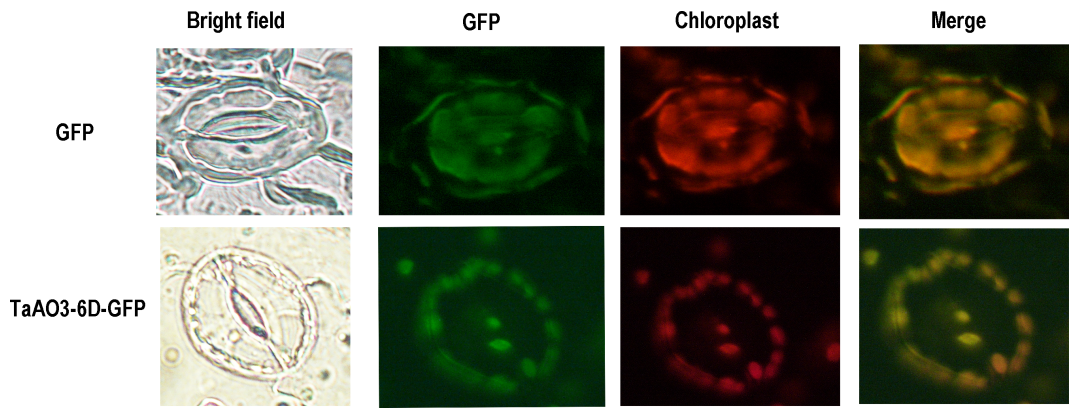

FIGURE 2
GFP-fused proteins of TaAO3-6D were localized to the chloroplasts of *Arabidopsis* guard cells. Chloroplast autofluorescence (red) and GFP fluorescence (green) in guard cells were simultaneously observed. Bright-field images (on the left) show the shapes of guard cells. Unfused GFP was found in the cytoplasm and nucleus, whereas TaAO3-6D-GFP was found in the chloroplasts. Scale bar = 10 μm.

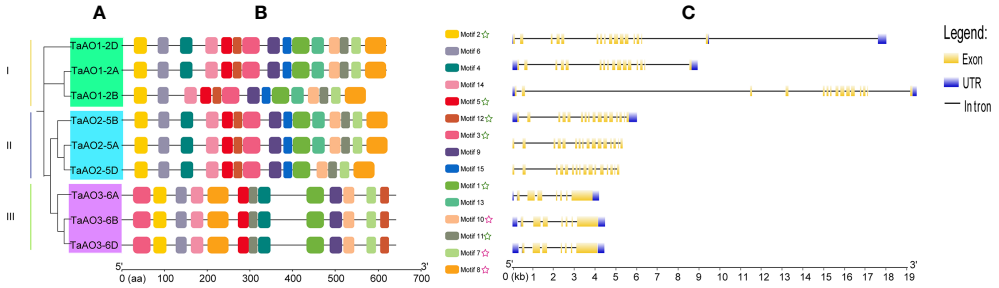

FIGURE 3
Phylogenetic analysis, conserved motifs, and gene structure of TaAOs. **(A)** Phylogenetic tree of TaAOs. The tree was built using the neighbor-joining (NJ) method with 1000 bootstrap repetitions in MEGA7. **(B)** Motifs of TaAO identified using MEME; MAST was used to visualize the patterns. Each motif is indicated with a specific color. The green star symbol represents the FAD binding domain; the purple star symbol represents the Succ_DH_flav_C domain. **(C)** Exon–intron structure of TaAOs, analyzed using GSDS. Untranslated regions (UTRs) are represented by blue frames; exons are represented by yellow frames; and introns are represented by black lines.

TaAOs located on chromosome 5 were grouped into Group II, and the three genes located on chromosome 6 were clustered into Group III. The results of a conserved motifs analysis of the TaAOs (Figure 3B; Table S6) showed that all TaAO proteins contained Motifs 1, 2, 3, 5, 7, 8, 10, 11, and 12. Motifs 7, 8, and 10 were contained in the Succ_DH_flav_C domain and Motifs 1, 2, 3, 5, 11, and 12 were contained in the FAD binding domain. The number and order of motifs in TaAOs belonging to Groups I and II were essentially consistent, with the exceptions of *TaAO1-2B* lacking Motif 4 and *TaAO2-5D* lacking Motif 13. The number of motifs of Group III members differed from that of members of Groups I and II. TaAOs in Group III only had 13 motifs, from which Motifs 13 and 15 were absent. Furthermore, the order of motifs in Group III also differed from that of the other two groups. Additionally, the results on intron/exon distribution patterns of *TaAO* genes appeared to indicate that the number of exons was significantly greater in Groups I and II than in Group III. Generally, *TaAOs* belonging to Groups I and II contained 16 exons, with the exception of *TaAO1-2D*, which only contained 15 exons. In contrast, the *TaAOs* belonging to Group III only contained seven exons (Figure 3C).

3.4 Phylogenetic and Ka/Ks analysis of *AO* genes of *T. aestivum* and its ancestor species

To further evaluate the phylogenetic relationships of TaAOs with other plant AOs, nine AOs from *T. aestivum*, four from *T. urartu*, three from *Ae. Tauschii*, six from *T. dicoccoides*, two from *Oryza sativa*, three from *Zea mays*, and three from *A. thaliana* were used to construct a phylogenetic tree. As shown in Figure 4, the set of all AOs could be divided into three groups, which was consistent

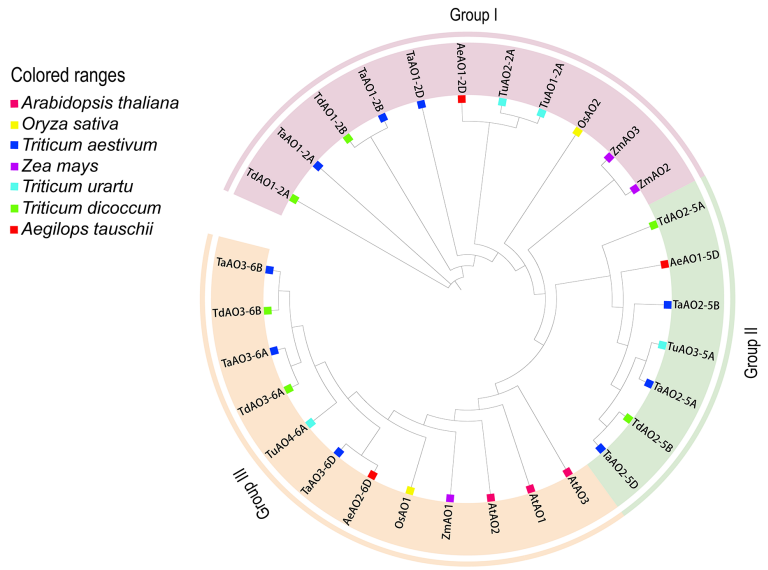

FIGURE 4
Phylogenetic tree of AOs from wheat, maize, rice, *Arabidopsis*, *T. urartu*, *T. dicoccoides*, and *Ae. tauschii*. The protein sequences were aligned using ClustalW2, and the phylogenetic tree was constructed using neighbor-joining (NJ) (1000 repeats) in the MEGA 7.0 software package. The AOs of wheat, maize, rice, *Arabidopsis*, *T. urartu*, *T. dicoccoides*, and *Ae. tauschii* can be distinguished by the use of different colors and shapes.

with the above-described results on the phylogenetic tree of wheat AOs. TaAOs located on chromosome 2 in different sub-genomes were classified into Group I, TaAOs located on chromosome 5 were in Group II, and TaAOs on chromosome 6 were in Group III (Table S7). It is interesting that all three AtAOs were clustered into Group III, which was found to have the closest relationship with TaAOs on chromosome 6. The AOs of rice and *Zea mays* were classified into Groups I and III, with none falling into Group II. With regard to sub-genome donor species, members were distributed across the three groups. These results indicate that AOs in these species may have evolved under different evolutionary directions, and furthermore, the functions of AOs in different groups may be at variance with one another.

A homology analysis of wheat and three sub-genome donor species was conducted, and the orthologs and paralogs were clustered. Orthologs are defined as genes in different species that are derived from a single gene in the last common ancestor, and paralogs are homologous genes within a single species, resulting from gene duplication (Remm et al., 2001). A total of 53 homologous gene pairs were associated with *T. aestivum* (Figure 5A), of which nine were paralog gene pairs and 44 were ortholog gene pairs were found. Among these 44 ortholog gene pairs, there were 7, 22, and 15 ortholog genes between *T. aestivum* and each of its ancestor species (*Ae. Tauschii*, *T. dicoccoides*, and *T. Urartu*, respectively). *TaAO* genes the AOs of *Ae. tauschii*, *T. dicoccoides*, *T. urartu* and *T. aestivum* can be divided into three groups (Figure 5B) were not found in either the domestication-related or the improvement-related sweep regions, and all the Ka/Ks values for AO replication gene pairs were <1 (Figure 5C; Table S8), indicating that *TaAO* genes were purified and selected, and their functions may be conserved.

3.5 Cis-element analysis of *TaAO* genes

In the process of plant growth and development, not only can cis-regulatory elements regulate the spatio-temporal expression of genes, but they also are involved in responses to phytohormone exposure and abiotic stresses (Davis, 2009). In the present study, 39 kinds of cis-elements were identified in the promoter regions of *AO* genes in wheat (Figure 6; Table S9). Cis-elements involved in growth and development, including the TATA box and CAAT box, were found in all TaAO promoters. For cis-elements associated with plant hormone responses, the largest set of cis-elements was

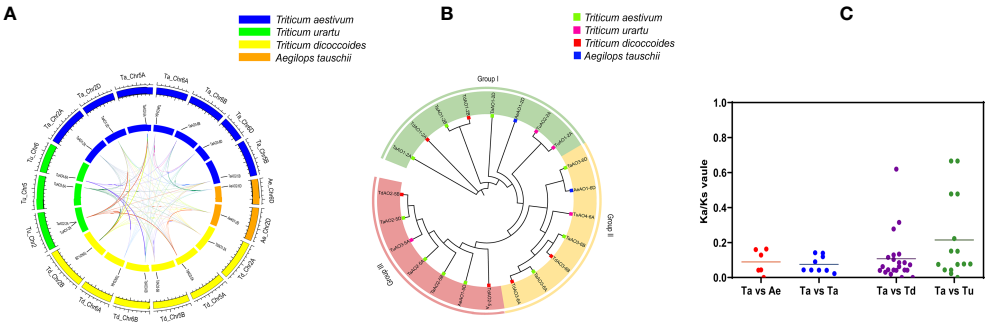

FIGURE 5
Analysis of **(A)** synteny and **(B)** phylogeny for *AO* genes in *T. aestivum* and its sub-genomic progenitors *T. urartu*, *T. dicoccoides*, and *Ae. Tauschii*. **(A)** Orange rectangles represent *Ae. tauschii* chromosomes, green rectangles represent *T. urartu* chromosomes, blue rectangles represent *T. aestivum* chromosomes, and yellow rectangles represent *T. dicoccoides* chromosomes. **(B)** This phylogenetic tree was constructed using 1000 bootstrap repetitions under the neighbor-joining (NJ) method in MEGA7. Blue, red, purple, and green squares represent *Ae. Tauschii*, *T. dicoccoides*, *T. urartu*, and *T. aestivum*, respectively. **(C)** Ka/Ks values for AO orthologous gene pairs between *T. aestivum*, *T. urartu*, *T. dicoccoides*, and *Ae. Tauschii*.

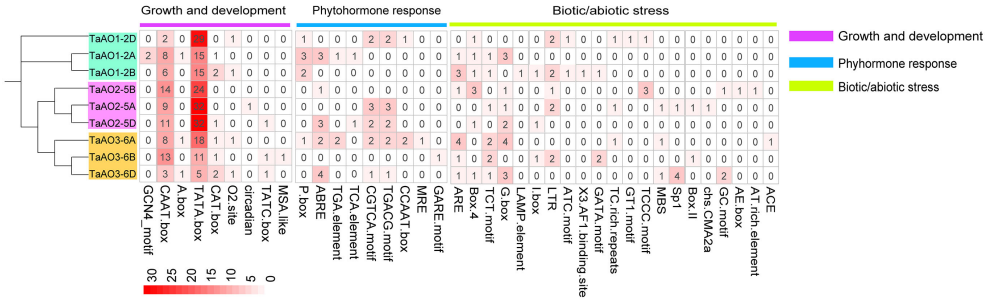

FIGURE 6
Identification of cis-acting elements of *TaAO* genes. The color gradient in each grid represents the number of promoter elements of these *AO* genes.

that of abscisic acid response elements (ABRE), of which 13 were identified. The second largest sets of cis-elements were salicylic acid-associated elements (CGTCA motif and TCA elements); the number of elements identified for each of these was 10. This suggests that the expression of *TaAOs* may be regulated by ABA and SA. The TGACG motif (methyl jasmonate), TGA element (auxin), CGTCA motif, and TCA element (salicylic acid) were identified in most of the *TaAO* gene promoters. In terms of biotic and abiotic stresses, the most abundant cis-element was the G-box, with 14 elements identified, followed by ARE, with 11. This suggests that the expression of *TaAOs* may be regulated by antioxidant/electrophile and photoregulatory factors. In summary, in addition to biotic stress regulation of AO, AO may also be regulated by ABA and SA hormones, as well as antioxidant/electrophile and photoregulatory abiotic stresses.

3.6 Molecular interaction networks

A network of the interactions between TaAOs and other wheat proteins was built using STRING v11.0. The results showed that all nine TaAO proteins interacted with 17 wheat proteins. Among these 17 wheat proteins, seven (Traes_5BL_402FB4A3F.1, Traes_7AL_C0609756B.1, Traes_7BL_8F49CE9D6.2, Traes_2AS_4AB51ACE2.1, Traes_2AS_BA55E613D.2, Traes_7AL_6405AB56F.2, Traes_4AS_2DCA42965.1) were unknown proteins, and the remaining ten were Succinate-CoA ligases (Traes_2DS_3AC11B9D8.1, Traes_2AS_3BA916807.1, Traes_2BS_8863D42E7.1), 4Fe-4S ferredoxin-type protein (Traes_5DL_885A58CBA.3), lactate/malate dehydrogenase (Traes_1BL_A93F9F079.2, Traes_1DL_5A31A68D3.2, Traes_1AL_2EC98608D.2), malate dehydrogenase (Traes_1BL_BD3E22844.1), succinate dehydrogenase (Traes_7DL_91E866851), and transket_pyr protein (Traes_2AL_1E2B26B7F.1) (Figure 7; Table S10). Succinate-CoA ligase (SUCL) can promote the production of ATP during the conversion of malate to succinate in the TCA cycle (Ostergaard, 2008). 4Fe-4S ferredoxin-type protein (4Fe-4S Fed) is involved in various redox processes in organisms, such as DNA repair, RNA and protein modification, and cofactor synthesis (Feng et al., 2021). Lactate/malate dehydrogenases (LDH/MDH) are involved in energy metabolism. Lactate dehydrogenase (LDH) operates at the final stage of aerobic glycolysis. Malate dehydrogenase (MDH) is a key enzyme in the regulation of malate metabolism; it catalyzes the reversible oxidative decarboxylation of malate to produce pyruvate and CO_2, as well as the reduction of $NAD(P)^+$ (Zhao et al., 2022). Succinate dehydrogenase (SDH) is the only enzyme that participates in both the tricarboxylic acid or citric acid cycle and the electron transport chain (Gill, 2012). Transket_pyr protein (TK) plays an important role in carbon metabolism (Liu et al., 2023). These AO-interacting proteins all play important functions in energy metabolism, which explains why AO also plays such an important role in energy metabolism. These results provide clues for further study of the function of *TaAO* genes.

3.7 Transcriptome analysis of *TaAOs*

In order to understand the expression patterns of *TaAOs*, wheat transcriptome data taken from different tissues and under exposure to different abiotic and biotic stresses were analyzed. From Figure 8, it is clearly evident that the expression levels of *TaAOs* belonging to Group II were the highest in all selected transcriptomes, which indicates that these three TaAOs may play essential roles in plant

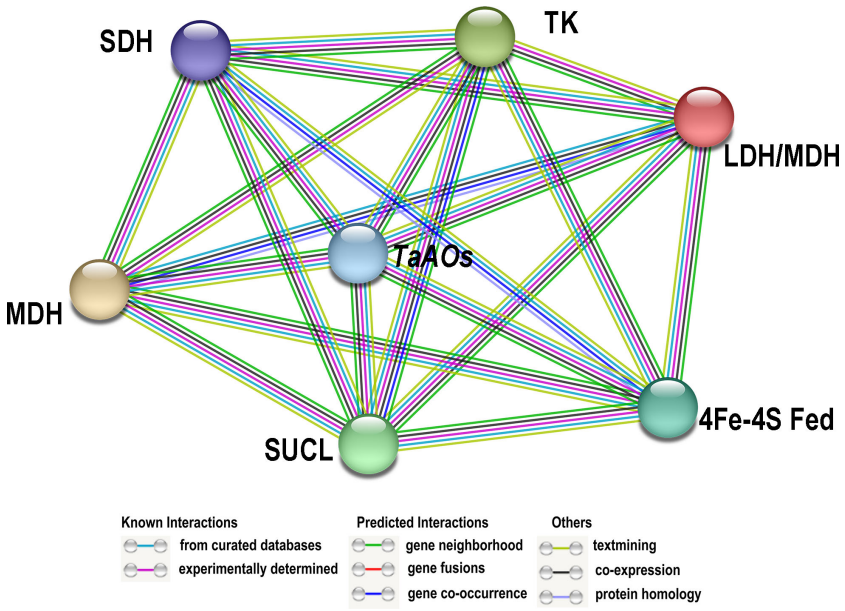

FIGURE 7
Protein–protein interaction (PPI) analysis of TaAO proteins. PPI network generated using STRINGV 11.5. Each node denotes a protein, and each edge represents an interaction.

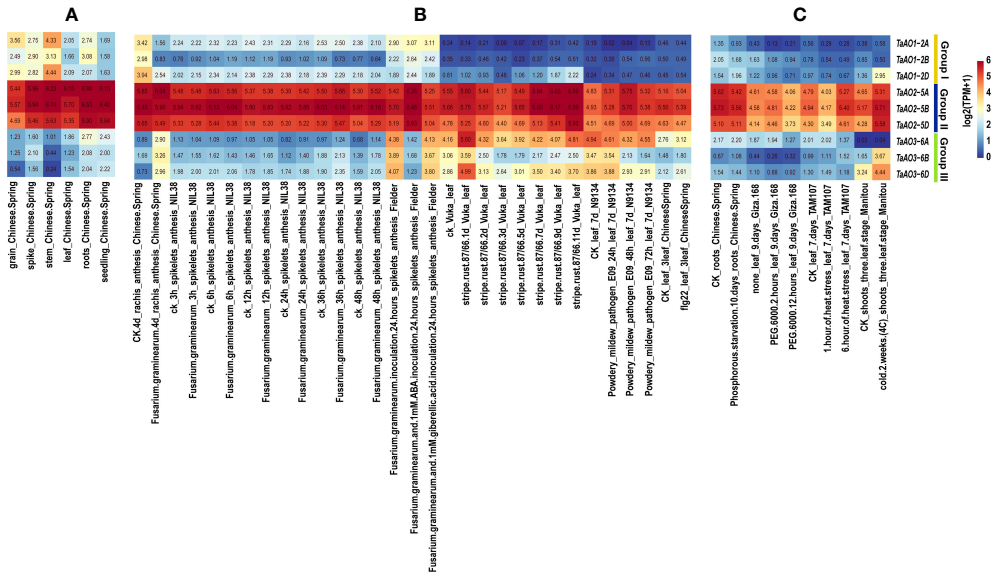

FIGURE 8
Transcriptome analysis of TaAOs. **(A)** Expression levels of nine *TaAO* genes in different tissues of Chinese Spring wheat. **(B)** Gene expression profiles of *TaAOs* under exposure to biological stress, plant hormone treatment, and pathogen-associated molecular patterns (PAMP). **(C)** Expression patterns of *TaAO* genes in wheat plants under exposure to different abiotic stresses. Different colors indicate the gene expression level: red indicates higher levels of expression, and blue lower.

growth and response to various treatments. In terms of the different tissues, *TaAOs* belonging to Group I were relatively highly expressed in the spike, grain, stem, and root, and *TaAOs* belonging to Group III were relatively highly expressed in the root and seedling, while *TaAOs* belonging to Group II were highly expressed in all tissues, with no clear tissue specificity observed (Figure 8A).

As shown in Figure 8B, the transcriptomes of TaAOs under biotic stress were analyzed. In general, the expression of *TaAOs* changed slightly after infection by stripe rust. With the exceptions of *TaAO1-2A* and *TaAO3-6B*, the expression of *TaAOs* was induced by this form of stress. Interestingly, expression of *TaAO1-2D* was induced to a large extent at the late stage of infection (9 d and 11 d), while expression of *TaAO3-6D* was significantly induced at the early stage of infection (1d). These findings suggest that *TaAOs* might play a role in the response to stripe rust infection, but the patterns of expression were different for different *TaAO*s. In wheat N9134 from leaf tissue infected by powdery mildew, the expression levels of *TaAO*s also changed slightly. The expression of *TaAO1-2A* and of TaAOs belonging to Group III was suppressed, while the expression of other *TaAOs* was induced. The expression of *TaAOs* was also slightly altered in wheat NIL38 from spikelet tissue infected by *F. graminearum*, but it was greatly altered in *F. graminearum*-infected rachis tissue of Chinese Spring. In rachis tissue infected by *F. graminearum*, the expression of *TaAOs* belonging to Group I was repressed. The *TaAOs* with the greatest decrease in expression were *TaAO1-2B*, the expression levels of which decreased to 11.2% of the levels observed in CK, while the expression of *TaAOs* belonging to Group III was induced. The *TaAOs* with the greatest increase in expression were *TaAO3-6D*, the expression level of which was 10.33 times that observed in CK. These findings indicate that TaAOs may be involved in the pathogenesis of Fusarium head blight, and that TaAOs belonging to Groups I and III play different roles. Additionally, we found that the expression levels of *TaAOs* belonging to Group III were much lower in *F. graminearum*-infected wheat spikelet tissue treated with 1 mM ABA than in non-ABA-treated wheat spikelet tissue. This indicates that ABA negatively regulates the expression of *TaAOs* belonging to Group III in *F. graminearum*-infected wheat spikelets.

As shown in Figure 8C, the transcriptomes of TaAOs under abiotic stress were also analyzed. The results showed that the most significant changes in expression levels of *TaAOs* were found in wheat in response to cold treatment. The expression of all *TaAOs* was induced, with the exception of *TaAO1-2B*, the expression level of which was decreased by half. In contrast, the expression of most *TaAOs* was repressed during exposure to heat stress and drought stress. These results indicate that most TaAOs may participate in the response to cold and that they play different roles in the responses to heat and drought.

3.8 Quantitative real-time PCR analysis

To further understand the potential role of *TaAO* genes in biotic and abiotic stresses, the patterns of expression of *TaAO1-2D*, *TaAO2-5A*, and *TaAO3-6D* in response to stripe rust infection, ABA, and PEG stress were quantified *via* qRT-PCR.

After PEG treatment (Figure 9), the expression levels of *TaAO1-2D* and *TaAO2-5A* were decreased for 36 hours, but they were subsequently increased at 48 hours after treatment. In contrast, the expression levels of *TaAO3-6D* were decreased for 48 hours following treatment. In the case of ABA treatment, similar expression patterns were detected in *TaAO2-5A* and *TaAO3-6D*, expression of which was suppressed for 48 hours following ABA

10.3389/fpls.2023.1210632

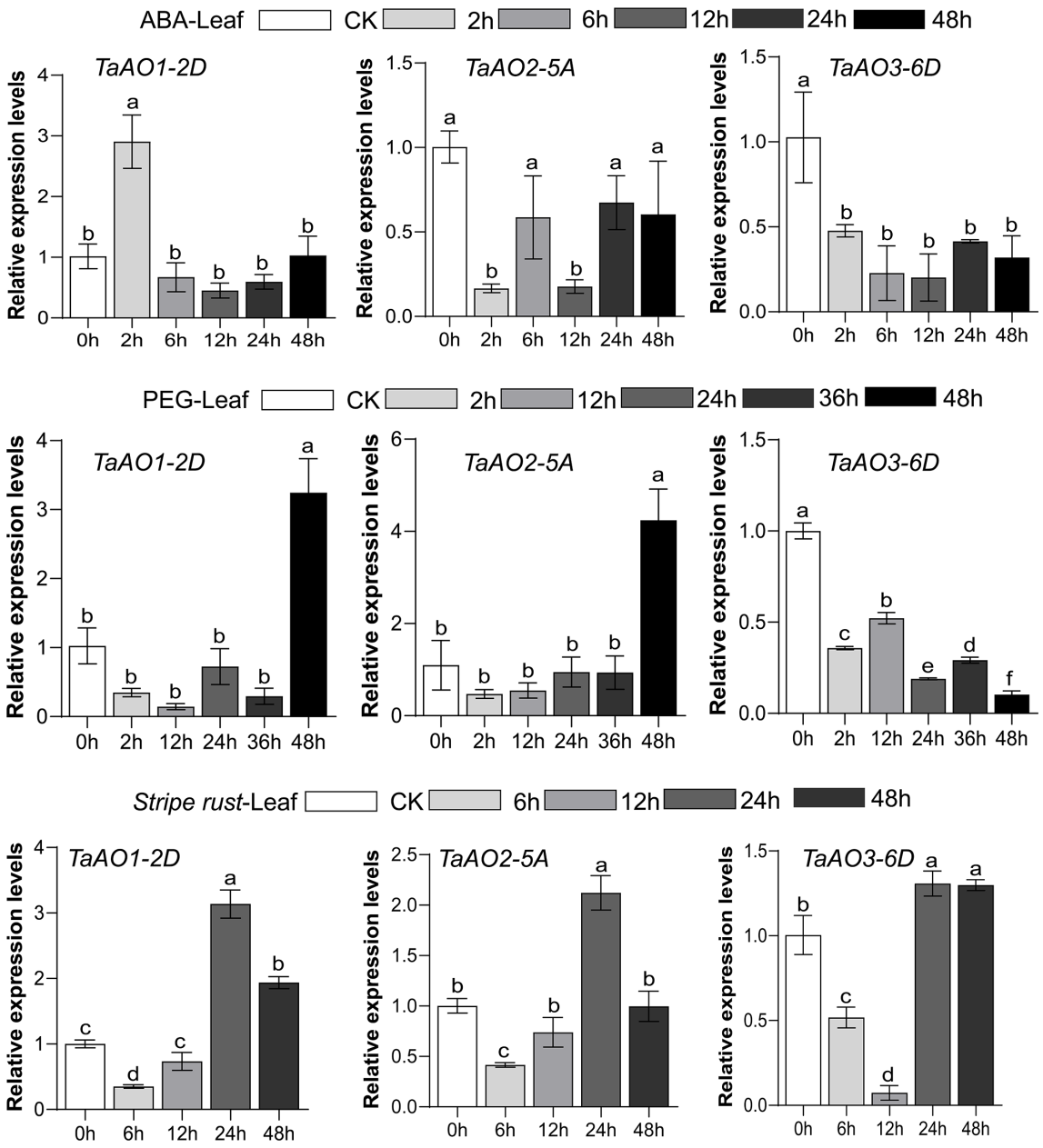

FIGURE 9
Expression levels of three *TaAO* genes in wheat leaves under exposure to abiotic stress (PEG), plant hormone treatment (ABA treatment), and biological stress (stripe rust infection), as indicated by qRT-PCR. The *x* axis represents time point, and the *y* axis represents expression level. Data from three independent replicates were analyzed; error bars represent the standard deviation. Lowercase letters (a-f) on the bars indicate significant differences determined via one-way ANOVA ($P < .05$). Plots created using GraphPad Prism 5.

treatment. The pattern of expression of *TaAO1-2D* differed slightly from that of the two aforementioned genes: an increase in the expression level of *TaAO1-2D* was observed 2 hours after ABA treatment.

Finally, in wheat inoculated with stripe rust, the general tendency of expression levels of *TaAO1-2D*, *TaAO2-5A*,and *TaAO3-6D* was to increase after an initial decrease. The lowest level of expression of *TaAO3-6D* was observed at 12 hpi, but the lowest levels for *TaAO1-2D* and *TaAO2-5A* were observed at 6 hpi. Compared with the expression level at 24 hpi, the expression levels of *TaAO1-2D* and *TaAO2-5A* were decreased at 48 hpi, while the expression level of *TaAO3-6D* at 48 hpi was roughly equal to that at 24 hpi.

4 Discussion

NAD^+ is an essential cofactor in energy metabolism and electron transfer. Additionally, several reports suggest that NAD^+ may be involved in plant defense responses (Dutilleul et al., 2003;

Zhang and Mou, 2009; Djebbar et al., 2012; Petriacq et al., 2012). Therefore, as the first enzyme of NAD^+ biosynthesis, AO may influence energy metabolism and plant defense by regulating NAD^+ content. However, this enzyme has previously only been reported in *Arabidopsis* and maize (Macho et al., 2012; Dong, 2019). In this study, we first conducted a systematic analysis of *AO*-family genes in wheat. The gene architectures, gene duplication events, chromosomal distributions, cis-elements in promoter regions, and expression patterns of *AO* genes in wheat were then further analyzed.

In this study, nine *AOs* were identified in wheat. Compared with other plants, the wheat genome encodes many more *AOs*, which may be due to the heterologous hexaploidy of the wheat genome. In this paper, homology analyses of wheat and three sub-genome donor species were carried out, as a result of which 44 homologous gene pairs were identified, accounting for 90.56% of the wheat orthologous gene pairs. These findings suggest that *TaAOs* are derived from three sub-genome donor species of wheat. Phylogenetic tree analysis of maize, *Arabidopsis*, rice, *T. aestivum*, and its ancestor species (*Ae. tauschii*, *T. dicoccoides*, and *T. urartu*) revealed that Group II only contained *T. aestivum* and its ancestor species. The expression of *AOs* in Group II was high during growth and development, and under biotic and abiotic stress (Figure 8), indicating that *AOs* of Group II play an important role in wheat, and that this group has been conserved in the evolution of wheat.

Although AOs are thought to be widely distributed in plants, there has been little investigation of the function of AOs in plants. Up to this point, only two reports on the function of plant AOs have been published (Macho et al., 2012; Dong, 2019). In one of these studies, a differentially expressed *ZmAO* gene involved in energy metabolism was screened from maize CMS-C sterile line C48-2. Compared with the control maintenance line 48-2, *ZmAO* was found to be significantly downregulated in C48-2 during the mononuclear stage of anther development. The *ZmAO* gene may be a positive energy regulator involved in plant growth and development through the NAD^+ synthesis pathway (Dong, 2019). Furthermore, AtAO2 of *Arabidopsis* is thought to participate in PTI and in resistance to *Pst* DC3000. The expression of *AO* has been found to be increased in non-virulent DC3000-inoculated *Arabidopsis* (Petriacq et al., 2012). Compared with the wild-type, flg22-triggered ROS bursts are significantly suppressed in *AtAO2* mutants, and *AtAO2* mutants are more susceptible to *Pst* DC3000 (Macho et al., 2012). These two *AOs* were both found to be members of Group III in the present study and are localized to chloroplasts (Katoh et al., 2006; Dong, 2019). Among the *TaAOs* identified in this study, *TaAO3-6A*, *TaAO3-6B*, and *TaAO3-6D* were also found to be clustered into Group III, and also located in chloroplasts, which suggests that *TaAO3-6A*, *TaAO3-6B*, and *TaAO3-6D* may have similar functions to those of the *AOs* reported in *Arabidopsis* and maize. Additionally, transcriptome analysis showed that the expression levels of *TaAO3-6A*, *TaAO3-6B*, and *TaAO3-6D* in flg22-treated wheat were increased by 33% to 53% compared with CK. This suggests that *TaAO3-6A*, *TaAO3-6B*, and *TaAO3-6D* may also play a role in PTI in wheat. Moreover, in our study, we found that the expression levels of *TaAOs* belonging to Group III were decreased in wheat treated with powdery mildew and increased in wheat treated with *F. graminearum* (Figure 8). As we know, the pathogen of wheat powdery mildew is a biotrophic parasite (Spanu et al., 2010), while *F. graminearum* is a hemi-biotrophic pathogen (Ma et al., 2020). These results suggest that TaAO may play opposing roles in the pathogenesis of hemi-biotrophic and biotrophic pathogens.

Previous studies have revealed that AO plays important roles in biotic stresses and plant development. In this study, we also found that AO may work in response to abiotic stress. The expression of most *TaAOs* was significantly upregulated under exposure to cold stress and downregulated under combined drought and heat stress. This indicates that *AOs* play an important role in the adaptation of plants to cold, heat, and drought stress. In summary, this research lays a foundation for further investigation of the function of *TaAOs*.

5 Conclusions

In this study, we systematically identified *AO* genes in wheat genomes. A total of nine *TaAO* genes were identified, which were distributed on three chromosomes of three sub-genomes. TaAOs were clustered into three groups. Gene structure and conserved motifs were similar within each group, but differed among the groups. Transcriptome analysis and real-time PCR assay indicated that TaAOs belonging to Group II were highly expressed in all tissues. *TaAOs* of Group III were found to be involved in PTI response and in the response to ABA treatment, and were found to play a positive role in wheat resistance to *F. graminearum* infection. Furthermore, *TaAOs* might positively regulate the response to cold treatment. These results provide systematic information on AO in wheat and lay a foundation for further research on the functions of *TaAOs*.

Data availability statement

The original contributions presented in the study are included in the article/Supplementary Material. Further inquiries can be directed to the corresponding authors.

Author contributions

WC, ZF, and WW designed the experiments and directed the writing of the manuscript. YF, MT, and JX performed the experiments and wrote the first draft. YF, PL, LW, and WC revised the manuscript. YF and MT contributed to the data analysis. All authors contributed to the article and approved the submitted version.

Funding

This research was supported by the Open Program of Engineering Research Center of Ecology and Agricultural Use of

Wetland Ministry of Education (KFT202107), the open project program of the State Key Laboratory for Biology of Plant Diseases and Insect Pests (NO. SKLOF202008), and the National Natural Science Foundation of China (31672088).

Conflict of interest

The authors declare that the research was conducted in the absence of any commercial or financial relationships that could be construed as a potential conflict of interest.

The reviewer XN declared a shared affiliation with the author WW to the handling editor at the time of review.

Publisher's note

All claims expressed in this article are solely those of the authors and do not necessarily represent those of their affiliated organizations, or those of the publisher, the editors and the reviewers. Any product that may be evaluated in this article, or claim that may be made by its manufacturer, is not guaranteed or endorsed by the publisher.

Supplementary material

The Supplementary Material for this article can be found online at: https://www.frontiersin.org/articles/10.3389/fpls.2023.1210632/full#supplementary-material

References

Abedi, T., and Mojiri, A. (2020). Cadmium uptake by wheat (Triticum aestivum l.): an overview. *Plants (Basel)* 9, 500. doi: 10.3390/plants9040500

Armenia, I., Balzaretti, R., Pirrone, C., Allegretti, C., D'arrigo, P., Valentino, M., et al. (2017). L-aspartate oxidase magnetic nanoparticles: synthesis, characterization and l-aspartate bioconversion. *Rsc Adv.* 7, 21136–21143. doi: 10.1039/c7ra00384f

Bacchella, L., Lina, C., Todone, F., Negri, A., Tedeschi, G., Ronchi, S., et al. (1999). Crystallization of l-aspartate oxidase, the first enzyme in the bacterial *de novo* biosynthesis of NAD. *Acta Crystallogr. D Biol. Crystallogr.* 55, 549–551. doi: 10.1107/s0907444998011913

Bifulco, D., Pollegioni, L., Tessaro, D., Servi, S., and Molla, G. (2013). A thermostable l-aspartate oxidase: a new tool for biotechnological applications. *Appl. Microbiol. Biotechnol.* 97, 7285–7295. doi: 10.1007/s00253-013-4688-1

Bishop, D. L., and Bugbee, B. G. (1998). Photosynthetic capacity and dry mass partitioning in dwarf and semi-dwarf wheat (Triticum aestivum l.). *J. Plant Physiol.* 153, 558–565. doi: 10.1016/s0176-1617(98)80204-6

Chen, C., Chen, H., Zhang, Y., Thomas, H. R., Frank, M. H., He, Y., et al. (2020). TBtools: an integrative toolkit developed for interactive analyses of big biological data. *Mol. Plant* 13, 1194–1202. doi: 10.1016/j.molp.2020.06.009

Cheng, H., Liu, J., Wen, J., Nie, X., Xu, L., Chen, N., et al. (2019). Frequent intra- and inter-species introgression shapes the landscape of genetic variation in bread wheat. *Genome Biol.* 20, 136. doi: 10.1186/s13059-019-1744-x

Chou, K. C., and Shen, H. B. (2010). Plant-mPLoc: a top-down strategy to augment the power for predicting plant protein subcellular localization. *PLoS One* 5, e11335. doi: 10.1371/journal.pone.0011335

Chow, C., Hegde, S., and Blanchard, J. S. (2017). Mechanistic characterization of escherichia coli l-aspartate oxidase from kinetic isotope effects. *Biochemistry* 56, 4044–4052. doi: 10.1021/acs.biochem.7b00307

Davis, S. J. (2009). Integrating hormones into the floral-transition pathway of arabidopsis thaliana. *Plant Cell Environ.* 32, 1201–1210. doi: 10.1111/j.1365-3040.2009.01968.x

Djebbar, R., Rzigui, T., Petriacq, P., Mauve, C., Priault, P., Fresneau, C., et al. (2012). Respiratory complex I deficiency induces drought tolerance by impacting leaf stomatal and hydraulic conductances. *Planta* 235, 603–614. doi: 10.1007/s00425-011-1524-7

Dong, B. (2019). The functional analysis of differentially expressed genes ZmAI and ZmAO in maize CMS-c CNKI. *CNKI* 7, 7–10. doi: 10.27345/d.cnki.gsnyu.2019.001308

Dutilleul, C., Garmier, M., Noctor, G., Mathieu, C., Chetrit, P., Foyer, C. H., et al. (2003). Leaf mitochondria modulate whole cell redox homeostasis, set antioxidant capacity, and determine stress resistance through altered signaling and diurnal regulation. *Plant Cell* 15, 1212–1226. doi: 10.1105/tpc.009464

Fang, Z. W., He, Y. Q., Liu, Y. K., Jiang, W. Q., Song, J. H., Wang, S. P., Yin, J. L., et al. (2020). Bioinformatic identification and analyses of the non-specific lipid transfer proteins in wheat. *J. Integr. Agric.* 19, 1170–1185. doi: 10.1016/S2095-3119(19)62776-0

Feng, J. Q., Shaik, S., and Wang, B. J. (2021). Spin-regulated electron transfer and exchange-enhanced reactivity in Fe4S4-mediated redox reaction of the Dph2 enzyme during the biosynthesis of diphthamide. *Angewandte Chemie-International Edition* 60, 20430–20436. doi: 10.1002/anie.202107008

Gakiere, B., Hao, J. F., De Bont, L., Petriacq, P., Nunes-Nesi, A., and Fernie, A. R. (2018). NAD(+) biosynthesis and signaling in plants. *Crit. Rev. Plant Sci.* 37, 259–307. doi: 10.1080/07352689.2018.1505591

Gasteiger, E., Gattiker, A., Hoogland, C., Ivanyi, I., Appel, R. D., and Bairoch, A. (2003). ExPASy: the proteomics server for in-depth protein knowledge and analysis. *Nucleic Acids Res.* 31, 3784–3788. doi: 10.1093/nar/gkg563

Gill, A. J. (2012). Succinate dehydrogenase (SDH) and mitochondrial driven neoplasia. *Pathology* 44, 285–292. doi: 10.1097/PAT.0b013e3283539932

Guo, G., Lei, M., Wang, Y., Song, B., and Yang, J. (2018). Accumulation of as, cd, and Pb in sixteen wheat cultivars grown in contaminated soils and associated health risk assessment. *Int. J. Environ. Res. Public Health* 15, 2601. doi: 10.3390/ijerph15112601

Hao, J., Petriacq, P., De Bont, L., Hodges, M., and Gakiere, B. (2018). Characterization of l-aspartate oxidase from arabidopsis thaliana. *Plant Sci.* 271, 133–142. doi: 10.1016/j.plantsci.2018.03.016

Katoh, A., Uenohara, K., Akita, M., and Hashimoto, T. (2006). Early steps in the biosynthesis of NAD in arabidopsis start with aspartate and occur in the plastid. *Plant Physiol.* 141, 851–857. doi: 10.1104/pp.106.081091

Kumar, S., Stecher, G., Li, M., Knyaz, C., and Tamura, K. (2018). MEGA X: molecular evolutionary genetics analysis across computing platforms. *Mol. Biol. Evol.* 35, 1547–1549. doi: 10.1093/molbev/msy096

Leese, C., Fotheringham, I., Escalettes, F., Speight, R., and Grogan, G. (2013). Cloning, expression, characterisation and mutational analysis of l-aspartate oxidase from pseudomonas putida. *J. Mol. Catalysis B-Enzymatic* 85-86, 17–22. doi: 10.1016/j.molcatb.2012.07.008

Letunic, I., and Bork, P. (2018). 20 years of the SMART protein domain annotation resource. *Nucleic Acids Res.* 46, D493–D496. doi: 10.1093/nar/gkx922

Letunic, I., and Bork, P. (2021). Interactive tree of life (iTOL) v5: an online tool for phylogenetic tree display and annotation. *Nucleic Acids Res.* 49, W293–W296. doi: 10.1093/nar/gkab301

Liu, G., Liu, Q., Han, Z., Wang, P., and Li, Y. (2023). Comparative proteomics analysis of adult haemonchus contortus isolates from ovis ammon. *Front. Cell Infect. Microbiol.* 13. doi: 10.3389/fcimb.2023.1087210

Ma, Z., Xie, Q., Li, G., Jia, H., Zhou, J., Kong, Z., et al. (2020). Germplasms, genetics and genomics for better control of disastrous wheat fusarium head blight. *Theor. Appl. Genet.* 133, 1541–1568. doi: 10.1007/s00122-019-03525-8

Macho, A. P., Boutrot, F., Rathjen, J. P., and Zipfel, C. (2012). Aspartate oxidase plays an important role in arabidopsis stomatal immunity. *Plant Physiol.* 159, 1845–1856. doi: 10.1104/pp.112.199810

Marinoni, I., Nonnis, S., Monteferrante, C., Heathcote, P., Hartig, E., Bottger, L. H., et al. (2008). Characterization of l-aspartate oxidase and quinolinate synthase from bacillus subtilis. *FEBS J.* 275, 5090–5107. doi: 10.1111/j.1742-4658.2008.06641.x

Mattevi, A., Tedeschi, G., Bacchella, L., Coda, A., Negri, A., and Ronchi, S. (1999). Structure of l-aspartate oxidase: implications for the succinate dehydrogenase/fumarate reductase oxidoreductase family. *Structure* 7, 745–756. doi: 10.1016/s0969-2126(99)80099-9

Mortarino, M., Negri, A., Tedeschi, G., Simonic, T., Duga, S., Gassen, H. G., et al. (1996). L-aspartate oxidase from escherichia coli. i. characterization of coenzyme binding and product inhibition. *Eur. J. Biochem.* 239, 418–426. doi: 10.1111/j.1432-1033.1996.0418u.x

Nasu, S., Wicks, F. D., and Gholson, R. K. (1982). L-aspartate oxidase, a newly discovered enzyme of escherichia coli, is the b protein of quinolinate synthetase. *J. Biol. Chem.* 257, 626–632. doi: 10.1016/S0021-9258(19)68239-6

Ostergaard, E. (2008). Disorders caused by deficiency of succinate-CoA ligase. *J. Inherit Metab. Dis.* 31, 226–229. doi: 10.1007/s10545-008-0828-7

Panchy, N., Lehti-Shiu, M., and Shiu, S. H. (2016). Evolution of gene duplication in plants. *Plant Physiol.* 171, 2294–2316. doi: 10.1104/pp.16.00523

Petriacq, P., De Bont, L., Hager, J., Didierlaurent, L., Mauve, C., Guerard, F., et al. (2012). Inducible NAD overproduction in arabidopsis alters metabolic pools and gene expression correlated with increased salicylate content and resistance to pst-AvrRpm1. *Plant J.* 70, 650–665. doi: 10.1111/j.1365-313X.2012.04920.x

Prunier, A. L., Schuch, R., Fernandez, R. E., Mumy, K. L., Kohler, H., Mccormick, B. A., et al. (2007). nadA and nadB of shigella flexneri 5a are antivirulence loci responsible for the synthesis of quinolinate, a small molecule inhibitor of shigella pathogenicity. *Microbiol. (Reading)* 153, 2363–2372. doi: 10.1099/mic.0.2007/006916-0

Remm, M., Storm, C. E., and Sonnhammer, E. L. (2001). Automatic clustering of orthologs and in-paralogs from pairwise species comparisons. *J. Mol. Biol.* 314, 1041–1052. doi: 10.1006/jmbi.2000.5197

Ren, Y., Liu, L. S., He, Z. H., Wu, L., Bai, B., and Xia, X. C. (2015). QTL mapping of adult-plant resistance to stripe rust in a "Lumai 21xJingshuang 16' wheat population. *Plant Breed.* 134, 501–507. doi: 10.1111/pbr.12290

Rombauts, S., Dehais, P., Van Montagu, M., and Rouze, P. (1999). PlantCARE, a plant cis-acting regulatory element database. *Nucleic Acids Res.* 27, 295–296. doi: 10.1093/nar/27.1.295

Sakuraba, H., Satomura, T., Kawakami, R., Yamamoto, S., Kawarabayasi, Y., Kikuchi, H., et al. (2002). L-aspartate oxidase is present in the anaerobic hyperthermophilic archaeon pyrococcus horikoshii OT-3: characteristics and role in the *de novo* biosynthesis of nicotinamide adenine dinucleotide proposed by genome sequencing. *Extremophiles* 6, 275–281. doi: 10.1007/s00792-001-0254-3

Sakuraba, H., Yoneda, K., Asai, I., Tsuge, H., Katunuma, N., and Ohshima, T. (2008). Structure of l-aspartate oxidase from the hyperthermophilic archaeon sulfolobus tokodaii. *Biochim. Biophys. Acta* 1784, 563–571. doi: 10.1016/j.bbapap.2007.12.012

Santra, D. K., Chen, X. M., Santra, M., Campbell, K. G., and Kidwell, K. K. (2008). Identification and mapping QTL for high-temperature adult-plant resistance to stripe rust in winter wheat (Triticum aestivum l.) cultivar 'Stephens'. *Theor. Appl. Genet.* 117, 793–802. doi: 10.1007/s00122-008-0820-5

Sobolewska, M., Wenda-Piesik, A., Jaroszewska, A., and Stankowski, S. (2020). Effect of habitat and foliar fertilization with K, zn and Mn on winter wheat grain and baking qualities. *Agronomy-Basel* 10, 276. doi: 10.3390/agronomy10020276

Spanu, P. D., Abbott, J. C., Amselem, J., Burgis, T. A., Soanes, D. M., Stuber, K., et al. (2010). Genome expansion and gene loss in powdery mildew fungi reveal tradeoffs in extreme parasitism. *Science* 330, 1543–1546. doi: 10.1126/science.1194573

Tedeschi, G., Negri, A., Mortarino, M., Ceciliani, F., Simonic, T., Faotto, L., et al. (1996). L-aspartate oxidase from escherichia coli. II. interaction with C4 dicarboxylic acids and identification of a novel l-aspartate: fumarate oxidoreductase activity. *Eur. J. Biochem.* 239, 427–433. doi: 10.1111/j.1432-1033.1996.0427u.x

Tedeschi, G., Nonnis, S., Strumbo, B., Cruciani, G., Carosati, E., and Negri, A. (2010). On the catalytic role of the active site residue E121 of e. coli l-aspartate oxidase. *Biochimie* 92, 1335–1342. doi: 10.1016/j.biochi.2010.06.015

Thompson, J. D., Higgins, D. G., and Gibson, T. J. (1994). CLUSTAL W: improving the sensitivity of progressive multiple sequence alignment through sequence weighting, position-specific gap penalties and weight matrix choice. *Nucleic Acids Res.* 22, 4673–4680. doi: 10.1093/nar/22.22.4673

Trapnell, C., Roberts, A., Goff, L., Pertea, G., Kim, D., Kelley, D. R., et al. (2012). Differential gene and transcript expression analysis of RNA-seq experiments with TopHat and cufflinks. *Nat. Protoc.* 7, 562–578. doi: 10.1038/nprot.2012.016

Zhang, X., and Mou, Z. (2009). Extracellular pyridine nucleotides induce PR gene expression and disease resistance in arabidopsis. *Plant J.* 57, 302–312. doi: 10.1111/j.1365-313X.2008.03687.x

Zhao, M. J., Yao, P. B., Mao, Y. X., Wu, J. J., Wang, W. H., Geng, C. H., et al. (2022). Malic enzyme 2 maintains protein stability of mutant p53 through 2-hydroxyglutarate. *Nat. Metab.* 4, 225–22+. doi: 10.1038/s42255-022-00532-w

frontiers | Frontiers in Plant Science

TYPE Original Research
PUBLISHED 28 August 2023
DOI 10.3389/fpls.2023.1232897

Check for updates

OPEN ACCESS

EDITED BY
Changlin Liu,
Chinese Academy of Agricultural Sciences (CAAS), China

REVIEWED BY
Hanif Khan,
Indian Institute of Wheat and Barley Research (ICAR), India
Yuefeng Ruan,
Agriculture and Agri-Food Canada (AAFC), Canada

*CORRESPONDENCE
Suizhuang Yang
yangszh@126.com
Xinli Zhou
eli6951@sina.com

†These authors have contributed equally to this work

RECEIVED 01 June 2023
ACCEPTED 31 July 2023
PUBLISHED 28 August 2023

CITATION
Yan Q, Jia G, Tan W, Tian R, Zheng X, Feng J, Luo X, Si B, Li X, Huang K, Wang M, Chen X, Ren Y, Yang S and Zhou X (2023) Genome-wide QTL mapping for stripe rust resistance in spring wheat line PI 660122 using the Wheat 15K SNP array. *Front. Plant Sci.* 14:1232897. doi: 10.3389/fpls.2023.1232897

COPYRIGHT
© 2023 Yan, Jia, Tan, Tian, Zheng, Feng, Luo, Si, Li, Huang, Wang, Chen, Ren, Yang and Zhou. This is an open-access article distributed under the terms of the Creative Commons Attribution License (CC BY). The use, distribution or reproduction in other forums is permitted, provided the original author(s) and the copyright owner(s) are credited and that the original publication in this journal is cited, in accordance with accepted academic practice. No use, distribution or reproduction is permitted which does not comply with these terms.

Genome-wide QTL mapping for stripe rust resistance in spring wheat line PI 660122 using the Wheat 15K SNP array

Qiong Yan[1†], Guoyun Jia[1†], Wenjing Tan[1], Ran Tian[1], Xiaochen Zheng[1], Junming Feng[1], Xiaoqin Luo[1], Binfan Si[1], Xin Li[1], Kebing Huang[1], Meinan Wang[2], Xianming Chen[2,3], Yong Ren[4], Suizhuang Yang[1*] and Xinli Zhou[1*]

[1]Wheat Research Institute, School of Life Sciences and Engineering, Southwest University of Science and Technology, Mianyang, Sichuan, China, [2]Department of Plant Pathology, Washington State University, Pullman, WA, United States, [3]Wheat Health, Genetics, and Quality Research Unit, US Department of Agriculture-Agricultural Research Service (USDA-ARS), Pullman, WA, United States, [4]Crop Characteristic Resources Creation and Utilization Key Laboratory of Sichuan Province, Mianyang Institute of Agricultural Science, Mianyang, Sichuan, China

Introduction: Stripe rust is a global disease of wheat. Identification of new resistance genes is key to developing and growing resistant varieties for control of the disease. Wheat line PI 660122 has exhibited a high level of stripe rust resistance for over a decade. However, the genetics of stripe rust resistance in this line has not been studied. A set of 239 recombinant inbred lines (RILs) was developed from a cross between PI 660122 and an elite Chinese cultivar Zhengmai 9023.

Methods: The RIL population was phenotyped for stripe rust response in three field environments and genotyped with the Wheat 15K single-nucleotide polymorphism (SNP) array.

Results: A total of nine quantitative trait loci (QTLs) for stripe rust resistance were mapped to chromosomes 1B (one QTL), 2B (one QTL), 4B (two QTLs), 4D (two QTLs), 6A (one QTL), 6D (one QTL), and 7D (one QTL), of which seven QTLs were stable and designated as *QYrPI660122.swust-4BS*, *QYrPI660122.swust-4BL*, *QYrPI660122.swust-4DS*, *QYrPI660122.swust-4DL*, *QYrZM9023.swust-6AS*, *QYrZM9023.swust-6DS*, and *QYrPI660122.swust-7DS*. *QYrPI660122.swust-4DS* was a major all-stage resistance QTL explaining the highest percentage (10.67%–20.97%) of the total phenotypic variation and was mapped to a 12.15-cM interval flanked by SNP markers *AX-110046962* and *AX-111093894* on chromosome 4DS.

Discussion: The QTL and their linked SNP markers in this study can be used in wheat breeding to improve resistance to stripe rust. In addition, 26 lines were selected based on stripe rust resistance and agronomic traits in the field for further selection and release of new cultivars.

KEYWORDS

stripe rust, wheat, resistance, QTL mapping, yellow rust

Introduction

Wheat stripe rust, caused by *Puccinia striiformis* Westend. f. sp. *tritici* Erikss. (*Pst*), is one of the most destructive diseases in the world (Chen, 2005; Milus et al., 2009). Losses from stripe rust typically range from 10% to 70% in commercial production environments, depending on the cultivar, prevailing climatic conditions, and inoculum pressure (Bariana et al., 2016; Zhou et al., 2022a). However, the disease can cause a 100% loss of yield for susceptible varieties (Bariana et al., 2016). Since 1950, the disease has occurred on an annual average of 4 million hectares in China. In particular, the five major outbreaks of wheat stripe rust in 1950, 1964, 1990, 2002, and 2017 all occurred on over 5.5 million hectares, resulting in a loss of 13.8 million tons of yield (Li and Zeng, 2000; Wan et al., 2004; Huang et al., 2018). Stripe rust can be controlled by resistant cultivars, fungicides, and some cultural practices. Compared to other approaches, planting resistant cultivars has been proven to be the most effective, easy-to-use, economical, and environmentally friendly way to control disease (Line, 2002; Chen, 2005).

Depending on phenotypic performance at different growth stages, wheat rust resistance can be classified into two types: all-stage resistance (ASR) and adult plant resistance (APR), sometimes also known as high-temperature adult plant (HTAP) resistance (Qayoum and Line, 1985; Chen, 2005; Lin and Chen, 2007; Rosewarne et al., 2013). All-stage resistance, also known as seedling resistance, can be detected at the seedling stage but is expressed at all growth stages. Such resistance is often race-specific and, thus, easily overcome by virulent races (Line, 2002; Chen, 2005; Chen, 2013). Due to race specificity, ASR often fails within 3–5 years of deployment (Jambuthenne et al., 2022). In contrast, HTAP resistance becomes more effective as plants grow older and the weather becomes warmer. It is usually non-race-specific, quantitatively inherited, and more likely to be durable. However, HTAP resistance is mostly incomplete, and the level is influenced by plant growth stage, temperature, and disease pressure (Chen, 2013).

To date, 84 permanently named and a large number of temporarily designated stripe rust resistance genes (*Yr* genes) and quantitative trait loci (QTLs) have been reported in wheat (Klymiuk et al., 2022). These resistance genes come mainly from common wheat cultivars, local germplasm, and wild relatives. Among them, *Yr5*/*Yr7*/*YrSP*, *Yr10*, *Yr15*, *Yr18*, *Yr36*, *Yr46*, *YrU1*, and *YrAS2388* were cloned and characterized (Fu et al., 2009; Krattinger et al., 2009; Liu et al., 2014; Moore et al., 2015; Klymiuk et al., 2018; Marchal et al., 2018; Zhang et al., 2019; Wang et al., 2020). Most ASR genes have been overcome by virulent races. ASR genes *Yr5* and *Yr15* are still effective against all *Pst* races identified in the United States and many other countries (Wang and Chen, 2017). However, races virulent on *Yr5* gene have been reported in Australia, India, China, and Turkey (Wellings and McIntosh, 1990; Zhang et al., 2020; Tekin et al., 2021), and the *Yr15* virulence has been documented in Afghanistan (Gerechter-Amitai et al., 1989). Most wheat cultivars that have shown durable resistance to stripe rust have APR or HTAP resistance controlled by variable numbers of genes or QTL (Lin and Chen, 2007; Lin and Chen, 2008b; Santra et al., 2008; Carter et al., 2009; Paillard et al., 2012; Ren et al., 2012a; Lu et al., 2014; Zhou et al., 2014; Dong et al., 2017; Feng et al., 2018; Liu et al., 2018; Liu et al., 2019; Liu et al., 2020). In order to obtain a high degree of durable resistance, combining the two types of resistance types in the same background is considered a preferred method to improve the resistance to stripe rust in wheat breeding (Chen, 2007; Ren et al., 2012a; Chen, 2013; Liu et al., 2018).

The development of molecular markers, especially single-nucleotide polymorphism (SNP) markers, has revolutionized QTL analysis. A SNP is caused by a single-nucleotide mutation due to the insertion, deletion, and replacement of a single base segment in the genome. SNPs exist in the entire genomes of biological individuals and are the most abundant. SNP markers are now widely used in genetic analysis and breeding (Ma et al., 2019). Recent advances in sequencing technology have led to the availability of many SNP arrays in wheat (Rasheed et al., 2017). High-throughput genotyping techniques, including Wheat 9K (Cavanagh et al., 2013), 15K (Soleimani et al., 2020), 90K (Wang et al., 2014; Wu et al., 2018), 660K (Cui et al., 2017), and 820K SNP (Winfield et al., 2016) arrays, are now available. Among these SNP arrays, the 15K array is generally adequate and cost-effective for mapping traits of interest (Soleimani et al., 2020).

PI 660122, a spring wheat germplasm, was developed by the Wheat Health, Genetics, and Quality Research Unit of the US Department of Agriculture, Agricultural Research Service (USDA-ARS), and Washington State University and deposited in the USDA-ARS National Small Grains Collections (NSGC). In previous studies, the germplasm showed a high level of resistance in field tests over multiple years (Wang et al., 2012; Zhou et al., 2015b). At the seedling stage, it was resistant to US races PST-43 and PST-127 and Chinese races CYR29, CYR31, CYR32, and CYR33 and moderately resistant to US races PST-100 and PST-114 and Chinese race PST-HY8 of *Pst* (Wang et al., 2012; Zhou et al., 2015b). A comparison of greenhouse and field tests indicated that PI 660122 had effective ASR and possible HTAP resistance. The objectives of the present study were to further characterize the stripe rust resistance in PI 660122, map QTL for ASR and APR, and identify the QTL by comparing their chromosomal locations with previously reported stripe rust resistance QTL.

Materials and methods

Plant materials

To map the QTL for stripe rust resistance in PI 660122, we developed a mapping population from a cross between Zhengmai (ZM9023, as the female parent) and PI 660122 (as the male parent). PI 660122 was developed from cross Avocet S/PI 610755 (Wang et al., 2012). Avocet S (AvS), an Australian spring wheat selection, is highly susceptible to most *Pst* races in China and many other countries and has been used as a susceptible control in stripe rust tests. PI 610755 is a Mexico spring wheat variety, selected from the cross Altar 84/*Aegilops tauschii (191)*//Opata M85. ZM9023, a spring wheat cultivar developed by the Wheat Research Institute of Henan Academy of Agricultural Sciences, is moderately or highly

susceptible to the currently predominant *Pst* races in China (Xue et al., 2014). We developed a total of 239 F_5 and F_6 recombinant inbred lines (RILs) from the ZM9023 × PI 660122 cross, using the single-seed descent method.

Greenhouse tests

Seedling tests were conducted in a greenhouse to evaluate the stripe rust responses of PI 660122 and Zhengmai 9023. For each genotype, 10–12 seeds were seeded in a 9 cm × 9 cm × 9 cm plot. At the one-leaf stage, seedlings were uniformly inoculated with fresh urediniospores of a *Pst* race mixed with talc at a ratio of 1:50. Three Chinese *Pst* races, CYR31, CYR32, and CYR34, were used in the seedling tests. Inoculated seedlings were kept in a dew chamber in the dark at 8°C and above 100% relative humidity for 24 h. The seedlings were then moved to a growth chamber at 16°C with a daily 16-h light for stripe rust development. The infection type (IT) data were recorded 18 days to 21 days after inoculation using the 0–9 scale (Line and Qayoum, 1992). Seedlings of AvS were included as the susceptibility check in each race test. Later, 15 RILs selected for each containing only one QTL were also tested together with the parents with the three races at the seedling stage in the greenhouse under the same conditions.

Field tests

The F_5 and F_6 RILs and their parents were tested for stripe rust responses to stripe rust in the experimental fields in Mianyang (MY; 31°33′N, 104°55′E) in 2021 (21) and both MY and Guangyuan (GY; 22:32°14′N, 106°17′E) in the Sichuan Province in 2022 (22). The field tests were conducted with one replicate at 21MY and 22GY and two replicates (completely randomized block design) at 22MY based on the available seed quantity. Each plot consisted of a single row, 1.0 m in length and with 25 cm between rows. Approximately 20 to 30 seeds were sown in each row. AvS was planted in a row every 20 rows as a susceptible check and spore spreader for increasing stripe rust pressure and uniformity in the nursery. To increase the *Pst* inoculum, AvS was also planted around the nursery. MY and GY are ideal regions for stripe rust, as *Pst* can over-winter and over-summer, and the nursery was naturally infected without artificial inoculation (Zhou et al., 2019).

The stripe rust IT of each parent or RIL was rated on a scale of 0–9 (Line and Qayoum, 1992). Disease severity (DS) was scored using a modified scale as previously described (Lin and Chen, 2007). Both IT and DS data were collected twice in each season. The first record was taken when susceptible AvS showed approximately 80% severity, and the second was approximately a week later (Nsabiyera et al., 2018). Agronomic traits such as plant height (PH), spike length (SL), productive tiller number (PTN), kernels per spike (KPS), and thousand-grain weight (TGW) were determined to select RILs. PH was measured from the ground to the top of the spike excluding awn after the milking stage; KPS, SL, and PTN of each plant were counted at maturity; TGW was measured after harvest.

DNA extraction and genotyping

Fresh young leaves of PI 660122, ZM9023, and 239 F_5 RILs were harvested from the experimental field in January 2021. DNA from the fresh leaves was extracted using a modified cetyltrimethyl ammonium bromide (CTAB) method (Li et al., 2013). DNA was dissolved in ddH_2O (100 µL), and DNA quality and concentration were determined by spectrophotometry (NanoDrop ND-1000, Thermo Scientific, Wilmington, DE, USA) after the DNA. DNA stock solutions were diluted with sterilized ddH_2O to different concentrations according to individual experimental requirements for molecular analyses.

The parents and the 239 RILs were genotyped by China Golden Marker (Beijing) Biotech Co., Ltd. (http://www.cgmb.com.cn/) using the 15K SNP chip (Soleimani et al., 2020).

Statistical analysis, genetic map construction, and QTL mapping

Analysis of variance (ANOVA) and analysis of Pearson's correlation coefficients were performed to analyze the stripe rust phenotypic data using the "AOV" tool in the QTL Ici Mapping V4.2 software (Wang, 2009; Meng et al., 2015). The same software was also used to analyze the genotypic data. After the genotypic data were scanned for missing and undetected data, redundant markers were deleted using the "Bin" function. Genetic maps were constructed using the Kosambi mapping function (Kosambi, 2016). QTL mapping was performed using the genetic maps and the IT and DS data based on inclusive composite interval mapping (ICIM) with preset parameters Step = 1 cM, value p for input variables (PIN) = 0.0001, and logarithm of odds (LOD) = 2.5. A QTL was identified when the logarithm of odds (LOD) score was greater than 2.5. To determine the additive effects of QTL, the effects of QTL combinations were demonstrated by plotting box plots for mean IT and mean DS of RILs sharing the same number of beneficial alleles.

Results

Stripe rust responses of the parents and RILs

In the greenhouse seedling tests, PI 660122 was highly resistant (IT of 2) to the tested three Chinese *Pst* races, whereas Zhengmai 9023 was highly susceptible (IT of 8–9) similar to the susceptible check AvS (Figure 1A). In the field tests under natural *Pst* infection, the final adult plant IT of PI 660122 was 2 across the two years and two locations, and its DS ranged from 5% to 10%, (Figure 1B). In contrast, Zhengmai 9023 was moderately resistant (IT of 5–6) with DS of 40%–50%. For comparison, AvS had IT of 9 and DS of 100%.

The RIL population had ITs ranging from 0 to 9 and DS from 0 to 90% across the years and locations (Figure 2). The IT and DS data from both sites and from both 2021 and 2022 at MY were each highly correlated (r = 0.76–0.81, $p < 0.001$ for IT; r = 0.61–0.75, $p < 0.001$ for DS) (Table 1). The ANOVA results showed significant

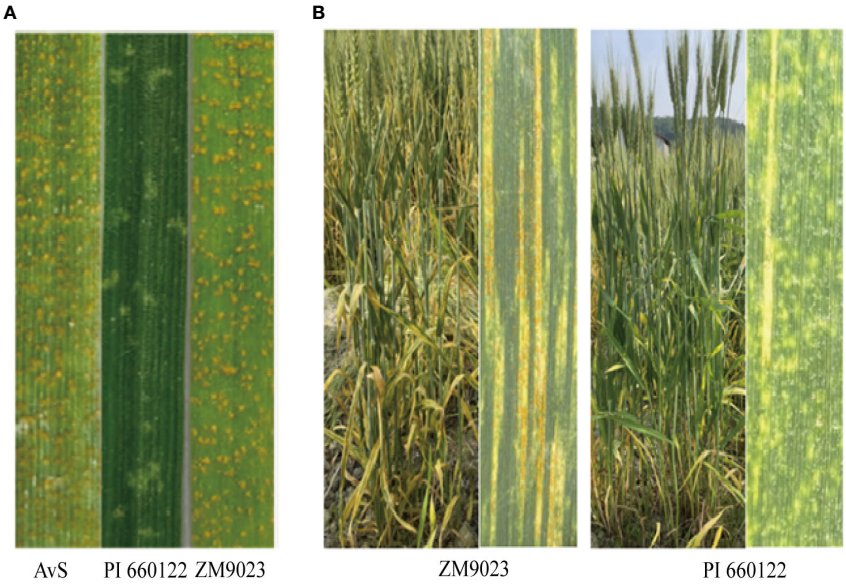

FIGURE 1
Stripe rust response of resistant parent PI 660122, susceptible parent Zhengmai 9023 (ZM9023), and susceptible check AvS with Chinese race CYR34 of *Puccinia striiformis* f sp. *tritici* at the seedling stage **(A)** and stripe rust reactions on flag leaves of ZM9023 and PI 660122 **(B)**.

variations ($p < 0.001$) among RILs, environments, and line × environment interactions for both IT and DS. The stripe rust phenotypes were influenced more by the environment than by the interaction of line and environment. The broad-sense heritability (h^2) was estimated at 0.92 using the IT data and 0.86 based on the DS data across the two sites (Table 2).

Genetic linkage map construction

A total of 5,432 SNPs in the 15K SNP array showed homozygous polymorphisms between the two parents. After the redundant markers were filtered out, 4,102 SNPs with known chromosome locations were obtained and used as inputs in the linkage analysis using QTL Ici Mapping V4.2. The 4,102 SNPs covered a total map length of 7,937.6 cM, with the genetic length ranging from 135.6 cM for chromosome 1B to 635.5 cM for chromosome 5A (Table 3). The number of markers per chromosome ranged from 60 for chromosome 6A to 322 for chromosome 2A, with an average of 189 SNPs. The mean distance between adjacent SNP markers ranged from 0.5 cM for chromosome 1B to 7.3 cM for chromosome 2D, with an overall mean of 1.9 cM. Genomes A, B, and D included 1,374 (33.50%), 1,672 (40.76%), and 1,056 (25.74%) SNPs covering lengths of 2,630.1 cM, 2,144.1 cM, and 3,163.4 cM with mean marker distance of 1.91 cM, 1.28 cM, and 3.00 cM, respectively. The map was used to identify significant associations between SNPs and stripe rust resistance.

QTL analysis of stripe rust resistance

QTL scans on all 21 chromosomes were performed using the ICIM method in the software QTL Ici Mapping V4.2. A total of nine QTLs contributing to stripe rust resistance in the Zhengmai 9023 × PI 660122 RIL population were identified with one QTL each on chromosomes 1B, 2B, 6A, 6D, and 7D and two QTLs each on 4B and 4D. Then, ICIM, single-marker analysis (SMA), and ICIM epistatic QTL (ICIM-EPI) for epistatic mapping were performed on QTL chromosome regions of these chromosomes. Among the QTL, seven (*QYrPI660122.swust-4BS*, *QYrPI660122.swust-4BL*, *QYrPI660122.swust-4DS*, *QYrPI660122.swust-4DL*, *QYrZM9023.swust-6AS*, *QYrZM9023.swust-6DS*, and *QYrPI660122.swust-7DS*) were detected in all environments, and two (*QYrZM9023.swust-1BL* and *QYrPI660122.swust-2BL*) were only detected in 22MY. Of the nine QTLs, six (*QYrPI660122.swust-2BL*, *QYrPI660122.swust-4BS*, *QYrPI660122.swust-4BL*, *QYrPI660122.swust-4DS*, *QYrPI660122.swust-4DL*, and *QYrPI660122.swust-7DS*) were from PI 660122 and three (*QYrZM9023.swust-1BL*, *QYrZM9023.swust-6AS*, and *QYrZM9023.swust-6DS*) from Zhengmai 9023.

QYrZM9023.swust-1BL, located at an 8.27-cM interval spanned by SNP markers *AX-89763895* and *AX-109273019*, explained 7.41% and 7.29% of phenotypic variation in IT and DS, respectively, and was detected only in 22MY. *QYrPI660122.swust-2BL*, located at a 1.83-cM interval spanned by SNP markers *AX-109849173* and *AX-109349804*, explained 4.65% and 5.57% of phenotypic variation in IT and DS, respectively, and was only detected in 22MY. *QYrPI660122.swust-4BS*, located at a 0.96-cM interval spanned by SNP markers *AX-108767762* and *AX-109309162*, explained 10.94%–15.00% and 5.84%–12.93% of phenotypic variation in IT and DS, respectively, across all environments. *QYrPI660122.swust-4BL*, mapped to a 1.54-cM interval flanked by SNP markers *AX-108935256* and *AX-108984536*, explained 8.25%–9.09% and 5.75%–13.51% phenotypic variation in IT and DS, respectively, and was detected in all environments. *QYrPI660122.swust-4DS*, located at a 12.15-cM interval spanned by SNP markers *AX-110046962* and *AX-111093894*, explained 11.64%–17.20% and 13.22%–20.97% phenotypic variation in IT and DS, respectively, across all environments. *QYrPI660122.swust-4DL*, located at a 1.23-cM

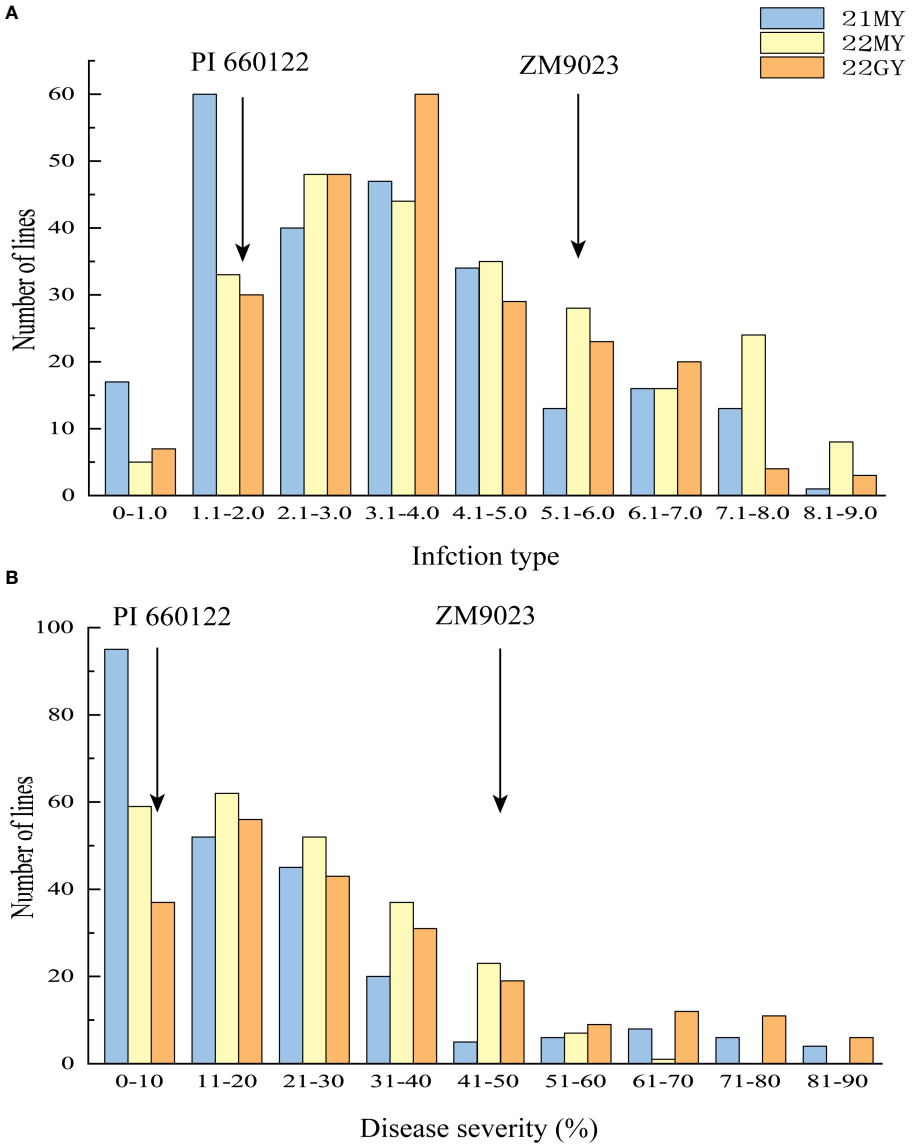

FIGURE 2
Frequency distributions of mean infection types (IT) **(A)** and disease severity (DS) **(B)** for 239 F_6 RILs from cross Zhengmai 9023 × PI 660122 tested in Mianyang (MY) in 2021 (21) and 2022 (22) and Guangyuan (GY) in 2022. Arrows indicate the values of the parent lines. RILs, recombinant inbred lines.

interval spanned by SNP markers *AX-94560848* and *AX-111557122*, explained 11.18%–18.24% and 6.60%–17.37% phenotypic variation in IT and DS, respectively, across all environments. *QYrZM9023.swust-6AS*, located at a 10.37-cM interval spanned by SNP markers AX-95124889 and *AX-110995858*, explained 5.43%–9.11% and 6.23%–7.92% of phenotypic variation in IT and DS, respectively, across all environments. *QYrZM9023.swust-6DS*, located at a 2.58-cM interval spanned by SNP markers *AX-11475193* and *AX-109317417*, explained 7.24%–13.33% and 7.25%–12.22% of phenotypic variation in IT and DS, respectively,

TABLE 1 Correlation coefficients (r) of infection type (IT) and disease severity (DS) of the recombinant inbred lines Zhengmai 9023 × PI 660122 tested in different environments.

Environment[a]	21MY	22MY	22GY
21MY	NA[b]		
22MY	0.81 (0.69)***[c]	NA	
22GY	0.77 (0.61)***	0.76 (0.76)***	NA

[a]21, 2021; 22, 2022; MY, Mianyang; GY, Guangyuan.
[b]NA, not applicable.
[c]The r values based on DS data are given in parentheses.
"***" denotes the r value is significant at $p < 0.001$.

TABLE 2 Analysis of variance and estimate of broad-sense heritability (h^2) of infection type (IT) and disease severity (DS) in the recombinant inbred line (RIL) population of Zhengmai 9023 × PI 660122 tested at Mianyang in 2021 and 2022 and Guangyuan in 2022.

Source of variation	DS			IT		
	df[a]	Mean square	F value	*df*	Mean square	F value
Lines	238	1,427.69	44.51***[b]	238	18.17	56.86***
Environments	2	7,683.04	239.53***	2	64.90	203.16***
Line × Environment	459	224.64	7.00***	459	1.65	5.17***
Error	689	32.08		689	0.32	
h^2	0.86			0.92		

[a]df, degree of freedom.
[b]"***" denotes the significance level of $p < 0.001$.

across all environments. *QYrPI660122.swust-7DS*, located at a 4.75-cM interval spanned by SNP markers *AX-110467729* and *AX-89378255*, explained 11.64%–17.20% and 13.22%–20.97% of phenotypic variation in IT and DS, respectively, and was detected in two environments, 21MY and 22GY (Figure 3, Table 4).

Identification of QTL resistance

Fifteen lines containing only one QTL were selected and tested for seedling reaction in the greenhouse using three Chinese *Pst* races (CYR31, CYR32, and CYR34). Among them, four lines contained

TABLE 3 Summary of chromosome assignment, number of SNPs, map length, and marker density of the genetic maps of the Zhengmai 9023 × PI 660122 recombinant inbred population.

Chromosome	No. of SNPs	Map length (cM)	Mean SNP distance (cM)
1A	156	311.4	2.0
1B	256	135.6	0.5
1D	82	561.9	6.9
2A	322	379.2	1.2
2B	254	339.4	1.3
2D	197	465.3	7.3
3A	249	362.0	1.5
3B	194	318.6	1.6
3D	190	428.1	2.3
4A	179	296.5	1.7
4B	193	281.5	1.5
4D	71	235.9	3.3
5A	235	635.5	2.7
5B	223	368.9	1.7
5D	138	500.5	3.6
6A	60	288.0	4.8
6B	303	390.1	1.3
6D	109	440.4	4.0
7A	173	357.5	2.1
7B	249	310.0	1.2
7D	269	531.3	2.0
Total	4102	7937.6	1.9
Average	195	376.7	1.9

SNPs, single-nucleotide polymorphisms.

QYrZM9023.swust-1BL, three lines contained *QyrPI660122.swust-4DS*, and eight lines contained *QYrPI660122.swust-7DS*. The lines containing *QYrZM9023.swust-1BL* or *QYrPI660122.swust-7DS* were susceptible (IT of 7–9) to all three races but showed moderate resistance at the adult-plant stage in the fields, indicating that these QTLs confer APR. In contrast, the lines containing *QYrPI660122.swust-4DS* were resistant (IT of 1–3) in the seedling tests, indicating that this QTL confers ASR (Figure 4, Table 5). The resistance types of *QYrPI660122.swust-2BL*, *QYrPI660122.swust-4BS*, *QYrPI660122.swust-4BL*, *QYrPI660122.swust-4DL*, *QYrZM9023.swust-6AS*, and *QYrZM9023.swust-6DS* were uncertain, as there were no single-QTL lines available from the RIL population.

QTL combinations

To determine the effects of the QTL in various combinations for *Pst* resistance, the 239 RILs were grouped into different genotypic groups based on the presence of markers closely

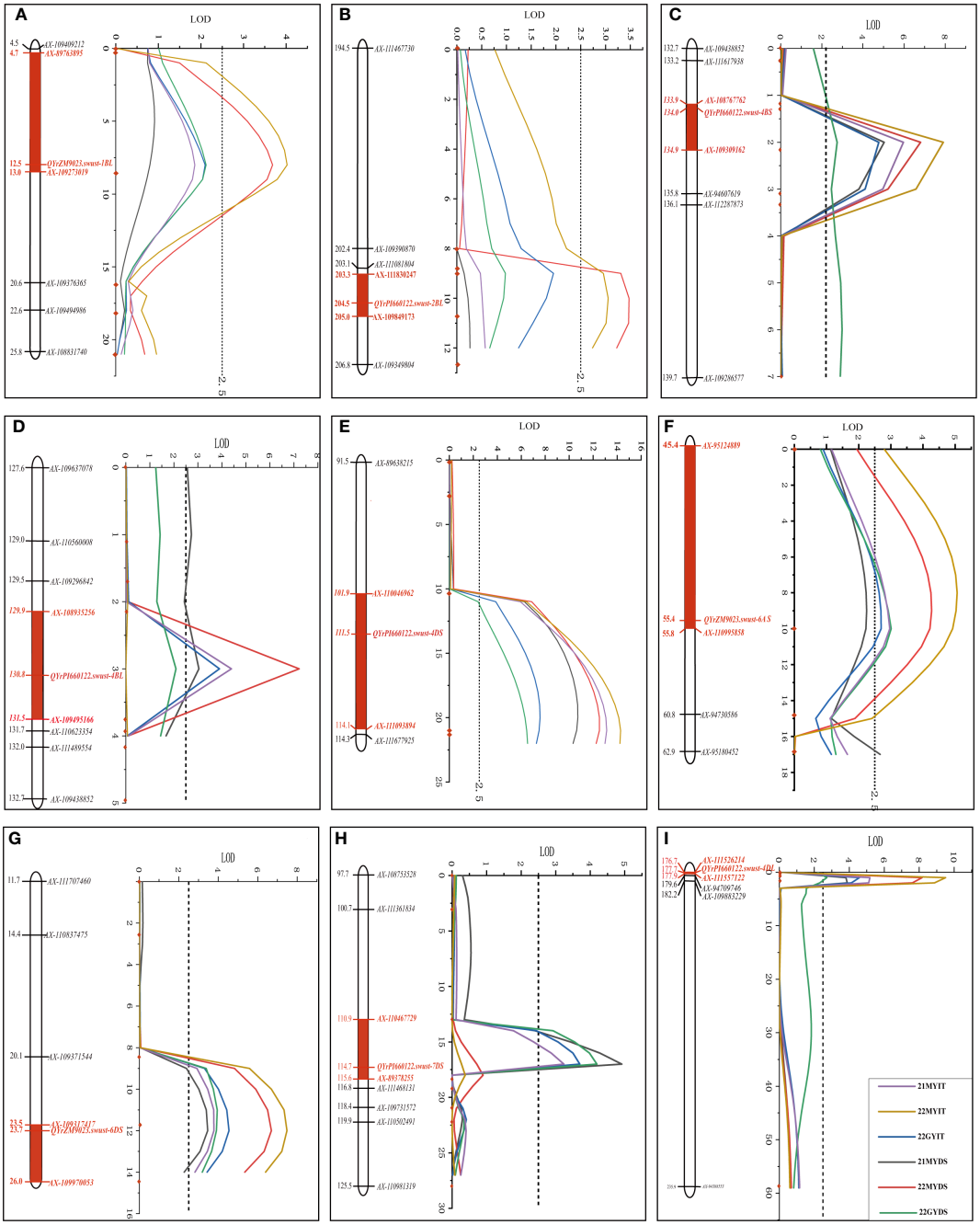

FIGURE 3
Stripe rust resistance QTLs on the genetic map of chromosomes 1BL **(A)**, 2BL **(B)**, 4BS **(C)**, 4BL **(D)**, 4DS **(E)**, 6AS **(F)**, 6DS **(G)**, 7DS **(H)**, and 4DS **(I)** based on infection type (IT) and disease severity (DS) data. The y-axis is in centimorgan (cM) distance, and the x-axis denotes LOD value. The red rectangle on the genetic map indicates the corresponding QTL region. QTLs, quantitative trait loci; LOD, limit of detection.

10.3389/fpls.2023.1232897

TABLE 4 Summary of nine stripe rust resistance QTLs identified based on mean disease severity (DS) and infection type (IT) of 239 RILs from Zhengmai 9023 × PI 660122 cross-tested in Mianyang 2021–2022 and Guangyuan 2022.

QTL	Environment	Center marker	Right marker	IT			DS		
				LOD[a]	PVE[b]	Add[c]	LOD	PVE	Add
QYrZM9023.swust-1BL	22MY	*AX-89763895*	*AX-109273019*	4.02	7.41	0.57	3.80	7.29	3.75
QYrPI660122.swust-2BL	22MY	*AX-109849173*	*AX-109349804*	2.52	4.65	−0.45	3.00	5.57	−.3.29
QYrPI660122.swust-4BS	21MY	*AX-108767762*	*AX-109309162*	5.97	14.15	−0.64	5.03	10.36	−5.69
	22MY			7.91	15.00	−0.76	6.72	12.76	−4.82
	22GY			4.77	10.940	−0.53	2.75	5.51	−4.84
QYrPI660122.swust-4BL	21MY	*AX-109495166*	*AX-108935256*	4.40	8.25	−0.56	3.04	5.75	−4.50
	22MY			–	–	–	7.19	13.51	−4.99
	22GY			3.90	9.09	−0.48	–	–	–
QYrPI660122.swust-4DS	21MY	*AX-110046962*	*AX-111093894*	13.13	21.82	−0.99	10.72	18.11	−8.83
	22MY			14.29	23.78	−1.06	12.65	21.04	−7.03
	22GY			7.57	13.81	−0.74	6.53	12.58	−7.57
QYrPI660122.swust-4DL	21MY	*AX-111526214*	*AX-111557122*	5.18	11.18	−0.60	3.81	7.22	−5.05
	22MY			9.51	18.23	−0.84	8.20	17.36	−5.33
	22GY			4.58	12.71	−0.52	2.71	6.60	−4.83
QYrZM9023.swust-6AS	21MY	*AX-95124889*	*AX-110995858*	2.97	5.53	0.46	–	–	–
	22MY			5.06	9.11	0.67	4.39	7.92	4.17
	22GY			2.70	5.43	0.41	3.01	6.23	5.13
QYrZM9023.swust-6DS	21MY	*AX-109317417*	*AX-111475193*	3.78	7.24	0.52	3.47	7.26	4.80
	22MY			7.48	13.33	0.75	6.85	12.44	4.87
	22GY			4.54	9.39	0.52	3.91	7.79	5.76
QYrPI660122.swust-7DS	21MY	*AX-110467729*	*AX-89378255*	3.24	6.91	−0.50	4.92	11.39	−5.85
	22GY			3.70	7.32	−0.50	4.19	8.26	−6.22

[a]LOD, logarithm of odds score.
[b]Add, additive effect of resistance allele.
[c]PVE, percentages of the phenotypic variance explained by individual QTL.
QTLs, quantitative trait loci; RILs, recombinant inbred lines.

associated with the nine QTL. These genotypes were further sorted into 10 groups based on the number of potential QTLs. Clearly, RILs carrying any number of QTL had lower mean DS than those without any of the QTL. Lines without any QTL had a mean IT of 6.6 and a mean DS of 46.91%. In comparison, when 0, 1, 2, 3, 4, 5, 6, and more than 6 QTLs were combined, the lines with one QTL had mean IT of 5.9 and mean DS of 36.04%, those with two QTLs had mean IT of 5.0 and mean DS of 31.81%, those with three QTLs had mean IT of 4.0 and mean DS of 23.25%, those with four QTLs had mean IT of 3.7 and mean DS of 19.52%, those with five QTLs had mean IT of 3.1 and mean DS of 14.76%, those with six QTLs had mean IT of 2.7 and mean DS of 10.45%, and those with seven or more QTL had mean IT of 2.4 and mean DS of 10.58%, close to the resistance level of PI 660122 (Figure 5).

Selection of breeding lines

Various agronomic traits, including PH, PTN, SL, KPS, and TGW, of the parents and the 239 RILs were assessed in 2021 and 2022 in Mianyang and 2022 in Guangyuan. The mean PH values of PI 660122 and ZM9023 were 90.3 cm and 79.3 cm, respectively, and the RILs were mainly distributed in the range of 81–110 cm. The mean PTN values of PI 660122 and ZM9023 were 5 and 4, respectively, and the mean PTN values of RILs were between 4 and 10. The mean SL values of PI 660122 and ZM9023 were 9.8 cm and 8.4 cm, respectively, and the mean SL values of RILs were between 7.3 cm and 11.3 cm. The mean KPS values of PI 660122 and ZM9023 were 48 and 44, respectively, and the mean KPS values of RILs were between 33 and 58. The mean TGW values of PI 660122 and ZM9023 were 48 g and 44 g,

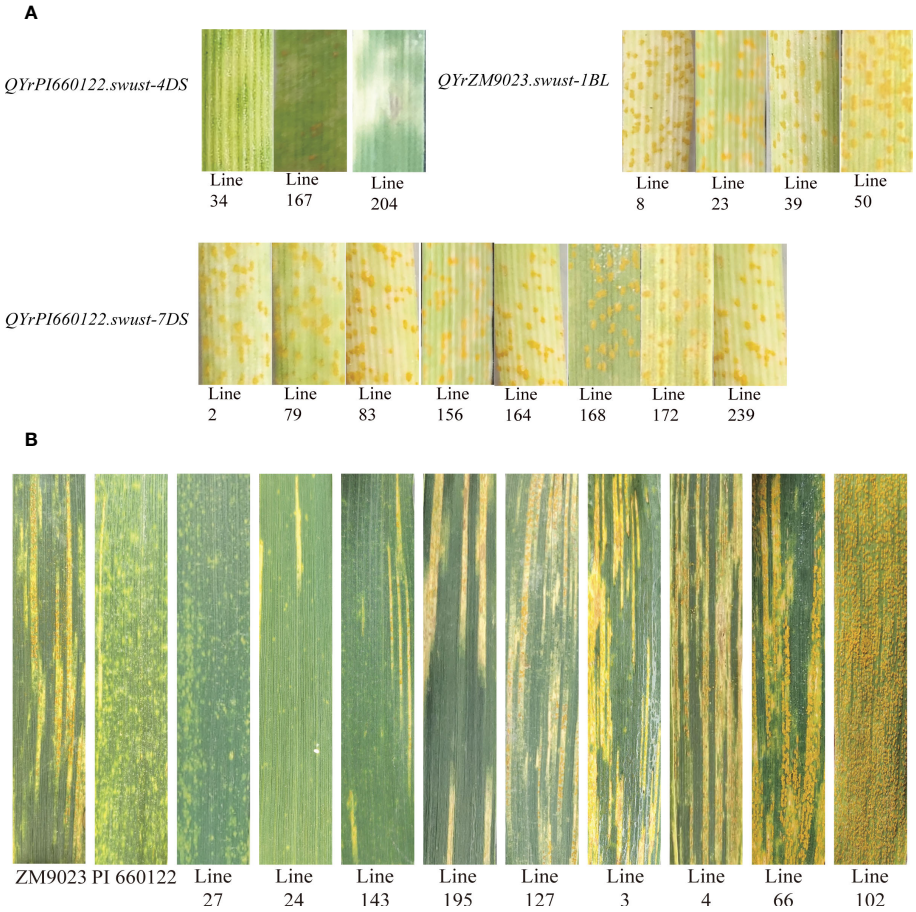

FIGURE 4
Stripe rust responses of lines containing only one QTL tested with Chinese race CYR32 of *Puccinia striiformis* f sp. *tritici* at the seedling stage **(A)** and on flag leaves of the resistant parent PI 660122, susceptible parent Zhengmai 9023 (ZM9023), and some selected recombinant inbred lines (RILs) **(B)**. Line 27 containing *QYrPI660122.swust-2BL*, *QYrPI660122.swust-4BS*, *QYrPI660122.swust-4BL*, *QYrPI660122.swust-4DS*, *QYrPI660122.swust-4DL*, *QYrZM9023.swust-6AS*, *QYrZM9023.swust-6DS*, and *QYrPI660122.swust-7DS*; Line 24 containing *QYrZM9023.swust-1BL*, *QYrPI660122.swust-2BL*, *QYrPI660122.swust-4BS*, *QYrPI660122.swust-4BL*, *QYrPI660122.swust-4DL*, and *QYrPI660122.swust-7DS*; Line 143 containing *QYrPI660122.swust-2BL*, *QYrPI660122.swust-4BS*, *QYrPI660122.swust-4BL*, *QYrPI660122.swust-4DL*, and *QYrPI660122.swust-7DS*; Line 195 containing *QYrPI660122.swust-4BS*, *QYrPI660122.swust-4BL*, *QYrPI660122.swust-4DL*, *QYrZM9023.swust-6AS*, and *QYrZM9023.swust-6DS*; Line 24 containing *QYrPI660122.swust-2BL* and *QYrPI660122.swust-4DS*; Line 3 containing *QYrZM9023.swust-1BL*, *QYrPI660122.swust-4BS*, *QYrPI660122.swust-4BL*, and *QYrPI660122.swust-4DL*; Line 4 containing *QYrPI660122.swust-2BL*, *QyrPI660122.swust-4BS*, *QyrPI660122.swust-4BL*, and *QyrPI660122.swust-4DL*; Line 66 and Line 102 without any QTLs. QTL, quantitative trait locus.

respectively, and the mean TGW values of RILs were between 30.6 g and 58.4 g.

In order to select RILs with desirable agronomic traits, the following criteria were used: PH between 80 cm and 100 cm, PTN 5 or more, SL greater than 9 cm, KPS not less than 45, and TGW over 42 g, with stripe rust IT of 1–3 and DS < 20%. Based on these criteria, 26 lines were selected. The QTLs detected by their highly associated SNP markers in the selected lines are listed in Table 6. These lines had at least two QTLs, and three lines (F_6-61, F_6-78, and F_6-86) had as many as seven QTLs. According to Table 7, the DS is negatively correlated with SL, PTN, KPS, and TGW, indicating that with the increase of DS, the SL, PTN, KPS, and TGW will decrease.

TABLE 5 Numbers of recombinant inbred lines from the Zhengmai 9023 × PI 660122 cross having only one stripe rust resistance and their infection types (ITs) at the seedling stage and mean IT and disease severity (DS) at the adult-plant stage in the fields of 2021 (21) and 2022 (22) at Mianyang (MY) and/or Guangyuan (GY).

QTL	No. of lines	Seedling ITs	Mean IT			Mean DS (%)		
			21MY	22MY	22GY	21MY	22MY	22GY
QYrZM9023.swust-1BL	4	8–9	5.6	7.1	5.8	39.5	36.2	40.0
QYrPI660122.swust-4DS	3	1–3	3.2	5.4	6.5	12.7	30.3	55.0
QYrPI660122.swust-7DS	8	7–9	6.4	7.3	5.9	26.6	40.2	42.5

QTL, quantitative trait locus.

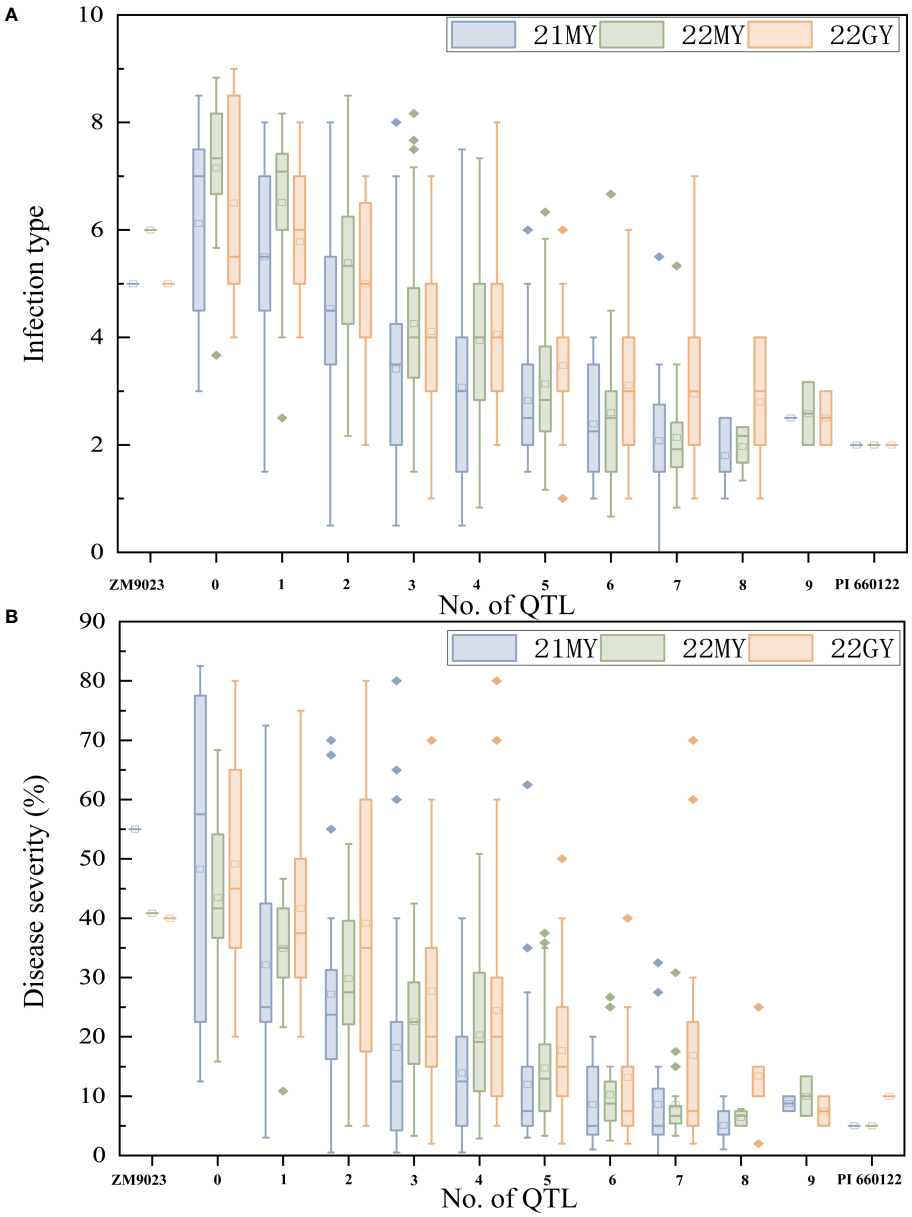

FIGURE 5
Effects of individual QTL and their combinations on stripe rust scores illustrated by mean infection type (IT) **(A)** and disease severity (DS) **(B)** scores of recombinant inbred lines from Zhengmai 9023 × PI 660122 (ZM9023 in three environments, 2021 Mianyang (21MY), 2022 Mianyang (22MY), and 2022 Guangyuan (22GY). Box plots indicate the infection type (IT) and disease severity (DS) associated with the identified QTL and their combination.

The correlation coefficients between DS and PH, and PTN were 0.13 and 0.15, respectively, and the correlation was significant ($p < 0.05$). The correlation coefficients between DS and SL, KPS, and TGW were 0.05, 0.08, and 0.02, respectively, and the correlation was not significant ($p > 0.05$).

Discussion

Developing durable resistance to stripe rust has been a top priority in wheat breeding over the past decade. Wheat line PI 660122 has exhibited high levels of stripe rust resistance for over a decade (Wang et al., 2012). In the present study, a RIL population containing 239 lines developed from a cross of PI 660122 with a Chinese elite cultivar, ZM9023, was phenotyped for stripe rust response in multiple environments and genotyped with the 15K wheat SNP array. We detected a total of nine QTLs, of which six (*QYrPI660122.swust-2BL*, *QyrPI660122.swust-4BS*, *QyrPI660122.swust-4BL*, *QyrPI660122.swust-4DS*, *QyrPI660122.swust-4DL*, and *QyrPI660122.swust-7DS*) came from PI 660122 and three (*QYrZM9023.swust-1BL*, *QYrZM9023.swust-6AS*, and *QYrZM9023.swust-6DS*) came from ZM9023.

QYrZM9023.swust-1BL, an APR QTL, was from Zhengmai 9023. This QTL was flanked by SNP markers *AX-89763895* and

TABLE 6 Mean stripe rust response, agronomic traits, and presence (+) and absence (–) of resistant QTLs detected with SNP markers in Zhengmai (ZM) 9023, PI 661022, and selected recombinant inbred lines[a].

Parent/line	Stripe rust		Agronomic trait					QTL								
	IT	DS (%)	PH	SL	PTN	KPS	TGW	1BL	2BL	4BS	4BL	4DS	4DL	6AS	6DS	7DS
ZM9023	5	45	79.3	8.4	4	44	40.9	+	–	–	–	–	–	+	+	–
PI 660122	2	7	90.3	9.8	5	49	45.1	–	+	+	+	+	+	–	–	+
F_6-5	2	9	95.0	9.5	5	49	46.4	+	–	+	+	+	+	–	–	–
F_6-13	1	3	93	9.7	5	50	52.1	–	+	+	+	+	+	–	–	–
F_6-18	3	13	83.0	9.4	6	48	53.7	+	–	–	–	–	–	+	+	–
F_6-22	2	5	97.0	9.1	7	46	47.5	+	+	+	+	–	+	–	–	+
F_6-27	1	3	93.7	9.4	8	52	50.7	–	+	+	+	+	+	+	+	+
F_6-32	3	9	99.3	10.4	6	52	56.8	+	+	–	–	–	–	–	–	+
F_6-48	3	11	95.7	9.1	6	51	46.9	+	–	–	–	+	–	–	–	+
F_6-54	2	7	84.3	9.1	6	49	45.0	–	–	+	+	–	+	–	–	–
F_6-56	2	5	83.7	9.0	6	45	53.5	–	–	–	–	+	–	+	+	+
F_6-61	3	10	86.7	10.2	7	52	46.3	+	–	+	+	+	+	+	+	–
F_6-78	2	6	96.3	9.5	6	49	44.2	–	+	+	+	+	+	+	+	–
F_6-86	3	14	90	9.6	7	50	47.9	+	+	+	+	–	+	+	+	–
F_6-115	3	12	98	9.7	5	48	52.6	+	+	–	–	+	+	–	–	+
F_6-124	2	6	90.7	9.4	8	57	53.2	+	+	–	–	–	–	+	+	–
F_6-150	3	13	98	9.6	6	47	51.9	–	+	–	–	+	–	+	+	–
F_6-161	3	15	93	9.4	7	54	50.1	–	–	–	–	–	–	–	+	+
F_6-162	3	11	94.7	9.1	7	49	49.5	–	+	–	–	+	–	–	–	–
F_6-170	3	11	93	9.6	7	50	52.0	–	+	–	–	–	–	+	+	+
F_6-178	3	11	89.5	9.5	7	51	48.3	+	–	+	–	–	+	+	+	–
F_6-186	2	8	96	9.9	5	45	46.0	–	–	–	–	+	–	–	–	+
F_6-187	2	4	80	9.4	5	49	52.4	+	–	+	+	+	+	–	–	–
F_6-207	2	3	82	9.7	6	52	44.0	–	–	+	+	+	+	+	+	+
F_6-211	2	3	82.0	9.7	6	52	49.6	–	–	+	–	+	+	–	–	–
F_6-228	3	10	92.7	9.5	6	48	49.3	–	–	–	–	+	–	+	+	+
F_6-231	3	14	93.7	9.3	5	56	45.6	+	–	–	–	–	–	+	+	+
F_6-235	3	13	97	9.5	7	48	49.9	+	+	–	–	+	–	+	+	–

[a]IT, infection type; DS, disease severity; PH, plant height; PTN, productive tiller number; SL, spike length; KPS, kernels per spike; TGW, thousand-grain weight.
QTLs, quantitative trait loci; SNP, single-nucleotide polymorphism.

AX-109273019, corresponding to the region from 670,429,611 bp to 681,685,826 bp of chromosome 1BL in the Chinese Spring (CS) genome (IWGSC RefSeq v1.0). Three permanently named stripe rust resistance genes, *Yr21* (Chen and Line, 1995), *Yr26* (Ma et al., 2001), and *Yr29* (William et al., 2006), were mapped to 1BL. Among them, *Yr21* and *Yr26* confer ASR, while *Yr29* is an APR gene linked with SSR markers *Xwmc44* and *Xwmc367* and located at the distal end of chromosome 1BL. The physical position of *Xwmc367* is in the range of 678,736,681–678,736,834 bp, which is within the genome range of *QYrZM9023.swust-1BL*. According to a previous study, ZM9023 has *Lr27*/*Yr30*/*Sr2* and *Lr46*/*Yr29*/*Pm39*/*Sr58* (Li et al., 2020). As both *Yr29* and *QYrZM9023.swust-1BL* confer APR, *QYrZM9023.swust-1BL* should be *Yr29*. *Yr29* has been reported and deployed widely in wheat varieties around the world (William et al., 2006; Melichar et al., 2008; Lan et al., 2014; Hou et al., 2015; Maccaferri et al., 2015; Muleta et al., 2017; Wang and Chen, 2017; Cobo et al., 2018; Godoy et al., 2018; Liu et al., 2019; Rosa et al., 2019; Liu et al., 2020).

QYrPI660122.swust-2BL was derived from PI 660122, and it was flanked by SNP markers *AX-109849173* and *AX-109349804*, corresponding to the region from 777,831,275 bp to 779,847,527 bp of chromosome 2BL in CS (IWGSC RefSeq v1.0). Seven

TABLE 7 Correlation coefficients (r) of important traits of the recombinant inbred lines Zhengmai 9023 × PI 660122.

Trait	IT	DS (%)	PH	SL	PTN	KPS	TGW
IT	NA[a]						
DS (%)	0.95***[b]	NA					
PH	0.16*	0.13*	NA				
SL	−0.01ns	−0.05	0.10ns	NA			
PTN	−0.12ns	−0.15*	−0.02ns	0.07ns	NA		
KPS	−0.03ns	−0.08ns	0.19**	0.45***	0.12ns	NA	
TGW	0.01ns	−0.02ns	0.06ns	0.06ns	0.02ns	−0.02ns	NA

[a]NA, not applicable.
[b]"***" denotes the r value is significant at <0.001, "**" denotes the r value is significant at <0.01, "*" denotes the r value is significant at <0.05, and "ns" denotes the r value is not significant at $p > 0.05$.

permanently named stripe rust resistance genes, including *Yr5* and *Yr7* (Macer, 1963; Marchal et al., 2018), *Yr43* (Cheng and Chen, 2010), *Yr44* (Sui et al., 2009), *Yr53* (Xu et al., 2013), *Yr72* (McIntosh et al., 2016), and *YrSP* (Feng et al., 2015), were mapped to 2BL. *Yr5*/*Yr7*/*YrSP* (Marchal et al., 2018) had been cloned, and it encoded nucleotide-binding (NB) and leucine-rich repeat (LRR) proteins. The physical map position of *Yr5*/*Yr7*/*YrSP* was 685.265–685.27 Mb. *Yr43*, an ASR gene, was flanked by *Xwgp110* and *Xwgp103*, but its physical map position is unknown. *Yr44*, an ASR gene, was derived from spring wheat cultivar Zak and flanked by *XpWB5*/*N1R1* and *Xwgp100*, but its physical map position is unknown. *Yr53*, an ASR gene, was derived from PI 480148 and flanked by *Xwmc441* and *XLRRrev*/*NLRRrev350*. The physical map position of *Xwmc441* was 598,064,318–598,064,477 bp. *Yr72*, an ASR gene, was derived from AUS27507 and flanked by *Xsun481* and *IWB12294*. The physical map position of *IWB12294* was 767,171,587–767,171,587 bp. In addition, several major QTLs have been mapped to the long arm of chromosome 2B. *QYr.hbaas-2BL* was located at 453.3 Mb (Jia et al., 2020). *Yr.niab-2B.1* was located at 683.05–750.12 Mb (Bouvet et al., 2022). *QYrpd.Swust-2BL.1*, *QYrpd.Swust-2BL.2*, *QYrpd.Swust-2BL.3*, and *QYrpd.Swust-2BL.4* were located at 773.79–775.17 Mb, 753.37–777.52 Mb, 793.15–798.00 Mb, and 782.53–784.55 Mb, respectively (Zhou et al., 2022b). *Qyr.gaas.2B.1* was located at 698.22–705.68 Mb (Cheng et al., 2022). *YrQz* was located at 557.37–630.40 Mb (Deng et al., 2004). *QYr.nafu-2BL* was located at 553.73–615.79 Mb (Zhou et al., 2015a; Hu et al., 2020). *QYrww.wgp.2B-4* was located at 524 Mb (Mu et al., 2020). *Yrdr.wgp-2BL* was located at 709.84 Mb (Hou et al., 2015). *QTL 2BL* was located at 779.11–783.89 Mb (Somers et al., 2004). *QYr.inra-2BL* was located at 615.79–621.47 Mb (Mallard et al., 2005). *QYraq.cau-2BL* was located at 670.60–739.40 Mb (Ramburan et al., 2004). *QYr.caas-2BL* was located at 693.74–733.16 Mb (Ren et al., 2012b). *Yrns.orz-2BL* was located at 685.74 Mb (Vazquez et al., 2015). *YrV23* is closely linked to *Xwmc356* at position 796,684,893–796,685,357 bp (Wang et al., 2006). Based on the chromosomal positions, *QYrPI660122.swust-2BL* is likely different from *Yr5*/*Yr7*/*YrSP* and *Yr53*, but its relationships with other genes or QTL on 2BL need to be further studied.

QYrPI660122.swust-4BS was derived from PI 660122, and it was flanked by SNP markers *AX-108767762* and *AX-109309162*, corresponding to the region from 32,961,964 bp to 36,395,734 bp of the CS (IWGSC RefSeq v1.0) chromosome 4BS. *QYr.caas-4BS* was located between markers *Xwmc652* and *Xgpw4388* (Wang et al., 2020). The physical map position of *QYr.caas-4BS* was 38.6–47.6 Mb. *QYrcl.sicau-4B* was located at the end of chromosome 4BS (Yao et al., 2020), which is different from the physical map position of *QYrPI660122.swust-4BS*. *QYrPI660122.swust-4BS* in PI 660122 is likely different from the previously mapped stripe rust resistance genes on chromosome 4BS.

QYrPI660122.swust-4BL was derived from PI 660122 and was flanked by SNP markers *AX-109495166* and *AX-108935256*, corresponding to the position from 396,263,280 bp to 445,689,397 bp of the CS chromosome 4BL. Three permanently named stripe rust resistance genes, *Yr50* (Liu et al., 2013), *Yr62* (Lu et al., 2014), and *Yr68* (McIntosh et al., 2016), were mapped to 4BL. *Yr50*, an ASR gene, was reported to be associated with *Xbarc1096* and *Xwmc47*. The map position of *Yr50* is 105.1 Mb–644.9 Mb. *Yr62*, a HTAP gene, was reported to be associated with *Xgwm192* and *Xgwm251*. The physical map position of *Yr62* was 482.8–568.6 Mb. *Yr68*, an APR gene, was reported to be associated with *IWB74301* and *IWB28394*, and its physical map position was 575.04–600.66 Mb. In addition, several major QTLs were located on chromosome 4BL. *QYrhm.nwafu-4B*, *Qyr.hbaas-4BL.1*, and *QYr.hbaas-4BL.2* overlapped *Yr62* (Yuan et al., 2018; Jia et al., 2020). *QYrhm.nwafu-4BL* was derived from Humai 15 and flanked by *AX-111150955* and *Xgwm251*, which was mapped to 523.4–568.6 Mb (Yuan et al., 2018). *QYr.hbaas-4BL.1* was linked with *IWB73717*, and its physical map position was 531.3 Mb (Jia et al., 2020). *QYr.hbaas-4BL.2* was linked with *IWB63337* at the physical map position of 558.1 Mb. *QYr.hbaas-4BL.3* was linked with *IWB32927* at the physical map position of 579.4 Mb. *QYr.sun-4B* was derived from the Australian wheat cultivar Janz and exhibited minor variation (9.4%–16.8%) (Zwart et al., 2010). It was flanked by *wPt-8543* and *Xwmc238*. The physical map position of *Xwmc238* was 236,742,906–236,743,133 bp. *QPst.jic-4B* (Melichar et al., 2008) was derived from the UK winter wheat cultivar Guardian and mapped to the region between *Xwmc652* and *Xwmc692* with a PVE of 12%. *QYr.crc-4BL* was flanked by markers *BS00048794_51* and *RAC875_rep_c72961_977*, and the physical map position of *QYr.crc-4BL* was 601.93–617.00 Mb (Rosa et al., 2019). *YrBm*, an APR QTL, was derived from Chinese winter wheat landrace

Baimangmai (Hu et al., 2022). It was flanked by markers *Xgpw7272* and *Xwmc652*. The physical map position of *YrBm* was 611.1–621.1 Mb. *QYrPI660122.swust-4BL* overlapped with *Yr50*, but further studies are needed to confirm the relationship between *QYrPI660122.swust-4BL* and *Yr50* and determine the relationships with other QTLs on chromosome 4BL.

QYrPI660122.swust-4DS, an ASR QTL, was derived from PI 660122, and it was flanked by SNP markers *AX-110046962* and *AX-111093894* and corresponds to the region from 1,702,954 bp to 9,555,772 bp of the CS 4DS chromosome. *Yr28* has been mapped to the short arm of chromosome 4D (Singh et al., 2000). *Yr28* is a major ASR gene conferring stripe rust resistance from *Ae. tauschii* and located between SSR markers *Xbcd265* and *Xmwg634*. *Yr28* has been cloned and characterized, which encoded a typical nucleotide oligomerization domain-like receptor (NLR) (Zhang et al., 2019). The gene was further mapped between *Xsdauw92* and *Xsdauw96*, approximately 0.13-cM interval, and its physical map position of *Yr28* was 1.820–1.826 Mb. Based on the physical map position, the resistance type, and the Mexican wheat genotype PI 610755 that has *Ae. tauschii* in the pedigree as stripe rust resistance donor of PI 660122 (Wang et al., 2012), *QYrPI660122.swust-4DS* is highly likely *Yr28*.

QYrPI660122.swust-4DL was derived from PI 660122 and was flanked by SNP markers *AX-94560848* and *AX-111557122* corresponding to 288,430,275 bp to 310,458,135 bp of the CS chromosome 4DL. So far, only one permanently named *Yr* gene, *Yr46* (Herrera-Foessel et al., 2011), has been reported on chromosome 4DL. *Yr46* is an APR gene from wheat cultivar RL6007 and flanked by SSR markers *Xgwm165* and *Xgwm192*, and its physical map position is approximately 417.2 Mb. Two QTLs, *QYr.ucw-4DL* (Cobo et al., 2018) and *QYr.hbaas-4DL* (Jia et al., 2020), have been also reported on chromosome 4DL. *QYr.ucw-4DL* was linked with the *IWA2395*, and its physical map position was 497.65 Mb (Cobo et al., 2018). *QYr.hbaas-4DL* is linked to SNP marker *IWB44356* (Jia et al., 2020), with the physical map position of approximately 477.9 Mb. Based on the different physical map positions of *QYrPI660122.swust-4DL* from those of *Yr46*, *QYr.ucw-4DL*, and *QYr.hbaas-4DL*, *QYrPI660122.swust-4DL* is likely a new QTL for stripe rust resistance.

QYrZM9023.swust-6AS is derived from Zhengmai 9023 and flanked by SNP markers *AX-95124889* and *AX-110995858* corresponding to the 27,748,586–71,705,701-bp region of the CS chromosome 6AS. Numerous genes or QTLs for stripe rust resistance have been mapped to 6AS. *Yr38* was mapped to 6AS (Marais et al., 2006), but its physical map position is unknown. *Yr81* is flanked by *KASP_3077* and *Xgwm459* (Gessese et al., 2019), and the physical map position of *Xgwm459* is within the 6,805,513–6,805,994-bp region. *YrP10090* is flanked by *AX-94460938* and *AX-110585473* (Liu et al., 2021), and its physical map position is within 107.1–446.5 Mb. *Qyr.gaas.6A* was flanked by *AX-109558600* and *AX-109542604* (Cheng et al., 2022), and its physical map position is within 609.11–609.89 Mb. *QYr-6A_Saar* derived from the CIMMYT variety Saar (Lillemo et al., 2008) is flanked by *XwPt-7063* and *Xbarc3*, and its physical map position is within 62.92–85.28 Mb. *QYr.uaf-6A.1* and *QYr.uaf-6A.4* were mapped with *IWA8028* and *IWB29623*, respectively (Habib et al., 2020). The physical map position of *QYr.uaf-6A.1* is at 105.02 Mb, and that of *QYr.uaf-6A.4* is at 18.71 Mb. *QYr.uga-6AS* is flanked by *wPt-671561* and *wPt-7840* (Hao et al., 2011), and its physical map position is within 24.09–85.28 Mb. *QYrex.wgp-6AS* is flanked by markers *Xgwm334* and *Xwgp56* (Lin and Chen, 2008a), which indicate the QTL physical map position within 9.25–61.02 Mb. *Yrq3* is flanked by SSR markers *Xgwm334* and *Xgwm169* (Cao et al., 2012), and its physical map position was found to be within 9.25–595.38 Mb. *QYrcl.sicau-6A.1* was detected by two adjacent DArT-seq markers (*3936688* and *1266956*) on chromosome 6A between 5.14 and 5.83 Mb (Yao et al., 2020). *QYr.sicau-6A* is flanked by SNP markers *AX-94548199* and *AX-111101235* (Ma et al., 2019), and its physical map position of *QYr.sicau-6A* is within 90.32–97.52 Mb. *QYrswp-6A* is linked with *IWA272* (Liu et al., 2019b), and its physical map position is 3.85 Mb. *QYrZM9023.swust-6AS* overlapped with *QYr-6A_Saar*, *Yr.uga-6AS*, and *QYrex.wgp-6AS*, but further studies are needed to determine if they are the same or different.

QYrZM9023.swust-6DS was also derived from Zhengmai 9023 and flanked by SNP markers *AX-11475193* and *AX-109317417* corresponding to the 35,630,857–44,498,347-bp region of the CS chromosome 6DS. Few genes or QTL for stripe rust resistance have been reported on 6DS. *Yr77* is an APR gene flanked by *Xbrac54* and *Xcfd188*, and the physical map position of *Xcfd188* is within the 238,118,148–238,118,395-bp region (R. McIntosh, personal communication). *QYr.ucw-6D* is linked with *IWA167* (Maccaferri et al., 2015), which is at the physical map position of 73.2 Mb. *QYr.ufs-6D* is flanked by *Xgwm325* and *Xbarc175* (Agenbag et al., 2012), and its physical map position is within the 79.96–411.88-Mb region. *QYR7* is flanked by *Xbcd1510* and *XksuD27* (Boukhatem et al., 2002), and its physical map position is approximately 12 Mb. Based on the physical positions, *QYrZM9023.swust-6DS* is likely different from these genes or QTLs for stripe rust resistance genes previously mapped on chromosome 6DS.

QYrPI660122.swust-7DS, an APR QTL derived from PI 660122, is flanked by SNP markers *AX-110467729* and *AX-89378255* corresponding to the 43,386,933–47,379,368-bp region of the CS 7DS chromosome. Only the permanently named stripe rust resistance gene *Yr18* has been mapped to chromosome 7DS. *Yr18* was mapped to 7DS in a number of different wheat cultivars, such as Jupateco 73R and Opata 85 (Singh, 1992; Singh et al., 2000), Australian cultivar Cook (Bariana et al., 2001), and Fukuho-komugi (Suenaga et al., 2003). *Yr18* is an APR gene flanked by *Xgwm1220* and *Xgwm29* and encodes a putative ATP-binding cassette transporter (Krattinger et al., 2009; Lagudah et al., 2009). The physical map position of *Yr18* is from 47.412 Mb to 47.424 Mb, similar to *QYrPI660122.swust-7DS*. *Yr18* is an important slow rusting gene and can confer high levels of resistance when combined with other minor genes (Singh and Rajaram, 1993; Navabi et al., 2004). Cultivars with *Yr18* have been widely used in the International Maize and Wheat Improvement Center (CIMMYT) wheat breeding program (Singh et al., 2005). PI 660122 was developed from a cross of AvS with Mexican wheat genotype PI 610755 (Wang et al., 2012), PI 610755 has Opata 85 in its pedigree (Altar 84/*Ae. tauschii* (191)//Opata M85) (https://npgsweb.ars-grin.gov/gringlobal/accessiondetail?id=1580210), *Yr18* was mapped in a RIL population for mapping *Yr28* (Singh

et al., 2000) as discussed above, and *QYrPI660122.swust-7DS* is most likely *Yr18*.

Conclusions

In the present study, we mapped nine QTLs conferring different types and levels of resistance to stripe rust. Among these QTLs, *QYrZM9023.swust-1BL* was identified as *Yr29*, *QYrPI660122.swust-4DS* as *Yr28*, and *QYrPI660122.swust-7DS* as *Yr18*, while *QYrPI660122.swust-4BS*, *QYrPI660122.swust-4BL*, and *QYrZM9023.swust-6DS* should be new. We demonstrated that combinations of different QTLs increased the levels of resistance. Furthermore, we selected lines from the RIL population with high adequate resistance to stripe rust combined with desirable agronomic traits, and these lines can be used in further evaluation for releasing commercial cultivars. The resistant lines and molecular markers for resistance QTL should be useful in developing wheat cultivars with high levels and durable resistance to stripe rust.

Data availability statement

The original contributions presented in the study are included in the article/supplementary material, further inquiries can be directed to the corresponding author/s.

Author contributions

QY and GJ detected the QTLs, analyzed the data, and prepared the first draft of the manuscript. QY, WT, RT, XQL, JF, XCZ and BS contributed to the collection of samples and phenotype data. XLZ contributed to the crosses and revised the manuscript. YR, XL, KH, and SY contributed to target line selection and population assessment. MW and XC provided seeds of the stripe rust-resistant parent. XLZ and XC conceived the project and generated the final version of the manuscript. All authors provided suggestions during the revision of the manuscript. All authors contributed to the article and approved the submitted version.

Funding

This study was financially supported by the Breakthrough in Wheat Breeding Material and Method Innovation and New Variety Breeding (Breeding Research Project, 2021YFYZ0002) and was partially funded by the Key Research and Development Program of the International Science and Technology Innovation Cooperation of Science and Technology Department of Sichuan Province, China (No. 2022YFH0032), National Natural Science Foundation of China (No. 32101707), PhD Foundation of Southwest University of Science and Technology (Nos. 19zx7116, 18zx7159, 16zx7162), and Longshan Academic Talent Research Support Program of SWUST (No. 17LZX5).

Conflict of interest

The authors declare that the research was conducted in the absence of any commercial or financial relationships that could be construed as a potential conflict of interest.

Publisher's note

All claims expressed in this article are solely those of the authors and do not necessarily represent those of their affiliated organizations, or those of the publisher, the editors and the reviewers. Any product that may be evaluated in this article, or claim that may be made by its manufacturer, is not guaranteed or endorsed by the publisher.

References

Agenbag, G. M., Pretorius, Z. A., Boyd, L. A., Bender, C. M., and Prins, R. (2012). Identification of adult plant resistance to stripe rust in the wheat cultivar Cappelle-Desprez. *Theor. Appl. Genet.* 125, 109–120. doi: 10.1007/s00122-012-1819-5

Bariana, H., Forrest, K., Qureshi, N., Miah, H., Hayden, M., and Bansal, U. (2016). Adult plant stripe rust resistance gene *Yr71* maps close to *Lr24* in chromosome 3D of common wheat. *Mol. Breed.* 36, 98. doi: 10.1007/s11032-016-0528-1

Bariana, H. S., Hayden, M. J., Ahmed, N. U., Bell, J. A., and McIntosh, R. A. (2001). Mapping of durable adult plant and seedling resistances to stripe rust and stem rust diseases in wheat. *Aust. J. Agric. Res.* 52, 1247–1255. doi: 10.1071/ar01040

Boukhatem, N., Baret, P. V., Mingeot, D., and Jacquemin, J. M. (2002). Quantitative trait loci for resistance against yellow rust in two wheat-derived recombinant inbred line populations. *Theor. Appl. Genet.* 104, 111–118. doi: 10.1007/s001220200013

Bouvet, L., Percival-Alwyn, L., Berry, S., Fenwick, P., Mantello, C. C., Sharma, R., et al. (2022). Wheat genetic loci conferring resistance to stripe rust in the face of genetically diverse races of the fungus *Puccinia striiformis* f. sp. tritici. *Theor. Appl. Genet.* 135, 301–319. doi: 10.1007/s00122-021-03967-z

Cao, X., Zhou, J., Gong, X., Zhao, G., Jia, J., and Qi, X. (2012). Identification and validation of a major quantitative trait locus for slow-rusting resistance to stripe rust in wheat. *J. Integ. Plant Biol.* 54, 330–344. doi: 10.1111/j.1744-7909.2012.01111.x

Carter, A. H., Chen, X. M., Garland-Campbell, K., and Kidwell, K. K. (2009). Identifying QTL for high-temperature adult-plant resistance to stripe rust (*Puccinia striiformis* f. sp. *tritici*) in the spring wheat (*Triticum aestivum* L.) cultivar 'Louise'. *Theor. Appl. Genet.* 119, 1119–1128. doi: 10.1007/s00122-009-1114-2

Cavanagh, C. R., Chao, S., Wang, S., Huang, B. E., Stephen, S., Kiani, S., et al. (2013). Genome-wide comparative diversity uncovers multiple targets of selection for improvement in hexaploid wheat landraces and cultivars. *Proc. Natl. Acad. Sci. U.S.A.* 110, 8057–8062. doi: 10.1073/pnas.1217133110

Chen, X. M. (2005). Epidemiology and control of stripe rust (*Puccinia striiformis* f. sp. *tritici*) on wheat. *Can. J. Plant Pathol.* 27, 314–337. doi: 10.1080/07060660509507230

Chen, X. M. (2007). Challenges and solutions for stripe rust control in the United States. *Aust. J. Agr. Res.* 58, 648–655. doi: 10.1071/AR07045

Chen, X. M. (2013). High-temperature adult-plant resistance, key for sustainable control of stripe rust. *Am. J. Plant Sci.* 4, 608–627. doi: 10.4236/ajps.2013.43080

Chen, X. M., and Line, R. F. (1995). Gene number and heritability of wheat cultivars with durable, highr-temperature, adult-plantresistance and race-specific resistance to *Puccinia striiformis*. *Phytopathology* 85, 573–578. doi: 10.1094/Phyto-85-573

Cheng, P., and Chen, X. M. (2010). Molecular mapping of a gene for stripe rust resistance in spring wheat cultivar IDO377s. *Theor. Appl. Genet.* 121, 195–204. doi: 10.1007/s00122-010-1302-0

Cheng, B., Gao, X., Cao, N., Ding, Y., Chen, T., Zhou, Q., et al. (2022). QTL mapping for adult plant resistance to wheat stripe rust in M96-5 × Guixie 3 wheat population. *J. Appl. Genet.* 63 (2), 265–279. doi: 10.1007/s13353-022-00686-z

Cobo, N., Pfluger, L., Chen, X. M., and Dubcovsky, J. (2018). Mapping QTL for resistance to new virulent races of wheat stripe rust from two argentinean wheat cultivars. *Crop Sci.* 58, 2470–2483. doi: 10.2135/cropsci2018.04.0286

Cui, F., Zhang, N., Fan, X., Zhang, W., Zhao, C., Yang, L., et al. (2017). Utilization of a wheat 660K SNP array-derived high-density genetic map for high-resolution mapping of a major QTL for kernel number. *Sci. Rep.* 7, 3788. doi: 10.1038/s41598-017-04028-6

Deng, Z. Y., Zhang, X. Q., Wang, X. P., Jing, J. K., and Wang, D. W. (2004). Identification and molecular mapping of a stripe rust resistance gene from a common wheat line Qz180. *Acta Bot. Sin.* 46, 236–241. doi: 10.1614/WS-03-091R

Dong, Z. Z., Hegarty, J. W., Zhang, J. L., Zhang, W. J., Chao, S. M., Chen, X. M., et al. (2017). Validation and characterization of a QTL for adult plant resistance to stripe rust on wheat chromosome arm 6BS (*Yr78*). *Theor. Appl. Genet.* 130, 2127–2137. doi: 10.1007/s00122-017-2946-9

Feng, J. Y., Wang, M. N., Chen, X. M., See, D. R., Zheng, Y. L., Chao, S. M., et al. (2015). Molecular mapping of *YrSP* and its relationship with other genes for stripe rust resistance in wheat chromosome 2BL. *Phytopathology* 105, 1206–1213. doi: 10.1094/PHYTO-03-15-0060-R

Feng, J. Y., Wang, M. N., See, D. R., Chao, S. M., Zheng, Y. L., and Chen, X. M. (2018). Characterization of novel gene *Yr79* and four additional QTL for all-stage and high-temperature adult-plant resistance to stripe rust in spring wheat PI 182103. *Phytopathology* 108, 737–747. doi: 10.1094/PHYTO-11-17-0375-R

Fu, D. L., Uauy, C., Distelfeld, A., Blechel, A., Epstein, L., Chen, X. M., et al. (2009). A kinase-START gene confers temperature-dependent resistance to wheat stripe rust. *Science* 323, 1357–1360. doi: 10.1126/science.1166289

Gerechter-Amitai, Z. K., van Silfhout, C. H., Grama, A., and Kleitman, F. (1989). *Yr15* — a new gene for resistance to *Puccinia striiformis* in *Triticum dicoccoides* sel. G-25. *Euphytica* 43, 187–190. doi: 10.1007/bf00037912

Gessese, M., Bariana, H., Wong, D., Hayden, M., and Bansal, U. (2019). Molecular mapping of stripe rust resistance gene *Yr81* in a common wheat landrace Aus27430. *Plant Dis.* 103, 1166–1171. doi: 10.1094/pdis-06-18-1055-re

Godoy, J., Rynearson, S., Chen, X. M., and Pumphrey, M. (2018). Genome-wide association mapping of loci for resistance to stripe rust in North American elite spring wheat germplasm. *Phytopathology* 108, 234–245. doi: 10.1094/PHYTO-06-17-0195-R

Habib, M., Awan, F. S., Sadia, B., and Zia, M. A. (2020). Genome-wide association mapping for stripe rust resistance in Pakistani spring wheat genotypes. *Plants* 9, 1056. doi: 10.3390/plants9091056

Hao, Y., Chen, Z., Wang, Y., Bland, D., Buck, J., Brown-Guedira, G., et al. (2011). Characterization of a major QTL for adult plant resistance to stripe rust in US soft red winter wheat. *Theor. Appl. Genet.* 123, 1401–1411. doi: 10.1007/s00122-011-1675-8

Herrera-Foessel, S. A., Lagudah, E. S., Huerta-Espino, J., Hayden, M. J., Bariana, H. S., Singh, D., et al. (2011). New slow-rusting leaf rust and stripe rust resistance genes *Lr67* and *Yr46* in wheat are pleiotropic or closely linked. *Theor. Appl. Genet.* 122, 239–249. doi: 10.1007/s00122-010-1439-x

Hou, L., Chen, X. M., Wang, M. N., See, D. R., Chao, S., Bulli, P., et al. (2015). Mapping a large number of QTL for durable resistance to stripe rust in winter wheat Druchamp using SSR and SNP markers. *PloS One* 10, e0126794. doi: 10.1371/journal.pone.0126794

Hu, C. Y., Wang, F. T., Feng, J., Sun, C., Guo, J. Y., Lang, X. W., et al. (2022). Identification and molecular mapping of *YrBm* for adult plan resistance to stripe rust in Chinese wheat landrace Baimangmai. *Theor. Appl. Genet.* 135, 2655–2664. doi: 10.1007/s00122-022-04139-3

Hu, T., Zhong, X., Yang, Q., Zhou, X. L., Li, X., Yang, S. Z., et al. (2020). Introgression of two quantitative trait loci for stripe rust resistance into three Chinese wheat cultivars. *Agronomy* 10, 483. doi: 10.3390/agronomy10040483

Huang, C., Jiang, Y. Y., Li, P. L., Peng, H., Cui, Y., Yang, J. J., et al. (2018). Epidemics analysis of wheat stripe rust in China in 2017. *Plant protection.* 44, 162–166. doi: 10.16688/j.zwbh.2017268

Jambuthenne, D. T., Riaz, A., Athiyannan, N., Athiyannan, N., Ng, W. L., Ziems, L., et al. (2022). Mining the Vavilov wheat diversity panel for new sources of adult plant resistance to stripe rust. *Theor. Appl. Genet.* 135, 1355–1373. doi: 10.1007/s00122-022-04037-8

Jia, M., Yang, L., Zhang, W., Rosewarne, G., Li, J., Yang, E., et al. (2020). Genome-wide association analysis of stripe rust resistance in modern Chinese wheat. *BMC Plant Biol.* 20, 491. doi: 10.1186/s12870-020-02693-w

Klymiuk, V., Chawla, H. S., Wiebe, K., Ens, J., Fatiukha, A., Govta, L., et al. (2022). Discovery of stripe rust resistance with incomplete dominance in wild emmer wheat using bulked segregant analysis sequencing. *Commun. Biol.* 5, 826. doi: 10.1038/s42003-022-03773-3

Klymiuk, V., Yaniv, E., Huang, L., Raats, D., Fatiukha, A., Chen, S., et al. (2018). Cloning of the wheat *Yr15* resistance gene sheds light on the plant tandem kinase-pseudokinase family. *Nat. Commun.* 9, 3735. doi: 10.1038/s41467-018-06138-9

Kosambi, D. D. (2016). *The estimation of map distances from recombination values*. Eds. R. Ramaswamy and D. D. Kosambi (New Delhi: Springer), 125–130. doi: 10.1007/978-81-322-3676-4_16

Krattinger, S. G., Lagudah, E. S., Spielmeyer, W., Singh, R. P., Huerta-Espino, J., McFadden, H., et al. (2009). A putative ABC transporter confers durable resistance to multiple fungal pathogens in wheat. *Science* 323, 1360–1363. doi: 10.1126/science.1166453

Lagudah, E. S., Krattinger, S. G., Herrera-Foessel, S., Singh, R. P., Huerta-Espino, J., Spielmeyer, Q., et al. (2009). Gene-specific markers for the wheat gene *Lr34/Yr18/Pm38* which confers resistance to multiple fungal disease. *Theor. Appl. Genet.* 119, 889–898. doi: 10.1007/s00122-009-1097-z

Lan, C. X., Rosewarne, G. M., Singh, R. P., Herrera-Foessel, S. A., Huerta-Espino, J., Basnet, B. R., et al. (2014). QTL characterization of resistance to leaf rust and stripe rust in the spring wheat line Francolin1. *Mol. Breed.* 34, 789–803. doi: 10.1007/s11032-014-0075-6

Li, W., Song, G. Q., Li, J. H., Li, Y. L., Zhang, S. J., Gao, J., et al. (2020). Molecular detection of four pleiotropic disease resistance genes in wheat. *J. Triti. Crops* 40, 395–400. doi: 10.7606/J.ISSN.1009-1041.2020.04.0

Li, J. L., Wang, S., Yu, J., Wang, L., and Zhou, S. L. (2013). A modified CTAB protocol for plant DNA extraction. *Chin. Bull. Bot.* 48, 72–78. doi: 10.3724/sp.j.1259.2013.00072

Li, Z. Q., and Zeng, S. M. (2000). *Wheat rusts in China* (Beijing: China Agricultural Press).

Lillemo, M., Asalf, B., Singh, R. P., Huerta-Espino, J., Chen, X. M., He, Z. H., et al. (2008). The adult plant rust resistance loci *Lr34/Yr18* and *Lr46/Yr29* are important determinants of partial resistance to powdery mildew in bread wheat line Saar. *Theor. Appl. Genet.* 116, 1155–1166. doi: 10.1007/s00122-008-0743-1

Lin, F., and Chen, X. M. (2007). Genetics and molecular mapping of genes for race-specific all-stage resistance and non-race-specific high-temperature adult-plant resistance to stripe rust in spring wheat cultivar Alpowa. *Theor. Appl. Genet.* 114, 1277–1287. doi: 10.1007/s00122-007-0518-0

Lin, F., and Chen, X. M. (2008a). Molecular mapping of genes for race-specific overall resistance to stripe rust in wheat cultivar Express. *Theor. Appl. Genet.* 116, 797–806. doi: 10.1007/s00122-008-0713-7

Lin, F., and Chen, X. M. (2008b). Quantitative trait loci for non-race-specific, high-temperature adult-plant resistance to stripe rust in wheat cultivar Express. *Theor. Appl. Genet.* 118, 631–642. doi: 10.1007/s00122-008-0894-0

Line, R. F. (2002). Stripe rust of wheat and barley in North America: a retrospective historical review. *Annu. Rev. Phytopathol.* 40, 75–118. doi: 10.1146/annurev.phyto.40.020102.111645

Line, R. F., and Qayoum, A. (1992). Virulence, aggressiveness, evolution and distribution of races of *Puccinia striiformis* (the cause of stripe rust of wheat) in North America 1968–87. *Tech. Bulletin United States Department Agric.* 1788, 1–44.

Liu, J., Chang, Z., Zhang, X., Yang, Z., Li, X., Jia, J., et al. (2013). Putative *Thinopyrum intermedium*-derived stripe rust resistance gene *Yr50* maps on wheat chromosome arm 4BL. *Theor. Appl. Genet.* 126, 265–274. doi: 10.1007/s00122-012-1979-3

Liu, W., Frick, M., Huel, R., Nykiforuk, C. L., Wang, X. M., Gaudet, D. A., et al. (2014). The stripe rust resistance gene *Yr10* encodes an evolutionary-conserved and unique CC-NBS-LRR sequence in wheat. *Mol. Plant* 7, 1740–1755. doi: 10.1093/mp/ssu112

Liu, S., Huang, S., Zeng, Q., Wang, X., Yu, R., Wang, Q., et al. (2021). Refined mapping of stripe rust resistance gene *YrP10090* within a desirable haplotype for wheat improvement on chromosome 6A. *Theor. Appl. Genet.* 134, 2005–2021. doi: 10.1007/s00122-021-03801-6

Liu, W., Kolmer, J., Rynearson, S., Chen, X., Gao, L., Anderson, J. A., et al. (2019b). Identifying loci conferring resistance to leaf and stripe rusts in a spring wheat population (*Triticum aestivum L.*) via genome-wide association mapping. *Phytopathology* 109, 1932–1940. doi: 10.1094/phyto-04-19-0143-r

Liu, L., Wang, M. N., Feng, J. Y., See, D. R., Chao, S. M., and Chen, X. M. (2018). Combination of all-stage and high-temperature adult-plant resistance QTL confers high level, durable resistance to stripe rust in winter wheat cultivar Madsen. *Theor. Appl. Genet.* 131, 1835–1849. doi: 10.1007/s00122-018-3116-4

Liu, L., Yuan, C. Y., Wang, M. N., See, D. R., and Chen, X. M. (2020). Mapping quantitative trait loci for high-temperature adult-plant resistance to stripe rust in spring wheat PI 197734 using a doubled haploid population and genotyping by multiplexed sequencing. *Front. Plant Sci.* 11. doi: 10.3389/fpls.2020.596962

Liu, L., Yuan, C. Y., Wang, M. N., See, D. R., Zemetra, R. S., and Chen, X. M. (2019). QTL analysis of durable stripe rust resistance in the North American winter wheat cultivar Skiles. *Theor. Appl. Genet.* 132, 1677–1691. doi: 10.1007/s00122-019-03307-2

Lu, Y., Wang, M., Chen, X., See, D., Chao, S., and Jing, J. (2014). Mapping of *Yr62* and a small-effect QTL for high-temperature adult-plant resistance to stripe rust in spring wheat PI 192252. *Theor. Appl. Genet.* 127, 1449–1459. doi: 10.1007/s00122-014-2312-0

Ma, J., Qin, N., Cai, B., Chen, G., Ding, P., Zhang, H., et al. (2019). Identification and validation of a novel major QTL for all-stage stripe rust resistance on 1BL in the winter wheat line 20828. *Theor. Appl. Genet.* 132, 1363–1373. doi: 10.1007/s00122-019-03283-7

Ma, J., Zhou, R., Dong, Y., Wang, L., Wang, X., and Jia, J. (2001). Molecular mapping and detection of the yellow rust resistance gene *Yr26* in wheat transferred from *Triticum turgidum* L. using microsatellite markers. *Euphytica* 120, 219–226. doi: 10.1023/a:1017510331721

Maccaferri, M., Zhang, J., Bulli, P., Abate, Z., Chao, S., Cantu, D., et al. (2015). A genome-wide association study of resistance to stripe rust (*Puccinia striiformis* f. sp.

tritici) in a worldwide collection of hexaploid spring wheat (*Triticum aestivum* L.). *G3-Genes Genom. Genet.* 5, 449–465. doi: 10.1534/g3.114.014563

Macer, R. (1963). The formal and monosomic genetic analysis of stripe rust (*Puccinia striiformis*) resistance in wheat, Hereditas. 2, 127–142

Mallard, S., Gaudet, D., Aldeia, A., Abelard, C., Besnard, A. L., Sourdille, P., et al. (2005). Genetic analysis of durable resistance to yellow rust in bread wheat. *Theor. Appl. Genet.* 110, 1401–1409. doi: 10.1007/s00122-005-1954-3

Marais, G. F., McCallum, B., and Marais, A. S. (2006). Leaf rust and stripe rust resistance genes derived from *Aegilops Sharonensis*. *Euphytica* 149, 373–380. doi: 10.1007/s10681-006-9092-9

Marchal, C., Zhang, J., Zhang, P., Fenwick, P., Steuernagel, B., Adamski, N. M., et al. (2018). BED-domain-containing immune receptors confer diverse resistance spectra to yellow rust. *Nat. Plant* 4, 662–668. doi: 10.1038/s41477-018-0236-4

McIntosh, R. A., Dubcovsky, J., Rogers, W. J., Morris, C., and Xia, X. C. (2016) *Catalogue of gene symbols for wheat: 2016 Supplement*. Available at: http://www.shigen.nig.ac.jp/wheat/komugi/genes/macgene/supplement2015-2016.pdf (Accessed 15 May, 2023).

Melichar, J. P., Berry, S., Newell, C., MacCormack, R., and Boyd, L. A. (2008). QTL identification and microphenotype characterisation of the developmentally regulated yellow rust resistance in the UK wheat cultivar Guardian. *Theor. Appl. Genet.* 117, 391–399. doi: 10.1007/s00122-008-0783-6

Meng, L., Li, H. H., Zhang, L. Y., and Wang, J. K. (2015). QTL IciMapping: Integrated software for genetic linkage map construction and quantitative trait locus mapping in biparental populations. *Crop J.* 3, 269–283. doi: 10.1016/j.cj.2015.01.001

Milus, E., Kristensen, K., and Hovmøller, M. S. (2009). Evidence for increased aggressiveness in a recent widespread strain of *Puccinia striiformis* f. sp. *tritici* causing stripe rust of wheat. *Phytopathology* 99, 89–94. doi: 10.1094/phyto-99-1-0089

Moore, J. W., Herrera-Foessel, S., Lan, C. X., Schnippenkoetter, W., Ayliffe, M., Huerta-Espino, J., et al. (2015). A recently evolved hexose transporter variant confers resistance to multiple pathogens in wheat. *Nat. Genet.* 47, 1494–1498. doi: 10.1038/ng.3439

Mu, J. M., Liu, L., Liu, Y., Wang, M. N., See, D. R., Han, D. J., et al. (2020). Genome-wide association study and gene specific markers identified 51 genes or QTL for resistance to stripe rust in US winter wheat cultivars and breeding lines. *Front. Plant Sci.* 11. doi: 10.3389/fpls.2020.00998

Muleta, K. T., Bulli, P., Rynearson, S., Chen, X. M., and Pumphrey, M. (2017). Loci associated with resistance to stripe rust (*Puccinia striiformis* f. sp. *tritici*) in a core collection of spring wheat (*Triticum aestivum*). *PloS One* 12, e0179087. doi: 10.1371/journal.pone.0179087

Navabi, A., Singh, R. P., Tewari, J. P., and Briggs, K. G. (2004). Inheritance of high levels of adult-plant resistance to stripe rust in five spring wheat genotypes. *Crop Sci.* 44, 1156–1162. doi: 10.2135/cropsci2004.1156

Nsabiyera, V., Bariana, H. S., Qureshi, W. D., Hayden, M. J., and Bansal, U. K. (2018). Characterisation and mapping of adult plant stripe rust resistance in wheat accession Aus27284. *Theor. Appl. Genet.* 131, 1459–1467. doi: 10.1007/s00122-018-3090-x

Paillard, S., Trotoux-Verplancke, G., Perretant, M. R., Mohamadi, F., Leconte, M., Coëdel, S., et al. (2012). Durable resistance to stripe rust is due to three specific resistance genes in French bread wheat cultivar Apache. *Theor. Appl. Genet.* 125, 955–965. doi: 10.1007/s00122-012-1885-8

Qayoum, A., and Line, R. F. (1985). High-temperature, adult-plant resistance to stripe rust of wheat. *Phytopathology* 75, 1121–1123. doi: 10.1094/phyto-75-1121

Ramburan, V. P., Pretorius, Z. A., Louw, J. H., Boyd, L. A., Smith, P. H., Boshoff, W. H. P., et al. (2004). A genetic analysis of adult plant resistance tostripe rust in the wheat cultivar Kariega. *Theor. Appl. Genet.* 108, 1426–1433. doi: 10.1007/s00122-003-1567-7

Rasheed, A., Hao, Y., Xia, X., Khan, A., Xu, Y., Varshney, R. K., et al. (2017). Crop breeding chips and genotyping platforms: progress, challenges, and perspectives. *Mol. Plant* 10, 1047–1064. doi: 10.1016/j.molp.2017.06.008

Ren, Y., He, Z. H., Li, J., Lillemo, M., Wu, L., Bai, B., et al. (2012b). QTL mapping of adult-plant resistance to stripe rust in a population derived from common wheat cultivars Naxos and Shanghai 3/Catbird. *Theor. Appl. Genet.* 125, 1211–1221. doi: 10.1007/s00122-012-1907-6

Ren, R. S., Wang, M. N., Chen, X. M., and Zhang, Z. J. (2012a). Characterization and molecular mapping of Yr52 for high-temperature adult-plant resistance to stripe rust in spring wheat germplasm PI 183527. *Theor. Appl. Genet.* 125, 847–857. doi: 10.1007/s00122-012-1877-8

Rosa, S. B., Zanella, C. M., Hiebert, C. W., Brûlé-Babel, A. L., Randhawa, H. S., Shorter, S., et al. (2019). Genetic characterization of leaf and stripe rust resistance in the Brazilian wheat cultivar Toropi. *Phytopathology* 109, 1760–1768. doi: 10.1094/PHYTO-05-19-0159-R

Rosewarne, G. M., Herrera-Foessel, S. A., Singh, R. P., Huerta-Espino, J., Lan, C. X., and He, Z. H. (2013). Quantitative trait loci of stripe rust resistance in wheat. *Theor. Appl. Genet.* 126, 2427–2449. doi: 10.1007/s00122-013-2159-9

Santra, D. K., Chen, X. M., Santra, M., Campbell, K. G., and Kidwell, K. K. (2008). Identification and mapping QTL for high-temperature adult-plant resistance to stripe rust in winter wheat (*Triticum aestivum* L.) cultivar 'Stephens'. *Theor. Appl. Genet.* 117, 793–802. doi: 10.1007/s00122-008-0820-5

Singh, R. P. (1992). Genetic association of leaf rust resistance gene *Lr34* with adult plant resistance to stripe rust in bread wheat. *Phytopathology* 82, 835–838. doi: 10.1094/phyto-82-835

Singh, R. P., Huerta-Espino, J., and William, H. M. (2005). Genetics and breeding for durable resistance to leaf and stripe rust of wheat. *Turk. J. Agric. Forest.* 29, 121–127.

Singh, R. P., Nelson, J. C., and Sorrells, M. E. (2000). Mapping *Yr28* and other genes for resistance to stripe rust in wheat. *Crop Sci.* 40, 1148–1155. doi: 10.2135/cropsci2000.4041148x

Singh, R. P., and Rajaram, S. (1993). Genetics of adult plant resistance to stripe rust in ten spring bread wheats. *Euphytica* 72, 1–7. doi: 10.1007/bf00023766

Soleimani, B., Lehnert, H., Keilwagen, J., Plieske, J., Ordon, F., Naseri, R. S., et al. (2020). Comparison between core set selection methods using different illumina marker platforms: a case study of assessment of diversity in wheat. *Front. Plant Sci.* 11. doi: 10.3389/fpls.2020.01040

Somers, D. J., Isaac, P., and Edwards, K. (2004). A high-density microsatellite consensus map for bread wheat (*Triticum aestivum* L.). *Theor. Appl. Genet.* 109, 1105–1114. doi: 10.1007/s00122-004-1740-7

Suenaga, K., Singh, R. P., Huerta-Espino, J., and William, H. M. (2003). Microsatellite markers for genes Lr34/Yr18 and other quantitative trait Loci for leaf rust and stripe rust resistance in bread wheat. *Phytopathology* 93, 881–890. doi: 10.1094/phyto.2003.93.7.881

Sui, X. X., Wang, M. N., and Chen, X. M. (2009). Molecular mapping of a stripe rust resistance gene in spring wheat cultivar Zak. *Phytopathology* 99, 1209–1215. doi: 10.1094/PHYTO-99-10-1209

Tekin, M., Cat, A., Akan, K., Catal, M., and Akar, T. (2021). A new virulent race of wheat stripe rust pathogen (*Puccinia striiformis* f. sp. *tritici*) on the resistance gene *Yr5* in Turkey. *Plant Dis.* 105, 3292. doi: 10.1094/pdis-03-21-0629-pdn

Vazquez, M. D., Zemetra, R., Peterson, C. J., Chen, X. M., Heesacker, A., and Mundt, C. C. (2015). Multi-location wheat stripe rust QTL analysis: genetic background and epistatic interactions. *Theor. Appl. Genet.* 128, 1307–1318. doi: 10.1007/s00122-015-2507-z

Wan, A. M., Zhao, Z. H., Chen, X. M., He, Z. H., Jin, S. L., Jia, Q. Z., et al. (2004). Wheat stripe rust epidemic and virulence of *Puccinia striiformis* f.sp. *tritici* in China in 2002. *Plant Dis.* 88, 896–940. doi: 10.1094/PDIS.2004.88.8.896

Wang, J. K. (2009). Inclusive composite interval mapping of quantitative trait genes. *Acta Agron. Sin.* 35, 239–245. doi: 10.3724/SP.J.1006.2009.00239

Wang, M. N., and Chen, X. M. (2017). *Stripe rust resistance*. Eds. X. M. Chen and Z. S. Kang (Dordrecht: Springer Netherlands), 353–558.

Wang, M. N., Chen, X. M., Xu, L. S., Cheng, P., and Bockelman, H. E. (2012). Registration of 70 common spring wheat germplasm lines resistant to stripe rust. *J. Plant Regist.* 6, 104–110. doi: 10.3198/jpr2011.05.0261crg

Wang, Y., Cheng, X., Shan, Q., Zhang, Y., Liu, J., Gao, C., et al. (2014). Simultaneous editing of three homoeoalleles in hexaploid bread wheat confers heritable resistance to powdery mildew. *Nat. Biotechnol.* 32, 947–951. doi: 10.1038/nbt.2969

Wang, Y. B., Xu, S. C., Xu, Z., Liu, T. G., and Lin, R. M. (2006). A microsatellite marker linked to the stripe rust resistance gene *YrV23* in the wheat variety Vilmorin23. *Hereditas* 28, 306–310. doi: 10.16288/j.yczz.2006.03.011

Wang, H., Zou, S. H., Li, Y. L., Lin, F. Y., and Tang, D. Z. (2020). An ankyrin-repeat and WRKY-domain-containing immune receptor confers stripe rust resistance in wheat. *Nat. Commun.* 11, 1353. doi: 10.1038/s41467-020-15139-6

Wellings, C. R., and McIntosh, R. A. (1990). *Puccinia striiformis* f.sp. *tritici* in Australasia: pathogenic changes during the first 10 years. *Plant Pathol.* 39, 316–325. doi: 10.1111/j.1365-3059.1990.tb02509.x

William, H. M., Singh, R. P., Huerta-Espino, J., Palacios, G., and Suenaga, K. (2006). Characterization of genetic loci conferring adult plant resistance to leaf rust and stripe rust in spring wheat. *Genome* 49, 977–990. doi: 10.1139/g06-052

Winfield, M. O., Allen, A. M., Burridge, A. J., Barker, G. L. A., Benbow, H. R., Wilkinson, P. A., et al. (2016). High-density SNP genotyping array for hexaploid wheat and its secondary and tertiary gene pool. *Plant Biotechnol. J.* 14, 1195–1206. doi: 10.1111/pbi.12485

Wu, J. H., Liu, S. J., Wang, Q. L., Zeng, Q. D., Mu, J. M., Huang, S., et al. (2018). Rapid identification of an adult plant stripe rust resistance gene in hexaploid wheat by high-throughput SNP array genotyping of pooled extremes. *Theor. Appl. Genet.* 131, 43–58. doi: 10.1007/s00122-017-2984-3

Xu, L. S., Wang, M. N., Cheng, P., Kang, Z. S., Hulbert, S. H., and Chen, X. M. (2013). Molecular mapping of *Yr53*, a new gene for stripe rust resistance in durum wheat accession PI 480148 and its transfer to common wheat. *Theor. Appl. Genet.* 126, 523–533. doi: 10.1007/s00122-012-1998-0

Xue, W. B., Xu, X., Mu, J. M., Wang, Q. L., Wu, J. H., Huang, L. L., et al. (2014). Evaluation of stripe rust resistance and genes in Chinese elite wheat varieties. *J. Tritic. Crops* 34, 1054–1060. doi: 0.7606/j.issn.1009-1041.2014.08.06

Yao, F. J., Long, L., Wang, Y. Q., Duan, L. Y., Zhao, X. Y., Jiang, Y. F., et al. (2020). Population structure and genetic basis of the stripe rust resistance of 140 Chinese wheat landraces revealed by a genome-wide association study. *Plant Sci.* 301, 110688. doi: 10.1016/j.plantsci.2020.110688

Yuan, F. P., Zeng, Q. D., Wu, J. H., Wang, Q. L., Yang, Z. J., Liang, B. P., et al. (2018). QTL mapping and validation of adult plant resistance to stripe rust in Chinese wheat landrace Humai 15. *Front. Plant Sci.* 9. doi: 10.3389/fpls.2018.00968

Zhang, C. Z., Huang, L., Zhang, H. F., Hao, Q. Q., Lyu, B., Wang, M. N., et al. (2019). An ancestral NB-LRR with duplicated 3'UTRs confers stripe rust resistance in wheat and barley. *Nat. Commun.* 10, 4023. doi: 10.1038/s41467-019-11872-9

Zhang, G. S., Zhao, Y. Y., Kang, Z. S., and Zhao, J. (2020). First report of a *Puccinia striiformis* f. sp. *tritici* race virulent to wheat stripe rust resistance gene *Yr5* in China. *Plant Dis.* 104, 284. doi: 10.1094/pdis-05-19-0901-pdn

Zhou, X. L., Fang, T. H., Li, K. X., Huang, K. B., Ma, C. H., Zhang, M., et al. (2022a). Yield losses associated with different levels of stripe rust resistance of commercial wheat cultivars in China. *Phytopathol* 112, 1244–1251. doi: 10.1094/phyto-07-21-0286-r

Zhou, X. L., Han, D. J., Chen, X. M., Mu, J. M., Xue, W. B., Zeng, Q. D., et al. (2015a). QTL mapping of adult-plant resistance to stripe rust in wheat line P9897. *Euphytica* 205, 243–253. doi: 10.1007/s10681-015-1447-7

Zhou, X. L., Hu, T., Li, X., Yu, M., Li, Y., Yang, S., et al. (2019). Genome-wide mapping of adult plant stripe rust resistance in wheat cultivar Toni. *Theor. Appl. Genet.* 132, 1693–1704. doi: 10.1007/s00122-019-03308-1

Zhou, X. L., Li, X., Han, D. J., Yang, S. Z., Kang, Z. S., and Ren, R. S. (2022b). Genome-wide QTL mapping for stripe rust resistance in winter wheat Pindong 34 using a 90K SNP array. *Front. Plant Sci.* 13. doi: 10.3389/fpls.2022.932762

Zhou, X. L., Wang, M. N., Chen, X. M., Lu, Y., Kang, Z. S., and Jing, J. X. (2014). Identification of *Yr59* conferring high-temperature adult-plant resistance to stripe rust in wheat germplasm PI 178759. *Theor. Appl. Genet.* 127, 935–945. doi: 10.1007/s00122-014-2269-z

Zhou, X. L., Zhang, G. M., Huang, L. L., Han, D. J., and Kang, Z. S. (2015b). Evaluation of resistance to stripe rust in eighty abroad spring wheat germplasms. *Sci. Agric. Sin.* 48, 1518–1526. doi: 10.3864/j.issn.0578-1752.2015.08.06

Zwart, R. S., Thompson, J. P., Milgate, A. W., Bansal, U. K., Williamson, P. M., Raman, H., et al. (2010). QTL mapping of multiple foliar disease and root-lesion nematode resistances in wheat. *Mol. Breed.* 26, 107–124. doi: 10.1007/s11032-009-9381-9

frontiers | Frontiers in Plant Science

TYPE Mini Review
PUBLISHED 18 September 2023
DOI 10.3389/fpls.2023.1269498

Check for updates

OPEN ACCESS

EDITED BY
Xinli Zhou,
Southwest University of Science and Technology, China

REVIEWED BY
Sudhir Navathe,
Agharkar Research Institute, India

*CORRESPONDENCE
Dingzhong Tang
dztang@fafu.edu.cn

RECEIVED 30 July 2023
ACCEPTED 01 September 2023
PUBLISHED 18 September 2023

CITATION
Zou S, Xu Y, Li Q, Wei Y, Zhang Y and Tang D (2023) Wheat powdery mildew resistance: from gene identification to immunity deployment.
Front. Plant Sci. 14:1269498.
doi: 10.3389/fpls.2023.1269498

COPYRIGHT
© 2023 Zou, Xu, Li, Wei, Zhang and Tang. This is an open-access article distributed under the terms of the Creative Commons Attribution License (CC BY). The use, distribution or reproduction in other forums is permitted, provided the original author(s) and the copyright owner(s) are credited and that the original publication in this journal is cited, in accordance with accepted academic practice. No use, distribution or reproduction is permitted which does not comply with these terms.

Wheat powdery mildew resistance: from gene identification to immunity deployment

Shenghao Zou, Yang Xu, Qianqian Li, Yali Wei, Youlian Zhang and Dingzhong Tang*

State Key Laboratory of Ecological Control of Fujian-Taiwan Crop Pests, Key Laboratory of Ministry of Education for Genetics, Breeding and Multiple Utilization of Crops, Plant Immunity Center, Fujian Agriculture and Forestry University, Fuzhou, China

Powdery mildew is one of the most devastating diseases on wheat and is caused by the obligate biotrophic phytopathogen *Blumeria graminis* f. sp. *tritici* (*Bgt*). Due to the complexity of the large genome of wheat and its close relatives, the identification of powdery mildew resistance genes had been hampered for a long time until recent progress in large-scale sequencing, genomics, and rapid gene isolation techniques. Here, we describe and summarize the current advances in wheat powdery mildew resistance, emphasizing the most recent discoveries about the identification of genes conferring powdery mildew resistance and the similarity, diversity and molecular function of those genes. Multilayered resistance to powdery mildew in wheat could be used for counteracting *Bgt*, including durable, broad spectrum but partial resistance, as well as race-specific and mostly complete resistance mediated by nucleotide-binding and leucine rich repeat domain (NLR) proteins. In addition to the above mentioned layers, manipulation of susceptibility (S) and negative regulator genes may represent another layer that can be used for durable and broad-spectrum resistance in wheat. We propose that it is promising to develop effective and durable strategies to combat powdery mildew in wheat by simultaneous deployment of multilayered immunity.

KEYWORDS

powdery mildew, *Blumeria graminis* f. sp. *tritici*, wheat, NLR, race-specific resistance

Introduction

Bread wheat (*Triticum aestivum* L.) is the most widely cultivated crop worldwide, providing approximately 20% of the total daily calories consumed by humans (Reynolds et al., 2012; Appels et al., 2018). Wheat powdery mildew, caused by *Blumeria graminis* f. sp. *tritici* (*Bgt*), is highly destructive, resulting in nearly 5% of the annual wheat yield loss globally (Singh et al., 2016; Savary et al., 2019). To combat this disease, researchers have cataloged over 100 powdery mildew (Pm) resistance alleles at nearly 65 loci in bread wheat

and its relatives (Table S1) (Mapuranga et al., 2022). Due to recent progress in large-scale genomic sequencing alongside innovative gene cloning strategies, more powdery mildew resistance genes have been cloned, broadening the disease resistance diversity in wheat.

To date, most of the identified wheat powdery mildew resistance genes encode CNL proteins with nucleotide-binding sites (NBS) and leucine-rich repeat (LRR) domains (NLR) associated with coiled-coils at the N-termini, such as Pm1a, Pm2, Pm3/Pm8/Pm17, Pm5e, Pm21/Pm12, Pm41, Pm60 and Pm69, which perceive the effectors secreted by *Bgt*, conferring effector triggered immunity (ETI) and showing race-specific resistance (Gupta et al., 2022). Race-specific resistance can mostly provide complete resistance to specific *Bgt* isolates when CNL immune receptors and their cognate effectors, encoded by pathogen avirulence (*Avr*) genes, are present. However, the gene-specific arms race, causing diversification of both immune receptor and Avr genes, can overcome this type of resistance rapidly, especially in wheat with a single race-specific immune receptor gene (Brunner et al., 2011). Apart from the mentioned CNL receptors, recently, two types of non-NLR immune receptors have also been reported to trigger race-specific resistance. (Lu et al., 2020; Sánchez-Martín et al., 2021; Gaurav et al., 2022). These non-NLR immune receptors contain (pseudo)kinase domains that may be responsible for detecting invading effectors (Sánchez-Martín and Keller, 2021). However, the cognate Avr effectors of these non-NLR immune receptors have not yet been identified. This discovery suggests that not only the typical intracellularly localized NLR proteins but also some non-NLR receptors may play a significant role in activating race-specific resistance against *Bgt* (Figure 1, Type 1).

Pattern-triggered immunity (PTI), in contrast to ETI, is the other tiered innate immune system that is activated by the recognition of pathogen-/damage-derived molecules via cell surface-localized pattern-recognition receptors (PRRs) (Jones and Dangl, 2006). PRRs mainly include receptor-like kinases (RLKs) and receptor-like proteins (RLPs). RLKs, found in plants, are a diverse family of proteins with an ectodomain (ECD), a single-pass transmembrane domain, and a cytoplasmic kinase domain, while RLPs lack the intracellular kinase domain (Tang et al., 2017). The ECDs of RLKs and RLPs are highly variable, encompassing leucine-rich repeat (LRR) domains, lysine motifs (LysMs), lectin domains, malectin-like domains, epidermal growth factor (EGF)-like domains, and others, allowing them to recognize a wide range of ligands, including steroids, peptides, polysaccharides, and lipopolysaccharides (Tang et al., 2017). Recently, several types of RLKs (such as TaRLK, LecRK-V, TtdLRK10L-1, HvLEMK1, and RLK-V) that trigger resistance in wheat have been identified, but the

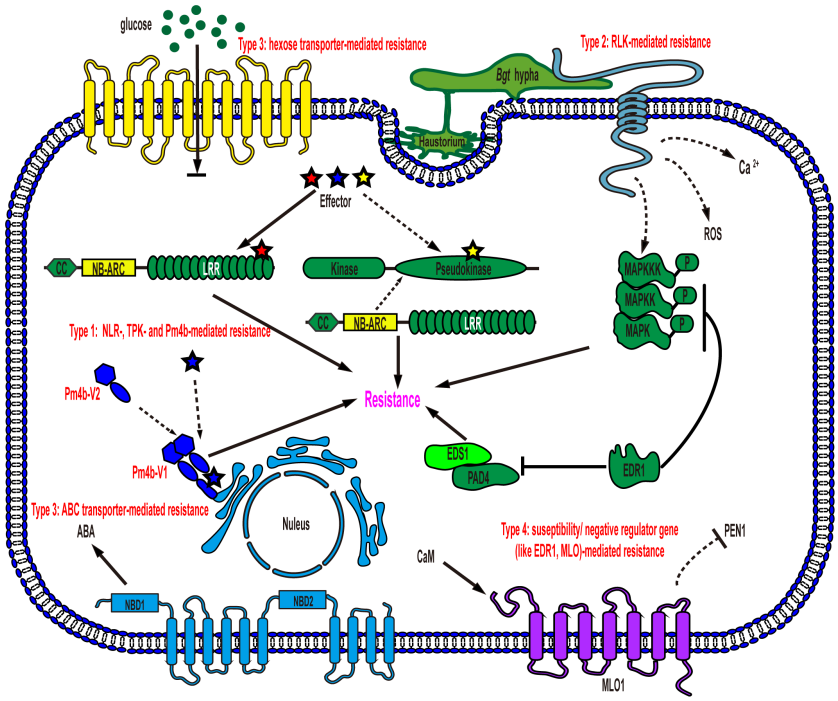

FIGURE 1
Schematic representation of models for wheat powdery mildew resistance gene function in an epidermal cell. Type 1: NLR-, TPK- and Pm4b-mediated resistance. NLRs and several non-NLRs, such as TPK and Pm4b, mediate race-specific resistance after recognizing cognate effectors secreted by *Bgt*, leading to the induction of cell death and resistance to powdery mildew. TKP: tandem kinase proteins; Type 2: RLK-mediated resistance. Plasma membrane-localized RLKs detect PAMPs of *Bgt*, triggering downstream signaling events such as mitogen-activated protein kinase (MAPK) cascades, calcium (Ca^{2+}) flux, and reactive oxygen species (ROS) bursts, ultimately providing defense against powdery mildew; Type 3: hexose transporter- and ABC transporter-mediated resistance. Membrane-localized transporters create a hostile environment for pathogen growth, resulting in resistance without requiring specific recognition of *Bgt*. NBD: nucleotide binding domain; Type 4: susceptibility/negative regulator gene-mediated resistance. Loss-of-function mutations in these genes, such as *EDR1* and *MLO*, enhance powdery mildew resistance in wheat. EDR1 negatively regulates key components of plant innate immunity, including MAPK, EDS1 and PAD4. MLO, on the other hand, modulates PEN1-associated vesicle fusion and exocytosis processes to support pathogenesis.

corresponding pathogen-associated molecular patterns (PAMPs) or ligands are yet to be identified. However, their conferred powdery mildew resistance is believed to be mainly activated through the recognition of the *Bgt*-associated molecular pattern (Figure 1, Type 2).

Unlike resistance genes that activate ETI or PTI, certain wheat powdery mildew resistance genes, such as *Pm38* and *Pm46*, do not require the perception of *Bgt* (Figure 1, Type 3). Intriguingly, both *Pm38* and *Pm46* encode membrane-localized transporter proteins (Krattinger et al., 2009; Moore et al., 2015). The powdery mildew resistance, conferred by either PTI or these two transporters, is mostly partial and quantitative, in contrast to the race-specific complete resistance. Notably, partial and quantitative resistance tends to be durable and broad-spectrum, providing protection against all races of the pathogen species (Moore et al., 2015; Sánchez-Martín and Keller, 2021).

In addition to the three types of resistance genes mentioned above, susceptibility genes such as *Mlo* and negative regulator genes such as *EDR1* provide a distinct form of powdery mildew resistance through loss-of-function, which is recessively inherited, with varying levels of resistance depending on the specific susceptibility gene's function (Figure 1, Type 4) (Wang et al., 2014; Zhang et al., 2017; Sánchez-Martín and Keller, 2021). MLO is a membrane-localized protein, while EDR1 is a cytoplasmic Raf-like mitogen-activated protein kinase (MAPK) kinase kinase (MAPKKK) (Büschges et al., 1997; Frye et al., 2001). Each of them plays a distinct role in wheat cell signaling pathways, and the extent of resistance conferred by knocking out them is determined by their intrinsic physiological and biochemical functions in plants. Overall, multilayered resistance to wheat powdery mildew has been identified in recent studies, and combining all the layers simultaneously and strategically would shed light on wheat resistance breeding, even though the molecular mechanism underlying some of the resistance remains to be fully understood.

The phytopathogen causing wheat powdery mildew

Blumeria graminis, a fungal plant pathogen, is responsible for powdery mildew (Savary et al., 2019). Based on their host specificity, multiple formae speciales are defined within the species, such as *Blumeria graminis* f. sp. *tritici* (*Bgt*), which specifically infects wheat and causes wheat powdery mildew. For typical images of the disease and pathogen, readers are referred to a previous review (Jankovics et al., 2015). To survive harsh conditions, *Bgt* can form chasmothecia and undergo a sexual life cycle (Jankovics et al., 2015). *Bgt* originated in the Fertile Crescent during wheat domestication, and historical human migration and trade facilitated its worldwide spread (Sotiropoulos et al., 2022). For the global races of *Bgt* and their spread, readers are referred to a recent review (Sotiropoulos et al., 2022). The sequencing and assembly of the 166 Mb *Bgt* genome, consisting of 11 chromosomes, revealed approximately 844 candidate effector genes (Müller et al., 2018). Hybridization of globally spread mildew isolates has further complicated the genome, accelerating adaptation to new wheat hosts (Müller et al., 2021).

NLR and several Non-NLR immune receptors activate race-specific resistance via effector recognition

An increasing number of race-specific resistance genes, providing efficient resistance to the rapidly evolving *Bgt*, have been identified in wheat and its wild relatives (Table 1). During molecular identification, most of the cloned race-specific resistance genes encode CNL immune receptors, with some identified as orthologous genes, such as *Pm12/Pm21* and *Pm8/Pm3* (Hurni et al., 2013; Zhu et al., 2023). *Pm60*, *Pm60a* and *Pm60b* are functional allelic variants found in different *Triticum urartu* accessions. Compared with *Pm60*, *Pm60b* contains a 240-nucleotide insertion, and its protein has two additional LRR motifs. In contrast, *Pm60a* has a 240-nucleotide deletion and two fewer LRR motifs in its protein, which narrows its *Bgt* resistance spectrum, whereas insertion of the two LRR motifs in Pm60b has comparatively little influence (Zou et al., 2022). Pm3b, Pm3a and Pm3d proteins are also allelic variants differing by a few amino acid (aa) point mutations, mainly in the NBS and LRR domains, which are responsible for recognizing different *Bgt* strains. The cognate Avr effectors of Pm3a, Pm3b and Pm3d were isolated, which belong to a large group of proteins with low sequence homology but predicted structural similarity (Bourras et al., 2019). In addition to *AvrPm3b*, *c*, and *d*, several other avirulence genes have been isolated (Table 1). However, the identification of *Bgt* avirulence effectors and the downstream pathways following perception still lags behind resistance gene cloning. Nonetheless, it is believed that there might be a direct interaction between CNLs and their corresponding effectors, resulting in the activation of the hypersensitive response and resistance, as seen with Pm1a and Pm3b (Bourras et al., 2015; Bourras et al., 2019).

Pm24 and WTK4 are tandem kinase proteins (TKP) composed of two tandem kinase domains, one of them is a pseudokinase domain, which are reported to confer resistance to *Bgt* (Table 1) (Lu et al., 2020; Gaurav et al., 2022). In addition to *Pm24* and *WTK4*, the barley stem rust resistance gene *Rpg1* and the wheat yellow rust resistance gene *Yr15* encode TKPs as well, which have been considered cytosolic localized and race-specific (Brueggeman et al., 2002; Klymiuk et al., 2018). Thus, although Pm24 is resistant to all of the tested 93 *Bgt* isolates collected from China and no virulent isolates have been discovered, by now, it suggests that Pm24 and WTK4 might confer race-specific resistance, similar to other reported TKPs. Furthermore, it has been hypothesized that the pseudokinase domain in these TKPs is the target of *Bgt* effectors and that the interaction activates either TKPs to phosphorylate downstream components or NLRs that guard the TKPs, consequently resulting in resistance (Sánchez-Martín and Keller, 2021; Fahima and Coaker, 2023).

TABLE 1 List of cloned genes conferring race-specific resistance to *Blumeria graminis* f. sp. *tritici* in wheat and their corresponding avirulence (*Avr*) genes cloned in the pathogens.

Gene	Gene Product	Donor species	Cognate *Avr*
Pm1a (Hewitt et al., 2021)	CNL [a]	*Triticum aestivum*	*AvrPm1a.1, AvrPm1a.2* (Hewitt et al., 2021; Kloppe et al., 2023)
Pm2 (Sanchez-Martin et al., 2016)	CNL	*Aegilops tauschii*	*AvrPm2* (Praz et al., 2017; Manser et al., 2021)
Pm3b (Yahiaoui et al., 2004)	CNL	*Triticum aestivum*	*AvrPm3b* (Bourras et al., 2019)
Pm3a, d (Srichumpa et al., 2005)	CNL	*Triticum aestivum*	*AvrPm3a, d* (Bourras et al., 2015; Bourras et al., 2019)
Pm5e (Xie et al., 2020)	CNL	*Triticum aestivum*	–
Pm8 (Hurni et al., 2013)	CNL	*Secale cereale*	–
Pm12 (Zhu et al., 2023)	CNL	*Aegilops speltoides*	–
Pm17 (Singh et al., 2018)	CNL	*Secale cereale*	*AvrPm17* (Müller et al., 2022)
Pm21 (He et al., 2018; Xing et al., 2018)	CNL	*Dasypyrum villosum*	–
Pm41 (Li et al., 2020)	CNL	*Triticum turgidum ssp. dicoccoides*	–
Pm60, 60a, 60b (Zou et al., 2018)	CNL	*Triticum urartu*	–
Pm69 (Kim et al., 2023)	CNL	*Triticum turgidum ssp. dicoccoides*	–
Pm24 (Lu et al., 2020)	TPK [b]	*Triticum aestivum*	–
WTK4 [c] (Gaurav et al., 2022)	TPK	*Aegilops tauschii*	–
Pm4b (Sánchez-Martín et al., 2021)	MCTP kinase [d]	*Triticum carthlicum*	–

[a]CNL, coiled-coil (CC), nucleotide binding site (NBS), leucine rich repeat (LRR) protein.
[b]TKP, tandem kinase protein.
[c]WTK, wheat tandem kinase.
[d]MCTP kinase, multiple C2-domains and transmembrane region kinase protein.
"-" is that no cognate gene has been reported there.

Pm4b is a novel race-specific wheat powdery mildew resistance gene (Figure 1, Type 1). Functional analysis has revealed that both protein variants resulting from alternative splicing are essential for the resistance function. These two protein isoforms share a kinase domain with serine/threonine specificity. However, in their C-terminus, one isoform has a single C2C domain, while the other contains a C2D domain coupled to a phosphoribosyl transferase C-terminal domain with two transmembrane domains. (Sánchez-Martín et al., 2021). Moreover, the two protein variants have the ability to form an ER-anchored heterocomplex. In this complex, the C2C/D or kinase domains may recognize the cognate effector, leading to the activation of kinase activity and subsequent disease resistance (Sánchez-Martín et al., 2021). Additionally, several functional allelic variants have been discovered in the *Pm4* locus, suggesting a diverse range of resistance capabilities.

Given the complexity of the enormous genome of wheat and its close relatives, it is predicted that more race-specific resistance genes, whether encoding NLR or non-NLR proteins, will likely be isolated in the future.

Putative powdery mildew resistance proteins responsible for recognizing PAMPs

Several RLKs were identified as conferring wheat powdery mildew resistance, such as RLK-V and LEMK1 with an LRR-malectin domain, LecRK-V with an L-type lectin domain, and TtdLRK10L-1, TaRLK1, and TaRLK2 with an LRR domain (Chen et al., 2016; Rajaraman et al., 2016; Hu et al., 2018; Wang et al., 2018; Xia et al., 2021). These RLKs may be responsible for recognizing PAMPs, as known in PTI, although the corresponding ligands have not yet been isolated (Figure 1, Type 2). Additionally, RLK-V has been shown to be required for resistance mediated by Pm21, supporting the model that ETI and PTI mutually potentiate and interdepend on each other (Yuan et al., 2021).

The powdery mildew resistance proteins that function independently of perceiving *Bgt*

Pm38 and Pm46 are two powdery mildew resistance proteins that confer protection against the pathogen without directly perceiving effectors or PAMPs originating from *Bgt* (Figure 1, type 3). Pm38 shares structural similarities with adenosine triphosphate-binding cassette (ABC) transporters of the pleiotropic drug resistance subfamily, which includes the well-known nonhost resistance protein PEN3 in Arabidopsis. Recently, it was reported that abscisic acid (ABA) is the substrate of the ABC transporter Pm38 and that ABA redistribution, mediated via the transporter, might contribute to resistance against not only *Bgt* but also multiple fungal pathogens in wheat (Krattinger et al., 2019; Bräunlich et al., 2021). On the other hand, Pm46 functions as a

plasma membrane-localized nonfunctional hexose transporter, leading to an increased hexose/sucrose ratio in the leaf apoplasm due to its blocking of apoplastic hexose retrieval in epidermal cells (Figure 1, Type 3)(Moore et al., 2015). Consequently, the altered sugar ratio triggers a sugar-mediated signaling response, creating a more hostile environment for pathogen growth (Proels and Hückelhoven, 2014). Notably, this type of resistance exhibits partial, durable, and broad-spectrum characteristics, similar to PTI, which stands in contrast to race-specific resistance. Remarkably, the perception of *Bgt* is not required for the activation of this type of resistance.

Modification of susceptibility/negative regulator genes for resistance to wheat powdery mildew

EDR1 is well conserved and is expected to function similarly in different plant species (Frye et al., 2001). In Arabidopsis, EDR1 negatively regulates PTI modulated by the RLP53-associated immune complex (Chen et al., 2022). Notably, EDR1 physically interacts with MKK4/MKK5 and negatively affects MPK3 and MPK6 protein levels and kinase activity (Zhao et al., 2014; Gao et al., 2021). Moreover, EDR1 directly associates with PAD4 and EDS1 and interferes with the heteromeric association of PAD4 and EDS1, which are key components of ETI (Neubauer et al., 2020) (Figure 1, Type 4). As a result, EDR1 acts as a negative regulator in innate immunity. Simultaneous modification of three homoeologs of *EDR1* in common wheat via genome editing relieves the suppression of EDR1 to immunity and significantly enhances powdery mildew resistance, although the resistance remains partial (Zhang et al., 2017). *MLO* encodes a transmembrane protein. The C-terminal domain in MLO is responsible for Ca^{2+}-dependent binding with calmodulin, which is associated with the negatively regulating ability of MLO to resistance (Kim et al., 2002). Furthermore, resistance mediated by knockout of MLO requires PEN1, suggesting that powdery mildew fungi may enlist MLO to regulate vesicle fusion and exocytosis processes for successful pathogenesis (Figure 1, Type 4)(Kusch and Panstruga, 2017; Jacott et al., 2021). Intriguingly, in *mlo* mutants, the development of powdery mildew is terminated at the stage of cell wall penetration, a phenomenon reminiscent of nonhost resistance mechanisms (Jacott et al., 2021). The *mlo* mutants also exhibit undesired pleiotropic phenotypes, including growth penalties and yield losses, which have hampered their widespread use (Consonni et al., 2006). However, a recently identified mutant, with a 304-kilobase pair targeted deletion in the *MLO-B1* locus of wheat, retains crop growth and yields while conferring robust powdery mildew resistance, although the precise mechanism by which to revert the growth penalties is not fully understood (Li et al., 2022; Najafi and Palmgren, 2022). Thus, disruption of this type of gene emerges as an attractive resistance breeding strategy in wheat.

Prospect

In race-specific powdery mildew resistance, some interactions between NLRs and cognate effectors have been subject to investigation, but the downstream signaling pathways resulting from these interactions remain to be fully understood. In contrast to NLR, the molecular analysis of non-NLR-based race-specific resistance is in its early stages, and the corresponding avirulence genes have not yet been identified. In addition, the ligands recognized by the RLKs for activating PTI to *Bgt* are also unknown. On the other hand, the characterization of resistance conferred by membrane-localized transporters, which do not require the perception of effectors or PAMPs from *Bgt*, has been more extensively studied. Although the resistance provided by these transporters is partial, similar to PTI triggered by RLKs, it tends to be more durable and broad-spectrum compared to race-specific powdery mildew resistance. Notably, resistance facilitated by genome modification of the susceptibility gene *MLO* is complete, durable, and broad-spectrum. Moreover, the undesirable growth penalties observed in *mlo* mutants can potentially be overcome by implementing additional precision genome editing to stack genetic changes.

Resistance to powdery mildew in wheat can be classified into different layers based on their specific characteristics. However, it is important to note that these layers of resistance should not be used individually to combat rapidly evolving *Bgt*. Studies have shown that even on *mlo* plants, powdery mildew isolates with enhanced virulence can emerge (Schwarzbach, 1979). The combination of multilayered resistance is necessary to create a high barrier, preventing *Blumeria graminis* f. sp. *tritici* from adapting to and overcoming (Dracatos et al., 2023). Thus, constant efforts are required to identify and understand various resistance genes in wheat and its close relatives, as well as analyze their molecular mechanisms. This ongoing research is essential for laying the foundation to develop effective and durable strategies to combat wheat powdery mildew.

Author contributions

SZ: Writing – original draft. YX: Writing – review & editing. QL: Writing – review & editing. YW: Writing – review & editing. YZ: Writing – review & editing. DT: Writing – review & editing.

Funding

The authors declare financial support was received for the research, authorship, and/or publication of this article. This work was supported by grants from the National Natural Science Foundation of China (31830077) and Natural Science Foundation of Fujian Province (2023J01284).

Conflict of interest

The authors declare that the research was conducted in the absence of any commercial or financial relationships that could be construed as a potential conflict of interest.

The author(s) declared that they were an editorial board member of Frontiers, at the time of submission. This had no impact on the peer review process and the final decision.

Publisher's note

All claims expressed in this article are solely those of the authors and do not necessarily represent those of their affiliated organizations, or those of the publisher, the editors and the reviewers. Any product that may be evaluated in this article, or claim that may be made by its manufacturer, is not guaranteed or endorsed by the publisher.

Supplementary material

The Supplementary Material for this article can be found online at: https://www.frontiersin.org/articles/10.3389/fpls.2023.1269498/full#supplementary-material

References

Appels, R., Eversole, K., Stein, N., Feuillet, C., Keller, B., Rogers, J., et al. (2018). Shifting the limits in wheat research and breeding using a fully annotated reference genome. *Science* 361 (6403), 1–13. doi: 10.1126/science.aar7191

Bourras, S., Kunz, L., Xue, M., Praz, C. R., Müller, M. C., Kälin, C., et al. (2019). The AvrPm3-Pm3 effector-NLR interactions control both race-specific resistance and host-specificity of cereal mildews on wheat. *Nat. Commun.* 10 (1), 2292–2292. doi: 10.1038/s41467-019-10274-1

Bourras, S., McNally, K. E., Ben-David, R., Parlange, F., Roffler, S., Praz, C. R., et al. (2015). Multiple avirulence loci and allele-specific effector recognition control the pm3 race-specific resistance of wheat to powdery mildew. *Plant Cell* 27 (10), 2991–3012. doi: 10.1105/tpc.15.00171

Bräunlich, S., Koller, T., Glauser, G., Krattinger, S. G., and Keller, B. (2021). Expression of the wheat disease resistance gene Lr34 in transgenic barley leads to accumulation of abscisic acid at the leaf tip. *Plant Physiol. Biochem.* 166, 950–957. doi: 10.1016/j.plaphy.2021.07.001

Brueggeman, R., Rostoks, N., Kudrna, D., Kilian, A., Han, F., Chen, J., et al. (2002). The barley stem rust-resistance gene Rpg1 is a novel disease-resistance gene with homology to receptor kinases. *Proc. Natl. Acad. Sci. U.S.A.* 99 (14), 9328–9333. doi: 10.1073/pnas.142284999

Brunner, S., Hurni, S., Herren, G., Kalinina, O., von Burg, S., Zeller, S. L., et al. (2011). Transgenic Pm3b wheat lines show resistance to powdery mildew in the field. *Plant Biotechnol. J.* 9 (8), 897–910. doi: 10.1111/j.1467-7652.2011.00603.x

Büschges, R., Hollricher, K., Panstruga, R., Simons, G., Wolter, M., Frijters, A., et al. (1997). The barley Mlo gene: a novel control element of plant pathogen resistance. *Cell* 88 (5), 695–705. doi: 10.1016/s0092-8674(00)81912-1

Chen, R., Sun, P., Zhong, G., Wang, W., and Tang, D. (2022). The RECEPTOR-LIKE PROTEIN53 immune complex associates with LLG1 to positively regulate plant immunity. *J. Integr. Plant Biol.* 64 (9), 1833–1846. doi: 10.1111/jipb.13327

Chen, T., Xiao, J., Xu, J., Wan, W., Qin, B., Cao, A., et al. (2016). Two members of TaRLK family confer powdery mildew resistance in common wheat. *BMC Plant Biol.* 16, 27. doi: 10.1186/s12870-016-0713-8

Consonni, C., Humphry, M. E., Hartmann, H. A., Livaja, M., Durner, J., Westphal, L., et al. (2006). Conserved requirement for a plant host cell protein in powdery mildew pathogenesis. *Nat. Genet.* 38 (6), 716–720. doi: 10.1038/ng1806

Dracatos, P. M., Lu, J., Sánchez-Martín, J., and Wulff, B. B. H. (2023). Resistance that stacks up: engineering rust and mildew disease control in the cereal crops wheat and barley. *Plant Biotechnol. J.* doi: 10.1111/pbi.14106

Fahima, T., and Coaker, G. (2023). Pathogen perception and deception in plant immunity by kinase fusion proteins. *Nat. Genet.* 55 (6), 908–909. doi: 10.1038/s41588-023-01396-w

Frye, C. A., Tang, D., and Innes, R. W. (2001). Negative regulation of defense responses in plants by a conserved MAPKK kinase. *Proc. Natl. Acad. Sci. U.S.A.* 98 (1), 373–378. doi: 10.1073/pnas.98.1.373

Gao, C., Sun, P., Wang, W., and Tang, D. (2021). Arabidopsis E3 ligase KEG associates with and ubiquitinates MKK4 and MKK5 to regulate plant immunity. *J. Integr. Plant Biol.* 63 (2), 327–339. doi: 10.1111/jipb.13007

Gaurav, K., Arora, S., Silva, P., Sánchez-Martín, J., Horsnell, R., Gao, L., et al. (2022). Population genomic analysis of Aegilops tauschii identifies targets for bread wheat improvement. *Nat. Biotechnol.* 40 (3), 422–431. doi: 10.1038/s41587-021-01058-4

Gupta, P., Balyan, H., Sharma, P., Gaurav, s.S., Sharma, S., Kumar, R., et al. (2022). Catalogue of gene symbols for wheat: 2022 supplement. *Annu. Wheat Newslett.* 68, 68–81.

He, H., Zhu, S., Zhao, R., Jiang, Z., Ji, Y., Ji, J., et al. (2018). Pm21, encoding a typical CC-NBS-LRR protein, confers broad-spectrum resistance to wheat powdery mildew disease. *Mol. Plant* 11 (6), 879–882. doi: 10.1016/j.molp.2018.03.004

Hewitt, T., Müller, M. C., Molnár, I., Mascher, M., Holušová, K., Šimková, H., et al. (2021). A highly differentiated region of wheat chromosome 7AL encodes a Pm1a immune receptor that recognizes its corresponding AvrPm1a effector from Blumeria graminis. *New Phytol.* 229 (5), 2812–2826. doi: 10.1111/nph.17075

Hu, P., Liu, J., Xu, J., Zhou, C., Cao, S., Zhou, W., et al. (2018). A malectin-like/leucine-rich repeat receptor protein kinase gene, RLK-V, regulates powdery mildew resistance in wheat. *Mol. Plant Pathol.* 19 (12), 2561–2574. doi: 10.1111/mpp.12729

Hurni, S., Brunner, S., Buchmann, G., Herren, G., Jordan, T., Krukowski, P., et al. (2013). Rye *Pm8* and wheat *Pm3* are orthologous genes and show evolutionary conservation of resistance function against powdery mildew. *Plant J.* 76 (6), 957-969. doi: 10.1111/tpj.12345

Jacott, C. N., Ridout, C. J., and Murray, J. D. (2021). Unmasking mildew resistance locus O. *Trends Plant Sci.* 26 (10), 1006–1013. doi: 10.1016/j.tplants.2021.05.009

Jankovics, T., Komáromi, J., Fábián, A., Jäger, K., Vida, G., and Kiss, L. (2015). New Insights into the Life Cycle of the Wheat Powdery Mildew: Direct Observation of Ascosporic Infection in *Blumeria graminis* f. sp. *tritici*. *Phytopathology* 105 (6), 797–804. doi: 10.1094/PHYTO-10-14-0268-R

Jones, J. D. G., and Dangl, J. L. (2006). The plant immune system. *Nature* 444 (7117), 323–329. doi: 10.1038/nature05286

Kim, H., Ahn, Y. J., Lee, H., Chung, E. H., Segonzac, C., and Sohn, K. H. (2023). Diversified host target families mediate convergently evolved effector recognition across plant species. *Curr. Opin. Plant Biol.* 74, 102398. doi: 10.1016/j.pbi.2023.102398

Kim, M. C., Panstruga, R., Elliott, C., Müller, J., Devoto, A., Yoon, H. W., et al. (2002). Calmodulin interacts with MLO protein to regulate defence against mildew in barley. *Nature* 416 (6879), 447–451. doi: 10.1038/416447a

Kloppe, T., Whetten, R. B., Kim, S. B., Powell, O. R., Lück, S., Douchkov, D., et al. (2023). Two pathogen loci determine Blumeria graminis f. sp. tritici virulence to wheat resistance gene Pm1a. *New Phytol.* 238 (4), 957-969. doi: 10.1111/nph.18809

Klymiuk, V., Yaniv, E., Huang, L., Raats, D., Fatiukha, A., Chen, S., et al. (2018). Cloning of the wheat Yr15 resistance gene sheds light on the plant tandem kinase-pseudokinase family. *Nat. Commun.* 9 (1), 3735. doi: 10.1038/s41467-018-06138-9

Krattinger, S. G., Kang, J., Bräunlich, S., Boni, R., Chauhan, H., Selter, L. L., et al. (2019). Abscisic acid is a substrate of the ABC transporter encoded by the durable wheat disease resistance gene Lr34. *New Phytol.* 223 (2), 853–866. doi: 10.1111/nph.15815

Krattinger, S. G., Lagudah, E. S., Spielmeyer, W., Singh, R. P., Huerta-Espino, J., McFadden, H., et al. (2009). A putative ABC transporter confers durable resistance to multiple fungal pathogens in wheat. *Science* 323 (5919), 1360–1363. doi: 10.1126/science.1166453

Kusch, S., and Panstruga, R. (2017). mlo-based resistance: An apparently universal "Weapon" to defeat powdery mildew disease. *Mol. Plant Microbe Interact.* 30 (3), 179–189. doi: 10.1094/mpmi-12-16-0255-cr

Li, M., Dong, L., Li, B., Wang, Z., Xie, J., Qiu, D., et al. (2020). A CNL protein in wild emmer wheat confers powdery mildew resistance. *New Phytol.* 228 (3), 1027–1037. doi: 10.1111/nph.16761

Li, S., Lin, D., Zhang, Y., Deng, M., Chen, Y., Lv, B., et al. (2022). Genome-edited powdery mildew resistance in wheat without growth penalties. *Nature* 602 (7897), 455–460. doi: 10.1038/s41586-022-04395-9

Lu, P., Guo, L., Wang, Z., Li, B., Li, J., Li, Y., et al. (2020). A rare gain of function mutation in a wheat tandem kinase confers resistance to powdery mildew. *Nat. Commun.* 11 (1), 680–680. doi: 10.1038/s41467-020-14294-0

Manser, B., Koller, T., Praz, C. R., Roulin, A. C., Zbinden, H., Arora, S., et al. (2021). Identification of specificity-defining amino acids of the wheat immune receptor Pm2

and powdery mildew effector AvrPm2. *Plant J.* 106 (4), 993–1007. doi: 10.1111/tpj.15214

Mapuranga, J., Chang, J., and Yang, W. (2022). Combating powdery mildew: Advances in molecular interactions between Blumeria graminis f. sp. tritici and wheat. *Front. Plant Sci.* 13. doi: 10.3389/fpls.2022.1102908

Moore, J. W., Herrera-Foessel, S., Lan, C., Schnippenkoetter, W., Ayliffe, M., Huerta-Espino, J., et al. (2015). A recently evolved hexose transporter variant confers resistance to multiple pathogens in wheat. *Nat. Genet.* 47 (12), 1494–1498. doi: 10.1038/ng.3439

Müller, M. C., Kunz, L., Graf, J. P., Schudel, S., and Keller, B. (2021). Host adaptation through hybridization: Genome analysis of triticale powdery mildew reveals unique combination of lineage-specific effectors. *Mol. Plant Microbe Interact.* 34 (12), 1350-1357. doi: 10.1094/mpmi-05-21-0111-sc

Müller, M. C., Kunz, L., Schudel, S., Lawson, A. W., Kammerecker, S., Isaksson, J., et al. (2022). Ancient variation of the AvrPm17 gene in powdery mildew limits the effectiveness of the introgressed rye Pm17 resistance gene in wheat. *Proc. Natl. Acad. Sci. U.S.A.* 119 (30), e2108808119. doi: 10.1073/pnas.2108808119

Müller, M. C., Praz, C. R., Sotiropoulos, A. G., Menardo, F., Kunz, L., Schudel, S., et al. (2018). A chromosome-scale genome assembly reveals a highly dynamic effector repertoire of wheat powdery mildew. *New Phytol.* 221 (4), 2176-2189. doi: 10.1111/nph.15529

Najafi, J., and Palmgren, M. (2022). Hexose transport reverts the growth penalty of mlo resistance. *Trends Plant Sci.* 27 (8), 739–741. doi: 10.1016/j.tplants.2022.04.003

Neubauer, M., Serrano, I., Rodibaugh, N., Bhandari, D. D., Bautor, J., Parker, J. E., et al. (2020). Arabidopsis EDR1 protein kinase regulates the association of EDS1 and PAD4 to inhibit cell death. *Mol. Plant Microbe Interact.* 33 (4), 693–703. doi: 10.1094/mpmi-12-19-0339-r

Praz, C. R., Bourras, S., Zeng, F., Sánchez-Martín, J., Menardo, F., Xue, M., et al. (2017). AvrPm2 encodes an RNase-like avirulence effector which is conserved in the two different specialized forms of wheat and rye powdery mildew fungus. *New Phytol.* 213 (3), 1301–1314. doi: 10.1111/nph.14372

Proels, R. K., and Hückelhoven, R. (2014). Cell-wall invertases, key enzymes in the modulation of plant metabolism during defence responses. *Mol. Plant Pathol.* 15 (8), 858–864. doi: 10.1111/mpp.12139

Rajaraman, J., Douchkov, D., Hensel, G., Stefanato, F. L., Gordon, A., Ereful, N., et al. (2016). An LRR/malectin receptor-like kinase mediates resistance to non-adapted and adapted powdery mildew fungi in barley and wheat. *Front. Plant Sci.* 7. doi: 10.3389/fpls.2016.01836

Reynolds, M., Foulkes, J., Furbank, R., Griffiths, S., King, J., Murchie, E., et al. (2012). Achieving yield gains in wheat. *Plant Cell Environ.* 35 (10), 1799–1823. doi: 10.1111/j.1365-3040.2012.02588.x

Sánchez-Martín, J., and Keller, B. (2021). NLR immune receptors and diverse types of non-NLR proteins control race-specific resistance in Triticeae. *Curr. Opin. Plant Biol.* 62, 102053. doi: 10.1016/j.pbi.2021.102053

Sanchez-Martin, J., Steuernagel, B., Ghosh, S., Herren, G., Hurni, S., Adamski, N., et al. (2016). Rapid gene isolation in barley and wheat by mutant chromosome sequencing. *Genome Biol.* 17 (1), 221. doi: 10.1186/s13059-016-1082-1

Sánchez-Martín, J., Widrig, V., Herren, G., Wicker, T., Zbinden, H., Gronnier, J., et al. (2021). Wheat Pm4 resistance to powdery mildew is controlled by alternative splice variants encoding chimeric proteins. *Nat. Plants* 7 (3), 327–341. doi: 10.1038/s41477-021-00869-2

Savary, S., Willocquet, L., Pethybridge, S. J., Esker, P., McRoberts, N., and Nelson, A. (2019). The global burden of pathogens and pests on major food crops. *Nat. Ecol. Evol.* 3 (3), 430–439. doi: 10.1038/s41559-018-0793-y

Schwarzbach, E. (1979). Response to selection for virulence against the ml-o based resistance in barley, not fitting the gene-for-gene hypothesis. *BARLEY Genet. Newslett.* 9, 85–89.

Singh, S. P., Hurni, S., Ruinelli, M., Brunner, S., Sanchez-Martin, J., Krukowski, P., et al. (2018). Evolutionary divergence of the rye *Pm17* and *Pm8* resistance genes reveals ancient diversity. *Plant Mol. Biol.* 98 (3), 249–260. doi: 10.1007/s11103-018-0780-3

Singh, R. P., Singh, P. K., Rutkoski, J., Hodson, D. P., He, X., Jorgensen, L. N., et al. (2016). Disease impact on wheat yield potential and prospects of genetic control. *Annu. Rev. Phytopathol.* 54, 303–322. doi: 10.1146/annurev-phyto-080615-095835

Sotiropoulos, A. G., Arango-Isaza, E., Ban, T., Barbieri, C., Bourras, S., Cowger, C., et al. (2022). Global genomic analyses of wheat powdery mildew reveal association of pathogen spread with historical human migration and trade. *Nat. Commun.* 13 (1), 4315. doi: 10.1038/s41467-022-31975-0

Srichumpa, P., Brunner, S., Keller, B., and Yahiaoui, N. (2005). Allelic series of four powdery mildew resistance genes at the Pm3 locus in hexaploid bread wheat. *Plant Physiol.* 139 (2), 885–895. doi: 10.1104/pp.105.062406

Tang, D., Wang, G., and Zhou, J.-M. (2017). Receptor kinases in plant-pathogen interactions: more than pattern recognition. *Plant Cell* 29 (4), 618–637. doi: 10.1105/tpc.16.00891

Wang, Z., Cheng, J., Fan, A., Zhao, J., Yu, Z., Li, Y., et al. (2018). LecRK-V, an L-type lectin receptor kinase in Haynaldia villosa, plays positive role in resistance to wheat powdery mildew. *Plant Biotechnol. J.* 16 (1), 50–62. doi: 10.1111/pbi.12748

Wang, Y., Cheng, X., Shan, Q., Zhang, Y., Liu, J., Gao, C., et al. (2014). Simultaneous editing of three homoeoalleles in hexaploid bread wheat confers heritable resistance to powdery mildew. *Nat. Biotech. advance Online Publ.* 32 (9), 947-951. doi: 10.1038/nbt.2969

Xia, T., Yang, Y., Zheng, H., Han, X., Jin, H., Xiong, Z., et al. (2021). Efficient expression and function of a receptor-like kinase in wheat powdery mildew defence require an intron-located MYB binding site. *Plant Biotechnol. J.* 19 (5), 897–909. doi: 10.1111/pbi.13512

Xie, J., Guo, G., Wang, Y., Hu, T., Wang, L., Li, J., et al. (2020). A rare single nucleotide variant in Pm5e confers powdery mildew resistance in common wheat. *New Phytol.* 228 (3), 1011-1026. doi: 10.1111/nph.16762

Xing, L., Hu, P., Liu, J., Witek, K., Zhou, S., Xu, J., et al. (2018). Pm21 from haynaldia villosa encodes a CC-NBS-LRR protein conferring powdery mildew resistance in wheat. *Mol. Plant* 11 (6), 874–878. doi: 10.1016/j.molp.2018.02.013

Yahiaoui, N., Srichumpa, P., Dudler, R., and Keller, B. (2004). Genome analysis at different ploidy levels allows cloning of the powdery mildew resistance gene *Pm3b* from hexaploid wheat. *Plant J.* 37 (4), 528–538. doi: 10.1046/j.1365-313X.2003.01977.x

Yuan, M., Ngou, B. P. M., Ding, P., and Xin, X.-F. (2021). PTI-ETI crosstalk: an integrative view of plant immunity. *Curr. Opin. Plant Biol.* 62, 102030. doi: 10.1016/j.pbi.2021.102030

Zhang, Y., Bai, Y., Wu, G., Zou, S., Chen, Y., Gao, C., et al. (2017). Simultaneous modification of three homoeologs of TaEDR1 by genome editing enhances powdery mildew resistance in wheat. *Plant J.* 91 (4), 714–724. doi: 10.1111/tpj.13599

Zhao, C., Nie, H., Shen, Q., Zhang, S., Lukowitz, W., and Tang, D. (2014). EDR1 physically interacts with MKK4/MKK5 and negatively regulates a MAP kinase cascade to modulate plant innate immunity. *PloS Genet.* 10 (5), e1004389. doi: 10.1371/journal.pgen.1004389

Zhu, S., Liu, C., Gong, S., Chen, Z., Chen, R., Liu, T., et al. (2023). Orthologous genes Pm12 and Pm21 from two wild relatives of wheat show evolutionary conservation but divergent powdery mildew resistance. *Plant Commun.* 4 (2), 100472. doi: 10.1016/j.xplc.2022.100472

Zou, S., Shi, W., Ji, J., Wang, H., Tang, Y., Yu, D., et al. (2022). Diversity and similarity of wheat powdery mildew resistance among three allelic functional genes at the Pm60 locus. *Plant J.* 110 (6), 1781–1790. doi: 10.1111/tpj.15771

Zou, S. H., Wang, H., Li, Y. W., Kong, Z. S., and Tang, D. Z. (2018). The NB-LRR gene Pm60 confers powdery mildew resistance in wheat. *New Phytol.* 218 (1), 298–309. doi: 10.1111/nph.14964

frontiers | Frontiers in Plant Science

TYPE Original Research
PUBLISHED 03 October 2023
DOI 10.3389/fpls.2023.1273306

Check for updates

OPEN ACCESS

EDITED BY
Runsheng Ren,
Jiangsu Academy of Agricultural Sciences (JAAS), China

REVIEWED BY
Aamir Iqbal,
International Maize and Wheat Improvement Center (CIMMYT), Pakistan
Muhammad Rameez Khan,
Directorate of Agriculture Research, Pakistan

*CORRESPONDENCE
Guangkuo Li
lgk0808@163.com
Haifeng Gao
ghf20044666@163.com

RECEIVED 05 August 2023
ACCEPTED 11 September 2023
PUBLISHED 03 October 2023

CITATION
Ma J, Awais M, Chen L, Yang H, Lai H, Shen Y, Wang H, Li G and Gao H (2023) Identification of *Puccinia striiformis* races from the spring wheat crop in Xinjiang, China.
Front. Plant Sci. 14:1273306.
doi: 10.3389/fpls.2023.1273306

COPYRIGHT
© 2023 Ma, Awais, Chen, Yang, Lai, Shen, Wang, Li and Gao. This is an open-access article distributed under the terms of the Creative Commons Attribution License (CC BY). The use, distribution or reproduction in other forums is permitted, provided the original author(s) and the copyright owner(s) are credited and that the original publication in this journal is cited, in accordance with accepted academic practice. No use, distribution or reproduction is permitted which does not comply with these terms.

Identification of *Puccinia striiformis* races from the spring wheat crop in Xinjiang, China

Jinbiao Ma[1], Muhammad Awais[2], Li Chen[3], Hong Yang[4], Hanlin Lai[5], Yuyang Shen[3], Huiqing Wang[6], Guangkuo Li[3]* and Haifeng Gao[3]*

[1]State Key Laboratory of Desert and Oasis Ecology, Key Laboratory of Ecological Safety and Sustainable Development in Arid Lands, Xinjiang Institute of Ecology and Geography, Chinese Academy of Sciences, Urumqi, China, [2]State Key Laboratory of Crop Stress Biology for Arid Areas, College of Plant Protection, Northwest A&F University, Shaanxi, Xianyang, China, [3]Institute of Plant Protection, Xinjiang Academy of Agricultural Sciences/Key Laboratory of Integrated Pest Management on Crop in Northwestern Oasis, Ministry of Agriculture and Rural Affairs, Urumqi, China, [4]College of Agriculture, Xinjiang Agricultural University/Key Laboratory of the Pest Monitoring and Safety Control of Crops and Forests, Urumqi, China, [5]College of Life Science, Xinjiang Agricultural University, Urumqi, China, [6]Xinjiang Plant Protection Station, Department of Xinjiang Agriculture, Urumqi, China

Stripe rust, caused by *Puccinia striiformis* f. sp. *tritici* (*Pst*), is a foliar disease that affects both winter and spring wheat crops in Xinjiang, China, which is linked to Central Asia. Race identification of *Pst* from spring wheat in Xinjiang was not done before. In this study, a total of 216 isolates were recovered from stripe rust samples of spring wheat in the region in 2021 and multiplied using the susceptible cultivar Mingxian 169. These isolates were tested on the Chinese set of 19 wheat differential lines for identifying *Pst* races. A total of 46 races were identified. Races *Suwon-11-1, Suwon11-12,* and *CYR32* had high frequencies in the spring wheat region. The frequencies of virulence factors on differentials "Fulhard" and "Early Premium" were high (>95%), whereas the virulence factor to differential "*Triticum spelta* var. Album" (*Yr5*) was not detected, while virulence to other differentials showed variable frequency within different counties. The predominant races in winter wheat in the same season were also detected from spring wheat cultivars, indicating Pst spreading from winter wheat to spring wheat crops. Deploying resistance genes in spring and winter wheat cultivars is critical for control stripe rust.

KEYWORDS

wheat stripe rust, race identification, virulence factor, spring wheat, China epidemic regions

1 Introduction

Wheat (*Triticum* spp.) is an important cereal crop worldwide. Wheat production must increase to keep pace with continued population growth. Various factors threaten wheat production, including biotic stresses (Singh et al., 2022). Stripe rust, also known as yellow rust (*Yr*), is one of the most destructive diseases of wheat and can cause 100% yield loss with susceptible cultivars and favorable environmental conditions (Begum et al., 2014).

The pathogen of wheat stripe rust, *Puccinia striiformis* f. sp. *tritici* (*Pst*), is highly aggressive and evolves quickly, and new races can overcome race-specific resistance in wheat cultivars and cause severe epidemics (Chen et al., 2010). Thus, it is crucial to identify new races and to develop wheat cultivars with effective and durable resistance to prevent potential disease epidemics (Elbasyoni et al., 2019). To date, 85 Yr genes for stripe rust resistance have been formally designated (*Yr1* to *Yr85*), and more than 100 temporarily named Yr genes or quantitative trait loci (QTL) have been reported (McIntosh et al., 2020; Feng et al., 2023).

The stripe rust fungus is notorious for its capability of long-distance dispersal in the world. Recently, high genetic diversity and recombination populations were reported in China's north and south epidemic regions. Moreover, these epidemic regions provide inoculum to cause epidemics in other regions of the country (Awais et al., 2022). China has been a primary focus of stripe rust for researchers after the Himalayan region was found as a center of diversity for the worldwide *Pst* populations (Ali et al., 2014).

Disease dynamics involve complex interactions among the host, pathogen, and environment (Newlands, 2018). The vast region of Xinjiang in northwestern China is important for stripe rust epidemics. As it is located in the potential center of diversity (Ali et al., 2014; Awais et al., 2022), the region links other Chinese epidemic regions to Central Asia (Chen et al., 2023). Also, both winter and spring wheat crops grown in this region and mild summer temperatures provide a long season of host plants and favorable environmental conditions for *Pst* to infect, develop, and survive. A recent study (Chen et al., 2023) was conducted to identify *Pst* races identification from winter wheat crops, but the races in spring wheat crops were not studied. The previous history of races on winter and spring wheat hosts is crucial for breaking the life cycle of *Pst*. Furthermore, identifying new stripe rust pathotypes creates an urgent need to develop new stripe rust-resistant lines.

Among different races identified in China using Chinese differential lines, the CYR32 is one of the most predominant races. It was first identified in red Abbondanza in Huangzhong, Qinghai Province, in 1991 (Wan et al., 2003). In 2009, a new Pst race G22 was virulent to cultivars Guinong and 92R lines, Moro, and Chuanmai 42 having resistance genes Yr10 and Yr26 (Liu et al., 2010), which were also virulent to cultivars rapidly spread to other regions (Liu et al., 2015). Races G22-9 (CYR34), CYR32, and CYR33 were China's most aggressive and predominant races (Liu et al., 2017; Bai et al., 2018; Huang et al., 2020).

Spring wheat in different parts of China is mainly grown in higher latitude or in the higher-elevation areas of Inner Mongolia, Heilongjiang, Qinghai, Ningxia, Xinjiang, Hebei, Tianjin, Shanxi, Gansu, and Tibet, and some small areas in Liaoning and Jilin province (Li et al., 2019). It has some serious drawbacks, especially its susceptibility to most diseases (Sears and Miller, 1985). One of the major reasons is the small breeding and research effort as spring wheat has a relatively small planting area compared to winter wheat. Another reason is that the environmental conditions during the spring wheat growing season is more suitable for disease infection.

This study aimed to identify races of *Pst* from the spring wheat crop of Xinjiang and determine the role of spring and winter wheat crops in the region for the survival of the pathogen, and to determine virulence frequencies of *Pst* in the spring wheat region to help deploy specific resistant cultivars to minimize future epidemics.

2 Materials and methods

2.1 Stripe rust collection

A total of 216 samples of wheat stripe rust were collected from spring wheat in Gongliu (GL), Nileke (NLK), Tekesi (TKS), Xinyuan (XY), and Zhaosu (ZS) in Yili, Xinjiang, China in the stripe rust surveys at the end of July, during cropping season of 2021 (Supplementary Table 1). Samples were collected from different fields at a minimum distance of 15–20 km following the protocol developed by Ali and Hodson (2017). The collected samples were put inside moisture-absorbent bags and labeled with specific sample codes, disease severity, GPS coordinates, crop growth stage, and cultivar information. The sample bags were placed on a table at room temperature overnight for drying and then put in a desiccator with silica at 4°C for later use.

2.2 Urediniospore multiplication

The leaf samples were moisturized and put on wet filter papers in petri dishes at 10°C for 10 h for urediniospore production. Urediniospores from individual uredinia were transferred onto a leaf of a susceptible wheat cultivar (Mingxian 169) 10–15 days after planting using a sterilized needle. The inoculated seedlings were sprayed with water, covered with moisturized plastic sheets to avoid contamination, kept in a dew chamber at 10 to 13°C for 24 h in darkness, and then placed in a growth chamber under a day/night thermoperiod of 17/13°C with a photoperiod of 16 h. Fifteen days after inoculation, urediniospores were collected into test tubes. The fresh urediniospores were used to inoculate Mingxian 169 seedlings to produce enough urediniospores. Urediniospores were kept in a desiccator in a refrigerator during the multiplication and stored in a −20°C freezer until further tests. If urediniospores from the freezer were needed for multiplication, the urediniospores were heat-shocked for 2 min by submerging the vials containing urediniospores in warm water (approximately 50°C). For each sample, spores from one uredinium were used to establish an isolate to represent the sample, and therefore, a total of 216 isolates were obtained for race identification.

2.3 Race identification

The set of 19 Chinese differential lines were used for identifying races of *Pst*, as described by Zhan et al. (2016). These differential lines carry single and multiple known and unknown *Yr* genes (Supplementary Table 2). Seeds of these differential lines, together with Mingxian-169 as a susceptible control, were planted in plastic pots with five lines in each pot. Seedlings (10 to 15 days old) were used for inoculation. Fresh uredospore were mixed with talcum

powder at a ratio of 1:30 in a 15-mL centrifuge tube, and the mixture was shaken gently onto seedlings of the differential lines. The inoculated seedlings were kept in the dew chamber for 24 h and then grown in the growth chambers under the conditions as described above. Fifteen days after inoculation, infection type was recorded for each differential using a 0–9 scale (Line and Qayoum, 1992). Infection types 0–6 were considered avirulent and infection types 7–9 were considered virulent (Wan and Chen, 2014). The differential test was repeated to validate the infection type data.

2.4 Data analysis

The virulence pattern of each isolate was used to identify the race. The virulence profile of isolates was compiled into an Excel sheet along with previously identified races (Zhan et al., 2016; Chen et al., 2023). Diversity for race and virulence in *P. striiformis* populations sampled from the Xinjiang region was calculated based on the Simpson diversity index "1-D" (Simpson, 1949). The frequencies of races and virulence factors were calculated for each location and the surveyed region. Cluster-based analysis was conducted based on the virulence profiles to assess the relationships of the isolates from different locations using the Ward method (1963) (Ward, 1963).

3 Results

3.1 Races and diversity

From the 216 isolates, 46 *Pst* races were identified, including 29 previously identified races and 17 new races (Table 1). As the new races had low frequencies, they were named with temporary numbers with the prefix of Nw standing for northwest. These races were clustered into six groups based on their virulence profiles (Figure 1).

In the overall population, Race *Suwon 11-1* had the highest frequency (15.74%). This race had a virulent pattern against

TABLE 1 Races of *Puccinia striiformis* f. sp. *tritici* from spring wheat in Xinjiang, China in 2021.

Race	Virulence profile	GL	NLK	TKS	XY	ZS	Overall population
CYR17	1,2,-,4,-,6,7,-,-,-,-,-,-,-,-,-,-,-	–	3.03	–	–	2.63	0.93
CYR23	1,2,3,4,-,6,7,8,9,-,11,-,-,-,-,-,-,-	2.08	3.03	–	–	–	0.93
CYR24	1,2,3,4,-,6,7,8,-,-,11,-,-,-,-,-,-,-	2.08	3.03	–	–	5.26	1.85
CYR25	1,2,3,4,5,6,7,8,9,-,11,-,-,-,-,-,-,-	2.08	–	–	–	2.63	0.93
CYR26	1,2,3,-,-,6,7,8,9,-,11,-,-,-,-,-,-,-	–	3.03	1.19	–	–	0.93
CYR28	1,2,3,4,5,6,7,8,9,-,11,-,-,-,-,16,-,-,-	2.08	3.03	3.57	–	5.26	3.24
CYR29	1,2,3,4,5,6,7,8,9,-,11,12,-,-,-,16,-,-,-	2.08	–	1.19	–	–	0.93
CYR30	1,2,3,4,5,6,7,8,9,-,11,12,-,-,-,16,17,-,-	–	–	1.19	7.69	2.63	1.39
CYR31	1,2,3,4,5,6,7,8,9,-,11,12,-,14,-,16,17,-,-	4.17	3.03	3.57	7.69	2.63	3.70
CYR32	1,2,3,4,5,6,7,8,9,10,11,12,13,14,-,16,17,-,-	4.17	9.09	4.76	7.69	13.16	6.94
CYR33	-,2,3,4,5,6,7,8,9,10,11,12,13,14,-,16,-,-,-	4.17	–	3.57	–	–	2.31
CYR34	1,2,3,4,5,6,7,8,9,10,11,12,13,14,-,16,17,-,19	6.25	–	7.14	15.38	5.26	6.02
Guinong22-13	-,2,3,-,-,6,7,8,9,10,11,12,13,14,-,16,17,-,19	4.17	9.09	4.76	15.38	2.63	5.56
Guinong22-14	1,2,3,4,5,6,7,8,9,10,11,12,13,14,15,-,-,-,19	–	–	2.38	–	2.63	1.39
Hy-4	1,2,3,4,5,6,7,8,9,10,11,-,13,14,-,16,17,-,-	–	–	1.19	–	–	0.46
Hy-6	1,2,3,4,5,6,7,8,9,-,11,-,-,14,-,-,17,-,-	4.17	–	–	–	–	0.93
Hy-7	-,2,3,4,5,6,7,8,9,10,11,-,13,14,-,16,17,-,-	2.08	–	–	–	–	0.46
Lovrin10-2	1,2,3,-,-,6,7,8,9,-,11,-,-,-,-,16,-,-,-	–	–	1.19	–	–	0.46
Lovrin13-2	1,2,3,4,-,6,7,8,9,-,11,12,-,-,-,16,-,-,-	–	–	–	–	5.26	0.93
Lovrin13-8	1,2,3,4,5,6,7,8,9,10,11,12,-,-,-,16,-,-,-	2.08	–	–	–	–	0.46
Nw-1	-,-,3,-,-,6,-,-,9,-,-,-,-,-,-,-,-,-	–	3.03	1.19	–	–	0.93
Nw-10	-,2,3,4,5,6,7,-,9,-,11,-,-,14,-,-,17,-,-	–	–	1.19	–	–	0.46
Nw-11	1,2,3,4,5,6,7,8,9,10,11,12,13,14,-,16,-,-,-	–	–	1.19	15.38	–	1.39

(Continued)

10.3389/fpls.2023.1273306

TABLE 1 Continued

Race	Virulence profile	GL	NLK	TKS	XY	ZS	Overall population
Nw-12	1,2,3,4,-,6,7,8,9,10,11,12,13,14,-,16,-,-,-	–	3.03	–	–	–	0.46
Nw-13	-,2,-,4,-,-,7,-,-,-,-,-,-,-,-,-,-,-	–	3.03	–	–	–	0.46
Nw-14	-,2,3,4,5,6,7,8,9,-,11,-,-,-,-,-,-,-	2.08	3.03	–	–	–	0.93
Nw-15	-,2,3,4,-,6,7,8,9,10,11,-,13,14,-,16,17,-,-	4.17	–	–	–	–	0.93
Nw-16	1,2,3,4,5,6,7,8,-,-,11,-,-,-,-,-,-,-	2.08	–	–	–	–	0.46
Nw-17	1,2,3,4,5,6,7,-,9,-,11,-,-,14,-,-,17,-,-	2.08	–	–	–	2.63	0.93
Nw-18	-,2,3,4,-,6,7,8,-,-,11,-,-,-,-,-,-,-	–	–	–	–	2.63	0.46
Nw-19	1,2,3,4,-,6,7,8,9,-,11,12,-,14,-,16,-,-,-	–	–	–	–	2.63	0.46
Nw-4	-,2,3,-,-,6,7,8,9,-,11,-,-,-,-,-,-,-	–	–	1.19	–	–	0.46
Nw-5	-,2,3,4,5,6,7,8,-,-,11,-,-,14,-,-,17,-,-	–	–	1.19	7.69	–	0.93
Nw-6	1,2,3,4,-,6,7,8,9,10,11,12,-,14,-,16,17,-,-	2.08	–	1.19	–	–	0.93
Nw-7	-,2,3,4,-,6,7,8,9,10,11,12,-,14,-,16,17,-,-	–	6.06	–	–	–	0.93
Nw-8	-,2,3,4,-,6,7,8,9,10,11,12,13,14,-,16,-,-,-	–	3.03	1.19	–	–	0.93
Nw-9	-,2,3,4,5,6,7,8,9,-,11,-,-,14,-,-,17,-,-	–	–	1.19	–	2.63	0.93
Suwon11-1	1,2,-,-,-,-,7,-,-,-,-,-,-,14,-,-,-,-,-	6.25	18.18	22.62	–	15.79	15.74
Suwon11-10	-,2,3,4,-,6,7,8,9,-,11,-,-,14,-,-,-,-,-	10.42	3.03	5.95	–	10.53	6.94
Suwon11-12	-,2,3,-,-,6,7,8,9,-,11,-,-,14,-,16,-,-,-	6.25	3.03	16.67	–	5.26	9.26
Suwon11-13	1,2,3,4,-,6,7,8,9,10,11,-,-,14,-,-,-,-,-	6.25	3.03	1.19	–	–	2.31
Suwon11-2	1,2,3,4,5,6,7,8,9,-,11,-,-,14,-,-,-,-,-	8.33	12.12	3.57	15.38	7.89	7.41
Suwon11-3	1,2,3,4,5,6,7,8,9,10,11,-,13,14,-,-,-,-,-	–	–	–	7.69	–	0.46
Suwon11-6	1,2,3,-,-,6,7,8,9,-,11,-,-,14,-,-,-,-,-	4.17	–	–	–	–	0.93
Suwon11-7	1,2,3,4,5,6,7,8,9,-,11,12,-,14,-,16,-,-,-	–	3.03	1.19	–	–	0.93
Suwon11-8	1,2,3,4,-,6,7,8,9,-,11,-,-,14,-,-,-,-,-	4.17	–	3.57	–	–	2.31
Total		**48**	**33**	**84**	**13**	**38**	**216**

[a]Virulence profile showed race virulence pattern against differential lines: 1 = Trigo Eureka, 2 = Fulhard, 3 = Lutescens 128, 4 = Mentana, 5 = Virgilio, 6 = Abbondanza, 7 = Early Premium, 8 = Funo, 9 = Danish 1, 10 = Jubilejina 2, 11 = Fengchan 3, 12 = Lovrin 13, 13 = Kangyin 655, 14 = Suwon 11, 15 = Zhong 4, 16 = Lovrin 10, 17 = Hybrid 46, 18 = Triticum spelta var. Album, and 19 = Guinong 22.

differentials Trigo Eureka (*Vr1*), Fulhard (*Vr2*), Early Premium (*Vr7*), and Suwon11 (*Vr14*), followed by race *Suwon 11-12* (9.26%). Races *CYR34* (*Vr1, Vr2, Vr3, Vr4, Vr5, Vr6, Vr7, Vr8, Vr9, Vr10, Vr11, Vr12, Vr13, Vr14, Vr16, Vr17*, and *Vr19*) and *CYR32* (*Vr1, Vr2, Vr3, Vr4, Vr5, Vr6, Vr7, Vr8, Vr9, Vr10, Vr11, Vr12, Vr13, Vr14, Vr16*, and *Vr17*) with broad virulence spectra had relative frequencies of 6.02% and 6.94%, respectively (Table 1).

Race diversities ranged from 0.88 to 0.95 with the highest race diversity observed in the Gongliu counties (Figure 2; Table 2). In the Gongliu county, the maximum relative frequency was noted by race *Suwon11-10* (10.42%). In Nileke races, *Suwon11-1* (18.18%) and *Suwon11-2* (12.12%) were predominant. In Tekesi, the predominant races were *Suwon11-1* (22.62%) and *Suwon11-12* (16.67%). In Xinyuan, high frequencies were observed for races *CYR34*, *Guinong22-13*, *Nw-11*, and *Suwon11-2* (15.3%). The highest frequency was observed for race *Suwon11-1* in the Zhaosu county.

3.2 Virulence

The virulence factors were simply designated as *Vr1*, *Vr2*, … *Vr19* corresponding to the sequential order of the 19 differential lines. Virulence factors *Vr2* and *Vr7*, which overcome the resistance genes in Fulhard and Early Premium, respectively, had greater than 95% frequencies. In contrast, virulence to resistance gene *Yr5* in differential *Triticum spelta* var. Album was not detected. Also, virulence to differential Zhong 4 had a low frequency (Table 3; Figure 3).

3.3 Comparison of predominant races in the winter and spring wheat regions

We compared races identified from the spring wheat region with the study on races identified in the winter wheat crop in the

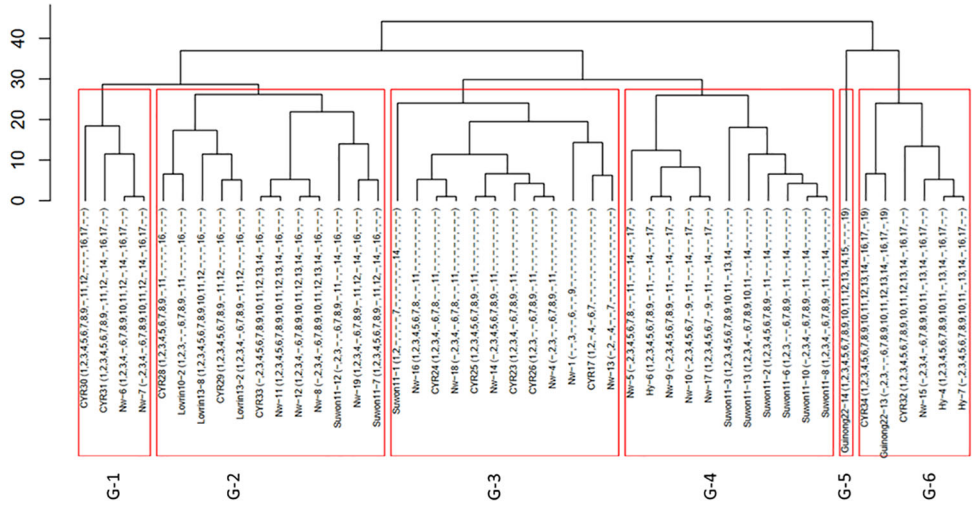

FIGURE 1
Clustering of 46 races of *Puccinia striiformis* f. sp. *tritici* collected from the spring wheat epidemic region in Xinjiang, China.

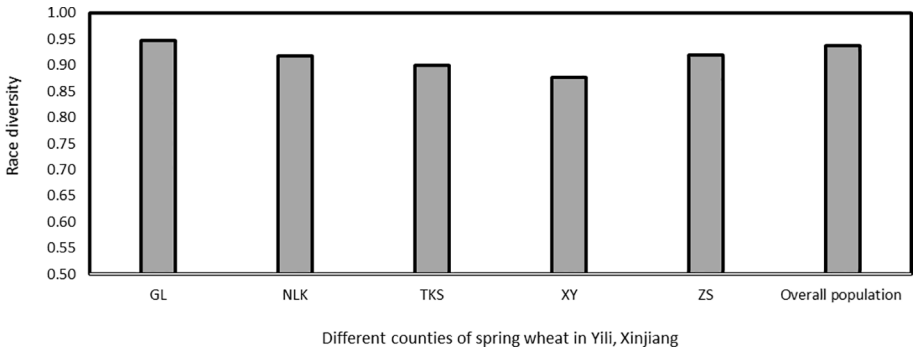

FIGURE 2
Race diversity in *Puccinia striiformis* f. sp. *tritici* isolates collected from spring wheat, Xinjiang, China in 2021. GL, Gongliu; NLK, Nileke; TKS, Tekesi; XY, Xinyuan; and ZS, Zhaosu.

same year in Xinjiang (Chen et al., 2023). The predominant races identified from winter wheat, such as *Suwon 11-1*, *Suwon11-2*, *Suwon 11-17*, *Loverin10-2*, *Hy-6*, *Guinong22-14*, *CYR34*, *CYR32*, *CYR30*, and *CYR28*, were also identified from spring wheat (Figure 4). The most predominant race in both winter wheat and spring wheat crops was *Suwon11-1*. Some races had big differences in frequencies between the crop regions. For example, races Hy6, CYR34, and CYR30 had much higher frequencies in the winter wheat crop than the spring wheat crop. The race diversity was higher in spring wheat than in winter wheat.

4 Discussion

Wheat crop is severely affected by stripe rust worldwide. Monitoring the disease and identifying races of the pathogen help researchers develop resistant cultivars. Understanding the dynamics of races within different host crops and seasons is vital to break up the regional pathogen life cycle. Xinjiang is one of the most important epidemic regions for wheat stripe rust not only for China but also for Central Asian countries due to its geographic proximity (Awais et al., 2022; Chen et al., 2023). Very limited research was conducted on race identification in this region. Recently, Chen et al. (2023) identified races from the winter wheat region but isolates from spring wheat were not included. In the present study, we obtained 216 isolates from spring wheat crops from Xinjiang and identified 46 races.

Our results showed that race *Suwon11-1* dominated the overall spring population, which was also the most predominant race in the same year in the winter wheat crop of Xinjiang (Chen et al., 2023). In addition, races *Suwon 11-2. Suwon 11-17, Loverin10-2, Hy-6, Guinong22-14, CYR34, CYR32, CYR30*, and *CYR28* were also found in both crops. This suggests that urediniospores produced on the winter wheat crop can carry over to the spring wheat crop, and vice versa. Also, barberry species near wheat fields may produce new races through sexual reproduction (Zhuang et al., 2019). Recently,

10.3389/fpls.2023.1273306

TABLE 2 Number of races, diversity, and virulences detected in the *Puccinia striiformis* f. sp. *tritici* isolates collected from the spring wheat crop in Xinjiang, China.

Region[a]	No. of isolates	No. of races detected	Race diversity	Frequency of the most frequent race	No. of virulences detected	Frequency of the most frequent virulence
GL	48	25	0.95	10.42	17	100.00
NLK	33	20	0.92	18.18	17	96.97
TKS	84	27	0.90	22.62	18	98.81
XY	13	9	0.88	15.38	17	100.00
ZS	38	19	0.92	15.79	18	100.00
Overall population	216	46	0.94	15.74	18	99.07

[a]GL, Gongliu; NLK, Nileke; TKS, Tekesi; XY, Xinyuan; and ZS, Zhaosu.

TABLE 3 Frequencies (%) of virulence factors in *Puccinia striiformis* f. sp. *tritici* isolates collected from spring wheat crops in Xinjiang, China.

Virulence [a]	Region [b]					Overall population
	GL	NLK	TKS	XY	ZS	
Vr1	66.67	66.67	61.90	76.92	76.32	67.13
Vr2	100.00	96.97	98.81	100.00	100.00	99.07
Vr3	93.75	75.76	77.38	100.00	81.58	82.87
Vr4	79.17	63.64	51.19	84.62	76.32	65.74
Vr5	47.92	33.33	38.10	84.62	47.37	43.98
Vr6	93.75	78.79	77.38	100.00	84.21	83.80
Vr7	100.00	96.97	98.81	100.00	100.00	99.07
Vr8	91.67	72.73	75.00	100.00	78.95	80.56
Vr9	89.58	72.73	76.19	92.31	73.68	79.17
Vr10	35.42	33.33	28.57	61.54	23.68	31.94
Vr11	93.75	72.73	76.19	100.00	81.58	81.94
Vr12	29.17	36.36	33.33	69.23	36.84	35.65
Vr13	25.00	24.24	26.19	61.54	23.68	27.31
Vr14	83.33	75.76	89.29	92.31	73.68	83.33
Vr15	0.00	0.00	2.38	0.00	2.63	1.39
Vr16	43.75	42.42	53.57	69.23	44.74	49.07
Vr17	33.33	27.27	27.38	61.54	31.58	31.48
Vr18	0.00	0.00	0.00	0.00	0.00	0.00
Vr19	10.42	9.09	14.29	30.77	10.53	12.96
Sample size	**48**	**33**	**84**	**13**	**38**	**216**

a Different virulent (Vr) corresponding differential lines: 1 = Trigo Eureka, 2 = Fulhard, 3 = Lutescens 128, 4 = Mentana, 5 = Virgilio, 6 = Abbondanza, 7 = Early Premium, 8 = Funo, C9 = Danish 1, 10 = Jubilejina 2, 11 = Fengchan 3, 12 = Lovrin 13, 13 = Kangyin 655, 14 = Suwon 11, 15 = Zhong 4, 16 = Lovrin 10, 17 = Hybrid 46, 18 = Triticum spelta var. Album, and 19 = Guinong 22.
b Regions GL = Gongliu, NLK = Nileke, TKS = Tekesi, XY = Xinyuan, and ZS = Zhaosu.

stripe rust found on volunteer wheat and various grasses during our field surveys (unpublished data) suggested that volunteer wheat and grasses may serve as the host bridges for *Pst* survival and transfer from late-maturing winter and spring wheat to autumn-sown winter wheat seedlings (Zeng et al., 2022).

Race identification from neighboring countries has not yet been done to understand whether Xinjiang plays any role in inter-regional migration, but it needs to be studied. The *Su11* race group that was virulent to Chinese differential Suwon 11 was dominant in China during 1994–1996 (Zhao and Kang, 2023)

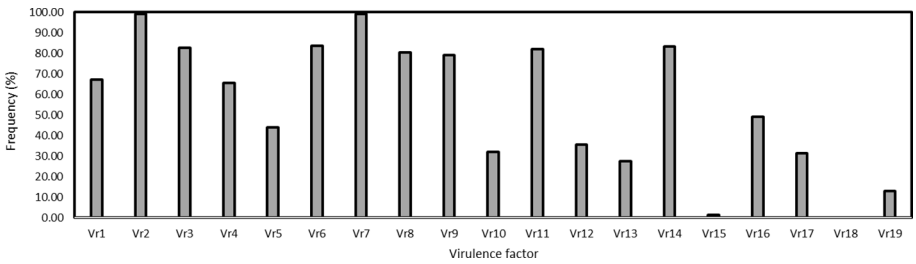

FIGURE 3
Frequencies of virulence factors detected in the *Puccinia striiformis* f. sp. *tritici* isolates collected from spring wheat crop of Xinjiang, China. The Chinese differentials are as follows: 1 = Trigo Eureka, 2 = Fulhard, 3 = Lutescens 128, 4 = Mentana, 5 = Virgilio, 6 = Abbondanza, 7 = Early Premium, 8 = Funo, C9 = Danish 1, 10 = Jubilejina 2, 11 = Fengchan 3, 12 = Lovrin 13, 13 = Kangyin 655, 14 = Suwon 11, 15 = Zhong 4, 16 = Lovrin 10, 17 = Hybrid 46, 18 = *Triticum spelta* var. Album, and 19 = Guinong 22.

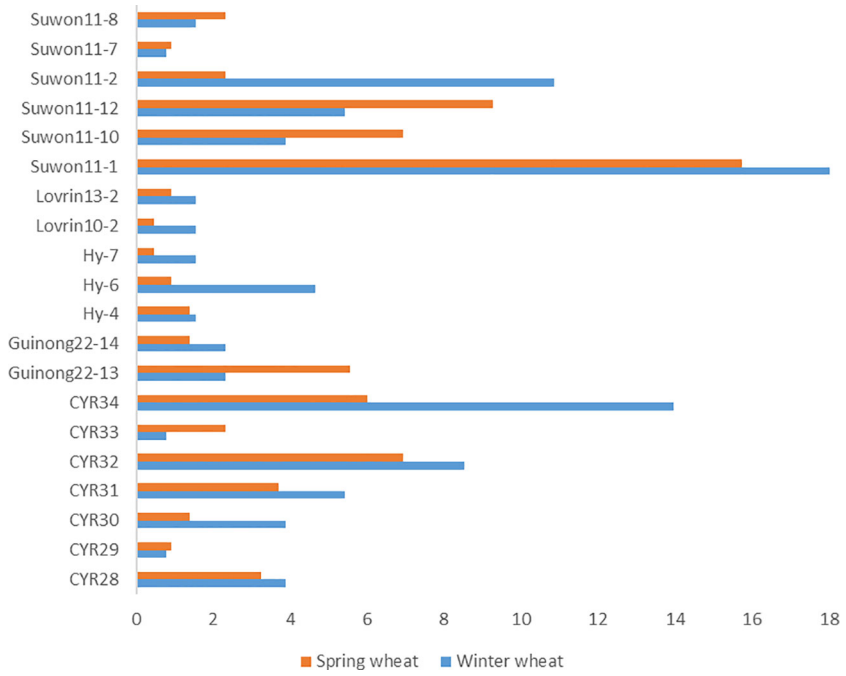

FIGURE 4
Puccinia striiformis f. sp. *tritici* races commonly detected from the winter and spring wheat regions of Xinjiang, China in 2021.

and was recently reported in Xinjiang in a previous study (Zhan et al., 2016). In the present study, we found that some of the *Su11* race group members were still predominant. These results suggest that the *Su11* race group has a high fitness, well adapting to the wheat cultivars and environments in Xinjiang. Although at relatively low frequencies, the recently identified races like CYR33 and CYR34 were detected in the present study and in the winter wheat region of Xinjiang (Chen et al., 2023). More importantly, we identified 17 new races with the virulence profiles that have not been found in any other regions of China. Continuous monitoring of the disease and the pathogen races in the vast Xinjiang region is needed for the effective control of stripe rust in this region and other regions of China.

The resistance genes in Fulhad and Early Premium are ineffective against the Pst population in Xinjiang and the other regions of China. In contrast, *Yr5* is still effective. Similar results were also found in the winter wheat region of Xinjiang (Chen et al., 2023). Rotations of host and non-host crops in different seasons may help farmers to reduce stripe rust damage (Bargués-Ribera and Gokhale, 2020). However, growing resistant cultivars is the most effective approach to control the diseases. Selecting resistant wheat cultivars from currently available ones in the region is the immediate step, but developing new cultivars with improved stripe rust resistance is an urgent and long task. Breeders should consider all race groups for developing wheat cultivars with effective resistance. It should be better to use various combinations of effective race-specific resistance genes with genes for durable resistance to develop wheat cultivars with adequate and long-lasting resistance. Also, collaborations within and beyond the Xinjiang region in stripe rust monitoring, research, and breeding

are necessary as the region is huge and the pathogen is capable of the long-distance migration.

5 Conclusions

This study conducted surveillance from the spring wheat region to identify the *Puccinia striiformis* f. sp. *Tritici* races. A total of 46 *Pst* races were identified, namely, 29 previously identified races and 17 new races from 216 isolates. Races *Suwon-11-1*, *Suwon11-12*, and *CYR32* had high frequencies in the spring wheat region. The predominant races in winter wheat in the same season were also detected from spring wheat cultivars, indicating Pst spreading from winter wheat to spring wheat crops. Deploying resistance genes and regular race identification from that region is vital to overcome future epidemic threats.

Data availability statement

The original contributions presented in the study are included in the article/Supplementary Material, further inquiries can be directed to the corresponding authors.

Author contributions

JM: Conceptualization, Formal Analysis, Investigation, Writing – original draft. MA: Formal Analysis, Writing – original draft. LC: Investigation, Writing – original draft. HY: Investigation, Validation, Writing – original draft. HL: Investigation, Writing – original draft. YS: Investigation, Writing – original draft. HW: Investigation, Writing – original draft. GL: Conceptualization, Methodology, Writing – original draft. HG: Conceptualization, Formal Analysis, Investigation, Writing – original draft.

Funding

The authors declare financial support was received for the research, authorship, and/or publication of this article. This research was funded by the Natural Science Foundation of Xinjiang Uygur Autonomous Region (2022D01A270), the Xinjiang Uygur Autonomous Region, Regional Coordinated Innovation Project (Shanghai Cooperation Organization Science and Technology Partnership Program) (No. 2022E01022), the Science and Technology Assistance Project of Xinjiang Uygur Autonomous Region (2022E02070), the Key Research & Development Program of Xinjiang (2022B02015-3 and 2021B02002-1), the Urumqi Integrated Experimental Station of China Agriculture Research System for Wheat (CARS-03-88), the Key Laboratory of Integrated Pest Management on Crop in Northwestern Oasis (KFJJ202104), and the Project of Fund for Stable Support to Agricultural Sci-Tech Renovation (xjnkywdzc-2022004).

Acknowledgments

We are highly grateful to Prof. Xianming Chen for his suggestions and spending valuable time to review this manuscript.

Conflict of interest

The authors declare that the research was conducted in the absence of any commercial or financial relationships that could be construed as a potential conflict of interest.

Publisher's note

All claims expressed in this article are solely those of the authors and do not necessarily represent those of their affiliated organizations, or those of the publisher, the editors and the reviewers. Any product that may be evaluated in this article, or claim that may be made by its manufacturer, is not guaranteed or endorsed by the publisher.

Supplementary material

The Supplementary Material for this article can be found online at: https://www.frontiersin.org/articles/10.3389/fpls.2023.1273306/full#supplementary-material

References

Ali, S., Gladieux, P., Rahman, H., Saqib, M. S., Fiaz, M., Ahmad, H., et al. (2014). Inferring the contribution of sexual reproduction, migration and off-season survival to the temporal maintenance of microbial populations: A case study on the wheat fungal pathogen *Puccinia striiformis* f. sp. *tritici*. *Mol. Ecol.* 23, 603–617. doi: 10.1111/mec.12629

Ali, S., and Hodson, D. (2017). "Wheat rust surveillance; field disease scoring and sample collection for phenotyping and molecular genotyping," in *Methods in Molecular Biology*. Ed. S. Periyannan (New York, USA: Humana Press).

Awais, M., Ali, S., Ju, M., Liu, W., Zhang, G., Zhang, Z., et al. (2022). Countrywide inter-epidemic region migration pattern suggests the role of southwestern population in wheat stripe rust epidemics in China. *Environ. Microbiol.* 24, 4684–4701. doi: 10.1111/1462-2920.16096

Bai, B. B., Liu, T. G., Liu, B., Gao, L., and Chen, W. Q. (2018). High relative parasitic fitness of G22 derivatives is associated with the epidemic potential of wheat stripe rust in China. *Plant Dis.* 102, 483–487. doi: 10.1094/PDIS-04-17-0511-SR

Bargués-Ribera, M., and Gokhale, C. S. (2020). Eco-evolutionary agriculture: Host-pathogen dynamics in crop rotations. *PloS Comput. Biol.* 16 (1), e1007546. doi: 10.1371/journal.pcbi.1007546

Begum, S., Iqbal, M., Ahmed, I., Fayyaz, M., Shahzad, A., and Ali, G. M. (2014). Allelic variation at loci controlling stripe rust resistance in spring wheat. *J. Genet.* 93, 579–586. doi: 10.1007/s12041-014-0413-9

Chen, X. M., Penman, L., Wan, A. M., and Cheng, P. (2010). Virulence races of Puccinia striiformis f. sp. tritici in 2006 and 2007 and development of wheat stripe rust and distributions, dynamics, and evolutionary relationships of races from 2000 to 2007 in the United States. *Can. J. Plant Pathol.* 32, 315–333. doi: 10.3390/jof9040436

Chen, L., Awais, M., Yang, H., Shen, Y., Li, G., Gao, H., et al. (2023). Races *CYR34* and *Suwon11-1* of *Puccinia striiformis* f. sp. *tritici* Played an Important Role in Causing the Stripe Rust Epidemic in Winter Wheat in Yili, Xinjiang, China. *J. Fungi.* 9, 436. doi: 10.3390/jof9040436

Elbasyoni, I. S., El-Orabey, W. M., Morsy, S., Baenziger, P. S., Al Ajlouni, Z., and Dowikat, I. (2019). Evaluation of a global spring wheat panel for stripe rust: Resistance loci validation and novel resources identification. *PloS One* 14 (11), e0222755. doi: 10.1371/journal.pone.0222755

Feng, J. Y., Yao, F. J., Wang, M. N., See, D. R., and Chen, X. M. (2023). Molecular mapping of *Yr85* and comparison with other genes for resistance to stripe rust on wheat chromosome 1B. *Plant Dis.* doi: 10.1094/PDIS-11-22-2600-RE

Huang, L., Xiao, X., Liu, B., Gao, L., Gong, G., Chen, W., et al. (2020). Identification of stripe rust resistance genes in common wheat cultivars from huang-huai-hai region of China. *Plant Dis.* 104, 1763–1770. doi: 10.1094/pdis-10-19-2119-re

Li, H., Zhou, Y., Xin, W., Wei, Y., Zhang, J., Guo, L., et al. (2019). Wheat breeding in northern China: achievements and technical advances. *Crop J.* doi: 10.1016/j.cj.2019.09.003

Line, R. F., and Qayoum, A. (1992). *Virulence, aggressiveness, evolution, and distribution of races of Puccinia striiformis (the cause of stripe rust of wheat) in North Americ-87.* 44, North America, USA: U.S. Department of Agriculture Technical Bulletin No. 1788.

Liu, B., Liu, T. G., Zhang, Z. Y., Jia, Q., Wang, B. T., Gao, L., et al. (2017). Discovery and pathogenicity of CYR34, a new race of Puccinia striiformis f. sp. *tritici* in China. *Acta Phytopathol. Sin.* 47, 682–688. doi: 10.13926/j.cnki.apps.000071

Liu, T. G., Peng, Y. L., Chen, W. Q., and Zhang, Z. Y. (2010). First detection of virulence in *Puccinia striiformis* f. sp. *tritici* in China to resistance genes *Yr24* (=*Yr26*) present in wheat cultivar Chuanmai 42. *Plant Dis.* 94, 1163. doi: 10.1094/PDIS-94-9-1163C

Liu, T. G., Zhang, Z. Y., Liu, B., Li, G., Peng, Y. L., and Chen, W. Q. (2015). Detection of virulence to *Yr26* and pathogenicity to Chinese commercial winter wheat cultivars at seedling stage. *Acta Phytopathol. Sin.* 45, 41–47.

McIntosh, R. A., Dubcovsky, W. J., Rogers, W. J., and Raupp, W. J. (2020) *Catalogue of gene symbols for wheat: In Annual Wheat Newsletter; The Wheat Genetic and Genomic Resources Center* (Manhattan, KS, USA: Kansas State University). Available at: https://wheat.pw.usda.gov/GG3/wgc (Accessed 28 June 2022).

Newlands, N. K. (2018). Model-based forecasting of agricultural crop disease risk at the regional scale, integrating airborne inoculum, environmental, and satellite-based monitoring data. *Front. Environ. Sci.* 6, 63. doi: 10.3389/fenvs.2018.00063

Sears, E. R., and Miller, T. E. (1985). The history of Chinese spring wheat. *Cereal Res. Commun.* 13, 261–263.

Sigh, B. H., Mandahal, K. S., Ankita,, Kaur Sarao, L., and Srivastava, P. (2022). Breeding wheat for biotic stress resistance: achievements, challenges and prospects. *Curr. Trends Wheat Res.* doi: 10.5772/intechopen.97359

Simpson, E. H. (1949). Measurement of diversity. *Nature* 163, 688. doi: 10.1038/163688a0

Wan, A. M., and Chen, X. M. (2014). Virulence characterization of *Puccinia striiformis* f. sp. *tritici* using a new set of *Yr* single-gene line differentials in the United States in 2010. *Plant Dis.* 98, 1534–1542. doi: 10.1094/PDIS-01-14-0071-RE

Wan, A. M., Wu, L. R., Jin, S. L., Yao, G., and Wan, B. T. (2003). Discovery and studied on CYR32, a new race of Puccinia striiformis f. sp. *tritici* in China. *Acta Phytophyl. Sin.* 30, 347–352.

Ward, J. H. (1963). Hierarchical grouping to optimize an objective function. *J. Am. Stat. Assoc.* 58, 236–244. doi: 10.1080/01621459.1963.10500845

Zeng, Q. D., Zhao, J., Wu, J. H., Zhan, G. M., Han, D. J., and Kang, Z. S. (2022). Wheat stripe rust and integration of sustainable control strategies in China. *Front. Agric. Sci. Eng.* 9, 37–51. doi: 10.15302/J-FASE-2021405

Zhan, G., Wang, F., Wan, C., Han, Q., Huang, L., Kang, Z., et al. (2016). Virulence and Molecular Diversity of the Puccinia striiformis f. sp. tritici Population in Xinjiang in Relation to Other Regions of Western China. *Plant Dis.* 100, 99–107. doi: 10.1094/PDIS-11-14-1142-RE

Zhao, J., and Kang, Z. (2023). Fighting wheat rusts in China: A look back and into the future. *Phytopathol. Res.* 5, 6. doi: 10.1186/s42483-023-00159-z

Zhuang, H., Zhao, J., Huang, L., Kang, Z., and Zhao, J. (2019). Identification of three Berberis species as potential alternate hosts for Puccinia striiformis f. sp. tritici in wheat-growing regions of Xinjiang, China. *J. Integr. Agric.* 18, 2786–2792. doi: 10.1016/S2095-3119(19)62709-7

frontiers | Frontiers in Plant Science

TYPE Original Research
PUBLISHED 10 October 2023
DOI 10.3389/fpls.2023.1223959

Check for updates

OPEN ACCESS

EDITED BY
Runsheng Ren,
Jiangsu Academy of Agricultural Sciences (JAAS), China

REVIEWED BY
Jaspal Kaur,
Punjab Agricultural University, India
Aamir W. Khan,
University of Missouri, United States
Satinder Kaur,
Punjab Agricultural University, India

*CORRESPONDENCE
Pawan Kumar Singh
pk.singh@cgiar.org

RECEIVED 16 May 2023
ACCEPTED 20 September 2023
PUBLISHED 10 October 2023

CITATION
Navathe S, He X, Kamble U, Kumar M, Patial M, Singh G, Singh GP, Joshi AK and Singh PK (2023) Assessment of Indian wheat germplasm for Septoria nodorum blotch and tan spot reveals new QTLs conferring resistance along with recessive alleles of *Tsn1* and *Snn3*.
Front. Plant Sci. 14:1223959.
doi: 10.3389/fpls.2023.1223959

COPYRIGHT
© 2023 Navathe, He, Kamble, Kumar, Patial, Singh, Singh, Joshi and Singh. This is an open-access article distributed under the terms of the Creative Commons Attribution License (CC BY). The use, distribution or reproduction in other forums is permitted, provided the original author(s) and the copyright owner(s) are credited and that the original publication in this journal is cited, in accordance with accepted academic practice. No use, distribution or reproduction is permitted which does not comply with these terms.

Assessment of Indian wheat germplasm for Septoria nodorum blotch and tan spot reveals new QTLs conferring resistance along with recessive alleles of *Tsn1* and *Snn3*

Sudhir Navathe[1], Xinyao He[2], Umesh Kamble[3], Manjeet Kumar[4], Madhu Patial[4], Gyanendra Singh[3], Gyanendra Pratap Singh[5], Arun Kumar Joshi[6] and Pawan Kumar Singh[2]*

[1]Genetics and Plant Breeding Group, Agharkar Research Institute, Pune, India, [2]Global Wheat Program, International Maize and Wheat Improvement Centre (CIMMYT), Texcoco, Mexico, [3]Division of Crop Improvement, ICAR-Indian Institute of Wheat and Barley Research, Karnal, India, [4]Division of Genetics, ICAR-Indian Agricultural Research Institute, New Delhi, India, [5]Indian Council of Agricultural Research (ICAR)-National Bureau of Plant Genetic Resources, New Delhi, India, [6]International Maize and Wheat Improvement Centre (CIMMYT) & Borlaug Institute for South Asia (BISA), New Delhi, India

The leaf blight diseases, Septoria nodorum blotch (SNB), and tan spot (TS) are emerging due to changing climatic conditions in the northern parts of India. We screened 296 bread wheat cultivars released in India over the past 20 years for seedling resistance against SNB (three experiments) and TS (two experiments). According to a genome-wide association study, six QTLs on chromosome arms 1BL, 2AS, 5BL, and 6BL were particularly significant for SNB across all three years, of which *Q.CIM.snb.1BL, Q.CIM.snb.2AS1, Q.CIM.snb.2AS.2, and Q.CIM.snb.6BL* appeared novel. In contrast, those on 5BS and 5BL may correspond to *Snn3* and *Tsn1*, respectively. The allelic combination of *tsn1*/*snn3* conferred resistance to SNB, whereas that of *Tsn1*/*Snn3* conferred high susceptibility. As for TS, *Tsn1* was the only stably significant locus identified in this panel. Several varieties like PBW 771, DBW 277, and HD 3319, were identified as highly resistant to both diseases that can be used in future wheat improvement programs as resistant donors.

KEYWORDS

Parastagonospora nodorum*, *Pyrenophora tritici-repentis*, quantitative inheritance, *Triticum aestivum*, *Tsn1

1 Introduction

Wheat (*Triticum* spp.) is a staple food and a crucial element of global food security. However, of several factors, fungal diseases are the most important that limit wheat production. Septoria nodorum blotch (SNB) is caused by the necrotrophic fungal pathogen *Parastagonospora nodorum* (syn. *Phaeosphaeria nodorum* [E. Müll.], syn. *Leptosphaeria*

nodorum [E. Müll.], syn. *Stagonospora nodorum* [Berk.], syn. *Septoria nodorum* [Berk.]). SNB frequently co-occurs with other necrotrophic fungal diseases like tan spot (TS, caused by *Pyrenophora tritici-repentis*) and Septoria tritici blotch (STB, caused by *Zymoseptoria tritici*). This disease is common in areas that experience frequent or high rainfall during the wheat growing season, such as Australia, Canada, Scandinavia, Central and Eastern Europe, eastern USA, and South America (Bearchell et al., 2005; Solomon et al., 2006; Shaw et al., 2008). In India, the disease was first recorded in the Nilgiri hills of south India (Chona and Munjal, 1952) and later from the Kumaon hills in Northern India (Joshi et al., 1971). In the last few decades, it has been encountered frequently in the northwestern plains zone (NWPZ) of the country, especially during cool and wet Rabi seasons (Rana et al., 2000). Due to the changing climatic conditions, SNB has been expanding into new niches. For example, it was first observed on emmer wheat (*T. dicoccoides*) in Turkey in 2017 and has been reported recently in Himachal Pradesh, India (Cat et al., 2018; Katoch et al., 2019).

Tan spot (TS), or yellow leaf spot, is a serious wheat disease affecting temperate and tropical wheat-growing regions. The fungal pathogen, a necrotroph that causes minor to severe spotting in wheat, was first described in 1823 (Hosford, 1982). The disease was subsequently reported in Europe, the USA, and Japan in the early 1900s (Wegulo, 2011). In India, reports on TS infection from northern plains and central regions were documented between 1934 and 1972 (Mitra, 1934; Misra and Singh, 1972), followed by a more recent one in 2007 (Singh, 2007). The development of the disease is encouraged by the favourable climate in South Asia, particularly in the Himalayan and eastern Gangetic plains, where low temperature and humidity favour prolonged leaf wetness. It has been reported that TS co-occurs with spot blotch in some parts of Nepal, causing yield losses of up to 20-30% (Duveiller et al., 2005). In Nepal, there is a higher incidence of foliar blight in the last week of January to mid-February when the temperature is still cool, and a few genotypes were identified as tolerant to the disease, like NL750, Milan, and Shanghai-7 (Dubin and Bimb, 1994; Duveiller et al., 2005; Gurung et al., 2012). So far, no systematic work has been done on SNB and TS in India except for reports on its occurrence. Moreover, no isolates have been deposited in the national fungal culture collection and type culture collections.

It is thought that *P. nodorum* obtains nutrients from dying plant tissue caused by secreted effectors. These effectors cause host hypersensitivity and result in programmed cell death (Friesen et al., 2007; Oliver et al., 2012). So far, eight effectors (SnToxA, SnTox1, SnTox2, SnTox3, SnTox4, SnTox5, SnTox6, and SnTox7) have been identified to date, along with nine major wheat sensitivity loci that correspond to them: *Tsn1, Snn1, Snn2, Snn3-B1/Snn3-D1, Snn4, Snn5, Snn6*, and *Snn7*, respectively (Friesen et al., 2007; Friesen and Faris, 2012; Tan et al., 2012; Phan et al., 2016).

Marker-trait associations (MTAs) of polygenetic traits in plants have been widely identified using genome-wide association studies (GWAS). Adhikari et al. (2011); Gurung et al. (2014); Liu et al. (2015), and Phan et al. (2018) have all discovered MTAs for SNB resistance at seedling resistance. In seedling experiments for resistance against a *P. nodorum* isolate lacking SnTox3, QTL was found on 2D, 3A, and 5B (Adhikari et al., 2011; Gurung et al., 2014). The 5B QTL's association with the *Tsn1* gene, which has been extensively studied (Liu et al., 2009; Gurung et al., 2014), supports the ability of GWAS to identify QTL for SNB resistance. TS resistance is both quantitatively and qualitatively inherited, where toxicity resistance genes and QTL have been identified. Tan spot resistance (Tsr) refers to the quality genes discovered through conidial inoculations, and "*Tsc*" and "*Tsn*" refer to genes for chlorosis and necrosis reactions against HST-containing cultures, respectively (McIntosh et al., 2008). In addition to the host susceptibility gene *Tsn1*, eight significant *Tsr* genes have so far been discovered, i.e., *Tsrl, Tsr2, Tsr3, Tsr4, Tsr5, Tsr6, TsrHar*, and *TsrAri*, being located on the chromosomes 2BS, 3AS, 3BL, 3DS, and 5BL (Kokhmetova et al., 2021; Lozano-Ramírez et al., 2022).

Though spot blotch remained a major concern in the Indian subcontinent among the foliar blotch diseases, it is important to do pre-emptive screening work on SNB and TS, considering the past reports and future outbreak risk under climate changing scenarios. In the present study, a panel of 296 bread wheat genotypes released in India over the past 20 years was screened at seedling stages for SNB and TS resistance. Further, the population was studied for the presence of the major toxin sensitivity gene *Tsn1*, and genome-wide association studies were performed for the genetic basis of the resistance.

2 Materials and methods

2.1 Plant material and genotyping

This study used a panel of 296 bread wheat genotypes from released varieties and advanced breeding lines developed primarily over the last twenty years from 25 research centres across India. DNA extraction and DArT sequencing of the genotypes were done per the protocol demonstrated by Li et al. (2016). The wheat accessions were sequenced with the DArTseq® technology at the Genetic Analysis Service for Agriculture (SAGA) at CIMMYT, Mexico. Markers with a minor allele frequency of less than 10% (2804 markers) or more than 30% missing data points (96 markers) were excluded from further analysis. A total of 9668 SNPs were finally used for the GWAS analysis, and their physical positions on the reference whole genome sequence (IWGSC: Chinese Spring RefSeq v1.0, International Wheat Genome Sequencing Consortium et al., 2018) were acquired from the database https://wheat-urgi.versailles.inra.fr/). The SNP markers were given names based on their chromosome location followed by clone ID, e.g., 5BL:3955588.

2.2 Disease screening for SNB and TS

The panel was evaluated for 3 years (2019, 2021, 2022) for SNB and 2 years for TS (2019, 2021) in greenhouse at the seedling stage. Mexican *P. tritici-repentis* (Ptr) isolate *MexPtr1* and *P. nodorum* isolate *MexSn4* were used for resistance screening against TS and SNB, respectively. Both isolates are ToxA producers based on inoculation experiments using differential genotypes, infiltration

experiments, and PCR with the ToxA-specific marker (data not shown). The isolates were grown on V8-PDA media (Lamari and Bernier, 1989), and conidiospore concentrations for inoculation were adjusted to 4×10^3 spores mL^{-1} (*MexPtr1*) and 1×10^7 spores mL−1 (*MexSn4*) (Singh et al., 2007; Singh et al., 2016). The response of TS and SNB was tested on seedlings in a greenhouse at 22°C day and 18°C night temperatures with a 16-h photoperiod. Experiments were set up in a randomized complete block design with two replicates, with four plants grown in plastic containers as experimental units to derive mean values for further analysis. Erik and Glenlea were used as resistant and susceptible controls, respectively. Inoculations were performed when the second leaf was fully expanded at around 14 days after planting. The inoculum was applied to seedlings with a hand sprayer until runoff (about 0.5 mL inoculum per plant). The trays were transferred to a humid chamber (RH 100%, 20°C) once the leaves were dry to promote infection, and the plants were returned to the greenhouse bench after 24 hours. Both diseases were rated on a linear scale of 1–5 at seven days after inoculation (dpi) (Feng et al., 2004; Hu et al., 2019).

2.3 Linkage disequilibrium and population structure

All 9668 SNP markers were used to calculate a kinship matrix, clusters among individual genotypes, and a heat map using the traditional Van Raden (2008) equation using TASSEL v5 (http://www.maizegenetics.net, accessed on 25 Oct 2022). Linkage disequilibrium (LD) was analysed with R^2 among SNP markers plotted against the physical distances in mega base pairs (Mb) across the 21 wheat chromosomes. The genotypic data was numerically transformed for population structure analysis utilizing XLSTAT (v. 2022.1). Structure 2.3.4 software was used to obtain the population structure (Pritchard et al., 2000). The admixture model was adjusted with a 100,000 burn-in period followed by 500,000 marker chain Monte Carlo (MCMC) iterations. The subpopulation test range was maintained at K1 - K5, with five iterations. The actual subpopulations were assessed using the DK approach (Earl and vonHoldt, 2012), which was verified using the Structure Harvester program (Web v0.6.94, Earl and vonHoldt, 2012) as per the method described by Evanno et al. (2005). The output summary calculated the standard deviation and average logarithm of the probability of the observed likelihood [LnP(D)]. The log-likelihood of the data was computed for each class (K = 1 to 5) to determine LnP(D) for each MCMC step. A neighbour-joining tree was created using TASSEL 5.0 (Bradbury et al., 2007) and visualized using the iTOL website (Letunic and Bork, 2021).

2.4 Genome-wide association analysis

For GWAS, three models (MLM, MLMM and FarmCPU) implemented in the R package GAPIT3 (Wang and Zhang, 2021) were used. The first was the mixed linear model (MLM=K+Q), which was based on the kinship matrix (K) and the principal component (PC) (Yu et al., 2006). The second method was the Multiple Loci Mixed Linear Model (MLMM), which employs forward-backward stepwise linear mixed-model regression to include associated markers as covariates. In contrast to MLM and MLMM, the third model FarmCPU (fixed and random, circulating probability unification); used all linked markers in a fixed-effect model and optimised the linked markers in a separate random-effect model, reducing false positives and false negatives and enabling quick computation. Population structure, principal components, and kinship were used as covariates in MLM and MLMM, and their QQ plots were compared. Our phenotypic data fit the FarmCPU model better, and QTL showed higher significance; therefore, only data analyzed by the FarmCPU model was chosen for additional examination. The Bonferroni correction (α=0.1) was used for an exploratory significance threshold to uncover putative QTL (Chan et al., 2010). QTL was recognized as robust when linked markers reached the strict -log10 (p) criteria of 3.0 in at least being detected across-year by either threshold adopted in this investigation and consistent across the models. The Quantile-Quantile (QQ) plots were also examined to determine the point at which the observed p-values diverge from those predicted by the null hypothesis. SNP marker annotations were obtained using the databases http://www.cerealsdb.uk.net and https://triticeaetoolbox.org. The physical positions of markers on the reference whole genome sequence (IWGSC: Chinese spring RefSeq v1.0, International Wheat Genome Sequencing Consortium et al., 2018) were acquired from the database https://wheat-urgi.versailles.inra.fr/ and https://plants.ensembl.org/Triticum_aestivum/Info/Index. If two significant markers shared a 10-Mbp interval or had substantial LD (R^2>0.8) with one another, they were regarded as belonging to the same QTL region.

2.5 KASP genotyping for *Tsn1*

Kompetitive Allele-Specific PCR (KASP) marker Ktsn1 specific for *Tsn1* (Dreisigacker et al., 2016) was used for genotyping the panel. Genomic DNA was isolated from 21-day-old seedling leaves, DNA concentration was measured with a Nanodrop 8000 spectrophotometer (Thermo Scientific), and the final concentration of 10 ng/ml was obtained by diluting the DNA with sterile PCR-grade water. KASP genotyping was undertaken using the PACE master mix per the manufacturer's guidelines (3CR biosciences). In brief, the assay mix for 25 samples was prepared as 3µl VIC primer, 7.5 µl common primer, and 14.5 µl of PCR grade H2O. Finally, for reaction assembly, individual reactions contained 5 µl 2X PACE, 0.138 µl assay mix, and 5 µl genomic DNA. The samples were run on a CFX96 Real-time PCR system (Bio-Rad). The PCR steps included 94°C for 15 min, 10 cycles of touch down program (94°C-0.20 min, 65 to 57°C-1 min), followed by 30 cycles of (94°C-0.20 min, 57°C-1 min). The results were analyzed in Bio-Rad CFX manager 3.1, and output was obtained as.csv files. The results obtained were compared against the linked SNP calls from the SNP array.

2.6 Haplotype analysis for the stable markers

For haplotype analysis, stable MTAs on chromosomes 1B, 2A, 5B, and 6B across experiments were selected. Eight markers that fitted the requirement that they were over the -log10(p) 3.0 threshold across the environments were chosen for the haplotype analysis: 5BS:1102120, 2AS:7487614, 2AS:1094287, 5BL:5324846, 5BL:3955588, 6B:1085698, 1B:1129298, and 5BL: Ktsn1. For TS, three markers, 5BL:5324846, 5BL:3955588, and 5BL : Ktsn1 were selected for the analysis. The corrected disease severities between haplotypes were compared using the Wilcoxon test implemented in R package ggpubr (Kassambara, 2020). The phenotypic data available for the seedling resistance to SNB in 2019, 2021, 2022, and TS in 2019 and 2021 was used for the analysis.

2.7 Stacking resistance allele and assessing interaction effect of *Tsn1* and *Snn3*

Data for three years (2019, 2021, and 2022) were used for this analysis. The corrected mean disease index from BLUP was used for haplotype analysis. Marker trait associations for SNB and TS were chosen from various models (MLM, MLMM, FarmCPU) to investigate the effect of stacking resistance alleles (Table S1). Resistant alleles were determined by mean comparison of corrected disease severity between alleles based on the Wilcoxon test, using the R package '*ggpubr*' (Kassambara, 2020). Wheat lines were classified according to the number of resistant alleles present. The t-test ($p < 0.05$) was implemented in the R package '*multcomView*' (Graves et al., 2015) to differentiate the significant groups.

To assess the gene effect of *Tsn1* and *Snn3*, two makers, 5BL:5324846 and 5BL:3955588, linked to *Tsn1* and data obtained from KASP assay Ktsn1 was compared with SNP 5BS:1102120 linked with *Snn3*. The interaction was discovered by comparing the mean between alleles using the t-test in the R package '*ggpubr*' (Kassambara, 2020).

2.8 Statistical analysis

The corrected disease index, genotypic and phenotypic variance, and heritability estimates were obtained from META-R software (Alvarado et al., 2020). Additionally, mean comparisons with the Wilcoxon test, t-test, and data visualization were executed using packages `*ggpubr*`, '*dplyr*', and '*multcomView*' using R software (Version 4.2.1, R Core Team, 2022).

3 Results

3.1 Disease evaluations

The population displayed significant phenotypic variation for SNB and TS resistance with a skewed distribution towards the lower disease in all experiments (Figure S1). A high proportion of genotypes exhibited high resistance to both diseases (See Table S1 for the disease scores) and the top 20 entries resistant to both diseases are presented in Table 1, including PBW 277, PBW 771, and HD 3319.

Analysis of variance revealed significant effects on genotype and genotype-by-environment for both diseases (Table 2). SNB showed higher overall heritability (0.87) than TS (0.75), with heritability in individual experiments ranging from 0.90 to 0.96.

3.2 Population structure and linkage disequilibrium analysis

Among the 9668 SNP markers selected for GWAS in the 296 bread wheat genotypes, 21.78% were from the A genome, 28.63% from the B genome, 12.03% from the D genome and 21.33% from unknown chromosomes. Population structure analysis based on the K means cluster approach divided the population into 4 major clusters that were depicted as a neighbour-joining tree (Figure 1). The kinship analysis also distinguished the population into 4 major groups and presented it as a kinship matrix-based heat map (Figure 2). The average extent of LD considered physical distance taken for the decay of R2 to reach a critical value of 0.10 across the genome, was approximately 10 Mb (Figures 2, S2, S3).

3.3 Genome-wide association study for SNB and TS

The exploratory -log10(p) threshold for the panel ranged from 2.92 to 11.53 for SNB and 2.96 to 15.86 for TS (Tables S1, S2). In total, 49 marker-trait associations (MTAs) were detected on various chromosomes for SNB (Table S1; Figures 3, S4). Six QTL on chromosomes 1BL, 2AS, 5BL, and 6BL were particularly significant for SNB over all three years and were considered robust QTLs. The QTL *Q.CIM.snb.1BL* on chromosome 1BL was identified with FarmCPU, and its peak marker 1BL:1129298 (p = 2.86E-04 to 8.97E-06) was located at 450.50Mbp on 1BL (Table 3). Two QTLs on 2AS, *Q.CIM.snb.2AS1 and Q.CIM.snb.2AS.2*, were detected in all models with their peak markers being 2AS:7487614 (59.43Mbp) and 2AS:1094287 (88.18Mbp), respectively. Another robust QTL, *Q.CIM.snb.5BS*, was identified at 5BS:1102120 (p=2.31E-05 to 5.99E-12) and was associated with *Snn3-B1*. Two *Tsn1*-associated markers 5BL:5324846 and 5BL:3955588 were detected across years and models on chromosome 5B at 566.04 and 588.4 Mbp, respectively (Table 3). The QTL *Q.CIM.snb.6BL* (p= 4.16E-04 to 1.61E-09) was detected using farmCPU, on the long arm of the chromosome 6B with peak marker 6BL:1085698 (669.13 Mbp).

For TS, 79 MTA (-log10(p) >3) were detected on various chromosomes (Table S2; Figure 3). Two *Tsn1*-associated markers 5BL:5324846 and 5BL:3955588 were significantly detected across years. The SNP 5BL:5324846 (p=3.51E-05 to 5.41E-06) was detected across the three models (MLM, MLMM, FarmCPU). While the SNP 5BL:3955588 (p=1.33E-05 to 3.63E-13) was

TABLE 1 List of wheat genotypes showing good resistance to Septoria nodorum blotch (SNB) and tan spot (TS), and their *Tsn1/tsn1* allele status.

No.	Genotype	Pedigree	SNB	TS	*Tsn1/tsn1*
1	PBW 771	BW9246/2*DBW17	1	1	*tsn1*
2	DBW 277	NI 5439/MACS 2496	1	1	*tsn1*
3	HD3319	18th HRWYT214/18th HRWYT229	1	1	*tsn1*
4	WH1256	SHA7//PRL/VEE#6/3/FASAN/4/HAAS8446/2*FASAN/5/CBRD/KAUZ/6/MILAN/AMSEL/7/FRET2*2/KUKUNA/8/2*WHEAR/SOKOLL	1	1	*Tsn1*
5	WH1258	CROC_1/Ae. Squarrosa (210)//WBLL1*2/BRAMBLING/3/VILLA JUAREZ F2009/5/BAV92//IRENA/KAUZ/3/HUITES*2/4/MURGA	1	1	*tsn1*
6	K1803	K 922/2K21	1	1	*tsn1*
7	K1805	K 922/2K21	1	1	*tsn1*
8	GW519	GW 394/PBW 519//AKAW 4627	1	1	*Tsn1*
9	TL 2969	JNIT-141/TL-1210//JNIT-141	1	1	*tsn1*
10	DBW93	WHEAR/TUKURU//WHEAR	1	1	*tsn1*
11	PBW802	HD2967*2/BWL3278	1.1	1	*tsn1*
12	UAS3002	RAJ4083/DWR195//HI 977	1.2	1	*tsn1*
13	UAS 3001	UAS259/GW322//HI 977	1.2	1	*tsn1*
14	UP3032	KAUZ//ALTAR84/AOS/3/MILAN/KAUZ/4/HUITES/UP2778	1.2	1	*tsn1*
15	MP3514	35IBWSN 244/DBW-17	1.3	1	*tsn1*
16	DBW285	PBW 550/SW89-5422	1.5	1	*Tsn1*
17	HD2733	ATTILA/3/HUITLE(HUI)/(CARC)CARCOMUN//CHEN/(CHTO)CHORLITO/4/ATTILA	1.5	1	*tsn1*
18	DBW 189	KACHU#1/4/CROC_1/Ae. Squarrosa (205)//BORL95/3/2*MILAN/5/KACHU	1.9	1	*tsn1*
19	DBW 168	SUNSU/CHIBIA	2	1	*tsn1*
20	DBW 273	FRANCOLIN #1*2//ND 643/2* WBLLI	1	1.1	*tsn1*
	Eric (Check)	Kitt//Waldron/Era	0	0	*tsn1*
	Glenlea (Check)	Sonora 64/Tezanos Pintos Precoz//Nainari 60	5	5	*Tsn1*

TABLE 2 Basic statistics for Septoria nodorum blotch (SNB) and tan spot (TS) and analysis of variance across the environments.

Statistic	Overall BLUP_Tan_Spot	Overall BLUP_SNB	BLUP_Tan_Spot 2019	BLUP_Tan_Spot 2021	BLUP_SNB 2019	BLUP_SNB 2021	BLUP_SNB 2022
Heritability	0.759906126	0.872762979	0.909059	0.920974941	0.939572	0.938598	0.967649
Genotype Variance	0.580347871	0.680425265	0.883009	0.849503872	0.836392	1.169902	0.770685
Env. Variance	0.157381034	0.022362639	-	-	-	-	-
Residual Variance	0.161262888	0.104236798	0.176669	0.145784844	0.107584	0.153066	0.051531
Grand Mean	2.154363684	1.830977394	2.436716	1.872596656	1.874347	1.95768	1.657822
LSD	1.043675952	0.824142849	0.787204	0.722395105	0.624506	0.744523	NA
CV	18.64009824	17.63305443	17.24945	20.38975204	17.4994	19.98472	13.69298
Genotype significance	2.03917E-34	4.66E-106	-	-	-	-	-
Gen × Env significance	1.54425E-59	9.35E-128	-	-	-	-	-

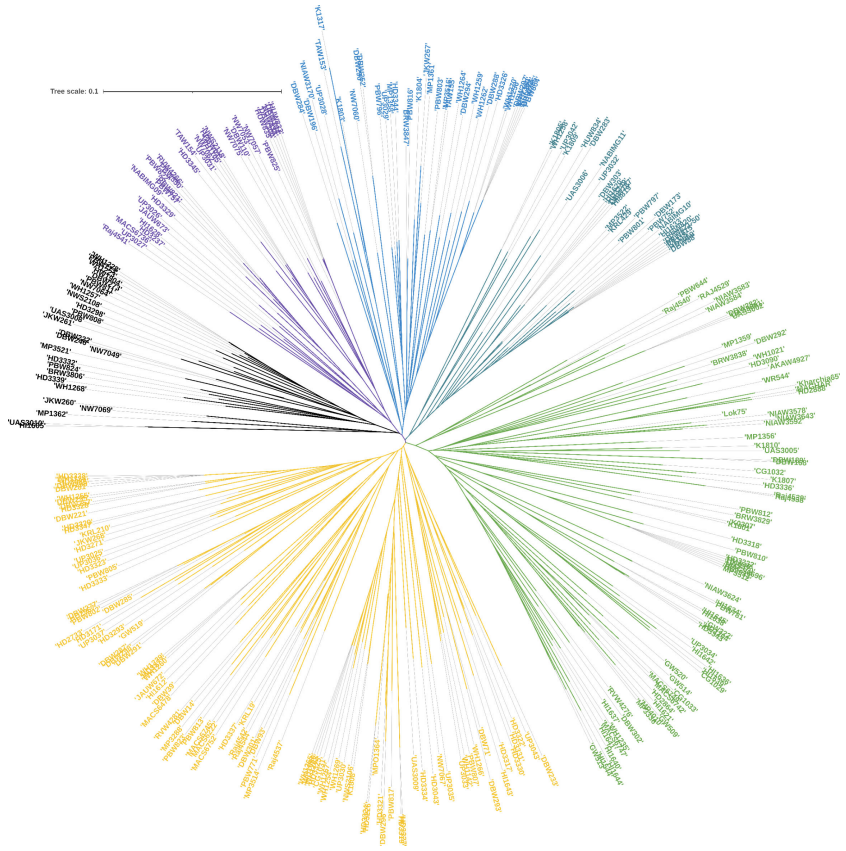

FIGURE 1
Population structures of 296 genotypes revealed by STRUCTURE 2.3.4 and neighbour-joining tree.

detected with a negative effect across the years (2019, 2021) from models MLM and MLMM only (Table 3).

Out of the 49 MTA identified for SNB resistance, 15 were selected to analyse their association with predicted genes and the corresponding biological functions. The criteria for shortlisting MTAs was that they were detected in at least two models or two experiments (See Table 4). Two *Tsn1*-associated markers, 5BL:5324846 and 5BL:3955588, were found to be associated with the transcripts *TraesCS5B02G409000*, *TraesCS5B02G387500*, and *TraesCS5B02G387000*. These transcripts are known to possess biological function pathogen stress response (PADRE) domain, Serine/threonine-protein kinase and Ubiquitin-like proteins respectively. Another marker, 2AS:7487614, has been found to be associated with two genes, namely *TraesCS2A02G107100* and *TraesCS2A02G107200*. These genes are known to have biological roles as a potassium transporter and a plant peroxidase, respectively. As for other MTAs, several noteworthy biological functions have been identified, including cysteine-type endopeptidase inhibitor activity (6B:1085698), NAD(P)-binding domain (4A:1082366), Cytochrome c oxidase subunit 5c, and Serine/threonine-protein kinase, active site (both for 3B:2251334). These functions are believed to play an active role in disease resistance (Table 4).

3.4 The significant role of *Tsn1* and *Snn3* on SNB resistance

The KASP assay revealed that 83 genotypes (25.85%) carry the susceptible allele *Tsn1*, whose SNB indices ranged mostly between 2.4 to 4.2 (Table S3). The allelic combinations at *Tsn1* and *Snn3* were tested using the results obtained from the *Ktsn1* marker and two *Tsn1* linked markers, 5B:5324846 and 5B:3955588, along with *Snn3-B1* linked marker 5BS:1102120. The comparison revealed that the allelic combination of recessive alleles *tsn1/snn3* imparts best resistance to SNB, followed by the *tsn1/Snn3* combination, whereas the allele combinations *Tsn1/snn3* and *Tsn1/Snn3* showed similar levels of resistance, indicating the higher phenotypic effects of *tsn1*(Figure 4).

3.5 Haplotype analysis and staking of R alleles

There were significant differences in the corrected SNB index between resistant and susceptible haplotypes. When compared to the resistance haplotypes “AA/TT” for *tsn1* (mean SNB index 1.69), the susceptibility haplotype “GG” for *Tsn1* had a higher disease

10.3389/fpls.2023.1223959

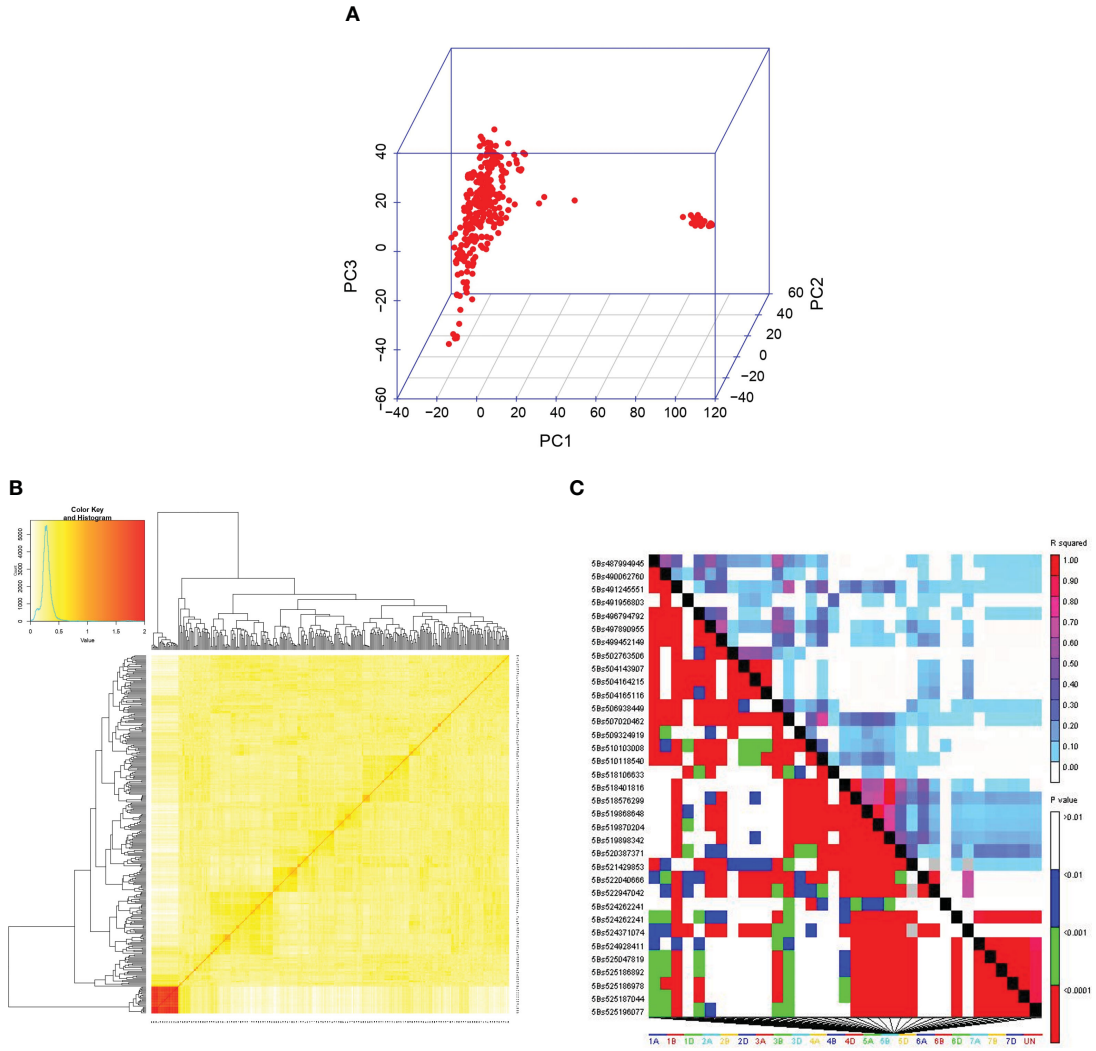

FIGURE 2
(A) 3D plots of principal components (PC). **(B)** The kinship matrix used in GWAS is visualized through a heat map. **(C)** LD matrix obtained from TASSEL 5.0.

index (3.4) (Figure 5). Furthermore, the haplotypes were tested for the four significant SNB QTLs, *Q.CIM.snb.1BL, Q.CIM.snb.2AS.1, Q.CIM.snb.2AS.2*, and *Q.CIM.snb.6BL* (Figure S5). Similarly, there was a significant difference between susceptible and resistant haplotypes for TS index (3.2 for the susceptibility haplotypes and 1.57 for the resistance haplotypes; Figure 5).

The stacking of resistance alleles for SNB and TS exhibited a clear trend that the number of resistance alleles is positively correlated with disease resistance (Figure 6). For example, cultivars DBW 242 and DBW 246, each possessing 35 resistant alleles, exhibited very high SNB resistance, whereas HD 2932 and Kharchiya 65 having the least number of resistance alleles were highly susceptible. A similar trend was observed for TS resistance.

4 Discussion

Utilizing resistant cultivars coupled with management approaches contribute to environmentally and economically sustainable wheat production. The discovery of host-specific gene-for-gene interactions determining the *P. nodorum*-wheat pathosystem and residual genetic resistance (Liu et al., 2004) offers immediate opportunities to further investigate host-genetic resistance in wheat breeding (Ruud and Lillemo, 2018; Peters Haugrud et al., 2022). Evaluations of the Indian wheat cultivars reveal at least 113 genotypes resistant for the TS, 174 genotypes for SNB, and 118 for both the SNB and TS. Out of the top 20 highly resistant genotypes, WH1256, GW 519 and DBW 285 carry the susceptibility allele *Tsn1*, implying that they must have other resistance genes/QTL to counteract the negative effects of *Tsn1*. By checking the pedigree information, it was found that WH1256 and DBW 285 have Chinese progenitors and might have inherited unknown resistance genes.

We found seedling resistance QTL *Q.CIM.snb.2AS* for SNB close to previously reported QTL *QSnb.nmbu-2AS* (4-24 Mbp), which may be associated with two adult-plant leaf blotch QTLs at 2-20 and 15-16 Mbp on the reference genome (Lin et al., 2022). Additionally, this region was also mapped near the seedling

10.3389/fpls.2023.1223959

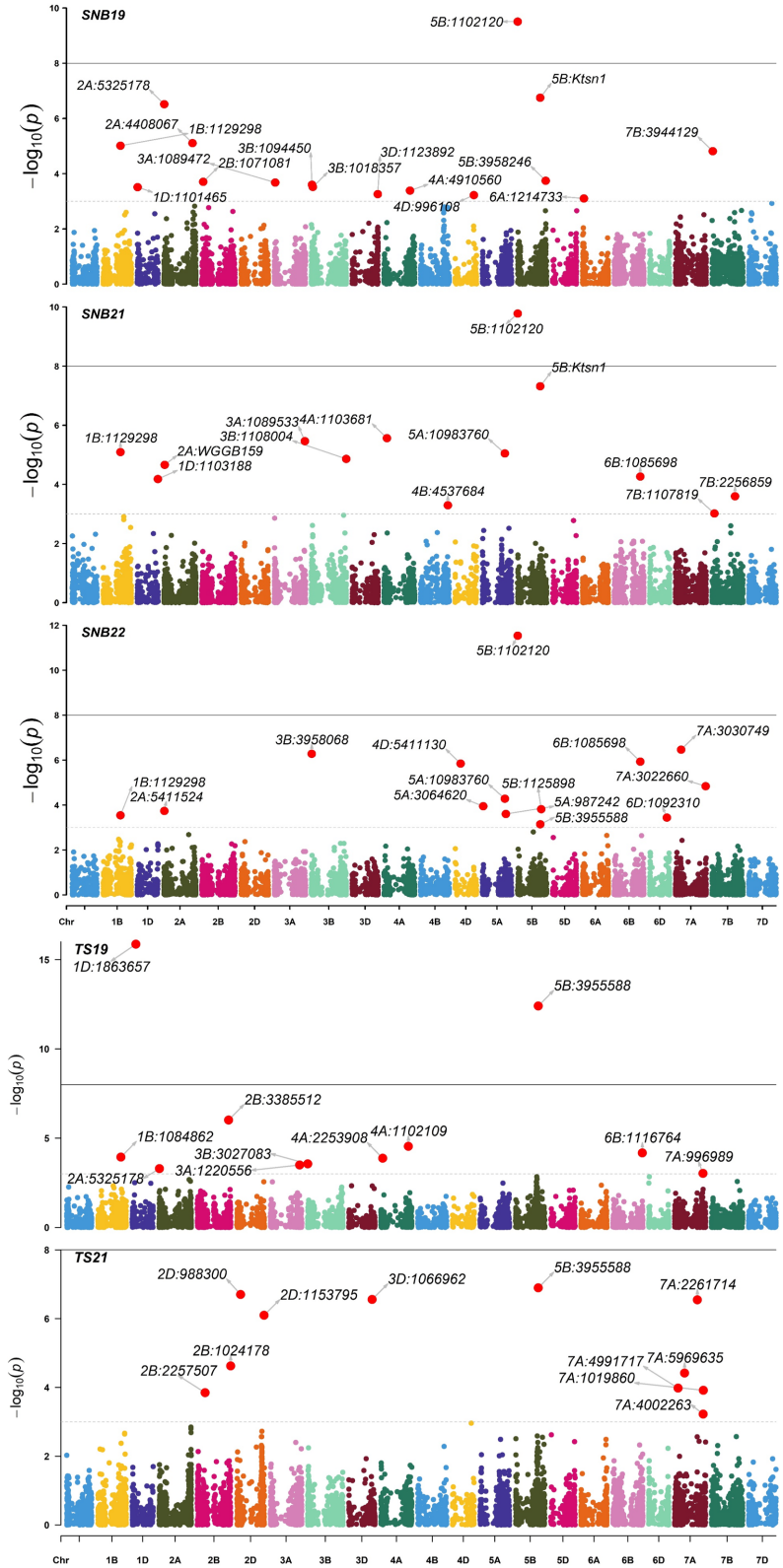

FIGURE 3
Manhattan plots of marker-trait associations detected by the FarmCPU model using 9668 single nucleotide polymorphisms in 296 Indian spring wheat genotypes evaluated for the seedling resistance to Septoria nodorum blotch (SNB) during years 2019, 2021, 2022 and tan spot (TS) during years 2019, 2021. The horizontal line represents the significant threshold −log10(P) = 5.00.

TABLE 3 Markers significantly associated with Septoria nodorum blotch (SNB) and tan spot (TS) resistance through genome-wide association mapping using a mixed linear model (MLM), multi-locus mixed model (MLMM) and fixed and random model circulating probability unification (FarmCPU).

QTL/Susceptibility locus	SNP	Chr	Position	P.value	maf	effect	Experiments	Significant models
Tsn1	5BL:5324846	5BL	566048753	2.02E-04 to 1.96E-05	0.3078	0.329 to 0.362	SNB19, SNB21, SNB22	MLM, MLMM, FarmCPU
Tsn1	5BL:3955588	5BL	584471793	3.80E-04 to 5.43E-09	0.2781	-0.166 to -0.299	SNB19, SNB21, SNB22	MLM, MLMM, FarmCPU
Snn3	5BS:1102120	5BS	6008757	2.31E-05 to 5.99E-12	0.3816	0.246 to 0.365	SNB19, SNB21, SNB22	MLM, MLMM, FarmCPU
Q.CIM.snb.2AS.1	2AS:7487614	2AS	59436678	8.21E-04 to 9.39E-04	0.1277	0.271 to 0.358	SNB19, SNB21, SNB22	MLM, MLMM, FarmCPU
Q.CIM.snb.2AS.2	2AS:1094287	2AS	88181233	1.13E-03 to 9.06E-04	0.4049	-0.258 to -0.320	SNB19, SNB21, SNB22	MLM, MLMM, FarmCPU
Q.CIM.snb.6BL	6BL:1085698	6BL	669137486	4.16E-04 to 1.61E-09	0.2133	0.207 to 0.333	SNB21, SNB22	FarmCPU
Q.CIM.snb.1BL	1BS:1129298	1BS	450506896	2.86E-04 to 8.97E-06	0.1339	0.232 to 0.309	SNB19, SNB21, SNB22	FarmCPU
Tsn1	5BL:5324846	5BL	566048753	3.51E-05 to 5.41E-06	0.3078	0.376 to 0.410	TS19, TS21	MLM, MLMM, FarmCPU
Tsn1	5BL:3955588	5BL	584471793	1.33E-05 to 3.63E-13	0.2781	-0.258 to -0.397	TS19, TS21	MLM, MLMM

TABLE 4 SNPs associated with SNB and TS resistance and possible function elucidated based on the gene annotation using wheat reference sequence (RefSeq V1.0).

Sr	SNP	Position	P.value	Experiment	Model	Genomic region	Transcript	Biological function
1	5B:3955588	584471793	3.80E-04 to 5.43E-09	SNB19, SNB21, SNB22	FarmCPU, MLM, MLMM	5B:584289532-584472557	TraesCS5B02G409000	IPR025322: Pathogen and abiotic stress response, cadmium tolerance, disordered region-containing (PADRE) domain
						5B: 566675237-566683367	TraesCS5B02G387500	IPR008271:Serine/threonine-protein kinase, active site, IPR001611: Leucine-rich repeat, IPR000719: Protein kinase domain
2	5B:5324846	566048753	2.02E-04 to 1.96E-05	SNB19, SNB22	MLM, MLMM	5B:566047792-566128622	TraesCS5B02G387000	IPR000626: Ubiquitin-like proteins
3	5B: 1102120	6008757	2.31E-05 to 5.99E-12	SNB19, SNB21, SNB22	FarmCPU, MLM, MLMM	5B:6006645-6224311	TraesCS5B02G004200	PTHR13523: Coiled coil helix domain containing 2/NUR77
4	2A:1094287	88181233	1.13E-03 to 9.06E-04	SNB21, SNB22	MLM, MLMM	2A:88116755-88181997	TraesCS2A02G143000	IPR013094:Alpha/beta hydrolase fold-3
5	2A:7487614	59436678	8.21E-04 to 9.39E-04	SNB21, SNB22	FarmCPU, MLM, MLMM	2A:59435139-59594492	TraesCS2A02G107100	IPR003855: Potassium transporter
							TraesCS2A02G107200	IPR000823: Plant peroxidase
6	6B:1085698	669137486	4.16E-04 to 1.61E-09	SNB21, SNB22	FarmCPU, MLM, MLMM	6B:669049914-669139405	TraesCS6B02G394200	IPR027214: cysteine-type endopeptidase inhibitor activity
7	1B:1129298	450506896	2.86E-04 to 8.97E-06	SNB19, SNB21, SNB 22	FarmCPU	1B:450449347-450507660	TraesCS1B02G255700	IPR039620: BKI1/Probable membrane-associated kinase regulator 1/3/4

(Continued)

TABLE 4 Continued

Sr	SNP	Position	P.value	Experiment	Model	Genomic region	Transcript	Biological function
8	4D:5411130	143306414	1.42E-06 to 4.05E-04	SNB22	FarmCPU, MLM, MLMM	4D:143303907-143585661	TraesCS4D02G147900	IPR002464: DNA/RNA helicase, ATP-dependent, DEAH-box type, conserved site
9	4A:1082366	82791100	8.54E-04	SNB21	MLM, MLMM	4A:82691100-82891100	TraesCS4A02G080300	IPR036291: NAD(P)-binding domain
10	5B:1092387	622950551	3.77E-04	SNB21	MLM, MLMM	5B:622947949-622988941	TraesCS5B02G451500	IPR009577:Putative small multi-drug export
11	5B:1093198	569332682	9.52E-04	SNB22	MLM, MLMM	5B:569240491-569341529	TraesCS5B02G390100	IPR012876: Protein of unknown function DUF1677, plant
12	5A:10983760	576671605	5.20E-05 to 2.74E-04	SNB22	FarmCPU, MLM, MLMM	5A:576592693-576675256	TraesCS5A02G379400	IPR011141: Polyketide synthase, type III, IPR001099:Chalcone/ stilbene synthase, N-terminal
13	5B:17335879	584572621	8.06E-05	SNB22	MLM, MLMM	5B:584569928-584622467	TraesCS5B02G409100	IPR025757: Ternary complex factor MIP1, leucine-zipper
14	3B:2251334	71642456	4.85E-04	SNB22	MLM, MLMM	3B:71639185-71816436	TraesCS3B02G105900	IPR008432: Cytochrome c oxidase subunit 5c
							TraesCS3B02G106100	IPR017441: Protein kinase, ATP binding site; IPR008271: Serine/ threonine-protein kinase, active site
15	7B:3029515	652894544	6.68E-04	SNB21	MLM, MLMM	7B:652891171-652981239	TraesCS7B02G386800	IPR036574: Knottin, scorpion toxin-like superfamily

resistance QTLs *Snb.niab-2A.1* (0.8-2.4 Mbp) and *Qsnb.cur-2AS2* (2.3-3.8 Mbp) reported by Lin et al. (2020) and Phan et al. (2016), respectively. *Snn3*-B1 has been associated with the short arm of chromosome 5B in previous research (Phan et al., 2016; Ruud et al., 2017; Ruud et al., 2019; Lin et al., 2020). Here, genetic analysis in the Indian wheat cultivars identified one marker 5BS:1102120 tightly linked to *Snn3*-B1 as representing the most significant genetic determinant of SnTox3 sensitivity in Indian germplasm.

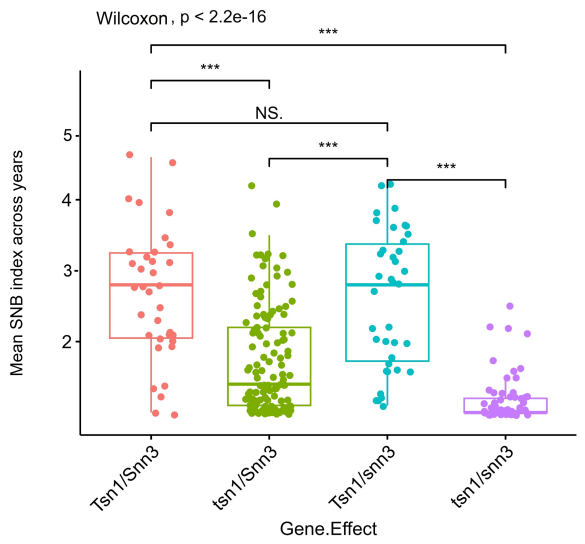

FIGURE 4
Boxplots showing gene interaction effect for *Tsn1* and *Snn3* in response to Septoria nodorum blotch (SNB). *** on boxplots indicates a significant difference in the mean disease index between groups by Wilcoxon test ($p < 0.05$).

Numerous shared QTLs between SNB and TS have been found in an increasing number of publications on the QTL mapping of both diseases (Phuke et al., 2020). A well-known example is *Tsn1* which confers sensitivity to both SnToxA and PtrToxA (Friesen et al., 2006). The current study has proven that *Tsn1* plays a major role in the susceptibility of the Indian panel to SNB and TS. TS resistance in seedlings and adult plants has also been discovered to be significantly influenced by the *P. nodorum* resistance/sensitivity QTL *Qsnb.cur-2AS.1* (Phan et al., 2016), discovered at the seedling and adult plant stage (Phan et al., 2016; Shankar et al., 2017). This phenomenon might suggest similar susceptibility/resistance mechanisms between the two diseases (Lin and Lillemo, 2021; Lin et al., 2022). It would be intriguing to learn if they share any additional effectors. To breed wheat varieties resistant to both diseases, wheat breeders can focus on mutual interactions, particularly for those QTL with relatively large effects and at both the seedling and adult stages.

The primary factor causing leaf necrosis is the HST ToxA, produced by the pathogens *P. nodorum* and *P. tritici-repentis* (produced by races 1, 2, 7, and 8). These pathogens are highly susceptible due to the sensitive gene *Tsn1*. The most prevalent Ptr race, Race 1, can also be found in South Asia and Mexico (Duveiller and Singh, 2009). However, *P. nodorum* from South Asia lacks information on the racial composition, variability, and toxins produced. In the last 25 years, South Asian breeding programs have incorporated new knowledge about resistance to leaf blight disease complex. Researchers and breeders worldwide could

10.3389/fpls.2023.1223959

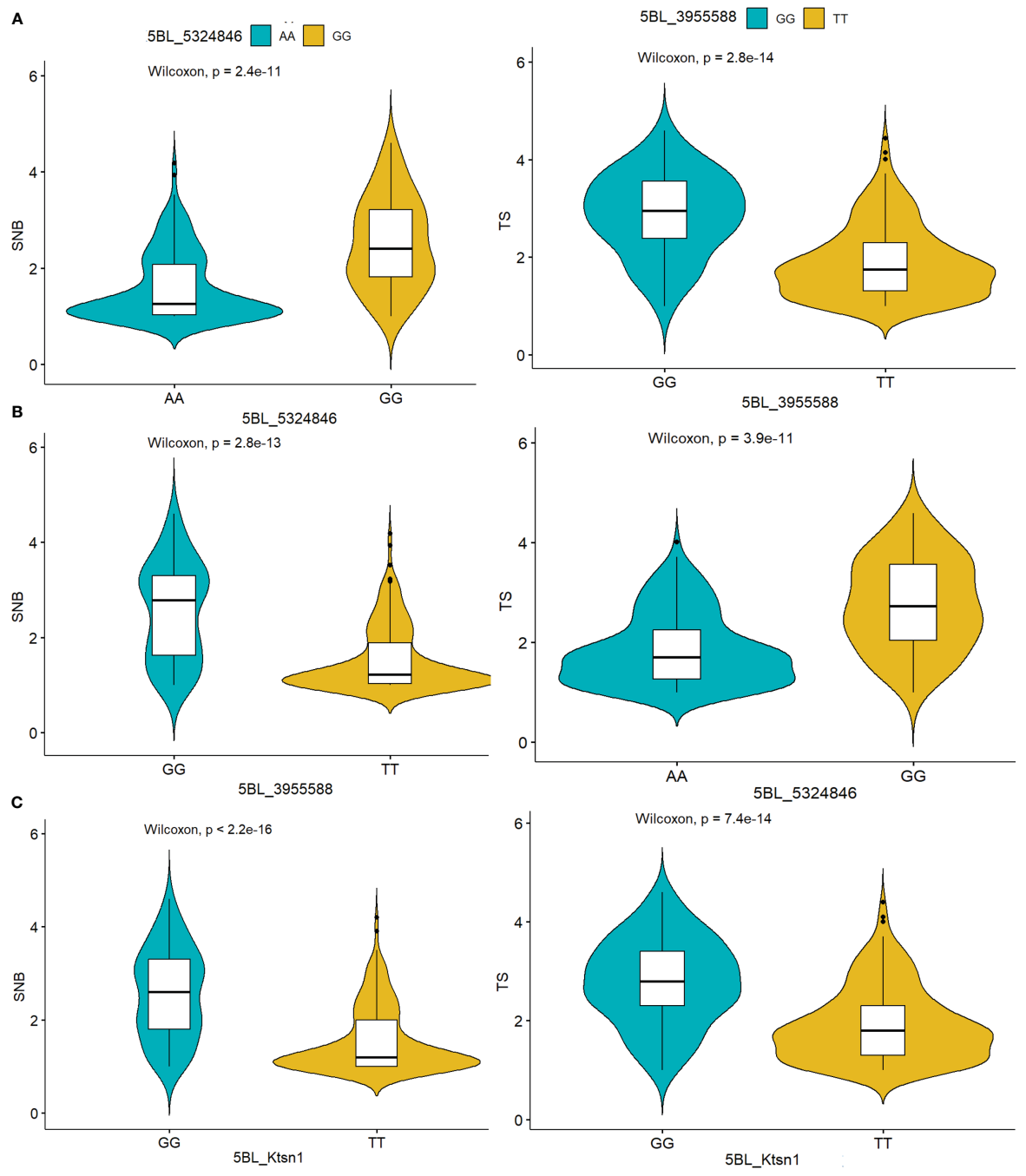

FIGURE 5
Haplotype analysis of the markers **(A)** 5BL:5324846 **(B)** 5BL:3955588 **(C)** KASP marker Ktsn1 indicated their significant association with Septoria nodorum blotch (SNB) and tans spot (TS) resistance determined by the Wilcoxon test.

ascertain the relationship between effector sensitivity and cultivar susceptibility using expressed ToxA since 2005 and Tox3 since 2011. The *ToxA* sequence in various *B. sorokiniana* isolates from India has been analyzed recently, and the results show that the gene is under positive selection (Navathe et al., 2020). The investigations on the pathogenicity factors, variability, and toxin profiling of *P. nodorum* and *P. tritici-repentis* from South Asia is lacking, irrespective of their numerous reports from India and Nepal. The horizontal transfer of *ToxA* between these three pathogens underlines that unless *Tsn1/Snn3* is selectively bred out of widely planted wheat germplasms, it is likely that ToxA will continuously evolve into forms that are more effective in inducing host cell death. Other cutting-edge technologies will accelerate the discovery and functional characterization of effector resistance genes in the coming years and offer effective methods for utilizing these in breeding programs.

India and Nepal have reported SNB, TS, and spot blotch occurrences individually or in the complex. Moreover, climate

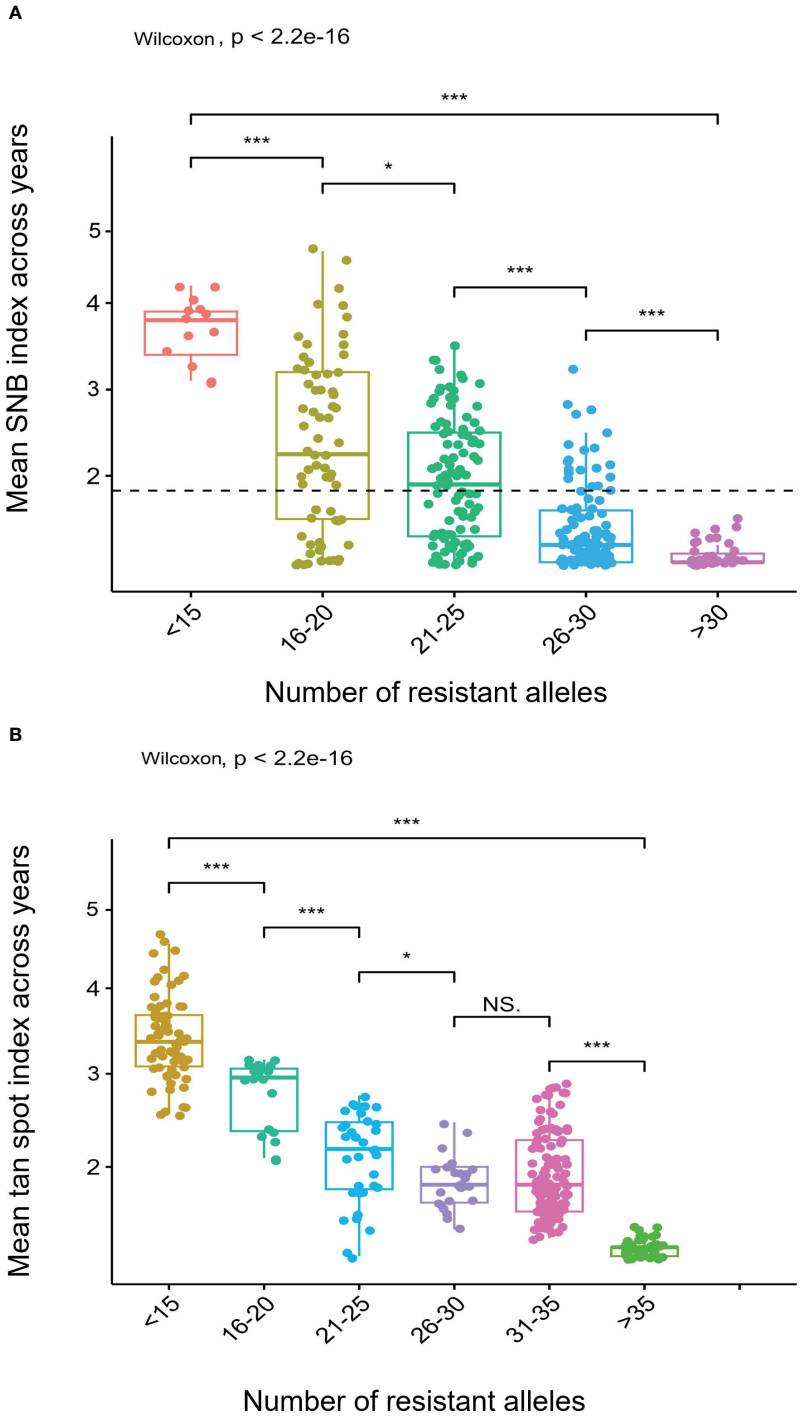

FIGURE 6
Boxplots showing effects of stacking resistant alleles for **(A)** Septoria nodorum blotch (SNB) and **(B)** Tan spot (TS). *** on boxplots indicates a significant difference in the mean disease index between groups by Wilcoxon test ($p < 0.05$).

change has warranted cross-continent jump in wheat diseases and we know very little about the interactions between these three diseases. Further, this subject is especially fascinating given that *P. nodorum, P. tritici-repentis* and *B. sorokiniana* share effectors. Because a new cultivar must be fully assessed at adult plant stage in field conditions, breeding for SNB/TS/SB resistance has always been difficult. The difficulties are made worse by inoculation using a representative group of isolates. Making significant annual isolate collections, especially from the cultivar that is currently most resistant, is one clear recommendation that has come out of recent studies. These novel isolates can be examined phenotypically for novel effectors and virulence traits and

genotypically to follow specific chromosomal regions. Any new effector can be expressed, and their contribution to virulence can be evaluated. The main benefit of isolate collections is that they make it possible to rationally choose the smallest set that accurately captures all the pathogen's phenotypic diversity, against which resistance should be sought.

At present, complete genetic resistance to SNB and TS has not been discovered. Therefore, a multifaceted strategy based on agronomic practices, disease surveillance, and genetic resistance will be required for the effective management of SNB and TS. Nevertheless, genetic resistance will continue to play a major role in managing these diseases. It was interesting to see that some varieties like PBW 771, DBW 277, and HD 3319 displayed high levels of resistance to both diseases. Hence, they must be deployed in the ongoing breeding programs for further enhancement of resistance for SNB and TS. Using field resistance and knowledge about new QTLs will certainly help breeders find much better resistance for these diseases facilitating higher production in the farmer's fields.

Data availability statement

The original contributions presented in the study are included in the article/supplementary material. The genotypic data is available at Dataverse CIMMYT data repository and can be accessed at https://hdl.handle.net/11529/10548934. Further inquiries can be directed to the corresponding author/s.

Author contributions

SN contributed to manuscript writing and data analysis, XH contributed to conceptualization, disease scoring and data analysis, and UK, MK, and MP helped in data analysis and manuscript writing. PKS and AJ contributed to the conceptualization, project monitoring, fund acquisition and revising. GPS and GS contributed to germplasm resources and fund acquisition. All authors contributed to the article and approved the submitted version.

Funding

Financial support from the Indian Council of Agriculture Research (ICAR), India, the Bill and Melinda Gates Foundation through project Accelerating Genetic Gain (AGG) in Maize and Wheat Project Grant INV-003439, USAID, and One CGIAR Initiatives for conducting this research is gratefully acknowledged.

Conflict of interest

The authors declare that the research was conducted in the absence of any commercial or financial relationships that could be construed as a potential conflict of interest.

Publisher's note

All claims expressed in this article are solely those of the authors and do not necessarily represent those of their affiliated organizations, or those of the publisher, the editors and the reviewers. Any product that may be evaluated in this article, or claim that may be made by its manufacturer, is not guaranteed or endorsed by the publisher.

Supplementary material

The Supplementary Material for this article can be found online at: https://www.frontiersin.org/articles/10.3389/fpls.2023.1223959/full#supplementary-material

References

Adhikari, T. B., Jackson, E. W., Gurung, S., Hansen, J. M., and Bonman, J. M. (2011). Association mapping of quantitative resistance to *Phaeosphaeria nodorum* in spring wheat landraces from the USDA National Small Grains Collection. *Phytopathology* 101, 1301–1310. doi: 10.1094/phyto-03-11-0076

Alvarado, G., Rodríguez, F. M., Pacheco, A., Burgueño, J., Crossa, J., Vargas, M., et al. (2020). META-R: a software to analyze data from multi-environment plant breeding trials. *Crop J.* 8, 745–756. doi: 10.1016/j.cj.2020.03.010

Bearchell, S. J., Fraaije, B. A., Shaw, M. W., and Fitt, B. D. L. (2005). Wheat archive links long-term fungal pathogen population dynamics to air pollution. *Proc. Natl. Acad. Sci. U.S.A.* 102, 5438–5442. doi: 10.1073/pnas.0501596102

Bradbury, P. J., Zhang, Z., Kroon, D. E., Casstevens, T. M., Ramdoss, Y., and Buckler, E. S. (2007). TASSEL: Software for association mapping of complex traits in diverse samples. *Bioinformatics* 23, 2633–2635. doi: 10.1093/bioinformatics/btm308

Cat, A., Tekin, M., Akar, T., and Catal, M. (2018). First report of *Stagonospora nodorum* blotch caused by *Parastagonospora nodorum* on emmer wheat (*Triticum dicoccum* Schrank) in Turkey. *J. Plant Pathol.* 17, 42161. doi: 10.1007/s42161-018-00205-2

Chan, E. K., Rowe, H. C., and Kliebenstein, D. J. (2010). Understanding the evolution of defense metabolites in *Arabidopsis thaliana* using genome-wide association mapping. *Genetics* 185, 991–1007. doi: 10.1534/genetics.109.108522

Chona, B. L., and Munjal, R. L. (1952). Glume blotch of wheat in India. *Indian Phytopathol.* 5, 17–20.

Dreisigacker, S., Sehgal, D., Reyes Jaimez, A. E., Luna Garrido, B., Muñoz Zavala, S., Núñez Ríos, C., et al. (2016). *CIMMYT wheat molecular genetics: laboratory protocols and applications to wheat breeding* (Mexico, D.F: CIMMYT).

Dubin, H. J., and Bimb, H. P. (1994). *Studies of soilborne diseases and foliar blights of wheat at the national wheat research experiment station, Bhairahawa, Nepal. Wheat Special Report No. 36* (Mexico DF, Mexico: CIMMYT).

Duveiller, E., Kandel, Y. R., Sharma, R. C., and Shrestha, S. M. (2005). Epidemiology of foliar blights (spot blotch and tan spot) of wheat in the plains bordering the Himalayas. *Phytopathology* 95, 248–256. doi: 10.1094/phyto-95-0248

Duveiller, E., and Singh, P. K. (2009). *Improving Wheat Resistance to Tan Spot caused by Pyrenophora tritici-repentis, Newsletter* (Mexico: CIMMYT). Available at: http://hdl.handle.net/10883/1293.

Earl, D. A., and vonHoldt, B. M. (2012). Structure Harvester: A website and program for visualizing STRUCTURE output and implementing the Evanno method. *Conserv. Genet. Resour.* 4, 359–361. doi: 10.1007/s12686-011-9548-7

Evanno, G., Regnaut, S., and Goudet, J. (2005). Detecting the number of clusters of individuals using the software structure: A simulation study. *Mol. Ecol.* 14, 2611–2620. doi: 10.1111/j.1365-294x.2005.02553.x

Feng, J., Ma, H., and Hughes, G. R. (2004). Genetics of resistance to *Stagonospora nodorum* blotch of hexaploid wheat. *Crop Sci.* 44, 2043–2048. doi: 10.2135/cropsci2004.2043

Friesen, T. L., and Faris, J. D. (2012). Characterization of plant-fungal interactions involving necrotrophic effector–producing plant pathogens. *Methods Mol. Biol.* 835, 191–207. doi: 10.1007/978-1-61779-501-5_12

Friesen, T. L., Meinhardt, S. W., and Faris, J. D. (2007). The *Stagonospora nodorum*–wheat pathosystem involves multiple proteinaceous host-selective toxins and corresponding host sensitivity genes that interact in an inverse gene-for-gene manner. *Plant J.* 51, 681–692. doi: 10.1111/j.1365-313x.2007.03166.x

Friesen, T. L., Stukenbrock, E. H., Liu, Z. H., Meinhardt, S., Ling, H., and Faris, J. D. (2006). Emergence of a new disease as a result of interspecific virulence gene transfer. *Nat. Genet.* 38, 953–956. doi: 10.1038/ng1839

Graves, S., Piepho, H., and Selzer, L. (2015) *Dorai-Raj, S. multcompView: visualizations of paired comparisons version 01–7*. Available at: https://cranr-project.org/web/packages/multcompView/index.html.

Gurung, S., Mamidi, S., Bonman, J. M., Xiong, M., Brown-Guedira, G., and Adhikari, T. B. (2014). Genome-wide association study reveals novel quantitative trait loci associated with resistance to multiple leaf spot diseases of spring wheat. *PloS One* 9, e108179. doi: 10.1371/journal.pone.0108179

Gurung, S., Sharma, R. C., Duveiller, E., and Shrestha, S. M. (2012). Comparative analyses of spot blotch and tan spot epidemics on wheat under optimum and late sowing period in South Asia. *Eur. J. Plant Pathol.* 134, 257–266. doi: 10.1007/s10658-012-9984-6

Hosford, R. M. Jr. (1982). *Tan spot of wheat and related diseases workshop*. Ed. R. M. Hosford Jr (North Dakota State Univ., Fargo USA), 1–24.

Hu, W., He, X., Dreisigacker, S., Sansaloni, C. P., Juliana, P., and Singh, P. K. (2019). A wheat chromosome 5AL region confers seedling resistance to both tan spot and Septoria nodorum blotch in two mapping populations. *Crop J.* 7, 809–818. doi: 10.1016/j.cj.2019.05.004

International Wheat Genome Sequencing Consortium, Appels, R., Eversole, K., Stein, N., Feuillet, C., Keller, B., Rogers, J., et al. (2018). Shifting the limits in wheat research and breeding using a fully annotated reference genome. *Science* 361, eaar7191. doi: 10.1126/science.aar7191

Joshi, L. M., Saari, E. E., and Wilcoxson, R. D. (1971). Epidemic of glume blotch on wheat and reaction of wheat varieties to. *Septoria nodorum. Indian Phytopathol.* 24, 413–415.

Kassambara, A. (2020). *ggpubr: 'ggplot2' based publication ready plots. R package version 0.4.0*. Available at: https://CRAN.R-project.org/package=ggpubr.

Katoch, S., Rana, S. K., and Sharma, P. N. (2019). Application of PCR based diagnostics in the exploration of *Parastagonospora nodorum* prevalence in wheat growing regions of Himachal Pradesh. *J. Plant Biochem. Biotechnol.* 28, 169–175. doi: 10.1007/s13562-018-0481-7

Kokhmetova, A., Sehgal, D., Ali, S., Atishova, M., Kumarbayeva, M., Leonova, I., et al. (2021). Genome-wide association study of tan spot resistance in a hexaploid wheat collection from Kazakhstan. *Front. Genet.* 11. doi: 10.3389/fgene.2020.581214

Lamari, L., and Bernier, C. C. (1989). Evaluation of wheat lines and cultivars to tan spot (*Pyrenophora tritici-repentis*) based on lesion type. *Can. J. Plant Pathol.* 11, 49–56. doi: 10.1080/07060668909501146

Letunic, I., and Bork, P. (2021). Interactive Tree of Life (iTOL) v5: an online tool for phylogenetic tree display and annotation. *Nucleic Acids Res.* 49 (W1), W293–W296. doi: 10.1093/nar/gkab301

Li, H., Vikram, P., Singh, R. P., Kilian, A., Carling, J., Song, J., et al. (2016). A high-density GBS map of bread wheat and its application for dissecting complex disease resistance traits. *BMC Genom.* 16, 216. doi: 10.1186/s12864-015-1424-5

Lin, M., Corsi, B., Ficke, A., Tan, K. C., Cockram, J., and Lillemo, M. (2020). Genetic mapping using a wheat multi-founder population reveals a locus on chromosome 2A controlling resistance to both leaf and glume blotch caused by the necrotrophic fungal pathogen *Parastagonospora nodorum*. *Theor. Appl. Genet.* 133, 785–808. doi: 10.1007/s00122-019-03507-w

Lin, M., Ficke, A., Dieseth, J. A., and Lillemo, M. (2022). Genome-wide association mapping of Septoria nodorum blotch resistance in Nordic winter and spring wheat collections. *Theor. Appl. Genet.* 135, 4169–4182. doi: 10.1007/s00122-022-04210-z

Lin, M., and Lillemo, M. (2021). "Advances in genetic mapping of Septoria nodorum blotch resistance in wheat and applications in resistance breeding," in *Achieving durable disease resistance in cereals*. Ed. R. P. Oliver (Burleigh Dodds Science Publishing, Cambridge, UK), 393–433. doi: 10.1201/9781003180715-15

Liu, Z., El-Basyoni, I., Kariyawasam, G., Zhang, G., Fritz, A., and Hansen, J. (2015). Evaluation and association mapping of resistance to tan spot and Stagonospora nodorum blotch in adapted winter wheat germplasm. *Plant Dis.* 99, 1333–1341. doi: 10.1094/pdis-11-14-1131-re

Liu, Z. H., Faris, J. D., Meinhardt, S. W., Ali, S., Rasmussen, J. B., and Friesen, T. L. (2004). Genetic and physical mapping of a gene conditioning sensitivity in wheat to a partially purified host-selective toxin produced by Stagonospora nodorum. *Phytopathology* 94, 1056–1060. doi: 10.1094/phyto.2004.94.10.1056

Liu, Z. H., Faris, J. D., Oliver, R. P., Tan, K. C., Solomon, P. S., and McDonald, M. C. (2009). SnTox3 acts in effector triggered susceptibility to induce disease on wheat carrying the *Snn3* gene. *PloS Pathog.* 5, e1000581. doi: 10.1371/journal.ppat.1000581

Lozano-Ramírez, N., Dreisigacker, S., Sansaloni, C. P., He, X., Islas, S. S., Pérez-Rodríguez, P., et al. (2022). Genome-wide association study for resistance to tan spot in synthetic hexaploid wheat. *Plants* 11, 433. doi: 10.3390/plants11030433

McIntosh, R. A., Yamazaki, Y., Dubcovsky, J., Rogers, J., Morris, C., Somers, D. J., et al. (2008). *Catalogue of gene symbols for wheat* (MacGene). Available at: http://wheat.pw.usda.gov/GG2/Triticum/wgc/2008/.

Misra, A. P., and Singh, R. A. (1972). Pathogenic differences among three isolates of *Helminthosporium tritici - repentis* and the performance of wheat varieties against them. *Indian Phytopathol.* 25, 350–353.

Mitra, M. (1934). A leaf spot disease of wheat caused by *Helminthosporium tritici-repentis* Died. *Indian J. Agric. Sci.* 4, 692–700.

Navathe, S., Yadav, P. S., Chand, R., Mishra, V. K., Vasistha, N. K., Meher, P. K., et al. (2020). *ToxA–Tsn1* interaction for spot blotch susceptibility in Indian wheat: An example of inverse gene-for-gene relationship. *Plant Dis.* 104, 71–81. doi: 10.1094/pdis-05-19-1066-re

Oliver, R. P., Friesen, T. L., Faris, J. D., and Solomon, P. S. (2012). *Stagonospora nodorum*: from pathology to genomics and host resistance. *Annu. Rev. Phytopathol.* 50, 23–43. doi: 10.1146/annurev-phyto-081211-173019

Peters Haugrud, A. R., Zhang, Z., Friesen, T. L., and Faris, J. D. (2022). Genetics of resistance to Septoria nodorum blotch in wheat. *Theor. Appl. Genet.* 135, 3685–3707. doi: 10.1007/s00122-022-04036-9

Phan, H. T., Rybak, K., Bertazzoni, S., Furuki, E., Dinglasan, E., Hickey, L. T., et al. (2018). Novel sources of resistance to Septoria nodorum blotch in the Vavilov wheat collection identified by genome-wide association studies. *Theor. Appl. Genet.* 131, 1223–1238. doi: 10.1007/s00122-018-3073-y

Phan, H. T., Rybak, K., Furuki, E., Breen, S., Solomon, P. S., and Oliver, R. P. (2016). Differential effector gene expression underpins epistasis in a plant fungal disease. *Plant J.* 87, 343–354. doi: 10.1111/tpj.13203

Phuke, R. M., He, X., Juliana, P., Bishnoi, S. K., Singh, G. P., Kabir, M. R., et al. (2020). Association mapping of seedling resistance to tan spot (*Pyrenophora tritici-repentis* race 1) in CIMMYT and South Asian wheat germplasm. *Front. Plant Sci.* 11. doi: 10.3389/fpls.2020.01309

Pritchard, J. K., Stephens, M., and Donnelly, P. (2000). Inference of population structure using multilocus genotype data. *Genetics* 155, 945–959. doi: 10.1093/genetics/155.2.945

Rana, S. K., Paul, Y. S., and Singh, D. (2000). Occurrence of glume blotch of wheat in Himachal Pradesh. *J. Mycol Plant Pathol.* 30, 427–428.

R Core Team. (2022). *R: A language and environment for statistical computing* (Vienna, Austria: R Foundation for Statistical Computing). Available at: https://www.R-project.org/.

Ruud, A. K., Dieseth, J. A., Ficke, A., Furuki, E., Phan, H. T., Oliver, R. P., et al. (2019). Genome-wide association mapping of resistance to *Septoria nodorum leaf blotch* in a Nordic spring wheat collection. *Plant Genome* 12, 180105. doi: 10.3835/plantgenome2018.12.0105

Ruud, A. K., and Lillemo, M. (2018). "Diseases affecting wheat: Septoria nodorum blotch," in *Integrated disease management of wheat and barley*. Ed. R. P. Oliver (Cambridge, UK: Burleigh Dodds Science Publishing Ltd.). doi: 10.19103/as.2018.0039.06

Ruud, A. K., Windju, S., Belova, T., Friesen, T. L., and Lillemo, M. (2017). Mapping of *SnTox3–Snn3* as a major determinant of field susceptibility to Septoria nodorum leaf blotch in the SHA3/CBRD Naxos population. *Theor. Appl. Genet.* 130, 1361–1374. doi: 10.1007/s00122-017-2893-5

Shankar, M., Jorgensen, D., Taylor, J., Chalmers, K. J., Fox, R., Hollaway, G. J., et al. (2017). Loci on chromosomes 1A and 2A affect resistance to tan (yellow) spot in wheat populations not segregating for *tsn1*. *Theor. Appl. Genet.* 130, 2637–2654. doi: 10.1007/s00122-017-2981-6

Shaw, M. W., Bearchell, S. J., Fitt, B. D. L., and Fraaije, B. A. (2008). Long term relationships between environment and abundance in wheat of *Phaeosphaeria nodorum* and *Mycosphaerella graminicola*. *New Phytol.* 177, 229–238. doi: 10.1111/j.1469-8137.2007.02236.x

Singh, D. P. (2007). First report of tan spot of wheat caused by *Pyrenophora tritici-repentis* in the Northern Hills and Northwestern Plains Zones of India. *Plant Dis.* 91, 460. doi: 10.1094/pdis-91-4-0460c

Singh, P. K., Crossa, J., Duveiller, E., Singh, R. P., and Djurle, A. (2016). Association mapping for resistance to tan spot induced by *Pyrenophora tritici-repentis race 1* in CIMMYTs historical bread wheat set. *Euphytica* 207, 515–525. doi: 10.1007/s10681-015-1528-7

Singh, P. K., Mergoum, M., Adhikari, T. B., Kianian, S. F., and Elias, E. M. (2007). Chromosomal location of genes for seedling resistance to tan spot and *Stagonospora nodorum* blotch in tetraploid wheat. *Euphytica* 155, 27–34. doi: 10.1007/s10681-006-9297-y

Solomon, P., Lowe, R. G. T., Tan, K.-C., Waters, O. D. C., and Oliver, R. P. (2006). *Stagonospora nodorum*: cause of Stagonospora nodorum blotch of wheat. *Mol. Plant Pathol.* 7, 147–156. doi: 10.1111/j.1364-3703.2006.00326.x

Tan, K. C., Ferguson-Hunt, M., Rybak, K., Waters, O. D., Stanley, W. A., Bond, C. S., et al. (2012). Quantitative variation in effector activity of ToxA isoforms from *Stagonospora nodorum* and *Pyrenophora tritici-repentis*. *MPMI* 25, 515–522. doi: 10.1094/mpmi-10-11-0273

Van Raden, P. M. (2008). Efficient methods to compute genomic predictions. *J. Dairy Sci.* 91, 4414–4423. doi: 10.3168/jds.2007-0980

Wang, J., and Zhang, Z. (2021). GAPIT Version 3: Boosting power and accuracy for genomic association and prediction. Genomics Proteomics. *Bioinformatics* 19, 629–640. doi: 10.1016/j.gpb.2021.08.005

Wegulo, S. N. (2011). *Tan spot of cereals* (The Plant Health Instructor, The American Phytopathological Society, St. Paul, MN, USA). doi: 10.1094/PHI-I-2011-0426-01

Yu, J., Pressoir, G., Briggs, W. H., Vroh Bi, I., Yamasaki, M., Doebley, J. F., et al. (2006). A unified mixed-model method for association mapping that accounts for multiple levels of relatedness. *Nat. Genet.* 38, 203–208. doi: 10.1038/ng1702

frontiers | Frontiers in Plant Science

TYPE Original Research
PUBLISHED 12 October 2023
DOI 10.3389/fpls.2023.1182548

Check for updates

OPEN ACCESS

EDITED BY
Runsheng Ren,
Jiangsu Academy of Agricultural Sciences (JAAS), China

REVIEWED BY
Filippo Maria Bassi,
International Center for Agricultural Research in the Dry Areas (ICARDA), Morocco
Qin Yang,
Northwest A&F University, China

*CORRESPONDENCE
Jemanesh K. Haile
jemanesh.haile@usask.ca;
hailej@canolacouncil.org

†PRESENT ADDRESSES
Jemanesh K. Haile,
Canola Council of Canada, Crop Productionand Innovation, Saskatoon, SK, Canada
Demissew Sertse,
Department of Plant Sciences, University of Manitoba, Winnipeg, MB, Canada

RECEIVED 08 March 2023
ACCEPTED 18 September 2023
PUBLISHED 12 October 2023

CITATION
Haile JK, Sertse D, N'Diaye A, Klymiuk V, Wiebe K, Ruan Y, Chawla HS, Henriquez M-A, Wang L, Kutcher HR, Steiner B, Buerstmayr H and Pozniak CJ (2023) Multi-locus genome-wide association studies reveal the genetic architecture of *Fusarium* head blight resistance in durum wheat. *Front. Plant Sci.* 14:1182548. doi: 10.3389/fpls.2023.1182548

COPYRIGHT
© 2023 Haile, Sertse, N'Diaye, Klymiuk, Wiebe, Ruan, Chawla, Henriquez, Wang, Kutcher, Steiner, Buerstmayr and Pozniak. This is an open-access article distributed under the terms of the Creative Commons Attribution License (CC BY). The use, distribution or reproduction in other forums is permitted, provided the original author(s) and the copyright owner(s) are credited and that the original publication in this journal is cited, in accordance with accepted academic practice. No use, distribution or reproduction is permitted which does not comply with these terms.

Multi-locus genome-wide association studies reveal the genetic architecture of *Fusarium* head blight resistance in durum wheat

Jemanesh K. Haile[1*†], Demissew Sertse[2†], Amidou N'Diaye[1], Valentyna Klymiuk[1], Krystalee Wiebe[1], Yuefeng Ruan[3], Harmeet S. Chawla[4], Maria-Antonia Henriquez[5], Lipu Wang[1], Hadley R. Kutcher[1], Barbara Steiner[6], Hermann Buerstmayr[6] and Curtis J. Pozniak[1]

[1]Department of Plant Sciences, Crop Development Centre, University of Saskatchewan, Saskatoon, SK, Canada, [2]Aquatic and Crop Resource Development, National Research Council Canada, Saskatoon, SK, Canada, [3]Swift Current Research and Development Centre, Agriculture and Agri-Food Canada, Swift Current, SK, Canada, [4]Department of Plant Sciences, University of Manitoba, Winnipeg, MB, Canada, [5]Morden Research and Development Centre, Agriculture and Agri-Food Canada, Morden, MB, Canada, [6]Department of Agrobiotechnology, Institute of Biotechnology in Plant Production, University of Natural Resources and Life Sciences Vienna, Tulln, Austria

Durum wheat is more susceptible to Fusarium head blight (FHB) than other types or classes of wheat. The disease is one of the most devastating in wheat; it reduces yield and end-use quality and contaminates the grain with fungal mycotoxins such as deoxynivalenol (DON). A panel of 265 Canadian and European durum wheat cultivars, as well as breeding and experimental lines, were tested in artificially inoculated field environments (2019–2022, inclusive) and two greenhouse trials (2019 and 2020). The trials were assessed for FHB severity and incidence, visual rating index, *Fusarium*-damaged kernels, DON accumulation, anthesis or heading date, maturity date, and plant height. In addition, yellow pigment and protein content were analyzed for the 2020 field season. To capture loci underlying FHB resistance and related traits, GWAS was performed using single-locus and several multi-locus models, employing 13,504 SNPs. Thirty-one QTL significantly associated with one or more FHB-related traits were identified, of which nine were consistent across environments and associated with multiple FHB-related traits. Although many of the QTL were identified in regions previously reported to affect FHB, the QTL *QFhb-3B.2*, associated with FHB severity, incidence, and DON accumulation, appears to be novel. We developed KASP markers for six FHB-associated QTL that were consistently detected across multiple environments and validated them on the Global Durum Panel (GDP). Analysis of allelic diversity and the frequencies of these revealed that the lines in the GDP harbor between zero and six resistance alleles. This study provides a comprehensive assessment of the genetic basis of FHB resistance and DON accumulation in durum wheat. Accessions with

multiple favorable alleles were identified and will be useful genetic resources to improve FHB resistance in durum breeding programs through marker-assisted recurrent selection and gene stacking.

KEYWORDS

durum wheat, FHB resistance, DON, GWAS, multi-locus, GDP, KASP markers

1 Introduction

According to FAO, food production needs to increase by 70% (baseline 2009) to feed a growing world population, which is projected to reach ~9.1 billion by 2050 (FAO, 2009). Reports that considered recent consumption behaviors and updated 2050 population projections (~10 billion) estimate that crop production of food crops will need to be increased by 119% to meet the demand (Berners-Lee et al., 2018). While achieving this production goal is feasible, major biotic and abiotic constraints further constrain crop production. For example, diseases and other pests account for up to 40% of annual yield loss in crop production (Savary et al., 2012). The prevalence of diseases and other pests has been exacerbated by increasing climate-change-related burdens and world trade and movements (Carvajal-Yepes et al., 2019; Prank et al., 2019).

Wheat is the most important cereal crop in the world; it is produced on 217 million hectares globally and is a major source of nutrition and caloric intake (OECD/FAO, 2019). However, diseases and other pests heavily constrain wheat production in general and durum wheat in particular. An average yield loss in wheat due to biotic stresses is estimated to be over 20% a year (Savary et al., 2019). Most wheat diseases are fungal-caused, and genetic resistance has been effective in controlling several diseases, like wheat rust. However, *Fusarium* head blight (FHB) (Miedaner et al., 2017) remains one of the most destructive diseases of wheat worldwide, especially for durum wheat, because it is generally the most susceptible of the small-grained cereals. Breeding for FHB resistance is a priority, but it is hindered by its complex genetic architecture, significant genotype-by-environment interaction, and high cost of phenotype testing. In addition to direct yield losses caused by FHB, indirect losses due to the contamination of infected kernels with *Fusarium* mycotoxins are becoming a primary concern.

Mycotoxins are toxic substances that cause a significant annual economic loss to the agriculture and food industries. Each year, approximately 25% of agricultural commodities are contaminated by mycotoxins. One of the major mycotoxins in the wheat supply chain with a critical health risk potential is deoxynivalenol (DON). DON is a trichothecene mycotoxin produced by *Fusarium graminearum* and *Fusarium culmorum* (Mirocha et al., 1994). It is also known as vomitoxin, which is harmful to humans and animals after consumption (Foroud et al., 2019) because it can cause vomiting, anorexia, growth retardation, immune suppression, inflammation and necrosis of various tissues, and diarrhea in animals (Pestka and Smolinski, 2005). The Codex Committee on Contaminants in Food develops and proposes international food safety standards and codes of practice and has set the maximum DON allowable at 2.0 mg/kg for cereal grains, including wheat (Canadian Grain Commission, 2019). Therefore, breeding for FHB-resistant cultivars, together with an integrated disease management strategy, is the most effective, economical, and environment-friendly way to combat the disease globally.

Most current durum wheat cultivars are highly susceptible to FHB, and breeding progress is hampered by the narrow genetic variation for FHB resistance in elite germplasm. Compared to hexaploid wheat, fewer resistance loci are reported for FHB resistance in tetraploid wheat. Furthermore, most of these quantitative trait loci (QTL) possess only minor or moderate effects compared to the major resistance loci in hexaploid wheat, e.g., *Fhb1* located on chromosome 3BS, *Fhb2* located on chromosome 6BS, and *Qfhs.ifa-5A* are all derived from the resistant Chinese cultivar "Sumai 3" (Prat et al., 2014). Introgression of resistance genes from hexaploid into durum wheat has been largely unsuccessful, except for a recent report where introgression of *Fhb1* from Sumai 3 into durum wheat resulted in an improved resistance response (Giancaspro et al., 2016; Prat et al., 2017). In addition, FHB resistance in wheat is usually negatively associated with agronomic traits such as semi-dwarfness and other plant phenological traits, a fact that complicates the genetic mapping of resistance loci or deploying them in breeding. There is compelling evidence supporting a negative correlation between FHB resistance and plant height (PH) and heading date (HD), which is often reflected in the colocalization of PH and HD QTL with FHB resistance QTL (Buerstmayr et al., 2003; Buerstmayr et al., 2012; Sari et al., 2018; Sari et al., 2020). In addition, the widely deployed dwarfing allele *Rht-B1* has been associated with FHB susceptibility (Buerstmayr and Buerstmayr, 2016; He et al., 2016a). Buerstmayr et al. (2020) summarized the influence of PH, anther extrusion/retention, and HD/flowering time on FHB response. This has motivated the phenotyping of agro-morphological traits along with FHB resistance for most recent FHB studies (Haile et al., 2020).

Despite the lack of genetic diversity for FHB resistance, several studies have identified FHB resistance QTL derived from tetraploid wheat, suggesting the presence of minor-effect resistance that could be the focus of gene pyramiding strategies. Several genome-wide

association studies (GWAS) have been reported using tetraploid wheat germplasm, including a Canadian durum wheat breeding panel (Sari et al., 2020), Tunisian-derived durum wheat populations (Ghavami et al., 2011), diverse durum lines from Northern America, the Mediterranean, Central Europe, Australia, and CIMMYT (Steiner et al., 2019b), and a durum association mapping panel mainly comprising Canadian breeding lines (Ruan et al., 2020). Most of the QTL mapping studies assessed type II resistance (resistance to fungal spread); however, other types of FHB resistance, such as resistance to DON accumulation, although more challenging to study, are also important. Moreover, most of the previous GWAS were performed based on single-locus models, such as the General Linear Model (GLM) and the Mixed Linear Model (MLM) (Bradbury et al., 2007). However, single-locus genome-wide association studies (SL-GWAS) are limited in detecting marginal effect quantitative trait nucleotides (QTNs) (Zhang et al., 2019b). Thus, many important loci associated with the target traits remain undiscovered because they do not satisfy the stringent criterion of the significance test. Current advances in multi-locus GWAS (ML-GWAS) models have improved the power and reliability of identifying causal loci for complex traits. to identify causal loci for complex traits. ML-GWAS also has a lower false-positive rate. It has been successfully applied to identify significant QTNs with subtle contributions to several agronomic traits in maize (Xu et al., 2018), rice (Misra et al., 2018), flax (Sertse et al., 2019), cotton (Li et al., 2018), and leaf rust in wheat (Fatima et al., 2020). At the same time, no studies have yet used ML-GWAS for FHB-related traits in durum wheat.

Thus, in the current study, we have analyzed a panel of Canadian and European durum wheat cultivars and breeding lines genotyped with the wheat 90K array and phenotyped for resistance to FHB to (1) determine the genetic architecture of FHB resistance, including resistance to DON accumulation, (2) test several GWAS models, including the SL and ML for FHB resistance-related traits, (3) identify potential candidate genes linked to the associated QTL, and (4) develop Kompetitive Allele-Specific PCR (KASP) markers from the QTL regions for utilization in plant breeding programs. In addition, we have addressed *Fusarium*-damaged kernels (FDK) and the relationship between FHB and quality traits such as protein content (PRO) and yellow pigment (YP). The results provide an insight into the complex genetic architecture of FHB resistance and reveal the QTL and genotypes of potential breeding value for FHB resistance. Additionally, the results should help better understand the genetic basis and diversity of DON accumulation in durum wheat and facilitate the reduction of DON contamination by stacking DON resistance QTL using marker-assisted selection (MAS).

2 Materials and methods

2.1 Plant materials

The germplasm used in this study consisted of 265 lines (Supplementary Table S1). This panel was primarily composed of durum from Canada, including elite Canadian and USA cultivars, advanced breeding lines, and recently developed germplasm from Canadian breeding programs (Crop Development Centre, University of Saskatchewan and Swift Current Research and Development Centre, Agriculture and Agri-food Canada) and research projects. The breeding lines and the cultivars were genotyped with *Rht-B1b* as per the previously published protocol (N'Diaye et al., 2017). The remaining lines were European *Triticum durum* cultivars and experimental lines developed by single seed descent by crossing a resistant tetraploid experimental line DBC-480 to Karur and Durobonus (susceptible European *T. durum* cultivars) and the advanced breeding line SZD1029K (Supplementary Table S1). These lines were developed and provided by the University of Natural Resources and Life Sciences, Vienna, Department of Agrobiotechnology, Institute of Biotechnology in Plant Production (IFA-Tulln), Austria, for this study. Karur and Durobonus are registered varieties in France and Austria, respectively. The DBC-480 line was developed at IFA-Tulln, Austria, by four generations of marker-assisted backcrossing of the highly resistant *Triticum aestivum* cultivar Sumai 3 into the background of the Austrian *T. durum* variety Semperdur and subjected to rigorous phenotypic selection for improved FHB resistance in field trials (Prat et al., 2017). The presence of the resistant *Fhb1* allele was verified using the SSR markers *Xgwm389, Xgwm533*, and *Xgwm493*. Cultivars Karur, Durobonus, and SZD1029K possess the semi-dwarfing allele *Rht-B1b*, while DBC-480 is a tall line harboring the *Rht-B1a* wild-type allele (Prat et al., 2017). Additionally, experimental lines descending from crosses of *T. durum* cultivars with moderately FHB-resistant *Triticum dicoccoum* and/or *Triticum dicoccoides* accessions from the IFA-Tulln, Austria, research program were also part of this study.

2.2 Phenotyping

Phenotypic data were obtained from multiple experiments conducted from 2019 to 2022 (inclusive) at FHB field nurseries (abbreviated afterward as FL) in Saskatoon (NSF), Saskatchewan, and Morden (MR), Manitoba, Canada, and in 2019 and 2020 in the University of Saskatchewan's Crop Development Centre's Greenhouse (GH), Saskatoon, SK (Supplementary Table S11). The infection recorded in 2021 was generally lower than normal because of extreme drought conditions (Supplementary Figure S1).

2.2.1 Screening in the field FHB nurseries

At Saskatoon, the 265 lines were planted at the FHB nursery in hill plots with FHB susceptible and resistant checks in a randomized complete block design with three replications. For artificial inoculation, the inoculum was prepared by mixing equal amounts of spores from two virulent DON-producing *Fusarium graminearum* isolates, *Fg003* and *Fg004*, 3-*O*-acetyl-DON (3-AcDON) and 15-*O*-acetyl-DON (15-AcDON), respectively, originally collected from Saskatchewan. Aliquots of conidia stock solutions were stored at −20°C, then thawed at 37°C and diluted with distilled water to obtain the anticipated final spore concentration just before inoculation. Inoculations were performed when 50% of the plants in the earliest plot reached anthesis using a motor-driven backpack sprayer in the

late afternoons. About 100 ml m^{-2} of conidial suspension at each inoculation cycle was sprayed onto the durum wheat heads. Inoculations were repeated at 2-day intervals and ended 2 days after the last plot flowered, resulting in up to six applications per plot. A sprinkler irrigation system provided adequate moisture after each inoculation to promote spore germination and fungal infection.

Agro-morphological traits, HD or anthesis (AD), days to maturity (MAT), and PH were assessed for all entries to determine their possible association with FHB traits. Heading date was recorded as the number of days from planting to the date when 50% of the heads in a plot had emerged, AD as days from planting until the first anther extruded out from the floret, and MAT when 50% of the plants reached physiological maturity. Plant height (cm) was measured as the distance from the base of the plant to the top of the spike, excluding awns. FHB incidence (INC) was the percentage of FHB-infected spikes/plots, and severity (SEV) was the percentage of symptomatic spikelets visually estimated 21 days after inoculation. At physiological maturity, 10 to 15 randomly infected spikes from each plot were collected and carefully threshed by hand to minimize the loss of FDKs. The grains were bulked, and a 10-g sample was milled in a Laboratory Mill 3610 grinder (2015 Perten Instruments®); 2 g subsample of flour was poured into a 15-ml polypropylene conical tube. DON quantification was performed using the high-throughput fast chromatography-tandem mass spectrometry (FC-MS/MS)-based method (Wang et al., 2022). LC-MS/MS conditions were developed on an Agilent Series 1260 Infinity HPLC system (Agilent Technologies, Mississauga, ON, Canada) coupled with an AB Sciex API 4000 hybrid triple quadrupole linear ion trap (QTRAP) mass spectrometer (AB Sciex, Concord, ON, Canada) equipped with a Turboionspray interface. Applied Biosystems/MDS Sciex Analyst software (Version 1.7) was used for system control and quantification. In addition, the FHB index (VRI) was calculated as (SEV × INC)/100 (Stack and McMullen, 1998), and INC-SEV-DON (ISD) index was calculated as (0.2 × INC) + (0.2 × SEV) + (0.6 × DON) following the protocol of the Prairie Recommending Committee for Wheat, Rye, and Triticale (PRCWRT, 2013).

The same lines were also evaluated at the Agriculture Agri-Food Canada (AAFC) FHB nursery near Morden, MB, in a randomized complete block design in a single 1-m-long row spaced 30 cm apart. *Fusarium graminearum* inoculum was prepared on corn kernels using four isolates: HSW-15-39 (3-ADON), HSW-15-87 (3-ADON), HSW-15-27 (15-ADON), and HSW-15-57 (15-ADON). Each isolate was inoculated in individual pans containing sterile corn and incubated for 1 month. After the corn was dried, it was stored in plastic tubs at 4°C until use. The inoculum was dispersed at a rate of 8 g per row, two times at weekly intervals, starting when the earliest lines were at the four- to five-leaf stage (Zadok's stage 31) (Zadoks et al., 1974). The inoculum application was followed by irrigation three times a week (Monday, Wednesday, and Friday) using Cadman Irrigations Travellers with Briggs Booms. FHB incidence and severity were rated at 21 days post-anthesis. Full-row plots were harvested manually (avoiding the borders) and combined threshed. The harvested samples were sent to a service provider (Central Testing Laboratory Ltd., Winnipeg, MB) to perform FDK and DON analyses. In addition, the effect of DON accumulation on YP and PRO was investigated for the DON samples collected from the 2020 NSF using a near-infrared spectroscopy (NIR) analyzer.

2.2.2 Screening in the greenhouse

Type II resistance to FHB was assessed in GH trials. Lines with check cultivars were planted in 1-gallon pots filled with a standard potting mix (type-3 soil). Six seeds per pot were sown, and after germination, only three plants were retained per pot for further growth and inoculation. Pots were designated as experimental units and arranged in a completely randomized design with two replications. Replicates were sown approximately 1–2 weeks apart, resulting in a 1–3-day difference in anthesis between replications. The temperature in the greenhouse was maintained at 22°C/18°C (day/night) with a 16-h photoperiod. The lines were inoculated with 3-ADON *F. graminearum* isolate SK-14-97 (obtained from the Cereal Pathology group, University of Saskatchewan, SK, Canada). First, a conidial suspension was plated onto potato dextrose agar media and exposed to permanent light for 4 to 7 days at 18°C. Then, a conidial suspension was adjusted to a concentration of 50,000 spores per mL using a hemocytometer. The anthesis date was recorded for each plant in a pot. Inoculations were performed at anthesis by pipetting 10 µl of conidia suspension between the lemma and palea of the two outer florets of one central spikelet per spike. A total of six heads per line was inoculated. The heads were then sprayed with sterile distilled water and covered with polyethylene transparent plastic bags for 24 hours to maintain high humidity. FHB symptoms were visually scored as the percentage of infected spikelets per spike at 21 days post-inoculation. At maturity, the inoculated heads of each line were harvested, combined from all replicates, threshed by hand to retain all the seeds, and ground into a fine powder for DON analysis following the procedure described in section 2.2.1.

2.3 Phenotypic data analyses

To obtain the best linear unbiased predictions (BLUPs) of the measured traits across test environments, the R package lme4 (version 3.4.2, https://www.r-project.org) was used for phenotypic data analysis using the following R-script: fitted to each genotype: Phenotype ~ (1|Genotype) + (1|Repeat%in%Environment) + (1|Genotype&Environment). Lines were treated as a random factor, and BLUPs were estimated for all traits within and across environments. Broad-sense heritability (H^2) was then estimated using the variance components estimated from the previous equation. Pearson correlations between the BLUPs of the observed traits were calculated in R (Benesty et al., 2009).

2.4 Genotyping and SNP filtering

The mapping panel was genotyped with the 90K Illumina SNP chip to identify single nucleotide polymorphisms (SNPs). SNPs with minor allele frequencies <5% and missing data >10% were removed to avoid spurious marker–trait associations, leaving 13,504

SNPs for subsequent analyses (Supplementary Table S10). The physical positions of SNP markers were obtained from the latest Chinese Spring reference genome sequences (RefSeqv2.1: https://doi.org/10.1111/tpj.15289) to compare the QTL intervals with previous studies because most of them used this reference sequence.

2.4.1 Genotyping with *Rht-B1b* marker

The *Rht-B1b* confers semi-dwarfism in durum (Peng et al., 1999). Therefore, we genotyped the lines with the *Rht-Blb* marker to see how this locus relates to FHB resistance. To compute the proportion of phenotypic variance explained by the marker *Rht-B1b*, we fitted a multiple linear regression model using *Rht-B1b* SNP as a predictor and FHB traits (mean FHB SEV and mean FHB INC) as a response. We also computed the proportion of mean PH variance explained by this marker for comparison. To implement the multiple linear regression model, we used the Ordinary Least Squares (OLS) regression function from the statsmodels library in Python 3.7.

2.5 Linkage disequilibrium and population structure

Linkage disequilibrium (LD) analysis was performed for each chromosome by computing r^2 values for all pairwise marker comparisons using the R genetics package (CRAN - Package genetics (r-project.org)). Marker positions were then used to investigate LD decay along each chromosome and across the entire genome. Background LD was estimated as the 90th percentile of the r^2 value of marker pairs on different chromosomes. LD decay distance was determined by fitting a non-linear model using the Hill and Weir method (Weir, 1979), with the r^2 threshold set at 0.2 and r^2 = half decay distance.

To define the appropriate number of subpopulations (K) for subsequent population structure and principal component analyses (PCA), the Bayesian information criterion (BIC) of each genotype was computed for 10 arbitrary clusters using the discriminant analysis of principal components (DAPC) function in the R package Adegenet 2.1.7 (Jombart, 2008; Jombart et al., 2020). Results were visualized into scree plots, and the number of clusters where the line trended horizontally was considered an appropriate number of ancestral subpopulations (K). The admixture proportion (ancestral coefficients) of genotypes was inferred based on sparse non-negative matrix factorization (sNMF) (Frichot et al., 2014) at the above (K + 1) estimated K as the number of subpopulations using the snmf function in R package LEA (Frichot and François, 2015). The admixture proportions of each genotype were summarized in bar plots using the plot function of the same package LEA. Principal component analysis was also performed based on the K subpopulation and the variation explained by each PC was computed. The clustering of the genotypes was visualized in a scatter plot based on the first two PCs. To confirm the population structure and the genetic relationships of the genotypes, phylogenetic analysis was performed following the Neighbor-Joining method using TASSEL 5 (Bradbury et al., 2007), and the web-based interactive tree of life (iTOL) (Letunic and Bork, 2016) was applied to visualize the trees.

2.6 Marker–trait association analysis

We applied seven ML and one SL GWAS method to capture loci underlying FHB and its related traits. The multi-locus methods include multi-locus random-SNP-effect MLM (mrMLM) (Wang et al., 2016), fast multi-locus random-SNP-effect EMMA (FASTmrEMMA) (Wen et al., 2017), Iterative Sure Independence Screening EM-Bayesian LASSO (ISIS EM-BLASSO) (Tamba et al., 2017), polygenic-background-control-based Kruskal–Wallis test plus empirical Bayes (pKWmEB) (Ren et al., 2018), fast mrMLM (FASTmrMLM) (Tamba and Zhang, 2018), and polygenic-background-control-based least angle regression plus empirical Bayes (pLARmEB) (Zhang et al., 2017), all implemented in the R package MrMLM v 5 (Wen et al., 2018). In addition, a haplotype (LD block) based on a restricted two-stage multi-locus multi-allele GWAS (RTM-GWAS) (He et al., 2017) was applied. The significant threshold for the first six in MrMLM was defined based on a logarithm of odds (LOD) >3, whereas for RTM GWAS Bonferroni corrected $p < \alpha/n$ was applied, where $\alpha = 0.05$ and n = the number of LD blocks. For single-locus GWAS, a mixed linear model (MLM, with $Q + K$ model) was applied using TASSEL 5 (Bradbury et al., 2007). The significant threshold of marker–trait association was set at a p-value adjusted based on Bonferroni correction (α/n, where $\alpha = 0.05$ or significant threshold before multiple comparisons and n was the number of markers used for GWAS) (Sun et al., 2017). Population structure and kinship were included as correcting factors for all eight methods. Finally, significant SNP markers within one LD (13 Mbp) on the same chromosome were considered to represent a single locus. Quantile–Quantile (Q–Q) plots were generated to visualize the goodness of fitting for the GWAS model accounted for by the population structure and familial relatedness. The negative logarithm of the p-value from the model was calculated against the expected value based on the null hypothesis.

After identifying consistent and significant QTL regions, representative SNPs were extracted from the QTL regions and further investigated for combined additive effects for the traits SEV, INC, and DON. These combinations were tested with across environment BLUP values of the traits to assess which combination contributed to better resistance. Lines that carry resistant alleles at multiple loci were then selected and recommended for future breeding for FHB resistance based on the number of resistance alleles they contained.

2.7 Analysis of potential candidate genes for DON accumulation

To identify potential candidate genes within the interval of the DON QTNs captured by the GWAS analyses, the Chinese Spring reference wheat genome (RefSeqv2.1: https://doi.org/10.1111/tpj.15289) was used. Three highly significant MTAs for DON, *Ra_c4159_2716* (*QFhb-1A.1*), *Ra_c41921_951* (*QFhb-4B.4*), and *Ra_c29107_289* (*QFhb-6A*), were subjected to candidate gene analysis to identify genes/gene networks associated with resistance. LD analysis was performed using the R package gpart

(Kim et al., 2019) by setting the coefficient of determination $r^2 > 0.5$ based on the genotype data and cv Chinese Spring's gene coordinates. All polymorphic genes within the LD block ($r^2 > 0.5$) were assessed for their potential functional role based on information in different databases, including Knetminer wheat (https://knetminer.com/Triticum_aestivum/) and wheatgmap (http://www.wheatgmap.org/), orthologs of other species from Ensembl Plants (https://plants.ensembl.org/). To search orthologs in well-studied species such as rice and *Arabidopsis*, corresponding databases were used: the Rice Genome Annotation Project Database (RGAP) (http://rice.uga.edu/) and the Arabidopsis Information Resource (TAIR) (https://www.arabidopsis.org/), respectively. Genes with potential roles in FHB and related trait regulations were identified and summarized.

2.8 KASP marker development and analysis

The six FHB-related traits QTL that were consistently detected in multiple environments and by multiple GWAS models were chosen for KASP marker conversion. The most significant SNP from each of these six QTL was selected from the iSelect 90K Infinium array, and their probe sequences (Wang et al., 2014) were used for PCR primer development. Primers were developed from this probe sequence with two allele-specific forward primers and one common reverse primer (Supplementary Table S9). The KASP genotyping assays were performed on a CFX Touch Real-Time PCR Detection System (BioRad, Hercules, CA, USA) following the LGC Biosearch Technologies' KASP genotyping manual (www.biosearchtech.com). Each KASP marker was verified on the GWAS panel to be congruent with the 90K iSelect genotyping scores. We then evaluated the genetic diversity of the SNPs significantly associated with the detected QTL in the Global Diversity Panel (GDP) of tetraploid wheat (Mazzucotelli et al., 2020). Six KASP markers, each representing a single locus detected by GWAS (see **KASP marker development and analysis**), were scored on the GDP, and data were recorded as "resistant" or "susceptible" alleles based on the marker effects estimated from the GWAS panel. Allelic frequencies of these loci were calculated separately in cultivars, landraces, domesticated, and wild emmer subsets of the GDP. Haplotypes were constructed based on the alleles at the six loci, and the number of accessions in GDP carrying each haplotype was summarized in a frequency bar plot. The top 10 most frequent haplotypes were georeferenced based on the coordinates of the country of origin of the accessions carrying the haplotypes and overlaid on the world map using the Quantum Geographic Information System (QGIS 3.8) (http://qgis.osgeo.org).

3 Results

3.1 Phenotypic variations

Descriptive statistics for all the traits tested under field and greenhouse conditions are presented in Supplementary Table S2. Analysis of variance of FHB traits showed significant ($p < 0.001$) variation among genotypes (data not shown). The phenotypic values ranged from 5% to 100% (GH) and 2% to 93% (FL) for SEV, 1% to 98% for INC, and 0.377 to 228.8 ppm (GH) and 0 to 97 ppm (FL) for DON. The mean values for all FHB traits were higher in 2020 at NSF, Saskatoon, than in the other environments, except where INC was higher in 2019 at the same location. In contrast, the lowest mean scores were recorded for 2021 at both field locations for all the traits. The frequency distribution of the mean values of the studied traits fit a normal distribution, except for DON (Figure 1). The broad-sense heritability (H^2, %) of the traits tested ranged from 38% (INC) to 93% (PH) (Supplementary Table S2).

Weak to strong correlations were detected between FHB SEV and INC and related traits. The correlations among BLUPs for FHB and morpho-physiological traits are presented in Figure 2. The correlation between BLUPs for SEV and INC ($r = 0.47$) was higher than that between SEV and DON ($r = 0.30$). BLUPs for DON were nearly equally correlated to SEV and FDK ($r = 0.27$). BLUPs for FDK correlated highest with SEV ($r = 0.46$). In contrast, BLUPs for PH, AD, and HD showed weak to moderate negative correlations with all FHB-related traits (Figure 2). The correlation coefficients of FHB response traits (SEV, INC, and DON) in all test environments ranged from 0.31 to 0.66 (Supplementary Figure S2). DON was highly correlated with SEV and FDK in individual environments (Supplementary Figure S2).

3.2 Population stratification

The final number of SNP markers used for the analysis of population structure and GWAS analysis was 13,504. The appropriate number of subpopulations (K) was identified as five subgroups, essentially consistent with the breeding program of origin and pedigree (Table S1). The admixture, PCA, and phylogenetic analyses showed a similar pattern of clustering of individuals (Figure 3). Most of the experimental lines carrying the major resistance QTL *Fhb1* derived from Sumai 3 are clustered in Pop1, whereas some progenies from crosses with Sumai 3 *Fhb1* sources to European durum wheat cultivars (Prat et al., 2017) were clustered in Pop2 and Pop3. Pop4 comprised all the Canadian durum wheat cultivars and breeding lines, whereas Pop5 consisted of experimental lines derived from the intercrossing of cultivated lines with *T. turgidum* ssp. *dicoccum* and *T. turgidum* ssp. *dicoccoides* lines from the IFA-Tulln breeding program.

3.3 Marker-trait associations

For GWAS analysis, we performed and compared several single and multi-locus models. The single-locus MLM detected a total of 204 QTNs for FHB-related traits (INC, SEV, FDK, and DON), 245 QTNs for agro-morphological traits (PH, HD/AD, and MAT), and 31 QTNs for quality traits (YP and PRO) (Supplementary Table S3), based on individual environment and across environment BLUPs. For FHB resistance-related traits, the QTNs identified were distributed on all 14 chromosomes. For the MLM, the Q–Q plots illustrating the associations observed between SNPs and FHB

10.3389/fpls.2023.1182548

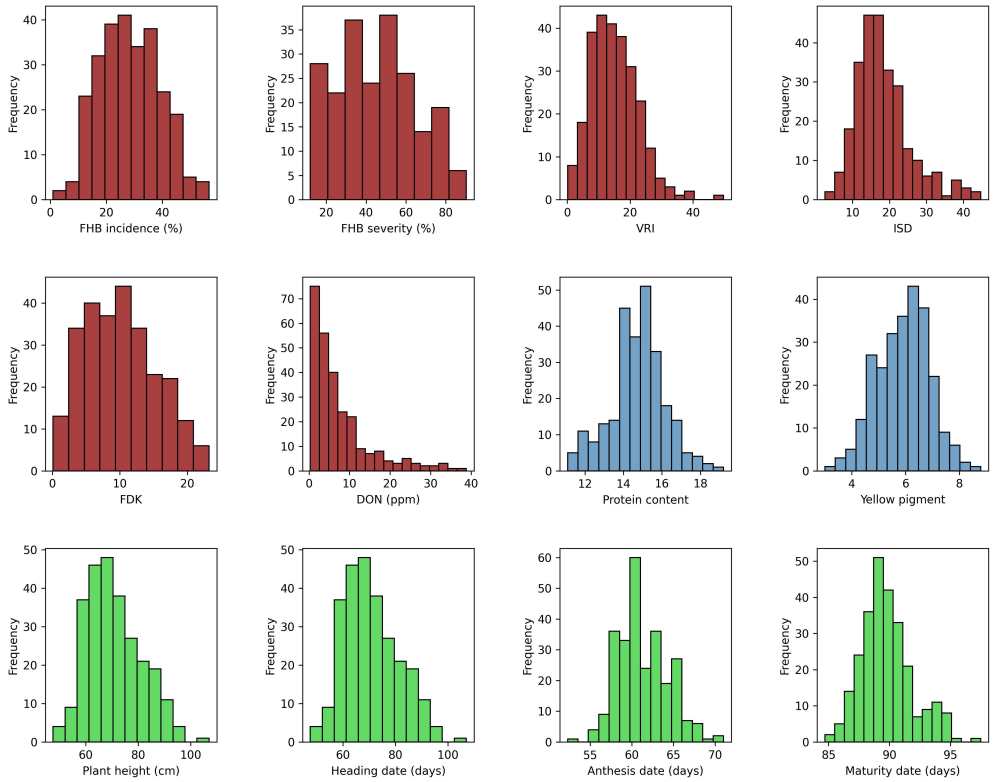

FIGURE 1
Phenotypic distribution of mean values for FHB incidence (INC; %), FHB severity (SEV; %), *Fusarium*-damaged kernels (FDK; %), deoxynivalenol concentration (DON; ppm), protein content (PRO; %), yellow pigment (YP, μg g^{-1}), visual rating index (VRI; %), INC-SEV-DON index (ISD), plant height (PH, cm), heading date (HD, days), anthesis date (AD, days), and maturity date (MAT, days).

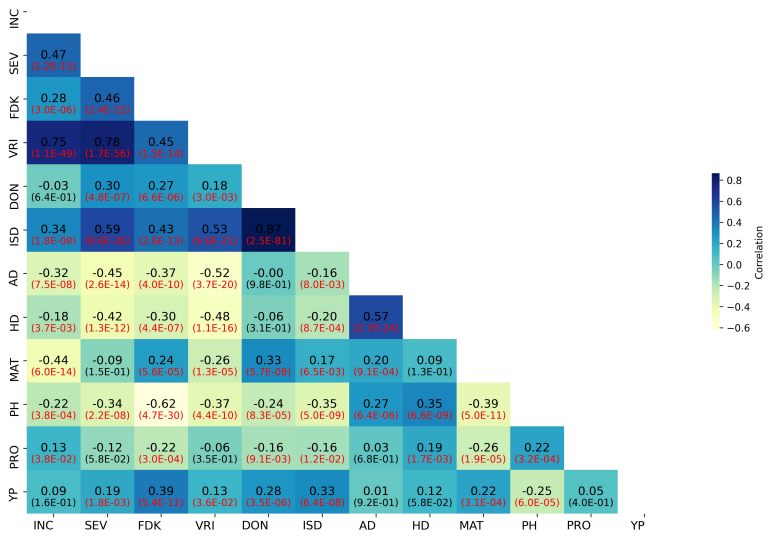

FIGURE 2
Correlation heatmap of FHB and agro-morphological trait BLUP values in the GWAS panel. INC, FHB incidence; SEV, FHB severity; FDK, *Fusarium*-damaged kernels; VRI, visual rating index; DON, deoxynivalenol; ISD, INC-SEV-DON index; AD, days to anthesis; HD, days to heading; MAT, days to maturity; PH, plant height; PRO, grain protein content; YP, yellow pigment.

10.3389/fpls.2023.1182548

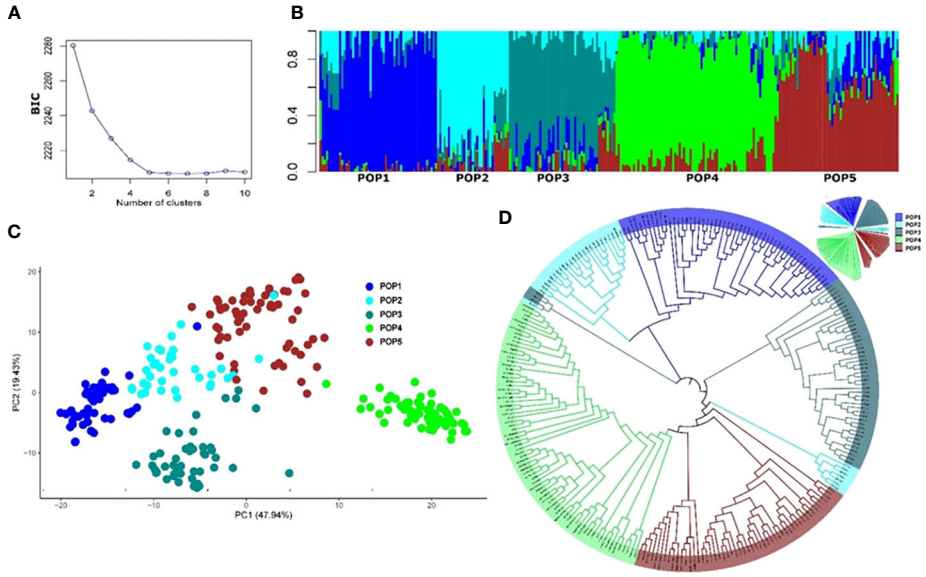

FIGURE 3
Population structure of the 265 durum wheat lines based on 13,504 SNP markers. **(A)** Cross-validation error showing the likely appropriate number of populations K to be 5. **(B)** Population structure based on genetic admixture for *K* = 5, where each bar represents a single line and the colored segments within each bar reflect the proportional contributions of each subgroup to that line. **(C)** Principal component analysis (PCA) plot of the first two principal components (PCs). Percentages in brackets indicate the variance explained by the PCs. **(D)** Topological view of the neighbor-joining phylogenetic tree.

resistance and related agro-morphological traits compared to expected associations after accounting for population structure and kinship relationships are presented in Supplementary Figure S3. The multi-locus models captured 288, 144, and 26 QTNs for FHB resistance, agro-morphological, and quality traits, respectively (Supplementary Table S3).

In total, 42 QTNs for FHB, 24 for agro-morphological, and six for quality traits were detected by two or more methods and explained greater than 15% of the phenotypic variation (Supplementary Tables S4, S5). Among the six ML-GWAS models used in our analysis, the ISIS EM-BLASSO model identified 93 QTNs, while FASTmrEMMA detected the lowest number of QTNs (37) for all the traits (Supplementary Table S3). We further grouped the 42 FHB QTNs into 31 QTL (Supplementary Table S4) based on the genome-wide LD of the panel (Supplementary Figure S4). Of these, *QFhb-1A.1*, *QFhb-2B.4*, *QFhb-3B.1*, *QFhb-3B.2* *QFhb-4B.1*, *QFhb-5A*, *QFhb-6B.3*, and *QFhb-7B.2* were associated with QTNs identified by BLUP values and/or from GH screening (Table 1).

QTNs for FHB SEV, INC, and DON that were detected in multiple environments with multiple models are presented in Table 1 and Supplementary Table S4. Most agro-morphology-related trait-associated QTNs were consistent with the position of FHB QTL *QFhb-4B.1* and *QFhb-5A* (Table 1; Supplementary Table S5). *QFhb-3B.1* localized to a similar region of chromosome 3B as that previously reported for *Fhb1* (Supplementary Figure S5), which we confirmed by marker analysis (Supplementary Table S1). Contrast analysis revealed that, on average, lines carrying *Fhb1* showed reduced SEV, DON, VRI, and ISD (Supplementary Figure S6). QTL *QFhb-2A.4* and *QFhb-4B.4* were associated only with DON. Similarly, another QTL on chromosome 2B, *QFhb-2B.4*, was captured by the LD block approach (RTM GWAS) associated with DON with the highest –log10(P) value of 26.58 (Supplementary Figure S7). *QFhb-4B.1* and *QFhb-5A* were detected by eight of the GWAS models and associated with all FHB response and agro-morphological traits, followed by *QFhb-7B.2*, which was associated with YP as well (Table 1). *QFhb-4B.1* represents the most prominent genomic region for PH and MAT, with the highest LOD score (43.0) and phenotypic variance (60.3), followed by *QFhb-5A* with an LOD score of 25.0 and phenotypic variance of 44.5% for HD, AD, and MAT. *QFhb-6A* explained the maximum phenotypic variance (29.7%) for PRO (Table 1; Supplementary Tables S4, S5). As an example, the phenotypic variation for VRI based on the representative SNP at the most significant and consistent QTL, *QFhb-5A*, is presented in Figure 4, and the QTL region that spanned 586–595 Mbp on chromosome 5A is associated with multiple FHB resistance, and agro-morphological traits are shown in Supplementary Figure S8. Significance –log10 (*p*-values) of the association of 13,504 SNPs based on RTM (LdBlock-based method) located on 14 chromosomes with BLUP values for DON, SEV, VRI, HD, MAT, and PH are depicted as Manhattan plot with multi-track Q–Q plots for each case (Supplementary Figure S9).

3.4 Candidate genes in the QTL regions for resistance to DON accumulation

The three loci strongly associated with DON, *Ra_c4159_2716 (QFhb-1A.1)*, *Ra_c41921_951 (QFhb-4B.4)*, and *Ra_c29107_289*

10.3389/fpls.2023.1182548

TABLE 1 Marker–trait associations detected by two or more GWAS models for FHB resistance and related traits using BLUP/field and GH data.

QTL	Representative SNP/sm	Chr	Marker position (Mbp)	Trait (environment)	LOD score	R^2 (%)	–log10 (P)	MAF	Method
QFhb-1A.1	*Ra_c4159_2716*	1A	490.5	**SEV** (GH), **DON** (GH)	3.6–3.8	9.1–35.7	4.37–4.58	0.3	1, 6
QFhb-2A.3	*BS00000209_51*	2A	746.8	**DON** (BLUP), **SEV** (BLUP, GH)	3.3–6.1	23.2–24.0	4.05–6.95	0.32	3, 5, 6
QFhb-2B.3	*Excalibur_c39451_68*	2B	683.2	**SEV** (BLUP, GH)	4.3–6.4	12.1–16.9	5.02–7.28	0.47	1, 4, 5, 6
QFhb-2B.4	*Kukri_c12804_620*	2B	114	**DON** (GH), **SEV** (GH)	3.3–4.8	5.3–15.1	4.05–5.54	0.48	1, 4, 5, 6, R
QFhb-3A.1*	*RAC875_c4954_943 wsnp_Ex_c23633_32868822*	3A	9.0–13.0	**SEV** (20NSF), **ISD, PRO**	3.3–6.2	5.6–7.8	4.04–7.02	0.46	3, 5, 6
QFhb-3B.1	*TA004185-0427 RAC875_c5966_1854*	3B	3.2–9.9	**SEV** (BLUP), **DON** (BLUP), **ISD**	3.6–5.0	7.2–20.1	3.87–5.73	0.46	2, 4, 5, T
QFhb-3B.2	*RAC875_rep_c109105_57, Excalibur_c62826_254*	3B	578.2–578.8	**SEV** (BLUP), D**ON** (BLUP)**INC** (BLUP), **VRI**	3.2–11.9	10.5–36.9	4.64–12.84	0.37	1, 3, 4, 5, 6, R, T
QFhb-3B.3	*BobWhite_c6462_373*	3B	793.1	**SEV** (BLUP, GH)	3.4–5.6	13.1–24.9	4.08–6.41	0.36	1, 3, 4, 5
*QFhb-4B.1***	*wsnp_BF482960B_Ta_1_4, RAC875_c27536_611, BS00021984_51, Ex_c101685_711*	4B	29.0–35.5	**SEV** (19NSF), **INC** (22MR), **DON** (21MR, 22MR), **FDK** (21MR), **PH**, **MAT**	3.8–20.1	5.3 – 52.3	4.52–21.23	0.29	1, 2, 3, 4, 5, 6, R, T
QFhb-4B.3	*Tdurum_contig14562_607*	4B	181.7	**INC** (BLUP)	3.9–5.2	10.1–11.3	4.64–6.03	0.38	3, 4, 6
QFhb-4B.4	*Ra_c41921_951*	4B	558.1	**DON** (BLUP), **ISD**	3.7–6.1	5.5–8.6	4.40–6.89	0.47	3, 4, 5, 6, R, T
*QFhb-5A****	*IAAV3365, BS00075959_51, wsnp_AJ612027A_Ta_2_5, BobWhite_c21949_150, wsnp_BF293620A_Ta_2_1, Kukri_c33022_198*	5A	586.6- 595.4	**INC** (19NSF, 20NSF, BLUP)**, SEV** (20NSF, 21NSF, BLUP)**, DON** (21MR, 22MR), **FDK** (21MR, 22MR), **VRI**, **HD, AD, HT, MAT**	3.3–25.0	5.9–44.5	3.74–28.49	0.40	1, 2, 3, 4, 5 6, R, T
QFhb-5B.1	*wsnp_Ra_c24619_34168104*	5B	508.8	**SEV** (BLUP, GH)	5.1–7.1	36.5–53.4	5.9–7.9	0.23	1, 4, 5, 6
QFhb-5B.2	*Ra_c2216_1442*	5B	591.1	**SEV** (GH), **FDK**	4.2–6.0	6.2–13.0	4.99–6.83	0.31	1, 4, 6
QFhb-6A*	*Ra_c29107_289, Excalibur_c25211_828*	6A	18.5–34.3	**DON** (GH),**INC** (BLUP), **MAT, PRO**	3.6-8.0	6.3–29.7	4.29-14.85	0.42	1, 3, 4, 5, T
QFhb-6B.1	*Excalibur_c30648_924, Kukri_c3009_267*	6B	11.5–18.5	**SEV** (GH, BLUP), **DON** (BLUP), I**SD**	3.9–9.1	5.7–26.6	4.68–9.98	0.3	1, 2, 3, 4, 5 6, T
QFhb-6B.3	*Tdurum_contig45714_427, RAC875_c34994_183*	6B	123.8–128.7	**INC** (BLUP), **SEV** (BLUP), **DON** (GH, BLUP)	3.5–6.7	5.2–13.8	4.18–7.55	0.41	2, 3, 4, 5, 6
*QFhb-7A***	*Tdurum_contig69067_405*	7A	662.0–671.0	**DON** (GH), **VRI,HD**	4.8–5.3	5.4–37.0	5.54–6.12	0.11	5, 6, T
*QFhb-7B.1***	*Kukri_c51101_351*	7B	630.1	**DON** (GH), **SEV** (BLUP, GH), **HD, MAT**	3.4–6.0	11.2–24.1	4.14–6.79	0.45	4, 5, 6
QFhb-7B.2*	*Excalibur_c49736_1197, IAAV3713*	7B	706.9–728.7	**DON** (GH), **SEV** (GH, BLUP), **YP**	4.1–6.8	14.8–19.4	4.90–7.70	0.48	4, 5

Models: 1, MrMLM; 2, FASTmrEMMA; 3, pKWmEB; 4, ISIS EM-BLASSO; 5, FASTmrMLM; 6v, pLARmEB; R, TM and T, TASSEL.

Traits: SEV, FHB severity; INC; FHB incidence; DON, deoxynivalenol; FDK, Fusarium-damaged kernel; VRI, visual rating index (SEV * INC/100); ISD, INC-SEV-DON index (0.2 * SEV + 0.2 * INC + 0.6 * DON); HD, days to heading; AD, days to anthesis, MAT, days to maturity; PH, plant height; YP, yellow pigment; PRO, grain protein content; Chr, chromosome; MAF. minor allele frequency.

Location and year: NSF, North Sed Farm, Saskatoon, SK; MR, Morden, MB; GH, greenhouse; 19, 2019; 20, 2020; 21, 2021; 22, 2022.

QTL with * colocalized with PRO or YP, ** colocalized with PH MAT and/or AD/HD, and *** colocalized with MAT, PH, and AD/HD. Underlined QTL for these representable QTNs were converted to KASP markers.

10.3389/fpls.2023.1182548

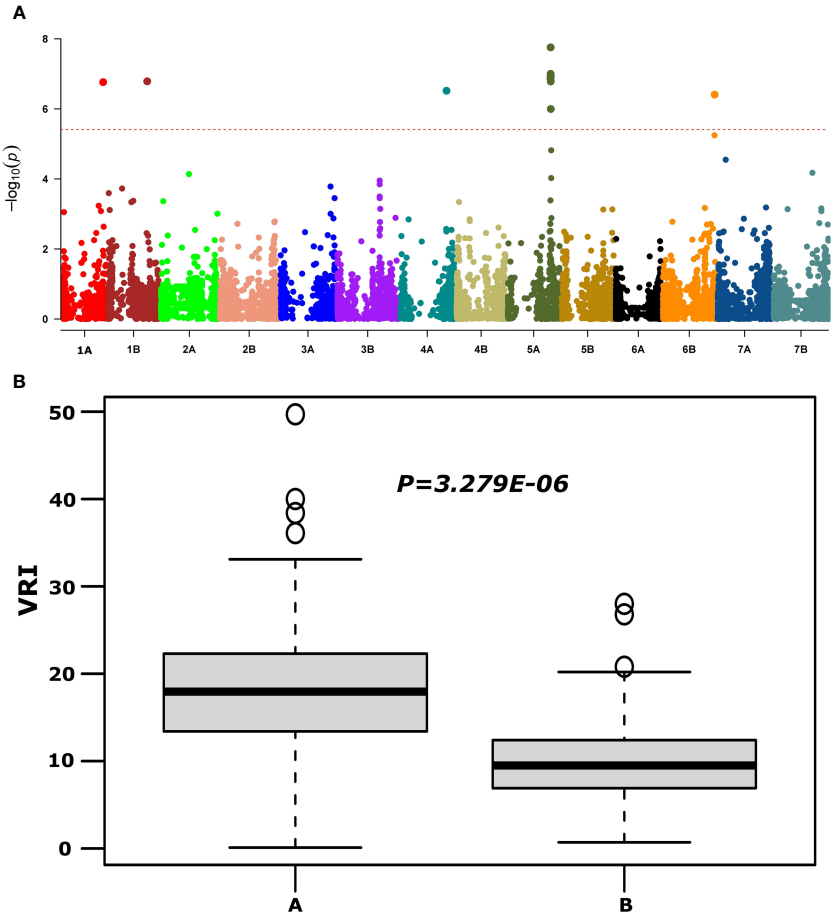

FIGURE 4
Manhattan plot reveals QTL for FHB visual rating index (VRI) using the MLM model (upper panel, **A**) and phenotypic variations at large effect QTL *QFhb-5A* (*IAAV3365*) for VRI (lower panel, **B**) based on overall mean.

(QFhb-6A), harbor candidate genes reported to be involved in disease resistance, defense, and stress responses, which were identified within their strong LD range of the associated genomic regions using Chinese Spring reference genome gene annotation (Table 2). The locus *Ra_c41921_951* on chromosome 4B associated with DON (FL) and detected by five different GWAS models harbors 11 genes, of which 10 were predicted to play a role in disease resistance; the remaining one is a stomatal opening gene. Two of the genes at this locus were predicted to contribute specifically to wheat stripe rust resistance. Of these, one was *TRAESCS4B02G280000*, which is an orthologue with genes encoding the SU (VAR)3-9 HOMOLOG 1 protein (SUVH1) that was assumed to regulate phenological traits such as days to flowering, heading, and maturity. Of the 11 genes, most (n = 8) were also predicted to regulate biological processes associated with drought resistance. The other GH_DON-associated locus on chromosome 6A, which was marked by *Ra_c29107_289*, harbors more than 20 genes that have been predicted to have a role in FHB resistance. This locus contains a higher density of genes (n = 13) that are orthologous with nitrate transporter 2.1 (NRT2.1). The QTL on chromosome 3B harbors *UDP-glucuronosyltransferases* (*UGTs*) gene families, which detoxify DON (Table 2).

3.5 KASP markers for the FHB-associated QTL

For MAS, we converted to KASP marker QTN representing six QTL that were (a) detected in multiple environments and (b) by multiple GWAS models (underlined QTL in Table 1). The markers were robust and clearly clustered lines into two discrete allelic groups (Supplementary Figure S12). These were then scored in the GWAS panel and a subset of the GDP and compared with available 90K data (Supplementary Table S9). The KASP markers developed from *Kukri_c12804_620* (*QFhb-2B.4*) scored two loci, one of which was much more congruent with the 90K data associated with the FHB resistance QTL, thus was used for further analysis (Supplementary Table S9). Analysis of the SNP markers in the GDP panel revealed that the frequency of FHB resistance alleles among the GDP wheat groups (cultivar, landrace, domesticated, and wild emmer) was highly variable, especially for *QFhb-5A* (Supplementary Figure 6A). Surprisingly, the frequencies of resistance alleles were low in cultivars (Figure 5; Supplementary Table S8). In contrast, wild and domesticated emmers present in the GDP all carried the resistance allele at *QFhb-6B.1* (Figure 5A; Supplementary Table S8). Next, we grouped the alleles from each

10.3389/fpls.2023.1182548

TABLE 2 Predicted candidate genes detected within the LD block of selected significant QTL with $R^2 > 15\%$ for resistance to DON accumulation.

QTL	Representative SNP from LD block	Accession	Gene name	Chr	Start	Role
QFhb-1A.1	*Ra_c4159_2716*	TRAESCS1A02G295400	*TRAESCS1A02G295400*	1A	490418247	Harvest index
		TRAESCS1A02G295200	*UGP3*	1A	490306427	Harvest index
		TRAESCS1A02G294700	*TRAESCS1A02G294700*	1A	489600057	Plant height
		TRAESCS1A02G295300	*AMT2*	1A	490411509	Disease resistance, drought
		TRAESCS1A02G295600	*HSP70-9*	1A	490509793	Proline content
		TRAESCS1A02G294500	*TRAESCS1A02G294500*	1A	489357467	Stripe rust resistance
QFhb-4B.4	*Ra_c41921_951*	TRAESCS4B02G278100	*HSFA2D*	4B	560012594	Disease resistance, harvest index, salt tolerance
		TRAESCS4B02G278000	*ARD*	4B	560007429	Stomatal opening, stomatal resistance, turgor pressure, drought
		TRAESCS4B02G277900	*PME8*	4B	559854826	Stripe rust
		TRAESCS4B02G279000	*SEC15A*	4B	562354948	Disease resistance
		TRAESCS4B02G279100	*TRAESCS4B02G279100*	4B	562419106	Disease resistance, drought
		TRAESCS4B02G279300	*TRAESCS4B02G279300*	4B	562436091	Disease resistance, drought
		TRAESCS4B02G279200	*TRAESCS4B02G279200*	4B	562425162	Disease resistance, drought
		TRAESCS4B02G279500	*TRAESCS4B02G279500*	4B	562628791	Disease resistance, drought
		TRAESCS4B02G279400	*TRAESCS4B02G279400*	4B	562439286	Disease resistance, drought
		TRAESCS4B02G280000	*SUVH1*	4B	562880284	Stripe rust, day to heading/flowering, seed dormancy
		TRAESCS4B02G279600	*TRAESCS4B02G279600*	4B	562697710	Disease resistance, drought
QFhb-6A	*Ra_c29107_289*	TRAESCS6A02G037900	*SKIP4*	6A	18709035	Disease resistance, seed dormancy, self-incompatibility
		TRAESCS6A02G037800	*TRAESCS6A02G037800*	6A	18704699	Day to flowering, days to heading
		TRAESCS6A02G037600	*TRAESCS6A02G037600*	6A	18596060	Disease resistance
		TRAESCS6A02G029100	*MIK1*	6A	15435891	Disease resistance, drought
		TRAESCS6A02G029900	*CNL*	6A	15626844	Drought
		TRAESCS6A02G030100	*RGA5*	6A	15652828	Defense
		TRAESCS6A02G031200	*NRT2.1*	6A	15781020	Disease resistance, drought, Nitrate
		TRAESCS6A02G030900	*NRT2.1*	6A	15747526	Disease resistance, drought, Nitrate
		TRAESCS6A02G030700	*NRT2.1*	6A	15727844	Disease resistance, drought, Nitrate
		TRAESCS6A02G031000	*NRT2.1*	6A	15756560	Disease resistance, drought, Nitrate
		TRAESCS6A02G030800	*NRT2.1*	6A	15734520	Disease resistance, drought, Nitrate
		TRAESCS6A02G031100	*NRT2.1*	6A	15765759	Disease resistance, drought, Nitrate
		TRAESCS6A02G032000	*PIK6-NP*	6A	15916289	Defense
		TRAESCS6A02G034200	*BRM*	6A	16562153	Stripe rust, bacterial blight, day to flowering
		TRAESCS6A02G032400	*NRT2.1*	6A	15951566	Disease resistance, drought, nitrate
		TRAESCS6A02G032500	*NRT2.1*	6A	16098637	Disease resistance, drought, nitrate
		TRAESCS6A02G033800	*NQR*	6A	16462020	Oxidative stress
		TRAESCS6A02G033000	*NRT2.1*	6A	16386427	Disease resistance, drought, nitrate

(Continued)

10.3389/fpls.2023.1182548

TABLE 2 Continued

QTL	Representative SNP from LD block	Accession	Gene name	Chr	Start	Role
		TRAESCS6A02G032800	*NRT2.1*	6A	16357746	Disease resistance, drought, nitrate
		TRAESCS6A02G033100	*NRT2.1*	6A	16398961	Disease resistance, drought, nitrate
		TRAESCS6A02G032900	*NRT2.1*	6A	16374353	Disease resistance, drought, nitrate
		TRAESCS6A02G033200	*NRT2.1*	6A	16408185	Disease resistance, drought, nitrate
		TRAESCS6A02G032600	*PRP39*	6A	16226818	Day to maturity
		TRAESCS6A02G033400	*HIDM*	6A	16443279	Disease resistance, drought

QTL into 58 haplotypes and identified their frequency within the GDP (Supplementary Figure 6B). The majority of the 10 most common resistant haplotypes were concentrated in accessions collected from the Mediterranean and Middle East countries (Figure 5C). The haplotype ID and frequencies for the selected six markers are presented in Supplementary Table S7.

4 Discussion

4.1 Trait heritability and correlation

This study identified QTL as having a major effect on DON accumulation based on both field and GH data, followed by SEV and INC. The heritability for DON was 86%, higher than for SEV (61%) and INC (38%). This is likely because we used the high-throughput fast chromatography-tandem mass spectrometry (FC-MS/MS) method, which is not subject to the same error rate as the visual scoring of FHB incidence and severity in the field (Wang et al., 2022). Similarly, the heritability for SEV was higher in the GH (72%) than in the field (61%). Conversely, He et al. (2016b) found low heritability estimates (0.34) for FHB traits in a point-inoculated trial. This could be because of genotypic differentiation that occurred due to point (GH) and spray (FL) inoculation, where some genotypes reacted differently to the two methods, resulting in a large interaction variance. According to Miedaner et al. (2003) and Schroeder et al. (1963), genotypes that are resistant to spray but susceptible to point inoculation should have type I resistance

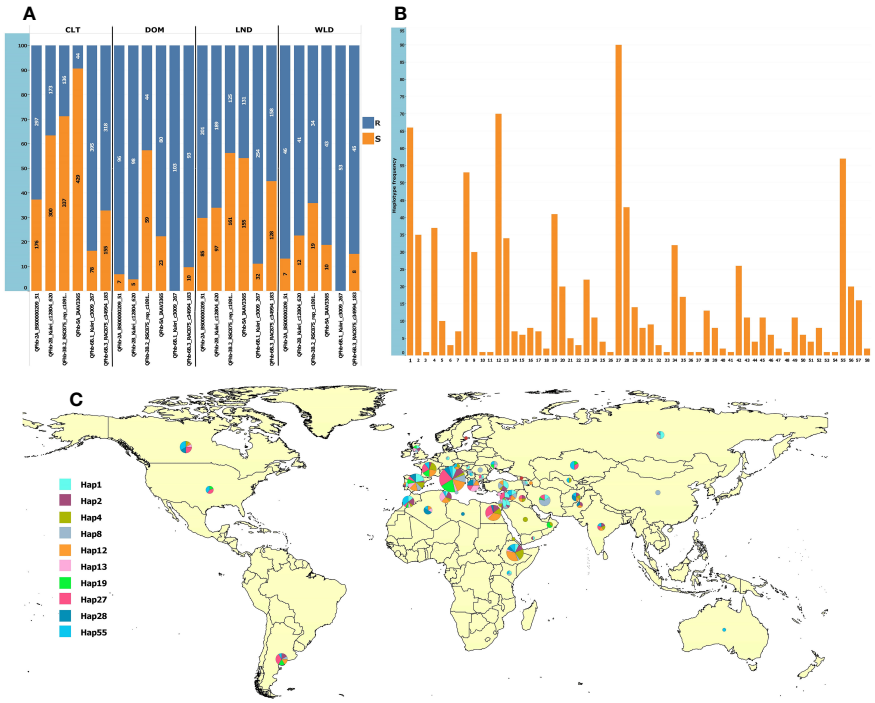

FIGURE 5
Allelic frequencies in the GDP panel and the geographic distribution of the 10 most frequent haplotypes. **(A)** Allelic frequencies of the six representative SNPs from the most consistent QTL in cultivars (CLT), domesticated emmer (DOM), landraces (LND), and wild emmer (WLD); the *y*-axis shows the percentage, and the labels show the absolute frequencies. **(B)** Haplotype frequencies based on the six loci. **(C)** Geographic distribution of the top 10 most frequent haplotypes. The haplotype pie chart circle size is proportional to the number of accessions from the corresponding country.

(resistance to initial infection), whereas genotypes susceptible to spray but resistant to point inoculation should possess type II resistance. Therefore, the QTL that were significant in two or more environments for FHB response should be emphasized for resistance breeding.

The negative correlations between FHB resistance and PH and HD/AD also agreed with previous findings summarized by (Prat et al., 2017; Steiner et al., 2017; Haile et al., 2018). The relationship between HD and PH with FHB was moderate and negative (Figure 2; Supplementary Figure S10), unlike the strong correlation reported by Ruan et al. (2020). Correlations between HD/AD and FHB may have a confounding effect on the association mapping results because these two traits can cause infection escape, and weather conditions such as humidity and temperature during anthesis can significantly affect the success of FHB infection. Therefore, it is vital to score FHB following the HD/AD days for individual germplasm (as used in this study) or correct for these factors in individual nurseries (Nannuru et al., 2022).

DON production plays a significant role in the spread of FHB within a spike (Bai et al., 2002); however, according to Bai et al. (2002), DON production is not necessary for initial infection by the fungus. The correlation between FHB SEV and DON accumulation in the present study was positive, with a coefficient of 0.43 (Figure 2). Reviews by Buerstmayr and Lemmens (2015) and Lemmens et al. (2016) also indicated a positive correlation between FHB severity traits and mycotoxins. However, He et al. (2014) found a negative relationship between FHB index and DON concentration, whereas Bai et al. (2002) reported a complicated relationship between SEV and DON, i.e., cultivars moderately resistant and moderately susceptible to FHB SEV usually had higher DON accumulation than resistant cultivars, but there also were exceptions, especially for cultivars with moderate resistance.

4.2 Marker–trait associations

Depending on the type of trait, applying appropriate model/s and statistical method/s is crucial for reliable results in GWAS. FHB resistance is a polygenic and multifactorial complex trait controlled by multiple small-effect loci. Multi-locus methods are more effective and efficient in capturing such small effect loci than single-locus models (Segura et al., 2012; Xu et al., 2018; Zhang et al., 2019a). However, combining multi- and single-locus methods is recommended to increase detection power and robustness (Li et al., 2018). It is also advantageous to integrate multiple GWAS methods to cross-check results to improve QTL confidence (Zhang et al., 2020).

Previous mapping studies have identified QTL for FHB resistance with minor to moderate effects that were repeatedly detected on 11 of the chromosomes of tetraploid wheat (Otto et al., 2002; Gladysz et al., 2007; Kumar et al., 2007; Ghavami et al., 2011; Buerstmayr et al., 2012; Ruan et al., 2012; Buerstmayr et al., 2013; Miedaner et al., 2017; Ruan et al., 2020). In our study, we identified QTN on all 14 chromosomes. Only minimal variation for resistance to FHB has been reported in cultivated durum wheat (*Triticum turgidum* ssp. *durum*); therefore, introgressions of resistance from its relatives (e.g., *T. turgidum* ssp. *dicoccum, T. turgidum* ssp. *dicoccoides*) are a priority and have shown promise, particularly in conferring resistance to FHB SEV (Buerstmayr et al., 2013). In this study, we identified QTN regions, *QFhb-1A.1*, *QFhb-2A.3*, *QFhb-6A*, and *QFhb-7B.2*, with significant contributions to the phenotypic variation that were identified from exotic sources. Several other studies also identified the main effect of QTL from exotic genetic resources, such as *T. carthlicum* (Sari et al., 2018), *T. turgidum* ssp. *dicoccoides* (Otto et al., 2002; Kumar et al., 2007; Ruan et al., 2012; Buerstmayr et al., 2013), and *T. turgidum* ssp. *dicoccum* (Buerstmayr et al., 2012; Zhang et al., 2014), stressing the importance of these germplasm collections as sources of FHB resistance genes to support breeding. The majority of the QTL detected by Ruan et al. (2020), were confirmed in this study, but the QTL effects were higher in this study. One potential explanation is that we tested a larger panel (265 lines) in five field environments and twice in the greenhouse, which may contribute to increased genetic variance and heritability expression.

4.2.1 QTL associated with multiple FHB resistance traits

Responses to different FHB resistance types are generally correlated, and complex biological and physiological mechanisms are involved in the coordination of their expression. Seven of the significant and stable QTL regions were detected for FHB resistance, *QFhb-1A.1*, *QFhb-2B.4*, *QFhb-3B.1*, *QFhb-3B.2*, *Fhb-4B.1*, *QFhb-5A*, and *QFhb-6B.3*, which affect SEV, INC, and DON. Moreover, *QFhb-3A.1* and *QFhb-7B.2* were associated with PRO and YP, respectively, in addition to SEV and DON. These QTL were of major importance based on consistency across models, their detection across multiple testing environments, and their association with agro-morphological traits like plant height and heading time.

Due to the colocalization of QTL, *QFhb-4B.1*, and *QFhb-5A* with PH and other agro-morphological traits, respectively, we discuss them independently. Simultaneously, we compared the locations of the QTL regions in this study with those of previous studies. For some of the QTL, comparisons across different findings were difficult due to the differences in the marker platforms and the lack of reliability in chromosome assignment among existing consensus maps.

4.2.1.1 Chromosome 1A

The QTL *QFhb-1A.1* contributed 35.1% to the phenotypic variance for DON in greenhouse (GH) trials. While we did not detect its effect in field trials, this QTL is coincident with minor QTL for FHB INC, and SEV in Canadian tetraploid germplasm (Ruan et al., 2020), Chinese elite germplasm (Wu et al., 2019), and US soft red winter wheat (Gaire et al., 2021). Our candidate gene analysis revealed that this QTL colocalizes with an ammonium transporter gene (AMT2), a family of proteins transporting ammonium salt and its analogs (Table 2). Several studies have reported that ammonium influences the interaction between plants and pathogens (Jiang et al., 2019); thus, this gene might influence the pathogen's ability to produce DON.

4.2.1.2 Chromosome 2A

Among the QTL, *QFhb-2A.3* was consistent for FHB SEV, as it was detected in five of the testing environments and using across-

environment BLUP values. In the same physical region of *QFhb-2A.3*, Gladysz et al. (2007) identified a QTL for resistance to FHB severity derived from the resistant *T. turgidum* ssp. *dicoccoides* accession Mt. Hermon#22 and a minor QTL from a diverse tetraploid population reported by Ruan et al. (2020) in the 762–769 Mb interval. Ruan et al. (2020) reported a QTL 16 Mb distant from *QFhb-2A.3*, whereas Steiner et al. (2019b) reported a QTL for FHB resistance in the same region. The physical positions of all the loci identified on chromosome 2A were physically distant from the photoperiod gene *Ppd-A1*, a major gene responsible for flowering time in wheat (Distelfeld et al., 2009). This is fortunate because these QTL are not being influenced by AD or HD, both of which could potentially limit their use in breeding programs.

4.2.1.3 Chromosome 3B

The two 3B QTL, *QFhb-3B.1* and *QFhb-3B.2*, were associated with all FHB response traits in this study. *QFhb-3B.1* was identified in a similar region as the 3B QTL identified in most previous studies (Anderson et al., 2001; Liu et al., 2006; Buerstmayr et al., 2009; Arruda et al., 2016; Steiner et al., 2019b; Ruan et al., 2020; Nannuru et al., 2022). This region also corresponds to the physical interval of the major FHB QTL, *Fhb1*, located on 3BS around 7.6–13.9 Mb (Anderson et al., 2001; Liu et al., 2006). This was expected as durum wheat lines that carry *Fhb1* introgressed from Sumai 3 (Prat et al., 2017) were included in our diversity panel, and most showed the favorable allele for this locus. Tetraploid landrace, TG3487, with mean FHB SEV 6.2% (Supplementary Table S11), also carried the favorable loci for *QFhb-3B.1* (Supplementary Table S1). *Fhb1* is well known for conferring resistance to FHB severity (Anderson et al., 2001; Buerstmayr et al., 2003; Cuthbert et al., 2006)). In this study, we also confirmed the importance of *QFhb-3B.1* to reduced DON accumulation in tetraploid wheat. Indeed, resistance to SEV conferred by *Fhb1* is associated with its ability to inactivate DON (Schweiger et al., 2016). Similarly, *QFhb-3B.2* is a pleiotropic locus associated with SEV, INC, DON, and VRI and contributed up to 36% of the phenotypic variance. It was considered a novel region, as we are not aware of previous studies reporting this region. *UDP-glucuronosyltransferases* (*UGTs*) reside in this QTL region; they are DON-responsive genes potentially involved in DON detoxification, are induced by *F. graminearum* and enhance resistance to FHB in wheat (Zhu et al., 2020; Wu et al., 2022). Plants can use UGTs to chemically modify DON to produce DON-3-glucosides, which are less toxic than DON (Jia et al., 2009). Accordingly, wheat could induce UGTs to respond to infection and detoxify the trichothecene mycotoxins. Interestingly, UGT genes had higher expression levels in FHB-resistant wheat genotypes such as "Sumai 3" (Gottwald et al., 2012).

4.2.1.4 Chromosome 5B

QTL *QFhb-5B.1* conferred up to 53% of the phenotypic variation for FHB SEV and DON and was detected around 508.8 Mb, 114.2 Mb away from the vernalization gene *VRN-B1* (613.0 Mb). It was not associated with agro-morphological traits. Ruan et al. (2020) identified a QTL for FHB INC and FHB index in the *VRN-B1* region (577–694 Mb) that affected HD, supporting that this QTL is indeed unique from that published previously.

4.2.1.5 Chromosome 7B

On 7BL, *QFhb-7B.2* was associated with FHB SEV and DON. The allele associated with reduced SEV and DON was also associated with elevated YP, an important end-use quality trait in durum wheat (Pozniak et al., 2007). The association with YP was perhaps not surprising since *QFhb-7B.2* is physically located near *Psy1-B1*, a critical gene in the carotenoid biosynthetic pathway that is partially responsible for the elevated yellow color in the grains of durum wheat (Pozniak et al., 2007). We did notice, however, that this QTL was also associated with a slight reduction in grain protein content. Indeed, DON showed a weak negative correlation with PRO (−0.17) (Figure 2). This is in contrast to previous reports that observed a positive correlation between FHB symptoms and PRO, likely because of the degradation of starchy content by *Fusarium* spp. and of proteins by the hyphae of the fungus causes the consequent increase in PRO (Boyacioglu et al., 1992). However, given the relatively small negative correlation, any potential loss in PRO is likely to be overcome in breeding programs by simultaneous selection for low DON and higher PRO, as has been done for other negatively correlated traits (Ruan et al., 2021).

4.2.2 QTL regions for FHB response colocalized with agro-morphological traits

Responses to FHB resistance involve complex biological mechanisms and environmental conditions. Wheat is most susceptible to FHB infection during anthesis, particularly if the flowering period coincides with warm, humid conditions that promote disease development (Hooker et al., 2002). For example, HD (or AD) might affect the disease scores when the germplasm differs in maturity, and correlations can be positive or negative, depending on weather conditions in different years. Consequently, FHB traits and flowering time QTL are often associated with mapping studies (Sari et al., 2019; Ruan et al., 2020). In our study, two of the major QTL for FHB responses, *QFhb-4B.1* and *QFhb-5A*, colocalized with all agro-morphological traits (Table 1). In addition, *QFhb-2B.1*, *QFhb-6A*, *QFhb-7A*, and *QFhb-7B.1* colocalized with minor PH and/or HD and MAT QTL. So, while these QTL may be useful for targeted selection breeding, their selection may result in undesirable influence on phenotypic expression of flowering time, time to maturity, and plant height. Indeed, taller plants have a greater chance to escape infection, and increased height likely reduces the relative humidity near the wheat spikes, but an excessive plant height is undesirable in commercial durum wheat production.

4.2.2.1 Chromosome 4B

Five QTL regions were identified on Chr 4B (Table 1; Supplementary Tables S4) in our study. Of these, QTL *QFhb-4B.4* was solely associated with DON and ISD, an index based on 60% of the DON value (PRCWRT, 2013). In the same interval, a QTL for FHB SEV was previously identified (Nannuru et al., 2022). *QFhb-4B.1* (spanning 29.0–35.5 Mb physical interval) was associated with all FHB response traits, including DON. However, this QTL consistently colocalized with major QTL (R^2 = 60.3 and LOD = 43.0) for PH and MAT. In a similar QTL region, Nannuru et al. (2022) identified QTL for resistance to FHB severity and DON in

the spring European wheat panel using scorings corrected for the confounding effect of PH and HD. Plant height has been reported to be associated with FHB (Mao et al., 2010; Miedaner et al., 2017; Sari et al., 2018; Steiner et al., 2019b; Buerstmayr and Buerstmayr, 2022). The correlation analysis in the present study further confirms these reports, as FHB SEV, INC, and DON were negatively correlated with PH.

Based on our analysis, *QFhb-4B.1* localizes to a similar genomic interval as *Rht1* (*Rht-B1*) on chromosome 4B. We confirmed this by assaying the allelic state of *Rht-B1* using a robust DNA marker for that gene (Ellis et al., 2002) (Supplementary Table S1). In our diversity panel, the *Rht-B1b* marker explained 4.1% and 5.7% of the phenotypic variance of the mean FHB SEV and INC, respectively, whereas it explained 49.3% of the mean PH variance. According to previous reports, there is an association between *Rht-B1a* (GA-sensitive allele), low FHB infection, and tall plant height (He et al., 2016a; Dhariwal et al., 2020; Nannuru et al., 2022). Given the strong influence of *Rht-B1b* on FHB susceptibility in our population, other dwarfing genes that do not impact the phenotypic expression of resistance should be considered by breeders. One GA-insensitive dwarfing gene, *Rht24*, may be a suitable alternative because it reduces plant height without influencing FHB (Herter et al., 2018).

4.2.2.2 Chromosome 5A

One of the most stable QTL regions identified in this study was *QFhb-5A* (Supplementary Figure S8), which spans 586.6–595.4 Mb and was associated with all the FHB response traits considered in the current study. However, this QTL also colocated within the interval of major QTL (R^2 = 44.5) for HD/AD and MAT. The physical position of this QTL supports that it is not *Fhb5* (Buerstmayr et al., 2009; Xue et al., 2011), which spans a physical interval between 105.4 and 214.2 Mb of chromosome 5A (Ma et al., 2020). However, *QFhb-5A* overlaps with other QTL reported previously—5A2 (Sari et al., 2020) with similar representative SNPs *wsnp_AJ612027A_Ta_2_5* and *Kukri_c33022_198*, spanning a physical interval of 550.5–556.8 Mb (Sari et al., 2018) and 551.0–556.6 Mb (Sari et al., 2020). Similarly, Ruan et al. (2020) reported a QTL for FHB response and flowering time in the same physical interval (585–591 Mb). *QFhb-5A* also appears to be congruent with a 5A QTL for FHB resistance derived from European winter wheat cultivars Arina, Pirat, and Apache (Gervais et al., 2003; Paillard et al., 2004; Draeger et al., 2007; Holzapfel et al., 2008; Gaire et al., 2021) and in Chinese spring wheat (Zhu et al., 2020) and European spring wheat (Nannuru et al., 2022).

Flowering time is an adaptive trait of wheat, and it is regulated by a complex pathway to ensure that grain filling occurs under favorable conditions (Royo et al., 2020). Allelic variation at the *Vrn1* loci in wheat regulates flowering time, plant height, spike, and spikelet morphology (Li et al., 2019). We determined that *Vrn-A1* correlates with the physical interval of *QFhb-5A* and has been associated with FHB response previously. A similar result is reported by Gervais et al. (2003); He et al. (2016b), and Klahr et al. (2007), where the QTL for the FHB response was likely to be conferred by the pleiotropic effects of *Vrn-A1*. According to He et al. (2016b), the effect of *Vrn-A1* on FHB resistance decreased substantially when DH was used as a covariate. Thus, current evidence supports that *QFhb-5A* is most likely pleiotropically associated with the effect of *Vrn-A1* on flowering time, despite this gene only having a moderate influence on flowering time in durum wheat (Ruan et al., 2020). However, as noted prior, *Vrn-A1* does not influence flowering time alone but also regulates spike and spikelet development, and plant height. Our current hypothesis is that *QFhb-5A* is not associated with HD per se but is likely associated with the pleiotropic effects on spikelet formation. Indeed, spike development impacts type II (resistance to FHB spread in the wheat spike), and mutants of *Vrn1* in wheat delay the formation of terminal spikelets and increase the overall number of spikelets per spike (Li et al., 2019). Therefore, caution should be taken when using this QTL in resistance breeding because the mechanism of colocalization between the vernalization genes and FHB resistance is still unclear.

4.3 Exploitation of FHB resistance QTL in durum wheat breeding

We identified *QFhb-3B.1* in our diversity panel as an effective QTL to reduce INC and SEV (Supplementary Figure S6), and based on marker data, we confirmed this QTL is congruent with *Fhb1* (Supplementary Table S1). *Fhb1* is the well-studied QTL for FHB resistance breeding in wheat and provides type II resistance and the ability to detoxify DON (Lemmens et al., 2005). However, the low frequency of resistance alleles in elite wheat breeding parents and concerns about the detrimental effect of linkage drag have limited the utilization of *Fhb1* in breeding programs (Brar et al., 2019). In addition, the introgression of *Fhb1* into durum wheat has been challenging due to unstable expression in a durum genetic background (Zhao et al., 2018). However, Prat et al. (2017) successfully introgressed *Fhb1* from Sumai 3 into two European durum cultivars (Karur and Durobonus) and an Austrian breeding line (SZD1029K), which we included in our diversity panel. We also included several breeding lines in our panel carrying *Fhb1* that are derived from introgression efforts (Supplementary Table S1). Allelic variation at *Fhb1* was associated with all FHB-related traits except for DON (Supplementary Figure S6), confirming the effectiveness of *Fhb1* introgression in some durum backgrounds. Moreover, we identified additional lines in our diversity panel that appear to be carriers of *Fhb1* based on KASP marker (*Fhb1-TaHRC*) data (Supplementary Table S1). However, the effect of *Fhb1* varied depending on the durum genetic background and the individual environments, explaining between 7% and 20% of the phenotypic variance, and indeed, some accessions harboring *Fhb1* showed moderate susceptibility to FHB in our studies. Previous studies have also demonstrated that *Fhb1* is neutral or does not effectively increase resistance to FHB alone in certain genotypes (Pumphrey et al., 2007). The discrepancies observed among *Fhb1* introgressions with different durum backgrounds may be due to differences in their respective genetic resistance architectures (Prat et al., 2017) or the presence of susceptibility factors and suppressor genes in its genome (Ghavami et al., 2011) that compromised the expression of FHB resistance in durum wheat. Furthermore, we noted that *Fhb1* introgressions showed reduced YP and PRO compared to non-carriers (Supplementary Figure S11).

In Canada, durum wheat cultivars such as Brigade (Clarke et al., 2009), Transcend (Singh et al., 2012), CDC Credence (Pozniak et al., 2020a), CDC Defy (Pozniak et al., 2020b), and AAC Schrader show improved FHB resistance relative to other elite durum wheat cultivars in Canadian production. These were developed by accumulating native resistance genes (Ruan et al., 2020; Sari et al., 2020) through phenotypic selection. Several Canadian durum wheat cultivars and advanced breeding lines—for example, Brigade, DT1021, DT696, Transcend, and DT2004—carry four favorable alleles for reduced DON accumulation. Therefore, these cultivars and breeding lines are a useful platform for stacking additional FHB resistance QTL (including *Fhb1*), which should result in further improvements in FHB resistance.

Because the QTL *QFhb-2A.3*, *QFhb-2B.4*, *QFhb-3B.2*, *QFhb-6B.1*, and *QFhb-6B.3* were not associated with the agro-morphological traits, these are likely a higher priority for immediate use in durum wheat breeding programs. Lines with resistance alleles at these QTL (ABAAA haplotype, Figure 6) showed relatively less mean FHB VRI and DON accumulation, whereas those lacking the resistance alleles showed high FHB SEV and more DON accumulation (Figure 6). Therefore, these lines carrying favorable haplotypes (such as ABAAA) could be good sources for FHB resistance breeding.

The GDP is an internationally established diversity panel comprising a wide representation of *Triticum turgidum* ssp. *durum* cultivars, modern germplasm, and landraces, along with a selection of emmer (*T. turgidum* ssp. *dicoccum*, *T. turgidum* ssp. *dicoccoides*) and primitive tetraploid wheats (Mazzucotelli et al., 2020). The panel is publicly available and is recognized by the durum wheat community as a vehicle to drive the discovery of useful alleles and their immediate deployment in breeding activities. To that end, we have developed KASP markers for utility in breeding programs (Supplementary Figure S12; Supplementary Table S9) and used these to characterize the six consistently expressed FHB-trait-associated QTL (see results section 3.5) and to describe their haplotypes in the GDP (Supplementary Table S9). This analysis revealed a relatively low frequency of resistance-associated haplotypes for some of the QTL in cultivated durum wheat, while a higher frequency of resistance alleles was detected in domesticated and wild emmer accessions (Figure 5). This trend of declining frequency of resistant alleles in commercial cultivars may reflect that the selection for other agronomically important traits may have reduced the frequency of FHB resistance in breeding programs. This may not be surprising, since many of the QTL we identified were associated with agro-morphological traits important to regional adaption (heading time, maturity time, plant height).

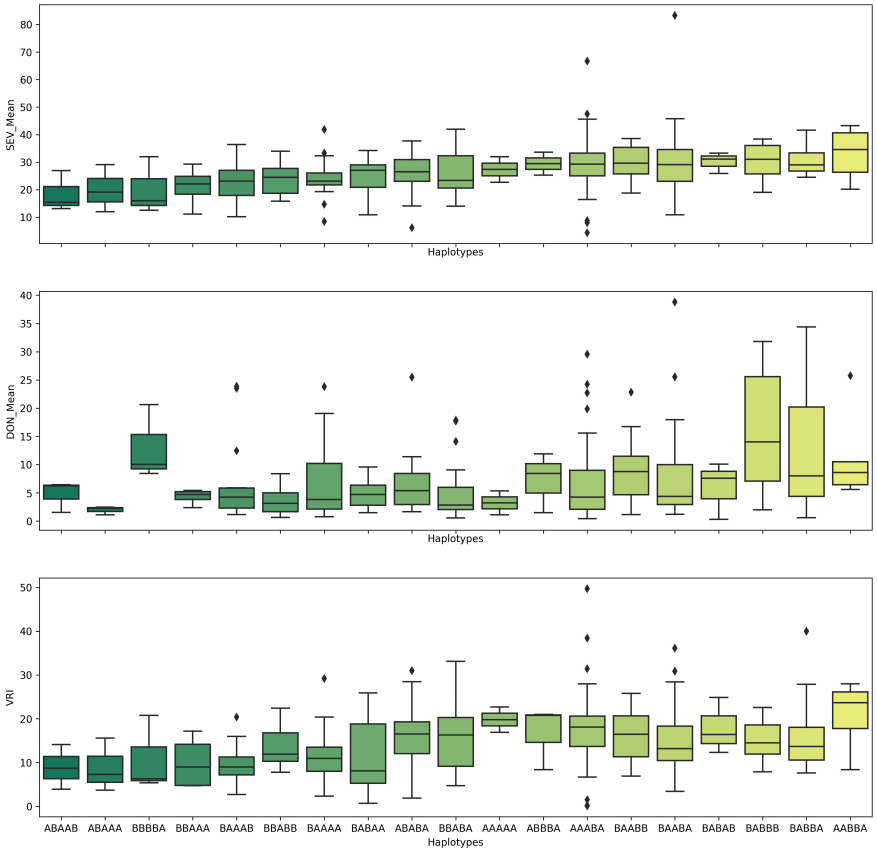

FIGURE 6
Pyramiding effects of *QFhb-2A.3*, *QFhb-3B.2*, *QFhb-6A*, *QFhb-6B.1*, and *QFhb-7B.2* provide resistance to FHB SEV, INC, and DON accumulation. SEV, severity (%); INC, incidence (%); DON, deoxynivalenol (ppm).

For example, *QFhb-5A* was strongly associated with FHB resistance but, as we noted above, was associated with HD, AD, HT, and MAT (Table 1). Both HD and MAT must be optimized for regional adaptation and to maximize grain yield potential (Alahmad et al., 2020), and selection for these two traits may have unintendedly reduced the frequency of FHB resistance alleles. At the same time, in a study by Gaire et al. (2021), the accumulation of FHB-resistance loci showed reduced DON but resulted in lower yield potential, highlighting a trade-off between FHB resistance and grain yield.

The wild relatives of wheat are a valuable resource for FHB resistance in wheat, and various studies have identified moderate levels of resistance in the wild (Ruan et al., 2012), cultivated emmer wheat (Ruan et al., 2012; Ruan et al., 2020), and Persian wheat (*T. carthlicum;* Somers et al., 2006). In our study, the frequency of resistant haplotypes at the six prominent QTL (Supplementary Table S6) was higher in the wild and domesticated emmer accessions from our panel (Supplementary Table S1), supporting their use in breeding. For example, we included several elite progenies of lines from *T. carthlicum* cv. "Blackbird" (Somers et al., 2006) and *T. turgidum* ssp. *dicoccum* TG3487 (Ruan et al., 2012; Ruan et al., 2020). Their progeny (D04X_84_030, D04X_84_033, and D04X_84_104), P48_19, A1200J_101, and A1200K_209, P49_7, and R11_27_1, carried the favorable alleles for the five FHB resistance QTL. Thus, exotic and wild germplasm is an important source of FHB resistance, and we are currently pyramiding the QTL identified from these native sources of resistance. Of course, we are mindful that linkage drag with other important durum traits is a reality when using these materials—as we observed for PRO and YP—but in our experience, these negative associations can be overcome by using a combination of marker-assisted selection, genomic selection, and coselection for FHB-related traits and agronomic performance (Haile et al., 2019).

5 Conclusions

Identifying and utilizing novel QTL and genes for resistance is a continuous and regular challenge in plant breeding to deal with the threats to crop production caused by diseases. Genome-wide association studies are one of the strategies to detect QTL associated with resistance. In this study, by applying ML-GWAS models to a panel of 265 durum wheat cultivars, breeding lines, and experimental populations, we provided comprehensive insight into the molecular genetic basis of FHB resistance and correlated agro-morphological and quality traits. SNPs associated with FHB resistance were identified across the 14 chromosomes. Among the major QTL identified in this study, six QTL regions on chromosomes 2A, 2B, 3B, 5A, and 6B were the most consistent across traits and environments and are recommended for marker-assisted gene stacking. Although most of them are identified in known regions, *QFhb-3B.2* associated with FHB SEV, INC, and DON could enhance our understanding and provide new resources for FHB resistance breeding. Stacking the QTL identified in this study and using the lines carrying the resistance alleles will facilitate further genetic improvement of FHB resistance and reduce DON accumulation in durum wheat. However, it is vital to integrate trait associations into breeding decisions, particularly when using QTL such as *QFhb.4B.1* and *QFhb.5A*, which colocalized with multiple agro-morphological traits.

Lastly, based on the results of our and previous studies (Prat et al., 2017; Ruan et al., 2020), *Fhb1* is effective in diverse durum backgrounds and in combination with other resistance QTL. Therefore, we suggest that pyramiding *Fhb1* with resistance QTL derived from exotic germplasm (*T. turgidum* ssp. *dicoccoides* and *T. turgidum* ssp. *dicoccum*) could improve FHB resistance in durum wheat. Finally, we have developed robust KASP markers for the six prominent QTL associated with FHB resistance and quantified their haplotypes in the Global Durum Panel. These markers, together with their assessment of the GDP, will be a useful resource to support marker-assisted breeding and/or as main effect markers in genomic selection programs.

Data availability statement

The datasets presented in this study can be found in online repositories. The names of the repository/repositories and accession number(s) can be found in the article/Supplementary Material.

Author contributions

JH and CJP designed the experiments. JH, M-AH, VK, KW, and LW conducted experiments and collected data under the supervision of CP. JH, DS, AN, KW, and HC performed data analysis. JH prepared the manuscript with input from DS and AN. CP, VK, BS, HB, HK, DS, M-AH, LW, and YR reviewed and edited the manuscript. All authors contributed to the article and approved the submitted version.

Funding

The authors acknowledge funding provided by the "4D Wheat: Diversity, Domestication, Discovery and Delivery" project, funded by Genome Canada, Agriculture and Agri-Food Canada, Western Grains Research Foundation, Saskatchewan Ministry of Agriculture, Saskatchewan Wheat Development Commission, Alberta Wheat Commission, Manitoba Crop Alliance, Ontario Research Fund, Viterra, Canadian Agricultural Partnership, and Illumina. We also acknowledge the administrative support of Genome Prairie.

Acknowledgments

The authors are grateful to Dr. Julia Lafferty (Saatzucht Donau GesmbH. & CoKG, Austria) and Agriculture and Agri-food-Canada for providing some of the breeding lines used in this study. The authors acknowledge Ens Jennifer, Lexie Gerl, Xue (Snow) Lin, Ayla Lichtenwald, Madison Kist, Maureen Troesch, Russel Lawrie, Ryan Babonich, Heidi Lazorko, and Eldon Simons for their assistance and technical support.

Conflict of interest

The authors declare that the research was conducted in the absence of any commercial or financial relationships that could be construed as a potential conflict of interest.

Publisher's note

All claims expressed in this article are solely those of the authors and do not necessarily represent those of their affiliated organizations, or those of the publisher, the editors and the reviewers. Any product that may be evaluated in this article, or claim that may be made by its manufacturer, is not guaranteed or endorsed by the publisher.

Supplementary material

The Supplementary Material for this article can be found online at: https://www.frontiersin.org/articles/10.3389/fpls.2023.1182548/full#supplementary-material

References

Alahmad, S., Kang, Y., Dinglasan, E., Mazzucorelli, E., Voss-Fels, K. P., Avle, J. A., et al. (2020). Adaptive traits to improve durum wheat yield in drought and crown rot environments. *Int. J. Mol. Sci.* 21 (15), 5260. doi: 10.3390/ijms21155260

Anderson, J. A., Stack, R. W., Liu, S., Waldron, B. L., Fjeld, A. D., Coyne, C., et al. (2001). DNA markers for Fusarium head blight resistance QTLs in two wheat populations. *Theor. Appl. Genet.* 102, 1164–1168. doi: 10.1007/s001220000509

Arruda, M. P., Lipka, A. E., Brown, P. J., Krill, A. M., Thurber, C., Brown-Guedira, G., et al. (2016). Comparing genomic selection and marker-assisted selection for Fusarium head blight resistance in wheat (*Triticum aestivum* L.). *Mol. Breed.* 36, 84. doi: 10.1007/s11032-016-0508-5

Bai, G. H., Desjardins, A. E., and Plattner, R. D. (2002). Deoxynivalenol-nonproducing *Fusarium graminearum* causes initial infection but does not cause disease spread in wheat spikes. *Mycopathologia* 153, 91–98. doi: 10.1023/A:1014419323550

Benesty, J., Chen, J., Huang, Y., and Cohen, I. (2009). "Pearson Correlation Coefficient," in *Noise Reduction in Speech Processing*. Eds. I. Cohen, Y. Huang, J. Chen and J. Benesty (Berlin, Heidelberg: Springer Berlin Heidelberg).

Berners-Lee, M., Kennelly, C., Watson, R., and Hewitt, C. N. (2018). Current global food production is sufficient to meet human nutritional needs in 2050 provided there is radical societal adaptation. *Elementa: Sci. Anthropocene* 6, 52. doi: 10.1525/elementa.310

Boyacioglu, D., Hettiarachchy, N. S., and Stack, R. W. (1992). Effect of three systemic fungicides on deoxynivalenol (vomitoxin) production by Fusarium graminearum in wheat. *Can. J. Plant Sci.* 72, 93–101. doi: 10.4141/cjps92-010

Bradbury, P. J., Zhang, Z., Kroon, D. E., Casstevens, T. M., Ramdoss, Y., and Buckler, E. S. (2007). TASSEL: software for association mapping of complex traits in diverse samples. *Bioinformatics* 23, 2633–2635. doi: 10.1093/bioinformatics/btm308

Brar, G. S., Pozniak, C. J., Kutcher, H. R., and Hucl, P. J. (2019). Evaluation of Fusarium head blight resistance genes Fhb1, Fhb2, and Fhb5 introgressed into elite Canadian hard red spring wheats: effect on agronomic and end-use quality traits and implications for breeding. *Mol. Breed.* 39, 44. doi: 10.1007/s11032-019-0957-8

Buerstmayr, H., Ban, T., and Anderson, J. A. (2009). QTL mapping and marker-assisted selection for Fusarium head blight resistance in wheat: a review. *Plant Breed.* 128, 1–26. doi: 10.1111/j.1439-0523.2008.01550.x

Buerstmayr, M., Alimari, A., Steiner, B., and Buerstmayr, H. (2013). Genetic mapping of QTL for resistance to Fusarium head blight spread (type 2 resistance) in a Triticum dicoccoides 9 Triticum durum backcross-derived population. *Theor. Appl. Genet.* 126, 2825–2834. doi: 10.1007/s00122-013-2174-x

Buerstmayr, M., and Buerstmayr, H. (2016). The semidwarfing alleles rht-D1b and rht-B1b show marked differences in their associations with anther-retention in wheat heads and with fusarium head blight susceptibility. *Phytopathology®* 106, 1544–1552. doi: 10.1094/PHYTO-05-16-0200-R

Buerstmayr, M., and Buerstmayr, H. (2022). The effect of the Rht1 haplotype on Fusarium head blight resistance in relation to type and level of background resistance and in combination with Fhb1 and Qfhs.ifa-5A. *Theor. Appl. Genet.* 135, 1985–1996. doi: 10.1007/s00122-022-04088-x

Buerstmayr, M., Huber, K., Heckmann, J., Steiner, B., Nelson, J. C., and Buerstmayr, H. (2012). Mapping of QTL for Fusarium head blight resistance and morphological and developmental traits in three backcross populations derived from Triticum dicoccum × Triticum durum. *Theor. Appl. Genet.* 125, 1751–1765. doi: 10.1007/s00122-012-1951-2

Buerstmayr, H., and Lemmens, M. (2015). Breeding healthy cereals: genetic improvement of Fusarium resistance and consequences for mycotoxins. *World Mycotoxin J.* 8, 591–602. doi: 10.3920/WMJ2015.1889

Buerstmayr, M., Steiner, B., and Buerstmayr, H. (2020). Breeding for Fusarium head blight resistance in wheat—Progress and challenges. *Plant Breed.* 139, 429–454. doi: 10.1111/pbr.12797

Buerstmayr, H., Stierschneider, M., Steiner, B., Lemmens, M., Griesser, M., Nevo, E., et al. (2003). Variation for resistance to head blight caused by Fusarium graminearum in wild emmer (Triticum dicoccoides) originating from Israel. *Euphytica* 130, 17–23. doi: 10.1023/A:1022324727780

Canadian Grain Commission (2019). *Grain and food safety* (600-303 Main Street, Winnipeg, MB R3C 3G8: Canadian Grain Commission).

Carvajal-Yepes, M., Cardwell, K., Nelson, A., Garrett, K. A., Giovani, B., Saunders, D. G. O., et al. (2019). A global surveillance system for crop diseases. *Science* 364, 1237–1239. doi: 10.1126/science.aaw1572

Clarke, J. M., Knox, R. E., Depauw, R. M., Clarke, F. R., Fernandez, M. R., Mccaig, T. N., et al. (2009). Brigade durum wheat. *Can. J. Plant Sci.* 89, 505–509. doi: 10.4141/CJPS08168

Cuthbert, P. A., Somers, D. J., Thomas, J., Cloutier, S., and Brule-Babel, A. (2006). Fine mapping *Fhb1*, a major gene controlling fusarium head blight resistance in bread wheat (Triticum aestivum L.). *Theor. Appl. Genet.* 112, 1465–1472. doi: 10.1007/s00122-006-0249-7

Dhariwal, R., Henriquez, M. A., Hiebert, C., Mccartney, C. A., and Randhawa, H. S. (2020). Mapping of major fusarium head blight resistance from Canadian wheat cv. AAC tenacious. *Int. J. Mol. Sci.* 21, 4497. doi: 10.3390/ijms21124497

Distelfeld, A., Li, C., and Dubcovsky, J. (2009). Regulation of flowering in temperate cereals. *Curr. Opin. Plant Biol.* 12, 178–184. doi: 10.1016/j.pbi.2008.12.010

Draeger, R., Gosman, N., Steed, A., Chandler, E., Thomsett, M., Srinivasachary,, et al. (2007). Identification of QTLs for resistance to Fusarium head blight, DON accumulation and associated traits in the winter wheat variety Arina. *Theor. Appl. Genet.* 115, 617–625. doi: 10.1007/s00122-007-0592-3

Ellis, M., Spielmeyer, W., Gale, K., Rebetzke, G., and Richards, R. (2002). "Perfect" markers for the *Rht-B1b* and *Rht-D1b* dwarfing genes in wheat. *Theor. Appl. Genet.* 105 (6–7), 1038–1042. doi: 10.1007/s00122-002-1048-4

FAO. (2009). *How to Feed the World in 2050.* Available at: https://www.fao.org/fileadmin/templates/wsfs/docs/expert_paper/How_to_Feed_the_World_in_2050.pdf.

Fatima, F., Mccallum, B. D., Pozniak, C. J., Hiebert, C. W., Mccartney, C. A., Fedak, G., et al. (2020). Identification of new leaf rust resistance loci in wheat and wild relatives by array-based SNP genotyping and association genetics. *Front. Plant Sci.* 11, 583738. doi: 10.3389/fpls.2020.583738

Foroud, N. A., Baines, D., Gagkaeva, T. Y., Thakor, N., Badea, A., Steiner, B., et al. (2019). Trichothecenes in cereal grains – an update. *Toxins* 11, 634. doi: 10.3390/toxins11110634

Frichot, E., and François, O. (2015). LEA: an R package for landscape and ecological association studies. *Methods Ecol. Evol.* 6, 925–929. doi: 10.1111/2041-210X.12382

Frichot, E., Mathieu, F., Trouillon, T., Bouchard, G., and François, O. (2014). Fast and efficient estimation of individual ancestry coefficients. *Genetics* 196, 973–983. doi: 10.1534/genetics.113.160572

Gaire, R., Brown-Guedira, G., Dong, Y., Ohm, H., and Mohammadi, M. (2021). Genome-wide association studies for fusarium head blight resistance and its trade-off with grain yield in soft red winter wheat. *Plant Dis.* 105, 2435–2444. doi: 10.1094/PDIS-06-20-1361-RE

Gervais, L., Dedryver, F., Morlais, J. Y., Bodusseau, V., Negre, S., Bilous, M., et al. (2003). Mapping of quantitative trait loci for field resistance to Fusarium head blight in an European winter wheat. *Theor. And Appl. Genet.* 106, 961–970. doi: 10.1007/s00122-002-1160-5

Ghavami, F., Elias, E. M., Mamidi, S., Ansari, O., Sargolzaei, M., Adhikari, T., et al. (2011). Mixed model association mapping for fusarium head blight resistance in Tunisian-derived durum wheat populations. *G3: Genes|Genomes|Genetics* 1, 209–218. doi: 10.1534/g3.111.000489

Giancaspro, A., Giove, S. L., Zito, D., Blanco, A., and Gadaleta, A. (2016). Mapping QTLs for fusarium head blight resistance in an interspecific wheat population. *Front. Plant Sci.* 7. doi: 10.3389/fpls.2016.01381

Gladysz, C., Lemmens, M., Steiner, B., and Buerstmayr, H. (2007). Evaluation and genetic mapping of resistance to Fusarium head blight in *Triticum dicoccoides*. *Israel J. Plant Sci.* 55, 263–266. doi: 10.1560/IJPS.55.3-4.263

Gottwald, S., Samans, B., Lück, S., and Friedt, W. (2012). Jasmonate and ethylene dependent defence gene expression and suppression of fungal virulence factors: two essential mechanisms of Fusarium head blight resistance in wheat? *BMC Genomics* 13, 369. doi: 10.1186/1471-2164-13-369

Haile, J. K., N'diaye, A., Clarke, F., Clarke, J., Knox, R., Rutkoski, J., et al. (2018). Genomic selection for grain yield and quality traits in durum wheat. *Mol. Breed.* 38, 75. doi: 10.1007/s11032-018-0818-x

Haile, J. K., N'diaye, A., Walkowiak, S, Nilsen, K. T., Clarke, J. M., Kutcher, H. R., et al. (2019). Fusarium head blight in durum wheat: recent status, breeding directions, and future research prospects. *Phytopathology* 109, 1664–1675. doi: 10.1094/phyto-03-19-0095-rvw

Haile, J. K., N'diaye, A., Sari, E., Walkowiak, S., Rutkoski, J. E., Kutcher, H. R., et al. (2020). Potential of genomic selection and integrating "Omics" Data for disease evaluation in wheat. *Crop Breed. Genet. Genomics* 2, e200016. doi: 10.20900/cbgg20200016

He, X., Lillemo, M., Shi, J., Wu, J., Bjørnstad, Å., Belova, T., et al. (2016b). QTL characterization of fusarium head blight resistance in CIMMYT bread wheat line soru1. *PloS One* 11, e0158052. doi: 10.1371/journal.pone.0158052

He, J., Meng, S., Zhao, T., Xing, G., Yang, S., Li, Y., et al. (2017). An innovative procedure of genome-wide association analysis fits studies on germplasm population and plant breeding. *Theor. Appl. Genet.* 130, 2327–2343. doi: 10.1007/s00122-017-2962-9

He, X., Singh, P. K., Dreisigacker, S., Singh, S., Lillemo, M., and Duveiller, E. (2016a). Dwarfing genes rht-B1b and rht-D1b are associated with both type I FHB susceptibility and low anther extrusion in two bread wheat populations. *PloS One* 11, e0162499. doi: 10.1371/journal.pone.0162499

He, X., Singh, P. K., Schlang, N., Duveiller, E., Dreisigacker, S., Payne, T., et al. (2014). Characterization of Chinese wheat germplasm for resistance to Fusarium head blight at CIMMYT, Mexico. *Euphytica* 195, 383–395. doi: 10.1007/s10681-013-1002-3

Herter, C. P., Ebmeyer, E., Kollers, S., Korzun, V., Leiser, W. L., Würschum, T., et al. (2018). Rht24 reduces height in the winter wheat population 'Solitär × Bussard' without adverse effects on Fusarium head blight infection. *Theor. Appl. Genet.* 131, 1263–1272. doi: 10.1007/s00122-018-3076-8

Holzapfel, J., Voss, H.-H., Miedaner, T., Korzun, V., Häberle, J., Schweizer, G., et al. (2008). Inheritance of resistance to Fusarium head blight in three European winter wheat populations. *Theor. Appl. Genet.* 117, 1119–1128. doi: 10.1007/s00122-008-0850-z

Hooker, D. C., Schaafsma, A. W., and Tamburic-Ilincic, L. (2002). Using weather variables pre- and post-heading to predict deoxynivalenol content in winter wheat. *Plant Dis.* 86, 611–619. doi: 10.1094/PDIS.2002.86.6.611

Jia, H., Cho, S., and Muehlbauer, G. J. (2009). Transcriptome analysis of a wheat near-isogenic line pair carrying fusarium head blight–resistant and –susceptible alleles. *Mol. Plant-Microbe Interactions®* 22, 1366–1378. doi: 10.1094/MPMI-22-11-1366

Jiang, J., Zhao, J., Duan, W., Tian, S., Wang, X., Zhuang, H., et al. (2019). TaAMT2;3a, a wheat AMT2-type ammonium transporter, facilitates the infection of stripe rust fungus on wheat. *BMC Plant Biol.* 19, 239. doi: 10.1186/s12870-019-1841-8

Jombart, T. (2008). adegenet: a R package for the multivariate analysis of genetic markers. *Bioinformatics* 24, 1403–1405. doi: 10.1093/bioinformatics/btn129

Jombart, T., Kamvar, Z. N., Collins, C., Luštrik, R., Beugin, M.-P., Knaus, B. J., et al. (2020). *Adegenet: exploratory analysis of genetic and genomic data*. Available at: http://adegenet.rforge.r-project.org/.

Kim, S. A., Brossard, M., Roshandel, D., Paterson, A. D., Bull, S. B., and Yoo, Y. J. (2019). gpart: human genome partitioning and visualization of high-density SNP data by identifying haplotype blocks. *Bioinformatics* 35, 4419–4421. doi: 10.1093/bioinformatics/btz308

Klahr, A., Zimmermann, G., Wenzel, G., and Mohler, V. (2007). Effects of environment, disease progress, plant height and heading date on the detection of QTLs for resistance to Fusarium head blight in an European winter wheat cross. *Euphytica* 154, 17–28. doi: 10.1007/s10681-006-9264-7

Kumar, S., Stack, R. W., Friesen, T. L., and Faris, J. D. (2007). Identification of a novel fusarium head blight resistance quantitative trait locus on chromosome 7A in tetraploid wheat. *Phytopathology* 97, 592–597. doi: 10.1094/PHYTO-97-5-0592

Lemmens, M., Scholz, U., Berthiller, F., Dall'asta, C., Koutnik, A., Schuhmacher, R., et al. (2005). The ability to detoxify the mycotoxin deoxynivalenol colocalizes with a major quantitative trait locus for Fusarium head blight resistance in wheat. *Mol. Plant Microbe Interact.* 18, 1318–1324. doi: 10.1094/MPMI-18-1318

Lemmens, M., Steiner, B., Sulyok, M., Nicholson, P., Mesterhazy, A., and Buerstmayr, H. (2016). Masked mycotoxins: does breeding for enhanced Fusarium head blight resistance result in more deoxynivalenol-3-glucoside in new wheat varieties? *World Mycotoxin J.* 9, 741–754. doi: 10.3920/WMJ2015.2029

Letunic, I., and Bork, P. (2016). Interactive tree of life (iTOL) v3: an online tool for the display and annotation of phylogenetic and other trees. *Nucleic Acids Res.* 44, W242–W245. doi: 10.1093/nar/gkw290

Li, C., Fu, Y., Sun, R., Wang, Y., and Wang, Q. (2018). Single-locus and multi-locus genome-wide association studies in the genetic dissection of fiber quality traits in upland cotton (Gossypium hirsutum L.). *Front. Plant Sci.* 9. doi: 10.3389/fpls.2018.01083

Li, C., Lin, H., Chen, A., Lau, M., Jernstedt, J., and Dubcovsky, J. (2019). Wheat *VRN1, FUL2* and *FUL3* play critical and redundant roles in spikelet development and spike determinacy. *Development* 146 (14), dev175398. doi: 10.1242/dev.175398

Liu, S., Zhang, X., Pumphrey, M. O., Stack, R. W., Gill, B. S., and Anderson, J. A. (2006). Complex microcolinearity among wheat, rice, and barley revealed by fine mapping of the genomic region harboring a major QTL for resistance to Fusarium head blight in wheat. *Funct. Integr. Genomics* 6, 83–89. doi: 10.1007/s10142-005-0007-y

Ma, Z., Xie, Q., Li, G., Jia, H., Zhou, J., Kong, Z., et al. (2020). Germplasms, genetics and genomics for better control of disastrous wheat Fusarium head blight. *Theor. Appl. Genet.* 133, 1541–1568. doi: 10.1007/s00122-019-03525-8

Mao, S.-L., Wei, Y.-M., Cao, W., Lan, X.-J., Yu, M., Chen, Z.-M., et al. (2010). *Confirmation of the relationship between plant height and Fusarium head blight resistance in wheat (Triticum aestivum L.) by QTL meta-analysis.*

Mazzucotelli, E., Sciara, G., Mastrangelo, A. M., Desiderio, F., Xu, S. S., Faris, J., et al. (2020). The global durum wheat panel (GDP): an international platform to identify and exchange beneficial alleles. *Front. Plant Sci.* 11, 569905. doi: 10.3389/fpls.2020.569905

Miedaner, T., Moldovan, M., and Ittu, M. (2003). Comparison of spray and point inoculation to assess resistance to fusarium head blight in a multienvironment wheat trial. *Phytopathology®* 93, 1068–1072. doi: 10.1094/PHYTO.2003.93.9.1068

Miedaner, T., Sieber, A.-N., Desaint, H., Buerstmayr, H., Longin, C. F. H., and Würschum, T. (2017). The potential of genomic-assisted breeding to improve Fusarium head blight resistance in winter durum wheat. *Plant Breed.* 136, 610–619. doi: 10.1111/pbr.12515

Mirocha, C. J., Xie, W., Xu, Y., Wilcoxson, R. D., Woodward, R. P., Etebarian, R. H., et al. (1994). Production of trichothecene mycotoxins by Fusarium graminearum and Fusarium culmorum on barley and wheat. *Mycopathologia* 128, 19–23. doi: 10.1007/BF01104274

Misra, G., Badoni, S., Domingo, C. J., Cuevas, R. P. O., Llorente, C., Mbanjo, E. G. N., et al. (2018). Deciphering the genetic architecture of cooked rice texture. *Front. Plant Sci.* 9. doi: 10.3389/fpls.2018.01405

Nannuru, V. K. R., Windju, S. S., Belova, T., Dieseth, J. A., Alsheikh, M., Dong, Y., et al. (2022). Genetic architecture of fusarium head blight disease resistance and associated traits in Nordic spring wheat. *Theor. Appl. Genet.* 135, 2247–2263. doi: 10.1007/s00122-022-04109-9

N'Diaye, A., Haile, J. K., Cory, A. T., Clarke, F. R., Clarke, J. M., Knox, R. E., et al. (2017). Single marker and haplotype-based association analysis of semolina and pasta colour in elite durum wheat breeding lines using a high-density consensus map. *PloS One* 12, e0170941. doi: 10.1371/journal.pone.0170941

OECD/FAO. (2019). *OECD-FAO Agricultural Outlook* (Paris: OECD Agriculture Statistics).

Otto, C. D., Kianian, S. F., Elias, E. M., Stack, R. W., and Joppa, L. R. (2002). Genetic dissection of a major Fusarium head blight QTL in tetraploid wheat. *Plant Mol. Biol.* 48, 625–632. doi: 10.1023/A:1014821929830

Paillard, S., Schnurbusch, T., Tiwari, R., Messmer, M., Winzeler, M., Keller, B., et al. (2004). QTL analysis of resistance to Fusarium head blight in Swiss winter wheat (Triticum aestivum L.). *Theor. Appl. Genet.* 109, 323–332. doi: 10.1007/s00122-004-1628-6

Peng, Z. S., Su, Z. X., and Cheng, K. C. (1999). Characterization of dwarf trait in the tetraptoid wheat landrace, Aiganfanma. *Wheat Inf Serv.* 89, 7–12.

Pestka, J. J., and Smolinski, A. T. (2005). Deoxynivalenol: toxicology and potential effects on humans. *J. Toxicol. Environ. Health B Crit. Rev.* 8, 39–69. doi: 10.1080/10937400590889458

Pozniak, C. J., Clarke, J. M., and Haile, T. A. (2020b). CDC Defy durum wheat. *Can. J. Plant Sci.* 100 (6), 725–730. doi: 10.1139/cjps-2020-0091

Pozniak, C. J., Clarke, J. M., Haile, J. K., and Haile, T. A. (2020a). CDC Credence durum wheat. *Can. J. Plant Sci.* 100 (6), 720–724. doi: 10.1139/cjps-2020-0092

Pozniak, C. J., Knox, R. E., Clarke, F. R., and Clarke, J. M. (2007). Identification of QTL and association of a phytoene synthase gene with endosperm colour in durum wheat. *Theor. Appl. Genet.* 114, 525–537. doi: 10.1007/s00122-006-0453-5

Prank, M., Kenaley, S. C., Bergstrom, G. C., Acevedo, M., and Mahowald, N. M. (2019). Climate change impacts the spread potential of wheat stem rust, a significant crop disease. *Environ. Res. Lett.* 14, 124053. doi: 10.1088/1748-9326/ab57de

Prat, N., Buerstmayr, M., Steiner, B., Robert, O., and Buerstmayr, H. (2014). Current knowledge on resistance to Fusarium head blight in tetraploid wheat. *Mol. Breed.* 34, 1689–1699. doi: 10.1007/s11032-014-0184-2

Prat, N., Guilbert, C., Prah, U., Wachter, E., Steiner, B., Langin, T., et al. (2017). QTL mapping of Fusarium head blight resistance in three related durum wheat populations. *Theor. Appl. Genet.* 130, 13–27. doi: 10.1007/s00122-016-2785-0

PRCWRT. (2013). *Operating procedures. Prairie grain recommending committee for wheat, rye and triticale operating procedures*. Available at: http://www.pgdc.ca/pdfs/wrt/Proposed%20PRCWRT%20OPS%20-%20FINAL%20DRAFT%20-%2027%20Nov%202013%20Updated%205%20December%202015.pdf.

Pumphrey, M. O., Bernardo, R., and Anderson, J. A. (2007). Validating the fhb1 QTL for fusarium head blight resistance in near-isogenic wheat lines developed from breeding populations. *Crop Sci.* 47, 200–206. doi: 10.2135/cropsci2006.03.0206

Ren, W.-L., Wen, Y.-J., Dunwell, J. M., and Zhang, Y.-M. (2018). pKWmEB: integration of Kruskal–Wallis test with empirical Bayes under polygenic background control for multi-locus genome-wide association study. *Heredity* 120, 208–218. doi: 10.1038/s41437-017-0007-4

Royo, C., Dreisigacker, S., Soriano, J. M., Lopes, M. S., Ammar, K., and Villegas, D. (2020). Allelic variation at the vernalization response (*Vrn-1*) and photoperiod sensitivity (*Ppd-1*) genes and their association with the development of durum wheat landraces and modern cultivars. *Front. Plant Sci.* 11, 00838. doi: 10.3389/fpls.2020.00838

Ruan, Y., Comeau, A., Langevin, F., Hucl, P., Clarke, J. M., Brule-Babel, A., et al. (2012). Identification of novel QTL for resistance to Fusarium head blight in a tetraploid wheat population. *Genome* 55, 853–864. doi: 10.1139/gen-2012-0110

Ruan, Y., Zhang, W., Knox, R. E., Berraies, S., Campbell, H. L., Ragupathy, R., et al. (2020). Characterization of the genetic architecture for fusarium head blight resistance in durum wheat: the complex association of resistance, flowering time, and height genes. *Front. Plant Sci.* 11, 592064. doi: 10.3389/fpls.2020.592064

Ruan, Y., Babonich, R., Clarke, J. M., Hucl, P. J., Clarke, F. R., Knox, R. E., et al. (2021). Differential reaction of hexaploid and tetraploid wheat to Fusarium graminearum chemotypes in a controlled environment. *Can. J. Plant Pathol.* 43 (5), 760–768. doi: 10.1080/07060661.2021.1907447

Sari, E., Berraies, S., Knox, R. E., Singh, A. K., Ruan, Y., Cuthbert, R. D., et al. (2018). High density genetic mapping of Fusarium head blight resistance QTL in tetraploid wheat. *PloS One* 13, e0204362. doi: 10.1371/journal.pone.0204362

Sari, E., Cabral, A. L., Polley, B., Tan, Y., Hsueh, E., Konkin, D. J., et al. (2019). Weighted gene co-expression network analysis unveils gene networks associated with the Fusarium head blight resistance in tetraploid wheat. *BMC Genomics* 20, 925. doi: 10.1186/s12864-019-6161-8

Sari, E., Knox, R. E., Ruan, Y., Henriquez, M. A., Kumar, S., Burt, A. J., et al. (2020). Historic recombination in a durum wheat breeding panel enables high-resolution mapping of Fusarium head blight resistance quantitative trait loci. *Sci. Rep.* 10, 7567. doi: 10.1038/s41598-020-64399-1

Savary, S., Ficke, A., Aubertot, J.-N., and Hollier, C. (2012). Crop losses due to diseases and their implications for global food production losses and food security. *Food Secur.* 4, 519–537. doi: 10.1007/s12571-012-0200-5

Savary, S., Willocquet, L., Pethybridge, S., Esker, P., Mcroberts, N., and Nelson, A. (2019). The global burden of pathogens and pests on major food crops. *Nat. Ecol. Evol.* 3, 1. doi: 10.1038/s41559-018-0793-y

Schroeder, H. W., Christensen, J. J., Christensen, J. D., Platz-Christensen, J., and Schroeder, H. W. (1963). Factors affecting resistance of Wheat to scab caused by Gibberella zeae. *Phytopathology* 53, 831–838. Available at: https://api.semanticscholar.org/CorpusID:80680493.

Schweiger, W., Steiner, B., Vautrin, S., Nussbaumer, T., Siegwart, G., Zamini, M., et al. (2016). Suppressed recombination and unique candidate genes in the divergent haplotype encoding Fhb1, a major Fusarium head blight resistance locus in wheat. *Theor. Appl. Genet.* 129, 1607–1623. doi: 10.1007/s00122-016-2727-x

Segura, V., Vilhjálmsson, B. J., Platt, A., Korte, A., Seren, Ü., Long, Q., et al. (2012). An efficient multi-locus mixed-model approach for genome-wide association studies in structured populations. *Nat. Genet.* 44, 825–830. doi: 10.1038/ng.2314

Sertse, D., You, F. M., Ravichandran, S., and Cloutier, S. (2019). The complex genetic architecture of early root and shoot traits in flax revealed by genome-wide association analyses. *Front. Plant Sci.* 10. doi: 10.3389/fpls.2019.01483

Singh, A. K., Clarke, J. M., Knox, R. E., Depauw, R. M., Mccaig, T. N., Fernandez, M. R., et al. (2012). Transcend durum wheat. *Can. J. Plant Sci.* 92 (4), 809–813. doi: 10.4141/cjps2011-255

Somers, D. J., Fedak, G., Clarke, J., and Cao, W. (2006). Mapping of FHB resistance QTLs in tetraploid wheat. *Genome* 49 (12), 1586–1593. doi: 10.1139/g06-127

Stack, R. W., and McMullen, M. P. (1998). *A visual scale to estimate severity of Fusarium head blight in wheat*. (Fargo, ND, United States: North Dakota State University Agriculture and University Extension Dept.)

Steiner, B., Buerstmayr, M., Michel, S., Schweiger, W., Lemmens, M., and Buerstmayr, H. (2017). Breeding strategies and advances in line selection for Fusarium head blight resistance in wheat. *Trop. Plant Pathol.* 42, 165–174. doi: 10.1007/s40858-017-0127-7

Steiner, B., Michel, S., Maccaferri, M., Lemmens, M., Tuberosa, R., and Buerstmayr, H. (2019b). Exploring and exploiting the genetic variation of Fusarium head blight resistance for genomic-assisted breeding in the elite durum wheat gene pool. *Theor. Appl. Genet.* 132, 969–988. doi: 10.1007/s00122-018-3253-9

Sun, J., Rutkoski, J. E., Poland, J. A., Crossa, J., Jannink, J. L., and Sorrells, M. E. (2017). Multitrait, random regression, or simple repeatability model in high-throughput phenotyping data improve genomic prediction for wheat grain yield. *Plant Genome* 10 (2). doi: 10.3835/plantgenome2016.11.0111

Tamba, C. L., Ni, Y.-L., and Zhang, Y.-M. (2017). Iterative sure independence screening EM-Bayesian LASSO algorithm for multi-locus genome-wide association studies. *PloS Comput. Biol.* 13, e1005357. doi: 10.1371/journal.pcbi.1005357

Tamba, C. L., and Zhang, Y.-M. (2018). A fast mrMLM algorithm for multi-locus genome-wide association studies. *bioRxiv*, 341784. doi: 10.1101/341784

Wang, S., Wong, D., Forrest, K., Allen, A., Chao, S., Huang, B. E., et al. (2014). Characterization of polyploid wheat genomic diversity using a high-density 90,000 single nucleotide polymorphism array. *Plant Biotechnol. J.* 12 (6), 787–796. doi: 10.1111/pbi.12183

Wang, S.-B., Feng, J.-Y., Ren, W.-L., Huang, B., Zhou, L., Wen, Y.-J., et al. (2016). Improving power and accuracy of genome-wide association studies *via* a multi-locus mixed linear model methodology. *Sci. Rep.* 6, 19444. doi: 10.1038/srep19444

Wang, L., Michel, D., Zhang, W., El-Aneed, A., Fobert, P. R., Ruan, Y., et al. (2022). A high-throughput fast chromatography tandem mass spectrometry (FC-MS/MS) based method for deoxynivalenol (DON) quantification in wheat grain. *PhytoFrontiers*™ 2 (4), 322–330. doi: 10.1094/PHYTOFR-03-22-0024-TA

Weir, B. S. (1979). Inferences about linkage disequilibrium. *Biometrics* 35, 235–254. doi: 10.2307/2529947

Wen, Y.-J., Zhang, H., Ni, Y.-L., Huang, B., Zhang, J., Feng, J.-Y., et al. (2017). Methodological implementation of mixed linear models in multi-locus genome-wide association studies. *Briefings Bioinf.* 19, 700–712. doi: 10.1093/bib/bbw145

Wen, Y.-J., Zhang, H., Ni, Y.-L., Huang, B., Zhang, J., Feng, J.-Y., et al. (2018). Methodological implementation of mixed linear models in multi-locus genome-wide association studies. *Briefings Bioinf.* 19, 700–712. doi: 10.1093/bib/bbw145

Wu, L., Zhang, Y., He, Y., Jiang, P., Zhang, X., and Ma, H. (2019). Genome-wide association mapping of resistance to fusarium head blight spread and deoxynivalenol accumulation in chinese elite wheat germplasm. *Phytopathology*® 109, 1208–1216. doi: 10.1094/PHYTO-12-18-0484-R

Wu, F., Zhou, Y., Shen, Y., Sun, Z., Li, L., and Li, T. (2022). Linking multi-omics to wheat resistance types to fusarium head blight to reveal the underlying mechanisms. *Int. J. Mol. Sci.* 23, 2280. doi: 10.3390/ijms23042280

Xu, Y., Yang, T., Zhou, Y., Yin, S., Li, P., Liu, J., et al. (2018). Genome-wide association mapping of starch pasting properties in maize using single-locus and multi-locus models. *Front. Plant Sci.* 9, 1311. doi: 10.3389/fpls.2018.01311

Xue, S., Xu, F., Tang, M., Zhou, Y., Li, G., An, X., et al. (2011). Precise mapping Fhb5, a major QTL conditioning resistance to Fusarium infection in bread wheat (Triticum aestivum L.). *Theor. Appl. Genet.* 123, 1055–1063.]. doi: 10.1007/s00122-011-1647-z

Zadoks, J. C., Chang, T. T., and Konzak, C. F. (1974). A decimal code for the growth stages of cereals. *Weed Res.* 14, 415–421. doi: 10.1111/j.1365-3180.1974.tb01084.x

Zhang, Q., Axtman, J. E., Faris, J. D., Chao, S., Zhang, Z., Friesen, T. L., et al. (2014). Identification and molecular mapping of quantitative trait loci for Fusarium head blight resistance in emmer and durum wheat using a single nucleotide polymorphism-based linkage map. *Mol. Breed.* 34, 1677–1687. doi: 10.1007/s11032-014-0180-6

Zhang, J., Feng, J. Y., Ni, Y. L., Wen, Y. J., Niu, Y., Tamba, C. L., et al. (2017). pLARmEB: integration of least angle regression with empirical Bayes for multilocus genome-wide association studies. *Heredity (Edinb)* 118, 517–524. doi: 10.1038/hdy.2017.8

Zhang, Y.-M., Jia, Z., and Dunwell, J. M. (2019a). The applications of new multi-locus GWAS methodologies in the genetic dissection of complex traits. *Front. Plant Sci.* 10, 100. doi: 10.3389/fpls.2019.00100

Zhang, Y.-M., Jia, Z., and Dunwell, J. M. (2019b). Editorial: the applications of new multi-locus GWAS methodologies in the genetic dissection of complex traits. *Front. Plant Sci.* 10. doi: 10.3389/fpls.2019.00100

Zhang, Y.-W., Tamba, C. L., Wen, Y.-J., Li, P., Ren, W.-L., Ni, Y.-L., et al. (2020). mrMLM v4. 0.2: an R platform for multi-locus genome-wide association studies. *Genom. Proteomics Bioinf.* 18, 481–487. doi: 10.1016/j.gpb.2020.06.006

Zhao, M., Leng, Y., Chao, S., Xu, S. S., and Zhong, S. (2018). Molecular mapping of QTL for Fusarium head blight resistance introgressed into durum wheat. *Theor. Appl. Genet.* 131, 1939–1951. doi: 10.1007/s00122-018-3124-4

Zhu, Z., Chen, L., Zhang, W., Yang, L., Zhu, W., Li, J., et al. (2020). Genome-wide association analysis of fusarium head blight resistance in Chinese elite wheat lines. *Front. Plant Sci.* 11. doi: 10.3389/fpls.2020.00206

frontiers | Frontiers in Plant Science

TYPE Original Research
PUBLISHED 20 October 2023
DOI 10.3389/fpls.2023.1270087

Check for updates

OPEN ACCESS

EDITED BY
Xinli Zhou,
Southwest University of Science and Technology, China

REVIEWED BY
Salim Bourras,
Swedish University of Agricultural Sciences, Sweden
Peng Cheng,
Northwest A&F University, China

*CORRESPONDENCE
Radivoje Jevtić
radivoje.jevtic@ifvcns.ns.ac.rs

RECEIVED 31 July 2023
ACCEPTED 06 October 2023
PUBLISHED 20 October 2023

CITATION
Jevtić R and Župunski V (2023) The challenge of managing yellow rust (*Puccinia striiformis* f.sp. *tritici*) in winter wheat: how combined climate and pathogen stressors impact variability in genotype reactions.
Front. Plant Sci. 14:1270087.
doi: 10.3389/fpls.2023.1270087

COPYRIGHT
© 2023 Jevtić and Župunski. This is an open-access article distributed under the terms of the Creative Commons Attribution License (CC BY). The use, distribution or reproduction in other forums is permitted, provided the original author(s) and the copyright owner(s) are credited and that the original publication in this journal is cited, in accordance with accepted academic practice. No use, distribution or reproduction is permitted which does not comply with these terms.

The challenge of managing yellow rust (*Puccinia striiformis* f.sp. *tritici*) in winter wheat: how combined climate and pathogen stressors impact variability in genotype reactions

Radivoje Jevtić* and Vesna Župunski

Laboratory for Phytopathology, Small Grains Department, Institute of Field and Vegetable Crops, Novi Sad, Serbia

Despite the ongoing evolution of wheat pathogens due to the selection pressures of agro-ecological conditions, many studies have often overlooked the combined impact of both biotic and abiotic factors on disease occurrence. From 2016 to 2023, a comprehensive screening of obligate pathogens, including *B. graminis* f. sp. *tritici, P. graminis* f. sp. *tritici*, *P. triticina*, and *P. striiformis* f. sp. *tritici*, was carried out. This screening was conducted on a phenotyping platform encompassing 2715 winter wheat genotypes and their wild relatives, both with and without resistant genes (Lr, Yr, and Sr) for rust diseases. The data were analyzed using PCAmix, best subsets regression, and linear regression modeling. The findings from this study reveal that the plant reactions to leaf and yellow rust infections is far from straightforward. It is heavily influenced not only by prevalent rust races and climatic factors that impact pathogen life cycles but also by variations in the susceptibility reactions of wheat genotypes to the broader agro-ecological conditions. We also observed a tendency for leaf rust and yellow rust to coexist within the same host plant, even though yellow rust is typically considered more aggressive. We reported for the first time genes related to yellow rust resistance breakdown in Serbia in 2023. Lastly, we underscored the importance of investigating resistance responses to rust diseases not exclusively through the interrelation between resistance genes and pathogen virulence, but also by considering how plants respond to the combined stresses of abiotic and biotic factors. Consequently, our study sets the groundwork for further research into how plants respond to multiple stressors and contributes for further investigations related with effective integrated rust management.

KEYWORDS

yellow rust, susceptibility, resistance, wheat, climatic factors

1 Introduction

Pest control in wheat production is challenging due to the continuous changes in wheat pathogens under selection pressure from resistant varieties, applied pesticides, and changing climatic conditions. The estimation suggests that as much as 40% of the global food supply is currently lost to pests, with the potential for further damage heightened by shifts in temperature, precipitation patterns, and the rise in extreme weather events, as highlighted by Heeb et al. (2019). The most important obligate pathogens of wheat are the causal agents of rust diseases (*Puccinia graminis* f. sp. *tritici*, *Puccinia triticina*, *Puccinia striiformis* f. sp. *tritici*) and powdery mildew (*Blumeria graminis* f. sp. *tritici*). Yield loss of rust diseases could reach 70% (Junk et al., 2016), while stem rust was also reported to cause yield losses of up to 100% (Afzal et al., 2007). Despite the continuous changes in wheat pathogens under the selection pressures of agro-ecological conditions, the impact of the combined effects of biotic and abiotic factors on disease occurrence has often been neglected in studies (White et al., 2011; Juroszek and von Tiedemann, 2013). Heeb et al. (2019) promoted a strategy for climate-smart pest management (CSPM) but also noted that developing a general model for predicting climate change-induced pest outbreaks on a local scale in the short term is highly unlikely.

Puccinia striiformis f.sp. *tritici* is a pathogen with the ability to spread over long distances through air currents, which is also its primary mode of transmission (Zadoks, 1961; Hovmøller et al., 2011). Although uredospores can be observed on the host plant's ears at high infection intensities, yellow rust is not transmitted through seeds. Telia production begins with the sexual stage of rust diseases in the late growing season, and teliospores from telia further infect alternative hosts. Pycniospores and aeciospores are formed on alternative hosts, and the life cycle is completed when aeciospores infect the host plants of wheat (Chen, 2005). During ideal conditions, 10 days are enough for yellow rust to complete its cycle from infection to the production of new spores. The disease cycle may repeat many times in one season.

There are six main genetic groups of yellow rust, each predominant in different regions worldwide: G1 in China; G2 in Nepal; G3 in Pakistan; G4 in the Middle East and Eastern Africa; G5 in the Mediterranean and Central Asia; and G6 in Northwestern Europe (Ali et al., 2014). The center of yellow rust diversity is the Himalayan region, where the greatest genetic changes occur, unlike the clonal population structure that dominates in Europe, America, and Australia (Wellings and Mcintosh, 1990; Hovmøller et al., 2011; Ali et al., 2014). Prior to 2011, the population of *P. striiformis* in Europe was predominantly clonal and depended on mutations with little influence from sexual recombination (Hovmøller et al., 2002). In a clonal population, mutations and subsequent selection would generate new virulent races against existing host resistance genes (Linde et al., 2002; de Vallavieille-Pope et al., 2012). The majority of clonal races were typical for the northwestern European genetic group, while exotic races had only a minor impact on wheat production (de Vallavieille-Pope et al., 2012). However, in 2011, two new races were discovered in many European countries, named Warrior and Kranich, which exhibited significantly greater genetic variability compared to the races of the previous clonal populations (Hovmøller et al., 2016). Warrior and Kranich caused immense problems in wheat production because of virulence against varieties carrying durable resistance to prevalent races of the yellow rust pathogen (Sørensen et al., 2014). These results emphasize the fact that, despite the continuous development of wheat varieties with resistance to the prevalent pathogen population, the introduction of new races of yellow rust can initiate infections of epidemic proportions, even at a continental level (Brown and Hovmøller, 2002).

Prevalent races (virulence phenotype) of yellow rust are grouped into genetic lineages and named Pst, followed by a sequential digit (Ali et al., 2014; Hovmøller et al., 2016; Thach et al., 2016). PstS1 is closely related with PstS2 and predominates in North America. PstS2 is predominant in East Africa (Hovmøller et al., 2008; Ali et al., 2014; Walter et al., 2016). PstS3 is prevalent in West Asia, southern Europe and North Africa (Ali et al., 2014). PstS4 consists of races prevalent on triticale in Northern Europe (Hovmøller et al., 2008; Hovmøller et al., 2016). Two races with specific microsatellite profiles belong to PstS5 (Ali et al., 2014; Hovmøller et al., 2016; Thach et al., 2016). PstS6 is a lineage prevalent in East Africa (Ali et al., 2014; Hovmøller et al., 2016; Thach et al., 2016). Yellow rust races belonging to lineages PstS7 (Warrior), PstS8 (Kranich), and PstS10 became prevalent in Europe from 2011, covering more than 80% of the investigated isolates (Ali et al., 2014). PstS10, formerly known as Warrior(-), became predominant in most parts of Europe since 2014 (Ali et al., 2014). Yellow rust races in the NW-European population detected before 2011 were part of a single clonal lineage termed PstS0 (Ali et al., 2014). PstS9 is related with PstS5 and was associated with epidemics in Central Asia since 2013 (Ali et al., 2014).

The presence of yellow rust in Serbia was first recorded in the genetic collection at Rimski šančevi by Jevtić et al. as early as 1997, and the first warning about the increased threat of its occurrence due to climate change was given by Jevtić and Jasnić in 2007 (Jevtić et al., 2023). Until 2014, the predominant rust species in Serbia was *Puccinia triticina*, which, in certain years (2001, 2004, and 2007), resulted in yield losses of up to 50% in experimental fields. However, in the 2013/2014 production season, *Puccinia striiformis* f.sp. *tritici* predominated over leaf rust and similarly, as in the rest of European countries, threatened wheat production (Jevtić et al., 2017; Jevtić et al., 2020). In 2014, winter temperatures in January (4.2°C) and February (6.1°C) exceeded the average temperatures (-0.1°C in January and 1.8°C in February) since 1964, and yellow rust prevailed over leaf rust and caused enormous damage in wheat production (Jevtić et al., 2020). During 2014, the disease indices of yellow rust ranged from 40% to 60% in wheat production areas (Jevtić et al., 2020). The outbreak of yellow rust in Serbia was caused by Warrior races (Jevtić et al., 2017; Jevtić et al., 2020).

Considering the mode of transmission of the yellow rust pathogen and its high ability to overcome host plant resistance, it was hypothesized in this study that the occurrence of rust diseases cannot be explained only by the influence of climatic factors on the life cycle of pathogens and the effectiveness of resistance genes. Rather, it can also be attributed to the overall genotype reaction to

combined abiotic and biotic stressors. Consequently, the aim of this study was to examine factors affecting variability in the predominance of yellow over leaf rusts and to highlight fundamental issues in the control of rust diseases.

2 Materials and methods

2.1 Plant material and field trials

The screening of obligate pathogens (*B. graminis* f. sp. *tritici*, *P. graminis* f. sp. *tritici*, *P. triticina*, *P. striiformis* f. sp. *tritici*) in the period 2016-2023 was conducted on a phenotyping platform comprising 2715 winter wheat genotypes and wild relatives (Supplementary Table 1). Winter wheat genotypes were characterized with diverse genetic backgrounds and included susceptible as well as genotypes carrying resistant genes for rust diseases (Lr, Yr, and Sr).

The phenotyping platform was established every year in the locality of Rimski šančevi (Vojvodina, the northern province of Serbia) according to the methodology recommended by CIMMYT (1979) in the "Instructions for the management and reporting of results for wheat program international yield and screening nurseries". The phenotyping platform is designed for the rapid assessment of a large number of advanced generation (F3-F7) lines of wheat genotypes under a wide range of climatic and disease conditions. Phenotyping was conducted under the direction of the Institute of Field and Vegetable Crops, Serbia (Laboratory for Phytopathology of the Small Grains Department) as a part of pre-breeding and breeding efforts in developing and promoting wheat lines with resistance to rust diseases and powdery mildew.

In the phenotyping platform, each genotype was sown in 1-m rows in five replicates with a row spacing of 20 cm, giving a plot area of 1 m^2. The establishment of the phenotyping platform was in accordance with the methodology recommended by CIMMYT, which indicated that each genotype should be sown in one unreplicated 5-m row or using smaller row lengths but with replicates so that the sum of all row lengths is equal to 5 m. Additionally, field trials were set up under naturally occurring inoculum, and the soft wheat variety Barbee (*Triticum aestivum* ssp. *compactum*), known for its susceptibility to *Blumeria* and *Puccinia*, was used to control pathogen pressure on all tested genotypes. The optimal time for winter wheat sowing in the agro-ecological conditions in Serbia is October, and the mean sowing date for genotypes in phenotyping platform in the eight-year period was 20 October.

2.2 Disease assessments

Assessments of obligate pathogens were made using disease indices (DIs) at the growth stage 71-73 BBCH (kernel watery; early milk) known for its high association with yield (Wegulo et al., 2009). The DIs (%) were calculated as follows: DI (%) = [sum (class frequency × score of rating class)]/[(total number of plants) × (maximal score of rating class)] × 100. Consequently, DI is a product of disease incidence (mean percentage of plants infected per plot) and average disease severity defined as the percentage of relevant host tissues or organs covered by symptoms (Seem, 1984). Disease severity was determined using the modified Cobb's scale (Peterson et al., 1948). The genotype reaction to yellow rust (GR YR) and leaf rust (GR LR) was categorized using the following scale: DI < 10% (GR=1) – resistant; 11 < DI < 20% (GR=2) – moderately resistant; 21 < DI < 30% (GR=3) – moderately susceptible; 31 < DI < 40% (GR=4) – moderately susceptible; 41 < DI < 50% (GR=5) – susceptible; 51 < DI < 60% – susceptible (GR=6); DI > 61 (GR=7) – susceptible.

2.3 Assessment of climatic factors in the phenotyping platform

Monthly mean temperatures and precipitation in the phenotyping platform were recorded for each growing season (from January to May) using data from the Republic Hydrometeorological Service of Serbia (http://www.hidmet.gov.rs/) (Figure 1). The weather station was placed on the same locality were the trials were conducted. On average, from 2016 to 2023, April was the least humid month in Novi Sad, with a relative humidity of 64.5%. Since it was still conducive enough for infection and development of rust diseases (El Jarroudi et al., 2017), relative humidity was not taken into account in the regression and PCAmix analysis. To provide a broader insight into climatic trends in Serbia, we are presenting the climatic conditions at the Rimski šančevi locality from 2006 to 2023 (Figure 1). The data on the outbreak of yellow rust in 2014 have already been published (Jevtić et al., 2017) and were not included in this study.

The minimum, optimum, and maximum temperatures affecting different stages of the life cycle of yellow and leaf rust (Singh et al., 2002) are provided in Table 1.

2.4 Statistical methods

Associations between qualitative variables (year) and quantitative variables (genotype reaction to yellow and leaf rust and climatic factors) were analyzed using principal component analysis with mixed data (PCAmix) since PCA requires quantitative variables and MCA requires qualitative variables only.

The factors influencing dependent variables (the disease index of leaf and yellow rust) were analyzed using a multiple linear stepwise regression model due to multicollinearity of the data and best subsets regression. The best subsets regression was performed to identify the best-fitting regression models with predictors of choice (abiotic and biotic factors) analyzed individually and in combination with each other. Genotypes were considered as categorical variables in multiple linear regression models, while obligate pathogens and climatic factors (temperature and total rainfall) were considered as continuous ones. Obligate pathogens were included in regression modelling as independent variables since different rust species can be habitant of the same host plant. The alpha level to enter and alpha level to remove the influencing

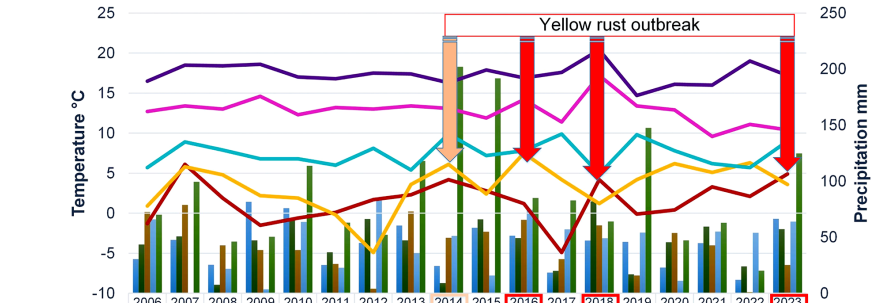

	2006	2007	2008	2009	2010	2011	2012	2013	2014	2015	2016	2017	2018	2019	2020	2021	2022	2023
Prec. January	30.5	47.7	25.4	81.6	76	25.2	44.9	60.5	24.3	58.4	51.3	18.5	47	45.8	22.9	44.7	12	66.4
Prec. February	43.5	50.7	7.6	47.3	65.7	36.7	66.3	47.2	9.2	65.9	49.2	20.1	81.9	17	45.5	59.5	24	57.2
Prec. March	72.5	78.8	42.8	38.7	38.7	26.2	4.1	73	49.5	54.9	65.5	30.5	60.6	15.9	53.8	42.8	1	25.3
Prec. April	66	0	21.9	3.6	63.7	22.8	82.8	35.8	51.2	15.9	74.5	57	49	54.1	11.1	55.1	54	63.9
Prec. May	70.1	99.4	46.2	50.4	113.7	63	52.2	118.1	202.1	191.7	85	82.9	64.2	147.6	47.3	62.9	20.2	124.8
T. January	-1.3	6.1	1.9	-1.5	-0.6	0.1	1.7	2.3	4.2	2.8	1.2	-4.9	4.2	-0.1	0.4	3.3	2.1	4.9
T. February	0.9	5.8	4.8	2.2	1.9	-0.2	-4.9	3.6	6.1	2.4	7.5	4.2	1.2	4.2	6.2	5.1	6.3	3.6
T. March	5.7	8.9	7.9	6.8	6.8	6	8.1	5.4	9.9	7.2	7.8	9.9	4.9	9.8	7.8	6.2	5.7	9
T. April	12.7	13.4	13	14.6	12.3	13.2	13	13.4	13.1	11.9	14.2	11.4	17.21	13.4	12.9	9.6	11.1	10.4
T. May	16.5	18.5	18.4	18.6	17	16.8	17.5	17.4	16.3	17.9	16.9	17.6	20.4	14.7	16.1	16	19	17.2

FIGURE 1
Climatic factors in the phenotyping platform at Rimski šančevi from 2006 to 2023 and yellow rust outbreaks in Serbia.

factors in the stepwise regression were set by default to 0.15 since it was reported that an alpha level of 0.05 could fail to identify important variables (Bursac et al., 2008).

Regression models were followed with the coefficient of determination (R^2), which is the percentage of variation in the response that is explained by the model. The analysis was performed using XLSTAT in Microsoft Excel (XLSTAT Statistical and Data Analysis Solution, 2022) and Minitab 17 Statistical Software (trial version). Package 'ggplot2' in R software was used for the visualization of PCAmix analysis (RStudio Team, 2022).

3 Results

In the period 2016-2023, the occurrence of the obligate pathogens in 2715 genotypes was not straightforward (Figure 2; Table 2). The predominance of yellow rust over leaf rust in the phenotyping platform had been recorded in 2016, 2018, and 2023 when 72%, 78%, and 96.5% of the genotypes were infected with yellow rust with a disease index exceeding 10%, respectively. In the rest of the years, no more than 11% of genotypes were infected with yellow rust. The average disease indices of yellow rust in 2016, 2018, and 2023 were 28.3%, 30.2%, and 52%, respectively (Table 2). It should be pointed out that in all years with yellow rust outbreak in the phenotyping platform at Rimski šančevi temperatures in January and/or February exceeded the eighteen-year average by 2.7°C (Figure 1).

The average disease indices of powdery mildew ranged from a trace level in 2023 to 22.2% in 2018. *P. triticina* was the predominant rust species in the years that were not conducive to yellow rust occurrence, except in 2022 when powdery mildew was the prevalent pathogen. In the years not conducive to yellow rust occurrence, the average disease DI of leaf rust was 13.5% in 2017, 40.8% in 2019, 31.85% in 2020, 53.1% in 2021 and 0.5% in 2022 (Table 2). The predominance of powdery mildew over rust diseases in 2022 can be attributed to the colder weather and significantly lower spring precipitation compared to the seasonal average (Figure 1). It is known that powdery mildew and leaf rust require different conditions for successful development. Powdery mildew typically emerges as the first leaf disease in spring, thriving in temperatures between 10 and 21°C. In the agro-ecological conditions of Serbia, it can even be observed as early as February. In contrast, optimal conditions for leaf rust initiation are usually met in the first half of April (Jevtić et al., 2020). Additionally, powdery mildew is unique compared to other fungi since its spores do not require dew or rain for germination (Salgado and Paul, 2016). Since the spring of 2022 (March-May) began with dry weather conditions, and recorded precipitation was minimal, with just 1 mm measured in March at the experimental site (Figure 1), it gave advantage to powdery mildew development over rust diseases.

TABLE 1 Minimum, optimum and maximum temperatures affecting life cycle of yellow and leaf rust.

	Leaf rust	Yellow rust	Leaf rust	Yellow rust	Leaf rust	Yellow rust	Leaf rust	Yellow rust
	Germination		Penetration		Growth		Sporulation	
Minimum T	2	0	10	2	2	3	10	5
Optimum T	20 12-15	9-13	20	9-13	25	12-15	25	12-15
Maximum T	30	23	30	23	35	20	35	20

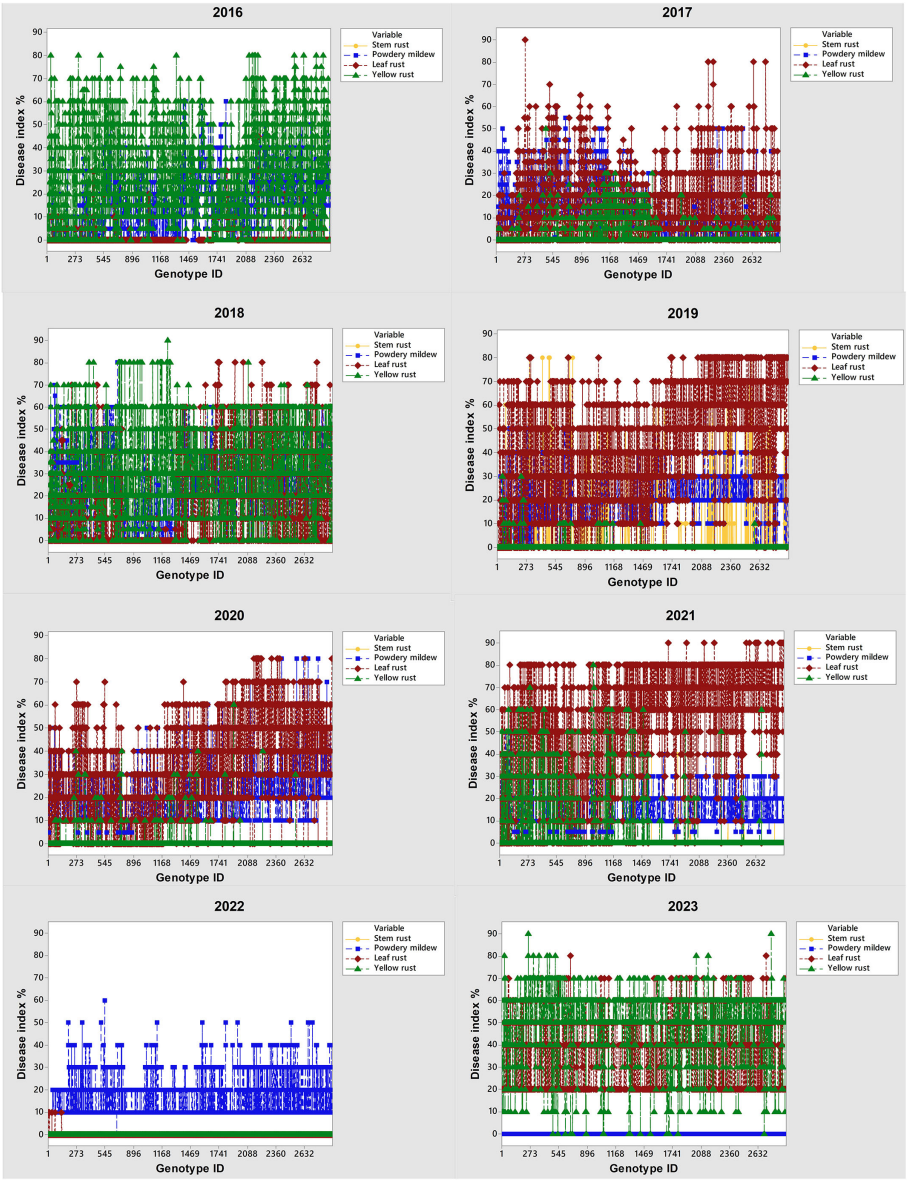

FIGURE 2
Changes in predominance of obligate pathogens (powdery mildew, leaf rust, yellow rust and stem rust) on 2715 winter wheat genotypes and wild relatives from 2016 to 2023. Phenotyping platform is located on Rimski šančevi (Vojvodina—north province of Serbia).

TABLE 2 Mean, minimum, median and maximum disease indices of obligate pathogens (powdery mildew, leaf rust, yellow rust and stem rust) in the phenotyping platform in Rimski šančevi from 2016 to 2023.

Obligate pathogen	Year	Mean DI	Minimum DI	Median DI	Maximum DI
Stem rust	2016	0.0	0.0	0.0	0.0
	2017	0.0	0.0	0.0	0.0
	2018	0.0	0.0	0.0	0.0
	2019	8.6	0.0	0.0	80
	2020	0.0	0.0	0.0	0.1
	2021	0.1	0.0	0.0	60

(Continued)

TABLE 2 Continued

Obligate pathogen	Year	Mean DI	Minimum DI	Median DI	Maximum DI
	2022	0.00004	0.0	0.0	0.1
	2023	0.0	0.0	0.0	0.0
Powdery mildew	2016	13.8	0.0	10	60
	2017	10.6	0.0	10	60
	2018	22.2	0.0	20	80
	2019	17.7	0.0	20	60
	2020	20.7	5.0	20	80
	2021	13.8	5.0	10	60
	2022	14.5	0.0	10	60
	2023	0.0	0.0	0.0	0.0
Leaf rust	2016	0.5	0.0	0.0	45
	2017	13.5	0.0	10	90
	2018	14.5	0.0	0.1	80
	2019	40.9	0.0	40	80
	2020	31.9	0.0	30	80
	2021	53.1	0.0	60	90
	2022	0.5	0.0	0.0	10
	2023	34.5	20	40	80
Yellow rust	2016	28.3	0.0	25	80
	2017	2.6	0.0	0.0	50
	2018	30.2	0.0	30	90
	2019	0.2	0.0	0.0	30
	2020	0.5	0.0	0.0	60
	2021	4.1	0.0	0.0	80
	2022	0.0003	0.0	0.0	0.1
	2023	51.9	0.1	50	90

Although the weather was sunnier and warmer in May than usual, it remained dry. Rainfall was mostly recorded during the final 10 days of the month, with an average total precipitation of 20.2 mm, which was 70 mm below the eighteen-year average of 91.2 mm (Figure 1). All these factors resulted in the predominance of powdery mildew in 2022.

Stem rust outbreaks in the phenotyping platform occurred only in 2019 when 32% of genotypes were infected with DI ranging from a trace level to 80%. Disease indices of stem rust above 10% were recorded in 18% of genotypes in 2019. In 2021, stem rust occurred only in 0.9% of genotypes with DI ranging from a trace level to 60%. Jevtić et al. (2020) reported that the delayed development of winter wheat genotypes, caused by extreme fluctuations in total rainfall during the winter period, can significantly increase their susceptibility to stem rust.

The range of disease indices of each obligate pathogen in the phenotyping platform indicates great diversity in susceptibility responses of genotypes to obligate pathogens. As a consequence, a more detailed analysis of factors affecting shifts in the predominance of leaf and yellow rust, increasing levels of coexistence of leaf and yellow rust, and yellow rust resistance breakdown are discussed in more detail further.

3.1 Shifts in predominance of leaf and yellow rust

To exclude the effect of powdery mildew on the relationship between leaf, yellow rust, and host plants, influencing factors on shifts in the predominance of leaf and yellow rust were analyzed using a set of 764 genotypes where the disease index of powdery mildew did not exceed 20% (Supplementary Table 1). The general association between years, genotype's reactions to leaf and yellow rust, and climatic factors from January to April in an eight-year

period was examined using PCAmix analysis (Figure 3). Since assessments of rust diseases were made in May/June when temperatures exceeded 15°C and slowed down yellow rust development, climatic conditions in May are excluded from PCAmix analysis.

In the subset of 764 genotypes, DI of yellow rust exceeding 41% (GR-5, GR-6) was highly associated only with 2023, indicating a higher pressure of yellow rust on wheat genotypes in 2023 than in previous years. In 2023, 81% of 764 genotypes were infected with yellow rust with DI exceeding 41%. In addition, leaf rust with moderate level of infection (from 31% to 50%) was associated with both 2023 and 2021, indicating a higher level of coexistence of leaf and yellow rust in 2023. Contrary to 2023, there were 8.6% and 23% of genotypes infected with yellow rust with DI exceeding 41% in 2016 and 2018, respectively. It resulted in the position of 2016 and 2018 on the opposite side of the factor map from 2023. A low level of yellow rust infection occurred in 2020 and 2022, with DI not exceeding 10% (2022) and 20% (2020). In these years, DI of leaf rust in the majority of genotypes was also at a low (GR-1) to moderate level of infection (GR-3). In the rest of the years (2017, 2019, and 2021), leaf rust was the predominant pathogen with disease indices exceeding 51%, especially in 2021.

Temperature in March was indicated as the most influencing factor on leaf rust infection in 2017 and 2019, while precipitation in April was the most associated with leaf rust infection in 2021. Temperature in January and precipitations in January were associated with the highest level of infection with yellow rust (GR-7) (Figure 3). The first two dimensions contributed 28.8% to the overall variability. The contribution of the first and second dimensions was 18.1% and 10.7%, respectively. Since PCAmix is used as a tool in exploratory data analysis, further analysis was performed with regression modeling.

Regression modelling of the most influencing factors on yellow rust infection in 764 genotypes confirmed that T in January ($P<0.001$), T in April ($P<0.001$), precipitation in January ($P<0.001$), precipitation in February ($P<0.001$), precipitation in March ($P<0.001$), leaf rust infection and genotype ($P<0.001$) significantly affected yellow rust occurrence giving the regression model with R^2 of 65.5% (Table 3). The same as in PCAmix analysis, regression modelling indicated significant effect of T in February ($P<0.001$), T in March ($P=0.003$) and total rainfall in April ($P<0.001$) on leaf rust occurrence in 764 genotypes. The genotype ($P<0.001$) and yellow rust infection ($P<0.001$) also affected leaf rust infection as shown by regression modelling but R^2 did not exceed 31% so there are additional factors that affected differences in leaf rust infection in phenotyping platform (Table 3).

In our study, the response of 764 susceptible genotypes to leaf and yellow rust over an eight-year period exhibited considerable dissimilarities, not only in terms of one pathogen's prevalence over the other but also in their coexistence. Although regression modeling indicated that fluctuations in January and April temperatures, as well as precipitation in January, February, and March, affected yellow rust occurrence on the 764 genotypes during the eight-year period, none of these factors were specifically associated with the year 2023 when the coexistence of both pathogens occurred. Consequently, we can assume that the reaction of the 764 genotypes to climatic conditions in 2023 was rather diverse, resulting in variability in their response to leaf and yellow rust infections. This also suggests that a more specific dataset should be analyzed to evaluate which climatic factors were most favorable in promoting the coexistence of both pathogens in the same year.

It should be pointed out that although 2016, 2018, and 2023 were favorable years for yellow rust infection, there was a set of

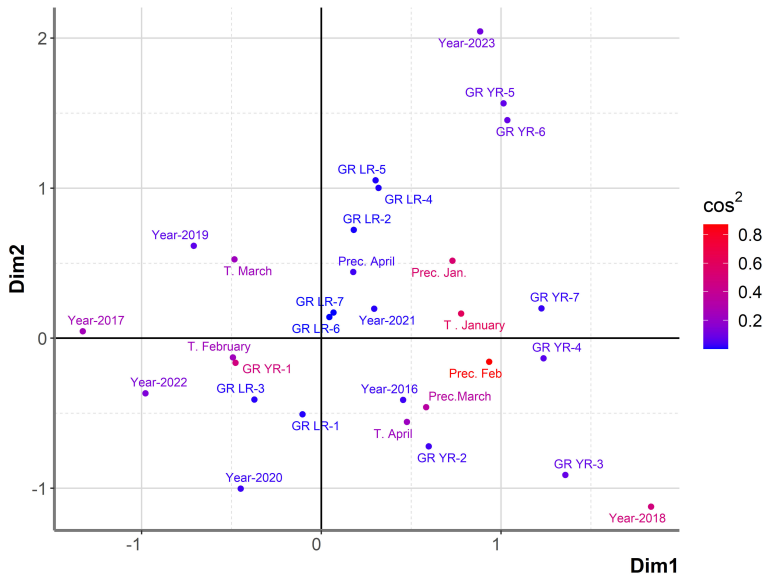

FIGURE 3
Graphical representation of PCAmix analysis on subset of 764 genotypes showing susceptibility to rust diseases in the period from 2016 to 2023. Factors included were: years (from 2016 to 2023), temperatures and precipitations from January to April from 2016 to 2023, reaction of 764 genotypes to leaf rust (GR LR) and reaction of 764 genotypes to yellow rust (GR YR).

TABLE 3 Regression modelling on the most influencing factors on yellow and leaf rust infection in 764 genotypes from 2016 to 2023.

Source	DF	Adj SS	ADj MS	F-Value	P-Value
Yellow rust					
Regression	769	1708410	2222	11.13	<0.001
T in January	1	53456	53456	267.75	<0.001
Prec. in January	1	301038	301038	1507.85	<0.001
Prec. in February	1	174997	174997	876.53	<0.001
Prec. in March	1	74176	74176	371.54	<0.001
T in April	1	16122	16122	80.75	<0.001
Leaf rust	1	143925	143925	720.90	<0.001
Genotype	763	281732	369	1.85	<0.001
Error	4499	898212	200		
Total	5268	2606622			
Leaf rust					
Regression	767	911665	1188.6	2.61	<0.001
Prec. in April	1	6586	6586.0	14.48	<0.001
T in March	1	3915	3915.1	8.61	0,003
T in February	1	27980	27979.9	61.52	<0.001
Yellow rust	1	40065	40065.2	88.09	<0.001
Genotype	763	789683	1035.0	2.28	<0.001
Error	4501	2047045	454.8		
Total	5268	2958711			

genotypes susceptible to yellow rust that showed different levels of susceptibility reactions over the three-year period, despite it being known that yellow rust is a more aggressive pathogen. All of them were susceptible to yellow rust in 2016 and 2023, but in 2018 showed moderate levels of susceptibility with DI below 30% (Figure 4). General liner modeling confirmed that yellow rust infection was significantly affected not only by year and competing leaf rust but also by genotype itself (Table 4).

Since PCAmix indicated the shifts in the predominance of leaf and yellow rust on 764 genotypes over an eight-year period, as well as increased levels of yellow rust infection together with the coexistence of leaf and yellow rust in 2023, further analysis on factors influencing yellow rust infection was conducted in two sets of genotypes showing: 1) coexistence between yellow and leaf rust in 2023 but not in 2016 and 2018; and 2) susceptibility reactions to yellow rust only in 2023.

3.2 Increased level of coexistence of leaf and yellow rust

Although yellow rust is known to be more aggressive than leaf rust, and despite favorable climatic conditions in 2016, 2018, and 2023 for yellow rust infection, the coexistence of yellow and leaf rust increased in 2023 when compared with 2018 and 2016 (Figure 2; Figure 5). Consequently, the subset of 99 genotypes (Supplementary Table 1) with a DI of yellow rust exceeding 41% in 2016, 2018, and 2023, and showing coexistence between leaf and yellow rust in 2023 (Figure 5), was analyzed using PCAmix and regression modeling to find out which climatic factors were most associated with leaf rust infection.

PCAmix analysis indicated that T in February, as well as precipitation in February, precipitation in March, and precipitation in April, significantly affected both leaf and yellow rust infection in the subset of 99 genotypes showing coexistence of leaf and yellow rust in 2023 (Figure 6). The first two dimensions contributed 60.7% to the overall variability. The contribution of the first and second dimensions was 49.4% and 11.3%, respectively. In the larger set of genotypes (764) in eight-year period, T in February and precipitation in April significantly affected leaf rust infection, while precipitation in February and precipitation in March were mostly associated with moderate levels of yellow rust infection.

Since PCAmix was used for reducing the dimensionality of a dataset, two types of regression modeling were carried out to estimate relationships between dependent variable (leaf rust infection) and independent variables (genotype, climatic factors, and competing yellow rust). For explaining leaf rust infection in the years conducive to yellow rust infection, the best subsets regression indicated that T in February, total rainfall in March, and DI of yellow rust formed the model with the smallest Mallows' Cp (4),

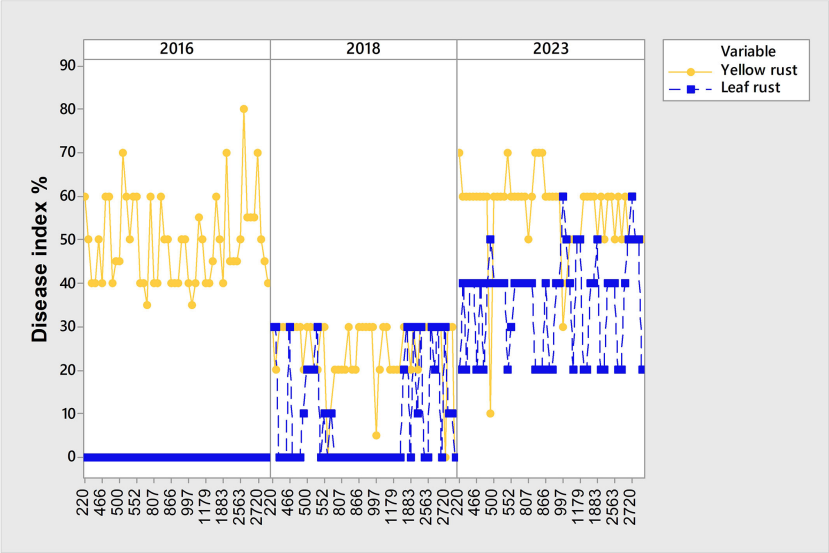

FIGURE 4
Set of 54 susceptible genotypes to yellow rust showing different levels of susceptibility in 2016, 2018 and 2023 that were conducive for yellow rust occurrence.

meaning that this model is relatively unbiased in estimating the true regression coefficients and predicting leaf rust infection (Table 5). Additionally, the best subsets regression showed that using only biotic or abiotic factors for regression modeling and prediction of leaf rust infection would give lower R^2, R^2_{pred}, and a much higher Mallows' Cp than using them as combined predictor variables.

Considering that the minimal temperature required for leaf rust penetration and sporulation is 10°C, typically achieved in April under Serbia's agro-ecological conditions, and that the latent period of leaf rust can be extended at temperatures between 5-10°C, it is plausible to suggest that the February temperature (3.6°C) and the below-average total rainfall in March (25 mm) created conditions more favorable for yellow rust infection and also delayed the development of leaf rust. Since duration of wheat phenological phases are also highly associated with earliness of genotypes and climatic conditions it can be inferred that these factors created an environment where leaf rust could thrive on the remaining green leaf tissue of susceptible genotypes only when the development of yellow rust was slowed down.

Stepwise regression confirmed the same set of predictors as significantly influencing leaf rust infection (P<0.001), together with the effect of genotype as a categorical predictor, giving the model with R^2 of 77% (Table 6).

Since DI of yellow rust in the subset of 99 genotypes did not change significantly in 2016, 2018 and 2023, we did not conduct analysis to find out if there are some additional climatic factors affecting yellow rust occurrence besides those obtained by PCAmix analysis.

3.3 Yellow rust resistance breakdown in 2023

In the phenotyping platform, there were 6.6% of genotypes (180 out of 2715) highly to moderately resistant to yellow rust in 2016 and 2018, but with yellow rust resistance breakdown in 2023, with yellow rust DI ranging from 40% to 60% (Figure 7; Supplementary Table 1). The same set of genotypes was resistant or moderately resistant to leaf rust in 2016 and 2018 as well.

Yellow rust resistance breakdown in 2023 was recorded in wild relatives as well as in winter wheat genotypes having all-stage (AS) race-specific genes (Lr1, Lr3, Lr10, Lr14a, Lr2a, Lr24, Yr2, Yr4, Yr6,

TABLE 4 General linear modelling on the most influencing factors on yellow rust infection in 54 genotypes in 2016, 2018 and 2023.

Source	DF	Adj SS	ADj MS	F-Value	P-Value
Leaf rust	1	466.0	466.0	7.37	0.008
Year	2	26930.7	13465.3	212.93	P<0.001
Genotype	53	7004.0	132.2	2.09	0.001
Error	104	6576.9	63.2		
Total	160	44871.1			

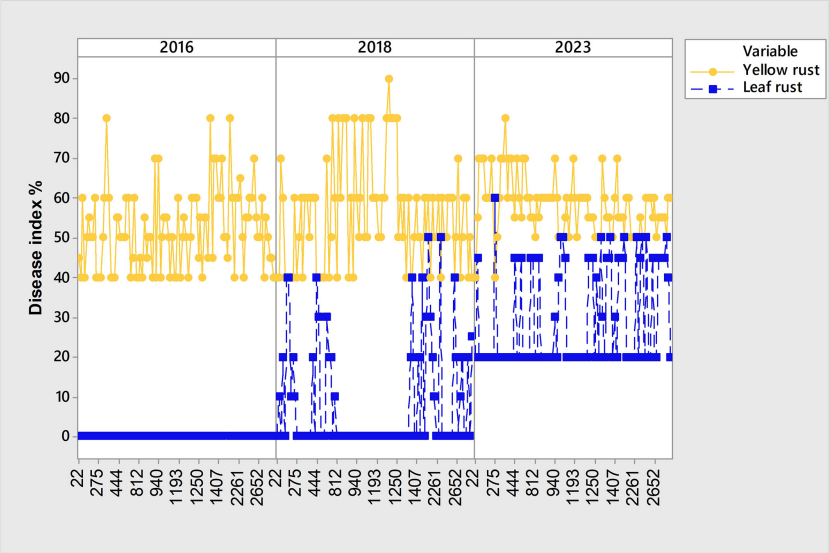

FIGURE 5
Set of 99 susceptible genotypes to yellow rust in 2016, 2018 and 2023 with higher level of coexistence of leaf and yellow rust in 2023.

Yr7, Yr9) and adult plant resistance genes (Lr13, Lr20, Yr14, Lr34). Wild relatives that showed susceptibility reaction to yellow rust in 2023 were: *Triticum paleocolchicum* Men.; *Triticum macha* var. *subletschchumicum*; *Triticum macha* var. *paleo-imereticum*; *Triticum dicoccoides* var. *aaronsohni* Flaksb; *T. macha* var. *submegrelicum* Dekapr. & Menabde; *Triticum dicoccum* Schrank ex Schübl. var. *atratum; Triticum dicoccum* var. *farum* Ja; *Triricum dicoccum* var. *rufum* (Schübl.); *Triticum durum* Desf. var. *affine* (Korn.); *Triticum polonicum* var. *vestitium*; *Triticum polonicum* L. var. *gracile* Flaksb; *Triticum polonicum* var. *villosum* Desv.

PCAmix indicated that T in January, precipitation in January, and T in April were associated with the highest level of infection with yellow rust (GR-6) (Figure 8). The first two dimensions contributed 58.4% to the overall variability. The contribution of the first and second dimensions was 48.8% and 9.6%, respectively. The same combination of climatic factors, with the exception of T in April, was associated with high levels of yellow rust infection in the set of 764 genotypes analyzed over an eight-year period. In that dataset T in April was more associated with a moderate level of yellow rust. However, T in February and precipitation in April,

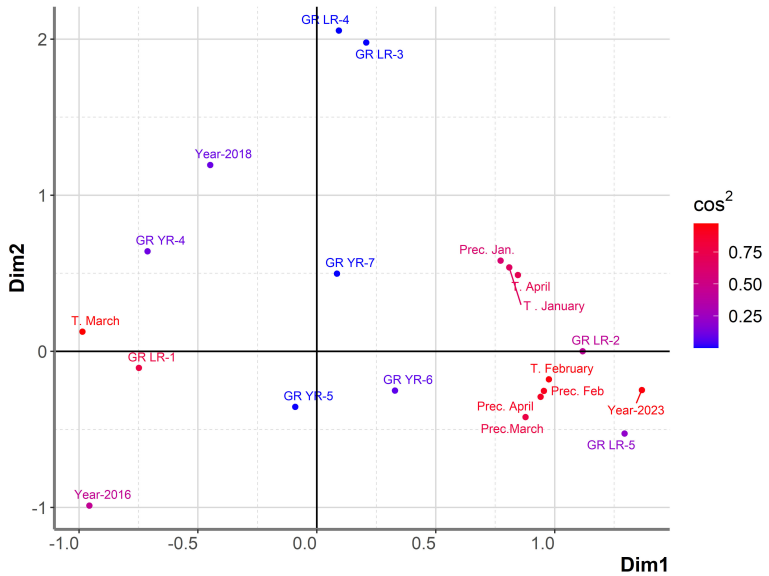

FIGURE 6
Graphical representation of PCAmix analysis on subset of genotypes showing coexistence between leaf and yellow rust in 2023. Factors included were: years (2016, 2018 and 2023), temperatures and precipitations from January to April in 2016, 2018 and 2023, reaction of 99 genotypes to leaf rust (GR LR) and reaction of 99 genotypes to yellow rust (GR YR).

TABLE 5 Best subsets regression for predicting leaf rust infection in 99 varieties in the years conducive for yellow rust occurrence (2016, 2018 and 2018).

Number of predictors	R^2	R^2_{pred}	Mallows' Cp	T in February (°C)	Precipitation in March (mm)	Yellow rust DI index (%)
1	53.6	52.9	65.2	X		
1	41.8	40.9	154.8		X	
2	57.4	56.5	38.1	X	X	
2	57.1	56.2	40.3	X		X
3	62.2	61.1	4.0	X	X	X

TABLE 6 Regression modelling on the most influencing factors on leaf rust infection in 99 genotypes in the years conducive for yellow rust occurrence (2016, 2018 and 2018).

Source	DF	Adj SS	ADj MS	F-Value	P-Value
Regression	101	58823	582.4	6.24	P<0,001
T in February	1	13060	13060.4	139.95	P<0,001
Prec. in March	1	3498	3498.4	37.49	P<0,001
Yellow rust	1	2957	2956.8	31.68	P<0,001
Genotype	98	11286	115.2	1.23	0.111
Error	189	17638	93.3		
Total	290	76461			

which highly affected leaf rust infection over the eight-year period, appeared to influence both leaf and yellow rust infection in the subset of genotypes showing yellow and leaf rust breakdown in 2023 (Figure 8). Precipitation in February and precipitation in March, which were associated with moderate levels of yellow rust infection in the eight-year period, were shown to affect leaf and yellow rust infection in 2023 with DI exceeding 31%. These results indicated that resistance breakdown to yellow rust was not associated with any specific climatic factors that were not already shown to be favorable for yellow rust infection of larger dataset comprising of 764 genotypes. Consequently, a more detailed study on changes in the race structure of yellow rust in the phenotyping platform and

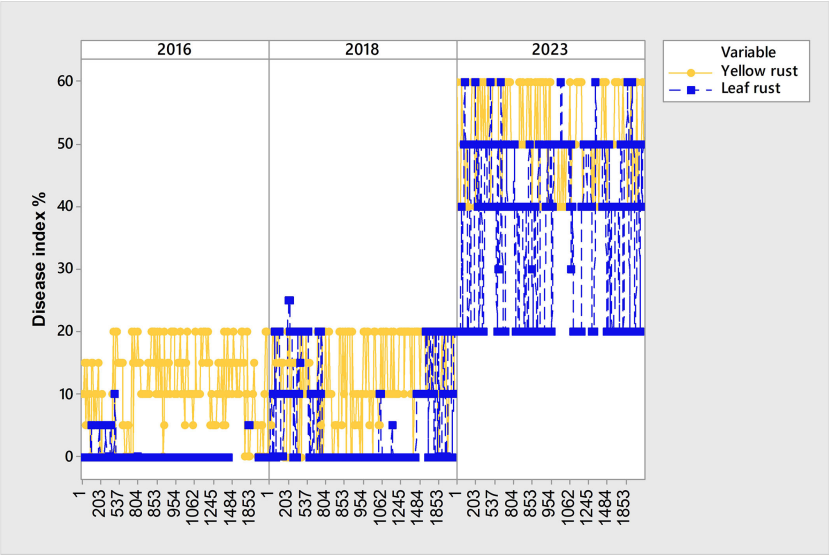

FIGURE 7
Set of 180 genotypes showing leaf and yellow rust resistance breakdown in 2023.

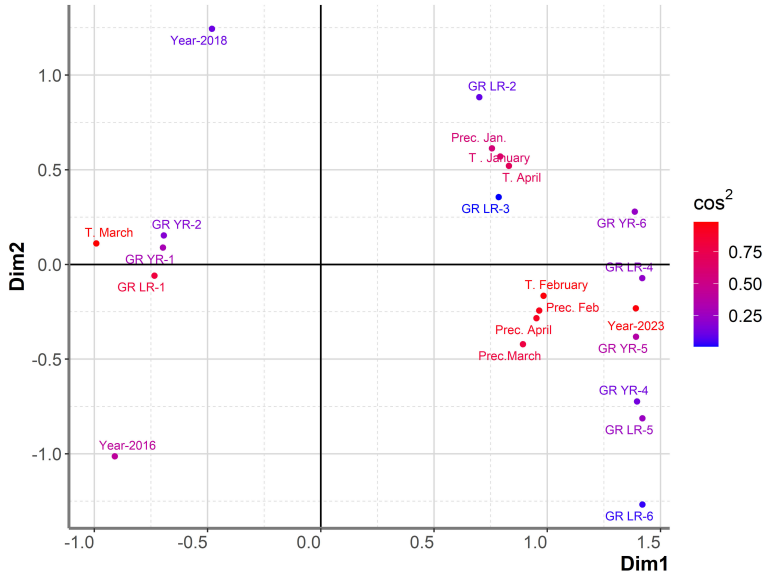

FIGURE 8
Graphical representation of PCAmix analysis on subset of genotypes showing resistance breakdown to leaf and yellow rust in 2023. Factors included were: years (2016, 2018 and 2023), temperatures and precipitations from January to April in 2016, 2018 and 2023, reaction of 180 genotypes to leaf rust (GR LR) and reaction of 180 genotypes to yellow rust (GR YR).

the individual response of each yellow rust resistance gene should be investigated in the future to explain the causes of yellow rust resistance breakdown in 2023.

4 Discussion

The results of this study indicated that the relationship between leaf and yellow rust is not straightforward and is strongly influenced not only by prevalent races and climatic factors affecting life cycle of pathogens, but also by differences in susceptibility reactions of wheat genotypes to agro-ecological conditions. In this study, we showed that the response of genotypes lacking resistance genes to yellow rust is not uniform in the years favorable for yellow rust infection, and we also observed the tendency of coexistence of leaf rust and yellow rust in the same host plant, although yellow rust is considered more aggressive. The effectiveness of resistance genes to rust diseases in Serbia is missing in reports related to European countries, making this study the first of its kind. Our study finally pointed out that resistance responses to rust diseases should not be investigated solely through the interaction between resistance genes and pathogen virulence capabilities but also through plants' response to combined abiotic and biotic stressors, which should be treated as a unique condition.

4.1 Shifts in predominance of leaf and yellow rust

The effect of climatic conditions on life cycle of the pathogens and susceptibility of host plants were always considered as primary precondition for pathogens outbreak. It is known that rust diseases have different requirements for initiation of infection and disease development, and that yellow rust is favored by elevated temperatures during the winter period (Hovmøller et al., 2016).

From 2016 to 2023, Serbia experienced extreme fluctuations in climatic elements, with temperatures in January and February varying by almost 10°C (ranging from -5 to +5°C in January) and 7°C (ranging from 1.2 to 7.5°C in February). In addition, there was a difference in total precipitation ranging from 1 to 65.5 mm in March and 11.1 to 74.5 mm in April. The results of our study indicated that winter temperatures (more specifically T in January) significantly affected yellow rust occurrence over the eight-year period. Although T in February was more associated with differences in leaf rust infection among years, in 2016, T in February exceeded the eighteen-year average by 4°C, setting the precondition for yellow rust predominance over leaf rust. In 2016, leaf rust infected only 4.8% of genotypes with DI above the trace level. PCAmix and regression modeling also indicated that precipitation in February and precipitation in March are associated with moderate levels of yellow rust infection. In the years with higher levels of yellow rust infection, total precipitation in February and/or March exceeded the eighteen-year average. This study's regression modeling on the most influencing factors on leaf rust infection gave an R^2 that did not exceed 31%, so a more specified dataset should be defined to explain differences in the effect of climatic factors on leaf rust infection. In the years with lower DI of leaf and yellow rust, extremely low T in January (-5°C) (2017) and lack of total rainfall in March (1 mm) (2022) resulted in the predominance of leaf rust over yellow rust in but with a lower DI than in the rest of the years. Powdery mildew predominated over all rust species in 2022 due to very dry conditions.

Jevtić et al. (2020) highlighted the significance of genotype reactions to climatic elements during specific phenological stages

as crucial factors affecting interactions among obligate pathogens and the dominance of one pathogen over another. The study also emphasized the need for increased attention to understanding how winter wheat genotypes can escape severe yellow rust infections during years initially conducive to pathogen development. Notably, the research revealed that, in the agro-ecological conditions of Serbia, elevated temperatures in February could lead to a higher prevalence of yellow rust in a larger number of susceptible winter wheat genotypes, compared to years where such high winter temperatures are observed only in January. The results of our study supported those of Jevtić et al. (2020) showing variability in the susceptibility reaction to yellow rust of a single genotype in years conducive to yellow rust occurrence. Significant effect of genotype itself was shown in the set of genotypes having high level of susceptibility to yellow rust in 2016 and 2023, but not in 2018 that was also conducive for yellow rust infection. In addition, the reaction of 764 susceptible genotypes to leaf and yellow rust over an eight-year period was quite different, not only with respect to the predominance of one pathogen over the other but also regarding their coexistence.

4.2 Increased level of coexistence of leaf and yellow rust

Until now, many efforts have been made in determining damage thresholds and developing mathematical as well as threshold-based weather model for forecasting wheat disease incidence and yield losses (Junk et al., 2016; El Jarroudi et al., 2017; Jevtić et al., 2017; El Jarroudi et al., 2020; Rodríguez-Moreno et al., 2020). However, prevalence of pathogens can hardly be predicted if studies are focused only on analysis of influence of individual abiotic and/or biotic factors (White et al., 2011; Juroszek and von Tiedemann, 2013).

It is known that abiotic stressors could affect plant-pest interactions (Pandey et al., 2017). High- and low-temperature, salinity and drought are reported to affect plant physiology and defense responses (Pandey et al., 2017). It was reported that stress combinations can have negative as well as positive effects on plants since regulatory network for plant responses to abiotic and biotic stresses consists of many components that may function antagonistically, or some responses can be prioritized over others (Glazebrook, 2005; Yasuda et al., 2008; Kissoudis et al., 2014). Consequently, plant responses to combined stressors cannot be predicted if only effect of individual stresses on plant response is investigated (Mittler, 2006; Rasmussen et al., 2013; Kissoudis et al., 2014; Suzuki et al., 2014; Pandey et al., 2017). In this study, a higher level of yellow rust infection has been recorded in 2016, 2018, and 2023, but the susceptibility reactions of wheat genotypes were not uniform in years conducive to yellow rust occurrence. In the subset of 99 genotypes with a DI of yellow rust exceeding 41% in 2016, 2018 and 2023, 72% of genotypes showed coexistence between leaf and yellow rust in 2023. Contrary to that, in 2018 in the same subset of genotypes, two pathogens coexisted in 11.3% genotypes. In 2016, yellow rust predominated over leaf rust with no records of coexistence. Regression modeling indicated that the combined effect of T in February, precipitation in March, and yellow rust infection significantly affected leaf rust infection in the subset of 99 genotypes. It could be suspected that the February temperature (4.2°C), exceeding the eighteen-year average, and the total rainfall in March (25 mm), which was below the eighteen-year average, were more conducive to yellow rust infection and postponed leaf rust development, creating favorable conditions for leaf rust to colonize the remaining green leaf tissue of susceptible genotypes when the development of yellow rust was slowed down. Interestingly, 38% of the genotypes exhibiting leaf-yellow rust coexistence in 2023 were early wheat genotypes with narrow leaf blades highly susceptible to leaf rust.

It is reported that plant responses to obligate pathogens could be either independent of resistance genes and determined by temperature changes. (Bryant et al., 2014). It has also been found that plant responses to obligate pathogens could be influenced by calcium-dependent phospholipid-binding proteins responsive to both pathogen infection and temperature changes (Zou et al., 2018). However, there are still open questions regarding plant responses to the combined effects of climatic factors influencing the life cycle of pathogens, the duration of development stages of wheat genotypes, and hormonal cross-talk in plant stress responses. Considering that the regression coefficient describes the size and direction of the relationship between a predictor and the response variable, it appears from our study that further investigations should be conducted to identify predictor variables that reflect the response of individual genotypes to combined abiotic and biotic stressors. This will help in developing models for rust occurrence that can be applied to a large number of genotypes with a high level of certainty.

4.3 Yellow rust resistance breakdown in 2023

The breeding for resistance to rust pathogens usually takes into account race-specific and race nonspecific resistance. Race-specific resistance is conferred by a major dominant gene, expressed at all growth stages, and is not durable. The race nonspecific resistance is primarily quantitative and usually effective in later growth stages. The race nonspecific resistance is known as adult plant resistance (APR) or slow-rusting resistance (Kumar et al., 2022). In this study, 6.6% of genotypes that were resistant or moderately resistant to yellow and leaf rust in the years conducive to yellow rust occurrence (2016 and 2018) exhibited resistance breakdown in 2023. Among them, there were genotypes carrying resistance genes for leaf rust (Lr) and yellow rust (Yr) with different modes of action. The resistance breakdown in 2023 was associated with all-stage (AS) race-specific genes (Lr1, Lr3, Lr10, Lr14a, Lr2a, Lr24, Yr2, Yr4, Yr6, Yr7, Yr9) and adult plant resistance genes (Lr13 race-specific, Lr20, Yr14 race-specific, Lr34 slow rusting), as well as resistance genes carried by wild relatives.

When examining the overall worldwide population of yellow rust using 19 Yr genes, Ali et al. (2017) indicated that virulence to Yr2, Yr6, Yr7, Yr9, and Yr25 was generally in high frequencies and across many regions (>70%). This finding is in accordance with the

results of our study, but it has to be pointed out that the virulences to Yr2, Yr6, Yr7, and Yr9 were recorded in Serbia for the first time in 2023, contrary to other European countries. Ali et al. (2017) also reported that virulence to Yr5 and Yr15 were absent in all regions, and virulence to Yr27 was not detected in Europe; virulence to Yr3, Yr4, Yr17, Yr32, YrSp, and YrAmb was absent in West Asia; virulence to Yr10 and Yr24 was absent in North Africa and South Asia; virulence to Yr10, Yr24, and YrSp was absent in Central Asia; and virulence to Yr10, Yr32, and YrSp was absent in East Africa.

Resistance to leaf rust in wheat is currently provided with more than 80 Lr genes and 14 other genes that have not been assigned a new number in the Lr series yet since they have not been subjected to the test of allelism with the known Lr genes (Dakouri et al., 2013). The majority of Lr genes provide race-specific resistance that is expressed with a hypersensitive response (HR) or programmed cell death (Flor, 1946). According to Dakouri et al. (2013), Lr1, Lr3, Lr10, and Lr20 were the most prevalent genes worldwide, but these have also been overcome in addition to Lr9 and Lr28 (Kolmer, 1996). In our study, Lr1, Lr3, Lr10, and Lr20 were present in genotypes that lost resistance to yellow rust in 2023 but also exhibited a susceptibility reaction to leaf rust more in 2023 than in previous years.

Adult plant resistance provided by Lr34 (Lr34/Yr18/Sr57/Pm38/Ltn1), Lr46 (Lr46/Yr29/Sr58/Pm39/Ltn2), and Lr67 (Lr67/Yr46/Sr56/Pm39/Ltn3) expresses pleiotropic effects against three rust species (*Puccinia graminis* f. sp. *tritici*, *Puccinia triticina*, *Puccinia striiformis* f. sp. *tritici*) and powdery mildew (*Blumeria graminis* f. sp. *tritici*) (Lagudah et al., 2006; Hulbert et al., 2007; Kolmer et al., 2008; Herrera-Foessel et al., 2014). Partial or slow resistance to leaf rust provided by Lr34, Lr46, and Lr67 is characterized by a shorter period of sporulation, smaller uredinia size, lower spore density, a longer latent period, and lower infection frequency (Caldwell et al., 1968). The mode of action of Lr34+, Lr46+, and Lr67+ genes does not fit any other previously described disease defense mechanisms (Hulbert et al., 2007), and it was also reported that their effectiveness is dependent on the geographic region (Hulbert et al., 2007). In the study of Dakouri et al. (2013), 79% accessions carring Lr34 had high to moderate levels of resistance ranging from trace level to 35%.

Characterization of APR-related defense responses was usually conducted on transgenic plants in controlled conditions (Risk et al., 2012; Risk et al., 2013), and it was shown that senescence, abiotic stress, and pathogenesis-related (PRs) genes were highly induced in genotypes having the Lr34+ gene. In addition, it was reported that Lr34+ can act synergistically with other leaf rust resistance genes such as Lr12, Lr13, Lr22a, Lr46, Lr67, and Lr68, or novel APR genes (Dyck, 1991; Dyck, 1992; Sawhney, 1992; Kloppers and Pretorius, 1997; Li et al., 2010; Dakouri et al., 2013). However, in our study, Lr34+Lr13 was less effective in providing rust resistance in 2023 than in previous years. Dakouri et al. (2013) reported the possibility of higher levels of rust infections (ranging from 36% to 52%) in genotypes carrying Lr34+, but the reasons for this were only speculated. Sha et al. (2005) reported that DNA methylation can play a role in the expression of APR genes in rice, with a high correlation between the repression of gene expression and hypermethylation but additional analysis of gene expression and methylation patterns is required to test this hypothesis.

According to a report by Kissoudis et al. (2014), 60% of expression changes resulting from combined stressors cannot be predicted based on individual stressor responses. This suggests that the differences between susceptible and resistant plant reactions may be more influenced by variations in the timing and intensity of plant responses to multiple stressors, rather than solely relying on the expression of individual genes (van Loon et al., 2006). Consequently, analyzing the association of morphological and physiological resistance traits conferred by APR genes with abiotic stressors and the expression of abiotic stress genes in field conditions could yield a more detailed genotype profile, facilitating informed breeding decisions to enhance resistance against combined biotic and abiotic stressors.

Nowadays, a lot of effort is being made to solve pest problems using integrated pest management (IPM) with the main goal of minimizing risks to people and the environment. IPM principles are combined to create IPM programs that include six major components: pest identification; monitoring and assessing pest numbers and damage; guidelines for when management action is needed; preventing pest problems; using a combination of biological, cultural, physical/mechanical, and chemical management tools; and, after the action is taken, assessing the effect of pest management. In addition, one of the most important IPM measures is developing pest-resistant genotypes. The breeding programs usually conduct high-throughput genotype screening to test the breeding material for its resistance, and molecular techniques have been constantly improved to map resistance genes. However, despite our increasing understanding of the genome, it may not fully explain the complexity of the phenotype, and identifying complete QTL interactions can be challenging (Velu and Singh, 2013). Our results contribute to all aspects of IPM components, especially those dealing with tracking rust diseases and assessing genotype susceptibility/resistance reactions to rust infection.

5 Conclusion

The ability to assess and predict the risk of pathogen development is one of the main goals in plant protection. We indicated that a single genotype could exhibit differences in susceptibility reactions to leaf and yellow rust even in years that are conducive to yellow rust outbreaks. The specificity in genotype reactions to combined abiotic and biotic stressors could directly influence the relationship between rust diseases, leading to the predominance of one pathogen over the other or their coexistence on the same host plant. Monitoring and assessing rust prevalence are important components of IPM, contributing not only to tracking the spread of rust diseases over large areas but also to developing a Decision-Support System for managing fungicide applications. In practice, there are many models for predicting rust occurrence that are based solely on weather data and developed using only a few wheat varieties as models. There is also a lack of information on their long-term efficacy. Therefore, our results indicate that more attention should be focused on multidisciplinary investigations when building models for rust occurrence. Finally, phenotypic plant breeding will always remain

an important practice, and our study points out that further investigations should be conducted to identify predictor variables that accurately reflect the response of individual genotypes to combined abiotic and biotic stressors, ensuring more reliable rust control management.

Data availability statement

The raw data supporting the conclusions of this article will be made available by the authors, without undue reservation.

Author contributions

RJ: Conceptualization, Funding acquisition, Investigation, Project administration, Resources, Supervision, Writing – review & editing. VŽ: Conceptualization, Formal Analysis, Investigation, Software, Visualization, Writing – original draft.

Funding

The author(s) declare financial support was received for the research, authorship, and/or publication of this article. This research was supported by the Ministry of Science, Technological Development and Innovation of the Republic of Serbia, grant number: 451-03-47/2023-01/200032.

Conflict of interest

The authors declare that the research was conducted in the absence of any commercial or financial relationships that could be construed as a potential conflict of interest.

Publisher's note

All claims expressed in this article are solely those of the authors and do not necessarily represent those of their affiliated organizations, or those of the publisher, the editors and the reviewers. Any product that may be evaluated in this article, or claim that may be made by its manufacturer, is not guaranteed or endorsed by the publisher.

Supplementary material

The Supplementary Material for this article can be found online at: https://www.frontiersin.org/articles/10.3389/fpls.2023.1270087/full#supplementary-material

References

Afzal, S. N., Haque, M. I., Ahmedani, M. S., Bashir, S., and Rattu, A. U. R. (2007). Assessment of yield losses caused by Puccinia striiformis triggering stripe rust in the most common wheat varieties. *Pakistan Journal of Botany* 39, 2127–2134.

Ali, S., Gladieux, P., Leconte, M., Gautier, A., Justesen, A. F., Hovmøller, M. S., et al. (2014). Origin, migration routes and worldwide population genetic structure of the wheat yellow rust pathogen *Puccinia striiformis* f.sp. *tritici*. *PloS Pathog.* 10, e1003903. doi: 10.1371/journal.ppat.1003903

Ali, S., Rodriguez-Algaba, J., Thach, T., Sørensen, C. K., Hansen, J. G., Lassen, P., et al. (2017). Yellow rust epidemics worldwide were caused by pathogen races from divergent genetic lineages. *Front. Plant Sci.* 8. doi: 10.3389/fpls.2017.01057

Brown, J. K. M., and Hovmøller, M. S. (2002). Aerial dispersal of pathogens on the global and continental scales and its impact on plant disease. *Science* 297, 537–541. doi: 10.1126/science.1072678

Bryant, R. R. M., McGrann, G. R. D., Mitchell, A. R., Schoonbeek, H., Boyd, L. A., Uauy, C., et al. (2014). A change in temperature modulates defense to yellow (stripe) rust in wheat line UC1041 independently of resistance gene Yr36. *BMC Plant Biol.* 14, 10. doi: 10.1186/1471-2229-14-10

Bursac, Z., Gauss, C. H., Williams, D. K., and Hosmer, D. W. (2008). Purposeful selection of variables in logistic regression. *Source Code Biol. Med.* 3, 17. doi: 10.1186/1751-0473-3-17

Caldwell, R. M., Kraybill, H. R., Sullivan, J. T., and Compton, L. E. (1968). Effect of leaf rust (*Puccinia triticina*) on yield, physical characters, and composition of winter wheats. *J. Agric. Res.* 48, 1049–1071.

Chen, X. M. (2005). Epidemiology and control of stripe rust [*Puccinia striiformis* f. sp. *tritici*] on wheat. *Can. J. Plant Pathol.* 27, 314–337. doi: 10.1080/07060660509507230

CIMMYT. (1979). *Instructions for the management and reporting of results for wheat program international yield and screening nurseries*. Available at: https://repository.cimmyt.org/handle/10883/3914?show=full.

Dakouri, A., McCallum, B. D., Radovanovic, N., and Cloutier, S. (2013). Molecular and phenotypic characterization of seedling and adult plant leaf rust resistance in a world wheat collection. *Mol. Breed.* 32, 663–677. doi: 10.1007/s11032-013-9899-8

de Vallavieille-Pope, C., Ali, S., Leconte, M., Enjalbert, J., Delos, M., and Rouzet, J. (2012). Virulence dynamics and regional structuring of *Puccinia striiformis* f. sp. *tritici* in France between 1984 and 2009. *Plant Dis.* 96, 131–140. doi: 10.1094/PDIS-02-11-0078

Dyck, P. L. (1991). Genetics of adult-plant leaf rust resistance in 'Chinese Spring' and 'Sturdy' wheats. *Crop Sci.* 31, cropsci1991.0011183X003100020016x. doi: 10.2135/cropsci1991.0011183X003100020016x

Dyck, P. L. (1992). Transfer of a gene for stem rust resistance from *Triticum araraticum* to hexaploid wheat. *Genome* 35, 788–792. doi: 10.1139/g92-120

El Jarroudi, M., Kouadio, L., Bock, C. H., El Jarroudi, M., Junk, J., Pasquali, M., et al. (2017). A threshold-based weather model for predicting stripe rust infection in winter wheat. *Plant Dis.* 101, 693–703. doi: 10.1094/PDIS-12-16-1766-RE

El Jarroudi, M., Lahlali, R., Kouadio, L., Denis, A., Belleflamme, A., El Jarroudi, M., et al. (2020). Weather-based predictive modeling of wheat stripe rust infection in Morocco. *Agronomy* 10 (2), 280. doi: 10.3390/agronomy10020280

Flor, H. H. (1946). Genetics of pathogenicity in melampsora lini. *J. Agric. Res.* 73, 335–357.

Glazebrook, J. (2005). Contrasting mechanisms of defense against biotrophic and necrotrophic pathogens. *Annu. Rev. Phytopathol.* 43, 205–227. doi: 10.1146/annurev.phyto.43.040204.135923

Heeb, L., Jenner, E., and Cock, M. J. W. (2019). Climate-smart pest management: building resilience of farms and landscapes to changing pest threats. *J. Pest Sci.* 92, 951–969. doi: 10.1007/s10340-019-01083-y

Herrera-Foessel, S., Singh, R., Lillemo, M., Huerta-Espino, J., Bhavani, S., Singh, S., et al. (2014). Lr67/Yr46 confers adult plant resistance to stem rust and powdery mildew in wheat. *TAG Theor. Appl. Genet. Theoretische Und Angewandte Genetik* 127 (4), 781–789. doi: 10.1007/s00122-013-2256-9

Hovmøller, M. S., Justesen, A. F., and Brown, J. K. M. (2002). Clonality and long-distance migration of *Puccinia striiformis* f.sp. *tritici* in north-west Europe. *Plant Pathol.* 51, 24–32. doi: 10.1046/j.1365-3059.2002.00652.x

Hovmøller, M. S., Sørensen, C. K., Walter, S., and Justesen, A. F. (2011). Diversity of *Puccinia striiformis* on cereals and grasses. *Annu. Rev. Phytopathol.* 49, 197–217. doi: 10.1146/annurev-phyto-072910-095230

Hovmøller, M. S., Walter, S., Bayles, R. A., Hubbard, A., Flath, K., Sommerfeldt, N., et al. (2016). Replacement of the European wheat yellow rust population by new races

from the center of diversity in the near-Himalayan region. *Plant Pathol.* 65, 402–411. doi: 10.1111/ppa.12433

Hovmøller, M. S., Yahyaoui, A. H., Milus, E. A., and Justesen, A. F. (2008). Rapid global spread of two aggressive strains of a wheat rust fungus. *Mol. Ecol.* 17, 3818–3826. doi: 10.1111/j.1365-294X.2008.03886.x

Hulbert, S. H., Bai, J., Fellers, J. P., Pacheco, M. G., and Bowden, R. L. (2007). Gene expression patterns in near isogenic lines for wheat rust resistance gene Lr34/Yr18. *Phytopathology*® 97, 1083–1093. doi: 10.1094/PHYTO-97-9-1083

Jevtić, R., Župunski, V., and Lalošević, M. (2023). "Climate change-induced alteration in biotic environment and its effect on cereal and pseudocereal quality," in *Developing Sustainable And Health Promoting Cereals And Pseudocereals Conventional and Molecular Breeding*. Eds. M. Rakszegi, M. Papageorgiou and J. M. Rocha (Academic Press is an imprint of Elsevier), 359–373.

Jevtić, R., Župunski, V., Lalošević, M., Jocković, B., Orbović, B., and Ilin, ,. S. (2020). Diversity in susceptibility reactions of winter wheat genotypes to obligate pathogens under fluctuating climatic conditions. *Sci. Rep.* 10, 19608. doi: 10.1038/s41598-020-76693-z

Jevtić, R., Župunski, V., Lalošević, M., and Župunski, L. (2017). Predicting potential winter wheat yield losses caused by multiple disease systems and climatic conditions. *Crop Prot.* 99, 17–25. doi: 10.1016/j.cropro.2017.05.005

Junk, J., Kouadio, L., Delfosse, P., and El Jarroudi, M. (2016). Effects of regional climate change on brown rust disease in winter wheat. *Climatic Change* 135, 439–451. doi: 10.1007/s10584-015-1587-8

Juroszek, P., and von Tiedemann, A. (2013). Climate change and potential future risks through wheat diseases: a review. *Eur. J. Plant Pathol.* 136, 21–33. doi: 10.1007/s10658-012-0144-9

Kissoudis, C., van de Wiel, C., Visser, R. G. F., and van der Linden, G. (2014). Enhancing crop resilience to combined abiotic and biotic stress through the dissection of physiological and molecular crosstalk. *Front. Plant Sci.* 5. doi: 10.3389/fpls.2014.00207

Kloppers, F. J., and Pretorius, Z. A. (1997). Effects of combinations amongst genes Lr13, Lr34 and Lr37 on components of resistance in wheat to leaf rust. *Plant Pathol.* 46, 737–750. doi: 10.1046/j.1365-3059.1997.d01-58.x

Kolmer, J. A. (1996). Genetics of resistance to wheat leaf rust. *Annu. Rev. Phytopathol.* 34, 435–455. doi: 10.1146/annurev.phyto.34.1.435

Kolmer, J. A., Singh, R. P., Garvin, D. F., Viccars, L., William, H. M., Huerta-Espino, J., et al. (2008). Analysis of the Lr34/Yr18 rust resistance region in wheat germplasm. *Crop Sci.* 48, 1841–1852. doi: 10.2135/cropsci2007.08.0474

Kumar, K., Jan, I., Saripalli, G., Sharma, P. K., Mir, R. R., Balyan, H. S., et al. (2022). An update on resistance genes and their use in the development of leaf rust resistant cultivars in wheat. *Front. Genet.* 13. doi: 10.3389/fgene.2022.816057

Lagudah, E. S., McFadden, H., Singh, R. P., Huerta-Espino, J., Bariana, H. S., and Spielmeyer, W. (2006). Molecular genetic characterization of the Lr34/Yr18 slow rusting resistance gene region in wheat. *Theor. Appl. Genet.* 114, 21–30. doi: 10.1007/s00122-006-0406-z

Li, Z. F., Xia, X. C., He, Z. H., Li, X., Zhang, L. J., Wang, H. Y., et al. (2010). Seedling and Slow rusting resistance to leaf rust in Chinese wheat cultivars. *Plant Dis.* 94, 45–53. doi: 10.1094/PDIS-94-1-0045

Linde, C. C., Zhan, J., and McDonald, B. A. (2002). Population structure of *Mycosphaerella graminicola*: From lesions to continents. *Phytopathology*® 92, 946–955. doi: 10.1094/PHYTO.2002.92.9.946

Mittler, R. (2006). Abiotic stress, the field environment and stress combination. *Trends Plant Sci.* 11, 15–19. doi: 10.1016/j.tplants.2005.11.002

Pandey, P., Irulappan, V., Bagavathiannan, M. V., and Senthil-Kumar, M. (2017). Impact of combined abiotic and biotic stresses on plant growth and avenues for crop improvement by exploiting physio-morphological traits. *Front. Plant Sci.* 8. doi: 10.3389/fpls.2017.00537

Peterson, R. F., Campbell, A. B., and Hannah, A. E. (1948). A diagrammatic scale for estimating rust intensity on leaves and stems of cereals. *Can. J. Res.* 26c, 496–500. doi: 10.1139/cjr48c-033

Rasmussen, S., Barah, P., Suarez-Rodriguez, M. C., Bressendorff, S., Friis, P., Costantino, P., et al. (2013). Transcriptome responses to combinations of stresses in arabidopsis. *Plant Physiol.* 161, 1783–1794. doi: 10.1104/pp.112.210773

Risk, J. M., Selter, L. L., Chauhan, H., Krattinger, S. G., Kumlehn, J., Hensel, G., et al. (2013). The wheat Lr34 gene provides resistance against multiple fungal pathogens in barley. *Plant Biotechnol. J.* 11, 847–854. doi: 10.1111/pbi.12077

Risk, J. M., Selter, L. L., Krattinger, S. G., Viccars, L. A., Richardson, T. M., Buesing, G., et al. (2012). Functional variability of the Lr34 durable resistance gene in transgenic wheat. *Plant Biotechnol. J.* 10, 477–487. doi: 10.1111/j.1467-7652.2012.00683.x

Rodríguez-Moreno, V. M., Jiménez-Lagunes, A., Estrada-Avalos, J., Mauricio-Ruvalcaba, J. E., and Padilla-Ramírez, J. S. (2020). Weather-data-based model: an approach for forecasting leaf and stripe rust on winter wheat. *Meteorol Appl.* 27, e1896. doi: 10.1002/met.1896

RStudio Team. (2022). *RStudio: Integrated Development for R*. Available at: http://www.rstudio.com/.

Salgado, J. D., and Paul, P. A. (2016). *Powdery Mildew of Wheat. Ohio State University Extension*. Available at: https://ohioline.osu.edu/factsheet/plpath-cer-11.

Sawhney, R. N. (1992). The role of Lr34 in imparting durable resistance to wheat leaf rust through gene interaction. *Euphytica* 61, 9–12. doi: 10.1007/BF00035541

Seem, R. C. (1984). Disease incidence and severity relationships. *Annu. Rev. Phytopathol.* 22, 133–150. doi: 10.1146/annurev.py.22.090184.001025

Sha, A. H., Lin, X. H., Huang, J. B., and Zhang, D. P. (2005). Analysis of DNA methylation related to rice adult plant resistance to bacterial blight based on methylation-sensitive AFLP (MSAP) analysis. *Mol Genet Genomics* 273, 484–490. doi: 10.1007/s00438-005-1148-3

Singh, R. P., Huerta-Espino, J., and Roelfs, A. P. (2002). "The wheat rusts," in *Bread Wheat*. Eds. B. C. Curtis, S. Rajaram and H. Gómez Macpherson (Rome, Italy: Food and agriculture organization of the united nations).

Sørensen, C. K., Hovmøller, M. S., Leconte, M., Dedryver, F., and de Vallavieille-Pope, C. (2014). New races of *Puccinia striiformis* found in Europe reveal race specificity of long-term effective adult plant resistance in wheat. *Phytopathology*® 104, 1042–1051. doi: 10.1094/PHYTO-12-13-0337-R

Suzuki, N., Rivero, R. M., Shulaev, V., Blumwald, E., and Mittler, R. (2014). Abiotic and biotic stress combinations. *New Phytol.* 203, 32–43. doi: 10.1111/nph.12797

Thach, T., Ali, S., de Vallavieille-Pope, C., Justesen, A. F., and Hovmøller, M. S. (2016). Worldwide population structure of the wheat rust fungus Puccinia striiformis in the past. *Fungal Genet. Biol.* 87, 1–8. doi: 10.1016/j.fgb.2015.12.014

van Loon, L. C., Rep, M., and Pieterse, C. M. J. (2006). Significance of inducible defense-related proteins in infected plants. *Annu. Rev. Phytopathol.* 44, 135–162. doi: 10.1146/ annurev.phyto.44.070505.143425

Velu, G., and Singh, R. P. (2013). Phenotyping in wheat breeding. In: S. Panguluri and A. Kumar (eds) *Phenotyping for Plant Breeding*. (New York, NY: Springer). doi: 10.1007/978-1-4614-8320-5_2

Walter, S., Ali, S., Kemen, E., Nazari, K., Bahri, B. A., Enjalbert, J., et al. (2016). Molecular markers for tracking the origin and worldwide distribution of invasive strains of Puccinia striiformis. *Ecol. Evol.* 6, 2790–2804. doi: 10.1002/ece3.2069

Wegulo, S. N., Breathnach, J. A., and Baenziger, P. S. (2009). Effect of growth stage on the relationship between tan spot and spot blotch severity and yield in winter wheat. *Crop Prot.* 28, 696–702. doi: 10.1016/j.cropro.2009.04.003

Wellings, C. R., and Mcintosh, R. A. (1990). *Puccinia striiformis* f.sp. *tritici* in Australasia: pathogenic changes during the first 10 years. *Plant Pathol.* 39, 316–325. doi: 10.1111/j.1365-3059.1990.tb02509.x

White, J. W., Hoogenboom, G., Kimball, B. A., and Wall, G. W. (2011). Methodologies for simulating impacts of climate change on crop production. *Field Crops Res.* 124, 357–368. doi: 10.1016/j.fcr.2011.07.001

XLSTAT Statistical and Data Analysis Solution. (2022). Available at: https://www.xlstat.com.

Yasuda, M., Ishikawa, A., Jikumaru, Y., Seki, M., Umezawa, T., Asami, T., et al. (2008). Antagonistic interaction between systemic acquired resistance and the abscisic acid–mediated abiotic stress response in Arabidopsis. *Plant Cell* 20, 1678–1692. doi: 10.1105/tpc.107.054296

Zadoks, J. C. (1961). Yellow rust on wheat studies in epidemiology and physiologic specialization. *Tijdschrift Over Plantenziekten* 67, 69–256. doi: 10.1007/BF01984044

Zou, B., Ding, Y., Liu, H., and Hua, J. (2018). Silencing of copine genes confers common wheat enhanced resistance to powdery mildew. *Mol. Plant Pathol.* 19, 1343–1352. doi: 10.1111/mpp.12617

frontiers | Frontiers in Plant Science

TYPE Original Research
PUBLISHED 24 October 2023
DOI 10.3389/fpls.2023.1279502

Check for updates

OPEN ACCESS

EDITED BY
Xinli Zhou,
Southwest University of Science and Technology, China

REVIEWED BY
Manoj Kumar Solanki,
University of Silesia in Katowice, Poland
Xin Li,
Southwest University of Science and Technology, China

*CORRESPONDENCE
Yi Chai
chaiyi123456@126.com
Wenli Wang
wliw@163.com

†These authors have contributed equally to this work

RECEIVED 18 August 2023
ACCEPTED 11 October 2023
PUBLISHED 24 October 2023

CITATION
Dong Y, Wang Y, Tang M, Chen W, Chai Y and Wang W (2023) Bioinformatic analysis of wheat defensin gene family and function verification of candidate genes. *Front. Plant Sci.* 14:1279502. doi: 10.3389/fpls.2023.1279502

COPYRIGHT
© 2023 Dong, Wang, Tang, Chen, Chai and Wang. This is an open-access article distributed under the terms of the Creative Commons Attribution License (CC BY). The use, distribution or reproduction in other forums is permitted, provided the original author(s) and the copyright owner(s) are credited and that the original publication in this journal is cited, in accordance with accepted academic practice. No use, distribution or reproduction is permitted which does not comply with these terms.

Bioinformatic analysis of wheat defensin gene family and function verification of candidate genes

Ye Dong[1†], Youning Wang[2†], Mingshuang Tang[3†], Wang Chen[1], Yi Chai[1*] and Wenli Wang[4*]

[1]Ministry of Agriculture and Rural Affairs (MARA) Key Laboratory of Sustainable Crop Production in the Middle Reaches of the Yangtze River (Co-Construction by Ministry and Province), College of Agriculture, Yangtze University, Jingzhou, China, [2]Hubei Key Laboratory of Quality Control of Characteristic Fruits and Vegetables, Hubei Engineering University, Xiaogan, Hubei, China, [3]Nanchong Academy of Agriculture Sciences, Nanchong, Sichuan, China, [4]College of Plant Protection, Northwest A&F University, Yangling, Shanxi, China

Plant defensins are widely distributed in the leaves, fruits, roots, stems, seeds, and tubers. Research shows that defensin in plants play a significant role in physiological metabolism, growth and development. Plant defensins can kill and suppress a variety of pathogenic bacteria. In this study, we understand the phylogenetic relationships, protein characterization, chromosomal localization, promoter and gene structural features of the *TaPDFs* family through sequence alignment and conserved protein structural domain analysis. A total of 73 *PDF* gene members in wheat, 15 *PDF* genes in maize, and 11 *PDF* genes in rice were identified. A total of 35, 65, and 34 *PDF* gene members were identified in the genomes of *Ae. tauschii*, *T. urartu*, and *T. dicoccoides*, respectively. *TaPDF4.9* and *TaPDF2.15* were constructed into pART27 vector with YFP by homologous recombination for subcellular localization analysis. Subcellular localization results showed that *TaPDF4.9* and *TaPDF2.15* were basically located in the cell membrane and cytoplasm, and *TaPDF4.9* was also located in the nucleus. *TaPDF4.9* and *TaPDF2.15* could inhibit the infection of *Phytophthora infestans* strain '88069'. The results suggest that *TaPDFs* may be able to improve disease resistance. The study of wheat defensins will be beneficial for improving wheat yield and provides a theoretical basis for research on resistance to wheat diseases.

KEYWORDS

defensins, gene structure, subcellular localization, gene expression, *Phytophthora infestans* infection

Introduction

Plants have their own defense systems, and when they are infected with external pathogens such as fungi and oomycetes, they will produce a series of antagonistic substances themselves (Sathoff et al., 2019). Antagonistic substances are mainly categorized into some low molecular weight secondary metabolites or some low molecular weight short peptides less than 100 amino acids to prevent the propagation and expansion of the pathogen and further invasion of the host plant (Terras et al., 1992). Plant defenses are among the short, low molecular weight peptides that are widely distributed in plants. (De Coninck et al., 2013).

There are 45-54 amino acid residues in plant defensins. The encoded proteins were approximately 5 kDa, which contain eight conserved cysteine residues forming four pairs of disulfide bonds (Cys4-Cys7, Cys3-Cys6, Cys2-Cys5 and Cys1-Cys8), among which, the most conserved are the two pairs, Cys2-Cys5 and Cys1-Cys8 (Thomma et al., 2002). It was shown that the solution structure of radish defensin (Rs-AFP1) by nuclear magnetic resonance (NMR) consists of three reverse parallel β-folded lamellae and one α-helix, forming a stable βαββββ structure with four pairs of disulfide bonds acting as support, and the Csαβ modal sequence (Cysteine stabilized αβ motif) was found, fixing a pair of disulfide bonds on the lamellae in the α-helix and β-fold (Vriens et al., 2016). The β-folded lamellar signature sequence (Cys-Xaa-Cys) and the α-helical signature sequence (Cys-Xaa-Xaa-Xaa-Cys) are common to most plant defensins (Parisi et al., 2019). The Cysteine stabilized αβ motif indicates that plant defensins are more structurally stable and can be stably expressed in many plants. Defensins have a special resistance mechanism. Defensins act mainly on the cell membranes of pathogenic microorganisms, binding to sphingolipids on the outer side of phospholipids. Defensins are able to disrupt the cell membranes of certain fungi, causing changes in the anions and cations on the cell membrane. Thus defensins disrupt the cell membrane of pathogenic microorganisms, altering their permeability and creating phenomena such as Ca^{2+} inward flow, K^+ outward, and medium liquefaction (Shahmiri et al., 2023).

Most phytodefensins are resistant to fungal pathogens and ward off diseases caused by fungi. It has been found that most defensins are induced to be expressed by fungal infection. GXCX3-9C has antifungal activity and is a core motif in plant defensins. (Sagaram et al., 2011). The core motif peptides of defensins in Medicago truncatula are MtDef4 and MtDef5. And these defensins show high activity against both plant and human bacterial pathogens (Andrew Edward Sathoff et al., 2019). The carrot defensin Rs-AFP2 binds to the nerve sphingolipid glucosylceramide (GlcCer) and acts on the cell membrane, with the binding site being the sphingolipid on the outside of the phospholipid. This in turn disrupts the cell membrane and alters its permeability, resulting in Ca^{2+} in-flow, K^+ out-flow, and liquefaction of the culture medium (Sadhu et al., 2023). In addition, it has been shown that the tolerance of certain plants to the heavy metal zinc is related to phyto-defensin. Reduced Expression of Plant Defensin 1 in Arabidopsis Leads to Increased Resistance to Pathogenic Bacteria and Zinc Toxicity (Nguyen et al., 2023). Phytodefensins have a very broad development prospect as a new antifungal drug. Research has shown that plant-derived AMPs can be used as alternative molecules to overcome pathogen resistance (Lima et al., 2022). This property can therefore be utilized to research new drugs to fight cancer. *Candida otitis* is a pan-resistant pathogenic yeast that can treat immunocompromised patients. Phytodefensins can influence the virulence properties of clinical strains of *C. auris* (Kamli et al., 2022). Plant defensins PaDef and γ-thionin are potential angiogenicmodulators of the VEGF activity on endothelial cells (Falcón-Ruiz et al., 2023). Therefore, plant defensins, with their broad-spectrum, antimicrobial and high efficiency, provide new ideas for the research and development of new antifungal and antitumor drugs. With the in-depth exploration of its mechanism of action, it is expected to be put more into the industrial, medical and other fields to play a role.

Wheat is one of the major grain crops in China and has an important position in food production, with more than 1/3 of the world's population taking it as their staple food. Since the growth of wheat is attacked by diseases, it is necessary to tap the relevant genes to breed disease-resistant varieties. A review of the literature shows that the *PDF* gene family is more fully reported in Arabidopsis. *PDF* gene family analysis is not currently reported in wheat, maize and rice. In study, using Arabidopsis PDF proteins (Araport11) as query, *PDF* genes in wheat were identified. Moreover, PDF protein characters and the phylogenetic relationships were analyzed. The function of *PDF* was explored through a series of analyses including chromosomal localization, conserved structure and gene structural domains of the wheat *PDF* gene. This study provides the first systematic certification and classification of the *PDF* genes family in wheat and its subgenomic donors. Genome-wide identification of *TaPDFs* will enrich the study of plant disease resistance genes and provide a basis for wheat varieties breeding.

Materials and methods

Screening and analysis of *PDF* genes in wheat, maize, and rice genomes

The 15 protein sequences from Arabidopsis *PDF* family were collected from TAIR database (http://www.Arabidopsis.org/index.jsp) (Mäser et al., 2001), and served as query sequences to research *PDF* genes in wheat genome (IWGSC v1.1), Maize genome (maizeGDB, B73 RefGen_v5, https://www.maizegdb.org/), and rice genome (RGAP, RGAP7, http://rice.plantbiology.msu.edu/index.shtml) using BLASTp with e-value < 10^{-10} (Clavijo et al., 2017). Subsequently, the PDF proteins containing the major intrinsic protein structural domain (gamma – thiionin, PF00304) were retained after searching in the Pfam database (http://pfam.xfam.org/) (Finn et al., 2016).

The length of CDS region, molecular weight (MW), isoelectric point (pI), stability, and hydrophilicity characteristics (GRAVY) of PDF proteins in wheat, maize, and rice were analyzed using ExPASy Server 10 (https://prosite.expasy.org/PS50011) (Li et al., 2018). Signal peptide of wheat *PDFs* was predicted by SignalP 4.1 (http://www.cbs.dtu.dk/services/SignalP/). The subcellular localization of wheat PDFs was predicted by WoLF PSORT

(https://wolfpsort.hgc.jp/) and Plant - mPLoc (http://www.csbio.sjtu.edu.cn/bioinf/plant-multi/).

Phylogeny, chromosome localization, conserved motif, gene structure, and *cis*-acting elements analysis

Comparison of all protein sequences from wheat, rice, maize and Arabidopsis using ClustalW2 (Thompson et al., 1994). Methods Phylogenetic trees were constructed with MEGA 7.0 and calculated according to the maximum likelihood (ML) method (Kumar et al., 2016). Drawing and landscaping the phylogenetic tree was accomplished through the Interactive Tree of Life website (IToL, version 3.2.317, http://itol.embl.de). *TaPDF* gene annotation file containing information on the chromosome position were extracted from the genome annotation information GFF3 file. Afterwards the physical map was then plotted using MapInspect software (Hu and Liu, 2011). *TaPDF* genome annotation information was used to map the gene (exon-intron) structure using GSDS2.0 (http://gsds.cbi.pku.edu.cn/index.php) (D.-M. Huang et al., 2022). The conserved motifs of TaPDF proteins were identified by MEME (v4.9.1, http://meme-suite.org/index.html) (Zheng et al., 2017). The conserved motifs are identified by the following criteria: (1) All sequences can include multiple non overlapping motifs; (2) Up to 20 different motifs; (3) The length of the motif is 6-50 aa. The protein sequences were uploaded to SWISS-MODEL website (https://www.swissmodel.expasy.org/) in order to identify protein structure with default parameters (Arnold et al., 2005).

The 1500 bp sequence upstream of the start codon of *TaPDFs* were submitted to the PlantCARE database to predict the *cis*-acting elements (Lescot et al., 2002). The enrichment analysis of *cis*-acting elements was performed using the pattern enrichment analysis (AME) function in the MEME program to identify the regulatory elements (İlhan et al., 2018).

Homology analysis

Genomic data for *T. dicoccoides* (v1.0.43), *Ae tauschii* (v4.0.43), and *T. urartu* (v1.43) was obtained from the EnsemblPlants database (http://plants.ensembl.org/index.html) (Alaux et al., 2018). The *PDF* homologous of urartu wheat (*T. urartu*), wild dicoccoides (*T. dicoccoides*), and rough goat grass (*Ae. tauschii*) were identified by BLASTp (threshold E<10^{-10}, match >80%). The protein which contains the structural domain of PF00304 (Gamma-thionin) was identified as *PDF* gene family member. The sequences of the identified *PDFs* were determined by whether the fragments were duplicated or tandem duplicated on the same chromosome, and homology mapping was performed using the R package "circlize".

Transcriptome analysis of *TaPDFs* gene and qRT-PCR analysis

In order to further study the expression patterns of *TaPDF* genes under different stresses, original RNA-seq data under various conditions was downloaded from the SRA database from NCBI (Appendix S1), and was mapped to the wheat reference genome using hisat2. The gene expression level was calculated by Cufflinks, which was normalized through the fragment by the exon base number per kilogram (FPKM) model per million bases (Trapnell et al., 2012). Finally, pheatmap package was used to generate the heatmap of *TaPDF* genes.

RNA was extracted from wheat leaves using TRIzol™ Reagent (Invitrogen). The cDNA obtained by reverse transcription was used as a template to amplify the target genes. The six highly expressed *TaPDF* genes *TaPDF4.9*, *TaPDF5.4*, *TaPDF2.12*, *TaPDF2.15*, *TaPDF2.23*, and *TaPDF2.20*, which were highly expressed in the transcriptome analysis, were selected for qRT-PCR analysis during *Fusarium graminearum* infestation. The wheat varieties used in this experiment were Yangmai 158 and Xinong 98710. The primers used in this study were listed in Appendix S2. The screened genes were analyzed by qRT-PCR on a CFX 96 Real-Time PCR System (Bio-Rad). (Mamidala et al., 2011). The fluorescence quantification reaction system consisted of 10 μL of 2× SYBR Green (Vazyme), 0.4 μL of each of the upstream and downstream primers, 2 μL of 50 ng/μL cDNA, and the addition of 7.2 μL of ddH_2O, for a total volume of 20 μL. The reaction conditions were 95°C for 3 min, 95°C for 5 s, primer annealing/extension, and 58°C for 30 s. A total of 45 cycles were started from step 2. Each gene requires the use of three technical repeats. The final resultant data were used to determine relative expression levels using the 2-ΔΔCt method (Livak and Schmittgen, 2001). Use of the ADP-ribosylation factor Ta2291, stably expressed under various conditions, as an internal reference gene for qRT-PCR analysis (Huang et al., 2021).

Inoculation of pathogenic phytophthora and subcellular localization

The target gene were ligated into the pART27 and pART27 vector with YFP using a homologous recombination kit (Vazyme). The connected *TaPDF2.15* and *TaPDF4.9* were selected for transient expression in *Nicotiana benthamiana* leaves. After two to three days, the leaves were cut off, and inoculated with *Phytophthora infestans* strain '88069', then they were placed in a humidor infecting box, stored with thetemperature at 20 °C. After four to six days, measure the lesion diameter of the inoculated leaves were measured (measure the longest and shortest). GFP signals from *TaPDF4.9*, *TaPDF5.4*, *TaPDF2.12*, and *TaPDF2.15* trans-overexpressed leaves were observed two days after injection using laser scanning confocal microscope (Leica TCS SP8).

Result

Screening and identification of *PDF* genes in wheat, maize, and rice genomes

The sequences containing the conserved domain of PF00304 (Gamma-thionin) were retained using Pfam online tool. Finally, 73 wheat *PDF* members, 15 members of maize, and 11 members of rice were identified (Table 1). The *PDF* genes of the four species were divided into five groups according to the rootless phylogenetic trees (Figure 1). The genes are named according to the location of the components, e.g. the first gene located in Group I is named as *TaPDF1.1*. Most of these *TaPDFs* are concentrated in Group II, IV and V. Group III is only *ZmPDF*.

As shown in Table 1, the average length of *TaPDF* is 80.57 aa. The average molecular weight of TaPDFs is 8.8 KD, and the average

TABLE 1 Protein characteristics of wheat PDF family.

Name	Accession numbers	Length/ aa	Molecular mass/kDa	Isoelectric point	Instability index	Aliphatic index	GRAVY	Predicted location(s)
TaPDF1.1	TraesCS6A02G157100.1	86	9.55	5.55	64.93	70.35	-0.134	Vacuole
TaPDF1.2	TraesCS6B02G184900.1	86	9.49	5.55	61.52	73.72	-0.117	Vacuole
TaPDF1.3	TraesCS6D02G146400.1	86	9.55	5.48	56.35	69.19	-0.205	Vacuole
TaPDF1.4	TraesCS6A02G126100.1	78	8.71	8.09	45.8	97.44	0.41	Nucleus
TaPDF2.1	TraesCS5B02G329100.1	77	8.4	9.41	55.84	78.57	-0.044	Vacuole
TaPDF2.2	TraesCS5A02G329000.1	77	8.28	9.08	33.58	83.64	0.058	Vacuole
TaPDF2.3	TraesCS5D02G334900.1	77	8.38	9.24	39.41	92.47	0.053	Vacuole
TaPDF2.4	TraesCS3D02G444200.1	128	14.33	8.7	64.43	63.91	-0.58	Nucleus. Vacuole.
TaPDF2.5	TraesCS3B02G488800.1	111	12.2	8.86	60.16	49.28	-0.45	Vacuole
TaPDF2.6	TraesCS5A02G329100.1	81	8.73	8.95	37.95	68.64	0.001	Nucleus
TaPDF2.7	TraesCS5B02G329200.1	80	8.77	8.8	42.58	64.62	-0.054	Nucleus. Vacuole.
TaPDF2.8	TraesCS5D02G335000.1	80	8.62	8.62	35.79	72	0.089	Nucleus
TaPDF3.1	TraesCS2B02G062000.1	75	7.85	5.72	70.96	79.33	0.299	Vacuole
TaPDF3.2	TraesCS2D02G048200.1	75	8.03	5.75	69.96	79.33	0.249	Vacuole
TaPDF3.3	TraesCS2D02G047900.1	75	8.04	5.75	69.83	78	0.22	Vacuole
TaPDF3.4	TraesCS2A02G049000.1	75	7.95	5.28	72.4	78	0.269	Vacuole
TaPDF3.5	TraesCS2A02G048900.1	78	8.39	8.48	47.07	85	0.385	Vacuole
TaPDF3.6	TraesCS2D02G047800.1	78	8.37	8.48	45.41	86.28	0.39	Vacuole
TaPDF3.7	TraesCS2B02G062100.1	78	8.36	8.48	42.82	85	0.373	Vacuole
TaPDF3.8	TraesCS5A02G525600.1	71	7.8	5.59	43.78	68.73	0.351	Nucleus. Vacuole.
TaPDF3.9	TraesCS4D02G349900.1	76	8.17	7.52	45.98	83.42	0.521	Vacuole
TaPDF3.10	TraesCS4B02G356200.1	76	8.09	8.17	46.61	88.55	0.621	Vacuole
TaPDF3.11	TraesCS3B02G476300.1	74	8.12	8.13	33.15	78.95	0.193	Vacuole
TaPDF3.12	TraesCS3A02G442500.1	74	8.13	8.46	38.15	84.19	0.264	Vacuole
TaPDF3.13	TraesCS1D02G388400.1	120	13.07	6.69	44.68	85.92	0.175	Vacuole
TaPDF3.14	TraesCS3D02G435100.1	76	8.44	8.14	21.79	84.47	0.212	Vacuole
TaPDF3.15	TraesCS3A02G442400.1	76	8.42	8.14	20.38	84.47	0.242	Vacuole
TaPDF3.16	TraesCS3B02G476200.1	72	8	8.47	22.45	84.36	0.215	Vacuole
TaPDF3.17	TraesCS3A02G442700.1	69	7.36	6.68	26.89	83.33	0.359	Vacuole

(Continued)

10.3389/fpls.2023.1279502

TABLE 1 Continued

Name	Accession numbers	Length/ aa	Molecular mass/kDa	Isoelectric point	Instability index	Aliphatic index	GRAVY	Predicted location(s)
TaPDF3.18	TraesCS3D02G435300.1	75	8.02	6.37	29.13	81.87	0.167	Vacuole
TaPDF3.19	TraesCS7A02G183500.1	70	7.56	8.72	42.16	84.86	0.467	Vacuole
TaPDF3.20	TraesCS7D02G185100.1	70	7.71	7.54	40.13	75	0.283	Vacuole
TaPDF3.21	TraesCS7B02G088300.1	76	8.26	8.72	44.81	81.97	0.295	Vacuole
TaPDF3.22	TraesCS7D02G185000.1	76	8.26	8.72	44.81	81.97	0.295	Vacuole
TaPDF3.23	TraesCS7A02G183400.1	76	8.31	8.72	45.93	79.34	0.301	Vacuole
TaPDF3.24	TraesCS7A02G183600.1	75	8.28	8.71	40.03	79.07	0.309	Vacuole
TaPDF3.25	TraesCS7D02G185200.1	75	8.19	8.49	36.71	76.53	0.337	Vacuole
TaPDF3.26	TraesCS7B02G088400.1	71	7.81	8.16	43.73	80.85	0.37	Vacuole
TaPDF4.1	TraesCS4D02G321100.1	81	8.59	9.33	37.46	79.63	0.127	Vacuole
TaPDF4.2	TraesCS5A02G496500.1	78	8.35	9.37	45.59	87.41	0.132	Vacuole
TaPDF4.3	TraesCS4D02G321000.1	82	9.09	9.68	62.49	70.2	-0.157	Vacuole
TaPDF4.4	TraesCS4B02G324000.1	82	9.08	9.6	63.91	70.24	-0.16	Vacuole
TaPDF4.5	TraesCS5A02G496600.1	82	8.95	9.69	26.52	67.93	-0.133	Vacuole
TaPDF4.6	TraesCS4B02G324100.1	82	8.91	9.49	26.87	66.71	-0.144	Vacuole
TaPDF4.7	TraesCS4D02G321200.1	82	8.93	9.69	27.84	66.71	-0.151	Vacuole
TaPDF4.8	TraesCS2B02G396100.1	85	9.86	8.91	33.9	55.06	-0.455	Vacuole
TaPDF4.9	TraesCS1A02G013600.1	82	8.97	8.9	46.25	73.9	-0.017	Nucleus. Vacuole.
TaPDF4.10	TraesCS1D02G012600.1	82	8.91	8.72	47.81	73.78	-0.072	Vacuole
TaPDF4.11	TraesCS1A02G014800.1	82	8.95	9.92	72.68	72.68	-0.084	Vacuole
TaPDF4.12	TraesCS1B02G017700.1	77	8.38	8.72	40.66	76.1	0.035	Vacuole
TaPDF4.13	TraesCS1D02G012100.1	76	8.42	7.56	31.42	64.21	-0.213	Vacuole
TaPDF4.14	TraesCS1B02G018100.1	81	8.98	8.5	58.07	59.26	-0.265	Vacuole
TaPDF4.15	TraesCS7B02G244000.1	83	9.17	8.16	37.04	60.12	-0.212	Vacuole
TaPDF4.16	TraesCS1D02G012000.1	82	9.06	8.7	43.39	28.41	-0.198	Vacuole
TaPDF4.17	TraesCS1A02G014100.1	74	8.42	6.79	23.04	27.7	-0.677	Vacuole
TaPDF4.18	TraesCS1A02G014000.1	82	9.1	7.6	44.51	64.27	-0.204	Vacuole
TaPDF4.19	TraesCS1D02G011900.1	86	9.41	8.17	45.61	66.05	-0.221	Vacuole
TaPDF4.20	TraesCS1B02G018000.2	79	8.69	7.57	49.64	54.43	-0.201	Vacuole
TaPDF4.21	TraesCS1B02G018000.1	82	9.14	8.48	59.81	53.66	-0.265	Vacuole
TaPDF4.22	TraesCS6B02G103000.1	82	8.89	9.08	58.38	70.37	0.113	Vacuole
TaPDF4.23	TraesCS6B02G102900.1	82	8.82	9.22	40.65	81.1	0.155	Vacuole
TaPDF4.24	TraesCSU02G027100.1	82	8.83	9.22	39.15	82.2	0.189	Vacuole
TaPDF4.25	TraesCSU02G026600.1	82	8.83	9.22	39.15	82.2	0.189	Vacuole
TaPDF4.26	TraesCS6A02G076800.1	82	8.76	9.22	43	79.88	0.195	Vacuole
TaPDF4.27	TraesCS1A02G050700.1	82	8.82	8.5	66.51	72.68	0.054	Vacuole

(Continued)

TABLE 1 Continued

Name	Accession numbers	Length/ aa	Molecular mass/kDa	Isoelectric point	Instability index	Aliphatic index	GRAVY	Predicted location(s)
TaPDF4.28	TraesCS1D02G053000.1	82	8.94	9.1	64.46	63.29	-0.14	Vacuole
TaPDF4.29	TraesCS1B02G067300.1	82	8.86	9.1	70.47	71.59	-0.015	Vacuole
TaPDF4.30	TraesCS1A02G050900.1	82	8.87	8.92	63.07	77.56	0.148	Vacuole
TaPDF4.31	TraesCS1A02G050800.1	82	8.98	9.08	54.27	66.83	-0.079	Vacuole
TaPDF4.32	TraesCS1D02G052900.1	81	8.89	8.72	63.95	65.19	-0.07	Vacuole
TaPDF4.33	TraesCS1B02G067100.1	84	9.29	8.43	63.35	70.95	-0.01	Vacuole
TaPDF4.34	TraesCS1B02G067000.1	82	8.92	8.49	59.01	79.88	0.143	Vacuole
TaPDF4.35	TraesCS1A02G050600.1	82	9.02	9.08	58.82	73.9	-0.01	Vacuole
TaPDF4.36	TraesCS1D02G052800.1	82	8.97	8.9	49.74	72.68	-0.024	Vacuole

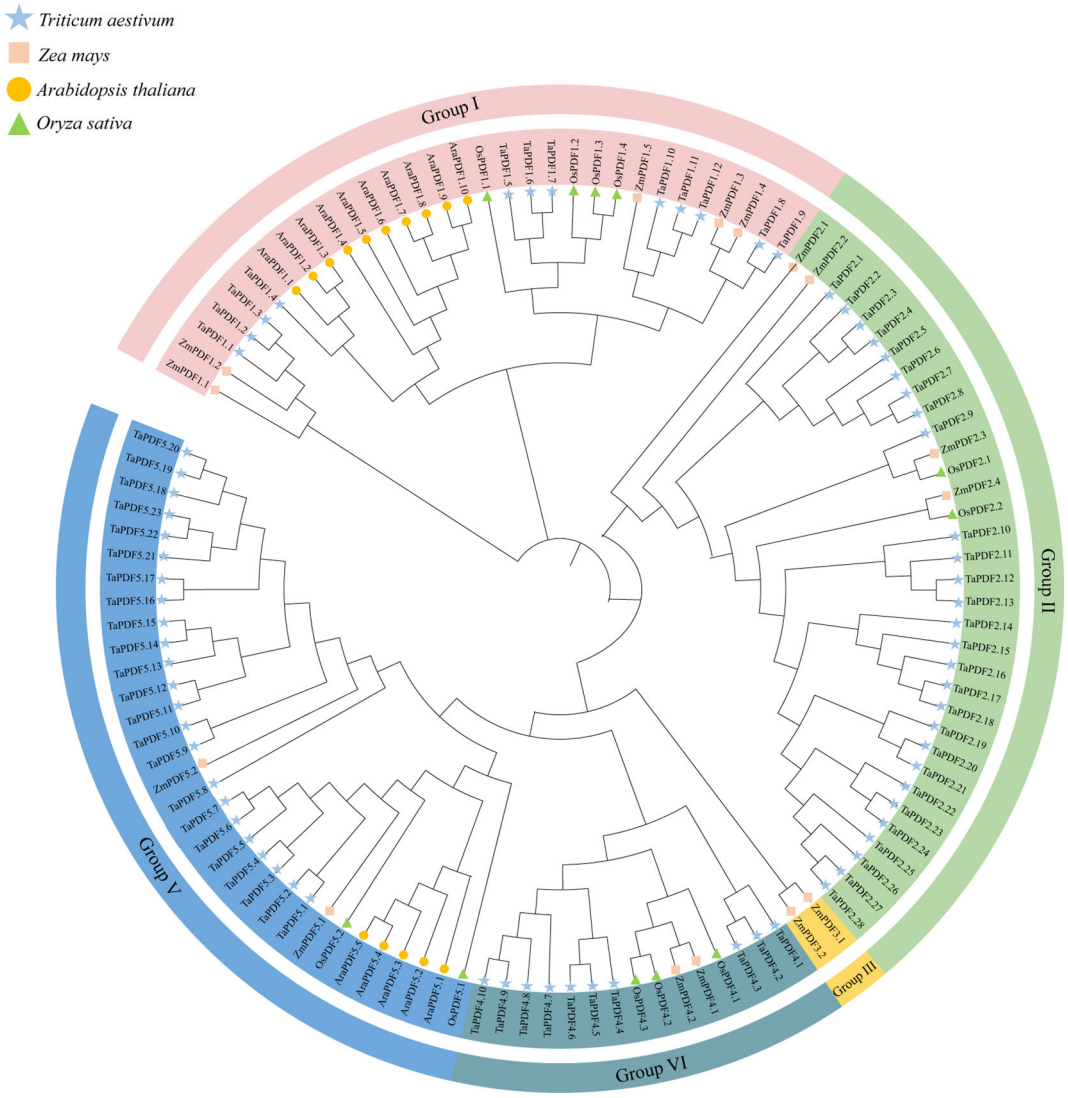

FIGURE 1
Phylogenetic tree of the PDF family of Triticum aestivum, Zea mays, Oryza sativa, and Arabidopsis thaliana.

isoelectric point is 8.27, which indicates that TaPDFs are alkaline proteins. The average instability index is 47.12, which reveals the TaPDFs are unstable proteins. The average value of the aliphatic index is 73.67. The average value of hydrophilicity is 0.06. Multi website prediction of subcellular localization results shows that most TaPDF proteins are located in vacuoles, with a small portion located in the nucleus.

Chromosomal mapping and gene duplication analysis of *TaPDF* genes

According to the chromosome distribution map (Figure 2), *PDF* genes were found to be widely distributed on each chromosome, with each chromosome containing multiple genes. As shown in Figure 2, wheat PDF contains multiple genes on its chromosomes during evolution. And each chromosome has duplicate genes. This shows that segmental duplication is the main reason for the expansion of the PDF family during the evolution of wheat.

Conserved motif and gene structure analysis of *TaPDF* gene family

Based on the *TaPDF* genomic information, the gene structure was mapped using GSDS2.0 (Figure 3). The vast majority of *TaPDF* genes contain non-coding regions at the 5' and 3' ends, and only a few *TaPDFs* do not contain non-coding regions. Most *TaPDF* genes contain two extrons.

TaPDFs all contain motifs 1, 2, 14 and 18. The sequence, position and identification of the conserved motifs in the TaPDF protein are shown in Figure 3. All identified wheat genes contain conserved structural domains of the PDF family. The wheat *PDF* gene family contains characterized amino acids, including a series of highly conserved active site residues consistent with previous studies on different plant species.

Identification of *PDF* members in common wheat, urartu wheat, wild emmer wheat, and coarse goat grass

A phylogenetic tree was constructed using MEGA 7.0 maximum likelihood (ML) method (Figure 4A). PDF proteins can be divided into five groups, of which groups I and V contain more PDF protein members. By gene duplication events, 2940 duplicate pairs were obtained. The common wheat positional information was put into the R package for circles plot analysis (Figure 4B). The results suggest that *PDFs* from each genomic donor may be ancestrally similar to each other. Alternatively, initially different *PDFs* may be stabilized after a long domestication process and lead to alterations in protein structure and function. Homology analysis of *TaPDF* suggests that wheat may be repeated multiple times in polyploidy, and we hypothesize that this may have made wheat more adapted to its environment and increased the number of wheat *PDF* genes during evolution.

Cis-acting elements of *TaPDFs* gene

A total of 60 *cis*-acting elements were screened by intercepting a 1500 bp region upstream of the *TaPDF* gene. These components are divided into three categories: phytohormones, biotic stress-abiotic

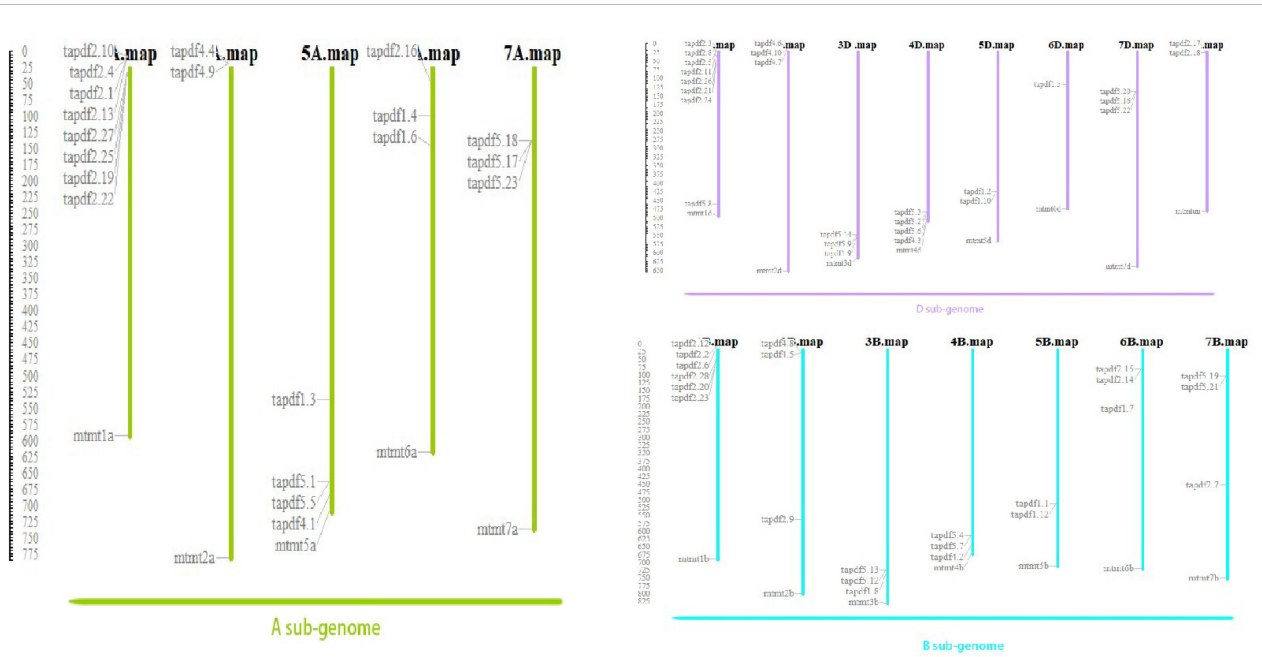

FIGURE 2
Chromosomal location of wheat *PDF* family.

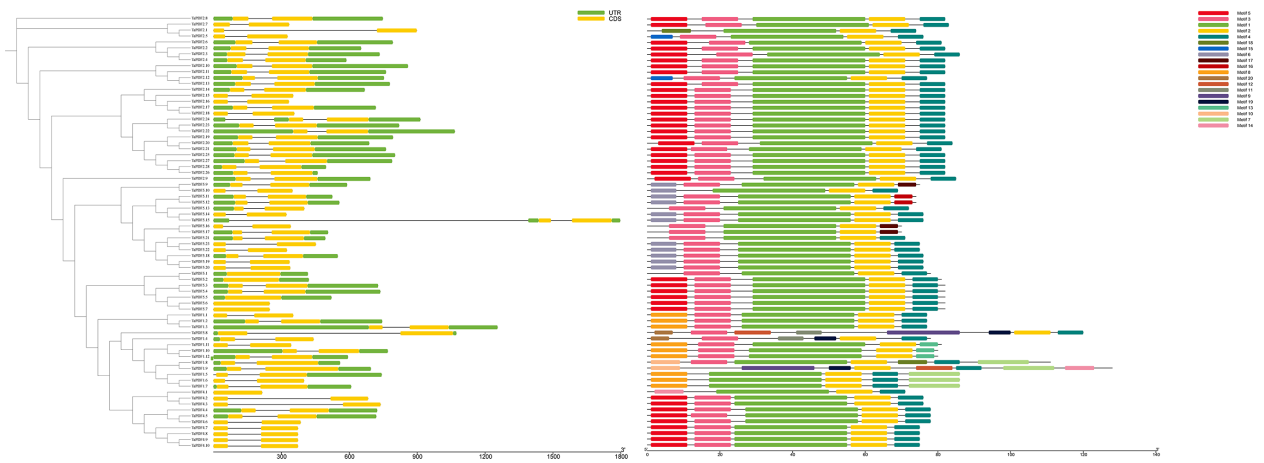

FIGURE 3
The evolutionary tree, motif analysis and gene structure analysis of 74 wheat *PDF* families.

stress, and growth and development (Figure 5). The results indicate that the promoter sequence of *TaPDF* gene has multiple cis-regulatory elements, including *cis*-acting elements involved in defense and stress response, light-responsive elements, low-temperature-inducible elements, anaerobic-inducible elements, and drought-inducible elements biotic-abiotic taxa. The most abundant original in *TaPDF* is CAAT-box as promoter-associated original. The most widely distributed *cis*-element is the abscisic acid-responsive *cis*-acting element ABRE. The two core promoter elements of the same growth and development-related element are TATA-box and CAAT-box. CGTCA motifs and TGACG motifs are the major motifs of jasmonate methyl ester response elements. The most common *cis*-element among all genes was the jasmonate methyl ester response element. And the light-responsive elements (g-boxes) are also more widely distributed. The next most common *cis*-elements are the methyl jasmonate response elements (CGTCA motif and TGACG motif), which are distributed in almost all genes. It suggests that *PDF* is associated with plant growth and development in wheat, and may also be associated with plant disease resistance.

Multi-conditional transcriptome of *TaPDF* genes

The transcriptome data downloaded and collated from the NCBI website were divided into three categories, including

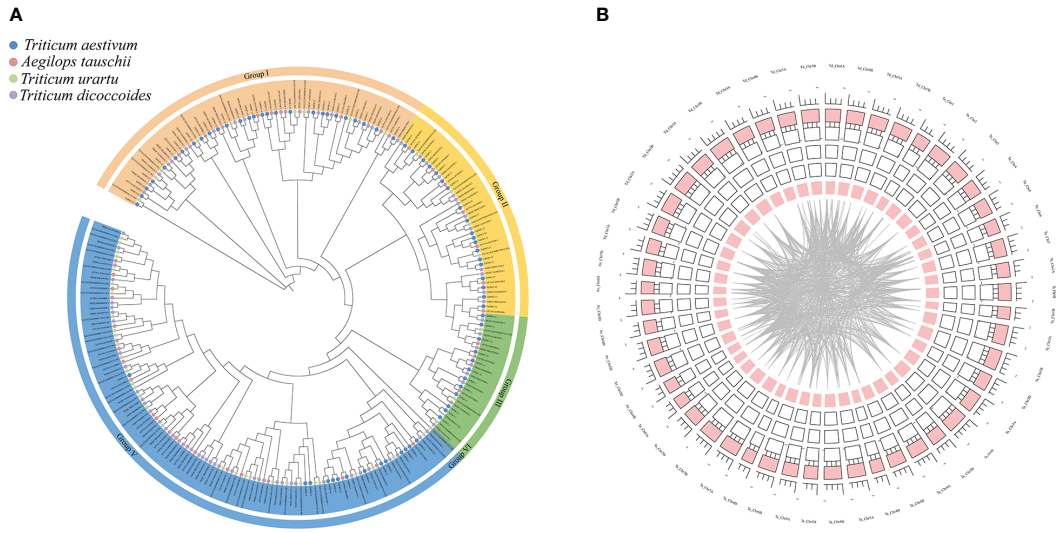

FIGURE 4
Phylogenetic tree and joint analysis circle diagram of the PDF family in T. aestivum, T. urartu, T. dicoccoides and Ae. tauschii. **(A)** is the T. aestivum, T. urartu, T. dicoccoides and Ae. tauschii evolutionary tree. **(B)** is the wheat homology analysis.

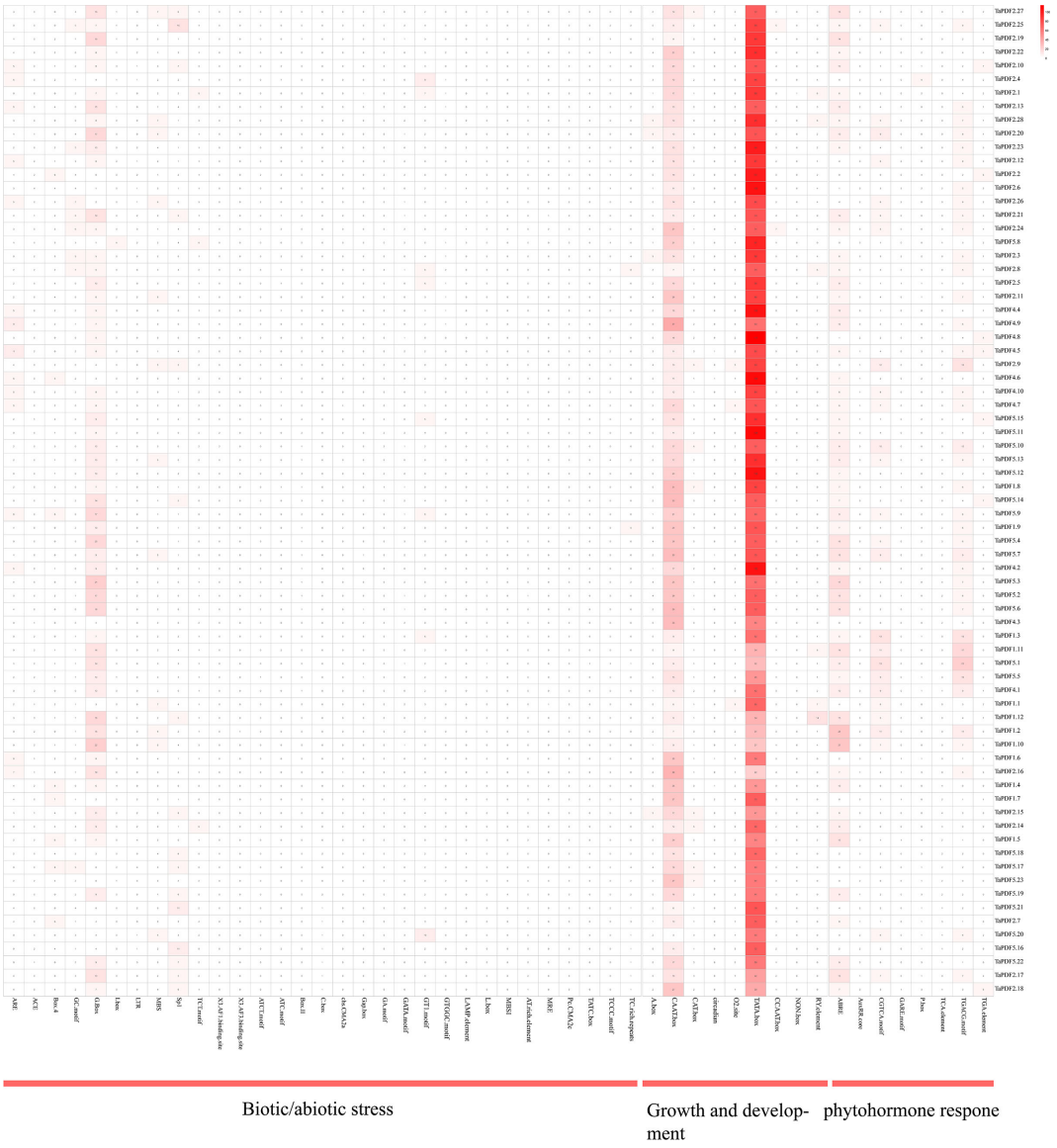

FIGURE 5
Cis-acting elements in wheat *PDF* gene promoter.

growth and development, abiotic stresses, and biotic stresses. As shown in the heat map in Figure 6, the overall expression of wheat *PDF* genes was low in the early stages of growth and development. *TaPDF5.4* was highly expressed at the apical meristem tiller stage, apical meristem trilobal stage, radicle seedling stage, root seedling stage, root tiller stage, root leaf stage, root trilobal stage and shoot apex meristem seedling stage. Therefore, the function of *TaPDF5.4* may be inseparably related to root growth and development. The overall expression of wheat *PDF* genes was also lower during abiotic stress. However, during the biotic stress treatment, *TaPDF4.9*, *TaPDF5.4*, *TaPDF2.12*, *TaPDF2.15*, *TaPDF2.23*, and *TaPDF2.20* were more highly expressed in spikelets inoculated by *Fusarium graminearum* at 3, 6, 12, and 24 h. The results suggest that the *TaPDF* genes may be associated with plant disease resistance, which was consistent with the prediction of *PDF* genes function.

Expression analyses of *TaPDF* genes

To further understand the role of *TaPDF* genes in reaction to biotic stresses, six highly expressed genes (*TaPDF2.12*, *TaPDF2.15*, *TaPDF2.20*, *TaPDF2.23*, *TaPDF4.9*, and *TaPDF5.4*) in the transcriptome (Figure 6) were selected. Expression of PDF genes in Yangmai 158 (disease-resistant) and Xinong 98710 (disease-susceptible) after inoculation with *F. graminearum* was analyzed by qRT-PCR (Figure 7). The overall expression level of *TaPDF* genes were up-regulated after inoculation of *F. graminearum* on the coleoptiles of two wheat species. However, *TaPDF4.9* gene expression level was down-regulated in Xinong 98710 and *TaPDF2.21* gene expression level was in a down-regulated state in Yangmai 158. According to the quantitative results, *PDF* gene may play different roles in wheat at 24h and 48h of *F. graminearum* infestation.

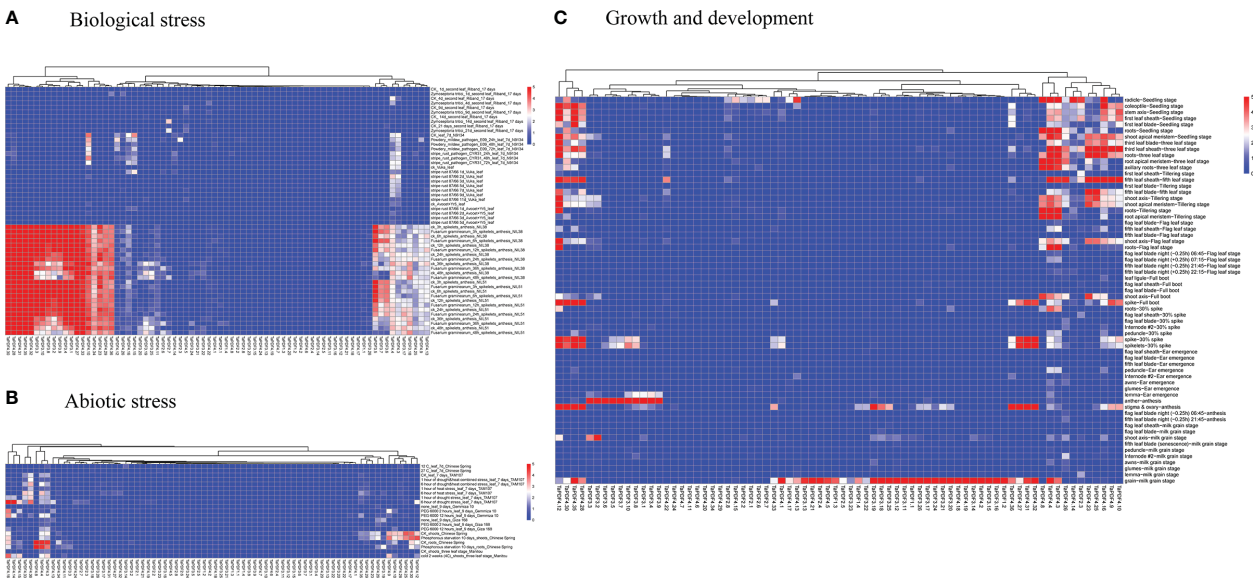

FIGURE 6
Heat map of growth and development of wheat *PDF* gene family. **A**, **B** and **C** represents transcriptomic data of TaPDFs in terms of biotic stress, abiotic stress and growth and development.

Subcellular localization of *TaPDF* genes

Most *PDF* genes were predicted to be located in vesicles, whereas only four genes were predicted to be on vesicles and nucleus. *TaPDF4.9*, *TaPDF5.4*, *TaPDF2.12*, and *TaPDF2.15* genes were selected as target genes for homologous recombination with the digested vector pART27. The results of Figure 8 showed that the four target genes were basically localized to the cytoplasm and cell membrane, and *TaPDF4.9* was also localized in the nucleus.

Agrobacterium-mediated transient overexpression and inoculation of *Phytophthora infestans*

After four to six days of inoculation with *Phytophthora infestans*, the lesion diameter was measured (Figures 9A, C). As shown in Figures 9B, D, the lesion area on the leaves, where *TaPDF2.15* and *TaPDF4.9* were transient overexpressed, was smaller (P value < 0.01) than the control. This result suggests that

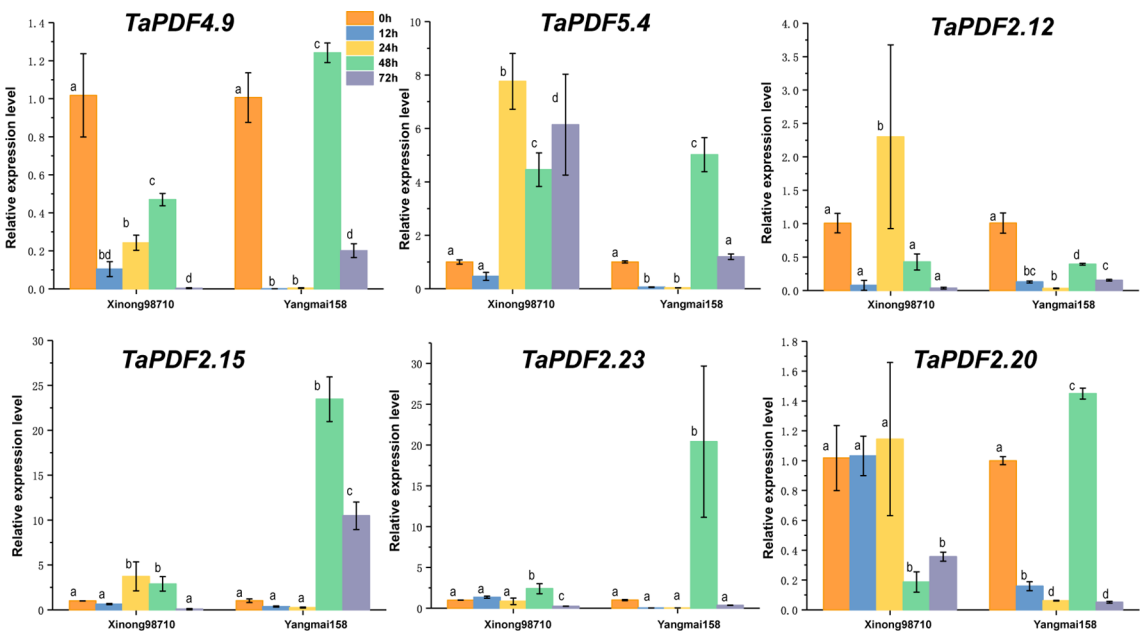

FIGURE 7
Expression patterns of six wheat (Triticum aestivum) *TaPDF* genes under *F. graminearum* treatments.

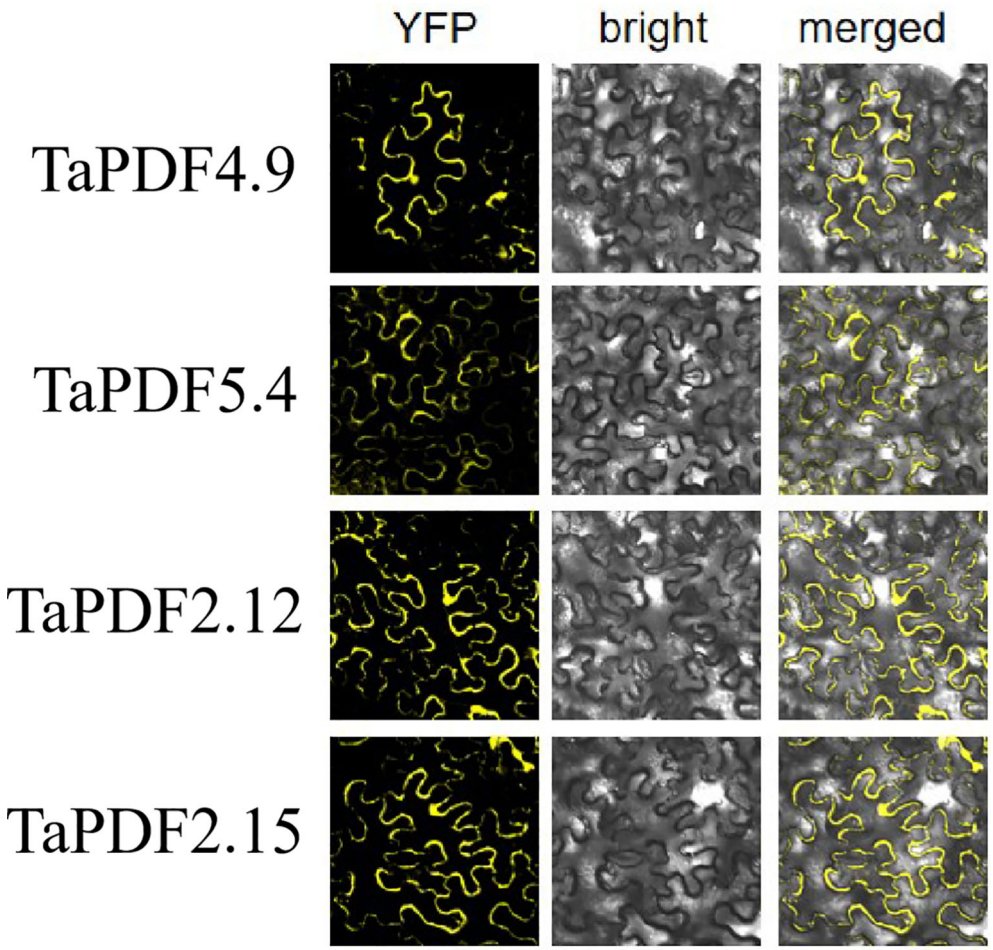

FIGURE 8
Subcellular localization of TaPDF4.9, TaPDF5.4, TaPDF2.12 and TaPDF2.15.

TaPDF may play positive roles in resistance to *Phytophthora infestans* strain '88069'.

Discussion

Plant defensins are widely distributed in the leaves, fruits, roots, stems, seeds, and tubers. Based on the genome-wide characterization of *PDFs* already performed in the literature in Arabidopsis thaliana (Mäser et al., 2001). However, there is a lack of systematic studies on the *PDF* family in wheat. In order to gain a deeper understanding of the functioning of wheat *PDFs*, this paper examines them. For the identification of family members, BLASTp searches were performed using known Arabidopsis PDF protein sequences (Kushmerick et al., 1998) and conserved structural domain sequences as query sequences (Clavijo et al., 2017). Sequences were queried in the wheat genome (IWGSC v1.1) and candidate hits were further checked by Pfam and InterProScan to exclude sequences without the Gamma - thiionin structural domain. Seventy-three wheat PDF proteins were finally identified. This study also identified *PDF* genes in rice and maize, which contained 15 maize *PDF* genes and 11 rice *PDF*s. The number of *PDF* genes varies in different plants. Differences in the number of genes from other species indicate functional redundancy in *TaPDFs*. However, genes do not correspond to changes in genome size.

Higher numbers of *PDFs* were identified in wheat than in Arabidopsis, maize and rice. The results illustrate the complexity of genetic traits in wheat. Homology analyses of *TaPDF* indicate that wheat may repeat multiple times in polyploidy, which we hypothesize may have made wheat more environmentally adapted and increased the number of wheat *PDF* genes during evolution. Based on gene structure and protein physicochemical property analyses, the wheat *PDF* gene has a highly conserved gene structure containing eight conserved cysteine residues forming four pairs of disulfide bonds (Cys4-Cys7, Cys3-Cys6, Cys2-Cys5, and Cys1-Cys8) (Thomma et al., 2002). The conclusions in the article are the same as those previously reported for the *PDF* family having the same structure. And the molecular weight size just shows that wheat *PDF* belongs to the shorter peptides with smaller molecular weight. The abscisic acid-responsive cis-acting element ABRE, the core promoter elements TATA box and CAAT box in the promoter of the wheat *PDF* gene are all growth and development-related elements. This suggests that *TaPDF* is

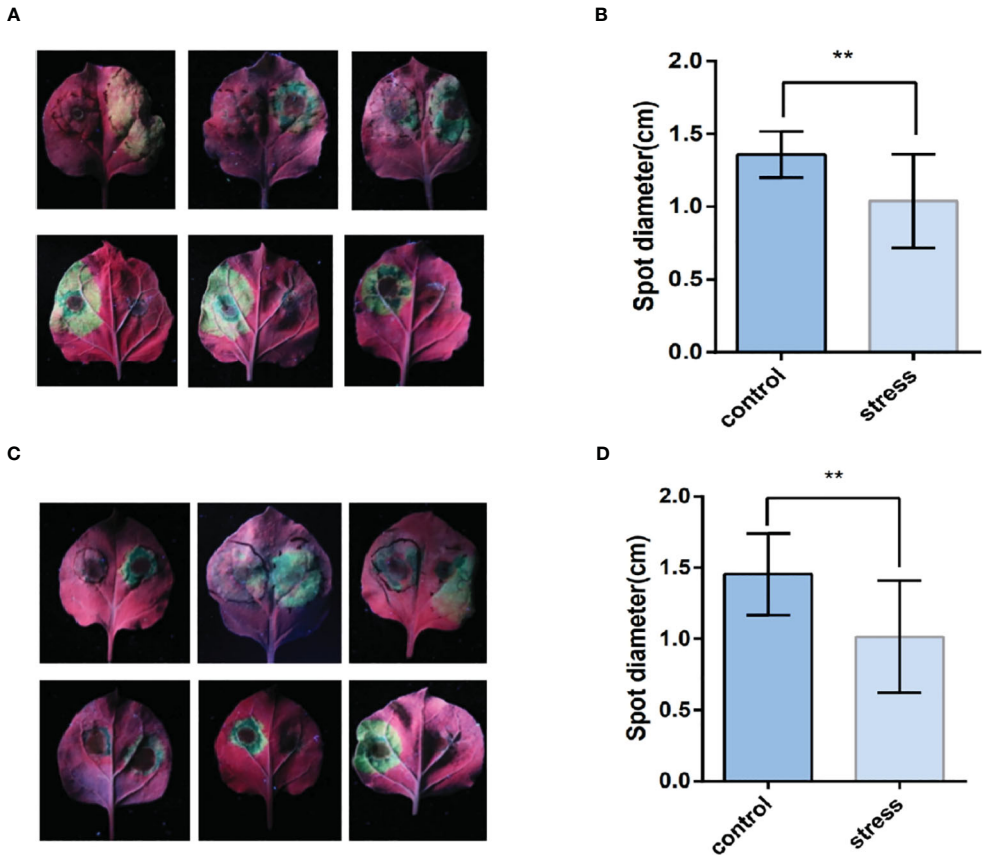

FIGURE 9
The leaf surface mediated by *TaPDF4.9* (AB) and *TaPDF2.15* (CD) inoculation with Phytophthora infestans. **(A)** is TaPDF4.9 infestation on tobacco, **(B)** is TaPDF4.9 infestation length. **(C)** is TaPDF2.15 infestation on tobacco and **(D)** is TaPDF2.15 infestation length. ** represents highly significant differences.

associated with plant growth and development. Whereas methyl jasmonate response elements are distributed in almost all genes, we can infer that *TaPDF* is associated with plant disease resistance. It has been shown that plant defensins are commonly considered to display antimicrobial activity against only fungi (Sathoff et al., 2019). To further reveal the function of *TaPDF*, six genes *TaPDF2.12*, *TaPDF2.15*, *TaPDF2.20*, *TaPDF2.23*, *TaPDF4.9* and *TaPDF5.4* were analyzed by qRT-PCR. The expression levels of *TaPDFs* were differentially up-regulated by *Fusarium graminearum*. The above results indicate that *TaPDFs* are not only involved in wheat growth and development, but also play a positive regulatory role in the stress response process. The effect of *TaPDF* on disease resistance was analyzed through the resistance of different wheat varieties to *F. graminearu*. The results showed that *TaPDF* has an effect on plant disease resistance. Relevant studies have shown that PsDef1 is significantly increased in Scots pine seedlings during germination and in their response to pathogenic infection with Heterobasidion annosum (Kovaleva et al., 2011).

And after inoculation with Phytophthora infestans, it can be seen that the plaque becomes smaller, indicating that both selected *TaPDF2.15* and *TaPDF4.9* can inhibit Phytophthora infestans. It shows that AhPDF1s and AtPDF1s were able to confer Zn tolerance and AhPDF1s also displayed antifungal activity (Shahzad et al., 2013). It can be seen that the *TaPDF* should be functionally similar to that in Arabidopsis thaliana, both of which have the function of inhibiting the infestation of pathogenic bacteria. Although the mechanism of amplification of such gene families is well understood in this paper, the genes are not well understood in different species, which will have to be studied in further depth. The gene family aspect could be further systematically analyzed for defensin gene families by combining more species. The results of subcellular localization showed that the selected genes were basically localized to cytoplasm and cell membrane, but the multisite predictions of the proteins were all on the vesicles and a few on the nucleus. The results indicate that by Agrobacterium alone mediated *Nicotiana benthamiana* leaves could not be accurately localized to the organelles, but also require organelle-corresponding stains, which need to be investigated in subsequent work.

Conclusions

In this study, we identified 73 wheat *PDF* family members using bioinformatics methods, 15 members of corn *PDF* genes and 11 members of rice *PDF* genes. With the hexaploid wheat as the main

research object and the amino acid sequence of *PDF* identified in Arabidopsis (Kushmerick et al., 1998), maize, and rice as reference, 35, 65, and 34 *PDF* gene family members were identified in the genomes of *T. dicoccoides*, *Ae. tauschii*, and *T. urartu*, respectively. As can be seen from the basic physicochemical properties, most of the TaPDFs are basic proteins and most are unstable. The genes are relatively evenly distributed across almost every chromosome. The high number of gene duplicate pairs indicates possible redundancy of function. The subcellular localization results of *TaPDF4.9*, *TaPDF5.4*, *TaPDF2.12*, and *TaPDF2.15* are basically located in the cytoplasm and cell membrane, and *TaPDF* 4.9 is also located on the nucleus. Transient overexpression of *TaPDF4.9* and *TaPDF2.15* could inhibit the infection of Phytophthora infestans strain '88069', which has the function of inhibiting the infection of Phytophthora infestans. According to the expression pattern, *TaPDF* is resistant to *F. graminearum*, and most of the selected genes showed an increase in transcript levels after being infested with *F. graminearum*. In this experiment we performed bioinformatic analysis of the wheat PDF family with subcellular localization, quantitative analysis and pathogenicity analysis. Wheat PDF was found to be effective in suppressing late blight in the Phytophthora infestans. As the genomes of more and more species are sequenced, it is believed that more members of the plant defensin family will be identified. With the development of functional genomics and proteomics, the role of such genes in wheat will become clearer and their mechanism of action will become clearer. Meanwhile, plant defensins have a very vast development prospect as a new antifungal drug, and researchers have also noticed the potential of plant defensins in the development of new anticancer drugs. Therefore, plant defensins, with their broad-spectrum, antimicrobial and high efficiency characteristics, provide new ideas for the research and development of new antifungal and antitumor drugs.

Data availability statement

The datasets presented in this study can be found in online repositories. The names of the repository/repositories and accession number(s) can be found in the article/Supplementary Material.

Author contributions

YD: Writing – original draft, Writing – review & editing. YW: Writing – original draft, Writing – review & editing. MT: Writing – original draft, Writing – review & editing. WC: Data curation, Investigation, Validation, Writing – review & editing. YC: Formal Analysis, Methodology, Writing – original draft. WW: Formal Analysis, Project administration, Writing – original draft.

Funding

The author(s) declare financial support was received for the research, authorship, and/or publication of this article. This research was supported by the Basic and long term scientific and technological work in agriculture (NAES083PP13) and Sichuan Provincial Science and Technology Plan Project (2022YFS0585).

Conflict of interest

The authors declare that the research was conducted in the absence of any commercial or financial relationships that could be construed as a potential conflict of interest.

Publisher's note

All claims expressed in this article are solely those of the authors and do not necessarily represent those of their affiliated organizations, or those of the publisher, the editors and the reviewers. Any product that may be evaluated in this article, or claim that may be made by its manufacturer, is not guaranteed or endorsed by the publisher.

Supplementary material

The Supplementary Material for this article can be found online at: https://www.frontiersin.org/articles/10.3389/fpls.2023.1279502/full#supplementary-material

References

Alaux, M., Rogers, J., Letellier, T., Flores, R., Alfama, F., Pommier, C., et al. (2018). Linking the International Wheat Genome Sequencing Consortium bread wheat reference genome sequence to wheat genetic and phenomic data. *Genome Biol.* 19 (1), 111. doi: 10.1186/s13059-018-1491-4

Arnold, K., Bordoli, L., Kopp, J., and Schwede, T. (2005). The SWISS-MODEL workspace: a web-based environment for protein structure homology modelling. *Bioinformatics* 22 (2), 195–201. doi: 10.1093/bioinformatics/bti770

Clavijo, B. J., Venturini, L., Schudoma, C., Accinelli, G. G., Kaithakottil, G., Wright, J., Clark, M. D., et al. (2017). An improved assembly and annotation of the allohexaploid wheat genome identifies complete families of agronomic genes and provides genomic evidence for chromosomal translocations. *Genome Res.* 27 (5), 885–896. doi: 10.1101/gr.217117.116

De Coninck, B., Cammue, B. P. A., and Thevissen, K. (2013). Modes of antifungal action and in planta functions of plant defensins and defensin-like peptides. *Fungal Biol. Rev.* 26 (4), 109–120. doi: 10.1016/j.fbr.2012.10.002

Falcón-Ruiz, E. A., López-Meza, J. E., and Ochoa-Zarzosa, A. (2023). The plant defensins PaDef and γ-thionin inhibit the endothelial cell response to VEGF. *Peptides* 165, 171008. doi: 10.1016/j.peptides.2023.171008

Finn, R. D., Coggill, P., Eberhardt, R. Y., Eddy, S. R., Mistry, J., Mitchell, A. L., et al. (2016). The Pfam protein families database: towards a more sustainable future. *Nucleic Acids Res.* 44 (D1), D279–D285. doi: 10.1093/nar/gkv1344

Hu, L., and Liu, S. (2011). Genome-wide identification and phylogenetic analysis of the ERF gene family in cucumbers. *Genet. Mol. Biol.* 34 (4), 624–633. doi: 10.1590/s1415-47572011005000054

Huang, D.-M., Chen, Y., Liu, X., Ni, D.-A., Bai, L., and Qin, Q.-P. (2022). Genome-wide identification and expression analysis of the SWEET gene family in daylily (Hemerocallis fulva) and functional analysis of HfSWEET17 in response to cold stress. *BMC Plant Biol.* 22 (1), 211. doi: 10.1186/s12870-022-03609-6

Huang, W., He, Y., Yang, L., Lu, C., Zhu, Y., Sun, C., et al. (2021). Genome-wide analysis of growth-regulating factors (GRFs) in Triticum aestivum. *PeerJ* 9, e10701. doi: 10.7717/peerj.10701

İlhan, E., Büyük, İ., and İnal, B. (2018). Transcriptome - Scale characterization of salt responsive bean TCP transcription factors. *Gene* 642, 64–73. doi: 10.1016/j.gene.2017.11.021

Kamli, M. R., Sabir, J. S. M., Malik, M. A., and Ahmad, A. (2022). Characterization of Defensin-like Protein 1 for Its Anti-Biofilm and Anti-Virulence Properties for the Development of Novel Antifungal Drug against Candida auris</i&gt. *J. fungi (Basel Switzerland)* 8 (12), 1298. doi: 10.3390/jof8121298

Kovaleva, V., Krynytskyy, H., Gout, I., and Gout, R. (2011). Recombinant expression, affinity purification and functional characterization of Scots pine defensin 1. *Appl. Microbiol. Biotechnol.* 89 (4), 1093–1101. doi: 10.1007/s00253-010-2935-2

Kumar, S., Stecher, G., and Tamura, K. (2016). MEGA7: molecular evolutionary genetics analysis version 7.0 for bigger datasets. *Mol. Biol. Evol.* 33 (7), 1870–1874. doi: 10.1093/molbev/msw054

Kushmerick, C., de Souza Castro, M., Santos Cruz, J., Bloch, C., and Beirão, P. S. L. (1998). Functional and structural features of γ-zeathionins, a new class of sodium channel blockers. *FEBS Lett.* 440(3), 302–306. doi: 10.1016/S0014-5793(98)01480-X

Lescot, M., Déhais, P., Thijs, G., Marchal, K., Moreau, Y., Van de Peer, Y., et al. (2002). PlantCARE, a database of plant cis-acting regulatory elements and a portal to tools for in silico analysis of promoter sequences. *Nucleic Acids Res.* 30 (1), 325–327. doi: 10.1093/nar/30.1.325

Li, R., An, J.-p., You, C.-x., Shu, J., Wang, X.-f., and Hao, Y.-j. (2018). Identification and expression of the CEP gene family in apple (Malus×domestica). *J. Integr. Agric.* 17 (2), 348–358. doi: 10.1016/s2095-3119(17)61653-8

Lima, A. M., Azevedo, M. I. G., Sousa, L. M., Oliveira, N. S., Andrade, C. R., Freitas, C. D. T., et al. (2022). Plant antimicrobial peptides: An overview about classification, toxicity and clinical applications. *Int. J. Biol. Macromol* 214, 10–21. doi: 10.1016/j.ijbiomac.2022.06.043

Livak, K. J., and Schmittgen, T. D. (2001). Analysis of relative gene expression data using real-time quantitative PCR and the 2(-Delta Delta C(T)) Method. *Methods* 25 (4), 402–408. doi: 10.1006/meth.2001.1262

Mäser, P., Thomine, S., Schroeder, J. I., Ward, J. M., Hirschi, K., Sze, H., et al. (2001). Phylogenetic relationships within cation transporter families of arabidopsis. *Plant Physiol.* 126 (4), 1646–1667. doi: 10.1104/pp.126.4.1646

Mamidala, P., Rajarapu, S. P., Jones, S. C., and Mittapalli, O. (2011). Identification and validation of reference genes for quantitative real-time polymerase chain reaction in Cimex lectularius. *J. Med. Entomol* 48 (4), 947–951. doi: 10.1603/me10262

Nguyen, N. N. T., Lamotte, O., Alsulaiman, M., Ruffel, S., Krouk, G., Berger, N., et al. (2023). Reduction in PLANT DEFENSIN 1 expression in Arabidopsis thaliana results in increased resistance to pathogens and zinc toxicity. *J. Exp. Bot.* 74(17): 5374–5393. doi: 10.1093/jxb/erad228

Parisi, K., Shafee, T. M. A., Quimbar, P., van der Weerden, N. L., Bleackley, M. R., and Anderson, M. A. (2019). The evolution, function and mechanisms of action for plant defensins. *Semin. Cell Dev. Biol.* 88, 107–118. doi: 10.1016/j.semcdb.2018.02.004

Sadhu, S., Jogam, P., Gande, K., Marapaka, V., Penna, S., and Peddaboina, V. (2023). Expression of radish defensin (RsAFP2) gene in chickpea (Cicer arietinum L.) confers resistance to Fusarium wilt disease. *Mol. Biol. Rep.* 50 (1), 11–18. doi: 10.1007/s11033-022-08021-9

Sagaram, U. S., Pandurangi, R., Kaur, J., Smith, T. J., and Shah, D. M. (2011). Structure-activity determinants in antifungal plant defensins MsDef1 and MtDef4 with different modes of action against Fusarium graminearum. *PloS One* 6 (4), e18550. doi: 10.1371/journal.pone.0018550

Sathoff, A. E., Velivelli, S. L. S., Shah, D. M., and Samac, D. A. (2019). Plant defensin peptides have antifungal and antibacterial activity against human and plant pathogens. *Phytopathology* 109 3, 402–408. doi: 10.1094/PHYTO-09-18-0331-R

Shahmiri, M., Bleackley, M. R., Dawson, C. S., van der Weerden, N. L., Anderson, M. A., and Mechler, A. (2023). Membrane binding properties of plant defensins. *Phytochemistry* 209, 113618. doi: 10.1016/j.phytochem.2023.113618

Shahzad, Z., Ranwez, V., Fizames, C., Marquès, L., Le Martret, B., Alassimone, J., et al. (2013). Plant Defensin type 1 (PDF1): protein promiscuity and expression variation within the Arabidopsis genus shed light on zinc tolerance acquisition in Arabidopsis halleri. *New Phytol.* 200 (3), 820–833. doi: 10.1111/nph.12396

Terras, F. R., Schoofs, H. M., De Bolle, M. F., Van Leuven, F., Rees, S. B., Vanderleyden, J., et al. (1992). Analysis of two novel classes of plant antifungal proteins from radish (Raphanus sativus L.) seeds. *J. Biol. Chem.* 267 (22), 15301–15309. doi: 10.1016/s0021-9258(19)49534-3

Thomma, B. P., Cammue, B. P., and Thevissen, K. (2002). Plant defensins. *Planta* 216 (2), 193–202. doi: 10.1007/s00425-002-0902-6

Thompson, J. D., Higgins, D. G., and Gibson, T. J. (1994). CLUSTAL W: improving the sensitivity of progressive multiple sequence alignment through sequence weighting, position-specific gap penalties and weight matrix choice. *Nucleic Acids Res.* 22 (22), 4673–4680. doi: 10.1093/nar/22.22.4673

Trapnell, C., Roberts, A., Goff, L., Pertea, G., Kim, D., Kelley, D. R., et al. (2012). Differential gene and transcript expression analysis of RNA-seq experiments with TopHat and Cufflinks. *Nat. Protoc.* 7 (3), 562–578. doi: 10.1038/nprot.2012.016

Vriens, K., Cools, T. L., Harvey, P. J., Craik, D. J., Braem, A., Vleugels, J., et al. (2016). The radish defensins RsAFP1 and RsAFP2 act synergistically with caspofungin against Candida albicans biofilms. *Peptides* 75, 71–79. doi: 10.1016/j.peptides.2015.11.001

Zheng, X.-W., Deng-Xia, Y. I., Lin-Hui, S., and Cong, L. I. (2017). In silico genome-wide identification, phylogeny and expression analysis of the R2R3-MYB gene family in Medicago truncatula. *J. Integr. Agric.* 016 (007), 1576–1591. doi: 10.1016/S2095-3119(16)61521-6

frontiers | Frontiers in Plant Science

TYPE Original Research
PUBLISHED 24 November 2023
DOI 10.3389/fpls.2023.1297580

Check for updates

OPEN ACCESS

EDITED BY
Xinli Zhou,
Southwest University of Science and Technology, China

REVIEWED BY
Xiaojun Nie,
Northwest A&F University, China
Haifeng Liu,
Chonnam National University, Republic of Korea

*CORRESPONDENCE
Dongfang Ma
madf@yangtzeu.edu.cn
Lijun Yang
Yanglijun1993@163.com

†These authors have contributed equally to this work

RECEIVED 20 September 2023
ACCEPTED 06 November 2023
PUBLISHED 24 November 2023

CITATION
Cao P, Wang Y, Ma Z, Xu X, Ma D and Yang L (2023) Genome-wide identification of long intergenic non-coding RNAs of responsive to powdery mildew stress in wheat (*Triticum aestivum*). *Front. Plant Sci.* 14:1297580. doi: 10.3389/fpls.2023.1297580

COPYRIGHT
© 2023 Cao, Wang, Ma, Xu, Ma and Yang. This is an open-access article distributed under the terms of the Creative Commons Attribution License (CC BY). The use, distribution or reproduction in other forums is permitted, provided the original author(s) and the copyright owner(s) are credited and that the original publication in this journal is cited, in accordance with accepted academic practice. No use, distribution or reproduction is permitted which does not comply with these terms.

Genome-wide identification of long intergenic non-coding RNAs of responsive to powdery mildew stress in wheat (*Triticum aestivum*)

Peina Cao[1†], Youning Wang[2†], Zhaolan Ma[1], Xiao Xu[1,3], Dongfang Ma[1,4*] and Lijun Yang[4*]

[1]Engineering Research Center of Ecology and Agricultural Use of Wetland, Ministry of College of Agriculture, Yangtze University, Jingzhou, China, [2]Hubei Key Laboratory of Quality Control of Characteristic Fruits and Vegetables, Hubei Engineering University, Xiaogan, Hubei, China, [3]Jiangsu Academy of Agricultural Sciences, Jiangsu Coastal Area Institute of Agricultural Sciences, Yancheng, China, [4]Key Laboratory of Integrated Pest Management on Crop in Central China, Ministry of Agriculture/Hubei Province Key Laboratory for Control of Crop Diseases, Pest and Weeds/Institute of Plant Protection and Soil Science, Hubei Academy of Agricultural Sciences, Wuhan, Hubei, China

Wheat powdery mildew caused by *Blumeria graminis* f. sp. *tritici* is one of the most serious foliar diseases of wheat, causing grain yield and quality degradation by affecting plant photosynthesis. It is an effective method to improve the disease resistance of wheat plants by molecular breeding. With the continuous development of sequencing technology, long intergenic noncoding RNAs (lincRNAs) have been discovered in many eukaryotes and act as key regulators of many cellular processes. In this study, 12 sets of RNA-seq data from wheat leaves pre- and post-pathogen infection were analyzed and 2,266 candidate lincRNAs were identified. Consistent with previous findings, lincRNA has shorter length and fewer exons than mRNA. The results of differential expression analysis showed that 486 DE-lincRNAs were selected as lincRNAs that could respond to powdery mildew stress. Since lincRNAs may be functionally related to their adjacent target genes, the target genes of these lincRNAs were predicted, and the GO and KEGG functional annotations of the predicted target genes were performed. Integrating the functions of target genes and the biological processes in which they were involved uncovered 23 lincRNAs that may promote or inhibit the occurrence of wheat powdery mildew. Co-expression patterns of lincRNAs with their adjacent mRNAs showed that some lincRNAs showed significant correlation with the expression patterns of their potential target genes. These suggested an involvement of lincRNAs in pathogen stress response, which will provide a further understanding of the pathogenic mechanism of wheat powdery mildew.

KEYWORDS

wheat, powdery mildew, lincRNAs, expression pattern, differential expression

Introduction

Noncoding RNAs (ncRNAs) have emerged as major components of the eukaryotic transcriptome compared to protein-coding genes (Ariel et al., 2015). The role of ncRNAs as potent and specific regulators of gene expression is now widely recognized in almost all species to date (Brosnan and Voinnet, 2009; Beermann et al., 2016; Yamada, 2017). The long non-coding RNAs (lncRNAs) are the largest family of the ncRNAs. There are three kinds of lncRNAs: long intergenic non-coding RNAs (lincRNAs), intronic lncRNAs, and antisense lncRNAs (Chen and Zhu, 2022). Based on the location and length information, long intergenic non-coding RNAs (lincRNAs, a type of lncRNA), longer than 200 nucleotides (nt), are an abundant class of endogenous RNA molecules that are transcribed from intergenic regions of the genome (Wang et al., 2017; Sanchita et al., 2020). Accumulating evidence revealed that lincRNAs have potential roles involved in pathogen-defense responses and abiotic stress. For example, lincRNA *XLOC_026030* in rice is involved in the biological response to Pi starvation, and its expression level has a significant upward trend on the third day after Pi starvation (Xu et al., 2016). LincRNAs in the soybean participate in stress response, signal transduction, and developmental processes (Golicz et al., 2017). In potato, there is high association between 17 lincRNAs and 12 defense-related genes, which suggest that lincRNAs have potential functional roles in defense responses (Kwenda et al., 2016).

Wheat is a major food crop, a staple food worldwide, and one of the sources of plant protein for humans (Dong et al., 2020). Increasing wheat yield by reducing the influence of biotic/abiotic stresses is still widely studied. The impact of plant diseases on wheat-growing regions is difficult to estimate (Morgounov et al., 2012). Powdery mildew (*Blumeria graminis* f. sp. *tritici*) disease could infect all aboveground tissues of wheat, especially in humid environment (Conner et al., 2003). Breeding and utilization of Pm-resistant varieties is the most cost-effective and environmentally acceptable approach to control damage caused by powdery mildew (Hu et al., 2020). High-throughput sequencing technology provides great convenience in RNA sequencing (RNA-seq) for transcriptome analysis, and has been applied to reveal the expression patterns of genes that respond to plant disease defense mechanisms and discover novel genes (Zhu et al., 2015; Zhang H. et al., 2016; Zhang J. C. et al., 2016). So far, a total of 89 resistance genes/alleles have been identified to confer resistance to powdery mildew in wheat (Dong et al., 2020). However, recent studies indicated that many resistance genes have lost their resistance to powdery mildew (Tan et al., 2019). Therefore, it is necessary to find new sources to resist powdery mildew.

Although the mechanism mediating wheat responses to the pathogens causing powdery mildew has been widely investigated for years, long intergenic noncoding RNAs (lincRNAs), which have been proven to regulate important processes in the stress responses of plants, are still poorly known in wheat against powdery mildew infection. In this work, the multi-study datasets from public RNA-seq bio-projects currently available for wheat have been analyzed to identify the potential expression pattern of lincRNAs in response to wheat powdery mildew infection. First, lincRNAs in wheat were identified using RNA-seq data from a previous time-series experiment in which plants were grown under infected or non-infected conditions (Zhang et al., 2014). Second, differential expression analysis of the identified lincRNAs was performed to obtain the lincRNAs that respond to powdery mildew infection. Third, based on genomic location analysis methods, mRNA–lincRNA target pairs were predicted and functional annotation of target genes was performed. Finally, to determine whether they play important roles in resisting or promoting powdery mildew infection, the expression patterns of eight mRNA–lincRNA target pairs were analyzed using qRT-PCR. This study will provide not only new ideas for further understanding the pathogenic mechanism of wheat powdery mildew but also information for a more comprehensive understanding of the molecular mechanism involved in wheat resistance to powdery mildew.

Materials and methods

Downloading the raw data

The RNA-seq data used in this study were from the NCBI SRA database (accession number PRJNA243835). The samples were leaves at the two-leaf stage of wheat seedlings, which are infected with two different fungi (*Puccinia striiformis* f. sp. *tritici* and *Blumeria graminis* f. sp. *tritici*). Samples were collected at 0 h, 24 h, 48 h, and 72 h after fungi infection. In this study, only the experimental data of wheat infection with powdery mildew were used.

RNA-Seq reads mapping and transcriptome assembly

The Fastq-dump_v2.8.0 tool was used to convert SRA files (paired-end sequencing data) into paired-end FASTQ format. FASTQC_v0.11.9 (FastQC Quality Control, version 0.11.9) software was used to assess the quality of all generated FASTQ files (Xiao et al., 2015). Trim_Galore_v0.6.7 tool was used for quality trimming and adapter removal with the default parameters. Subsequently, the clean reads were then mapped to the wheat (version 2.1, International Wheat Genome Sequencing Consortium) reference genome with the default parameters by the software HISAT2_v4.8.2 (Pertea et al., 2016). The file containing all mapped readings for each sample was saved in SAM format. SAM files contain the alignment position of sequencing data on the reference genome and other relevant information (Li et al., 2009). The parameter "sort -o" in software samtools_v1.9 was used to convert SAM format files into sorted BAM files (Pertea et al., 2016). BAM files are in binary format and are often used in subsequent analyses, such as mutation detection and gene expression analysis (McKenna et al., 2010). Using StringTie_v2.1.7 software, all BAM files were assembled into one complete GTF file with the default parameters (Pertea et al., 2015). In addition, StringTie software can estimate the expression levels of genes and transcripts in all samples (Pertea et al., 2016).

Identification of lincRNAs in wheat

Refer to previous research for lincRNA detection (Chen et al., 2019). Firstly, the parameter "- r" of gffcompare in StringTie was used to filter transcripts without the "u" character to ensure the preservation of intergenic transcripts (Pertea and Pertea, 2020). All of PLEK, CNCI, and CPC2 can be used to predict the encoding potential of transcripts. The transcript sequence with class_code = " u " was predicted by these three software to obtain three sets of transcripts that did not have coding capabilities. To reduce the impact of false positives, the intersection of the a, b, and c datasets was taken, and the final intersection was analyzed for subsequent analysis. To minimize the impact of false positives predicted by the software, the intersection of the three datasets was taken. The transcripts that were predicted to be non-coding in all three software were continued for subsequent analysis. LongOrfs is a core tool in software TransDecoder for predicting long open reading frames (ORFs) in transcripts. ORFs with a length of at least 100 amino acids are recognized by default. LincRNAs do not have long ORFs, so transcript sequences containing long ORFs were removed (Harrow et al., 2012). To further rule out the ability of the remaining sequences to encode proteins, the transcript sequence was translated into six possible protein sequences using the transeq command, each corresponding to a different reading frame. HMMER was used to identify whether these translated protein sequences contain specific protein domains, families, patterns, etc. (Finn et al., 2011). Protein sequences without special structures were used for subsequent analysis. Using BLAST search in the NR database, sequences similar to the query sequences can be found in known protein sequences. Protein sequences with an E-value greater than 1e-5 compared to known protein sequences were preserved. Retained transcripts as candidate lincRNAs (Figure 1A).

Analysis of differentially expressed lincRNA (DE-lincRNA)

The GTF file from stringtie analysis contains information such as transcripts and their expressions. After converting them to the form required for DESeq2, differential expression analysis of the transcriptome data was performed using DESeq2 (Love et al., 2014). The online software Omicshare (https://www.omicshare.com/tools/) was used for differential expression analysis, and the parameter was $p < 0.05$.

Prediction of adjacent target genes and functional annotation of target genes

Genomic location analysis method was used to predict adjacent target genes of lincRNA. In general, genes within a certain distance range are considered potential adjacent target genes. The distance of 100 kb is relatively close on the genomic scale. Genes closer to lincRNA may have a closer association and possibly functional relationship with lincRNA (Luo et al., 2016). Therefore, mRNA in the range of 100 kb expands in both upstream and downstream directions based on the location of differentially expressed lincRNA (DE-lincRNA) on chromosomes as possible target genes of lincRNA. GO and KEGG functional annotation of target genes was implemented using the online tool Omicshare (https://www.omicshare.com/tools/). The potential interaction between lincRNA and mRNA was plotted using software Cytoscape_v3.9.1. The software TBtools was used to generate the heat map of gene expression.

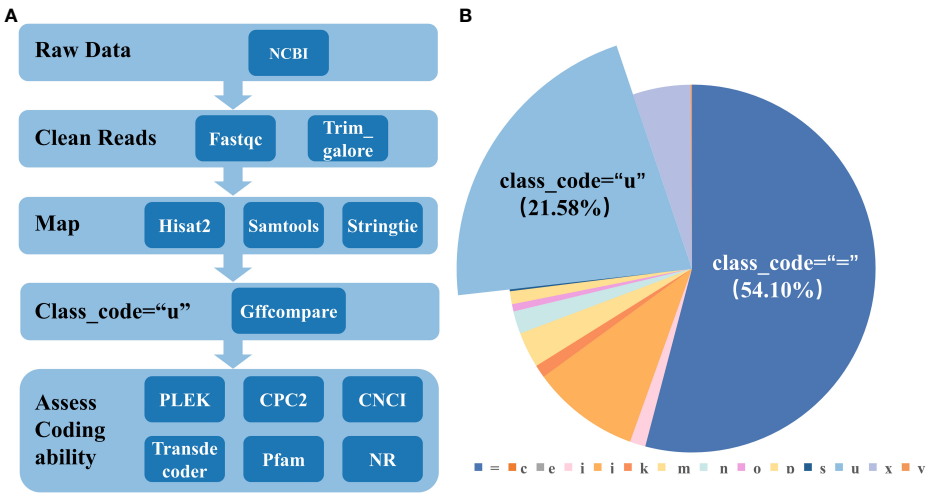

FIGURE 1
The identification process of lincRNA. **(A)** The specific identification process of lincRNA and the software and tools used at each step (Chen et al., 2019). **(B)** Location comparison of transcripts to reference genomes and the proportion of each species, as generated by GffCompare. Classification is based on previous studies (Pertea and Pertea, 2020).

Plant material and powdery mildew infestation

Wheat (Yangmai 20 variety) seeds were germinated in a greenhouse at 25 ± 2°C. After 2–3 days, healthy wheat seedlings were selected and transferred to a round flowerpot. There are three to five seedlings in each pot at the greenhouse. Seedlings about the two-leaf stage were inoculated with *Blumeria graminis* f. sp. *tritici* race E09 from infected wheat leaves under 18 ± 2°C (Guo et al., 2021). The infected wheat leaves were presented from Professor Lijun Yang (Institute of Plant Protection and Soil Science Hubei Academy of Agricultural Sciences). The wheat leaves were collected at 0 h, 24 h, 48 h, and 72 h after inoculation, and then maintained in a −80°C cryogenic refrigerator. This experiment used non-infected wheat leaves (0 h) as the control group.

Total RNA extraction and qRT-PCR

Total RNA was extracted from wheat leaves (infected and non-infected leaves) with TRIzol reagent (Aidlab, Beijing, China) and was reverse transcribed using HiScript II Reverse transcriptase (Vazyme, Nanjing, China). Quantitative PCR was carried out in triplicate with the ChamQ SYBR Color qPCR Master Mix (Vazyme, Nanjing, China). The reactions were conducted in a 20-μL volume containing 10 μL of 2×ChamQ SYBR Color qPCR Master Mix, 0.4 μL of each primer (10 μmol/mL), 0.4 μL 50×ROX Reference Dye 1, and 2 μL of the cDNA, and the remaining double-distilled water was replenished to 20 μL. The annealing temperature of the primer was 60°C. Primers used in present study are listed in Supplementary Table 3.

Results

Characterization of lincRNA

After the low-quality sequencing fragments in the RNA seq data (Supplementary Table 1), wheat leaves under different stages of powdery mildew infection were filtered out, and 95.56% of the clean reads were successfully mapped. There are a total of 244,636 transcripts, of which 52,789 were recorded as class_code = "u", accounting for 21.58% (Figure 1B), about half of the mRNA (class_code = "="). After comparison with the genome and removal of coding sequences, a total of 2,266 lincRNAs were identified in wheat. The result of the number of exons of mRNA and lincRNA showed that the number of the number of exons gradually increases, and the number of mRNA and lincRNA showed a significant decrease (Figure 2A). In addition, there are also differences in sequence length between mRNA and lincRNA. The gene length of lincRNA ranged from 200 to 2,000 bp, and only a few lincRNAs had a length greater than 2,000 bp, and the number of lincRNA decreased with the increase of length. However, mRNA has a wide range of gene length distribution, and there are a large number of gene distributions in each length interval, and their number was not significantly different (Figure 2B).

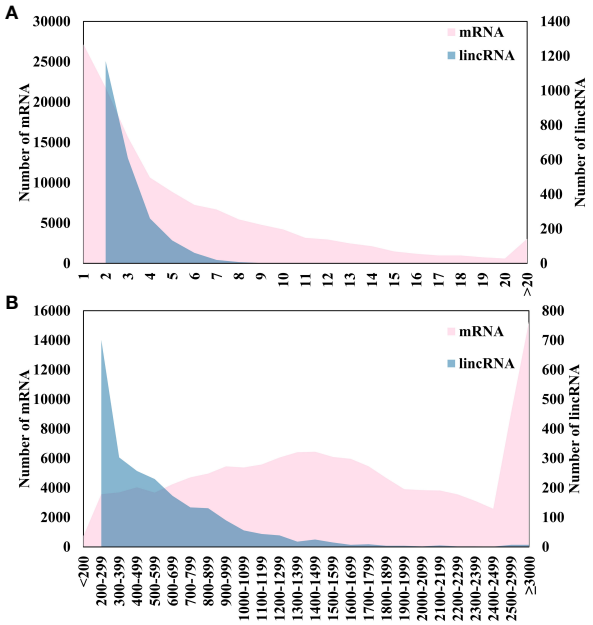

FIGURE 2
Analysis of the characteristics of lincRNA and mRNA. Pink represents mRNA and blue represents lincRNA. The primary ordinate was used for mRNA and the secondary ordinate was used for lincRNA. **(A)** Exon number analysis. **(B)** Gene length analysis.

Identify the lincRNAs that can respond to powdery mildew infection

According to the transcriptome data of four groups of wheat samples, the non-infected samples (0h) were compared with infected samples at three different time points (24h, 48h, and 72h). There were 107, 176, and 176 differentially expressed lincRNAs. Notably, although the number of DE-lincRNAs was the same in the latter two groups, the sequence of DE-lincRNAs was different (Figures 3A–C; Supplementary Table 2). Differential expression analysis was also performed in pairs among three infected samples of different time points, and 134, 154, and 85 DE-lincRNAs were obtained (Figures 3D–F; Supplementary Table 2). To identify the lincRNAs that can respond to powdery mildew infection, all the DE-lincRNAs in these six comparison groups were combined and repeated DE-lincRNAs in different groups were removed, resulting in a total of 486 DE-lincRNAs that could respond to powdery mildew infection in wheat.

Prediction of adjacent target genes

Considering the physical distance, the 100-kb distance falls within the close range on the genome scale, and relatively close genes may have a closer association and possible functional relationship with lincRNAs. From the perspective of regulatory scope, many regulatory sequences and elements are located in the upstream and downstream regions of genes. Therefore, the choice of a distance range of 100 kb in our study allows a more

10.3389/fpls.2023.1297580

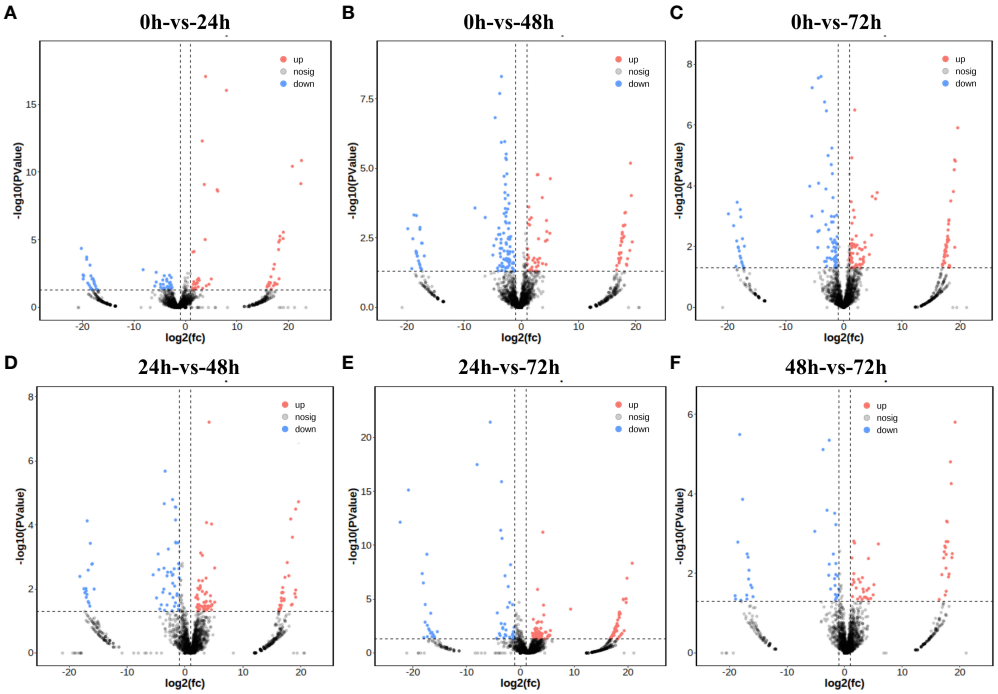

FIGURE 3
Differential expression analysis. Red indicates an upward expression and blue indicates a downward expression. Gray represents no significant difference. **(A–F)** Volcano plot for difference analysis for each comparison group.

comprehensive consideration of the potential regulatory effect of lincRNA on genes close to it. A total of 1,062 adjacent genes were obtained by locating 486 lincRNAs within 100 kb of both 5' and 3' directions. This was not a one-to-one relationship, because a lincRNA responds to multiple coding genes nearby.

Functional annotations of target genes

To clarify the function of the adjacent target genes and the biological processes involved, GO and KEGG functional annotations were used to analyze the function of target genes. A total of 727 target genes from the 1,062 adjacent target gene list were successfully mapped to terms in the GO database. There were three main categories for GO terms: Molecular Function, Cellular Component, Biological Process, and the number of genes was 592, 327, and 424, respectively (Figure 4; Supplementary Table 4). Some target genes were involved in more than one biological process. According to the KEGG annotation results (Figure 5), pathways related to the regulation of plant disease resistance mechanisms were selected, including fructose and mannose metabolism, MAPK signaling pathway-plant, plant hormone signal transduction, plant-pathogen, and starch and sucrose metabolism—five processes of interaction. A total of 28 genes involved in these processes were selected for further analysis (Table 1). The correspondence between lincRNAs and mRNAs is shown in Figure 6.

Analysis of expression patterns of disease-resistant lincRNAs and their target genes

Since the target genes are identified by the genomic location analysis method, more than one mRNA is contained near a lincRNA. A total of 23 lincRNA–mRNA pairs were formed between 28 target genes and their nearby lincRNAs (Supplementary Table 5). There was clear evidence for higher expression of mRNAs than lincRNAs (Figure 7). Among them, eight pairs of genes with high expression were selected for expression pattern analysis. There were four pairs of mRNA whose changes in expression showed the same trend as the predicted results: the first, third, sixth, and eighth pairs (Figures 8A, C, F, H). The results of the expression pattern analysis of lincRNA show that the experiments of the second, fourth, fifth, and eighth pairs were consistent with the predicted results (Figures 8B, D, E, H). From the results of qRT-PCR, changes in the expression of mRNA in the first, third, fifth, and seventh pairs correlated with changes in lincRNA (Figures 8A, C, E, G). The expression patterns of the second, fourth, sixth, and eighth pairs were not significantly correlated (Figures 8B, D, F, H). As expected, some lincRNAs may have potential regulatory relationships with their corresponding target genes. Both lincRNAs and their target genes with the same expression pattern showed an increase in expression levels. This phenomenon indicates that these genes may be susceptible genes for powdery mildew.

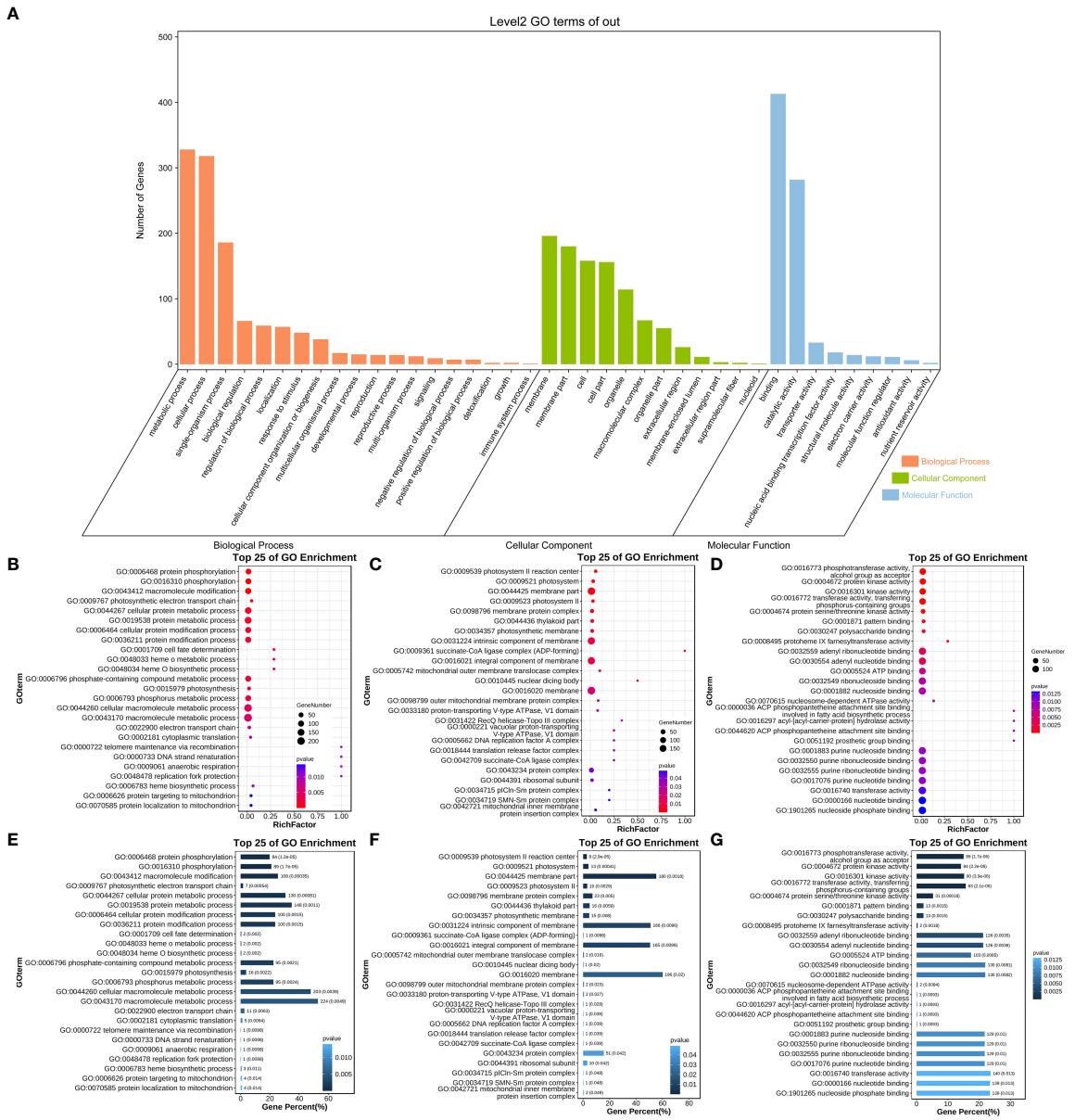

FIGURE 4
GO function analysis of neighboring target genes. **(A)** GO annotated secondary classification histogram of results. The abscissa represents the first-level classification of GO's three ontology, the first of which is the biological pathway (BP), the second is the cellular component (CC), and the third is molecular function (MF). **(B–D)** GO-enriched bubble chart of the top 25 terms. The *x*-axis is the Rich Factor, the ratio of the number of genes enriched into the pathway by the set of selected genes to the number of genes enriched into the pathway by background genes. The *y*-axis is the name of the enriched pathway, arranged from smallest to largest according to *p*-value. The size of the dot indicates the number of genes, and the larger the dot, the more genes are enriched into that pathway. The color of the dot represents the level of the *p*-value, and the smaller the *p*-value, the more significant the pathway. **(E–G)** GO Enrichment Analysis Bar Chart. The abscissa is the proportion of the number of genes, and the ordinate is the GO Term and the details of each GO number. The different color depths in the figure represent different gene numbers, and the color gradually decreases from dark to light. From left to right, it corresponds to the specific classification of BP, CC, and MF.

Discussion

To obtain lincRNA in wheat that can respond to powdery mildew infection, four groups of sequencing data from non-infected wheat samples and infected wheat samples at three different time points were analyzed. All the significantly DE-lincRNAs were aggregated to obtain the lincRNAs in wheat in response to powdery mildew infection, totaling 486 lincRNAs. A similar study identified 283 DE-lincRNAs that were tightly correlated with the fungi-responsive lincRNAs in wheat, of which 254 DE-lincRNAs responded to the powdery mildew stress (Zhang H. et al., 2016). The difference between this study and previous studies is that we selected a new reference genome of wheat. There are subtle differences in the identification of lincRNA, and the identification criteria of previous studies are more stringent. The transcripts containing ORF greater than 300 bp were removed in this study, while the transcripts from previous studies were required not to contain ORF more than 150 bp. This may be the reason for the

10.3389/fpls.2023.1297580

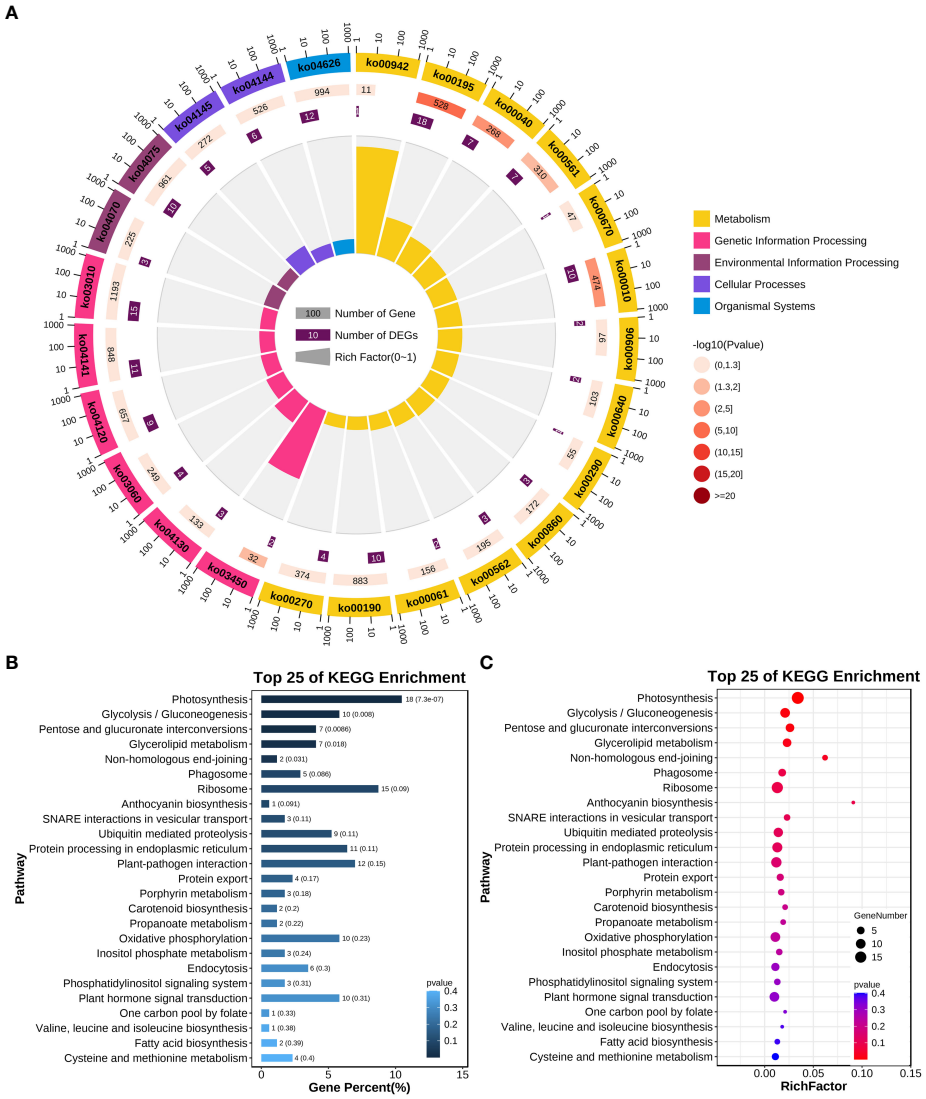

FIGURE 5
KEGG annotation results of adjacent target genes. **(A)** Enrichment circle chart. The first circle is the classification of enrichment. Outside the circle is the coordinate of the number of genes, and different colors represent different classifications. The second circle shows the total number of background genes in that category. The third circle is the number of selected genes enriched into the classification as well as the *p*-value. The more genes, the longer the bar, the smaller the value, the darker the color. **(B)** KEGG Enrichment Analysis Bar Chart. **(C)** KEGG-enriched bubble chart of the top 25 terms.

TABLE 1 Pathways associated with plant disease resistance and their corresponding genes.

Pathway	Pathway ID	Genes
Fructose and mannose metabolism (2)	ko00051	TraesCS2A03G1155100; TraesCS3D03G0638600
MAPK signaling pathway - plant (6)	ko04016	TraesCS4A03G0706000; TraesCS4A03G0705900; TraesCS5B03G0484700; TraesCS3D03G0407400; VTraesCS1A03G0813700; TraesCS5B03G0483900
Plant hormone signal transduction (10)	ko04075	TraesCS3B03G0153700; TraesCS2D03G0863900; TraesCS5A03G0126700; TraesCS5B03G0484700; TraesCS3D03G1093100; TraesCS4A03G0040600; TraesCS2A03G1155100; TraesCS1A03G0813700; TraesCS5B03G0483900; TraesCS3B03G0833700
Plant-pathogen interaction (12)	ko04626	TraesCS6B03G1287600; TraesCS5B03G1159600; TraesCS4A03G0706000; TraesCS4A03G0705900; TraesCS5A03G0725600; TraesCS7B03G0962800; TraesCS3D03G0407400; TraesCS5A03G0824000; TraesCS6D03G0428100; TraesCS5D03G0595900; TraesCS2D03G0419900; TraesCS5B03G0483900
Starch and sucrose metabolism (6)	ko00500	TraesCS2D03G0711200; TraesCS4A03G0706200; TraesCS2D03G0711600; TraesCS4A03G0706400; TraesCS3D03G0638600; TraesCS6D03G0658300

The numbers in parentheses represent how many genes of the pathway were included.

10.3389/fpls.2023.1297580

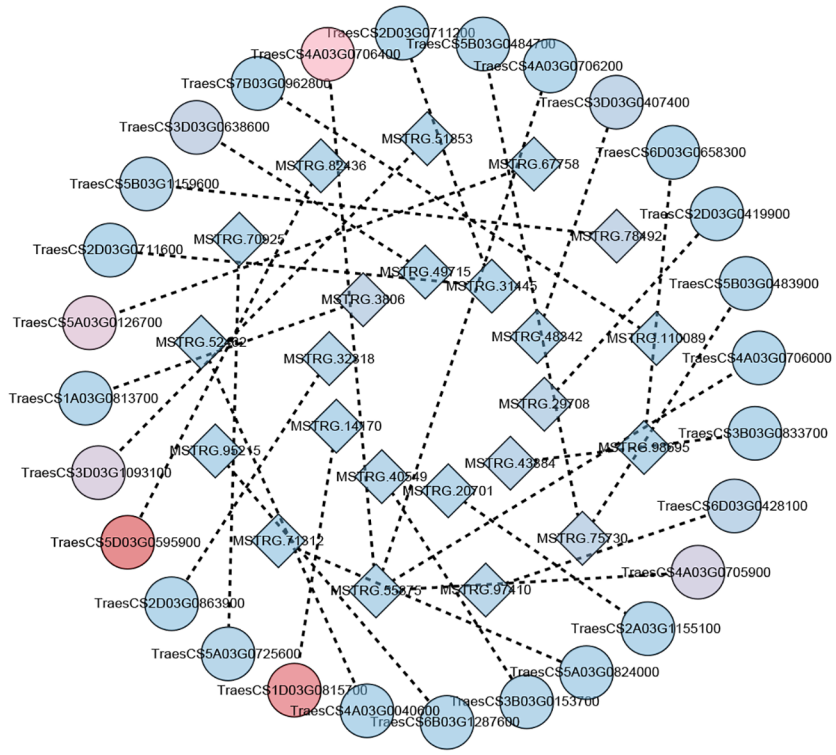

FIGURE 6
The correspondence between lincRNAs and mRNAs. The circle represents mRNAs and the square represents lincRNAs. Lines represent the presence of potential regulatory relationships between genes. The shade of color represents the level of gene expression. A change in color from blue to red indicates higher and higher levels of gene expression (the sum of expression at all time points was taken).

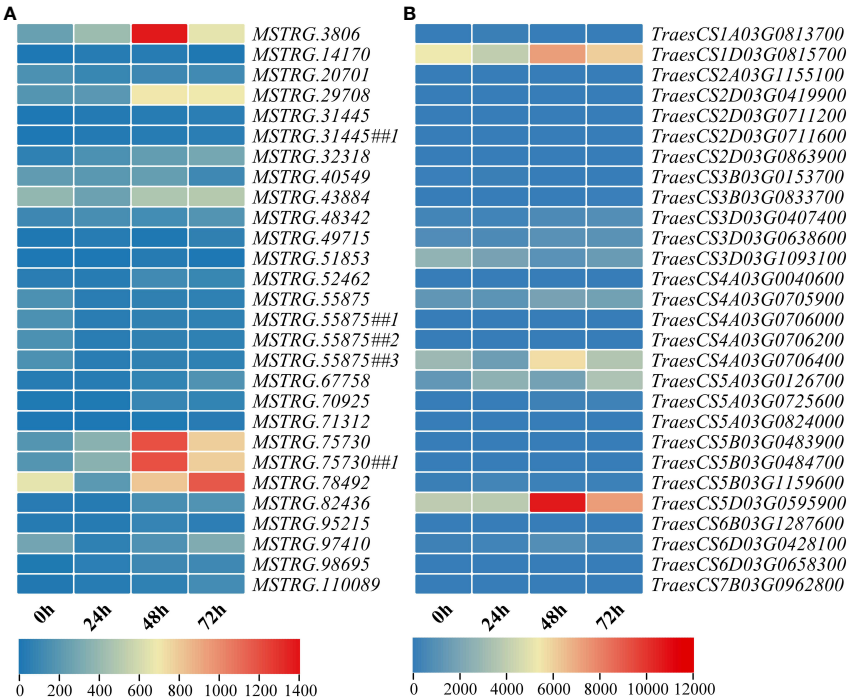

FIGURE 7
Heat map of expression levels of genes involved in the regulation of plant disease resistance mechanisms at four different time points (0 h, 24 h, 48 h, and 72 h). **(A)** Expression of 23 lincRNAs at different time points. **(B)** Expression of 28 mRNAs at different time points. To demonstrate the one-to-one correspondence of mRNAs to lincRNAs, several lincRNAs are repeated.

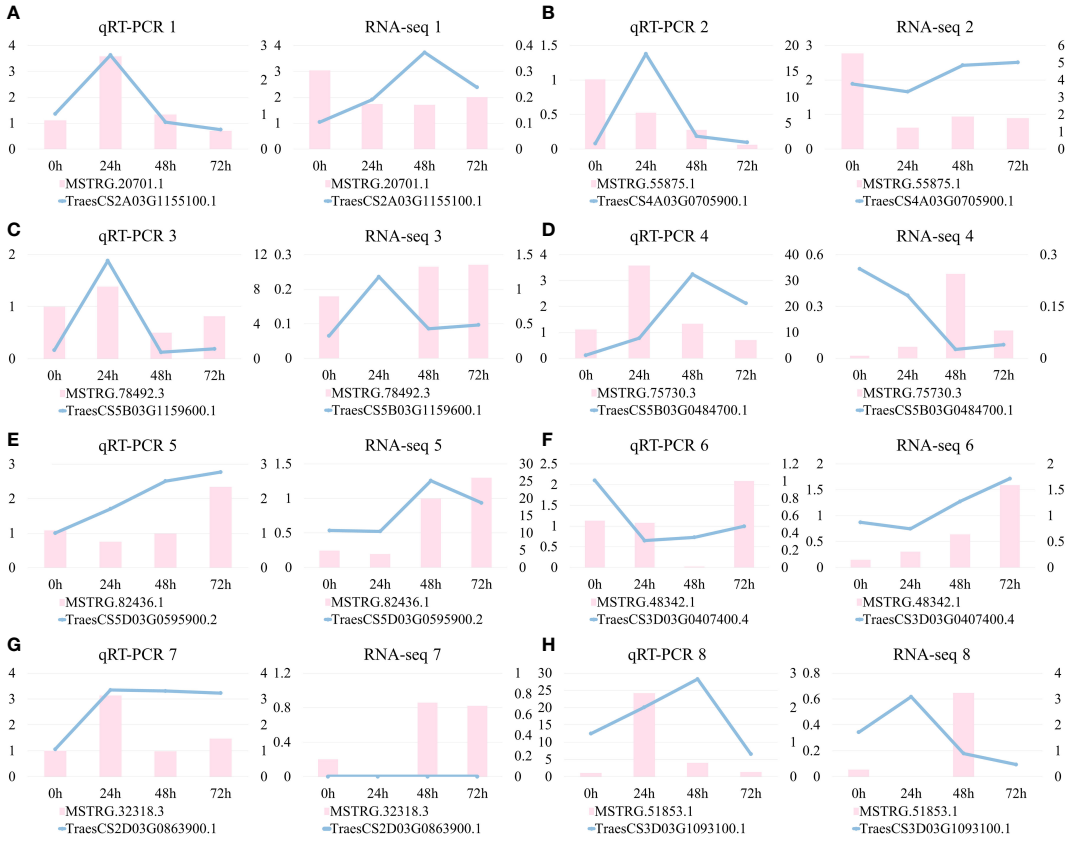

FIGURE 8
Analysis of expression patterns of lincRNAs and neighboring target genes. **(A–H)** The experimental and predicted results of eight pairs of mRNA–lincRNA correspond in turn. The figure on the left is plotted from the results of qRT-PCR and the figure on the right is plotted based on the gene expression obtained from RNA-seq data.

difference in prediction results for lincRNA. Our study analyzed the co-expression patterns of lincRNAs with their adjacent protein-coding genes, and previous studies analyzed the co-expression patterns of selected miRNAs targeting lincRNAs and functional genes (Zhang H. et al., 2016). The diversity of prediction methods contributes to a comprehensive understanding of the disease defense mechanism of wheat powdery mildew.

Possible expression correlations between lincRNAs and their adjacent target genes were assessed to further clarify the specific mode of action of lincRNA in response to powdery mildew infection. The method based on genomic location analysis suggests that genes within a certain distance near lincRNAs may be potential adjacent target genes (Ørom et al., 2010; Engreitz et al., 2016). In our study, a range of 100 kb was chosen, which is a common choice rather than an absolute value. Different lincRNAs may have different regulatory ranges, and the regulatory distance range may be affected by other factors (Ørom and Shiekhattar, 2013; Kopp and Mendell, 2018). Consistent with the expected results, some lincRNAs showed significant correlation with the expression patterns of their potential target genes, while others did not show any association. It should be noted that the existing prediction methods only make preliminary predictions, and further experimental verification and functional studies are required to find the real target genes of lincRNA.

LincRNAs are becoming a key regulatory factor in various cellular processes, but it is still difficult to clarify the function of individual lincRNA (Ransohoff et al., 2018). The function of adjacent target genes can be used as a reference to identify the function of lincRNA (Guttman et al., 2009). To further understand the specific functions of lincRNA in response to powdery mildew infection, GO and KEGG function annotations were performed on potential target genes of DE-lincRNAs. The annotation results help us to better understand the functions of lincRNA and their roles in biological processes. However, there are still some inevitable defects. GO functional analysis is usually the annotation of the whole genome, which may lead to the omission or masking of the functional information of some genes. The annotation information in the GO database is based on known functions and biological processes, but functional annotation may be limited for some genes that are not fully understood (Gene Ontology Consortium, 2019). Our study was limited by the fact that 335 genes have not yet been successfully annotated. This part of the bias will narrow the scope of research that matches our target genes. The KEGG database is also mainly based on known signaling and metabolic pathways, which have not yet covered all biological processes and may not account for some newly discovered functions (Hucka et al., 2003; Kanehisa et al., 2017).

The functional annotation information indicates that *TraesCS2A03G1155100* is involved in pathway “Fructose and

mannose metabolism" and "Plant hormone signal transduction". Fructose and mannose are part of the process of sugar metabolism in plant. Sugar signaling contributes to plant immune responses to pathogens, and may act as a signal molecule to induce plant defense responses to invading pathogens (Bolouri Moghaddam and Van den Ende, 2012). Based on the functional similarities, it is speculated that lincRNA *MSTRG.20701* with the same expression pattern as the genes mentioned above may regulate fructose and mannose metabolism and thus participate in plant defense responses. Both *TraesCS2A03G1155100* and *TraesCS2D03G0863900* are involved in the process of plant hormone signal transduction. Numerous studies have shown that plants can produce hormones for disease resistance and defense (Yan et al., 2023). In addition, *TraesCS5D03G0595900* and *TraesCS5B03G1159600* participate in plant–pathogen interaction. This information provides a reference for further understanding the role of lincRNA in response to powdery mildew infection. However, the exact mechanisms of lincRNA in plant immunity require further research for confirmation.

Data availability statement

The original contributions presented in the study are included in the article/Supplementary Material. Further inquiries can be directed to the corresponding authors.

Author contributions

PC: Writing – original draft. YW: Data curation, Writing – original draft. ZM: Validation, Writing – review & editing. XX: Methodology, Supervision, Writing – review & editing. DM: Writing – review & editing. LY: Resources, Writing – review & editing.

Funding

The author(s) declare financial support was received for the research, authorship, and/or publication of this article. This research was funded by the Open Project Program of Key Laboratory of Integrated Pest Management on Crop in Central China, the Ministry of Agriculture/Hubei Province Key Laboratory for Control of Crop Diseases, Pest and Weeds (2021ZTSJJ8), the China Agriculture Research System (CARS-3), and the National Key Research and Development Program of Jiangsu (BE2021335).

Acknowledgments

The authors thank LY (Institute of Plant Protection and Soil Science Hubei Academy of Agricultural Sciences, Wuhan, China) for providing the pathogenesis of *Blumeria graminis* f. sp. *tritici* race E09.

Conflict of interest

The authors declare that the research was conducted in the absence of any commercial or financial relationships that could be construed as a potential conflict of interest.

Publisher's note

All claims expressed in this article are solely those of the authors and do not necessarily represent those of their affiliated organizations, or those of the publisher, the editors and the reviewers. Any product that may be evaluated in this article, or claim that may be made by its manufacturer, is not guaranteed or endorsed by the publisher.

Supplementary material

The Supplementary Material for this article can be found online at: https://www.frontiersin.org/articles/10.3389/fpls.2023.1297580/full#supplementary-material

References

Ariel, F., Romero-Barrios, N., Jegu, T., Benhamed, M., and Crespi, M. (2015). Battles and hijacks: Noncoding transcription in plants. *Trends Plant Sci.* 20, 362–371. doi: 10.1016/j.tplants.2015.03.003

Beermann, J., Piccoli, M. T., Viereck, J., and Thum, T. (2016). Non-coding RNAs in development and disease: background, mechanisms, and therapeutic approaches. *Physiol. Rev.* 96 (4), 1297–1325. doi: 10.1152/physrev.00041.2015

Bolouri Moghaddam, M. R., and Van den Ende, W. (2012). Sugars and plant innate immunity. *J. Exp. Bot.* 63 (11), 3989–3998. doi: 10.1093/jxb/ers129

Brosnan, C. A., and Voinnet, O. (2009). The long and the short of noncoding RNAs. *Curr. Opin. Cell Biol.* 21, 416–425. doi: 10.1016/j.ceb.2009.04.001

Chen, L., Shi, G., Chen, G., Li, J., Li, M., Zou, C., et al. (2019). Transcriptome analysis suggests the roles of long intergenic non-coding RNAs in the growth performance of weaned piglets. *Front. Genet.* 10. doi: 10.3389/fgene.2019.00196

Chen, L., and Zhu, Q. H. (2022). The evolutionary landscape and expression pattern of plant lincRNAs. *RNA Biol.* 19 (1), 1190–1207. doi: 10.1080/15476286.2022.2144609

Conner, R., Kuzyk, A., and Su, H. (2003). Impact of powdery mildew on the yield of soft white spring wheat cultivars. *Can. J. Plant Sci.* 83, 725–728. doi: 10.4141/p03-043

Dong, Z., Tian, X., Ma, C., Xia, Q., Wang, B., Chen, Q., et al. (2020). Physical mapping of Pm57, a powdery mildew resistance gene derived from Aegilops searsii. *Int. J. Mol. Sci.* 21 (1), 322. doi: 10.3390/ijms21010322

Engreitz, J. M., Haines, J. E., Perez, E. M., Munson, G., Chen, J., Kane, M., et al. (2016). Local regulation of gene expression by lncRNA promoters, transcription and splicing. *Nature* 539 (7629), 452–455. doi: 10.1038/nature20149

Finn, R. D., Clements, J., and Eddy, S. R. (2011). HMMER web server: interactive sequence similarity searching. *Nucleic Acids Res.* 39 (suppl_2), W29–W37. doi: 10.1093/nar/gkr367

Gene Ontology Consortium (2019). The Gene Ontology Resource: 20 years and still GOing strong. *Nucleic Acids Res.* 47 (D1), D330–D338. doi: 10.1093/nar/gky1055

Golicz, A., Singh, M. B., and Bhalla, P. L. (2017). The long intergenic noncoding RNA (LincRNA) Landscape of the soybean genome. *Plant Physiol.* 176 (3), 2133–2147. doi: 10.1104/pp.17.01657

Guo, H., Zhang, H., Wang, G. H., Wang, C. Y., Wang, Y. J., Liu, X. L., et al. (2021). Identification and evaluation of resistance to powdery mildew and yellow rust in a wheat mapping population. *Plant Genome* 14 (2), 1–15. doi: 10.1002/tpg2.20092

Guttman, M., Amit, I., Garber, M., French, C., Lin, M. F., Feldser, D., et al. (2009). Chromatin signature reveals over a thousand highly conserved large non-coding RNAs in mammals. *Nature* 458 (7235), 223–227. doi: 10.1038/nature07672

Harrow, J., Frankish, A., Gonzalez, J. M., Tapanari, E., Diekhans, M., Kokocinski, F., et al. (2012). GENCODE: the reference human genome annotation for The ENCODE Project. *Genome Res.* 22 (9), 1760–1774. doi: 10.1101/gr.135350.111

Hu, W. G., Wang, Q. H., Wang, S. W., Wang, M. M., Wang, C. Y., Tian, Z. R., et al. (2020). Gene co-expression network analysis provides a novel insight into the dynamic response of wheat to powdery mildew stress. *J. Genet.* 99, 44. doi: 10.1007/s12041-020-01206-w

Hucka, M., Finney, A., Sauro, H. M., Bolouri, H., Doyle, J. C., Kitano, H., et al. (2003). The systems biology markup language (SBML): a medium for representation and exchange of biochemical network models. *Bioinformatics* 19 (4), 524–531. doi: 10.1093/bioinformatics/btg015

Kanehisa, M., Furumichi, M., Tanabe, M., Sato, Y., and Morishima, K. (2017). KEGG: new perspectives on genomes, pathways, diseases and drugs. *Nucleic Acids Res.* 45 (D1), D353–D361. doi: 10.1093/nar/gkw1092

Kopp, F., and Mendell, J. T. (2018). Functional classification and experimental dissection of long noncoding RNAs. *Cell* 172 (3), 393–407. doi: 10.1016/j.cell.2018.01.011

Kwenda, S., Birch, P. R. J., and Moleleki, L. N. (2016). Genome-wide identification of potato long intergenic noncoding RNAs responsive to Pectobacterium carotovorum subspecies brasiliense infection. *BMC Genomics* 17, 614. doi: 10.1186/s12864-016-2967-9

Li, H., Handsaker, B., Wysoker, A., Fennell, T., Ruan, J., Homer, N., et al. (2009). The sequence alignment/Map format and SAMtools. *Bioinformatics* 25 (16), 2078–2079. doi: 10.1093/bioinformatics/btp352

Love, M. I., Huber, W., and Anders, S. (2014). Moderated estimation of fold change and dispersion for RNA-seq data with DESeq2. *Genome Biol.* 15, 550. doi: 10.1186/s13059-014-0550-8

Luo, S., Lu, J. Y., Liu, L., Yin, Y., Chen, C., Han, X., et al. (2016). Divergent lncRNAs regulate gene expression and lineage differentiation in pluripotent cells. *Cell Stem Cell* 18 (6), 637–652. doi: 10.1016/j.stem.2016.01.024

McKenna, A., Hanna, M., Banks, E., Sivachenko, A., Cibulskis, K., Kernytsky, A., et al. (2010). The Genome Analysis Toolkit: a MapReduce framework for analyzing next-generation DNA sequencing data. *Genome Res.* 20 (9), 1297–1303. doi: 10.1101/gr.107524.110

Morgounov, A., Tufan, H. A., Sharma, R., Akin, B., Bagci, A., Braun, H. J., et al. (2012). Global incidence of wheat rusts and powdery mildew during 1969–2010 and durability of resistance of winter wheat variety Bezostaya 1. *Eur. J. Plant Pathol.* 132, 323–340. doi: 10.1007/s10658-011-9879-y

Ørom, U. A., Derrien, T., Beringer, M., Gumireddy, K., Gardini, A., Bussotti, G., et al. (2010). Long noncoding RNAs with enhancer-like function in human cells. *Cell* 143 (1), 46–58. doi: 10.1016/j.cell.2010.09.001

Ørom, U. A., and Shiekhattar, R. (2013). Long noncoding RNAs usher in a new era in the biology of enhancers. *Cell* 154 (6), 1190–1193. doi: 10.1016/j.cell.2013.08.028

Pertea, M., Kim, D., Pertea, G. M., Leek, J. T., and Salzberg, S. L. (2016). Transcript-level expression analysis of RNA-seq experiments with HISAT, stringtie and ballgown. *Nat. Protoc.* 11, 1650–1667. doi: 10.1038/nprot.2016.095

Pertea, G., and Pertea, M. (2020). Gff utilities: gffread and gffcompare. *F1000 Res.* 9, 304. doi: 10.12688/f1000research.23297.1

Pertea, M., Pertea, G. M., Antonescu, C. M., Chang, T. C., Mendell, J. T., and Salzberg, S. L. (2015). StringTie enables improved reconstruction of a transcriptome from RNA-seq reads. *Nat. Biotechnol.* 33 (3), 290–295. doi: 10.1038/nbt.3122

Ransohoff, J., Wei, Y., and Khavari, P. (2018). The functions and unique features of long intergenic non-coding RNA. *Nat. Rev. Mol. Cell Biol.* 19, 143–157. doi: 10.1038/nrm.2017.104

Sanchita, Trivedi, P. K., Asif, M. H. (2020). Updates on plant long non-coding RNAs (lncRNAs): the regulatory components. *Plant Cell Tissue Organ Cult.* 140 (2), 259–269. doi: 10.1007/s11240-019-01726-z

Tan, C., Li, G., Cowger, C., Carver, F. B., and Xu, X. (2019). Characterization of Pm63, a powdery mildew resistance gene in Iranian landrace PI 628024. *Theor. Appl. Genet.* 132, 1137–1144. doi: 10.1007/s00122-018-3067-9

Wang, H., Wang, Y., Xie, S., Liu, Y., and Xie, Z. (2017). Global and cell-type specific properties of lincRNAs with ribosome occupancy. *Nucleic Acids Res.* 45 (5), 2786–2796. doi: 10.1093/nar/gkw909

Xiao, H., Yuan, Z., Guo, D., Hou, B., Yin, C., Zhang, W., et al. (2015). Genome-wide identification of long noncoding RNA genes and their potential association with fecundity and virulence in rice brown planthopper, Nilaparvata lugens. *BMC Genomics* 16, 749. doi: 10.1186/s12864-015-1953-y

Xu, X. W., Zhou, X. H., Wang, R. R., Peng, W. L., An, Y., and Chen, L. L. (2016). Functional analysis of long intergenic non-coding RNAs in phosphate-starved rice using competing endogenous RNA network. *Sci. Rep.* 6, 20715. doi: 10.1038/srep20715

Yamada, M. (2017). Functions of long intergenic non-coding (linc) RNAs in plants. *J. Plant Res.* 130, 67–73. doi: 10.1007/s10265-016-0894-0

Yan, W. Y., Jian, Y. Q., Duan, S. G., Guo, X., Hu, J., Yang, X. H., et al. (2023). Dissection of the plant hormone signal transduction network in late blight-resistant potato genotype SD20 and prediction of key resistance genes. *Mol. Physiol. Plant Pathol.* 113 (3), 523–538. doi: 10.1094/PHYTO-04-22-0124-R

Zhang, H., Hu, W., Hao, J., Lv, S., Wang, C., Tong, W., et al. (2016). Genome-wide identification and functional prediction of novel and fungi-responsive lincRNAs in Triticum aestivum. *BMC Genomics* 17 (1), 1–11. doi: 10.1186/s12864-016-2570-0

Zhang, H., Yang, Y., Wang, C., Liu, M., Li, H., Fu, Y., et al. (2014). Large-scale transcriptome comparison reveals distinct gene activations in wheat responding to stripe rust and powdery mildew. *BMC Genomics* 15 (1), 898. doi: 10.1186/1471-2164-15-898

Zhang, J. C., Zheng, H. Y., Li, Y. W., Li, H. J., Liu, X., Qin, H. J., et al. (2016). Coexpression network analysis of the genes regulated by two types of resistance responses to powdery mildew in wheat. *Sci. Rep.* 6, 23805. doi: 10.1038/srep23805

Zhu, Y., Li, Y., Fei, F., Wang, Z., Wang, W., Cao, A., et al. (2015). E3 ubiquitin ligase gene CMPG1–V from Haynaldia villosa L. contributes to powdery mildew resistance in common wheat (Triticum aestivum L.). *Plant J.* 84, 154–168. doi: 10.1111/tpj.12966

frontiers | Frontiers in Plant Science

TYPE Original Research
PUBLISHED 27 November 2023
DOI 10.3389/fpls.2023.1283567

Check for updates

OPEN ACCESS

EDITED BY
Xinli Zhou,
Southwest University of Science and Technology, China

REVIEWED BY
Xiaojun Nie,
Northwest A&F University, China
Gang Li,
Nanjing Agricultural University, China

*CORRESPONDENCE
Yingxin Zhang
zhangyingxin1985@126.com
Wenli Wang
wliw@163.com

†These authors have contributed equally to this work

RECEIVED 26 August 2023
ACCEPTED 08 November 2023
PUBLISHED 27 November 2023

CITATION
Wang M, Hong W, Wang Y, Han X, Chen W, Wang S, Zhang Y and Wang W (2023) Identification, characterization and expression analysis of wheat RSH family genes under abiotic stress. *Front. Plant Sci.* 14:1283567. doi: 10.3389/fpls.2023.1283567

COPYRIGHT
© 2023 Wang, Hong, Wang, Han, Chen, Wang, Zhang and Wang. This is an open-access article distributed under the terms of the Creative Commons Attribution License (CC BY). The use, distribution or reproduction in other forums is permitted, provided the original author(s) and the copyright owner(s) are credited and that the original publication in this journal is cited, in accordance with accepted academic practice. No use, distribution or reproduction is permitted which does not comply with these terms.

Identification, characterization and expression analysis of wheat RSH family genes under abiotic stress

Mengru Wang[1†], Wei Hong[1†], Youning Wang[2†], Xiaowen Han[1], Wang Chen[1], Shuping Wang[1], Yingxin Zhang[1*] and Wenli Wang[3*]

[1]Ministry of Agriculture and Rural Affairs (MARA) Key Laboratory of Sustainable Crop Production in the Middle Reaches of the Yangtze River (Co-Construction by Ministry and Province), College of Agriculture, Yangtze University, Jingzhou, China, [2]Hubei Key Laboratory of Quality Control of Characteristic Fruits and Vegetables, Hubei Engineering University, Xiaogan, Hubei, China, [3]College of Plant Protection, North West Agriculture and Forestry (A&F), University, Yangling, Shaanxi, China

Guanosine pentaphosphate and guanosine tetraphosphate are collectively called (p)ppGpp (Guanosine tetraphosphate and pentaphosphate). (p)ppGpp content in plants is affected by conditions such as light, salt, pH, UV light, and environmental phytohormones. The synthesis and hydrolysis of (p)ppGpp in plants is accomplished by a class of proteins called RSH (RelA/SpoT homologs). To date, a systematic and comprehensive genome-wide analysis of the RSH gene family in wheat and its closely related species has not been conducted. In this study, 15, 14, 12, and 8 members of RSH were identified in wheat (*Triticum aestivum*), *Triticum dicoccoides*, *Triticum urartu* and *Aegilops tauschii* respectively. Based on the conserved structural domains of the RSH genes, the *TaRSHs* have been categorized into *TaRSH* and *TaCRSH*. The gene duplications in the TaRSH gene family were all identified as segmental duplications indicating that the TaRSH family plays a significant role in expansion and that segmental duplications maintain a degree of genetic stability. Through the analysis of transcriptome data and RT-qPCR experiments, it was observed that the expression levels of TaRSHs were upregulated in response to abiotic stress. This upregulation suggests that TaRSHs play a crucial role in enhancing the resilience of wheat to adverse environmental conditions during its growth and development. Their increased expression likely contributes to the acquisition of stress tolerance mechanisms in wheat. Especially under NaCl stress, the expression levels increased most significantly. The more detailed systematic analysis provided in this article will help us understand the role of *TaRSHs* and provide a reference for further research on its molecular biological functions in wheat.

KEYWORDS

RSH genes, bioinformatics, RT-qPCR, transcriptome analysis, abiotic stress

1 Introduction

Wheat (*Triticum aestivum*) is a herbaceous plant and a cereal crop widely grown around the world. The safe and stable production of wheat is crucial for ensuring food security (Albahri et al., 2023). However, wheat quality and yield are often affected by abiotic stresses including drought, saline-alkali, and extreme temperatures during growth and development (Yin et al., 2018), As a consequence, it is of great importance for wheat genetic improvement to explore stress resistance-related genes and screen wheat germplasm resources with high resistance (Kosová et al., 2014).

When living organisms are under environmental stress, they can regulate their metabolism to slow down their metabolic activity, save resources, and resist adverse conditions (Rossnerova et al., 2020). The strict response is a kind of stress signaling system in response to nutritional deprivation (Irving et al., 2021). It has the ability to and promote cell survival under challenging environmental circumstances (Braeken et al., 2006). Guanosine tetra- and pentaphosphate, commonly known as (p)ppGpp or alarmones, are key molecules involved in the strict response. They are synthesized and hydrolyzed by proteins belonging to the RSH superfamily, which are homologues of RelA/SpoT proteins (Sinha and Winther, 2021). The strict response was first identified in bacteria and it is marked by the accumulation of (p)ppGpp molecules synthesized by RelA/SpoT (Jain et al., 2006).

For the past few years, with the evolution of genomics, RSH has been identified in *Arabidopsis thaliana* (van der Biezen et al., 2000), *Nicotiana tabacum* (Givens et al., 2004), *Oryza sativa* (Du et al., 2019), *Brassica napus* (Dąbrowska et al., 2021) and other plants. Furthermore, previous research has shown that RSH plays a vital role in plant response to biotic/abiotic stresses. The expression level of *AtRSH2* was significantly increased under salt stress (Mizusawa et al., 2008). Abscisic acid (ABA) is a plant hormone involved in signals transduction under environmental stress (Nakashima and Yamaguchi-Shinozaki, 2013), which can induce the *AtRSH2* expression (Mizusawa et al., 2008). Takahashi study has been found that mechanical damage can down-regulate the expression level of *AtRSH1* while up-regulate that of *AtRSH2* (Takahashi et al., 2004). In *O. sativa*, Du's study found that the expression of *OsRSHs* are induced to varying degrees by abiotic stresses such as salt, low temperature, high temperature, and mechanical damage (Du et al., 2019). In *Brassica napus*, the expression of *BnRSHs* remains unaffected by salt stress. However, when exposed to PGPR bacteria, particularly *Serratia* sp., there is a notable increase in the expression of *BnRSHs* (Dąbrowska et al., 2021).

So far, there are no studies have systematically studied the RSH gene family in wheat. To conduct a comprehensive analysis of the wheat RSH gene family and elucidate the expression patterns of *TaRSHs* under abiotic stress, this study employed bioinformatics techniques to analyze the *TaRSH* genes. In the end, we successfully identified 15 *TaRSH* genes and conducted a comprehensive analysis of their phylogeny, protein characteristics, structural features, chromosomal distribution, transcriptome profiling, promoter analysis, Subcellular localization analysis, and their expression patterns under various abiotic stress conditions. This study elucidates the functional genes within the wheat RSH gene family, thereby yielding significant insights that pave the way for further in-depth exploration of their biological roles. The findings offer valuable information that can guide future research endeavors aimed at unraveling the intricate molecular mechanisms and regulatory networks associated with the *RSH* genes in wheat.

2 Materials and methods

2.1 Identification of RSH genes in *T. aestivum*

The wheat reference genome, IWGSC RefSeqv2.1, was acquired from Ensembl Plants database (http://plants.ensembl.org/index.html) through a download procedure. The Hidden Markov Model of RelA/SpoT (RSH) homologs (PF04607) was retrieved from Pfam database (http://pfam.xfam.org/) via a download process. And the RSH protein sequences were collected from relevant literature reports and other species databases, including four *Arabidopsis thaliana* RSHs (AtRSHs) (van der Biezen et al., 2000), six *Oryza sativa* RSHs (OsRSHs), four *Solanum lycopersicum* (SlRSHs) and eight *Zea mays* (ZmRSHs). The obtained protein sequences were employed as reference sequences to identify potential TaRSHs by performing BLASTp searches (e-value <$1e^{-5}$) against the wheat protein database (Jiang et al., 2020). Then the protein sequences containing RelA/SpoT protein domain were detected through the Pfam (v35.0, http://Pfam.xfam.org) and InterProScan (v94.0, http://www.ebi.ac.uk/InterProScan). After eliminating the redundant and incompletely annotated sequences, the finally retained genes were identified as the members of wheat RSH family. Moreover, the *RSH* genes of the other nine wheat cultivars were obtained by blast in the 10+ Wheat Genome Project database (https://galaxy-web.ipk-gatersleben.de/).

2.2 Phylogenetic analysis of RSHs

The multiple sequence alignment of the identified RSHs were analyzed by ClustalW2 in MEGA 11 software (Polyakova et al., 2022). The phylogenetic tree containing TaRSHs, AtRSHs (van der Biezen et al., 2000), OsRSHs (Du et al., 2019), SlRSHs and ZmRSHs was constructed by neighbor-joining method (1000 bootstrap replicates) and modified by iTol online tool (Interactive tree of Life, http://ITOL.embl.de). The original name of SlRSHs and ZmRSHs are shown in Supplement File Table S1. TaRSHs were named according to the phylogenetic relationships and pfam conserved domains. And the Phylogenetic tree for the RSHs in Chinese spring and nine other wheat cultivars (SY Mattis, CDC Stanley, CDC Landmark, Norin 61, PI190962 (spelt wheat), LongReach Lancer, Julius and Jagger) were also constructed using the above methods.

2.3 Chromosomal location, collinearity, and Ka/Ks analysis of TaRSHs

The gene annotation information of *TaRSHs* was extracted from IWGSC v2.1 GFF3 file. The start and end location information about *TaRSHs* in correspondence chromosomes were used to draw the physical map via the MapInspect software (Song and Peng, 2019). The homologous gene pairs between *TaRSHs* and the reference genomes of *T. aestivum*, *T. urartu*, *T. dicoccoides*, and *Ae. Tauschii* (Nan et al., 2018) were identified by BLASTp (e-value<10^{-10}, similarity>80%). The non-synonymous replacement rate (Ka), synonymous replacement rate (Ks) and Ka/Ks values among the *RSHs* gene pairs from the four species were calculated by TBtools (Chen et al., 2020). Finally, the interspecific collinearity map was drawn by TBtools, and the scatter map of Ka/Ks values was drawn by Excel. Collinearity analysis between wheat and between wheat and rice calculated with TBtools.

2.4 Analysis of the conserved domains and motifs of TaRSHs

The exon/intron structures of *TaRSH* genes were precisely delineated by employing TBtools, utilizing the comprehensive information from the GFF3 gene structure annotation (Chen et al., 2020). Conserved motifs within *TaRSH* genes were identified by employing the MEME (version 5.5.1, http://meme-suite.org/tools/meme). The motif sequence are shown in Supplement File Table S2.

The analysis was conducted with the following parameters: allowing each sequence to contain an arbitrary number of non-overlapping motifs, identifying a total of 10 distinct motifs, and considering motif widths ranging from 10 to 100 amino acids. This approach facilitated a comprehensive investigation of conserved motifs within *TaRSH* genes.The protein motif structure was mapped using TBtools. TaRSH conserved domain information was obtained from the pfam website and the results were visualized by TBtools.

2.5 Protein characterization and three-dimensional homology modeling of TaRSH

The protein fundamental characteristics of TaRSHs, such as protein molecular weight (MW), sequence length (Len), total hydrophilicity (GRAVY) and isoelectric point (pI), were assessed utilizing the ExPASy Server10 (https://prosite.expasy.org/PS50011). This analysis facilitated a comprehensive examination of the essential properties of the TaRSH proteins (Wilkins et al., 1999). To determine the subcellular localization of *TaRSH* genes, the Plant-mPLoc tool (http://www.csbio.sjtu.edu.cn/bioinf/Plantmulti) was employed. his computational approach enabled the prediction of the precise cellular compartments within plant cells where these TaRSH proteins are expected to be localized (Fang et al., 2020). The three-dimensional (3D) structure of TaRSHs was computationally modeled using SWISS-MODEL (https://www.swissmodel.expasy.org/).

2.6 *cis*-element analysis and protein-protein interaction network

In order to identify the *cis*-elements in the promoter sequence of the *TaRSH* genes, the upstream sequences (1-1500 bp) of *TaRSHs* were extracted from the wheat genome, and were uploaded to the PlantCARE (http://bioinformatics.psb.ugent.be/webtools/plantcare/html/plant) to identify *cis*-elements (Lescot et al., 2002). Then, the prediction result was displayed using the R package "pheatmap" (Hu, 2021). The model protein interaction networks of TaRSHs are predicted through STRING database (http://string-db.org) (Szklarczyk et al., 2015). The minimum interaction score required is set to a high confidence level (0.700); the maximum number of interactive displays no more than 10 on the first housing, the display is not more than 10 on the second housing. Then the visual image is exported from its website.

2.7 TaRSHs expression pattern analysis

Wheat transcriptome sequencing datas (PRJEB25639, PRJEB23056, PRJNA436817, SRP133837, PRJEB25640, and PRJEB25593) were downloaded from the NCBI-SRA database and were mapped to the wheat reference genome using Hisat (Ramírez-González et al., 2018). The *TaRSHs* expression level were calculated by Cufflinks (normalized as TPM value) (Trapnell et al., 2012). Expression patterns of TaRSHs under different conditions were heatmapped using Log_2(TPM+1) values by R package pheatmap.

2.8 Targeting relationship prediction between miRNAs and TaRSHs

To identify miRNAs targeting to *TaRSHs*, the *TaRSHs* CDS sequences were uploaded to the psRNATarget online website (https://www.zhaolab.org/psRNA/) to determine the potential targeting relationships between *TaRSHs* and miRNAs (Dai et al., 2018). Afterwards, the results were visualized using R package "ggplot2" and "ggalluvial".

2.9 Growth and stress treatments at the seedling stage of wheat

Wheat (Yangmai 20) seeds were sterilized by immersing them in a 1% sodium hypochlorite solution. Then, seeds were thoroughly rinsed with double distilled water. Subsequently, sterilized seeds were placed onto petri dishes layered with two sheets of saturated filter paper, and cultured for 2 days at a temperature of 25°C (Zhang et al., 2019). The germinated seeds were transferred to petri dishes containing a 1/4 strength Hoagland solution. After 3 days, the concentration of the Hoagland solution was increased to 1/2 strength. The growth conditions during the experiment are as follows: a 16-hour light period followed by an 8-hour dark

period, a temperature was maintained at 25°C (Yang et al., 2022). At the one-leaf and one-heart stage of growth, the wheat seedlings were exposed to solutions of 150 mM NaCl, 20% PEG6000 and 100 µm ABA, while distilled water (ddH_2O) was used as a control. Samples of leaf and root tissues were collected at specific time points, including 2, 12, 24, 48, 72 and 120 hours after the treatment initiation (Sahin et al., 2015).

2.10 RNA extraction and RT-qPCR analysis

With the aim of show the specific expression profile of *TaRSHs* in wheat tissues and during development, RT-qPCR was performed to detect the expression level of *TaRSHs*. Total RNA was extracted using the TRizol reagent (Life, USA). RNA was subjected to reverse transcription using RevertAid Reverse Transcriptase (Vazyme, Nanjing, China), followed by dilution of the resulting cDNA to a concentration of 100 ng/µL using RNase-free water. Real-time quantitative PCR (RT-qPCR) was performed on the CFX 96 Real-Time PCR system (Bio Rad, Hercules, CA, USA) using ChamQ SYBR qPCR Master Mix (Vazyme, Nanjing, China). The 20 µL RT-qPCR reaction system was consisted of 10 µL 2 × SYBR Premix Extaq, 1 µL of each primer (10 µM), 2 µL template (approximately 100 ng/µl) and 6 µl ddH_2O. The procedure is as follows: denaturation at 95°C for 30 s (step 1), denaturation at 95°C for 5 s (step 2), primer annealing/extension and fluorescence signal collection at 60°C for 20 s (step 3). The next 40 cycles start in step 2. Three biological replicates were performed for each sample, and three technical repeats were performed for each replicate. Relative expression levels were determined with the $2^{-\Delta\Delta Ct}$ method (Livak and Schmittgen, 2001). ADP-ribosylation factor *Ta2291* whose expression was stable under various conditions, was used as an internal reference gene for RT-qPCR analysis. The primers shown in Supplement File Table S3.

2.11 Subcellular localization analysis of TaRSH2.7

To validate the subcellular localization of TaRSH2.7, the full length of TaRSH2.7 was amplified by 2 × Phanta Max Master Mix (Vazyme, Nanjing, China). The TaRSH2.7 sequences were recombined into 16318:TaRSH2.7:GFP vector with the restriction enzymes BamHI (NEB, Beijing, China) and ClonExpress II One Step Cloning Kit (Vazyme, Nanjing, China). Protoplasts were prepared from 30 healthy and tender wheat (Yangmai 20) leaves that grew for seven days. For the preparation method, refer to the wheat protoplast preparation and transformation kit (Coolaber, Beijing, China) (Liu et al., 2017). Observation with fluorescence microscopy (Nikon, Japan) 16 h after transformation.

3 Results

3.1 Identification and phylogenetic analysis of RSH members

By employing a comprehensive bioinformatics approach, a total of 15 *RSH* genes were identified within the wheat genome. Aiming to study the evolutionary relationship of RSH genes of *T. aestivum*, *A. thaliana*, *O. sativa*, *S. lycopersicum* and *Z. mays*. a phylogenetic tree was constructed based on their amino acid sequence comparison. As illustrated in Figure 1A, based on the phylogenetic relationship and conserved domain, the 15 TaRSH proteins were named as TaRSH1.1 to TaRSH1.3, TaRSH2.1 to TaRSH2.6, and TaCRSH1 to TaCRSH3. The identified *TaRSH* genes were classified into three distinct groups: Group I contained three members, Group II contained three ones, and Group III contained nine members. In addition, all of the 15 TaRSHs possess RelA_SpoT and HD domain. Among them, TaRSH1.1, TaRSH1.2,

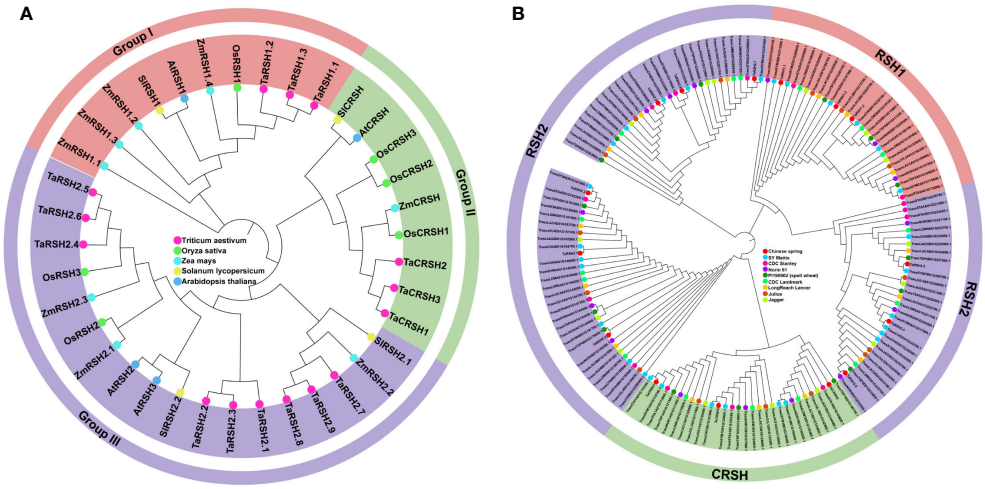

FIGURE 1
Phylogenetic analysis. **(A)** Phylogenetic analysis of *Triticum aestivum*, *Oryza sativa*, *Arabidopsis thaliana*, *Solanum lycopersicum* and *Zea mays* RSHs. **(B)** Phylogenetic analysis of Chinese spring, SY Mattis, CDC Stanley, CDC Landmark, Norin 61, PI190962 (spelt wheat), LongReach Lancer, Julius and Jagger RSHs.

and TaRSH1.3 belonging to Group I, contain TGS domain, which is a unique domain in Group I. TaCRSH1, TaCRSH2, and TaCRSH3 are members of Group II and possess the EF-Hand domain, which is a distinctive domain found exclusively in Group II (Figure 2). As shown in Figure 1B, phylogenetic analyses showed that the number and grouping of *RSH* genes in the cultivars were consistent with those of Chinese Spring, except for ArinaLrFor (No hits found), SY mattis (30) and CDC stanley (14, and lacked a RSH1).

3.2 Protein characterization and three-dimensional structure of TaRSHs

As shown in Table 1, protein characterization revealed that the amino acid number of TaRSHs with a distribution range of 534-899 aa, and the molecular weight with a distribution range of 58.85-98.91 kDa. The mean isoelectric point was pI of 6.78 with a distribution range of 6.03-7.62. The distribution range of instability index was 39.71-50.06, except for TaRSH1.2, other TaRSHs belonged to unstable proteins. The mean value of hydrophilicity was -0.26 and the distribution range was -0.39~-0.13. All the values of hydrophilicity were less than 0, These findings suggest that TaRSHs exhibit hydrophilic properties, indicating their tendency to interact with water molecules.

Subcellular localization prediction analysis revealed that TaCRSH2, TaCRSH3, TaRSH2.2, TaRSH1.1, TaRSH1.2, TaRSH1.3, TaRSH2.7, TaRSH2.8, TaRSH2.9 were distributed in chloroplasts, while TaCRSH2 may be distributed in the cell membrane, and TaCRSH3, TaRSH2.4, TaRSH2.5 and TaRSH2.2 may be distributed in mitochondria; TaRSH2.4, TaRSH2.5, and TaRSH2.6 were distributed in peroxisome. In addition, TaCRSH1 is localized only in the cell membrane, while TaRSH2.1 is localized only in the nucleus.

Three-dimensional homology modelling of TaRSHs was analyzed by SWISS-MODEL. As shown in Figure 3, all TaRSHs mainly consisted of α-helix, β-turn, random coil and extended strand. The proportion of these four structures in TaRSHs proteins varied, with α-helix accounting for the largest proportion (48.16%-58.43%), followed by Random coil (24.57%-37.33%), Extended strand (8.96%-16.64%), and the smallest proportion of β-turns (5.62%-9.76%). The Group II has the least amount of α-helix (47.55%), and the most amount of Extended strand (14.11%), β-turns (8.27%) and Random coil (30.08%).

3.3 Gene structure, motif and conserved domain analysis of TaRSHs

The structural diversity of exons and introns frequently influences the evolutionary trajectory of gene families, offering supplementary evidence that strengthens the phylogenetic clustering. (Shiu and Bleecker, 2003; Wang et al., 2014). In order to understand the structure characteristics of *TaRSHs*, the exon-intron structure of *TaRSH* genes was analyzed using GFF3 annotation of wheat. The gene structure of *TaRSH* gene has a relatively complex structure (Figure 2). Furthermore, the intron number of *TaRSH* ranging from 3-23. TaRSH1.3 contains 24 exons, while *TaCRSHs* only contains 3 exons of different lengths. The exon-intron structure shows that most *TaRSHs* have UTR non-coding regions at both ends of the sequence, and only *TaRSH2.5*,

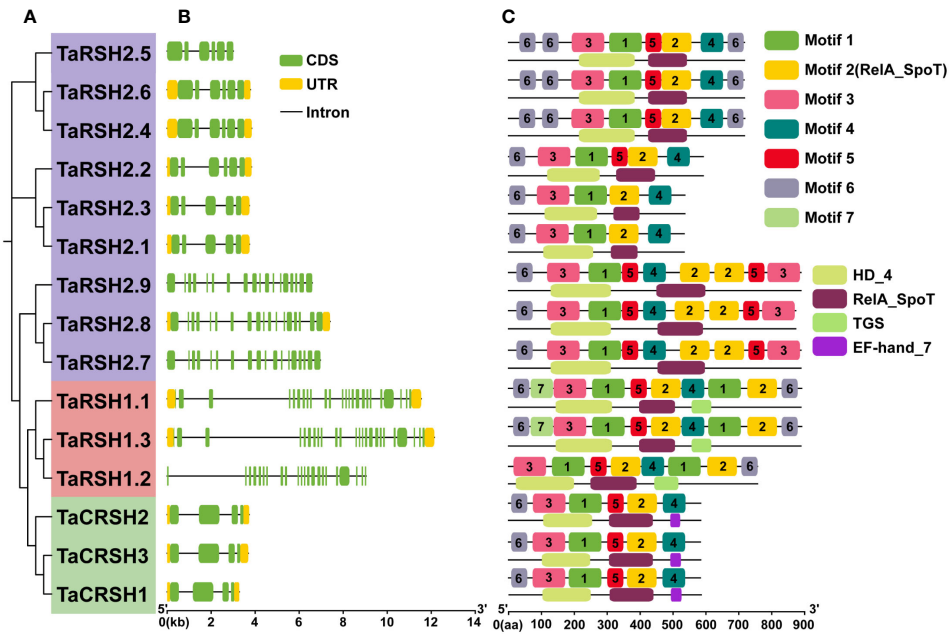

FIGURE 2
Exon–intron structure and conserved domain and motif analyses. **(A)** Phylogenetic tree of 15 TaRSHs; **(B)** Exon–intron analysis of 15 TaRSHs, the yellow and green box represent untranslated region (UTR) and coding sequence (CDS), and the black line represents intron. **(C)** Motif analysis of TaRSHs, Motifs were represented in different colors.

10.3389/fpls.2023.1283567

TABLE 1 The specific details of TaRSH protein characterization.

Name	Gene ID	Length[1]	MW[2]	pI[3]	Ins[4]	GRAVY[5]	Sub[6]
TaCRSH1	TraesCS1A03G0255000.1	582	64.18	6.74	44.55	-0.308	Cell membrane
TaCRSH2	TraesCS1B03G0355400.1	584	64.22	6.63	42.59	-0.258	Chloroplast
TaCRSH3	TraesCS1D03G0258800.1	583	64.21	6.61	44.41	-0.290	Cell membrane Chloroplast
TaRSH2.1	TraesCS2A03G0355800.1	534	58.85	7.06	49.27	-0.298	Cytoplasm Mitochondrion Nucleus
TaRSH2.2	TraesCS2B03G0475100.1	592	65.57	7.62	48.71	-0.318	Mitochondrion
TaRSH2.3	TraesCS2D03G0372500.1	536	59.12	7.30	50.47	-0.285	Chloroplast Mitochondrion
TaRSH1.1	TraesCS4A03G0311500.3	891	98.90	7.13	41.59	-0.223	Chloroplast
TaRSH1.2	TraesCS4B03G0469400.1	759	85.06	6.03	39.71	-0.205	Chloroplast
TaRSH1.3	TraesCS4D03G0420700.2	891	98.91	7.31	42.83	-0.229	Chloroplast
TaRSH2.4	TraesCS5A03G0543300.1	718	78.80	6.19	48.67	-0.374	Peroxisome
TaRSH2.5	TraesCS5B03G0552800.1	717	78.84	6.15	49.77	-0.369	Mitochondrion Peroxisome
TaRSH2.6	TraesCS5D03G0507200.1	716	78.79	6.28	50.06	-0.388	Mitochondrion Peroxisome
TaRSH2.7	TraesCS6A03G0717200.1	889	97.89	6.89	49.09	-0.132	Chloroplast
TaRSH2.8	TraesCS6B03G0851000.1	873	96.02	6.75	48.51	-0.153	Chloroplast
TaRSH2.9	TraesCS6D03G0600800.1	899	97.96	7.07	48.82	-0.137	Chloroplast

[1](Amino acid length, aa); [2](Molecular weight, KD); [3](Isoelectric point); [4](Instability index); [5](Grand average of hydropathy); [6](predicted subcellular location.

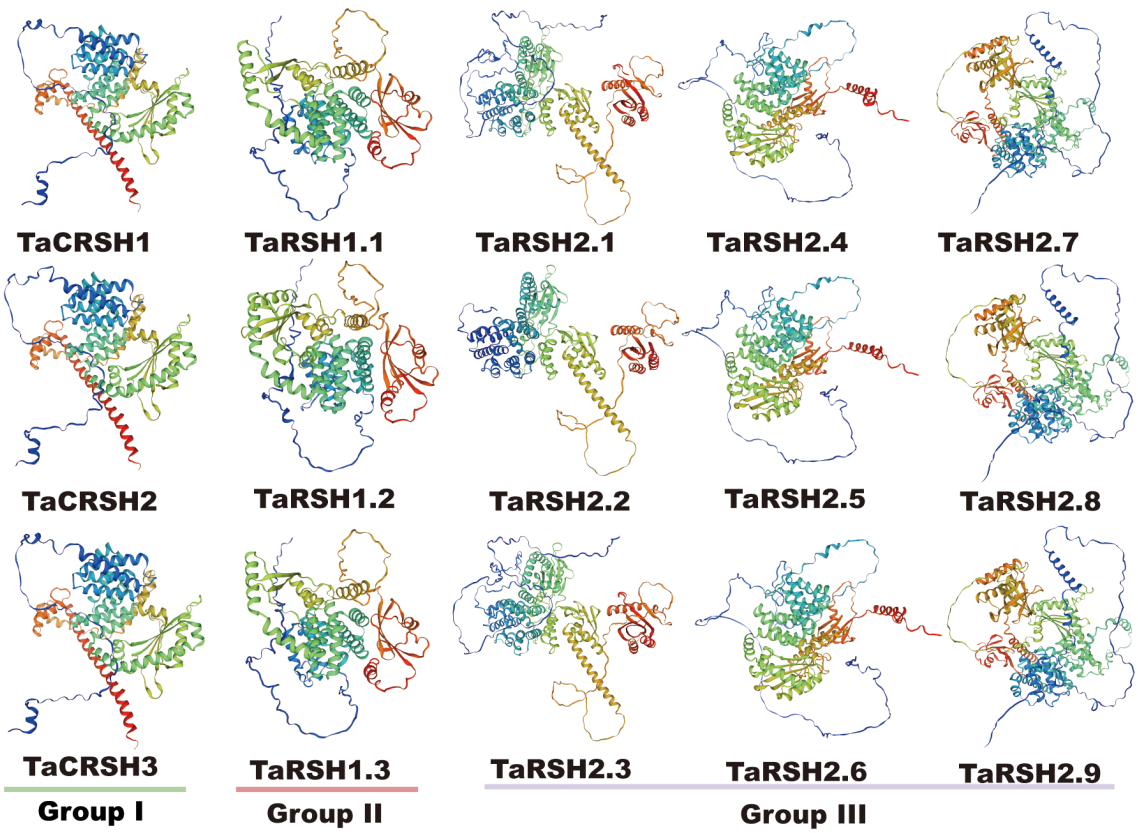

FIGURE 3
Predicted 3D models of TaRSHs. Models were generated by using SWISS-MODEL.

TaRSH2.7, *TaRSH2.9*, and *TaRSH1.2* have no UTR, indicating that the TaRSH family sequence is highly conserved.

Conservative motif analysis revealed that seven kinds of Motifs were identified from TaRSHs, among which TaRSH2.1 and TaRSH2.3 contained the least number of Motifs (four); TaRSH1.1 and TaRSH1.3 contained the most Motifs (10). By integrating phylogenetic analysis, it was observed that TaRSHs exhibiting a higher degree of relatedness also displayed a greater consistency in their motif composition. As shown in Figure 2, structural domain analysis revealed that Motif 2 contains the RelA_SpoT structural domain, which constitutes the key functional structural domain of RSH. There were additional motifs identified that did not exhibit a match with known key functional structural domains. The intricate and diverse structure of the *TaRSH* gene suggests its potential involvement in numerous crucial biological processes in plants.

3.4 Chromosomal mapping, collinearity and Ka/Ks analysis of *RSH* genes

Based on the gene structure annotation information of TaRSHs, a chromosome distribution map was generated using MapInspect software. As exhibited in Figure 4A, 15 *TaRSHs* are evenly distributed on 15 chromosomes, and each sub-genome contains 5 *TaRSHs*. It is crucial of Tandem duplication and segmental duplication for the evolution of gene families (Liu et al., 2021). Through analysis of sequence similarity and chromosome positioning, it was observed that among the 15 *TaRSH* genes, a total of 13 pairs exhibited fragment duplications, whereas no tandem duplication events were detected. The findings indicate that the expansion of the RSH gene family in *T. aestivum* during evolution can primarily be attributed to fragment duplications (Figure 4B).

Through BLASTp analysis, 14, 12, and 8 *RSH* genes were identified from the reference genomes in *T. urartu, T. dicoccoides, and A. tauschii*. The Ka/Ks ratios for non-synonymous substitution rates (Ka) and synonymous substitution rates were calculated using TBtools. The results of Ka/Ks analysis revealed that all homologous gene pairs exhibited values below 1, indicating a notable presence of strong purifying selection pressure acting on the *RSH* gene within wheat species (Figure 4C). Based on the sequence similarity and chromosome position, a total of 13 pairs of fragment duplications were found among 15 *TaRSHs*, while no tandem duplication event was identified (Figure 4D).

3.5 *Cis*-acting element analysis of *TaRSHs*

Cis-elements are one of the important factors in the modulation of gene expression. They are involved in regulating the expression of relevant genes for growth and developmental processes and adaptation to environmental changes (Liu et al., 2013). As indicated in Figure 5, 40 kinds of *cis*-elements were identified in total. In addition to a significant repertoire of fundamental components, such as TATA box and CAAT box, there are also many light response and hormone response elements. Among them, light responsive element includes 23 types, such as G-box, GA1 motif, Sp1, and MRE. Hormone response elements include regulatory gibberellin (GARE-motif, TATC-box and P-box), auxin (AuxRR-core and TGA-element), abscisic acid (ABRE), salicylic acid (TCA-element), and methyl jasmonate response element (TGACG-motif and CGTCA-motif), with abscisic acid and methyl jasmonate response element in the majority. Meanwhile, it also includes growth and development related *cis*-elements that circadian rhythm (circadian), meristem expression (CAT-box), and endosperm expression (GCN4_motif). In addition, anaerobic induction (ARE), anoxic specific inducibility (GC-motif), low-temperature (LTR), drought inducibility (MBS), wound responsive element (WUN-motif), and defense and stress responsiveness (TC-rich repeats) element also exist in the *TaRSHs* promoter region.

3.6 Protein interaction network analysis of TaRSHs

Functional and physical interactions of TaRSH proteins were revealed with STRING software by association modelling. The protein interaction results (Figure 6) showed that TaRSH2.1, TaRSH2.2 and TaRSH2.3 may have potential interactions with Traes_2AS_128CFF290.2, while TaRSH2.4, TaRSH2.5 and TaRSH2.6 interact with Traes_5DL_D4DB081FF.1. TaRSH2.7, TaRSH2.8 and TaRSH2.9 have a low probability of interacting with Traes_6DL_9DFF7CA97.1. And the likelihood of TaRSH2.8 and Traes_6BL_A652B6412.2 interoperating is also low. We will follow up with yeast two-hybrid experiments to verify the accuracy of this result and explore their potential mutualistic networks even further.

3.7 Transcriptome analysis unveiled diverse expression patterns exhibited by *TaRSH* genes

The analysis of expression patterns revealed that *TaRSH* genes exhibit diverse and distinct patterns of gene expression (Figure 7). During various growth and developmental stages, the expression levels of four *TaRSH* genes (*TaRSH1.3*, *TaRSH2.5*, *TaRSH2.4*, and *TaRSH2.3*) were significantly upregulated, whereas *TaCRSH1* were highly expressed only in the first leaf Seedling stage and the fifth leaf stage. In response to different biotic stresses such as *Zymoseptoria tritici*, *Magnaporthe oryzae*, stripe rust, and *Fusarium graminearum* infection, six *TaRSH* genes (*TaRSH1.1*, *TaRSH1.2*, *TaRSH1.3*, *TaRSH2.1*, *TaRSH2.2*, and *TaRSH2.3*) exhibited pronounced upregulation of their expression levels. In contrast, the expression levels of *TaCRSH1* were specifically upregulated only in response to stripe rust treatment. Under abiotic stress conditions, three *TaRSH* genes demonstrated significant induction, albeit at relatively lower expression levels individually. These findings imply the potential involvement of *TaRSH* genes in the defense response against abiotic stresses in wheat.

10.3389/fpls.2023.1283567

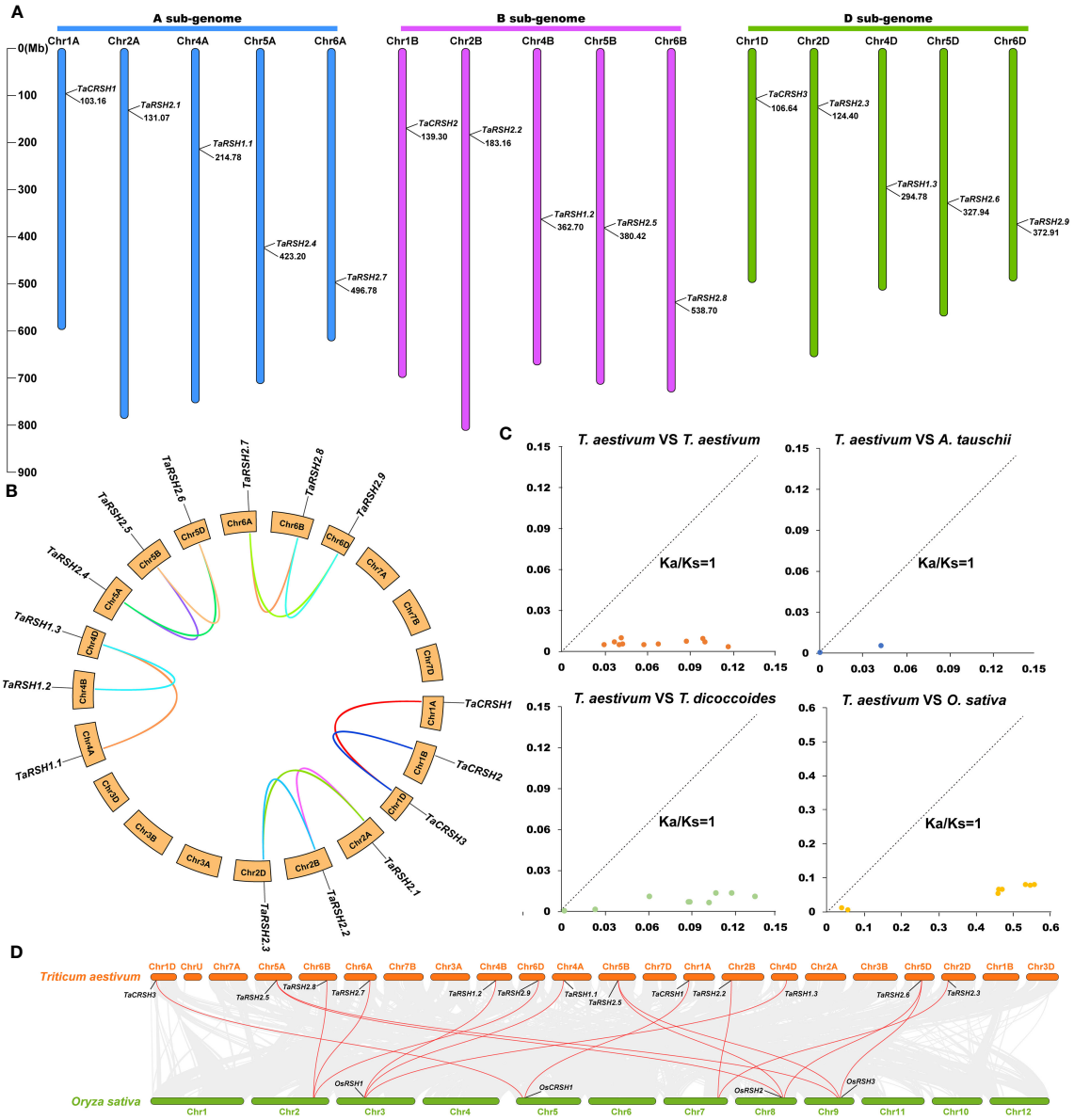

FIGURE 4
Chromosome location on wheat RSH gene and analysis of gene duplication. **(A)** Chromosomal location of 15 *TaRSH* genes in wheat genome. The lines represent gene duplication events. **(B)** TaRSHs collinearity analysis. **(C)** Ka/Ks ratio between RSH genes of Triticum aestivum, Triticum urartu, Triticum dicoccoides and Aegilops tauschii. **(D)** Collinearity analysis between wheat and between wheat and rice.

3.8 MicroRNA targeting analysis of *TaRSH* genes

MicroRNA (miRNA) have important functions in the modulation of gene expression. It can inhibit the degradation of the target gene mRNA or protein translation (Zhu et al., 2019). Consequently, we conducted a comprehensive analysis of potential miRNAs that could potentially target *TaRSH* genes, aiming to elucidate the regulatory mechanisms governing the expression of *TaRSH* genes and provide valuable insights into their regulation in wheat. As shown in Figure 8, 12 wheat miRNAs targeted 15 *TaRSH* genes by cleavage and translational repression, of which 10 miRNAs targeted 15 *TaRSH* genes by cleavage, and only tai-miR9676-5p targeted *TaRSH2.7*, *TaRSH2.8*, and *TaRSH2.9* by translational repression; and tai-miR531 targeted *TaRSH2.8* and *TaRSH2.9* by translational repression. It's worth noting that tae-miR5062-5p only targets Group II members, and members in Group I are only targeted by tae-miR9658-3p, which imply tae-miR5062 and tae-miR9658 may have specificity and selectivity. The analysis showed that multiple miRNAs targeted *TaRSHs* and formed a miRNA-miRNA regulatory network to participate in the post-transcriptional expression regulation of *TaRSHs*.

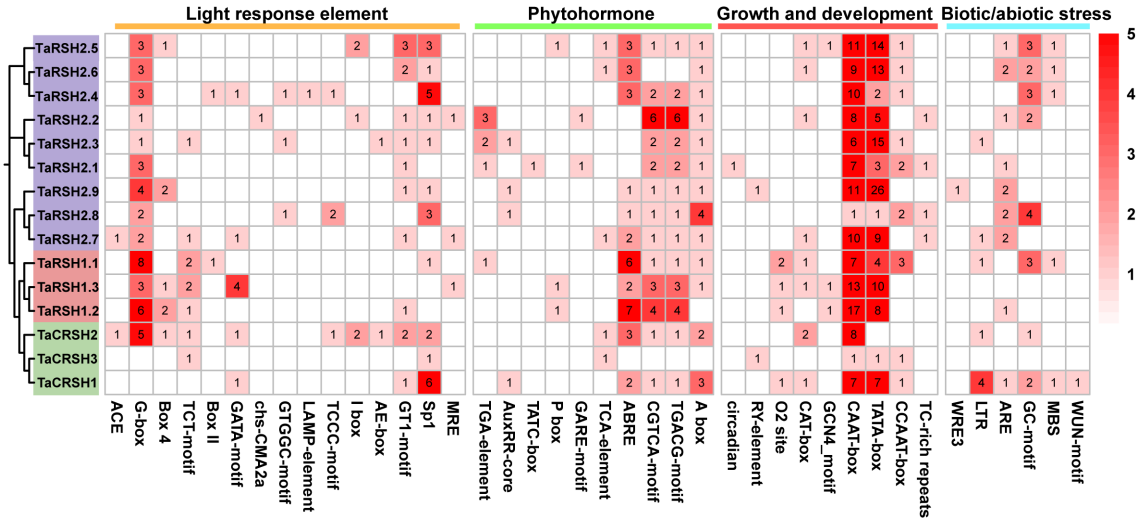

FIGURE 5
Statistical analysis of *cis*-acting elements in the promoter of TaRSH genes. The color and number of the grid represent the number of *cis*-acting elements in corresponding TaRSHs.

3.9 RT-qPCR analysis of *TaRSH* genes

To obtain a comprehensive comprehension of the functional significance of *TaRSH* genes in response to biotic and abiotic stresses, the expression patterns of three selected genes (*TaCRSH2*, *TaRSH2.1*, and *TaRSH2.7*) were analyzed using quantitative real-time PCR (RT-qPCR) in response to drought, ABA, and NaCl stresses (Figure 9).

In the presence of NaCl treatment, the expression patterns of *TaCRSH2* in both roots and leaves demonstrated notable divergence. In roots, the expression of *TaCRSH2* reached the maximum at 24 hours. Whereas in leaves, the maximum expression level was observed at 48 hours. Conversely, *TaRSH2.1* and *TaRSH2.7* showed their highest expression levels at 24 hours in both roots and leaves, implying that *TaRSH2.1* and *TaRSH2.7* exhibit a rapid response to salt stress in both above-ground and below-ground organs.

Under ABA treatment, the expression level of *TaCRSH2* showed a biphasic regulation pattern in roots, being initially down-regulated and subsequently up-regulated with the peak expression occurring at 24 hours. In contrast, in leaves, *TaCRSH2* was up-regulated followed by down-regulation, reaching its lowest expression level at 24 h. Remarkably, TaRSH2.1 and TaRSH2.7 demonstrated robust upregulation in both roots and leaves within 24 hours of ABA treatment, highlighting their rapid response to drought stress.

Under PEG treatment, the expression level of *TaRSH2.1*, *TaRSH2.7* and *TaCRSH2* was significantly upregulated at 2 hours in roots. In leaves, differentially expressed at 2 hours in leaves of *TaRSH2.7* and *TaCRSH2*, which implied that the two genes responded rapidly to drought stress and may play important regulatory roles in the response to adversity.

3.10 Subcellular localization of TaRSH2.7

The predictions of subcellular localization showed that TaRSH2.7 is predicted localization in chloroplast. In order to validate the localization of TaRSH2.7 in the chloroplast, we employed a GFP tagging approach at the C-terminal of the protein and expressed it in wheat protoplasts. As a control, we also included free GFP (Figure 10A). Through fluorescence microscopy, we observed a distinct fluorescence signal specifically localized in the chloroplasts for TaRSH2.7:GFP, further confirming its chloroplast localization (Figure 10B). As a result, Consistent with the predicted results, TaRSH2.7 is localized in chloroplasts, suggesting its potential roles within this organelle.

4 Discussion

The (p)ppGpp not only plays a crucial role in microbial adaptation to adverse environments, but it also serves as a key regulator in plant growth, development, and stress response (Du et al., 2019). At present, genome-wide identification of RSH proteins has been performed in various plant species, including rice, *Arabidopsis*, and *B. napus* (Dąbrowska et al., 2021). Unfortunately, there is a lack of functional studies on wheat RSH, which significantly restricts our understanding of its biological roles and hinders the effective utilization of TaRSH in resistance breeding. Therefore, the systematic identification and analysis of wheat *RSH* gene at the genome level and understanding its expression pattern in drought and salt stresses, can lay the foundation for studying the stress response function of *TaRSH*.

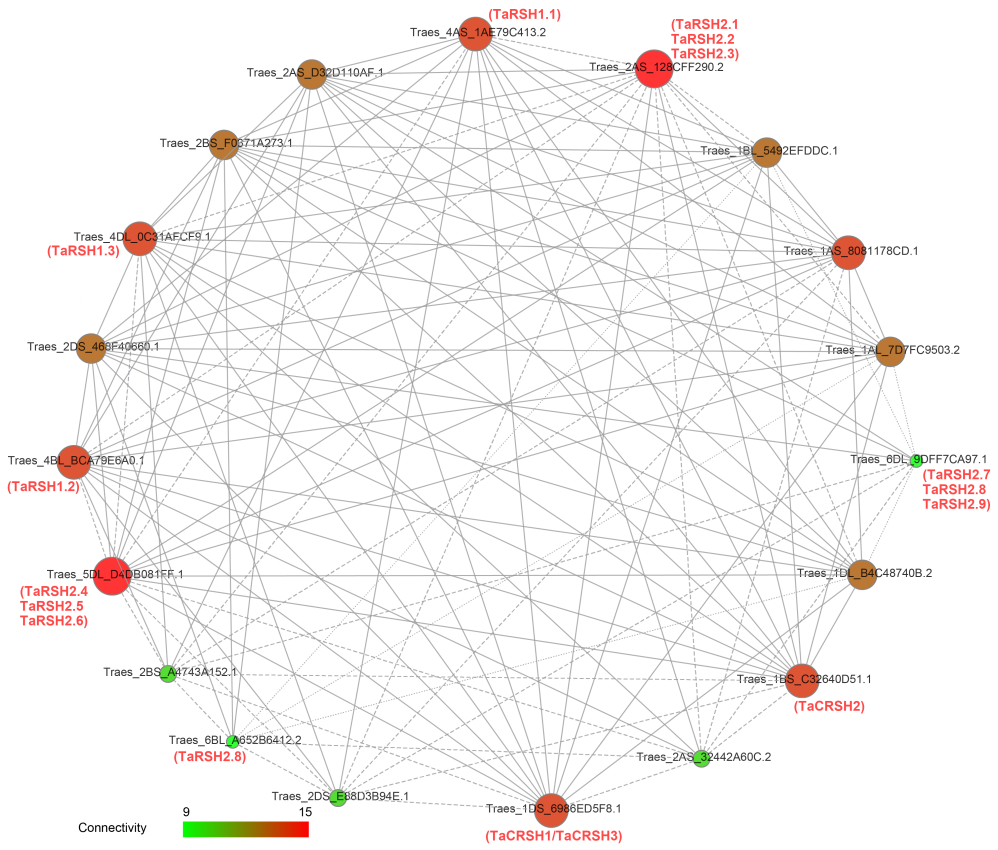

FIGURE 6
Network mapping between wheat RSH proteins. The interaction network between 15 TaRSH proteins and wheat-related transcription factors. The size of the ball and the intensity of the color both represent the intensity of the interaction. Green represents a small effect, and red represents a large effect.

In this study, 15 *TaRSH* family members were identified from the wheat genome, which encoded proteins have a length of 534-899 aa (Table 1), and their protein lengths are similar to those of AtRSHs (558-883 aa) (van der Biezen et al., 2000) and OsRSHs (559-892 aa) (Ito et al., 2022). Meanwhile, combined with phylogenetic relationships and conservative domain analysis, it was found that OsRSHs and TaRSHs were located in the same subgroup exhibiting significant structural similarity. For example, OsRSHs have EF-hand structural domains and are only specifically present in CRSH, which may be involved in Ca^{2+} metabolism or play a crucial role in Ca^{2+} metabolism, and TaCRSHs also contain EF-hand structural domains. So we speculate that TaCRSHs may be

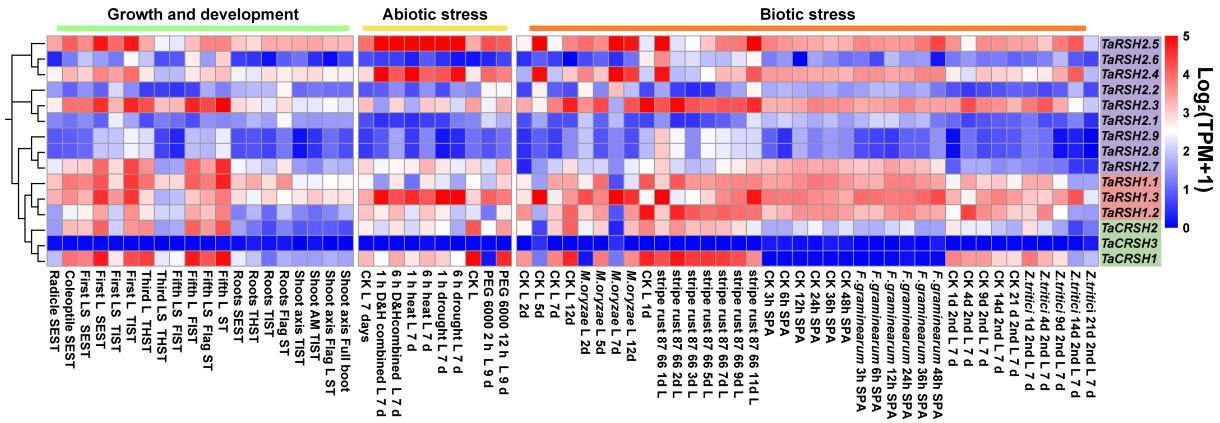

FIGURE 7
Expression pattern profiling of TaRSH genes under growth, development, and biotic/abiotic stresses. L, leaf; LS, leaf sheath; SEST, seeding Stage; TIST, tillering Stage; THST, three leaf Stage; FLST, fifth leaf Stage; SPA, spikelets anthesis; AM, apical meristem.

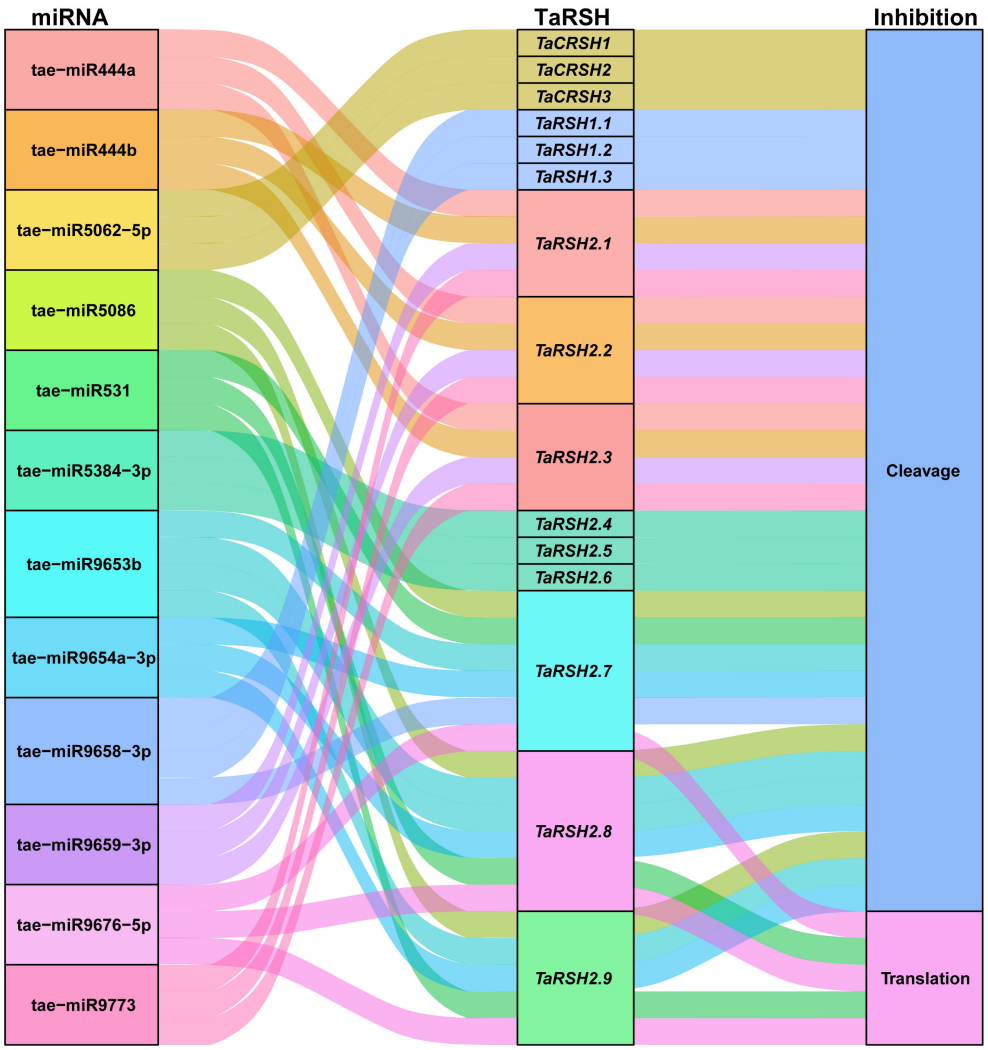

FIGURE 8
Sankey diagram for the targeting relationships between miRNA and ApCAT and corresponding inhibition pattern. The three columns represent miRNA, mRNA, and inhibition pattern.

involved in Ca^{2+} metabolism as well. In addition, OsRSH1 contains a conserved TGS functional domain, which may have a (p)ppGpp hydrolysis function, and TaRSH1 also contains a TGS structural domain, so we speculate that TaRSH1 may also be involved in the hydrolysis of (p)ppGpp (Du et al., 2019).

Segmental duplication and tandem duplication are two primary mechanisms underlying gene copy number variations, subsequently leading to the expansion of plant gene families (Huang et al., 2002). In this study, we identified 13 pairs of segmental duplicated gene pairs based on chromosomal location and collinearity analysis, while no tandem duplication events were detected. Therefore, segmental duplication is considered as the primary mechanism driving the expansion of the wheat *RSH* gene family during the evolutionary process (Li et al., 2022). The Ka/Ks value, also known as the ratio of non-synonymous to synonymous substitution rates, serves as a quantitative indicator for assessing the rate of genetic evolution (Hurst, 2002). The Ka/Ks value of 1 suggests neutral selection, while a Ka/Ks value higher than 1 indicates positive selection leading to accelerated evolution. Conversely, a Ka/Ks value lower than 1 suggests purifying selection due to functional constraints (Kawaura et al., 2009). To further investigate selective pressures, we calculated the Ka/Ks values for inter-specific wheat and wheat with three ancestral wheat homologous gene pairs. The result showed that Ka/Ks values of all homologous gene pairs were all less than 1. This result suggests that *RSH* is highly conserved not only in wheat, but also among ancestral wheat.

The *cis*-regulatory elements in the promoter region are the major factors regulating gene expression, which play a crucial role in regulating the expression of target genes in response to developmental processes and environmental changes (Yin et al., 2020). Previous studies have shown that *OsRSHs* contains a large number of light-responsive elements, and its expression is regulated by light (Du et al., 2019). Similarly, in this study, we observed that *TaRSHs* contain the highest number of light-responsive elements, suggesting a potential correlation between the expression of *TaRSHs* and light conditions. Meanwhile, a variety of elements

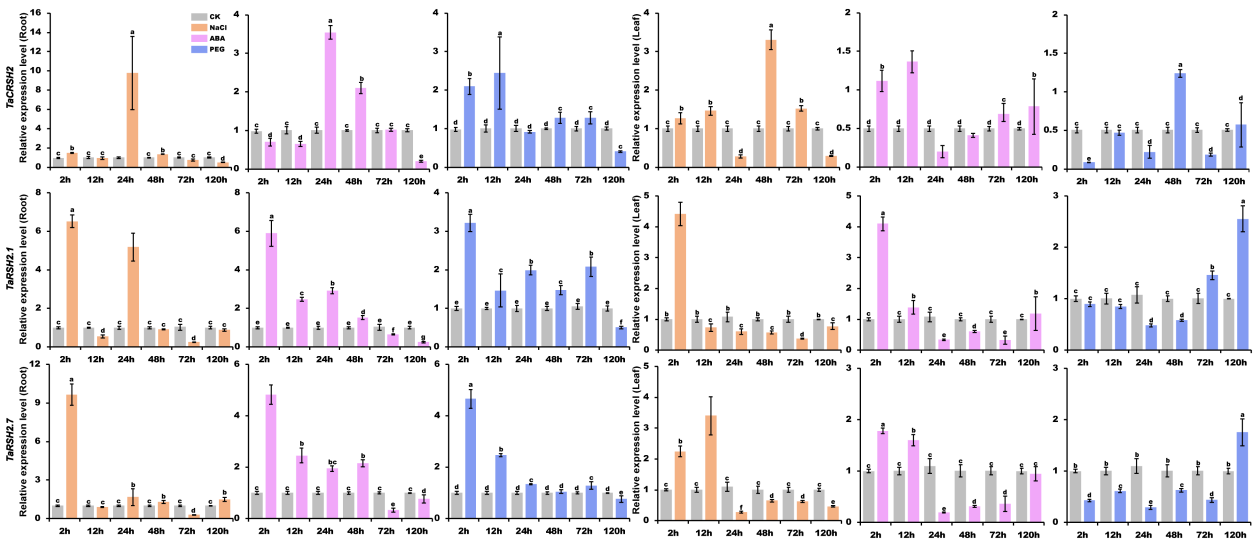

FIGURE 9
Analysis of TaRSH expression under abiotic stress. By using yangmai 20 for quantitative analysis, the treatments performed include 20% PEG, 150 mM NaCl and 100 μM ABA. Different colors represent different stress treatments. The Y axis represents the relative expression level, and the X axis represents the time point after stress treatment. Different letters in a column indicate significant differences between the treatments at $p < 0.05$ level.

related to biotic/abiotic stress response were also detected, which indicate that *TaRSHs* play a role in the stress response. In addition, plant hormone response elements such as abscisic acid (ABRE), jasmonic acid (CGTCA-motif and TGACG-motif), gibberellin (TATC-box) and salicylic acid (TCA-element) were also found in the *TaRSHs* promoter. Related studies have shown that these plant hormones play an important role in plant response to stress. For example, TaIAA15-1A can enhance drought tolerance in *Brachypodium* by regulating abscisic acid signal pathway (Su et al., 2023). Ellen H Colebrook study shows that plants can flexibly adjust the level of gibberellin in response to a variety of stresses, such as salt, drought, cold, shading and submergence (Colebrook et al., 2014). These results further imply that *TaRSHs* have a crucial function in plant response to multiple stresses.

To further reveal the participating roles of *TaRSHs* in different growth and development stages and biotic/abiotic stresses, its expression pattern profiling was performed by mining massive RNA-seq data. The results showed that the expression level of *TaRSHs* in leaves was much higher than that in roots and stems, suggesting *TaRSHs* expression was tissue-specific. This result is consistent with the conclusion that RSH plays a biological role in chloroplasts (Boniecka et al., 2017). Meanwhile, Du's study show that during the initial stages of high-temperature treatment, the relative expression levels of *OsRSH1* are significantly reduced, while *OsRSH2* is significantly induced with expression levels gradually increasing within 6 hours (Du et al., 2019). Similarly, multiple *TaRSHs*, such as *TaCRSH2*, *TaRSH1.1*, and *TaRSH2.3*, were significantly upregulated under high temperature stress within 6 hours. In addition, the expression level of *TaRSHs* is

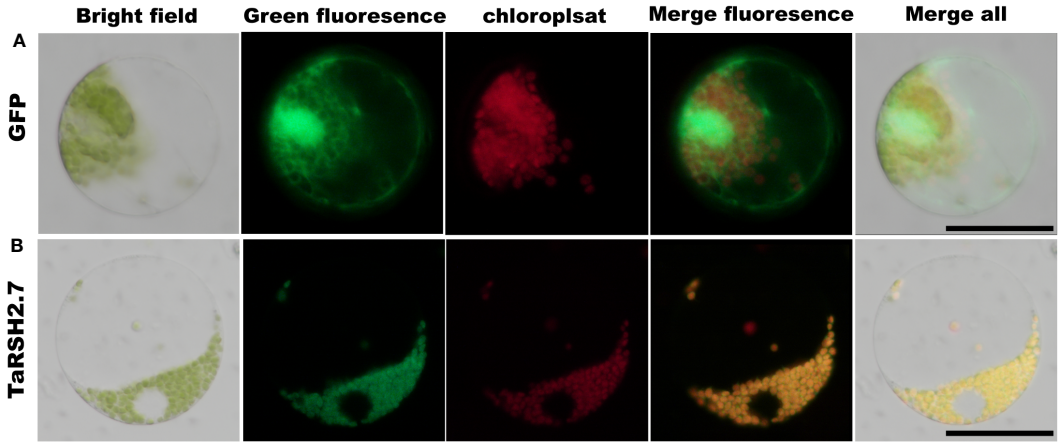

FIGURE 10
Subcellular location analysis of TaRSH2.7 was performed in wheat protoplast. The free GFP was as control **(A)**. TaRSH2.7 is localized on chloroplasts **(B)**. Green fluorescence represents free GFP and TaRSH2.7:GFP fusion protein, while red fluorescence indicates chloroplasts.

also up-regulated to varying degrees by fungal pathogens such as *F. graminearum*, *Z. tritici*, and *M. oryzae*. The above results showed that *TaRSHs* not only participates in the growth and development of wheat, but also plays a positive regulatory role in stress response processes.

To explore the biological function of *TaRSHs* and reveal its expression characteristics in response to abiotic stress, in this study, based on the transcriptomic expression profiling results, three differential expression genes (*TaCRSH2*, *TaRSH2.1*, and *TaRSH2.7*) were selected for further analyzing their expression characteristics under salt and drought. The results showed that the results indicate that under drought, ABA, and salt stress, *TaCRSH2*, *TaRSH2.1*, and *TaRSH2.7* in both leaf and root tissues are induced and upregulated to varying degrees at specific time points, which suggest *TaRSHs* can participate in the response process of wheat to stresses including drought, ABA, and salt. Previous study had shown that *OsRSHs* (Du et al., 2019) and *AtRSHs* (Hirayama and Shinozaki, 2007; Mizusawa et al., 2008) also can be induced by drought, salt, and ABA, which is consistent with our research results.

5 Conclusions

In this study, a total of 15 *RSH* genes were discovered within the wheat genome. These genes were categorized into three distinct groups based on their conserved domains and evolutionary relationships. Interestingly, the 15 *TaRSHs* were found to be evenly distributed among the 15 chromosomes of wheat. Furthermore, the *RSH* gene exhibited a high degree of conservation not only within wheat species but also across its three ancestral wheat species. It was evident that RSH has experienced significant selective pressure, leading to substantial purification during its evolutionary process. Protein characterization showed that TaRSH proteins are mostly hydrophilic unstable acidic protein. The analysis of *cis*-elements and transcriptome show that TaRSH plays a significant role in plant growth, stress response and development. The results of RT-qPCR analysis showed that *TaCRSH2*, *TaRSH2.1* and *TaRSH2.7* participated in the process of wheat response to drought, ABA and NaCl stresses. These studies show that the *RSH* gene family of wheat is closely related to plant growth and development, stress response and plant hormones. At the same time, it is necessary to identify and study functional genes to provide useful information for further exploring the biological functions of the wheat *RSH* gene family.

Data availability statement

The original contributions presented in the study are included in the article/Supplementary Material. Further inquiries can be directed to the corresponding authors.

Author contributions

MW: Writing – original draft, Writing – review & editing. WH: Writing – review & editing. YW: Writing – original draft. XH: Data curation, Formal Analysis, Software, Writing – review & editing. WC: Data curation, Investigation, Writing – original draft. SW: Funding acquisition, Project administration, Writing – original draft. YZ: Methodology, Writing – original draft. WW: Funding acquisition, Writing – review & editing.

Funding

The author(s) declare financial support was received for the research, authorship, and/or publication of this article. This research was supported by the Basic and long term scientific and technological work in agriculture (NAES083PP13) and Sichuan Provincial Science and Technology Plan Project (2022YFS0585).

Conflict of interest

The authors declare that the research was conducted in the absence of any commercial or financial relationships that could be construed as a potential conflict of interest.

Publisher's note

All claims expressed in this article are solely those of the authors and do not necessarily represent those of their affiliated organizations, or those of the publisher, the editors and the reviewers. Any product that may be evaluated in this article, or claim that may be made by its manufacturer, is not guaranteed or endorsed by the publisher.

Supplementary material

The Supplementary Material for this article can be found online at: https://www.frontiersin.org/articles/10.3389/fpls.2023.1283567/full#supplementary-material

References

Albahri, G., Alyamani, A. A., Badran, A., Hijazi, A., Nasser, M., Maresca, M., et al. (2023). Enhancing essential grains yield for sustainable food security and bio-safe agriculture through latest innovative approaches. *Agronomy* 13, 1709. doi: 10.3390/agronomy13071709

Boniecka, J., Prusińska, J., Dąbrowska, G. B., and Goc, A. (2017). Within and beyond the stringent response-RSH and (p)ppGpp in plants. *Planta* 246, 817–842. doi: 10.1007/s00425-017-2780-y

Braeken, K., Moris, M., Daniels, R., Vanderleyden, J., and Michiels, J. (2006). New horizons for (p)ppGpp in bacterial and plant physiology. *Trends Microbiol.* 14, 45–54. doi: 10.1016/j.tim.2005.11.006

Chen, C. J., Chen, H., Zhang, Y., Thomas, H. R., Frank, M. H., He, Y. H., et al. (2020). TBtools: an integrative toolkit developed for interactive analyses of big biological data. *Mol. Plant* 13, 1194–1202. doi: 10.1016/j.molp.2020.06.009

Colebrook, E. H., Thomas, S. G., Phillips, A. L., and Hedden, P. (2014). The role of gibberellin signalling in plant responses to abiotic stress. *J. Exp. Biol.* 217, 67–75. doi: 10.1242/jeb.089938

Dąbrowska, G. B., Turkan, S., Tylman-Mojżeszek, W., and Mierek-Adamska, A. (2021). *In silico* study of the RSH (RelA/spoT homologs) gene family and expression analysis in response to PGPR bacteria and salinity in Brassica napus. *Int. J. Mol. Sci.* 22, 10666. doi: 10.3390/ijms221910666

Dai, X. B., Zhuang, Z. H., and Zhao, P. X. C. (2018). psRNATarget: a plant small RNA target analysis server, (2017 release). *Nucleic Acids Res.* 46, W49–W54. doi: 10.1093/nar/gky316

Du, L. E., Huang, J., Wang, L., Liang, H., Jin, X. W., and Chen, J. (2019). Bioinformatics analysis of rice osRSH gene family. *Mol. Plant Breed.* 17, 7277–7285. doi: 10.13271/j.mpb.017.007277

Fang, Z. W., Jiang, W. Q., He, Y. Q., Ma, D. F., Liu, Y. K., Wang, S. P., et al. (2020). Genome-wide identification, structure characterization, and expression profiling of dof transcription factor gene family in wheat (Triticum aestivum L.). *Agronomy* 10, 294. doi: 10.3390/agronomy10020294

Givens, R. M., Lin, M.-H., Taylor, D. J., Mechold, U., Berry, J. O., and Hernandez, V. J. (2004). Inducible expression, enzymatic activity, and origin of higher plant homologues of bacterial RelA/SpoT stress proteins in Nicotiana tabacum. *J. Biol. Chem.* 279, 7495–7504. doi: 10.1074/jbc.M311573200

Hirayama, T., and Shinozaki, K. (2007). Perception and transduction of abscisic acid signals: keys to the function of the versatile plant hormone ABA. *Trends Plant Sci.* 12, 343–351. doi: 10.1016/j.tplants.2007.06.013

Hu, K. (2021). Become competent in generating RNA-seq heat maps in one day for novices without prior R experience. *Methods Mol. Biol. (Clifton N.J.)* 2239, 269–303. doi: 10.1007/978-1-0716-1084-8_17

Huang, S., Sirikhachornkit, A., Su, X., Faris, J., Gill, B., Haselkorn, R., et al. (2002). Genes encoding plastid acetyl-CoA carboxylase and 3-phosphoglycerate kinase of the Triticum/Aegilops complex and the evolutionary history of polyploid wheat. *Proc. Natl. Acad. Sci.* 99, 8133–8138. doi: 10.1073/pnas.072223799

Hurst, L. D. (2002). The Ka/Ks ratio: diagnosing the form of sequence evolution. *Trends genetics: TIG* 18, 486. doi: 10.1016/S0168-9525(02)02722-1

Irving, S. E., Choudhury, N. R., and Corrigan, R. M. (2021). The stringent response and physiological roles of (pp)pGpp in bacteria. *Nat. Rev. Microbiol.* 19, 256–271. doi: 10.1038/s41579-020-00470-y

Ito, K., Ito, D., Goto, M., Suzuki, S., Masuda, S., Iba, K., et al. (2022). Regulation of ppGpp Synthesis and Its Impact on Chloroplast Biogenesis during Early Leaf Development in Rice. *Plant Cell Physiol.* 63, 919–931. doi: 10.1093/pcp/pcac053

Jain, V., Kumar, M., and Chatterji, D. (2006). ppGpp: stringent response and survival. *J. Microbiol. (Seoul Korea)* 44, 1–10.

Jiang, W. Q., Geng, Y. P., Liu, Y. K., Chen, S. H., Cao, S. L., Li, W., et al. (2020). Genome-wide identification and characterization of SRO gene family in wheat: Molecular evolution and expression profiles during different stresses. *Plant Physiol. biochemistry: PPB* 154, 590–611. doi: 10.1016/j.plaphy.2020.07.006

Kawaura, K., Mochida, K., Enju, A., Totoki, Y., Toyoda, A., Sakaki, Y., et al. (2009). Assessment of adaptive evolution between wheat and rice as deduced from full-length common wheat cDNA sequence data and expression patterns. *BMC Genomics* 10, 271. doi: 10.1186/1471-2164-10-271

Kosová, K., Vítámvás, P., Oldřich Urban, M., Kholová, J., and Tom Prášil, I. (2014). Breeding for enhanced drought resistance in barley and wheat – drought-associated traits, genetic resources and their potential utilization in breeding programmes. *Czech J. Genet. Plant Breed.* 50, 247–261. doi: 10.17221/118/2014-CJGPB

Lescot, M., Déhais, P., Thijs, G., Marchal, K., Moreau, Y., Van De Peer, Y., et al. (2002). PlantCARE, a database of plant cis-acting regulatory elements and a portal to tools for in silico analysis of promoter sequences. *Nucleic Acids Res.* 30, 325–327. doi: 10.1093/nar/30.1.325

Li, Y. T., Liu, X., Xiao, Y. X., Wen, Y., Li, K. K., Ma, Z. L., et al. (2022). Genome-wide characterization and function analysis uncovered roles of wheat LIMs in responding to adverse stresses and TaLIM8-4D function as a susceptible gene. *Plant Genome* 15, e20246. doi: 10.1002/tpg2.20246

Liu, Y., Wang, L., Xing, X., Sun, L. P., Pan, J. W., Kong, X. P., et al. (2013). ZmLEA3, a multifunctional group 3 LEA protein from maize (Zea mays L.), is involved in biotic and abiotic stresses. *Plant Cell Physiol.* 54, 944–959. doi: 10.1093/pcp/pct047

Liu, X., Wei, X. N., Zhang, X. W., and Zhang, Z. Y. (2017). Establishment of a highly-efficient transformation system of wheat protoplasts. *J. Plant Genet. Resour.* 18, 117–124. doi: 10.13430/j.cnki.jpgr.2017.01.015

Liu, C., Wu, Y. H., Liu, Y. X., Yang, L. Y., Dong, R. S., Jiang, L. Y., et al. (2021). Genome-wide analysis of tandem duplicated genes and their contribution to stress resistance in pigeonpea (Cajanus cajan). *Genomics* 113, 728–735. doi: 10.1016/j.ygeno.2020.10.003

Livak, K. J., and Schmittgen, T. D. (2001). Analysis of relative gene expression data using real-time quantitative PCR and the 2(-Delta Delta C(T)) Method. *Methods (San Diego Calif.)* 25, 402–408. doi: 10.1006/meth.2001.1262

Mizusawa, K., Masuda, S., and Ohta, H. (2008). Expression profiling of four RelA/SpoT-like proteins, homologues of bacterial stringent factors, in Arabidopsis thaliana. *Planta* 228, 553–562. doi: 10.1007/s00425-008-0758-5

Nakashima, K., and Yamaguchi-Shinozaki, K. (2013). ABA signaling in stress-response and seed development. *Plant Cell Rep.* 32, 959–970. doi: 10.1007/s00299-013-1418-1

Nan, W. Z., Shi, S. D., Jeewani, D. C., Quan, L., Shi, X., and Wang, Z. H. (2018). Genome-wide identification and characterization of wALOG family genes involved in branch meristem development of branching head wheat. *Genes (Basel)* 9:510. doi: 10.3390/genes9100510

Polyakova, T., Shatokhina, A., and Politov, D. (2022). Molecular Phylogeny of Russian Species of the Genus Spiraea (Rosaceae) according to the Nucleotide Variability of the ITS Nuclear rDNA Region. *Russian J. Genet.* 58, 1297–1305. doi: 10.1134/S1022795422110084

Ramírez-González, R. H., Borrill, P., Lang, D., Harrington, S. A., Brinton, J., Venturini, L., et al. (2018). The transcriptional landscape of polyploid wheat. *Science* 361, eaar6089. doi: 10.1126/science.aar6089

Rossnerova, A., Izzotti, A., Pulliero, A., Bast, A., Rattan, S. I. S., and Rossner, P. (2020). The molecular mechanisms of adaptive response related to environmental stress. *Int. J. Mol. Sci.* 21, 7053. doi: 10.3390/ijms21197053

Sahin, U., Ekinci, M., Kiziloglu, F. M., Yildirim, E., Turan, M., Kotan, R., et al. (2015). Ameliorative effects of plant growth promoting bacteria on water-yield relationships, growth, and nutrient uptake of lettuce plants under different irrigation levels. *HortScience horts* 50, 1379–1386. doi: 10.21273/HORTSCI.50.9.1379

Shiu, S. H., and Bleecker, A. B. (2003). Expansion of the receptor-like kinase/Pelle gene family and receptor-like proteins in Arabidopsis. *Plant Physiol.* 132, 530–543. doi: 10.1104/pp.103.021964

Sinha, A. K., and Winther, K. S. (2021). The RelA hydrolase domain acts as a molecular switch for (p)ppGpp synthesis. *Commun. Biol.* 4, 434. doi: 10.1038/s42003-021-01963-z

Song, M., and Peng, X. Y. (2019). Genome-wide identification and characterization of DIR genes in medicago truncatula. *Biochem. Genet.* 57, 487–506. doi: 10.1007/s10528-019-09903-7

Su, P. S., Sui, C., Li, J. Y., Wan, K., Sun, H. N., Wang, S. H., et al. (2023). The Aux/IAA protein TaIAA15-1A confers drought tolerance in Brachypodium by regulating abscisic acid signal pathway. *Plant Cell Rep.* 42, 385–394. doi: 10.1007/s00299-022-02965-9

Szklarczyk, D., Franceschini, A., Wyder, S., Forslund, K., Heller, D., Huerta-Cepas, J., et al. (2015). STRING v10: protein-protein interaction networks, integrated over the tree of life. *Nucleic Acids Res.* 43, D447–D452. doi: 10.1093/nar/gku1003

Takahashi, K., Kasai, K., and Ochi, K. (2004). Identification of the bacterial alarmone guanosine 5′-diphosphate 3′-diphosphate (ppGpp) in plants. *Proc. Natl. Acad. Sci.* 101, 4320–4324. doi: 10.1073/pnas.0308555101

Trapnell, C., Roberts, A., Goff, L., Pertea, G., Kim, D., Kelley, D. R., et al. (2012). Differential gene and transcript expression analysis of RNA-seq experiments with TopHat and Cufflinks. *Nat. Protoc.* 7, 562–578. doi: 10.1038/nprot.2012.016

van der Biezen, E. A., Sun, J., Coleman, M. J., Bibb, M. J., and Jones, J. D. (2000). Arabidopsis RelA/SpoT homologs implicate (p)ppGpp in plant signaling. *Proc. Natl. Acad. Sci. United States America* 97, 3747–3752. doi: 10.1073/pnas.060392397

Wang, B., Sun, Y. F., Song, N., Wei, J. P., Wang, X. J., Feng, H., et al. (2014). MicroRNAs involving in cold, wounding and salt stresses in Triticum aestivum L. *Plant Physiol. biochemistry: PPB* 80, 90–96. doi: 10.1016/j.plaphy.2014.03.020

Wilkins, M. R., Gasteiger, E., Bairoch, A., Sanchez, J. C., Williams, K. L., Appel, R. D., et al. (1999). Protein identification and analysis tools in the ExPASy server. *Methods Mol. Biol. (Clifton N.J.)* 112, 531–552. doi: 10.1385/1-59259-584-7:531

Yang, F., Zhang, J. J., Liu, Q. E., Liu, H., Zhou, Y. H., Yang, W. Y., et al. (2022). Improvement and re-evolution of tetraploid wheat for global environmental challenge and diversity consumption demand. *Int. J. Mol. Sci.* 23, 2206. doi: 10.3390/ijms23042206

Yin, J. L., Liu, M. Y., Ma, D. F., Wu, J. W., Li, S. L., Zhu, Y. X., et al. (2018). Identification of circular RNAs and their targets during tomato fruit ripening. *Postharvest Biol. Technol.* 136, 90–98. doi: 10.1016/j.postharvbio.2017.10.013

Yin, J. L., Wang, L. X., Zhao, J., Li, Y. T., Huang, R., Jiang, X. C., et al. (2020). Genome-wide characterization of the C2H2 zinc-finger genes in Cucumis sativus and functional analyses of four CsZFPs in response to stresses. *BMC Plant Biol.* 20, 359. doi: 10.1186/s12870-020-02575-1

Zhang, P. G., Zhu, Y. X., Ma, D. F., Xu, W. J., Zhou, J. J., Yan, H. W., et al. (2019). Screening, identification, and optimization of fermentation conditions of an antagonistic endophyte to wheat head blight. *Agronomy* 9, 476. doi: 10.3390/agronomy9090476

Zhu, Y. X., Jia, J. H., Yang, L., Xia, Y. C., Zhang, H. L., Jia, J. B., et al. (2019). Identification of cucumber circular RNAs responsive to salt stress. *BMC Plant Biol.* 19, 164. doi: 10.1186/s12870-019-1712-3

frontiers | Frontiers in Plant Science

TYPE Review
PUBLISHED 23 February 2024
DOI 10.3389/fpls.2024.1355178

Check for updates

OPEN ACCESS

EDITED BY
Xinli Zhou,
Southwest University of Science and Technology, China

REVIEWED BY
Huamin Chen,
Chinese Academy of Agricultural Sciences, China
Qinhu Wang,
Northwest A&F University, China
Jiajie Wu,
Shandong Agricultural University, China

*CORRESPONDENCE
Xiaodong Wang
zhbwxd@hebau.edu.cn

RECEIVED 13 December 2023
ACCEPTED 22 January 2024
PUBLISHED 23 February 2024

CITATION
Zhao S, Li M, Ren X, Wang C, Sun X, Sun M, Yu X and Wang X (2024) Enhancement of broad-spectrum disease resistance in wheat through key genes involved in systemic acquired resistance.
Front. Plant Sci. 15:1355178.
doi: 10.3389/fpls.2024.1355178

COPYRIGHT
© 2024 Zhao, Li, Ren, Wang, Sun, Sun, Yu and Wang. This is an open-access article distributed under the terms of the Creative Commons Attribution License (CC BY). The use, distribution or reproduction in other forums is permitted, provided the original author(s) and the copyright owner(s) are credited and that the original publication in this journal is cited, in accordance with accepted academic practice. No use, distribution or reproduction is permitted which does not comply with these terms.

Enhancement of broad-spectrum disease resistance in wheat through key genes involved in systemic acquired resistance

Shuqing Zhao[1], Mengyu Li[1], Xiaopeng Ren[1], Chuyuan Wang[1], Xinbo Sun[2], Manli Sun[1], Xiumei Yu[3] and Xiaodong Wang[1]*

[1]State Key Laboratory of North China Crop Improvement and Regulation, College of Plant Protection, Hebei Agricultural University, Baoding, Hebei, China, [2]College of Agronomy, Hebei Agricultural University, Baoding, Hebei, China, [3]College of Life Sciences, Hebei Agricultural University, Baoding, Hebei, China

Systemic acquired resistance (SAR) is an inducible disease resistance phenomenon in plant species, providing plants with broad-spectrum resistance to secondary pathogen infections beyond the initial infection site. In *Arabidopsis*, SAR can be triggered by direct pathogen infection or treatment with the phytohormone salicylic acid (SA), as well as its analogues 2,6-dichloroisonicotinic acid (INA) and benzothiadiazole (BTH). The SA receptor non-expressor of pathogenesis-related protein gene 1 (NPR1) protein serves as a key regulator in controlling SAR signaling transduction. Similarly, in common wheat (*Triticum aestivum*), pathogen infection or treatment with the SA analogue BTH can induce broad-spectrum resistance to powdery mildew, leaf rust, *Fusarium* head blight, and other diseases. However, unlike SAR in the model plant *Arabidopsis* or rice, SAR-like responses in wheat exhibit unique features and regulatory pathways. The acquired resistance (AR) induced by the model pathogen *Pseudomonas syringae* pv. *tomato* strain DC3000 is regulated by *NPR1*, but its effects are limited to the adjacent region of the same leaf and not systemic. On the other hand, the systemic immunity (SI) triggered by *Xanthomonas translucens* pv. *cerealis* (*Xtc*) or *Pseudomonas syringae* pv. *japonica* (*Psj*) is not controlled by *NPR1* or SA, but rather closely associated with jasmonate (JA), abscisic acid (ABA), and several transcription factors. Furthermore, the BTH-induced resistance (BIR) partially depends on *NPR1* activation, leading to a broader and stronger plant defense response. This paper provides a systematic review of the research progress on SAR in wheat, emphasizes the key regulatory role of NPR1 in wheat SAR, and summarizes the potential of pathogenesis-related protein (*PR*) genes in genetically modifying wheat to enhance broad-spectrum disease resistance. This review lays an important foundation for further analyzing the molecular mechanism of SAR and genetically improving broad-spectrum disease resistance in wheat.

KEYWORDS

wheat, systemic acquired resistance, genetic improvement, NPR1, *PR* genes

Introduction

As early as 1901, researchers found that plants infected with pathogens develop higher levels of resistance to secondary infections (Görlach et al., 1996). Over the next 30 years, several descriptive studies were conducted, which collectively indicated the presence of systemic immunity in plants. Among them, the concept of SAR was widely accepted, referring to the ability of plants to develop broad-spectrum resistance against secondary pathogens during the response to primary pathogen infection (Görlach et al., 1996). Tobacco mosaic virus and its *Solanaceae* hosts were used in the early study of SAR (Görlach et al., 1996). With the deepening of research, SAR has been demonstrated to exist widely in various plants, and effectively combat viral, bacterial, and fungal diseases, and induce disease resistance responses with long-term and systematic nature (Zhang et al., 1999).

SAR in *Arabidopsis* and rice

Usually caused by local infection of pathogenic bacteria, SAR is an important part of plant disease resistance system, and is an inducible broad-spectrum immunity of plant resistance to pathogenic bacteria, lacks specificity toward the initial infection (Görlach et al., 1996). When a non-lethal pathogen causes localized programmed cell death, it triggers the accumulation of the plant hormone SA and the expression of *PR* genes, thereby protecting the rest of the plant from secondary infections for weeks to months. SAR can even be transmitted to offspring through epigenetic regulation (Fu and Dong, 2013).

In the model plant *Arabidopsis thaliana*, infection with pathogenic microorganisms or treatment with SA and its analogs INA and BTH can induce SAR response, associated with the transcriptional activation of *PR* genes (Fu and Dong, 2013). Specifically, the SA receptor protein NPR1 in *Arabidopsis* is a key transcriptional regulatory factor for SAR. Upon infection with a primary pathogen or treatment with SA analogs, the intracellular SA level significantly increases, and NPR1 protein undergoes redox modification to translocate from cytoplasm to nucleus. After phosphorylation, it forms a complex with TGA transcription factors, promoting the expression of various *PR* genes and enhancing the plant resistance to secondary pathogens (Delaney et al., 1995; Mou et al., 2003). The endogenous level of SA in plant defense responses is largely dependent on the intensity of the hypersensitive response (HR) induced by the pathogen (Mou et al., 2003).

In *Arabidopsis*, the homologous proteins of NPR1, NPR3 and NPR4, participate in E3 ligase-mediated degradation of NPR1 in an SA-dependent manner (Fu et al., 2012). When the SA level is low, proteases bind to NPR4 and degrade NPR1. However, during pathogen infection, when the SA level increases, it competitively binds to NPR4. This binding leads to the accumulation of NPR1 and activates the NPR1-mediated defense response. When plants develop HR as part of the defense response, SA levels reach very high levels in the plant, and in this scenario, SA binds to NPR3 to promote its interaction with NPR1, ultimately leading to the transformation of NPR1 (Fu et al., 2012; Moreau et al., 2012). Recently, the crystal structure of the NPR1 protein in *Arabidopsis* has been resolved, revealing its existence as a "bird-shaped" dimer. NPR1-induced defense gene reprogramming in response to various biotic and abiotic stresses may involve not only TGA homodimers but also heterologous transcription activators, repressors, and lipid metabolites (Kumar et al., 2022).

In rice, infection with *Pseudomonas syringae* or treatment with BTH can induce SAR-like response against the rice blast fungus and is associated with the transcriptional activation of *PR* genes (Smith and Métraux, 1991; Schweizer et al., 1999) However, compared to *Arabidopsis*, rice has relatively higher endogenous levels of SA, which do not increase upon pathogen infection (Silverman et al., 1995; Chen et al., 1997). The protein interaction between rice NPR1 homolog (rNH1) and TGA transcription factors is conserved (Chern et al., 2001). Overexpression of the *Arabidopsis AtNPR1* gene in rice significantly enhances the broad-spectrum resistance of plant to various pathogens, including *Xanthomonas oryzae* pv. *oryzae* (*Xoo*), *Magnaporthe oryzae*, and *Cochliobolus miyabeanus* (Quilis et al., 2008; Xu et al., 2017). Further studies indicate that the overexpression of the *rNH1* gene in rice not only enhances resistance to *Xoo* but also increases sensitivity to light and BTH treatment (Chern et al., 2005; Xu et al., 2017). Additionally, the WRKY transcription factor *OsWRKY45* is a key regulator of the SA/BTH signaling pathway independent of *rNH1* in rice (Shimono et al., 2007; Nakayama et al., 2013).

SAR-like responses in *Triticeae* crops of wheat and barley

In *Triticeae* crops of wheat and barley, both primary pathogen infection and BTH treatment can induce broad-spectrum resistance against diseases like powdery mildew, rust, and *Fusarium* head blight. However, SAR in *Triticeae* crops such as wheat and barley, when induced by pathogen infection or BTH treatment, displays distinct characteristics and regulatory pathways compared to model plants like *Arabidopsis* and rice. As a result, three different "SAR-like responses" have been observed in wheat and barley: acquired resistance (AR), systemic immunity (SI), and BTH-induced resistance (BIR) (Wang et al., 2018) (Table 1, Figure 1).

In *Triticeae* crops of wheat and barley, AR like the SAR in model plant can be observed in the neighboring area after injection with *Pseudomonas syringae* pv. *tomato* strain DC3000. This AR response enhances resistance against the secondary pathogen *M. oryzae* by upregulating *PR* genes (Colebrook et al., 2012). However, unlike SAR in *Arabidopsis*, the AR response in barley does not extend to other leaves, meaning it lacks systemic properties. Inducing AR response in wheat by injecting *P. syringae* DC3000 significantly enhances resistance to the highly virulent *Puccinia tritici* pathotype THTT (Gao et al., 2018). Overexpression of the wheat *NPR1* gene in barley (*wNPR1-OE*) significantly enhances resistance to the *M. oryzae* strain Guy11, while gene silencing of the barley *HvNPR1* gene (*HvNPR1-Kd*) significantly reduces AR response to Guy11, indicating that the *NPR1* gene directly regulates the AR response in barley. Using quantitative real-time

TABLE 1 Features and molecular mechanism of SAR response in *Arabidopsis*, rice, and *Triticeae* crops of wheat and barley.

SAR response	Inducible factor	Resistance features	Molecular mechanism	Reference
Arabidopsis	Infection of pathogen; Treatment of SA, INA, and BTH	HR induced by the pathogen, Enhanced resistance in systemic leaf, Increased SA content, Systemic.	Transcriptional activation of *PR* genes, Regulated by NPR1, Involvement of WRKY transcription factors.	Fu and Dong (2013)
Rice	Infection of *Pseudomonas syringae* pv *tomato* DC3000, Treatment of BTH	Pathogens induce HR, Plants exhibit high basal SA content, Systemic	*PR* gene transcription activation, WRKY45 independently regulates BTH-induced resistance	Smith and Métraux (1991); Schweizer et al. (1999); Shimono et al. (2007); Nakayama et al. (2013);
Wheat and barley acquired resistance (AR)	Infection of *Pseudomonas syringae* pv *tomato* DC3000,	Pathogenic bacteria trigger HR, Resistance is enhanced in adjacent areas of HR, SA content in necrotic leaves increases, Not systemic	*PR* gene transcription activation, Regulated by *NPR1*, Regulated by *WRKY6*.	Li et al. (2020); Li et al. (2022);
Barley systemic immunity (SI)	Infection of *Xanthomonas translucens* pv *cerealis* (*Xtc*) and *Pseudomonas syringae* pv *japonica* (*Psj*)	Pathogenic bacteria trigger HR, Resistance is enhanced in systemic leaf, Low association with SA, High association with JA and ABA, Systemic	Regulated independently of *NPR1*, Regulated by *WRKY* and *ERF*	Dey et al. (2014);
Wheat and barley BTH-induced resistance (BIR)	Treatment of BTH	Enhanced resistance to multiple fungal diseases, Systemic	Transcriptional activation of wheat *WCI* and barley *BCI* genes, Transcriptional activation of *PR* genes, Partial involvement of *NPR1*, Regulated by *WRKY70*	Görlach et al. (1996); Li et al. (2020); Hafez et al. (2014);

polymerase chain reaction (qRT-PCR), it was found that the induction levels of barley *PR* genes, including *HvPR1b*, *HvPR2*, *HvPR3_Chit2b*, and *HvPR5*, were closely correlated with the expression levels of *NPR1* transgene in *wNPR1-OE* and *HvNPR1-Kd* barley transgenic plants (Wang et al., 2016). Further transcriptomic analysis revealed that the expression of *HvPR1*, *HvPR2*, *HvPR3*, *HvPR5*, *HvPR9*, and *HvPR13* genes was significantly induced in the AR response to DC3000 in barley, and the induction patterns were positively correlated with the expression levels of the *NPR1* gene, suggesting that these genes are regulated by the *NPR1* gene in the AR response (Gao et al., 2018).

By transcriptome sequencing, it was found that barley transcription factor gene *HvWRKY6* may act as a regulatory factor for AR in wheat (Li et al., 2020). The AR response was induced by injecting DC3000, and the resistance level of wheat transgenic lines overexpressing *HvWRKY6* (*HvWRKY6-OE*) to *M. oryzae* strain P131 was significantly improved. The expression levels of *TaPR1a, TaPR2* and *TaPR4b* genes in *HvWRKY6-OE* were significantly increased, indicating that *HvWRKY6* gene plays an important regulatory role in AR response. *HvWRKY6-OE* have shown enhanced resistance to *P. tritici* pathotype THTT, *Puccinia striiformis* f. sp. *tritici* pathotype CYR32, *Fusarium* crown rot, and sharp eyespot to varying degrees (Li et al., 2020; Li et al., 2022). Transcriptome sequencing analysis showed that *HvWRKY6* gene activated wheat defense response in a pathogen-independent manner. *HvWRKY6* partially activates the SAR-associated transcripts, including calcium-associated disease resistance pathways and part of the effector-triggered immunity (ETI) (Li et al., 2022). *HvWRKY6*-mediated resistance response is related to the activation of SA pathway and the inhibition of ABA and JA pathways (Li et al., 2022).

Injecting *Xanthomonas translucens* pv. *cerealis* (*Xtc*) or *Pseudomonas syringae* pv. *japonica* (*Psj*) into barley leaves can induce SI against *Xtc* infection in other systemic healthy leaves (Dey et al., 2014). However, unlike SAR in *Arabidopsis*, the SI process in barley is not induced by SA or BTH, but is closely associated with jasmonic acid (JA) and abscisic acid (ABA). Further studies have shown that the SI process in barley is regulated by several *WRKY* and *ERF* transcription factors but has a relatively low correlation with the *NPR1* gene.

BTH has been successfully developed as a commercial plant resistance inducer and applied in agricultural production. In *Arabidopsis* and tobacco, induction of resistance and *PR* gene expression by INA/BTH has been observed (Uknes et al., 1992; Lawton et al., 1995). It is likely that SA/INA/BTH induce SAR

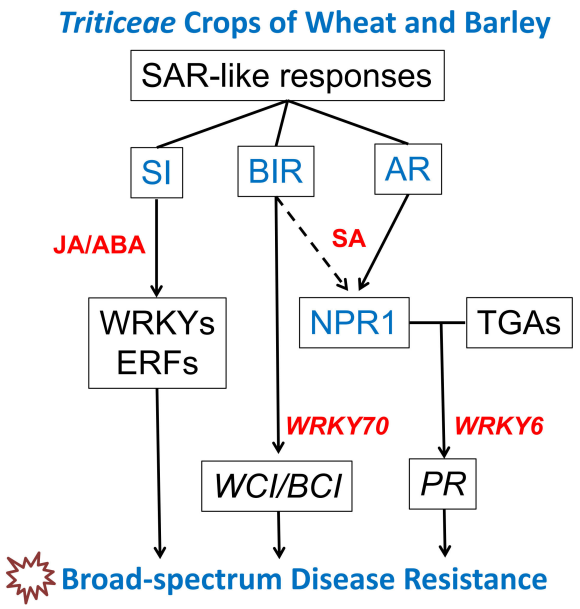

FIGURE 1
Regulatory network of SAR-like responses in *Triticeae* crops of wheat and barley. This network encompasses three SAR-like responses: acquired resistance (AR), systemic immunity (SI), and benzothiadiazole-induced resistance (BIR). Recent studies utilizing transcriptome sequencing and wheat transgenic lines have contributed to the prediction of this regulatory network. Understanding the molecular mechanisms that underlie SAR-like responses provides valuable gene resources for enhancing the broad-spectrum resistance of wheat to diseases such as stripe/leaf rust, powdery mildew, *Fusarium* head blight, *Fusarium* crown rot, sharp eyespot, and others.

through the same signal transduction pathway (Görlach et al., 1996). Treatment of wheat with BTH induces systemic BIR against multiple diseases such as powdery mildew, leaf rust, and *Fusarium* head blight. However, most *PR* genes are insensitive to SA and BTH, while another class of BTH-induced genes, such as the wheat chemical induced (*WCI*) gene and the barley chemical induced (*BCI*) gene, may play important roles in the BIR (Beßer et al., 2000; Hafez et al., 2014). Transcriptome sequencing showed that the barley transcription factor gene *HvWRKY70* may act as a regulatory factor of BIR in wheat. BTH-induced SAR reaction showed that several *PR* genes and *BCI* genes in wheat transgenic lines overexpressing *HvWRKY70* (*HvWRKY70-OE*) were significantly up-regulated by BTH, indicating that *HvWRKY70* gene was involved in the regulation of BIR. In addition, *HvWRKY70-OE* showed increased resistance to *P. striiformis* f. sp. *tritici* pathotype CYR32 and *Blumeria graminis* f. sp. *tritici* pathotype E20 (Li et al., 2020).

Interactors of the NPR1 protein in plant-pathogen interaction

NPR1, as a SA receptor protein, possesses three conserved domains: the N-terminal broad-complex, tramtrack, and bricabrac/poxvirus, zinc finger (BTB/POZ) domain, the central ankyrin-repeat (ANK) domain, and the C-terminal NPR1/NIM1-like domain. The BTB/POZ domain is a potential target for the E3 ubiquitin degradation pathway (Petroski and Deshaies, 2005), while the ANK domain is mainly involved in the interaction with TGA transcription factors (Cao et al., 1997; Sedgwick and Smerdon, 1999). The NPR1/NIM1-like domain participates in SA binding along with the BTB/POZ domain (Wu et al., 2012).

NIMIN is a protein family first discovered in *Arabidopsis* and plays a crucial role in regulating the NPR1-mediated immune signaling pathway. It finely regulates the dynamic defense process against diseases. Hermann et al. reported that during different stages of SAR, different NIMIN-NPR1 complexes are formed to promote the activation of defense genes. In normal plant growth, the binding of NIMIN3 to NPR1 prevents excessive activation of immune responses (Hermann et al., 2013). However, upon pathogen attack, NIMIN2 and NIMIN1 sequentially bind to NPR1, promoting the binding with SA and the expression of *PR* genes, thereby enhancing plant immune responses (Maier et al., 2011). NIMIN proteins regulate the dynamic balance of NPR1 and contribute to the rapid upregulation of defense genes, ensuring successful resistance against invading pathogens (Hermann et al., 2013). TEOSINTE BRANCHED 1, CYCLOIDEA, PCF (TCP) transcription factors are also essential participants in the SA signaling pathway. NPR1 interacts with nuclear TCP transcription factors TCP8, TCP14 and TCP15, promoting SAR function. TCP15 directly binds to the TCP binding site in the *PR5* promoter, enhancing *PR5* expression, contributing to ETI, and playing an important role in SAR (Li et al., 2018). NPR1 has also been reported to interact with cyclin-dependent kinase 8 (CDK8) and WRKY18 in *Arabidopsis*, and SA can promote their interaction. CDK8 facilitates the expression of *NPR1* and *PR1* genes by recruiting RNA polymerase II to their promoter and coding regions. NPR1, in turn, recruits CDK8, promoting its own and target gene expression and contributing to the establishment of plant immunity (Chen et al., 2019).

Both fungal pathogen *Colletotrichum fructicola* effector protein CfEC12 and apple MdNPR1 interact with NIM1-interacting (MdNIMIN2) protein. CfEC12 competes with MdNIMIN2 in binding to the 13-63 amino acid position of MdNPR1, thereby suppressing the expression of downstream *PR* genes and immune responses (Shang et al., 2023). NPR1 plays a key role in limiting co-infection of TuMV, a member of the largest RNA virus genus in plant, and this resistance is counteracted by viral RNA-dependent RNA polymerase nuclear inclusion body B (NIb). NIb interacts with NPR1 and targets its SUMO interacting motif 3 (SIM3); NIb interferes with NPR1-SIM3 interaction and subsequent SUMoization; NIb also affects the SUMO-dependent phosphorylation of NPR1; targeting NPR1-SIM3 is a conserved ability of NIBs from different descendant viruses. *Potyvirus* uses NIb to suppress NPR1-mediated resistance by disrupting NPR1 SUMO (Liu et al., 2023a). The RXLR effector protein RXLR48 in *Phytophthora capsica* interacts with NPR1 and inhibits plant defense. RxLR48 promotes nuclear localization of NPR1 and inhibits its proteasome-mediated degradation, suggesting that RxLR48 inhibits SA signaling by targeting the transcriptional regulator NPR1 (Li et al., 2019). Using yeast two-hybrid

screening, a virulent effector protein, PNPi, that directly targets the NPR1 protein was identified in wheat rust, inhibiting the interaction between NPR1 and TGA2, and suppressing wheat SAR (Wang et al., 2016). There were 19 PNPi-like secreted proteins with RlpA-like double-psi beta-barrel (DPBB_1) conserved structure in wheat leaf rust. Twelve PNPi-like effector protein genes were cloned and their interaction with wheat NPR1 protein was verified by yeast two-hybrid system. Among them, four PNPi-like effector proteins could interact with wheat NPR1 protein (Zhao et al., 2020).

NPR1 protein in *Triticeae* crops of wheat and barley

In the *Triticeae* crops of wheat and barley, significant progress has been made in the study of *NPR1* gene (Table 2). For example, overexpression of *Arabidopsis AtNPR1* or oat *ScNPR1* in common wheat significantly enhances plant resistance against *Fusarium graminearum* (Gao et al., 2013; Yu et al., 2017). The interaction between NPR1 homologous proteins and TGA transcription factor homologous proteins is highly conserved in wheat and rice, suggesting that wheat NPR1 homologous proteins have conserved disease resistance functions (Cantu et al., 2013). Bioinformatics analysis revealed the presence of nine *NPR1* homologous genes (*TaNPR1*) in wheat, with six members located on the homoeologous group 3 chromosomes named *TaG3NPR1*, and three members located on the homoeologous group 7 chromosomes named *TaG7NPR1*. *TaG3NPR* regulates the expression of *PR* genes in the SA signaling pathway. Additionally, a novel fusion pattern of NPR1 protein, as NPR1 fused with nucleotide-binding adaptor shared by APAF-1, R proteins, and CED-4 (NB-ARC-NPR1) was discovered on the 7A chromosome in common wheat (Ta7ANPR1). Under biotic stress conditions, the *Ta7ANPR1* gene simultaneously transcribes two mRNAs, one encoding an NB-ARC protein and the other encoding an NB-ARC-NPR1 fusion protein. The *Ta7ANPR1* gene negatively regulates plant defense responses against wheat rust through the NB-ARC-NPR1 fusion protein (Wang et al., 2020b). Calcineurin B-like interacting protein kinases (CIPKs) have been shown to be essential for biological stress tolerance in plant-pathogen interactions. A CIPK homolog, *TaCIPK10*, was identified and cloned from wheat. TaCIPK10 physically interacts and phosphorylates with AtNPR3/4 homologous TaNH2 to regulate wheat resistance to *P. striiformis* f. sp. *tritici* (Liu et al., 2019a).

Furthermore, it has been reported that about 40 *NPR1* homologous genes or *NPR* family coding genes can be identified in *Triticum aestivum*, *Triticum urartu*, *Triticum dicoccoides*, and *Aegilops tauschii*. *NPR1* homologous genes exhibit good collinearity in common wheat and its close relatives. Based on RNA-seq data, *TaNPR1* homologous genes exhibit different tissue-specific expression patterns, and *TaNPR1-A/B/D*, *TaNPR3-A/B/D*, and *TaNPR4-A/B/D* are significantly induced under biotic stress conditions (Liu et al., 2019b). Through gene expression profile analysis, three *NPR1* homologous genes named *TaNPR1*, *TaNPR2*, and *TaNPR3* were cloned from wheat near-isogenic lines resistant to *Fusarium* head blight (Yang et al., 2013). Among them, *TaNPR1* and *TaNPR3* showed significant upregulation in response to *Fusarium graminearum*, suggesting their involvement in wheat defense against *Fusarium* head blight. Association analysis using a natural population consisting of 178 winter wheat genotypes revealed that two *NPR* genes located on the 2AL and 2DL chromosomes of common wheat were associated with resistance to *Fusarium* head blight (Diethelm et al., 2014). Both SA and the biocontrol agent *Trichoderma* induce the expression of the wheat *NPR1* gene and enhance plant resistance against powdery mildew (Ahangar et al., 2017).

TABLE 2 Functional characterized *NPR* genes in wheat.

Gene Name	Gene accession	Role in wheat resistance	Reference
NPR1-3A/3B/3D	TraesCS3A02G105400 TraesCS3B02G123800 TraesCS3D02G107500	Positive regulator of AR and BIR, Targeted by rust effector PNPi	Wang et al. (2016); Liu et al. (2019b);
TaG3NPR1	KAF7021350 KAF7028198	Regulation of expression of *PR* genes in SA signaling pathway	Wang., et al. (2020b);
TaG7NPR1/NB-ARC-NPR1	KAF7046550 KAF7105730 TraesCS7D02G023000	Simultaneously transcribes two mRNAs and negative regulation of plant defense response to wheat rust disease	Wang., et al. (2020b);
TaNH2	KU736862	Interacted with TaCIPK10 and enhance disease resistance to wheat stripe rust	Liu et al. (2019a);

PR genes act as the downstream of SAR

PR proteins are a class of water-soluble proteins produced by plants in response to pathogen invasion or non-biological stimuli. When subjected to biotic or abiotic stress, the expression levels of *PR* genes rapidly increase and are often used as markers of plant immune activation. Numerous studies have shown that PR proteins play important roles in plant disease resistance and SAR (Hamamouch et al., 2011). To date, a total of 18 *PR* gene families have been identified in various plant species in response to different pathogens (van Loon et al., 2006; Ferreira et al., 2007; Sels et al., 2008; Wang et al., 2018). In addition, *PR* gene has been widely used as indicator gene for wheat resistance response to monitor the intensity of resistance response (Wu et al., 2019).

The PR1 protein family, as the earliest identified defense-related proteins, has been extensively studied for its disease resistance mechanisms. *PR1* homologous genes (*PR1a* and *PR1b*) have been successfully cloned in wheat and barley and induced to express by a

variety of pathogens (Molina et al., 1999; Gao et al., 2015). These genes are considered as key downstream regulatory genes of NPR1 in SAR-like responses in *Triticeae* crops of wheat and barley (Wang et al., 2016). RNA-seq transcriptome sequencing was performed on resistant wheat line carrying leaf rust resistance gene *TcLr19* and susceptible wheat variety "Chinese Spring" inoculated with the *P. tritici* pathotype PHNT, and seven SA-induced *TaPR1* genes associated with plant disease resistance were identified. qRT-PCR results showed that among these *TaPR1* genes, *TaPR1-4* had the largest induction effect by the infection of leaf rust (Wang et al., 2022a). The *TdPR1.2* gene identified from *Trticum turgidum* also plays a vital role in enhancing plant resistance to abiotic stress (Ghorbel et al., 2021). The expression and genetic polymorphisms of *PR1, PR2, PR4, PR9* and *PR10* in sixteen Egyptian wheat genotypes were analyzed to clarify the expression mechanism of *PR* genes during stripe rust infection (Esmail et al., 2020).

The PR1 protein plays a pivotal role as an interaction hub in the extracellular space. TaPR1a protein in wheat interacts with lipid transfer protein TaLTP3 (PR14) in the extracellular matrix, and overexpression of *TaLTP3* in wheat transgenic line can specifically activate the transcription of *TaPR1a* gene, as well as multiple plant hormone pathways including SA, JA, and auxin, providing new insights into the synergistic mechanism of PR proteins (Zhao et al., 2021). TaPR1-4 interacts with thaumatin-like protein TaPR5/TaTLP1 through the αIV helix and participates in the defense process against wheat leaf rust through the CAPE1 motif (Wang et al., 2022a).

Research has shown that wheat TaPR1 protein can directly interact with the fungal toxin ToxA produced by the tan spot pathogen (*Pyrenophora tritici-repentis*) and mediate the induction of necrotic reactions in susceptible wheat (Lu et al., 2014). The effector SnTox3 from *Parastagonospora nodorum* elicits a strong necrotic response in susceptible wheat and also interacts with wheat TaPR-1, SnTox3 prevented CAPE1 from being released from TaPR1 *in vitro*, SnTox3 independently induced necrosis through Snn3 recognition, and inhibited host defense through direct interaction with the TaPR1 protein (Sung et al., 2021). The wheat transgenic lines overexpressing *TaPR1a* gene (*TaPR1a-OE*) showed increased resistance to both wheat leaf rust and stripe rust. By targeting TaPR1a protein in the extracellular space, wheat rust effector protein PNPi inhibits plant disease resistance and is conducive to rust infection (Bi et al., 2020).

Significant efforts have been dedicated to the genome-wide identification of *PR1* genes in wheat. Twelve *PR-1* genes encoding the CAP superfamily domain were identified in the genome of the *Triticum turgidum* subspecies. Phylogenetic analysis showed that *PR1* gene could be divided into three groups according to variations in conserved domain. Most TdPR1 proteins present an N-terminal signaling peptide. The expression profile analysis showed that the *PR-1* gene family was organism specific and could be induced by different abiotic stresses (Zribi et al., 2023). Bioinformatics tools and RNA sequencing discovered 86 potential wheat *TaPR1* genes, and *TaPR1* genes were involved in SA signaling pathway, MAPK signaling pathway, and phenylalanine metabolism in response to infection of *P. striiformis* f. sp. *tritici* pathotype CYR34. One particular gene, *TaPR1-7*, was found to be associated with resistance to *P. striiformis* f. sp. *tritici* in a biparental wheat population (Liu et al., 2023b). *TaPR1*, as the representative of wheat SAR downstream defense related protein genes, holds significant potential and is deserving of further exploration and investigation.

PR2 and *PR3* genes encode β-1,3-endoglucanases and chitinase proteins, respectively. Molecular docking analysis of β-1,3-endoglucanases and chitinase proteins revealed key amino acid residues involved in ligand binding and important interactions, which may play an important role in plant defense against fungal pathogens (Numan et al., 2021). The PR4 family features a Barwin domain at the C-terminus, which endows the host plant with disease resistance. A total of four *PR-4* genes were identified from the genome of the Qingke (*Hordeum vulgare* L. var. *nudum*) by HMM analysis. Expression profile analysis confirmed that *PR-4* was involved in the defense response to drought, cold, and powdery mildew infection, and the transcription of two barley *PR4* genes were differentially regulated by MeJA and SA (Wang et al., 2022b).

Wheat thaumatin-like protein (TaTLP/TaPR5) are secreted into the apoplastic space, and when stimulated by biological or abiotic stresses, their expression levels increase rapidly, and they show antifungal activity in various plant species, which is an important component of plant SAR and a sign of plant disease resistance (Han et al., 2023). Wheat TaTLP1 is involved in the resistance to leaf rust. TaPR1 and TaTLP1 also have direct protein interaction in the extracellular space, positively regulating wheat resistance to leaf rust in a reactive oxygen species (ROS)-dependent and direct germicidal manner (Wang et al., 2022a). Leaf rust effector protein Pt_21 directly targets wheat TaTLP1 and inhibits host defense response by inhibiting the antifungal activity of TaTLP1 (Wang et al., 2023).

Currently, other *PR* genes in barley and wheat have been rarely reported. However, considering the research potential and application prospects of *PR* genes in other crops, they hold great promise for genetic improvement of wheat disease resistance. Drawing from information on *PR* genes reported in other plant species, we conducted a preliminary prediction and classification of 18 *PR* gene families in wheat (Table 3).

Conclusion and future prospective

The SAR-like responses observed in *Triticeae* crops of wheat and barley (AR, SI, and BIR) exhibit significant differences compared to those in *Arabidopsis* and rice. In recent years, studies on the *NPR1* homologous genes in wheat have provided preliminary clues to understanding the molecular mechanisms underlying these differences. The key regulatory factors and downstream functional proteins in SAR, including the SA receptor proteins NPR3/4, WRKY transcription factors, and PR proteins, still require further exploration. Uncovering the key nodal genes involved in SAR-like responses in wheat, as well as the co-regulated downstream genes involved in these biological processes, will provide important genetic resources for broad-spectrum disease resistance improvement in wheat. Additionally, with the continuous advancement of genomics and the

10.3389/fpls.2024.1355178

TABLE 3 Predicted and characterized *PR* genes in wheat in this study.

Gene Name	Encoded protein	Gene accession	Role in wheat resistance	Reference
PR1	Secretion protein with C-terminal CAPE1 peptide	TraesCS5A02G183300, TraesCS7D02G201400, TraesCS7B02G105300, TraesCS7A02G198900, TraesCS7A02G198800, TraesCS7D02G201300, TraesCS7B02G105200, TraesCS7B02G110000, TraesCS5D02G259800, TraesCS7D02G161200	Interact with PR5, Interact with LTP3 (PR14), Targeted by rust effector PNPi, Positive regulator in resistance to leaf rust and stripe rust, Downstream of AR, Downstream of BIR.	Zhao et al. (2021); Wang., et al. (2020a); Bi et al. (2020); Sung et al. (2021)
PR2	β-1,3-endoglucanases	TraesCS3D02G478300, TraesCS3D02G478000, TraesCS3B02G529700, TraesCS2D02G349400, TraesCS3A02G483000, TraesCS3B02G529300, TraesCS7B02G105100, TraesCS7B02G105000, TraesCS7B02G104900	*Pst-milR1* targets silencing wheat TaPR2, Downstream of AR, Downstream of BIR.	Numan et al. (2021);
PR3/ PR8/ PR11	Chitinase	TraesCS2D02G349400, TraesCS2D02G349000, TraesCS2D02G348900, TraesCS2B02G369100, TraesCS2A02G350800, TraesCS3D02G260500, TraesCS3D02G260300, TraesCS3B02G293200, TraesCS3A02G260200, TraesCS2A02G350900, TraesCS3B02G293400, TraesCS3A02G260100	Downstream of AR, Downstream of BIR.	van Loon et al. (2006); Giżyńska et al. (2018); Numan et al. (2021);
PR4	Chitinase and chitin-binding proteins	TraesCS3D02G524700, TraesCS3B02G584700, TraesCS3A02G517100	Inhibite growth of *Fusarium culmorum*, Downstream of AR	Wang et al. (2022b);
PR5	Thaumatin-like protein	TraesCS7B02G417700, TraesCS5B02G016000, TraesCS5B02G015700, TraesCS5B02G015500, TraesCS5A02G017900, TraesCS7D02G551400, TraesCS7B02G483400, TraesCS7A02G558500, TraesCS5A02G018200, TraesCS5A02G019100, TraesCS5A02G019000, TraesCS5A02G018900, TraesCS5A02G018800, TraesCS5A02G018700, TraesCS5A02G018600, TraesCSU02G146600, TraesCS6B02G473800, TraesCS4A02G498000, TraesCS2A02G110300	Interact with PR1, Targeted by leaf rust effector Pt_21, Positive regulator in resistance to leaf rust, Downstream of AR, Downstream of BIR.	Wang., et al. (2020a); Wang., et al.(2022a); Wang., et al. (2023)
PR6	Protease inhibitor	TraesCS1A02G265600, TraesCS1D02G266000, TraesCS1B02G276800, TraesCS1B02G276300, TraesCS1B02G276200, TraesCS1A02G265800	Unknown	Gaddour et al. (2001); Gao et al. (2013);
PR7	Endogenous protease	TraesCS5A02G520700, TraesCS5A02G693100, TraesCS4D02G456100, TraesCS4D02G456000, TraesCS4B02G352100,	Unknown	Jordá et al. (2000);
PR9	Peroxidase	TraesCS2B02G124800, TraesCS2D02G107800, TraesCS2B02G125200, TraesCS2A02G107500	Induce by powdery mildew, Downstream of AR.	Passardi et al. (2004);
PR10	Ribonuclease-like protein	TraesCS5D02G102700, TraesCS5B02G096300, TraesCS5A02G090600	Unknown	Aglas et al. (2020);
PR12	Small cysteine-rich antifungal protein	TraesCS2D02G047800, TraesCS2B02G062100, TraesCS2A02G048900	Unknown	Terras et al. (1995);
PR13	Thionins	TraesCS5B02G228600, TraesCS1A02G398200, TraesCS5A02G230000, TraesCS1D02G405700, TraesCS1B02G426100, TraesCS5A02G229900, TraesCS5A02G229800, TraesCS7D02G008100, TraesCS4A02G492000, TraesCS4A02G491800, TraesCSU02G200700, TraesCSU02G219800, TraesCSU02G066300, TraesCS4A02G491900, TraesCSU02G066400, TraesCS4A02G491700, TraesCSU02G219800, TraesCSU02G193300, TraesCS1B02G426000, TraesCS1D02G405600, TraesCS5D02G473800, TraesCS5B02G471300	Downstream of AR	Epple et al. (1995);
PR14	Lipid transfer protein	TraesCSU02G253500, TraesCSU02G056900, TraesCSU02G056700, TraesCS3B02G064000, TraesCS3B02G063700, TraesCS3B02G063500, TraesCS3B02G063100, TraesCSU02G258000, TraesCSU02G147300, TraesCS3B02G064300, TraesCS3B02G064200, TraesCS3B02G063900, TraesCSU02G056600, TraesCSU02G251500, TraesCSU02G237900, TraesCSU02G154200, TraesCSU02G147200, TraesCSU02G147100, TraesCS3B02G064100, TraesCS3B02G063600, TraesCS3B02G063400, TraesCS3B02G063200, TraesCS3B02G063000, TraesCS3B02G062700, TraesCS3B02G062600, TraesCS3B02G064400	PR14 (LTP3) activates *PR1* transcription, Downstream of BIR.	Blein et al. (2002); Bi et al. (2020); Zhao et al. (2021);

(Continued)

TABLE 3 Continued

Gene Name	Encoded protein	Gene accession	Role in wheat resistance	Reference
PR15	Oxalate oxidase	TraesCS4D02G032200, TraesCS4D02G032000, TraesCS4D02G031700, TraesCS4D02G031600, TraesCS4B02G033600, TraesCS4B02G033400, TraesCS4B02G033300, TraesCS4B02G033200, TraesCS4B02G033100, TraesCS4A02G181700, TraesCS4D02G030800, TraesCS4A02G279300, TraesCS4A02G279200, TraesCS4A02G279100, TraesCS3B02G282500, TraesCS3B02G282400	Unknown	Gregersen et al. (1997);
PR16	Oxalate oxidase-like protein	TraesCSU02G256400, TraesCSU02G253400, TraesCSU02G245800, TraesCSU02G238600, TraesCSU02G222000, TraesCSU02G172100, TraesCSU02G161300, TraesCSU02G152900, TraesCSU02G152800, TraesCSU02G152000, TraesCSU02G151939, TraesCSU02G151900, TraesCSU02G150800, TraesCSU02G150700, TraesCSU02G150600, TraesCSU02G145700, TraesCSU02G145600, TraesCSU02G145500, TraesCSU02G145300, TraesCSU02G128800, TraesCSU02G128700, TraesCSU02G128600, TraesCSU02G128500, TraesCSU02G128400, TraesCSU02G128300, TraesCSU02G128200, TraesCSU02G128100, TraesCSU02G128000, TraesCSU02G127900, TraesCS5A02G545400, TraesCS5A02G545300, TraesCS5A02G545250, TraesCS5A02G545200, TraesCS5A02G544521, TraesCS5A02G544500, TraesCS5A02G544400, TraesCS5A02G544200, TraesCS5A02G544196, TraesCS5A02G544189, TraesCS5A02G544100, TraesCS5A02G544000, TraesCS5A02G543800, TraesCS5A02G543756, TraesCS5A02G543700, TraesCS5A02G543600, TraesCS4B02G378400, TraesCS4B02G378300, TraesCS4B02G378200, TraesCS4B02G378100, TraesCS4B02G378000, TraesCS4B02G377900, TraesCS4B02G377800, TraesCS4B02G377700, TraesCS4B02G377500, TraesCS4B02G377400, TraesCS4B02G377300, TraesCS4B02G377200, TraesCS4B02G377100, TraesCS4B02G377000, TraesCS4B02G376900, TraesCS4B02G376700	Unknown	Zhou et al. (1998);
PR17	Plant basic secretory family protein	TraesCS6D02G072100, TraesCS1D02G174100, TraesCS6B02G105400, TraesCS1A02G166600, TraesCS6A02G078400, TraesCS1B02G183100	Downstream of BIR	Christensen et al. (2002); Zhang et al. (2012);
PR18	Carbohydrate oxidases FAD-binding Berberine family protein	TraesCS7B02G273700, TraesCS7D02G368800, TraesCS7A02G353900, TraesCS4D02G101000, TraesCS4B02G104000, TraesCS4A02G212100, TraesCS2A02G542600, TraesCS5A02G555000, TraesCS2B02G572400, TraesCS2D02G543700, TraesCSU02G034600, TraesCS4B02G391900, TraesCS4B02G358600, TraesCS7D02G393900, TraesCS7B02G300200, TraesCS7A02G400100, TraesCS7B02G273600, TraesCS7D02G368700, TraesCS7B02G273500, TraesCS3A02G066000LC, TraesCS7A02G354000, TraesCS7D02G368500, TraesCS7A02G126600, TraesCS2B02G145300, TraesCS3D02G113700, TraesCS7D02G124500, TraesCS5A02G261400, TraesCS3A02G111600, TraesCS7B02G273800, TraesCS2D02G126200, TraesCS7D02G369000, TraesCS5D02G268800, TraesCS7D02G472000, TraesCS3B02G132200, TraesCS2A02G052700, TraesCS2A02G123200, TraesCS7B02G388200, TraesCS7A02G484600, TraesCS7A02G353800, TraesCS7B02G273900, TraesCS2D02G052300, TraesCS2B02G066900, TraesCS2A02G052800, TraesCS2D02G126400, TraesCS2D02G052500, TraesCS2B02G145500, TraesCS2B02G066800, TraesCS2A02G052600, TraesCS2A02G052900, TraesCS2D02G052700	Unknown	Custers et al. (2004);

widespread application of gene editing technologies, knockout of key negative regulatory genes involved in SAR-like responses in wheat can generate innovative disease-resistant germplasm resources, demonstrating significant research prospects and application potential.

Author contributions

SZ: Data curation, Investigation, Visualization, Writing – original draft, Software. ML: Data curation, Investigation, Software, Visualization, Writing – original draft. XR: Data curation, Investigation, Writing – original draft. CW: Data curation, Investigation, Writing – original draft. XS: Formal analysis, Funding acquisition, Supervision, Writing – review & editing. MS: Formal analysis, Funding acquisition, Supervision, Writing – review & editing. XY: Formal analysis, Supervision, Writing – review & editing. XW: Conceptualization, Funding acquisition, Project administration, Supervision, Writing – review & editing, Formal analysis.

Funding

The author(s) declare financial support was received for the research, authorship, and/or publication of this article. This work was supported by the National Key Research and Development Program of China (2023YFD1201002), Provincial Natural Science Foundation of Hebei for Outstanding Young Scientists (C2022204010), Provincial Natural Science Foundation of Hebei (C2021204008 and C2021204010), Local Science and Technology Development Fund Projects Guided by the Central Government (236Z6501G and 236Z6302G), Provincial Natural Science Foundation of Hebei for Excellent Young Scientists (C2023204188), the State Key Laboratory of North China Crop Improvement and Regulation (NCCIR2021ZZ-17), and S&T Program of Hebei (23567601H).

Conflict of interest

The authors declare that the research was conducted in the absence of any commercial or financial relationships that could be construed as a potential conflict of interest.

Publisher's note

All claims expressed in this article are solely those of the authors and do not necessarily represent those of their affiliated organizations, or those of the publisher, the editors and the reviewers. Any product that may be evaluated in this article, or claim that may be made by its manufacturer, is not guaranteed or endorsed by the publisher.

References

Aglas, L., Soh, W. T., Kraiem, A., Wenger, M., Brandstetter, H., and Ferreira, F. (2020). Ligand binding of PR-10 proteins with a particular focus on the bet v 1 allergen family. *Curr. Allergy Asthm. Rep.* 20, 1–11. doi: 10.1007/s11882-020-00918-4

Ahangar, L., Ranjbar, G. A., Babaeizad, V., Najafi Zarrini, H., and Biabani, A. (2017). Assay of *NPR1* gene expression in wheat under powdery mildew stress. *J. Crop Prot.* 6, 157–166.

Beßer, K., Jarosch, B., Langen, G., and Kogel, K. H. (2000). Expression analysis of genes induced in barley after chemical activation reveals distinct disease resistance pathways. *Mol. Plant Pathol.* 1, 277–286. doi: 10.1046/j.1364-3703.2000.00031.x

Bi, W., Zhao, S., Zhao, J., Su, J., Yu, X., Liu, D., et al. (2020). Rust effector PNPi interacting with wheat TaPR1a attenuates plant defense response. *Phytopathol. Res.* 2, 1–14. doi: 10.1186/s42483-020-00075-6

Blein, J. P., Coutos-Thévenot, P., Marion, D., and Ponchet, M. (2002). From elicitins to lipid-transfer proteins: a new insight in cell signalling involved in plant defence mechanisms. *Trends Plant Sci.* 7, 293–296. doi: 10.1016/S1360-1385(02)02284-7

Cantu, D., Yang, B., Ruan, R., Li, K., Menzo, V., Fu, D., et al. (2013). Comparative analysis of protein-protein interactions in the defense response of rice and wheat. *BMC Genomics* 14, 1–12. doi: 10.1186/1471-2164-14-166

Cao, H., Glazebrook, J., Clarke, J. D., Volko, S., and Dong, X. (1997). The *Arabidopsis NPR1* gene that controls systemic acquired resistance encodes a novel protein containing ankyrin repeats. *Cell* 88, 57–63. doi: 10.1016/S0092-8674(00)81858-9

Chen, J., Mohan, R., Zhang, Y., Li, M., Chen, H., Palmer, I. A., et al. (2019). NPR1 promotes its own and target gene expression in plant defense by recruiting CDK8. *Plant Physiol.* 181, 289–304. doi: 10.1104/pp.19.00124

Chen, Z., Iyer, S., Caplan, A., Klessig, D. F., and Fan, B. (1997). Differential accumulation of salicylic acid and salicylic acid-sensitive catalase in different rice tissues. *Plant Physiol.* 114, 193–201. doi: 10.1104/pp.114.1.193

Chern, M., Fitzgerald, H. A., Canlas, P. E., Navarre, D. A., and Ronald, P. C. (2005). Overexpression of a rice *NPR1* homolog leads to constitutive activation of defense response and hypersensitivity to light. *Mol. Plant-Microbe Interact.* 18, 511–520. doi: 10.1094/MPMI-18-0511

Chern, M. S., Fitzgerald, H. A., Yadav, R. C., Canlas, P. E., Dong, X., and Ronald, P. C. (2001). Evidence for a disease-resistance pathway in rice similar to the NPR1-mediated signaling pathway in Arabidopsis. *Plant J.* 27, 101–113. doi: 10.1046/j.1365-313x.2001.01070.x

Christensen, A. B., Cho, B. H., Næsby, M., Gregersen, P. L., Brandt, J., Madriz-Ordeñana, K., et al. (2002). The molecular characterization of two barley proteins establishes the novel PR-17 family of pathogenesis-related proteins. *Mol. Plant Pathol.* 3, 135–144. doi: 10.1046/j.1364-3703.2002.00105.x

Colebrook, E. H., Creissen, G., McGrann, G. R. D., Dreos, R., Lamb, C., and Boyd, L. A. (2012). Broad-spectrum acquired resistance in barley induced by the *Pseudomonas* pathosystem shares transcriptional components with *Arabidopsis* systemic acquired resistance. *Mol. Plant-Microbe Interact.* 25, 658–667. doi: 10.1094/MPMI-09-11-0246

Custers, J. H., Harrison, S. J., Sela-Buurlage, M. B., Van Deventer, E., Lageweg, W., Howe, P. W., et al. (2004). Isolation and characterisation of a class of carbohydrate oxidases from higher plants, with a role in active defence. *Plant J.* 39, 147–160. doi: 10.1111/j.1365-313X.2004.02117.x

Delaney, T. P., Friedrich, L., and Ryals, J. A. (1995). *Arabidopsis* signal transduction mutant defective in chemically and biologically induced disease resistance. *Proc. Natl. Acad. Sci. U.S.A.* 92, 6602–6606. doi: 10.1073/pnas.92.14.6602

Dey, S., Wenig, M., Langen, G., Sharma, S., Kugler, K. G., Knappe, C., et al. (2014). Bacteria-triggered systemic immunity in barley is associated with *WRKY* and *ETHYLENE RESPONSIVE FACTORs* but not with salicylic acid. *Plant Physiol.* 166, 2133–2151. doi: 10.1104/pp.114.249276

Diethelm, M., Schmolke, M., Groth, J., Friedt, W., Schweizer, G., and Hartl, L. (2014). Association of allelic variation in two NPR1-like genes with *Fusarium* head blight resistance in wheat. *Mol. Breed.* 34, 31–43. doi: 10.1007/s11032-013-0010-2

Epple, P., Apel, K., and Bohlmann, H. (1995). An *Arabidopsis thaliana* thionin gene is inducible *via* a signal transduction pathway different from that for pathogenesis-related proteins. *Plant Physiol.* 109, 813. doi: 10.1104/pp.109.3.813

Esmail, S. M., Aboulila, A. A., and Abd El-Moneim, D. (2020). Variation in several pathogenesis-related (PR) protein genes in wheat (*Triticum aestivum*) involved in defense against *Puccinia striiformis* f. sp. *tritici*. *Physiol. Mol. Plant Pathol.* 112, 101545. doi: 10.1016/j.pmpp.2020.101545

Ferreira, R. B., Monteiro, S. A. R. A., Freitas, R., Santos, C. N., Chen, Z., Batista, L. M., et al. (2007). The role of plant defence proteins in fungal pathogenesis. *Mol. Plant Pathol.* 8, 677–700. doi: 10.1111/j.1364-3703.2007.00419.x

Fu, Z. Q., and Dong, X. (2013). Systemic acquired resistance: turning local infection into global defense. *Annu. Rev. Plant Biol.* 64, 839–863. doi: 10.1146/annurev-arplant-042811-105606

Fu, Z. Q., Yan, S., Saleh, A., Wang, W., Ruble, J., Oka, N., et al. (2012). NPR3 and NPR4 are receptors for the immune signal salicylic acid in plants. *Nature* 486, 228–232. doi: 10.1038/nature11162

Gaddour, K., Vicentecarbajosa, J., Lara, P., Isabellamoneda, I., Díaz, I., and Carbonero, P. (2001). A constitutive cystatin-encoding gene from barley (Icy) responds differentially to abiotic stimuli. *Plant Mol. Biol.* 45, 599–608. doi: 10.1023/A:1010697204686

Gao, J., Bi, W., Li, H., Wu, J., Yu, X., Liu, D., et al. (2018). *WRKY* transcription factors associated with NPR1-mediated acquired resistance in barley are potential resources to improve wheat resistance to *Puccinia triticina*. *Front. Plant Sci.* 9, 1486. doi: 10.3389/fpls.2018.01486

Gao, C. S., Kou, X. J., Li, H. P., Zhang, J. B., Saad, A. S. I., and Liao, Y. C. (2013). Inverse effects of *Arabidopsis NPR1* gene on *Fusarium* seedling blight and *Fusarium* head blight in transgenic wheat. *Plant Pathol.* 62, 383–392. doi: 10.1111/j.1365-3059.2012.02656.x

Gao, L., Wang, S., Li, X. Y., Wei, X. J., Zhang, Y. J., Wang, H. Y., et al. (2015). Expression and functional analysis of a pathogenesis-related protein 1 gene, *TcLr19PR1*, involved in wheat resistance against leaf rust fungus. *Plant Mol. Biol. Rep.* 33, 797–805. doi: 10.1007/s11105-014-0790-5

Ghorbel, M., Zribi, I., Haddaji, N., Besbes, M., Bouali, N., and Brini, F. (2021). The wheat pathogenesis related protein (TdPR1. 2) ensures contrasting behaviors to *E. coli* transformant cells under stress conditions. *Adv. Microbiol.* 11, 453–468. doi: 10.4236/aim.2021.119034

Giżyńska, M., Witkowska, J., Karpowicz, P., Rostankowski, R., Chocron, E. S., Pickering, A. M., et al. (2018). Proline-and arginine-rich peptides as flexible allosteric modulators of human proteasome activity. *J. Med. Chem.* 62, 359–370. doi: 10.1021/acs.jmedchem.8b01025

Görlach, J., Volrath, S., Knauf-Beiter, G., Hengy, G., Beckhove, U., Kogel, K. H., et al. (1996). Benzothiadiazole, a novel class of inducers of systemic acquired resistance, activates gene expression and disease resistance in wheat. *Plant Cell.* 8, 629–643. doi: 10.1105/tpc.8.4.629

Gregersen, P. L., Thordal-Christensen, H., Förster, H., and Collinge, D. B. (1997). Differential gene transcript accumulation in barley leaf epidermis and mesophyll in response to attack by *Blumeria graminis* f. sp. *hordei* (syn. *Erysiphe graminis* f. sp. *hordei*). *Physiol. Mol. Plant Pathol.* 51, 85–97. doi: 10.1006/pmpp.1997.0108

Hafez, Y. M., Soliman, N. K., Saber, M. M., Imbabi, I. A., and Abd-Elaziz, A. S. (2014). Induced resistance against *Puccinia triticina*, the causal agent of wheat leaf rust by chemical inducers. *Egypt. J. Biol. Pest Control* 24, 173.

Hamamouch, N., Li, C., Seo, P. J., PARK, C. M., and Davis, E. L. (2011). Expression of *Arabidopsis* pathogenesis-related genes during nematode infection. *Mol. Plant Pathol.* 12, 355–364. doi: 10.1111/j.1364-3703.2010.00675.x

Han, Z., Guang, D., Schneiter, R., and Tian, C. (2023). The function of plant PR1 and other members of the CAP protein superfamily in plant–pathogen interactions. *Mol. Plant Pathol.* 24, 651–668. doi: 10.1111/mpp.13320

Hermann, M., Maier, F., Masroor, A., Hirth, S., Pfitzner, A. J., and Pfitzner, U. M. (2013). The arabidopsis NIMIN proteins affect NPR1 differentially. *Front. Plant Sci.* 4. doi: 10.3389/fpls.2013.00088

Jordá, L., Conejero, V., and Vera, P. (2000). Characterization of P69E and P69F, two differentially regulated genes encoding new members of the subtilisin-like proteinase family from tomato plants. *Plant Physiol.* 122, 67–74. doi: 10.1104/pp.122.1.67

Kumar, S., Zavaliev, R., Wu, Q., Zhou, Y., Cheng, J., Dillard, L., et al. (2022). Structural basis of NPR1 in activating plant immunity. *Nature* 605, 561–566. doi: 10.1038/s41586-022-04699-w

Lawton, K., Weymann, K., Friedrich, L., Vernooij, B., Uknes, S., and Ryals, J. (1995). Systemic acquired resistance in *Arabidopsis* requires salicylic acid but not ethylene. *Mol. Plant-Microbe Interact.* 8, 863–870. doi: 10.1094/MPMI-8-0863

Li, M., Chen, H., Chen, J., Chang, M., Palmer, I. A., Gassmann, W., et al. (2018). TCP transcription factors interact with NPR1 and contribute redundantly to systemic acquired resistance. *Front. Plant Sci.* 9, 1153. doi: 10.3389/fpls.2018.01153

Li, Q., Chen, Y., Wang, J., Zou, F., Jia, Y., Shen, D., et al. (2019). A *Phytophthora capsica* virulence effector associates with NPR1 and suppresses plant immune responses. *Phytopathol. Res.* 1, 1–11. doi: 10.1186/s42483-019-0013-y

Li, H., Wu, J., Shang, X., Geng, M., Gao, J., Zhao, S., et al. (2020). *WRKY* transcription factors shared by BTH-induced resistance and *NPR1*-mediated acquired resistance improve broad-spectrum disease resistance in wheat. *Mol. Plant-Microbe Interact.* 33, 433–443. doi: 10.1094/MPMI-09-19-0257-R

Li, M., Zhao, S., Yang, J., Ren, Y., Su, J., Zhao, J., et al. (2022). Exogenous expression of barley *HvWRKY6* in wheat improves broad-spectrum resistance to leaf rust, *Fusarium* crown rot, and sharp eyespot. *Int. J. Biol. Macromolecules* 218, 1002–1012. doi: 10.1016/j.ijbiomac.2022.07.138

Liu, P., Guo, J., Zhang, R., Zhao, J., Liu, C., Qi, T., et al. (2019a). TaCIPK10 interacts with and phosphorylates TaNH2 to activate wheat defense responses to stripe rust. *Plant Biotechnol. J.* 17, 956–968. doi: 10.1111/pbi.13031

Liu, X., Liu, Z., Niu, X., Xu, Q., and Yang, L. (2019b). Genome-wide identification and analysis of the NPR1-like gene family in bread wheat and its relatives. *Int. J. Mol. Sci.* 20, 5974. doi: 10.3390/ijms20235974

Liu, R., Lu, J., Xing, J., Xue, L., Wu, Y., and Zhang, L. (2023b). Characterization and functional analyses of wheat *TaPR1* genes in response to stripe rust fungal infection. *Sci. Rep.* 13, 3362. doi: 10.1038/s41598-023-30456-8

Liu, J., Wu, X., Fang, Y., Liu, Y., Bello, E. O., Li, Y., et al. (2023a). A plant RNA virus inhibits NPR1 sumoylation and subverts NPR1-mediated plant immunity. *Nat. Commun.* 14, 3580. doi: 10.1038/s41467-023-39254-2

Lu, S., Faris, J. D., Sherwood, R., Friesen, T. L., and Edwards, M. C. (2014). A dimeric PR-1-type pathogenesis-related protein interacts with ToxA and potentially mediates ToxA-induced necrosis in sensitive wheat. *Mol. Plant Pathol.* 15, 650–663. doi: 10.1111/mpp.12122

Maier, F., Zwicker, S., Hueckelhoven, A., Meissner, M., Funk, J., Pfitzner, A. J., et al. (2011). NONEXPRESSOR OF PATHOGENESIS-RELATED PROTEINS1 (NPR1) and some NPR1-related proteins are sensitive to salicylic acid. *Mol. Plant Pathol.* 12, 73–91. doi: 10.1111/j.1364-3703.2010.00653.x

Molina, A., Görlach, J., Volrath, S., and Ryals, J. (1999). Wheat genes encoding two types of PR-1 proteins are pathogen inducible, but do not respond to activators of systemic acquired resistance. *Mol. Plant-Microbe Interact.* 12, 53–58. doi: 10.1094/MPMI.1999.12.1.53

Moreau, M., Tian, M., and Klessig, D. F. (2012). Salicylic acid binds NPR3 and NPR4 to regulate NPR1-dependent defense responses. *Cell Res.* 22, 1631–1633. doi: 10.1038/cr.2012.100

Mou, Z., Fan, W., and Dong, X. (2003). Inducers of plant systemic acquired resistance regulate NPR1 function through redox changes. *Cell* 113, 935–944. doi: 10.1016/S0092-8674(03)00429-X

Nakayama, A., Fukushima, S., Goto, S., Matsushita, A., Shimono, M., Sugano, S., et al. (2013). Genome-wide identification of WRKY45-regulated genes that mediate benzothiadiazole-induced defense responses in rice. *BMC Plant Biol.* 13, 1–11. doi: 10.1186/1471-2229-13-150

Numan, M., Bukhari, S. A., Rehman, M. U., Mustafa, G., and Sadia, B. (2021). Phylogenetic analyses, protein modeling and active site prediction of two pathogenesis related (*PR2* and *PR3*) genes from bread wheat. *PloS One* 16, e0257392. doi: 10.1371/journal.pone.0257392

Passardi, F., Penel, C., and Dunand, C. (2004). Performing the paradoxical: how plant peroxidases modify the cell wall. *Trends Plant Sci.* 9, 534–540. doi: 10.1016/j.tplants.2004.09.002

Petroski, M. D., and Deshaies, R. J. (2005). Function and regulation of cullin–RING ubiquitin ligases. *Nat. Rev. Mol. Cell Biol.* 6, 9–20. doi: 10.1038/nrm1547

Quilis, J., Peñas, G., Messeguer, J., Brugidou, C., and Segundo, B. S. (2008). The *Arabidopsis AtNPR1* inversely modulates defense responses against fungal, bacterial, or viral pathogens while conferring hypersensitivity to abiotic stresses in transgenic rice. *Mol. Plant-Microbe Interact.* 21, 1215–1231. doi: 10.1094/MPMI-21-9-1215

Schweizer, P., Schlagenhauf, E., Schaffrath, U., and Dudler, R. (1999). Different patterns of host genes are induced in rice by *Pseudomonas syringae*, a biological inducer of resistance, and the chemical inducer benzothiadiazole (BTH). *Eur. J. Plant Pathol.* 105, 659–665. doi: 10.1023/A:1008791223608

Sedgwick, S. G., and Smerdon, S. J. (1999). The ankyrin repeat: a diversity of interactions on a common structural framework. *Trends Biochem. Sci.* 24, 311–316. doi: 10.1016/S0968-0004(99)01426-7

Sels, J., Mathys, J., De Coninck, B. M., Cammue, B. P., and De Bolle, M. F. (2008). Plant pathogenesis-related (PR) proteins: a focus on PR peptides. *Plant Physiol. Biochem.* 46, 941–950. doi: 10.1016/j.plaphy.2008.06.011

Shang, S., Liu, G., Zhang, S., Liang, X., Zhang, R., and Sun, G. (2023). A fungal CFEM-containing effector targets NPR1 regulator NIMIN2 to suppress plant immunity. *Plant Biotechnol. J.* 22, 82–97. doi: 10.1111/pbi.14166

Shimono, M., Sugano, S., Nakayama, A., Jiang, C. J., Ono, K., Toki, S., et al. (2007). Rice *WRKY45* plays a crucial role in benzothiadiazole-inducible blast resistance. *Plant Cell* 19, 2064–2076. doi: 10.1105/tpc.106.046250

Silverman, P., Seskar, M., Kanter, D., Schweizer, P., Métraux, J. P., and Raskin, I. (1995). Salicylic acid in rice (biosynthesis, conjugation, and possible role). *Plant Physiol.* 108, 633–639. doi: 10.1104/pp.108.2.633

Smith, J. A., and Métraux, J. P. (1991). *Pseudomonas syringae* pv. *syringae* induces systemic resistance to *Pyricularia oryzae* in rice. *Physiol. Mol. Plant Pathol.* 39, 451–461. doi: 10.1016/0885-5765(91)90011-6

Sung, Y. C., Outram, M. A., Breen, S., Wang, C., Dagvadorj, B., Winterberg, B., et al. (2021). PR1-mediated defence via C-terminal peptide release is targeted by a fungal pathogen effector. *New Phytol.* 229, 3467–3480. doi: 10.1111/nph.17128

Terras, F. R., Eggermont, K., Kovaleva, V., Raikhel, N. V., Osborn, R. W., Kester, A., et al. (1995). Small cysteine-rich antifungal proteins from radish: Their role in host defense. *Plant Cell* 7, 573. doi: 10.2307/3870116

Uknes, S., Mauch-Mani, B., Moyer, M., Potter, S., Williams, S., Dincher, S., et al. (1992). Acquired resistance in *arabidopsis*. *Plant Cell* 4, 645–656. doi: 10.1105/tpc.4.6.645

van Loon, L. C., Rep, M., and Pieterse, C. M. (2006). Significance of inducible defense-related proteins in infected plants. *Annu. Rev. Phytopathol.* 44, 135–162. doi: 10.1146/annurev.phyto.44.070505.143425

Wang, X., Bi, W. S., Gao, J., Yu, X., Wang, H., and Liu, D. (2018). Systemic acquired resistance, *NPR1*, and pathogenesis-related genes in wheat and barley. *J. Integr. Agricult.* 17, 60345–60347. doi: 10.1016/S2095-3119(17)61852-5

Wang, L., Lu, H., Zhan, J., Shang, Q., Wang, L., Yin, W., et al. (2022b). Pathogenesis-related protein-4 (*PR-4*) gene family in Qingke (*Hordeum vulgare* L. var. *nudum*): Genome-wide identification, structural analysis and expression profile under stresses. *Mol. Biol. Rep.* 49, 9397–9408. doi: 10.1007/s11033-022-07794-3

Wang, F., Shen, S., Zhao, C., Cui, Z., Meng, L., Wu, W., et al. (2022a). TaPR1 interacts with TaTLP1 via the αIV helix to be involved in wheat defense to *Puccinia triticina* through the CAPE1 motif. *Front. Plant Sci.* 13, 874654. doi: 10.3389/fpls.2022.874654

Wang, X., Yang, B., Li, K., Kang, Z., Cantu, D., and Dubcovsky, J. (2016). A conserved *Puccinia striiformis* protein interacts with wheat NPR1 and reduces induction of pathogenesis-related genes in response to pathogens. *Mol. Plant-Microbe Interact.* 29, 977–989. doi: 10.1094/MPMI-10-16-0207-R

Wang, F., Yuan, S., Wu, W., Yang, Y., Cui, Z., Wang, H., et al. (2020a). TaTLP1 interacts with TaPR1 to contribute to wheat defense responses to leaf rust fungus. *PloS Genet.* 16, e1008713. doi: 10.1371/journal.pgen.1008713

Wang, X., Zhang, H., Nyamesorto, B., Luo, Y., Mu, X., Wang, F., et al. (2020b). A new mode of NPR1 action via an NB-ARC–NPR1 fusion protein negatively regulates the defence response in wheat to stem rust pathogen. *New Phytol.* 228, 959–972. doi: 10.1111/nph.16748

Wang, F., Shen, S., Cui, Z., Yuan, S., Qu, P., Jia, H., et al. (2023). *Puccinia triticina* effector protein Pt_21 interacts with wheat thaumatin-like protein TaTLP1 to inhibit its antifungal activity and suppress wheat apoplast immunity. *Crop J.* 11, 1431–1440. doi: 10.1016/j.cj.2023.04.006

Wu, J., Gao, J., Bi, W., Zhao, J., Yu, X., Li, Z., et al. (2019). Genome-wide expression profiling of genes associated with the *Lr47*-mediated wheat resistance to leaf rust (*Puccinia triticina*). *Int. J. Mol. Sci.* 20, 4498. doi: 10.3390/ijms20184498

Wu, Y., Zhang, D., Chu, J. Y., Boyle, P., Wang, Y., Brindle, I. D., et al. (2012). The *Arabidopsis* NPR1 protein is a receptor for the plant defense hormone salicylic acid. *Cell Rep.* 1, 639–647. doi: 10.1016/j.celrep.2012.05.008

Xu, G., Yuan, M., Ai, C., Liu, L., Zhuang, E., Karapetyan, S., et al. (2017). uORF-mediated translation allows engineered plant disease resistance without fitness costs. *Nature* 545, 491–494. doi: 10.1038/nature22372

Yang, Z., Ma, X., Wu, S., Wang, H., Sun, X., Ji, X., et al. (2013). Cloning of *NPR1-like* genes and their response to *Fusarium graminearum* infection in wheat. *Acta Agronom. Sin.* 39, 1775–1782. doi: 10.3724/SP.J.1006.2013.01775

Yu, G., Zhang, X., Yao, J., Zhou, M., and Ma, H. (2017). Resistance against *Fusarium* Head Blight in transgenic wheat plants expressing the *ScNPR1* gene. *J. Phytopathol.* 165, 223–231. doi: 10.1111/jph.12553

Zhang, Y., Fan, W., Kinkema, M., Li, X., and Dong, X. (1999). Interaction of NPR1 with basic leucine zipper protein transcription factors that bind sequences required for salicylic acid induction of the *PR-1* gene. *Proc. Natl. Acad. Sci. U.S.A.* 96, 6523–6528. doi: 10.1073/pnas.96.11.6523

Zhang, W. J., Pedersen, C., Kwaaitaal, M., Gregersen, P. L., Mørch, S. M., Hanisch, S., et al. (2012). Interaction of barley powdery mildew effector candidate CSEP0055 with the defence protein PR17c. *Mol. Plant Pathol.* 13, 1110–1119. doi: 10.1111/j.1364-3703.2012.00820.x

Zhao, J., Bi, W., Zhao, S., Su, J., Li, M., Ma, L., et al. (2021). Wheat apoplast-localized lipid transfer protein TaLTP3 enhances defense responses against *Puccinia triticina*. *Front. Plant Sci.* 12, 771806. doi: 10.3389/fpls.2021.771806

Zhao, S., Shang, X., Bi, W., Yu, X., Liu, D., Kang, Z., et al. (2020). Genome-wide identification of effector candidates with conserved motifs from the wheat leaf rust fungus *Puccinia triticina*. *Front. Microbiol.* 11, 1188. doi: 10.3389/fmicb.2020.01188

Zhou, F., Zhang, Z., Gregersen, P. L., Mikkelsen, J. D., de Neergaard, E., Collinge, D. B., et al. (1998). Molecular characterization of the oxalate oxidase involved in the response of barley to the powdery mildew fungus. *Plant Physiol.* 117, 33–41. doi: 10.1104/pp.117.1.33

Zribi, I., Ghorbel, M., Haddaji, N., Besbes, M., and Brini, F. (2023). Genome-wide identification and expression profiling of pathogenesis-related protein 1 (*PR-1*) genes in durum wheat (*Triticum durum* desf.). *Plants* 12, 1998. doi: 10.3390/plants12101998

frontiers | Frontiers in Plant Science

TYPE Original Research
PUBLISHED 21 March 2024
DOI 10.3389/fpls.2024.1369330

Check for updates

OPEN ACCESS

EDITED BY
Runsheng Ren,
Jiangsu Academy of Agricultural Sciences (JAAS), China

REVIEWED BY
Giorgio Mariano Balestra,
University of Tuscia, Italy
Juanni Chen,
Southwest University, China

*CORRESPONDENCE
Lifang Wu
lfwu@ipp.ac.cn

†These authors share first authorship

RECEIVED 12 January 2024
ACCEPTED 26 February 2024
PUBLISHED 21 March 2024

CITATION
Zhang H, Yuan M, Gao Y, Su P, Jia H, Tang C, Meng H and Wu L (2024) Nano protective membrane coated wheat to resist powdery mildew.
Front. Plant Sci. 15:1369330.
doi: 10.3389/fpls.2024.1369330

COPYRIGHT
© 2024 Zhang, Yuan, Gao, Su, Jia, Tang, Meng and Wu. This is an open-access article distributed under the terms of the Creative Commons Attribution License (CC BY). The use, distribution or reproduction in other forums is permitted, provided the original author(s) and the copyright owner(s) are credited and that the original publication in this journal is cited, in accordance with accepted academic practice. No use, distribution or reproduction is permitted which does not comply with these terms.

Nano protective membrane coated wheat to resist powdery mildew

Huilan Zhang[1,2,3,4†], Meng Yuan[1,5†], Yameng Gao[1], Pengfei Su[1,5], Huiling Jia[1], Caiguo Tang[1,2,3,4], He Meng[1,6] and Lifang Wu[1,2,3,4*]

[1]The Center for Ion Beam Bioengineering & Green Agriculture, Hefei Institutes of Physical Science, Chinese Academy of Sciences, Hefei, Anhui, China, [2]Zhongke Taihe Experimental Station, Taihe, Anhui, China, [3]CNSIG Anhui Hongsifang Fertilizer Co., Ltd., Hefei, Anhui, China, [4]Institute of Hefei Artificial Intelligence Breeding Accelerator, Hefei, Anhui, China, [5]School of Life Sciences, University of Science and Technology of China, Hefei, Anhui, China, [6]School of Life Sciences, Anhui Agricultural University, Hefei, China

The plant pathogenic fungus *Blumeria graminis* f. sp. *tritici* infects wheat and reduces its yield. The policy of reducing fertilizer and biocide use in sustainable agriculture has prompted researchers to develop more green and efficient management strategies. In this study, a novel nanoprotective membrane (kaolin-nano titanium dioxide-liquid paraffin, referred to as KTP) that could effectively prevent powdery mildew of wheat was prepared by using 1 g/L kaolin, 2 g/L nanotitanium dioxide and 8% (v/v) liquid paraffin. The prevention and control effects of KTP spraying in advance in the pot and field experiments were 98.45% and 83.04%, respectively. More importantly, the weight of 1000 grains of wheat pretreated with KTP was 2.56 g higher than that of wheat infected with powdery mildew, significantly improving wheat yield. KTP delayed the germination of powdery mildew spores on the leaf surface, and inhibited the formation of mycelia. In addition, KTP did not affect the growth of wheat or the survival of earthworms. KTP nanoprotective membrane are a green and safe prevention and control materials that are which is expected to be widely used in agriculture to control wheat powdery mildew.

KEYWORDS

wheat, powdery mildew, KTP (kaolin - TiO2-NPs - liquid paraffin), disease index, green prevention and control

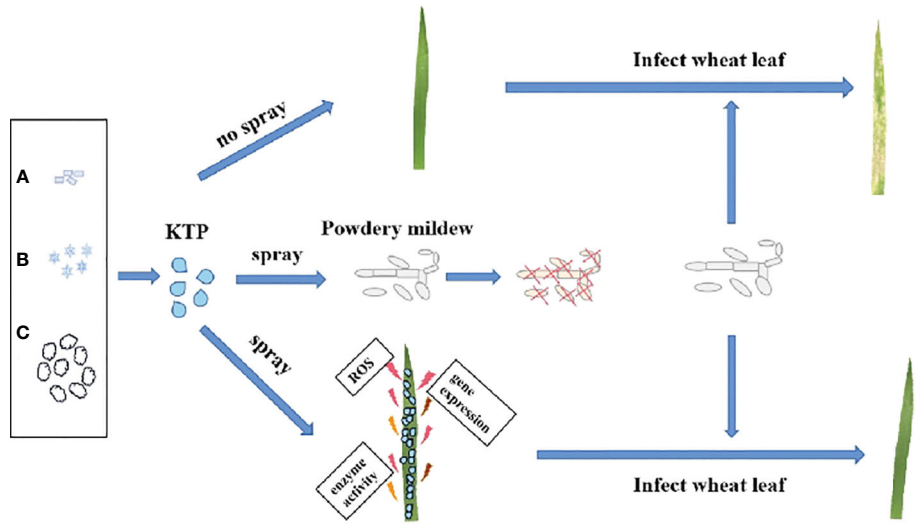

GRAPHICAL ABSTRACT

Highligts

- The powdery mildew inhibitor KTP is composed of 1 g/L kaolin, 2 g/L nanotitanium dioxide and 8% (v/v) liquid paraffin.
- KTP is formed by hydrogen bonding and electrostatic attraction between components.
- The prevention effects of KTP in the pot and field experiments were 98.45% and 83.04%, respectively.
- The yield of wheat increased significantly after the control of powdery mildew by KTP.
- KTP delayed the germination of powdery mildew spores on the leaf surface and inhibited the formation of mycelia.

1 Introduction

Wheat is one of the most important food crops worldwide, and its sustainable production directly affects the stable development of a country (Yinghui et al., 2016). Wheat powdery mildew is a wheat leaf disease caused by the obligate parasitic ascomycetous fungus *Blumeria graminis* f. sp. *tritici* (*Bgt*) that is endemic in warm and humid regions of the world, such as China, the United Kingdom, Germany, Japan, and the southeastern United States (Saari and Wilcoxson, 1974; Merchan and Kranz, 1986; Mandal et al., 2014), but especially in northern Europe (Reignault et al., 2001). Under nutrient-rich conditions, *Bgt* spores germinate and produce appressoria, form penetration pegs, enter host cells to form haustoria, absorb nutrients from host cells for the rapid growth of secondary hyphae, and, finally, form colonies (Zheng et al., 2020). Colonies cover the surface of wheat leaves, resulting in chlorophyll degradation and a decrease in the photosynthetic rate (Kuckenberg et al., 2009; Walters et al., 2008; Wright et al., 1995). Therefore, powdery mildew destroys the vegetative growth of the aboveground parts of wheat plants directly, causing an annual yield loss of 14 to 30% (Griffey et al., 1993), and is one of the most destructive diseases in the global wheat industry (Reignault et al., 2001).

To date, the control of powdery mildew relies mainly on the cultivation of disease-resistant plant varieties and the spraying of pesticides. Planting disease-resistant varieties is considered to be one of the most cost-effective ways to prevent and control of wheat powdery mildew (Summers and Brown, 2013; Xin et al., 2012). However, pathogenic bacterial variants alter the physiological effects of antimicrobial agents on plants, causing most cultivated plant varieties to lose resistance after 3-5 years (Vallavieille-Pope et al., 2012). The use of fungicides for many years has led to many problems, such as pathogen resistance, induced plant toxicity and environmental pollution. Therefore, manufacturers urgently need to develop new green and safe preparations for the prevention and control of wheat powdery mildew in the field.

Currently, the practical application of nanotechnology in the agricultural industry has received widespread attention (Santhoshkumar et al., 2014). And NPs have broad potential for agricultural application (Ali et al., 2014). However, research on the management of wheat powdery mildew with nanomaterials is relatively limited, and the expected effect has not been achieved. Moreover, the lack of a control mechanism limits the application of nanomaterials in wheat powdery mildew management. Here, we explored the feasibility of using nanotitanium dioxide (TiO_2-NPs) and kaolin as nanopesticides to control wheat powdery mildew. Wherein, TiO_2-NPs has been widely used for its antibacterial and antifungal properties (Santhoshkumar et al., 2014; Waghmode et al., 2019; Rodríguez-González et al., 2019), which can help plants resist some bacterial and fungal diseases (De Filpo et al.,

2013; Javed et al., 2020; Owolade and Ogunleti, 2008). Kaolin is a nonmetallic mineral with good plasticity that can be used in pesticide production (Cantore et al., 2009). Then, the novel nanocomposite was obtained by combining it with the modifier liquid paraffin.

In this study, 1 g/L kaolin, 2 g/L nanotitanium dioxide, and 8% (v/v) liquid paraffin were used to prepare the nanoprotective membrane (kaolin- nanotitanium dioxide -liquid paraffin, referred to as KTP). We explored the mechanism by which KTP controls wheat powdery mildew at the molecular, physiological and biochemical levels. KTP plays an important role in regulating the expression of the pathogenesis-related protein-encoding gene *PR1*, the oxalate oxidase gene (*OXO*) and the chitinase gene (*CHI1*). We found that KTP delayed the germination of powdery mildew spores on the leaf surface and inhibited mycelium formation. The physicochemical properties of KTP showed that it was formed by hydrogen bonding and electrostatic attraction among the components, and KTP could be uniformly applied to the surface of wheat leaves with good hydrophobicity and thermal stability, meeting the needs of the field. Furthermore, spraying KTP in the field could effectively prevent wheat powdery mildew incidence and reduce the loss of wheat yield and quality. The above results showed that the nanoprotective membrane could effectively control wheat powdery mildew. And KTP has the ability to control wheat powdery mildew on a large scale. We believe that this new plant protection material will provide farmers with a novel management strategy to prevent powdery mildew, which will have a positive impact on sustainable agricultural production.

2 Materials and methods

2.1 Materials

Kaolin (CAS:1332-58-7, 1250 mesh) was purchased from Yuejiang New Materials Co., Ltd (Guangzhou, Guangdong, China). Nanotitanium dioxide (TiO_2-NPs, CAS:13463-67-7, 99.8% anatase type) was purchased from Shanghai Aladdin Biochemical Technology Co., Ltd. (Shanghai, China). Liquid paraffin (CAS: 8042-47-5) was obtained Sangon Biotech (Shanghai) Co., Ltd (Shanghai, China). The other chemicals used in this work were all of analytical reagent grade and purchased from Sinopharm Chemical Reagent Co., Ltd.

The winter wheat (*Triticum aestivum L.*) variety Bainong 207 (provided by Professor Hao Chenyang of the Institute of Crop Sciences, Chinese Academy of Agricultural Sciences), which is sensitive to powdery mildew infection, was used for all the experiments in this study. The grains of Bainong 207 that were of uniform in size and not damaged were selected and planted in pots containing rich nutritive soil (diameter = 10 cm), with 20 seeds in each pot. The wheat plants were grown in a constant temperature and light incubator with a light intensity of 300 μmol photons $m^{-2}s^{-1}$, 22°C/20°C, 16 h light/8 h dark cycle, and 85% relative humidity.

2.2 Preparation of KTP

A total of 0.1 g of kaolin, 0.2 g of TiO2-NPs and 8 mL of liquid paraffin were added, after which the volume was brought to 100 mL with deionized water. The resulting suspension was stirred at 1500 rpm/min for 2 h, followed by ultrasonic treatment for 1 h. The resulting mixture was named KTP (kaolin - TiO_2-NPs - liquid paraffin) and was incubated at room temperature condition.

2.3 Characterization of KTP

The prepared sample was directly analyzed via contact angle (CA), Fourier transform infrared (FTIR) spectroscopy, the thermal gravimetric analysis (TGA), differential thermal analysis (DTA), zeta potential analysis and scanning electron microscopy -energy dispersive spectrometer (SEM-EDS).

The contact angle (CA) (JY-82, Dataphysics Co., Germany.) was detected according to the sessile drop method at room temperature. Detailed steps are as follows: appropriate amounts of kaolin and titanium dioxide were tabletted, and then a drop of water was dropped directly above the surface of the slide containing each sample tablet and photographed during the process, and the contact angle between the water droplet and the surface of each sample was measured by goniophotometric method. Subsequently, the contact angle of KTP was determined by applying it uniformly to the slide surface.

The samples were also characterized by Fourier transform infrared spectroscopy (FTIR) (iS10, Nicolet Co., U.S.A.) in a KBr pellet at ambient temperature, wherein the sample content in KBr was 0.5%. For each sample, 32 scans were recorded in a 400–4000 cm^{-1} spectral range at a resolution of 4 cm^{-1}. The infrared spectra of kaolin and titanium dioxide nanoparticles were collected. Then, the ATR (Attenuated Total Refraction, ATR) accessory was placed in the optical path of the spectrometer, and 1 drop of liquid paraffin and KTP were pipetted onto the crystal surface of the ATR accessory, and the infrared spectra of the liquid paraffin and KTP were collected with an air background as a blank control.

The thermal gravimetric analysis and differential thermal analysis were performed by a thermogravimetric analyzer (TG-DSC) (STA 449F3, NETZSCH Co., Germany.) at a scan rate of 10 °C/min from room temperature to 800°C in nitrogen. And used the scanning electron microscope (SEM) (Sirion 200, FEI Co., U.S.A.) to observe the morphology of the leaves.

Scanning electron microscope and energy dispersive spectrometer(SEM-EDS)analysis of KTP nano protective membrane distribution on leaf surface. Detailed steps are as follows: wheat leaves of normal growth for 7 days, and the following 4 different treatments: normally grown wheat leaves (CK group), wheat leaves sprayed with KTP (KTP group), wheat leaves inoculated with Bgt after KTP spraying (KTP + Bgt group), and wheat leaves inoculated with Bgt (Bgt group) were carried out. After 144 h, suitable size of leaves were cut and stuck directly to the

conductive adhesive and sprayed gold for 30 s. Subsequently, a scanning electron microscope (SEM) was used, in which an accelerating voltage of 15 kV was selected for the energy spectrum, and a detector was used to analyze the surface morphology of the samples as well as the elemental distribution.

The charged nature of the components was analyzed using a zeta potential analyzer (ZS90, Malvern Co., England.). The samples of kaolin, titanium dioxide, liquid paraffin and KTP were placed in deionized water and ultrasonicated for 5 min, and the average value of each group of samples was taken from three measurements.

2.4 Inoculation and control of powdery mildew

Bainong 207 wheat seeds were planted into pots (DI = 10 cm) and placed in a constant -temperature and constant-light incubator. After 7 days of culture in an incubator, sufficient amounts of powdery mildew fungus were cultured for inoculation. Two different treatment methods were employed: one was sprayed with KTP composites which wre subsequently inoculated with powdery mildew after drying. The other was sprayed with the KTP complex 48 hours after infection. The incidence of wheat powdery mildew and seedling growth index (plant height, fresh weight and dry weight) were investigated after 7 days of continuous culture in a light incubator. Moreover, the normal-growing wheat without treatment and that sprayed with KTP were analyzed. The wheat powdery mildew disease index DI was calculated as follows: $DI = \sum_{t=1}^{n}(xi * si)/\sum_{t=1}^{n} xi * I * 100$, where i is the incidence level (0%-100%), xi is the number of leaves with incidence level i, si is the severity value of incidence level i, and I is the incidence rate.7

2.5 Powdery mildew spore germination growth experiment

The wheat plants were subjected to the following 4 different treatments: normally grown wheat leaves (CK group), wheat leaves sprayed with KTP (KTP group), wheat leaves inoculated with *Bgt* after KTP spraying (KTP + *Bgt* group), and wheat leaves inoculated with *Bgt* (*Bgt* group). All the samples were collected in 3 biological replicates at 7 different time points (12,24.48,72,96,120,144 h) after powdery mildew inoculation. After sampling, the wheat leaves in each group were cut into 3 cm long segments, which were subsequently immersed in an ethanol/acetic acid solution (1:1, v/v) and placed at room temperature for 24 h until decolorization. After complete decolorization, the translucent leaves were washed in an aqueous solution of lactic acid and glycerin (lactic acid/glycerin/water, 1/1/1, V/V/V) for 48 h. After complete cleaning, the leaves were dyed by immersing them in 0.6% (W/V) Coomassie Bright Blue R-250 methanol solution for 1 min. Subsequently, the leaves were gently washed with deionized water to remove the excess dye. Finally, the treated leaves were preserved in an aqueous solution of lactic acid and glycerin for microscopic observation.

In addition, the number of powdery mildew spores that formed mature mycelia was counted at 48 h, and 200 spores were counted each time.

2.6 Changes in gene expression in leaves

Wheat leaves from the 4 different treatment groups were collected at each time point, with three biological replicates each time. After sampling, each group of wheat leaves was cut into 2 small sections, each weighing 0.5 g, placed in a centrifuge tube equipped with steel balls, transferred to liquid nitrogen for freezing, and placed in a -80°C freezer for subsequent physiological biochemical and real-time fluorescence quantitative PCR (RT–qPCR) detection.

Total RNA was isolated from the samples using a Plant RNA Isolation Kit (Omega, R6827) according to the manufacturer's instructions. Isolated RNA samples were reverse-transcribed into cDNA using TransScript One-Step gDNA Removal and cDNA Synthesis SuperMix (TransGen Biotech, AT311) following the manufacturer's protocol. Each cDNA sample was diluted 32X with double distilled water. RT-qPCR was performed using a Roche Light Cycler 96 following the standard protocol; three biological replicates were used for RT-qPCR. The housekeeping gene actin (ACT) was used as the internal control and the relative expression of the target genes was calculated using the $2^{-\Delta\Delta CT}$ method. The primer sequences for real-time quantitative reverse transcription polymerase chain reaction are detailed in Table 1.

2.7 Field trial

A large number of powdery mildew fungi were cultivated in an artificial climatic chamber, and the powdery mildew spores on the leaves were rinsed off with sterile water, and the powdery mildew spore suspension with a concentration of 1000 U/mL was adjusted to be used for inoculation of wheat powdery mildew fungi in the field. The experimental field located in Science Island (31°54'N, 117°10'E) with planting Bainong 207 of wheat variety. The experimental areas were divided to 3 plots. Each treatment area consisted of 5 rows (2 m per row, 0.2 m between rows), and each treatment was set up with three replicates. In the evening of wheat flowering, spray the leaf surface with KTP nanofilm, tebuconazole, and powdery mildew spore suspension (1000 U/mL) respectively. The specific methods are as follows: a. Bgt + KTP group: spray the powdery mildew spore suspension first, and 2 days later, spray KTP nanofilm; b. KTP + Bgt group: spray KTP nanofilm first, let it dry naturally, and then spray the powdery mildew spore suspension; c. Tebuconazole + Bgt group: spray the pesticide tebuconazole first, let it dry naturally, and then spray the powdery mildew spore suspension; d. Bgt group: spray with an equal amount of sterile water instead of KTP, let it dry naturally, and then spray the powdery mildew spore suspension; e. KTP + Bgt + KTP group: 15 days later, perform a second spray of KTP nanofilm on the KTP 3+ Bgt group. After 30 days, the disease index of powdery

TABLE 1 qRT-PCR primer sequence information.

Gene	Accession number	Forward sequence(5′-3′)	Reverse sequence (5′-3′)	Gene description
OXO	M21962.1	CAGGGTCGTGG AACTTCTCAAG	TTATCATTTCAG GGAAGGCTCCTA	Oxalate oxidase (Tayeh et al., 2015)
PR1	HQ848391	CATGCACCTTCG TATGCCTAACT	TGGCTTATTAC GGCATTCCTTT	Pathogenesis-related protein 1 (Tayeh et al., 2015)
CHI1	AB029934	GCCACGTCCCC ACCATACTAT	CCGGCAAGAT CGTAGTTGGA	Class 1 basic chitinase (Tayeh et al., 2015)
Act	AB181991	AACCTTCAGT TGCCCAGCAA	TGTTCGACCG CTGGCATAC	Actin (26)

mildew was counted in each of the above plots, during which normal field management such as fertilization and weed control was carried out.

2.8 Biosafety experiment of KTP

Ten earthworms of consistent size and vitality were picked and placed in a 1000 ml rice box containing earthy materials and incubated at room temperature for 2 days. KTP was subsequently sprayed on the soil surface layer, and the control group was sprayed with an equal volume of deionized water and incubated at room temperature for 7 days to observe the survival status of the earthworms.

2.9 Statistical analysis

The experimental data are presented as the average of the measurements obtained from three independent assays and are expressed as the mean ± standard error of the mean. Significant differences between treatments were further analyzed using analysis of variance (ANOVA), and the significance between pairs was tested by Duncan's test (SPSS 26.0; IBM, Somers, NY). $P < 0.05$ was considered to indicate statistical significance.

3 Results and discussion

3.1 Prevention and control of wheat powdery mildew by KTP

Through pot experiments, we examined the efficacy of KTP in controlling powdery mildew. After 1 week, the tips of the wheat leaves in the *Bgt* group began to turn yellow and chlorotic, and powdery mildew colonies covered the leaf surface (Figure 1Aa). Sporadically distributed white punctate plaques appeared on the surface of wheat leaves sprayed with KTP after inoculation with powdery mildew (Figure 1Ac). Notably, no obvious colonies had grown on the surface of the leaves of wheat plants treated with KTP in advance, the leaves still appeared green, and the plants were in good growth condition (Figure 1Abf1). The disease index of the wheat plants from each group were also counted in this trial (Figure 1B). The results showed that the wheat disease index of the *Bgt* group was 96.06. Moreover, we sprayed KTP on wheat plants that had been sick for 2 days, the disease index was reduced to 32.13 and the prevention and control effect was 33.39%. The wheat disease index in the advanced KTP treatment group was 1.49, and the prevention and control effect was 98.45%, which was significantly lower than that in the *Bgt* group and sprayed KTP after inoculation with powdery mildew. This shows that the prespraying KTP prevention and control effect is the best. This result may indicate that the protective film formed on the surface of wheat leaves by spraying KTP in advance effectively hindered the germination and proliferation of powder spores on wheat leaves.

To determine the effect of spraying KTP on the control of powdery mildew in the field, we treated Bainong 207 differently and counted the disease index 30 days later (Figure 1C). It could be seen that the disease index of the KTP + *Bgt*, *Bgt* + KTP and Tebuconazole + *Bgt* groups were 9.33, 14.33 and 3.67 respectively. After 15 days, the KTP + *Bgt* group was sprayed with KTP for the second time, and there was no significant difference between the disease index of the KTP + *Bgt* + KTP group and that of the KTP + *Bgt* group. The disease index of the plants in each treatment proup were significantly lower than those in the *Bgt* group (55), indicating that KTP could be used to control wheat powdery mildew efficiently in the field.

Furthermore, we determined the 1000-grain weight (TGW) of wheat under different treatments (Figure 1D), and the results showed that there was no significant difference between the CK group and the KTP group. The TGWs of the tebuconazole + *Bgt* and KTP + *Bgt* groups were 46.53 g and 47.06 g, respectively. These values were significantly greater in the treatment groups than in the of *Bgt* group (44.5 g). It was worth noting that TGW of KTP + *Bgt* group was not significantly different from that of the CK group, which demonstrated that KTP could completely prevent wheat yield loss caused by powdery mildew infection (the TGW was reduced by 2.56 g). Therefore, KTP is suitable for large-scale promotion and application as powdery mildew prevention and control agent.

3.2 Characterization of the KTP complex

The hydrophobic properties of kaolin, TiO_2-NPs and their complex KTP were investigated. As shown in Figure 2A, the

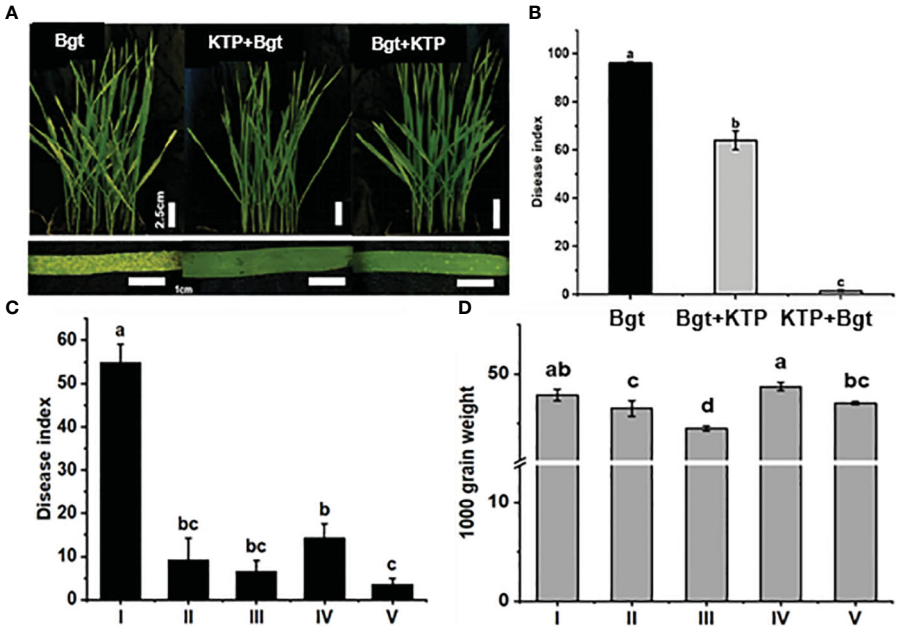

FIGURE 1
(A) Prevention and control of powdery mildew phenotypes in wheat cultivars under different treatments. **(B)** Disease index of wheat plants grown in pots under different treatment conditions for 7 days post infection. **(C)** Disease index of wheat in field under different treatment conditions. (I) *Bgt* group; (II) *Bgt* + KTP group; (III) KTP + *Bgt* + KTP group; (IV) KTP + *Bgt* group; (V) Tebuconazole + *Bgt* group. **(D)** Thousand grain weight of wheat under different treatments. (I) CK group; (II) Tebuconazole + *Bgt* group; (III) *Bgt* group; (IV) KTP group; (V) KTP + *Bgt* group.

hydrophobic angles of kaolin and TiO_2-NPs were 33.89° and 18.83°, respectively, while that of KTP was 102.48°. These results indicated that kaolin and TiO_2-NPs were hydrophilic, while the nanoprotective membrane KTP was hydrophobic. The hydrophobic angle of wheat leaves treated with KTP was 106.36°, and the hydrophobic effect was stronger than that of KTP. This indicated that KTP was strongly compatible with wheat leaves, and could attach to the surface of wheat leaves better, mitigating losses caused by complex environments such as rain washing in the field.

As shown in Figure 2B, the peak value at 3436 cm^{-1} was ascribed to the stretching vibrations of kaolin-OH. The peak at 1098 cm^{-1} was ascribed to the stretching vibrations of kaolin Si-O-Si (Zhou et al., 2016). The peak at 3415 cm^{-1} was the -OH stretching vibration of TiO_2-NPs, and the peak at 1384 cm^{-1} was attributed to -CH_3. The peak at 615 cm^{-1} was ascribed to the Ti-O-Ti vibration of the TiO_2-NPs (Irshad et al., 2020; Li-Chun et al., 2007). There was a large amount of hydrophilic -OH groups on the kaolin and TiO_2-NP surfaces, which was also the reason why kaolin and TiO_2-NPs exhibited hydrophilicity in the contact angle determination experiment. The peak at 3735 cm^{-1} was attributed to the free water -OH of liquid paraffin, and the peak at 2924 cm^{-1} was attributed to the symmetric and asymmetric structure of -CH_2. The peaks at 1460 cm^{-1} and 1374 cm^{-1} attributed to -CH_3. The peaks at 723 cm^{-1} and 661 cm^{-1} were attributed to in-plane swings of liquid paraffin -CH_2.

The corresponding positions in the FTIR spectra of KTP could be found in the abovementioned stretching vibration of -OH, the stretching vibration of Si-O-Si, the O-Ti-O bond, the symmetry and asymmetry of - CH_2, the in-plane swing of -CH_2, and the in-plane swing of -CH_3. This indicated that kaolin, TiO_2-NPs and liquid paraffin were indeed present in KTP. Kaolin and TiO_2-NPs were effectively modified with liquid paraffin. Compared with those in kaolin, the stretching those in of -OH and Si-O-Si in KTP were blueshifted from 3436 cm^{-1} to 3425 cm^{-1} and from 1098 cm^{-1} to 1087 cm^{-1}, respectively. Compared with that of TiO_2-NPs, the stretching vibration of KTP-OH shifted from 3415 cm^{-1} to 3425 cm^{-1} and from 1384 cm^{-1} to 1375 cm^{-1}, and the O-Ti-O bond shifted from 615 cm^{-1} to 611 cm^{-1}. Compared with liquid paraffin, the peak of -OH was weakened, but the peak was not changed, the -CH_3 of KTP blueshifted from 1460 cm^{-1} to 1459 cm^{-1}, redshifted from 1374 cm^{-1} to 1375 cm^{-1}, the symmetric and asymmetric -CH_2 blueshifted from 2924 cm^{-1} to 2923 cm^{-1}, and the in-plane swing of -CH_2 blueshifted from 661 cm^{-1} to 642 cm^{-1}, and redshifted from 723 cm^{-1} to 726 cm^{-1}. Therefore, complex KTP is formed between kaolin, TiO_2-NPs and liquid paraffin through a large number of hydrogen bond interactions. It may ensure that KTP can form a stable protective film on the leaves, effectively resisting the invasion of powdery spores.

The TG-DSC analysis results for KTP are shown in Figure 2C. There was only one weight loss stage in the KTP thermogravimetric curve. The weight loss stage ranged from 273.1°C to 394°C, and the total weight loss rate was 96.3%. The reason for the quality loss was the thermal decomposition of liquid paraffin. The results of thermal analysis showed that KTP could stably persist below 273.1 °C. Therefore, KTP has good thermal stability at room temperature and could meet practical application requirements in the field.

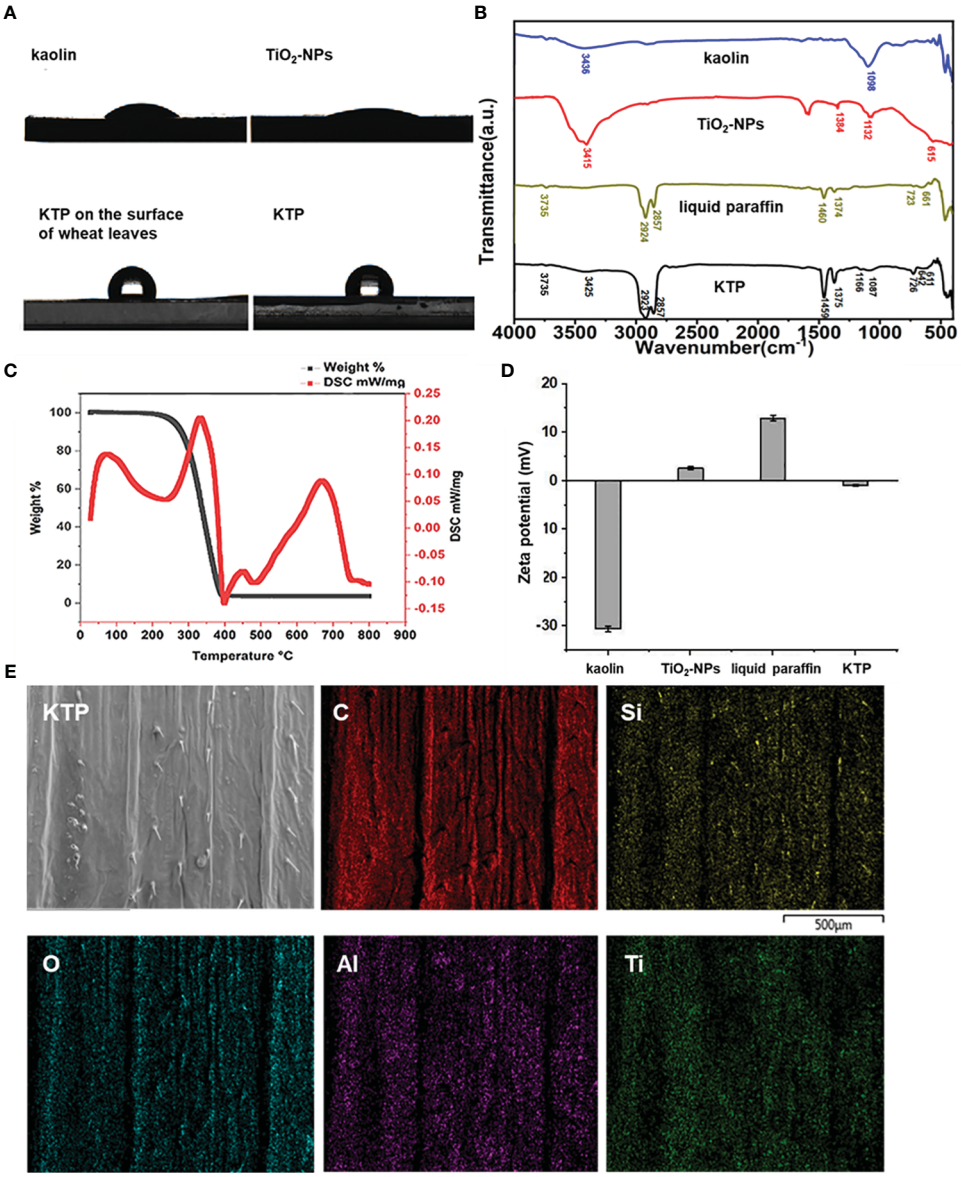

FIGURE 2
(A) The result of contact angle. **(B)** The results of fourier transform infrared. **(C)** The thermogravimetric curve of KTP. **(D)** Zeta potential diagram. **(E)** KTP energy spectrum scanning diagram.

To examine the electrical chargeability of each material, the zeta potentials of kaolin, TiO_2-NPs, liquid paraffin, and KTP were tested in this experiment (Figure 2D). The results showed that, compared with that of each component, the charge of KTP was numerically lower and electroneutral, which indicated that KTP was successfully synthesized. These results indicated that kaolin, TiO_2-NPs, and liquid paraffin further promoted the synthesis of KTP nanoprotective membranes by relying on electrostatic attraction.

To explore whether KTP was uniformly distributed on the surface of the wheat leaves, we performed energy spectral scanning analysis of C, O, Al, Si, and Ti on the surface of the wheat leaves sprayed with KTP. As shown in Figure 2E, the elements in KTP were distributed relatively evenly on the surface of the wheat leaves. This indicated that the KTP nanoprotective membrane could be used to uniformly cover the surface of wheat leaves, which guaranteed its disease prevention and control efficacy.

3.3 KTP inhibits powder spore germination

To further investigate how KTP prevents the occurrence of powdery mildew, we conducted a spore germination growth test. After inoculation with powdery mildew for 7 days, the surface of the wheat leaves not subjected to KTP treatment was covered with a large number of powdery mildew colonies, while no powdery mildew colonies formed on the surface of the wheat leaves treated

with KTP (Figures 3Aa, a'). The results showed that KTP significantly inhibited the formation of the mycelia structure of powdery mildew spores on the leaf surface.

Subsequently, we examined the samples at different infection times under an optical microscope. The germination growth of powdery mildew spores was a dynamic process (Figures 3Ab–h). At 12 h, the powdery mildew spores of the *Bgt* group had already started to infect the leaves of wheat, and the spores germinated and produced a short primary germ tube, a process that involved the germination of the spores and the development of a germ tube. The germ tubes subsequently developed appressorium structures and underwent deformation to grow invading nails that penetrated the cell wall of the host epidermal cells, forming haustoria that parasitize the cytoplasm. Some of the spores began to grow secondary hyphae at 48 h to form mature mycelia, and at 144 h, the spores of the *Bgt* group all had notable hyphae (Figure 3Ah). In contrast to those in the *Bgt* group (Figures 3Ab'–h'), the spores in the KTP + *Bgt* group did not germinate long budding tubes at 12 h and did not form hyphal structures at 24 h; only a few spores those in at 144 h, and the hyphal growth state was significantly weaker than that of the *Bgt* group, while the remaining spores mostly remained in the appressorium status and did not grow exuberant hyphal structures. These results indicated that KTP delayed the germination of wheat powdery mildew spores.

In addition, the mature mycelium formation rate at 48 h was also determined in this test. As shown in Figure 3B, at 48 h after inoculation with powdery mildew, 19% of the germinated powdery mildew spores had germinated into mature mycelia in the KTP + *Bgt* group, which was significantly lower than that in the *Bgt* group (87%). In conclusion, KTP delayed the germination of powdery mildew spores from wheat and significantly inhibited the formation of mycelia of powdery mildew.

Besides, the morphologies of the wheat leaves infected with powdery mildew spores (144 h) were observed via SEM. Figure 3C shows that the mycelia of powdery mildew in the *Bgt* group grew vigorously and covered the surface of the wheat leaves, while the spores in the KTP + *Bgt* group were still in the state of an appressorium; moreover, an obvious mycelial structure was not

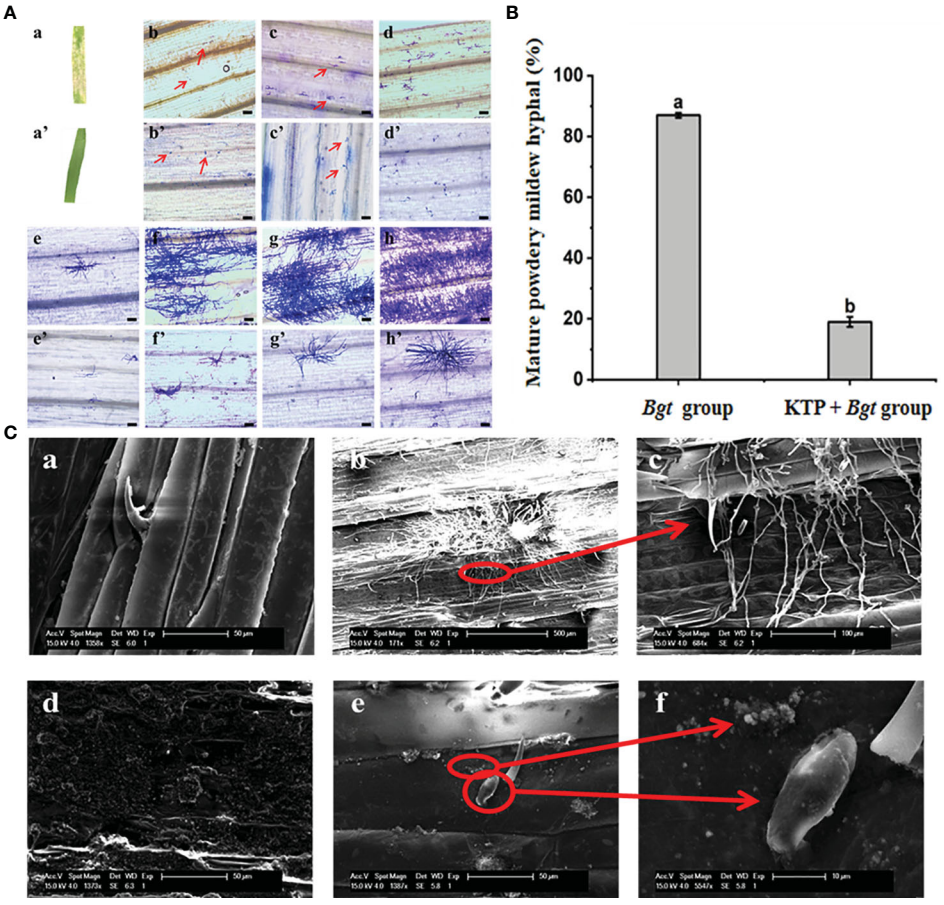

FIGURE 3
(A) Effect of KTP on germination and development of powdery mildew spores in wheat leaves, bar = 100 µm. (a) Occurrence of wheat powdery mildew in *Bgt* group. (a') Occurrence of wheat powdery mildew in KTP + *Bgt* group. (b - h) and (b '- h') *Bgt* group and KTP + *Bgt* group showed the spore germination and growth of powdery mildew at 12, 24, 48, 72, 96, 120 and 144 hours. **(B)** The ratio of mature powdery mildew hyphal at 48h **(C)** SEM image of KTP inhibiting conidial germination of powdery mildew. (a) Wax layer on the surface of wheat leaves; (b, c) *Bgt* group wheat leaf surface; (d) Wheat leaves sprayed with KTP; (e, f) The surface of wheat leaves pretreated by KTP.

observed. KTP was attached to the surface of the wheat leaves. The normally growing wheat leaves were covered with a layer of wax, while the wheat leaves of the KTP group had an uneven granular structure. Therefore, the above results indicated that the growth of powdery mildew spores was inhibited by the KTP nanoprotective membrane.

3.4 Differential gene expression analysis

PR1 is a defense protein involved in plant-pathogen interactions. The expression of *PR1* is widely considered a reliable marker for activating the hypersensitivity (HR)-mediated defense pathway or establishing salicylic acid (SA)-mediated disease resistance in different plants (Xin et al., 2012). Chitinase plays an important role in plant defense against fungal pathogens and is also a type of pathogen-related protein (Ahmed et al., 2022). CHI1 protects plants from fungi by degrading fungal cell walls and inhibiting the growth of mycelia (Tayeh et al., 2015). Additionally, OXO is considered a marker of pathogen infection resulting from the interaction between powdery mildew and grains (Lane, 2002). OXO can produce H_2O_2, which is a kind of ROS (Christensen et al., 2004).

We examined the changes in the *PR1*, *CHI1* and *OXO* genes over time after KTP spraying and powdery mildew invasion into wheat (Figures 4A, B). The relative transcript levels of *PR1* in the CK and KTP groups did not significantly differ at 0 h, 6-24 h, or 72 h. Except for at 144 h, the transcript level of *PR1* in the KTP + *Bgt* group was lower than that in the *Bgt* group throughout the measurement period. These findings indicated that KTP spray decreased *PR1* transcription in response to powdery mildew invasion and that KTP did not affect the transcript levels of *PR1* in normal wheat. Additionally, the expression of *CHI1* in the *Bgt* group was 16.67 times greater than that in the KTP + *Bgt* group (72 h). Taken together, these findings indicated that the transcript level of *CHI1* in wheat plants strongly promoted the production of chitinase to play a protective role against powdery mildew, while spraying KTP reduced the level of powdery mildew-related stress on the plants, so the transcript level of *CHI1* in the KTP + *Bgt* group was relatively low. However, there was no significant difference in the transcript levels of *CHI1* between the CK and KTP groups at 0 h, 24 h, 48 h and 72 h. These findings indicated that KTP did not affect the transcription of *CHI1* but rather reduced it by alleviating the infestation of wheat by powdery mildew. In addition, after spraying KTP or inoculating powdery mildew, the expression of *OXO* increased rapidly and then began to decline slowly. These findings suggested that the expression of *OXO* decreased with increasing time. Notably, at 72 h, the expression of *OXO* in the KTP group was 3 times that in the CK group, while that in the *Bgt* group was 10 times that in the KTP + *Bgt* group, and 50 times that at 144 h. Thus, KTP decreased the transcription of *OXO* induced by powdery mildew and played a protective role in wheat. The above data indicated that wheat infection with powdery mildew tended to increase the expression of *OXO* and subsequently induce the production of ROS to resist the invasion of powdery mildew. Therefore, these findings could help wheat to resist the invasion of powdery mildew, and reduce the expression of *PR* genes.

3.5 Biosafety Assessment of KTP

To explore the effect of KTP on the growth of wheat, we measured the plant height, fresh weight and dry weight of each group of wheat plants for 7 days. The *Bgt* group yielded the shortest wheat plants, with a plant height of 23.60 cm, which was significantly lower than that of the other three groups (Figure 5A). The fresh weight and dry weight of the wheat plants in the *Bgt* group were 4.52 g and 0.36 g respectively, which were significantly lower than those in the other three groups (Figures 5B, C). Therefore, spraying KTP prevents a reduction in the fresh weight and dry weight of wheat plants caused by powdery

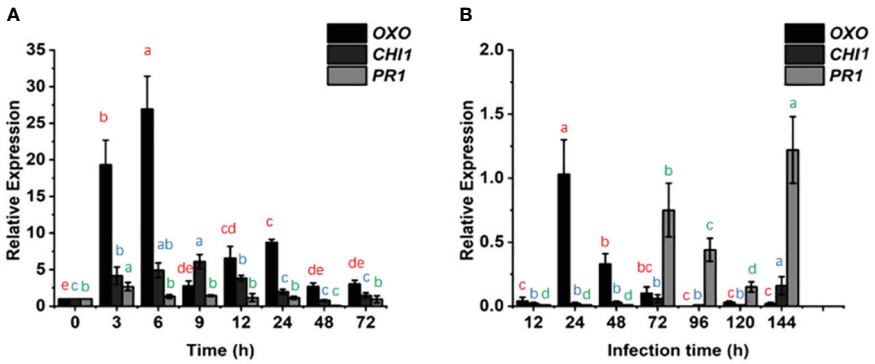

FIGURE 4
Effects of different experimental treatments on the expression of *OXO*, *CHI1* and *PR1* in wheat seedling leaves with time. **(A)** The transcription levels of *OXO*, *CHI1* and *PR1* in the KTP group and CK group were examined and compared by qRT-PCR. **(B)** The transcription levels of *OXO*, *CHI1* and *PR1* in the KTP + *Bgt* group and *Bgt* group were examined and compared by qRT-PCR. The expression of 3 genes in CK group and *Bgt* group were averaged as 1 (0).

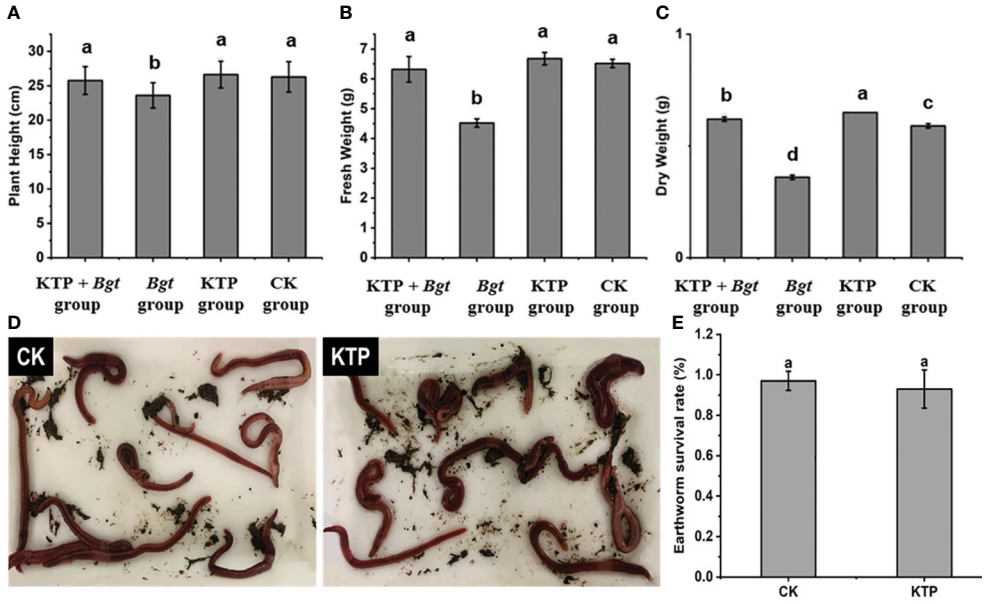

FIGURE 5
(A) Effects of different treatments on wheat plant height. **(B)** Effects of different treatments on wheat fresh weight. **(C)** Effects of different treatments on wheat dry weight. **(D)** Earthworm survival state. **(E)** Effect of KTP for earthworm survival.

mildew infection, and KTP has no side effects on the growth of wheat plants.

KTP might leach into the soil after rain, so the safety of KTP for soil organisms was evaluated. There was no significant difference in the survival status of earthworms in the KTP-treated soil compared to that in the CK group, in which survival rates were 93% and 97%, respectively (Figures 5D, E). It could be concluded that KTP had no effect on plants or soil organisms and had good biosafety.

4 Conclusion

Kaolin, TiO_2-NPs, and liquid paraffin form KTP through the interaction of hydrogen bonding as well as electrostatic attraction. KTP delayed the germination of powdery mildew spores and inhibited the formation of mycelia. KTP has good physicochemical properties and meets field conditions, which could significantly reduce the occurrence of powdery mildew, thus preventing yield loss caused by powdery mildew. Therefore, this study provides an efficient, safe, and green management strategy for powdery mildew infection in large field areas.

Data availability statement

The original contributions presented in the study are included in the article/supplementary material. Further inquiries can be directed to the corresponding author.

Author contributions

HZ: Writing – review & editing, Conceptualization, Investigation, Methodology, Resources, Writing – original draft. MY: Writing – review & editing, Formal analysis, Investigation, Methodology, Writing – original draft. YG: Methodology, Writing – original draft, Formal analysis, Writing – review & editing. PS: Formal analysis, Writing – review & editing, Methodology, Resources, Writing – original draft. HJ: Writing – original draft, Formal analysis, Funding acquisition, Resources, Validation, Visualization, Writing – review & editing. CT: Writing – review & editing, Funding acquisition, Supervision, Validation, Visualization, Writing – original draft. HM: Investigation, Project administration, Writing – review & editing. LW: Writing – review & editing, Conceptualization, Resources, Supervision.

Funding

The author(s) declare that financial support was received for the research, authorship, and/or publication of this article. This work was funded by the National Key Research and Development Program of China (2022YFD2301403), the major special project of Anhui province (202103a06020002), the China Postdoctoral Science Foundation Funded Project (2021M703254), the Grant of the President Foundation of Hefei Institutes of Physical Science of Chinese Academy of Sciences (YZJJ2022QN31).

Conflict of interest

Authors HZ, CT, and LW was/were employed by the company CNSIG Anhui Hongsifang Fertilizer Co.

The remaining authors declare that the research was conducted in the absence of any commercial or financial relationships that could be construed as a potential conflict of interest.

Publisher's note

All claims expressed in this article are solely those of the authors and do not necessarily represent those of their affiliated organizations, or those of the publisher, the editors and the reviewers. Any product that may be evaluated in this article, or claim that may be made by its manufacturer, is not guaranteed or endorsed by the publisher.

References

Ahmed, T., Noman, M., Jiang, H., Shahid, M., Ma, C., Wu, Z., et al. (2022). Bioengineered chitosan-iron nanocomposite controls bacterial leaf blight disease by modulating plant defense response and nutritional status of rice (Oryza sativa L.). *NANO Today* 45, 101547. doi: 10.1016/j.nantod.2022.101547

Ali, M. A., Rehman, I., and Iqbal, A. (2014). Nanotechnology: A new frontier in Agriculture. *Adv. Life Sci.* 1, 129–138.

Cantore, V., Pace, B., and Albrizio, R. (2009). Kaolin-based particle film technology affects tomato physiology, yield and quality. *Environ. Exp. Bot.* 66, 279–288. doi: 10.1016/j.envexpbot.2009.03.008

Christensen, A. B., Thordal-Christensen, H., Zimmermann, G., Gjetting, T., Lyngkjær, M. F., Dudler, R., et al. (2004). The germinlike protein GLP4 exhibits superoxide dismutase activity and is an important component of quantitative resistance in wheat and barley. *Mol. Plant Microbe IN* 17, 109–117. doi: 10.1094/MPMI.2004.17.1.109

De Filpo, G., Palermo, A. M., Rachiele, F., and Nicoletta, F. P. (2013). Preventing fungal growth in wood by titanium dioxide nanoparticles. *Int. Biodeter. Biodegr.* 85, 217–222. doi: 10.1016/j.ibiod.2013.07.007

Griffey, C. A., Das, M. K., and Stromberg, E. L. (1993). Effectiveness of adult-plant resistance in reducing grain yield loss to powdery mildew in winter wheat. *Plant Dis.* 77, 618–622. doi: 10.1094/PD-77-0618

Irshad, M. A., Nawaz, R., ur Rehman, M. Z., Imran, M., Ahmad, J., Ahmad, S., et al. (2020). Synthesis and characterization of titanium dioxide nanoparticles by chemical and green methods and their antifungal activities against wheat rust. *Chemosphere* 258, 127352. doi: 10.1016/j.chemosphere.2020.127352

Javed, B., Nadhman, A., and Mashwani, Z.-u. (2020). Phytosynthesis of Ag nanoparticles from Mentha longifolia: their structural evaluation and therapeutic potential against HCT116 colon cancer, Leishmanial and bacterial cells. *Appl. Nanosci.* 10, 3503–3515. doi: 10.1007/s13204-020-01428-5

Kuckenberg, J., Tartachnyk, I., and Noga, G. (2009). Temporal and spatial changes of chlorophyll fluorescence as a basis for early and precise detection of leaf rust and powdery mildew infections in wheat leaves. *Precis. Agric.* 10, 34–44. doi: 10.1007/s11119-008-9082-0

Lane, B. G. (2002). Oxalate, germins, and higher-plant pathogens. *IUBMB Life* 53, 67–75. doi: 10.1080/15216540211474

Li-Chun, X., Jia, L., and Bai-Fu, X. (2007). Study on photocatalytic performance of TiO_2 modified with CTAB. *J. Natural Sci. Heilongjiang Univ.* 24. doi: 10.13482/j.issn1001-7011-2007-03-022

Mandal, M. S. N., Fu, Y., Zhang, S., and Ji, W. (2014). Proteomic analysis of the defense response of wheat to the powdery mildew fungus, Blumeria graminis f. sp. tritici. *Protein J.* 33, 513–524. doi: 10.1007/s10930-014-9583-9

Merchan, V. M., and Kranz, J. (1986). *The effect of rain on the development of wheat powdery mildew (Erysiphe graminis DC. f. sp. tritici Marchal)* (Germany, FR: Zeitschrift fuer Pflanzenkrankheiten und Pflanzenschutz).

Owolade, O., and Ogunleti, D. (2008). "Effects of titanium dioxide on the diseases, development and yield of edible cowpea," in *Agricultural and Food Sciences (Journal of plant protection research)*. doi: 10.2478/v10045-008-0042-5

Reignault, P. H., Cogan, A., Muchembled, J., Lounes-Hadj Sahraoui, A., Durand, R., and Sancholle, M. (2001). Trehalose induces resistance to powdery mildew in wheat. *New Phytol.* 149, 519–529. doi: 10.1046/j.1469-8137.2001.00035.x

Rodríguez-González, V., Terashima, C., and Fujishima, A. (2019). Applications of photocatalytic titanium dioxide-based nanomaterials in sustainable agriculture. *J. Photoch. Photobio. C* 40, 49–67. doi: 10.1016/j.jphotochemrev.2019.06.001

Saari, E. E., and Wilcoxson, R. D. (1974). Plant disease situation of high-yielding dwarf wheats in asia and africa. *Annu. Rev. Phytopathol.* 12, 49–68. doi: 10.1146/annurev.py.12.090174.000405

Santhoshkumar, T., Rahuman, A. A., Jayaseelan, C., Rajakumar, G., Marimuthu, S., Kirthi, A., et al. (2014). Green synthesis of titanium dioxide nanoparticles using Psidium guajava extract and its antibacterial and antioxidant properties. *Asian PAC J. Trop. Med.* 12), 9. doi: 10.1016/S1995-7645(14)60171-1

Summers, R., and Brown, J. (2013). Constraints on breeding for disease resistance in commercially competitive wheat cultivars. *Plant Pathol.* 62, 115–121. doi: 10.1111/ppa.12165

Tayeh, C., Randoux, B., Tisserant, B., Khong, G., Jacques, P., and Reignault, P. (2015). Are ineffective defence reactions potential target for induced resistance during the compatible wheat-powdery mildew interaction. *Plant Physiol. Bioch.* 96, 9–19. doi: 10.1016/j.plaphy.2015.07.015

Vallavieille-Pope, C. D., Ali, S., Leconte, M., Enjalbert, J., and Rouzet, J. (2012). Virulence Dynamics and Regional Structuring of Puccinia striiformis f. sp. tritici in France Between 1984 and 2009. *Lant Dis.* 96, 131–140. doi: 10.1094/PDIS-02-11-0078

Waghmode, M. S., Gunjal, A. B., Mulla, J. A., Patil, N. N., and Nawani, N. N. (2019). Studies on the titanium dioxide nanoparticles: Biosynthesis, applications and remediation. *SN Appl. Sci.* 1, 310. doi: 10.1007/s42452-019-0337-3

Walters, D. R., McRoberts, N., and Fitt, B. D. L. (2008). Are green islands red herrings Significance of green islands in plant interactions with pathogens and pests. *Biol. Rev.* 83, 79–102. doi: 10.1111/j.1469-185X.2007.00033.x

Wright, D. P., Baldwin, B. C., Shephard, M. C., and Scholes, J. D. (1995). Source-sink relationships in wheat leaves infected with powdery mildew. I. Alterations in carbohydrate metabolism. *Physiol. Mol. Plant P* 47, 237–253. doi: 10.1006/pmpp.1995.1055

Xin, M., Wang, X., Peng, H., Yao, Y., Xie, C., Han, Y., et al. (2012). Transcriptome comparison of susceptible and resistant wheat in response to powdery mildew infection. *Genom. Proteom. Bioinform.* 10, 94–106. doi: 10.1016/j.gpb.2012.05.002

Yinghui, L., Na., S., Chuanzhi, Z., Feng., L., Miaomiao, G., Yuhui, W., et al. (2016). Application of glycerol for induced powdery mildew resistance in triticum aestivum L. *Front. Physiol.* 7, 413. doi: 10.3389/fphys.2016.00413

Zheng, H., Dong, L., Han, X., Jin, H., Yin, C., Han, Y., et al. (2020). The TuMYB46L-TuACO3 module regulates ethylene biosynthesis in einkorn wheat defense to powdery mildew. *New Phytol.* 225, 2526–2541. doi: 10.1111/nph.16305

Zhou, L., Xu, S., Zhang, G., Cai, D., and Wu, Z. (2016). A facile approach to fabricate self-cleaning paint. *Appl. Clay Sci.* 132, 290–295. doi: 10.1016/j.clay.2016.06.015

frontiers | Frontiers in Plant Science

TYPE Original Research
PUBLISHED 16 May 2024
DOI 10.3389/fpls.2024.1387427

Check for updates

OPEN ACCESS

EDITED BY
Jing Feng,
Chinese Academy of Agricultural Sciences, China

REVIEWED BY
Sudhir Navathe,
Agharkar Research Institute, India
Zhu-Qing Shao,
Nanjing University, China

*CORRESPONDENCE
Pengtao Ma
ptma@ytu.edu.cn
Yuli Jin
yulijin@ytu.edu.cn
Cheng Liu
lch6688407@163.com

†These authors have contributed equally to this work

RECEIVED 17 February 2024
ACCEPTED 30 April 2024
PUBLISHED 16 May 2024

CITATION
Qian Z, Liu R, Liu X, Qie Y, Wang J, Yin Y, Xin Q, Yu N, Zhang J, Li Y, Li J, Dai Y, Liu C, Jin Y and Ma P (2024) Bulked segregant RNA-seq reveals complex resistance expression profile to powdery mildew in wild emmer wheat W762.
Front. Plant Sci. 15:1387427.
doi: 10.3389/fpls.2024.1387427

COPYRIGHT
© 2024 Qian, Liu, Liu, Qie, Wang, Yin, Xin, Yu, Zhang, Li, Li, Dai, Liu, Jin and Ma. This is an open-access article distributed under the terms of the Creative Commons Attribution License (CC BY). The use, distribution or reproduction in other forums is permitted, provided the original author(s) and the copyright owner(s) are credited and that the original publication in this journal is cited, in accordance with accepted academic practice. No use, distribution or reproduction is permitted which does not comply with these terms.

Bulked segregant RNA-seq reveals complex resistance expression profile to powdery mildew in wild emmer wheat W762

Zejun Qian[1†], Ruishan Liu[1†], Xueqing Liu[2†], Yanmin Qie[3], Jiangchun Wang[2], Yan Yin[2], Qingguo Xin[2], Ningning Yu[1], Jiadong Zhang[1], Yaoxue Li[1], Jiatong Li[1], Yintao Dai[1], Cheng Liu[4*], Yuli Jin[1*] and Pengtao Ma[1*]

[1]Yantai Key Laboratory of Characteristic Agricultural Bioresource Conservation & Germplasm Innovative Utilization, College of Life Sciences, Yantai University, Yantai, China, [2]Institute of Grain and Oil Crops, Yantai Academy of Agricultural Sciences, Yantai, China, [3]Institute of Cereal and Oil Crops, Hebei Academy of Agricultural and Forestry Sciences/Hebei Laboratory of Crop Genetic and Breeding, Shijiazhuang, China, [4]Crop Research Institute, Shandong Academy of Agricultural Sciences, Jinan, China

Powdery mildew, caused by *Blumeria graminis* f. sp. *tritici* (*Bgt*), is one of the most destructive fungal diseases threatening global wheat production. Exploring powdery mildew resistance (*Pm*) gene(s) and dissecting the molecular mechanism of the host resistance are critical to effectively and reasonably control this disease. Durum wheat (*Triticum turgidum* L. var. *durum* Desf.) is an important gene donor for wheat improvement against powdery mildew. In this study, a resistant durum wheat accession W762 was used to investigate its potential resistance component(s) and profile its expression pattern in responding to *Bgt* invasion using bulked segregant RNA-Seq (BSR-Seq) and further qRT-PCR verification. Genetic analysis showed that the powdery mildew resistance in W762 did not meet monogenic inheritance and complex genetic model might exist within the population of W762 × Langdon (susceptible durum wheat). After BSR-Seq, 6,196 consistently different single nucleotide polymorphisms (SNPs) were called between resistant and susceptible parents and bulks, and among them, 763 SNPs were assigned to the chromosome arm 7B. Subsequently, 3,653 differentially expressed genes (DEGs) between resistant and susceptible parents and bulks were annotated and analyzed by Gene Ontology (GO), Cluster of Orthologous Groups (COG), and Kyoto Encyclopedia of Genes and Genomes (KEGG) pathway enrichment. The potential regulated genes were selected and analyzed their temporal expression patterns following *Bgt* inoculation. As a result, nine disease-related genes showed distinctive expression profile after *Bgt* invasion and might serve as potential targets to regulate the resistance against powdery mildew in W762. Our study could lay a foundation for analysis of the molecular mechanism and also provide potential targets for the improvement of durable resistance against powdery mildew.

KEYWORDS

durum wheat, powdery mildew, BSR-seq, expression profiling, DEG

Introduction

Wheat (*Triticum aestivum* L., 2*n* = 6X = 42, AABBDD) is a globally significant staple crop closely associated with food security worldwide (Li et al., 2019; Han et al., 2020). As a primary source of nutrition, wheat provides essential macronutrients such as carbohydrates, proteins, and a variety of vitamins. However, wheat production often faces the threat from various fungal diseases. Powdery mildew, caused by *Blumeria graminis* f. sp. *tritici* (*Bgt*), is one of the most devastating diseases of wheat and can significantly reduce wheat yield by 10%–15% and even up to 62% in severe cases (Singh et al., 2016; Li et al., 2019; Wang et al., 2021). Therefore, it is important and urgent to explore and utilize more novel and broad-spectrum powdery mildew resistance (*Pm*) genes to effectively control this disease.

To date, more than 100 *Pm* genes/alleles have been identified in common wheat and its relatives, including 69 officially designated *Pm* genes at 64 loci (*Pm1-Pm69*, *Pm8* = *Pm17*, *Pm18* = *Pm1c*, *Pm22* = *Pm1e*, *Pm23* = *Pm4c*, *Pm31* = *Pm21*) as well as dozens of provisionally named genes (McIntosh et al., 2020; He et al., 2021; Wang et al., 2023; Li et al., 2024). Among them, the genes derived from common wheat can be directly introduced into susceptible cultivars for resistance breeding, such as *Pm1a* (Sears and Briggle, 1969), *Pm3b* (Briggle, 1969), *Pm5e* (Huang et al., 2003), *Pm24* (Xue et al., 2012), *Pm38/Lr34/Yr18/Sr57* (Krattinger et al., 2009), and *Pm46/Yr46/Lr67/Sr55* (Moore et al., 2015), but these genes often have low genetic diversity compared to wheat cultivars and are easy to be defeated after long-term of promotion in production. In comparison, the genes originated from the wheat relatives often possess higher genetic variations and exhibit strong ability to withstand *Bgt* variations, such as *Pm12* from *Aegilops speltoides* Tausch (Zhu et al., 2023) and *Pm21* from *Dasypyrum villosum* L. Candagy (He et al., 2018) and, hence, have higher value in wheat improvement against powdery mildew in the future (Han et al., 2024a, Han et al., 2024b, Han et al., 2024c). Meanwhile, more and more *Pm* genes have gradually lost their resistance to powdery mildew and also many effective *Pm* genes are difficult to be utilized in breeding due to linkage drags and other negative effects in the breeding practices. For example, *Pm1a* and *Pm8* have been widely used in wheat production and breeding for many years, but their resistance have gradually lost in all or part of wheat planting areas due to the continuous variation of powdery mildew pathogens (Cowger et al., 2018). The *Pm12* was not only highly resistant to powdery mildew but also accompanied by poor yield and quality traits, making it difficult to directly utilize in breeding (Zhu et al., 2023). Therefore, mining more novel effective *Pm* genes and introducing them into wheat cultivars are significant for wheat production and disease resistance breeding.

Durum wheat (*T. turgidum* L. var. *durum* Desf., simply *T. durum*, 2*n* = 4*X* = 28, AABB) is a tetraploid wheat species and often possesses multiple resistances to leaf rust, stem rust, stripe rust and powdery mildew (Miedaner et al., 2019). Four *Pm* genes have been identified in the past decades, including *Mld*, *Pm3h*, *PmDR147*, and *Pm68*. Among them, *Mld* is a recessive gene located on chromosome 4B which could be solely used or pyramided with other *Pm* genes in wheat breeding (Bennett, 1984); *Pm3h* is a dominant resistance gene located on chromosome arm 1AS, probably originates from an Ethiopian durum wheat accession (Srichumpa et al., 2005); *Pm3h* was also originally identified in durum wheat, and subsequently confirmed to be same as *Pm3d* after cloning (Yahiaoui et al., 2006); *PmDR147* is also a dominant gene mapped on chromosome arm 2AL in durum wheat accession DR147 (Zhu et al., 2004).

Bulked segregant RNA-Seq (BSR-Seq), which combined the bulked segregant analysis (BSA) and RNA sequencing (RNA-Seq), is a high-efficiency strategy in genomics research of the complex polyploid species. In this strategy, RNA-seq is independent on pre-existing databases of expressed genes and can provide an unbiased view of gene expression profiling (Pearce et al., 2015; Pankievicz et al., 2016; Han et al., 2024a), thus is an effective and low-cost method to comprehensively evaluate the gene expression pattern of the *Pm* genes after inoculation by *Bgt* isolates. Additionally, BSR-seq can also overcome the adverse effects of the genome sequences and obtain sequence and expression information of almost all transcripts of a specific cell or tissue in a certain stage, so it is an efficient method for rapid gene mapping (Wang et al., 2017; Hao et al., 2019), especially for the crop species with complex genomes, such as wheat and its relatives (Zhang et al., 2017).

W762 is a durum wheat accession that shows high resistant to powdery mildew at the whole stage. To dissect its genetic basis against powdery mildew, in this study, we intended to (i) clarify the genetic pattern of powdery mildew resistance, (ii) identify differentially expressed genes (DEGs) at the whole-genome scale, and (iii) profile the expression of the key genes associated with resistance to powdery mildew. Our study could lay a foundation for analysis of the molecular mechanism and also provide potential targets for the improvement of durable resistance against powdery mildew.

Materials and methods

Plant materials and pathogens

The durum wheat accession W762, provided by International Maize and Wheat Improvement Center (CIMMYT), was used to test its reaction pattern against powdery mildew. The susceptible durum wheat accession Langdon (LDN), also provided by CIMMYT, was crossed with W762 to produce F_1, F_2, and $F_{2:3}$ generations for genetic analysis and BSR-Seq analysis. Wheat cultivar Mingxian 169, which was susceptible to all the *Bgt* isolates tested in this study (Ma et al., 2018), was used as the susceptible control in phenotypic assessment experiment. Thirty-two *Bgt* isolates B05, E07, E09, E15, E17, E18, E20, E21, E23–1, E31, F01, F02, F03, F05, F06, F07, F08, F09, F10, F11, F13, F16, F17, F18, F19, F21, F22, F23, F24, F25, F28, and F32, provided by Prof. Hongxing Xu, Henan University, Kaifeng, China and Prof. Yilin Zhou, Institute of Plant Protection, Chinese Academy of Agricultural Sciences, Beijing, China, were used to evaluate the resistant spectrum of W762. These *Bgt* isolates were previously and

preserved on the susceptible seedlings which were put in independent glass tubes with three layers of gauze to avoid cross infection.

Phenotypic assessment to different *Bgt* isolates

Phenotypic assessment of W762 to the 32 *Bgt* isolates was determined in the greenhouse of Yantai University, Yantai, China. At least five seeds of W762 and LDN were sown in a 128-cell (3.2 cm× 3.2 cm× 4.2 cm) rectangular tray (54 cm× 28 cm× 4.2 cm) and the susceptible control Mingxian 169 was planted randomly in the trays. These trays were put in an independent growth chamber separately to be infected with different *Bgt* isolates. When the seedlings grown to the two-leaf stage, all the seedlings were inoculated with fresh conidiospores increased on Mingxian 169 seedlings and incubated in a chamber at 18°C for 24h with 100% humidity and then cultivated with a daily cycle of 14h of light at 22°C and 10h of darkness at 18°C. After 10–14 days, the spores were fully developed on the first leave of susceptible check Mingxian 169. Infection types (ITs) on each plant were assessed on a 0–4 scale, with IT 0, 0; 1, and 2 being regarded as resistant, and IT 3 and 4 as susceptible (Si et al., 1992; Wang et al., 2009). All tests were repeated three times to assure the reliability of the data.

Microscopic analyses of reaction process after *Bgt* invasion

Microscopic analyses were performed as previously described (Wang et al., 2014). The 2 cm leaf segments were cut at 0h, 0.5h, 2h, 4h, 12h, 24h, 36h, 48h, and 72h after inoculating the *Bgt* isolate E09 and immediately fixed at 37°C for 24h in 2 ml of Carnoy's Fluid (ethanol: acetic acid, 3:1, v/v), then stained with 2 ml of 0.6% (w/v) Coomassie blue solution for 3 min. Excess dye was rinsed off carefully with distilled water. Samples were observed under an Olympus BX-53 microscope (Olympus, Japan).

Genetic analysis and preparation of samples for BSR-Seq

To determine the inheritance of powdery mildew resistance in W762, the *Bgt* isolate E09, a prevalent *Bgt* isolate in North China (Zhou et al., 2005), was selected to inoculate W762, LDN, and their F_1, F_2, and $F_{2:3}$ progenies for genetic analysis. After phenotypic evaluation, the numbers of resistance and susceptible plants were counted, and then a goodness-of-fit assessment was performed to determine the resistant/susceptible ratio using a chi-squared (χ^2) test. The deviations of the observed phenotypic data from the theoretically expected segregation ratios were then evaluated using the SPSS 16.0 software (SPSS Inc., Chicago, United States) at $p < 0.05$.

More than 20 seeds of each $F_{2:3}$ family were sown for further genetic analysis and preparation of the samples for BSR-Seq. Resistant and susceptible RNA bulks were constructed by separately mixing equal amounts of RNA from the 30 homozygous resistant and susceptible $F_{2:3}$ families, respectively. When the spores were fully developed on the first leaves of Mingxian 169, the total RNA of W762, LDN, resistant, and susceptible RNA bulks were extracted from the young leaves using TRIzol reagent (Invitrogen, Carlsbad, California, USA) following the manufacturer's recommendations.

BSR-Seq analysis

First, the RNA samples underwent quality and integrity testing. The eligible mRNA was isolated from total RNA by using Oligo (dT) magnetic beads paired with poly(A) tails of mRNA through A-T complementary nature. Then, the mRNA was randomly fragmented by adding the fragmentation buffer. The cDNAs were synthesized based on the mRNA template, random hexamers, dNTPs, buffer, and DNA polymerase I. After cDNA purification, end reparation, 3′ add A-tail, and sequencing adaptors ligation, fragment sizes were selected with AMPure XP beads. Finally, a cDNA library was obtained through polymerase chain reaction (PCR) amplification. After passing the library inspection, high-throughput sequencing was performed using the platform of Illumina HiSeq 4000 in Beijing Biomics Technology Co. Ltd. (Beijing, China). The sequencing indicator was set as 10 Gb clean data for the parents W762 and LDN and 20 Gb clean data for the bulks. After filtering on raw reads, and removing the adaptors and low-quality reads using software Trimmomatic v0.36 (Bolger et al., 2014) with default parameters, the clean reads were obtained. The high-quality reads were aligned to the Chinese Spring reference genome sequence v2.1 (RefSeq v2.1) (Zhu et al., 2021) and its annotation files by using software TopHat2 (Dobin et al., 2013). The mapped reads were used for further analysis. The read alignments were masked for PCR duplications and split for reads spanning introns before they were used to call SNPs and InDels using module "HaplotypeCaller" of software GATK v3.6 (McKenna et al., 2010). The resulting SNPs and InDels with sequencing depth less than four were abandoned, and the remaining ones were used for BSA analysis. Only variants with *P*-value of Fisher's exact test on read count data $< 1e^{-8}$ and allele frequency difference (AFD) > 0.6 were considered to be related to powdery mildew resistance. The RefSeq v2.1 was further used as a reference to call SNPs and InDels.

Identification and statistics of DEGs

The genes expression levels were evaluated using FPKM (fragments per kilo base of transcript per million fragments mapped) (Trapnell et al., 2010). Using the software EBSeq (http://www.bioconductor.org/packages/release/bioc/html/EBSeq.html), DEGs were identified based on the standard of error detection rate (EDR) <0.01 and fold change (FC; ratio test/common reference) ≥2. The statistical significance of DEGs was performed using multiple tests and EDR was adjusted with the Benjamini–Hochberg procedure (Reiner et al., 2003).

Functional annotation and enrichment analysis

The DEGs, which showed consistent expression difference between the resistant and susceptible parents and bulks, were annotated on the platform WheatOmics 1.0 (http://202.194.139.32/). Then, Gene Ontology (GO), Cluster of Orthologous Groups (COG), and Kyoto Encyclopedia of Genes and Genomes (KEGG) pathways enrichment analysis of DEGs were performed using an R package referred to Sherman et al. (2022), and among them, significance enrichment analysis for KEGG pathway was performed on the DEGs to further determine the signal transduction pathway(s) that these DEGs may be involved in.

Quantitative real-time polymerase chain reaction

The seedlings of W762 and LDN were inoculated with the *Bgt* isolate E09 at the two-leaf stage. Then, the first leaves were sampled at 0h, 0.5h, 2h, 4h, 12h, 24h, 36h, 48h, and 72h post-inoculation (hpi) for RNA extraction using TRIzol reagent (Invitrogen, USA) following the manufacturer's recommendations. The FastKing gDNA Dispelling RT SuperMix kit (Tiangen, Beijing, China) was employed to remove residual DNA and synthesize the corresponding cDNA using the following PCR procedure: 42°C for 15 min and 95°C for 3 min. The qRT-PCR procedure was performed using SYBR Premix Ex Taq (Takara, Beijing, China) on the Bio-Rad CFX Connect real-time PCR system (BIO-RAD, USA). The expression pattern of each gene was calculated as a fold change using the comparative CT method (Livak and Schmittgen, 2001). For each sample, three technical replications were set. The gene *TaActin* was used as the internal control for normalization.

Results

Powdery mildew resistance evaluation and its genetic analysis

After inoculated with 32 *Bgt* isolates, W762 conferred resistance to 10 isolates with IT 0, six isolates with IT 1, and five isolates with IT 2, whereas 11 isolates with ITs 3 and 4 (Table 1), which suggested the resistance to powdery mildew is moderate.

Then, W762 was crossed with LDN to obtain F_1, F_2, and $F_{2:3}$ progenies. When inoculated with the *Bgt* isolate E09, W762 showed no visible symptoms on the first leaves (IT 0). In contrast, the susceptible parent, LDN, had abundant sporulation which covered an area of more than 50% of the first leaves (IT 4) (Figure 1). Coomassie blue staining also showed large number of spores produced in LDN, and meanwhile had very mild cell death (Figure 2). All the F_1 plants of W762 × LDN showed resistance at the level of IT 0 as similar as W762. Among the 200 F_2 plants, the segregation ratio of the resistant (66) and susceptible (134) individuals did not fit for 3:1, the theoretical Mendelian segregation ratio for monogenic inheritance. The $F_{2:3}$ families

TABLE 1 Seedling infection types of W762 and Langdon to 32 different *Blumeria graminis* f. sp. *tritici* (*Bgt*) isolates.

Bgt isolates	W762	Langdon	*Bgt* isolates	W762	Langdon
B05	1	4	F08	4	4
E07	1	4	F09	0	4
E09	0	4	F10	1	4
E15	3	4	F11	4	4
E17	0	4	F13	2	4
E18	1	4	F16	2	4
E20	1	4	F17	0	4
E21	2	4	F18	4	4
E23–1	3	4	F19	4	4
E31	0	4	F21	1	4
F01	4	4	F22	4	4
F02	0	4	F23	0	4
F03	2	4	F24	0	4
F05	4	4	F25	0	4
F06	3	4	F28	2	4
F07	0	4	F32	4	4

Infection type (IT) described as Si et al. (1992), and 0–4 scale was used to score the infection types: 0, 0; among which 1 and 2 were regarded as resistant phenotypes, 3 and 4 were susceptible phenotypes.

10.3389/fpls.2024.1387427

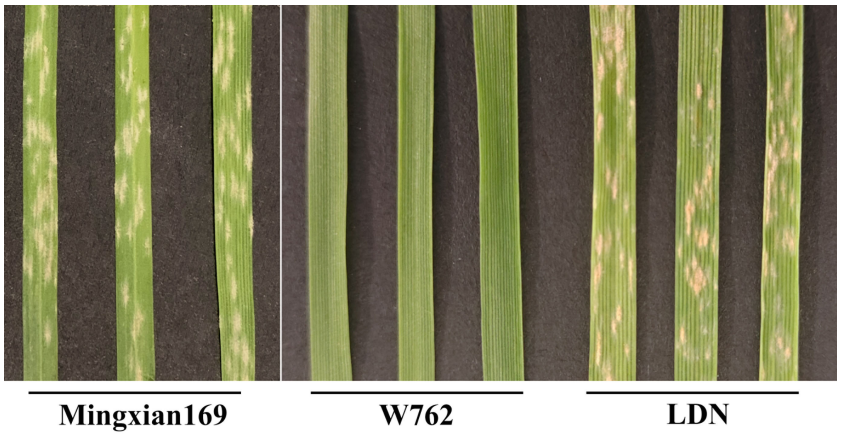

FIGURE 1
Reaction patterns of susceptible control Mingxian 169, durum wheat accessions W762, and Langdon (LDN) to the *Blumeria graminis* f. sp. *tritici* (*Bgt*) isolate E09 at the seedling stage.

segregated 31 homozygous resistant: 94 segregating: 75 homozygous susceptible, also not fitting for the ratio 1:2:1 with monogenic inheritance. Therefore, the powdery mildew resistance in W762 did not meet monogenic inheritance and complex genetic model might exist within this population.

Summary of the RNA-Seq data

After filtering low-quality reads and adaptors, the clean reads of 26,390,677,800 (W762), 34,391,335,500 (LDN), 40,197,188,700 (resistant bulks), and 38,205,766,800 (susceptible bulks) were obtained, respectively. The data size was more than the transcript size of the wheat genome. Therefore, it was considered to cover most expressed genes in the wheat genome. The percentage of clean reads with a Q30 was greater than 94.00% and a Q20 was greater than 97.00% for all the four samples, and the GC content ranged from 54.02% to 55.48%. After mapping the four sets of clean reads to RefSeq v2.1 individually, the percentage of reads mapping to the reference genome ranged from 81.51% to 83.31%, and the coverage of uniquely mapped reads was 99.16%–99.33%. In conclusion, the sequencing quality was high and suitable for subsequent analysis.

Confirmation of candidate intervals

To evaluate the candidate intervals associated with the powdery mildew resistance, a total of 63,641, 727,819, 52,093, and 64,438 SNPs were detected from the clean data of W762, LDN, resistance and susceptible bulks, respectively. Among them, 6,196 SNPs were confirmed to be consistently different between the resistant and susceptible parents and bulks, and used for subsequent SNP index analysis. Using 99% confidence as the threshold, the putative candidate regions of 66,805,294–404,438,437 and 525,703,735–645,084,093 on chromosome 7B were identified (Figure 3). In this interval, 763 SNPs were identified to be consistently different between resistance and susceptible parents and bulks, account for a proportion of 34.7%. This revealed a high confidence of these candidate regions. These SNPs were used for subsequent DEGs analysis.

Analysis of DEGs at the whole-genome scale

A total of 124,200 genes were identified from the parents and bulks after BSR-Seq. Among them, 10,431 DEGs were detected

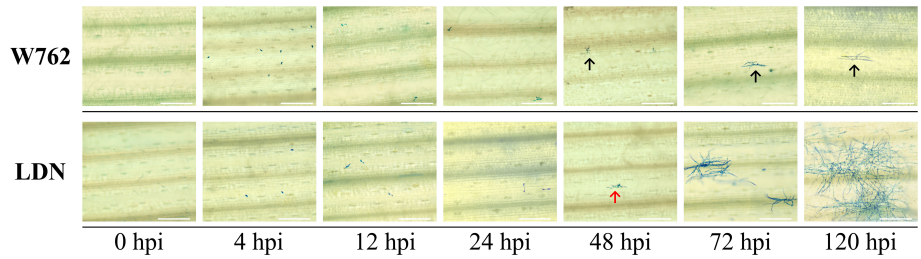

FIGURE 2
Infection process of the *Blumeria graminis* f. sp. *tritici* (*Bgt*) isolate E09 on the first leaves of W762 and Langdon (LDN). Wheat leaf samples were taken at different hpi for Coomassie blue staining. Bar = 200 μm. The black arrows indicate deformed appressorium, and the red arrows indicate normal appressorium.

between parents W762 and LDN, of which, 5,512 ones were upregulated and 4,919 ones were downregulated compared to LDN (Figure 4). Furthermore, 9,088 DEGs were detected between the resistance and susceptible bulks, of which 4,803 and 4,285 DEGs were downregulated and upregulated, respectively. For further screening, 3,653 DEGs showed consistent expression difference between the parents and bulks (Figure 4). Combined with the candidate interval analysis, only 21 DEGs were located in this interval. These genes were considered as prime candidates in the resistance response pathway to powdery mildew in W762.

After GO analysis, the DEGs were mainly involved in three branches: biological processes, cellular components and molecular function. Among them, biological processes included metabolic processes and cellular processes; cellular components included cells, cell parts, membranes, membrane's part and organelles; and molecular functions contained binding and catalytic activity (Figure 5). However, the results of the GO analysis mainly focused on the processes after *Bgt* inoculation. The "response to stimuli" process was significantly enriched and may be involved in disease defense, but no known DEGs related to defense mechanism (s) were detected. Therefore, cluster of COG analysis was carried out using the same DEGs above mentioned. The data showed that the DEGs were mainly involved in signal transduction mechanisms (13.75%), transcription (13.38%), and replication, recombination and repair (12.25%). Among them, a few DEGs were directly involved in defense mechanisms, but accounting for only 2.18% (Figure 6). These results demonstrated that except for defense-related genes themselves, genes related to biological metabolism and synthesis also responded to the biological defense process.

After KEGG analysis, a total of 50 pathways were significantly enriched using these DEGs, involving cellular processes, environmental adaptation processing, genetic information processing, metabolism, and organismal system. Among them, a plant-pathogen interaction pathway as well as a plant hormone signal transduction pathway emerged (Figures 7, 8). These genes might be potential candidates for understanding the interaction between pathogen and plants and were also the candidate targets for molecular mechanism against wheat powdery mildew.

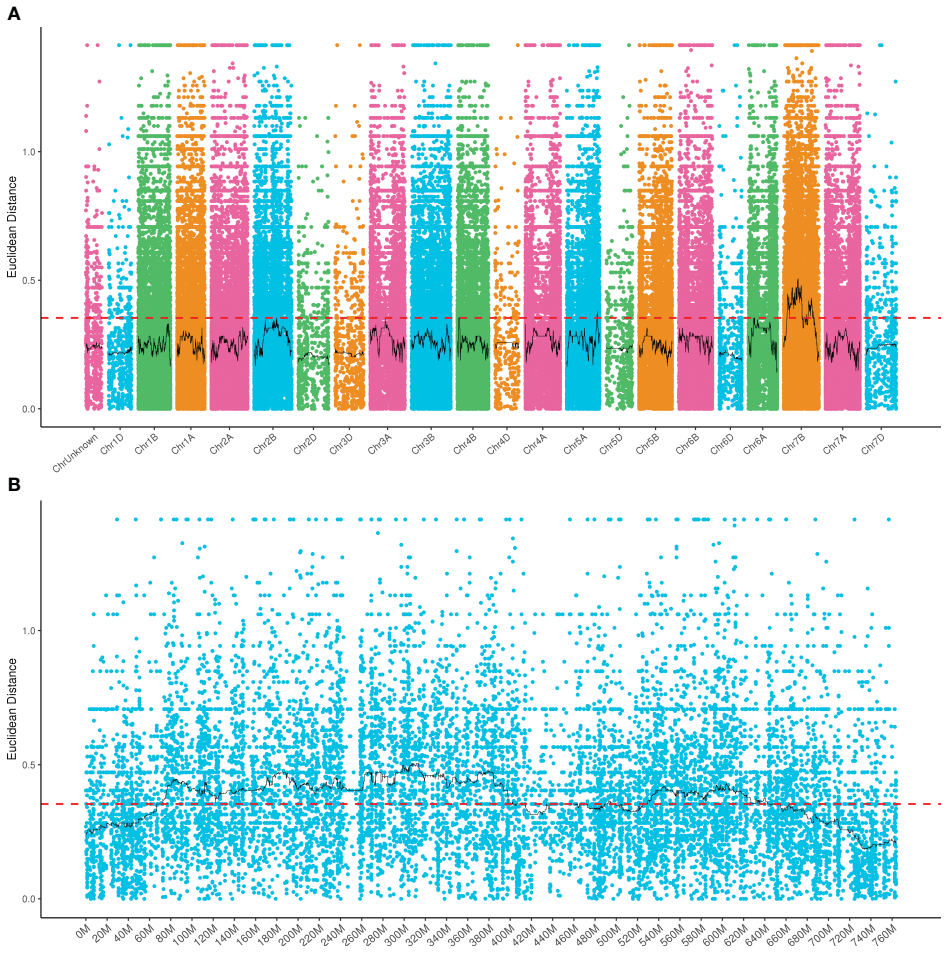

FIGURE 3
Distribution of the SNPs with consistent differences between the resistant parent W762 and susceptible parent Langdon (LDN) and their derived resistant and susceptible bulks on 21 chromosomes **(A)** and chromosome 7B **(B)**.

10.3389/fpls.2024.1387427

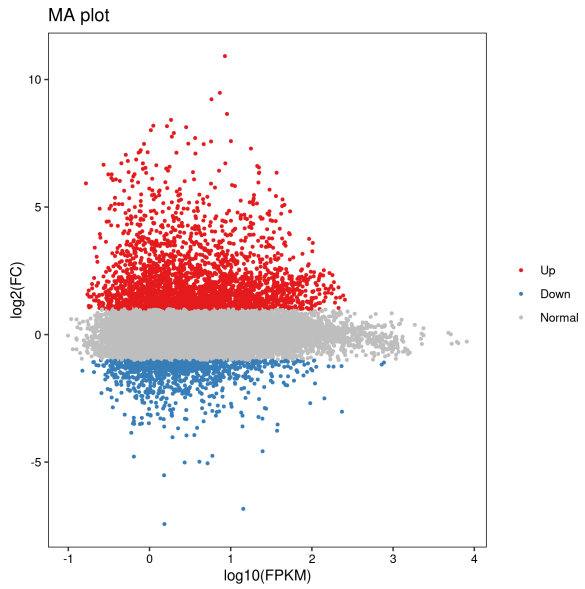

FIGURE 4
M-versus-A (MA) plot of the differentially expressed genes (DEGs) with consistent differences between the resistant parent W762 and susceptible parent Langdon (LDN) and their derived resistant and susceptible bulks. *X* and *Y* axes showed overall signal strength and output difference of the DEGs between resistant and susceptible parents and bulks.

Expression pattern of the key genes related to the powdery mildew resistance in W762

To screen and verify the potential candidate genes responding to *Bgt* invasion, we monitored the infection process using the *Bgt* isolate E09. From the microscopic analyses of reaction process after *Bgt* invasion, we can see that 0 hpi can be used as blank control, 2–4 hpi as primary germ tube formation, 12 hpi as penetration, 24 hpi as haustorium formation, 48 hpi as secondary penetration, and 72 hpi as microcolony formation (Figure 2). Then, we designed the point-in-time for sampling based on the process of microcolony formation, and monitored the transcription levels of 18 potential target genes (including 12 DEGs in the candidate intervals) at different time after inoculating with the *Bgt* isolate E09. Nine genes showed significant differences expression patterns between W762 and LDN. Among them, *TraesCS7B03G0190200.1* and *TraesCS7B03G0320300* encoding serine/threonine protein kinases, *TraesCS7B03G0319700.1* and *TraesCS7B03G1012000.1* encoding protein kinase domain, *TraesCS7B03G0910400.1* encoding disease resistance protein expressed at low levels in LDN, while upregulated in W762 from 0.5 hpi, indicating that they were likely to play roles at the early stage in fighting *Bgt* invasion. *TraesCS7B03G0812600* encoding transcription factor expressed at high level at almost all the invasion process and can be considered as a key gene in the process of fighting *Bgt* invasion. While, *TraesCS7B03G0272100.1* encoding a

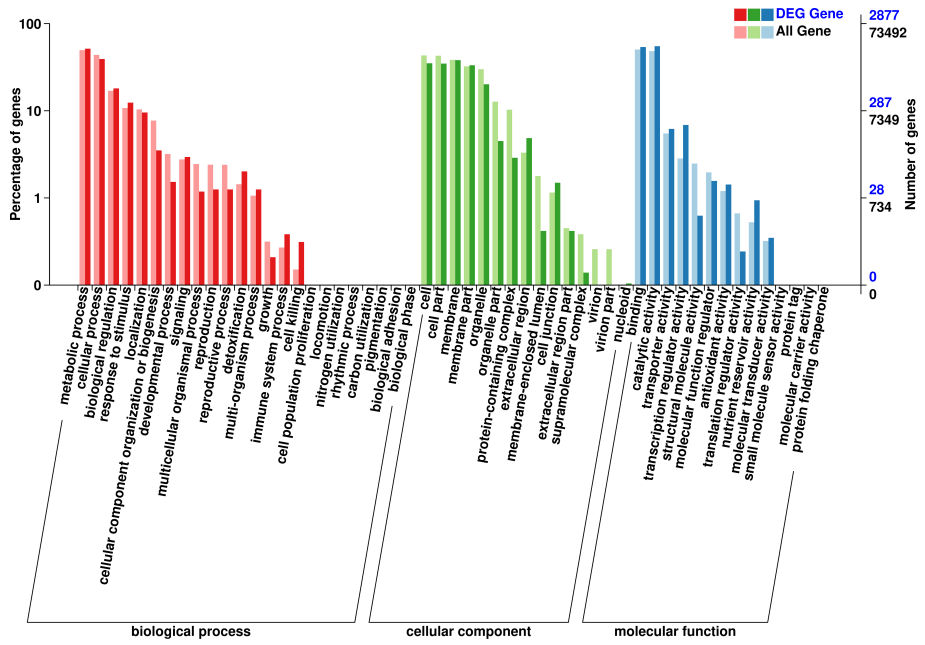

FIGURE 5
Gene ontology (GO) analysis of the differentially expressed genes (DEGs) with consistent differences between the resistant parent W762 and susceptible parent Langdon (LDN) and their derived resistant and susceptible bulks.

10.3389/fpls.2024.1387427

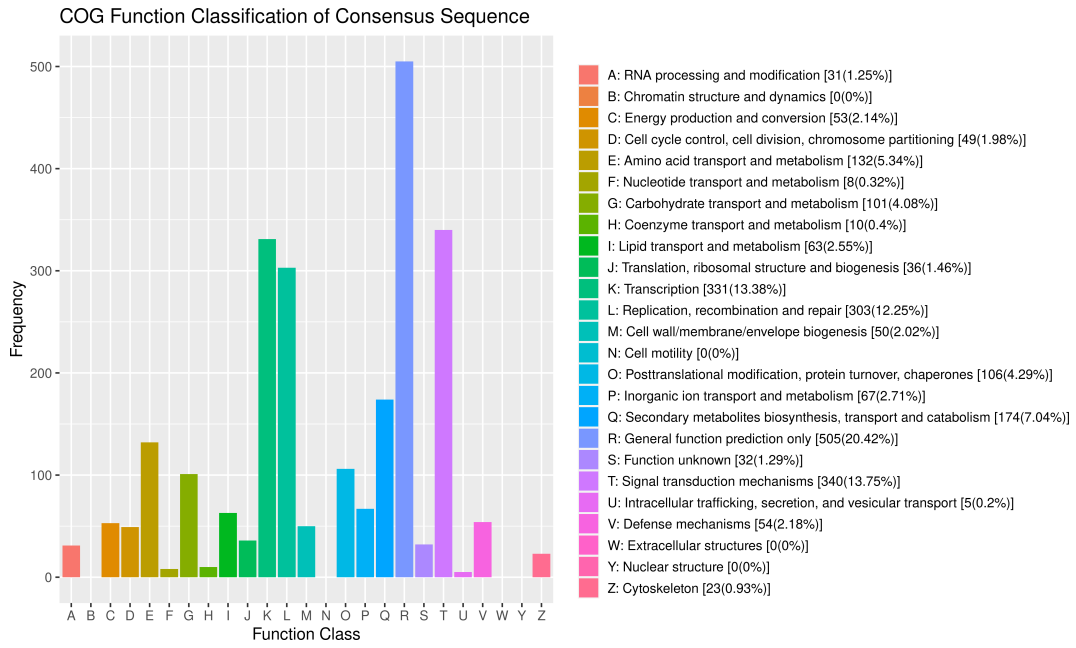

FIGURE 6
Clusters of orthologous groups (COG) analysis of the differentially expressed genes (DEGs) with consistent differences between the resistant parent W762 and susceptible parent Langdon (LDN) and their derived resistant and susceptible bulks.

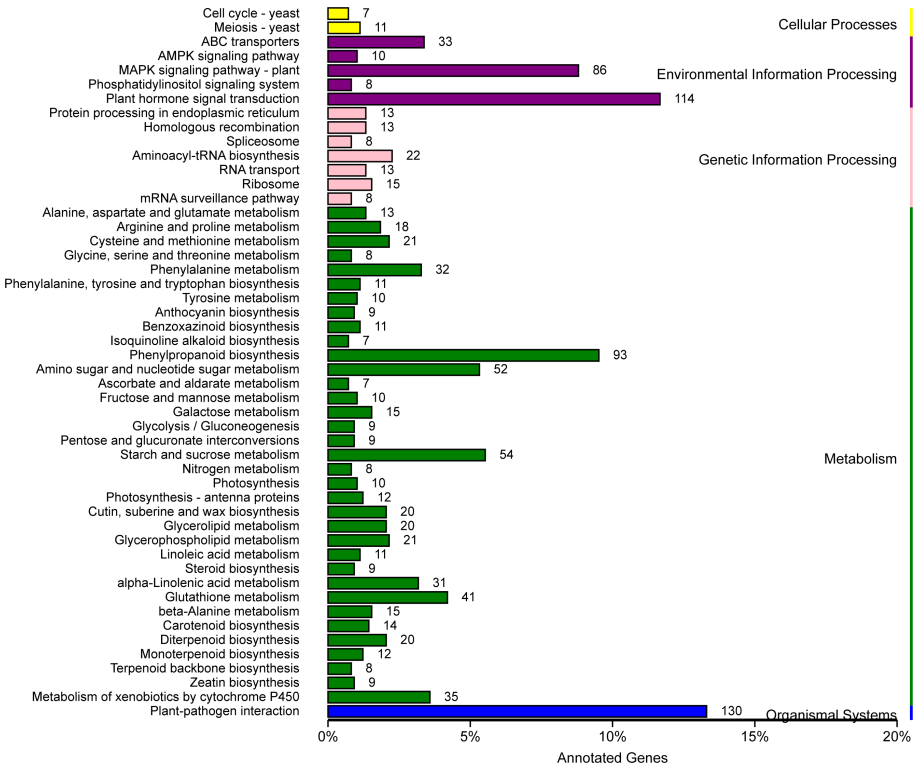

FIGURE 7
Kyoto Encyclopedia of Genes and Genomes (KEGG) pathways enrichment analysis for differentially expressed genes (DEGs) with consistent differences between the resistant parent W762 and susceptible parent Langdon (LDN) and their derived resistant and susceptible bulks.

10.3389/fpls.2024.1387427

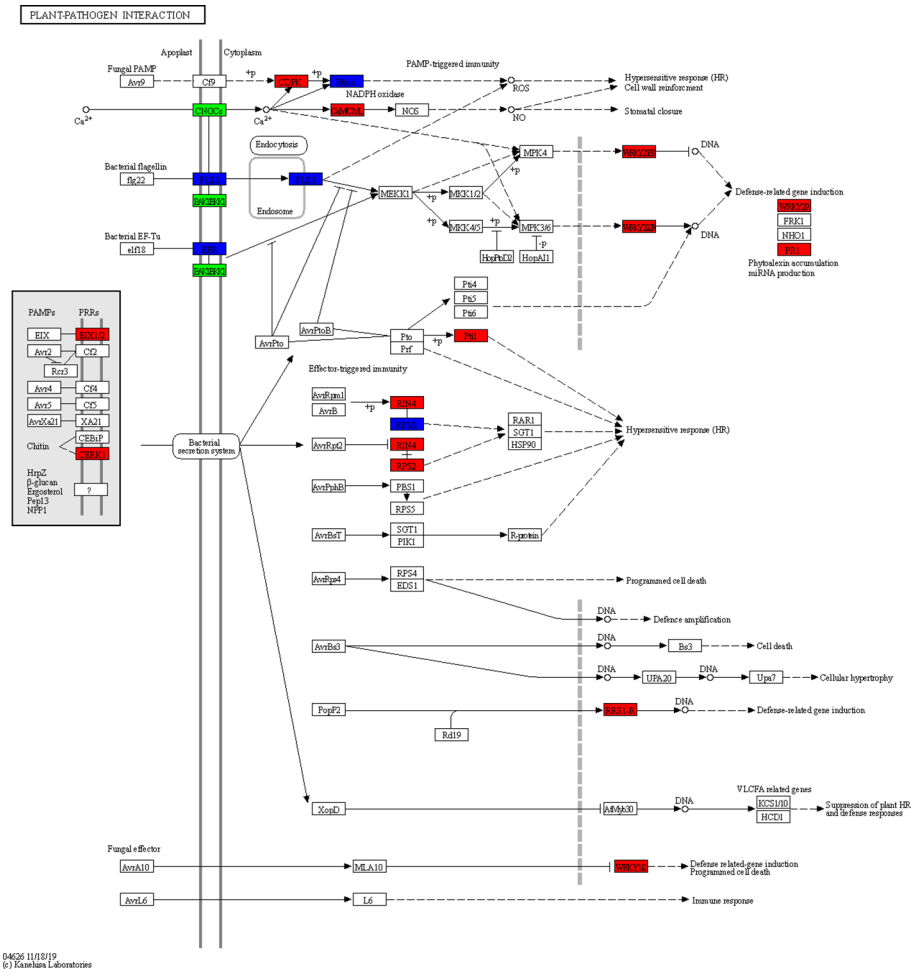

FIGURE 8
Plant-pathogen interaction pathway enriched from differentially expressed genes (DEGs) with consistent differences between the resistant parent W762 and susceptible parent Langdon and their derived resistant and susceptible bulks.

leucine rich repeat (LRR) protein, *TraesCS7B03G0925400.1* encoding a homologous gene of *Arabidopsis thaliana RPM1* protein, *TraesCS7B03G0959700.1* encoding serine/threonine protein kinases, and *TraesCS7B03G0812600.1* encoding transcription factor expressed after *Bgt* invasion in both W762 and LDN, and reached the peak at 2 hpi in LDN (Table 2; Figure 9), suggesting that they may be involved in other pathways related to *Bgt* invasion. Therefore, these genes and their expression patterns can be used as valuable references for

TABLE 2 Partial candidate genes of W762 on chromosome 7B and the primers for quantitative real-time PCR (qRT-PCR).

Gene	Physical genomic location	Functional annotation	Forward primer(5′–3′)	Reverse primer(5′–3′)
TraesCS7B03G0190200	77775536.77786594	Belongs to the protein kinase superfamily	AACGCGGTGATGGAGACTGT	CCGACGGCTGCTTCTTGGT
TraesCS7B03G0272100	122453467.122459516	LRR-repeat protein	GTCGTGCTGTCCTTTCTGC	ATAATGCGTAGGGTGGGTG
TraesCS7B03G0319700	147090873.147093400	Protein kinase domain	AAGCGTCCCGTCTTCTCCCT	TGTTCTTCTGTTTGCCACCACC
TraesCS7B03G0320300	147700331.147707756	Serine/Threonine protein kinases	GACTGGTGGACCTTTGGTA	GCTCACGACTGGGTATTCT
TraesCS7B03G0345700	163329488.163332909	disease resistance protein	ATACCTCCTCATCAAGCAA	ATCCCACAATAGATACCACTT
TraesCS7B03G0378900	189804519.189808558	Protein kinase domain	TATGTCCTACGGCGTCCTGG	TCGTTGGCTCTGCGTTGAT
TraesCS7B03G0446100	241732753.241736063	LRR-repeat protein	CACCAAGGGCGTCAAGCAG	GGGAACACCCAGGCACAGAT

(Continued)

10.3389/fpls.2024.1387427

TABLE 2 Continued

Gene	Physical genomic location	Functional annotation	Forward primer(5′–3′)	Reverse primer(5′–3′)
TraesCS7B03G0506300	299127491.299151515	Protein kinase domain	GCGTCAACTTCTGCGACAT	TGCTGTTCCCAACCGAGTA
TraesCS7B03G0532100	327508868.327510511	Zinc finger CCCH domain-containing protein	GCCCGTATGTGACAAACTGC	CATCCCTCCTCGGTGTAGAA
TraesCS7B03G0569800	370388905.370393531	Serine/Threonine protein kinases	CGAGGATTGAAGTATGTGC	AAGTCAGTCTCAGTGGTGG
TraesCS7B03G0577700	378060043.378068505	Serine threonine-protein kinase Rio1	ACGAGCCACCAGCGGATAA	TCCTTCCGAGCAGCCTTCC
TraesCS7B03G0581800	381059421.381062323	LRR-repeat protein	TGACGCCGTGGGAGATTGT	TTGATGCGGAGCCAGAACG
TraesCS7B03G0812600	545776588.545785098	transcription factor	GTGGAGCTGAGCTGAAAGG	GAAGGCATACGACCAAGAA
TraesCS7B03G0863700	578446982.578448448	Disease resistance protein	ACATGGCGGATACCTGAGCG	TCCGGCGTCTCGAACCACT
TraesCS7B03G0910400	598101444.598107287	disease resistance protein	CCGCTTATCTTAGAGGTCC	AACTCGTGCAATCCAATAC
TraesCS7B03G0925400	605759635.605761734	Disease resistance protein RPM1	CAAGGGTCGTTGGAGGAGT	AGAAAGCGATGGCAGTGGG
TraesCS7B03G0959700	622253623.622256064	Serine threonine-protein kinase	CCTCCGTAGCAGCGTAGACA	CCATTCACGTTTGCCATTTT
TraesCS7B03G1012000	647238432.647243000	Protein kinase domain	GGATGATGTTCCCGGTGAG	TCGGAGGCTTGGCTTTATT

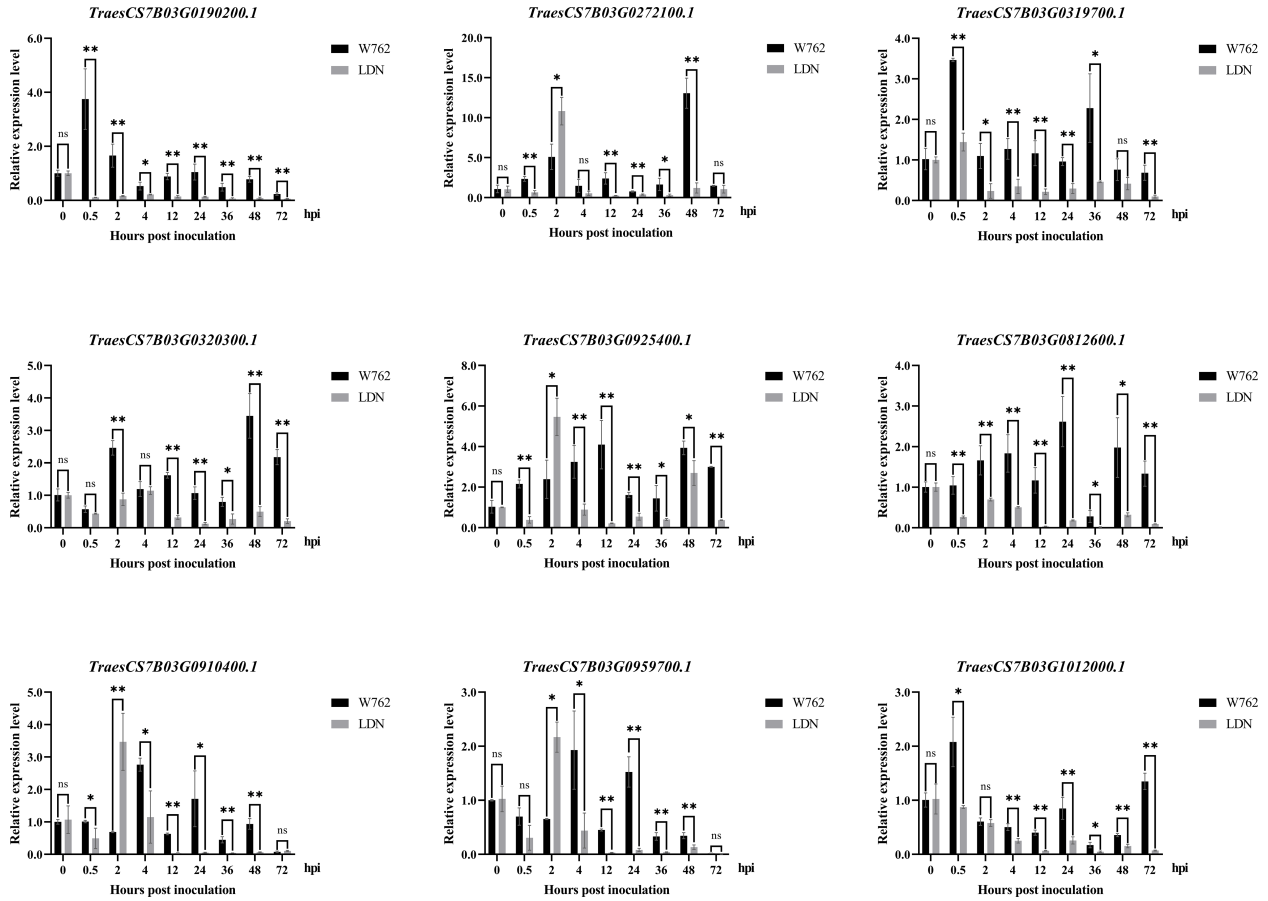

FIGURE 9
Expression profiles of nine genes in W762 and Langdon (LDN) after inoculating with the *Blumeria graminis* f. sp. *tritici (Bgt)* isolate E09 at 0, 0.5, 2, 4, 12, 24, 36, 48 and 72 hours post inoculation (hpi). Normalized values of target genes expression relative to *TaActin* were given as mean ± SD from three replicates. Statistically significant differences (Student's t-test): *, $P < 0.05$; **, $P < 0.01$. ns: not significant.

dissecting the genetic and molecular basis of the powdery mildew resistance in W762.

Discussion

Durum wheat is an important germplasm for wheat improvement against powdery mildew. In this study, a durum wheat accession W762 was resistant to 21 of 32 tested *Bgt* isolates, indicating that it was a valuable resistance donor for wheat improvement against powdery mildew. Genetic analysis showed that the powdery mildew resistance in W762 did not meet monogenic inheritance and complex genetic model might exist in W762. There are several reasons that may be related to this phenomenon, including alien translocation and gametocidal genes and quantitative inheritance. For example, there were evidences that the homologous group two chromosomes of *Triticeae* spp. carried genes favoring the transmission of specific gametes (Tsujimoto and Tsunewaki, 1988). Fu et al. (2013) identified a recessive *Pm* gene (*pmX*) located on chromosome arm 2AL that showed abnormal segregation. Inheritances of the two stem rust resistance genes *Sr36* and *Sr40* showed segregation distortion and recombination suppression which involved alien translocations (Tsilo et al., 2008; Wu et al., 2009). In the present study, molecular genetic analysis of F_2 populations of the cross W762 × LDN and their derived $F_{2:3}$ families deviated significantly from monogenic inheritance. It was supposed that the resistance to powdery mildew in W762 may be controlled by quantitative trait loci or several major *Pm* genes. Further studies on isolating single genes through multiple generations of backcrossing and self-crossing were needed in the future.

BSR-Seq is an efficient method for both rapid gene mapping and differential gene expression profiling (Wang et al., 2017; Hao et al., 2019). Using BSR-Seq, the resistance genes in W762 were postulated to be located on the intervals of 66.8–404.4 Mb and 525.7–645.1 Mb on chromosome 7B. The candidate regions have a total of 740 DEGs, and the resistance gene(s) in responding to *Bgt* invasion in W762 may be located in these candidate intervals. To further identify candidate genes/regulatory genes, we selected 18 potential targeted genes in the candidate intervals to analyze their response patterns against *Bgt* invasion. Nine of these genes did not express in both resistant parent W762 and susceptible parent LDN, and hence can be eliminated. The remaining genes were all upregulated in W762 after *Bgt* invasion, suggesting these genes may play important roles in responding *Bgt* invasion.

Plant resistance is a complex process in the course of host-pathogen interaction (Hikichi, 2016). To respond to the invasion of pathogen, a lot of genes will be activated in plants. Invasion of the pathogens could be prevented at different layers, such as cell wall, plasma membrane, and various enzymes in cytoplasm (Braeken et al., 2008; Soto et al., 2011; Siddiqui et al., 2012). In this study, following *Bgt* inoculation, a large number of DEGs, including the targeted genes in the candidate intervals, which are important for defense against *Bgt* invasion, were identified and analyzed using GO, COG, and KEGG enrichment. And three types of genes accounted for the greater proportions, including those involved in biological process, cellar component and molecular function. This result is consistent with the model of signal transduction and activation of defense mechanisms: when pathogens invade, signal transduction mechanisms are activated to transduce the stress signal; then, defense mechanisms are expected to be mobilized to fight the *Bgt* invasion; both these processes need the support of biosynthesis and metabolism.

Conclusion

W762 is a durum wheat accession that shows high resistance to powdery mildew. We clarified the genetic pattern of powdery mildew resistance, identified DEGs at the whole-genome scale and profiled the expression of several key genes associated with resistance to powdery mildew using qRT-PCR. Our study could lay a foundation for analysis of the molecular mechanism and also provide potential targets for the improvement of durable resistance against powdery mildew.

Data availability statement

The datasets presented in this study can be found in online repositories. The names of the repository/repositories and accession number(s) can be found in the article/supplementary material.

Author contributions

ZQ: Writing – original draft, Writing – review & editing. RL: Writing – original draft, Writing – review & editing. XL: Writing – original draft, Writing – review & editing. YQ: Writing – original draft, Writing – review & editing. JW: Writing – original draft, Writing – review & editing. YY: Writing – original draft, Writing – review & editing. QX: Writing – original draft, Writing – review & editing. NY: Writing – original draft, Writing – review & editing. JZ: Writing – original draft, Writing – review & editing. YL: Writing – original draft, Writing – review & editing. JL: Writing – original draft, Writing – review & editing. YD: Writing – original draft, Writing – review & editing. CL: Writing – original draft, Writing – review & editing. YJ: Writing – original draft, Writing – review & editing. PM: Writing – original draft, Writing – review & editing.

Funding

The author(s) declare financial support was received for the research, authorship, and/or publication of this article. This research was financially supported by Key R&D Plan of Shandong

Province (2022LZG002–4), Wheat Industry Technology System of Shandong Province (SDAIT-01–01), National Natural Science Foundation of China (32072053 and 32301923), Natural Science Foundation of Shandong Province (ZR202211200155), and Key R&D Plan of Yantai City (2022XCZX092).

Acknowledgments

We are grateful to Prof. Yilin Zhou, Institute of Plant Protection, Chinese Academy of Agricultural Sciences, Beijing, China, and Prof. Hongxing Xu, Henan University, Kaifeng, China, for providing the *Blumeria graminis* f. sp. *tritici* isolates.

Conflict of interest

The authors declare that the research was conducted in the absence of any commercial or financial relationships that could be construed as a potential conflict of interest.

Publisher's note

All claims expressed in this article are solely those of the authors and do not necessarily represent those of their affiliated organizations, or those of the publisher, the editors and the reviewers. Any product that may be evaluated in this article, or claim that may be made by its manufacturer, is not guaranteed or endorsed by the publisher.

References

Bennett, F. G. A. (1984). Resistance to powdery mildew in wheat: a review of its use in agriculture and breeding programmes. *Plant Pathol.* 33, 279–300. doi: 10.1111/j.1365-3059.1984.tb01324.x

Bolger, A. M., Marc, L., and Bjoern, U. (2014). Trimmomatic: a flexible trimmer for illumina sequence data. *Bioinformatics* 15, 2114–2120. doi: 10.1093/bioinformatics/btu170

Braeken, K., Daniels, R., Ndayizeye, M., Vanderleyden, J., and Michiels, J. (2008). ""Quorum sensing in bacteria-plant interactions,"," in *Molecular mechanisms of plant and microbe coexistence*, vol. 15 . Eds. C. S. Nautiyal and P. Dion (Springer, Berlin).

Briggle, L. W. (1969). Near-isogenic lines of wheat with genes for resistance to *erysiphe graminis* f. sp. *tritici*. *Crop Sci.* 9, 70–72. doi: 10.2135/cropsci1969.0011183X000900010023x

Cowger, C., Mehra, L., Arellano, C., Meyers, E., and Murphy, J. P. (2018). Virulence 376 differences in *Blumeria graminis* f. sp. *tritici* from the central and eastern United 377 States. *Phytopathology* 108, 402–411. doi: 10.1094/PHYTO-06-17-0211-R

Dobin, A., Davis, C. A., Schlesinger, F., Drenkow, J., Zaleski, C., Jha, S., et al. (2013). STAR: ultrafast universal RNA-seq aligner. *Bioinf. (Oxford England)* 29, 15–21. doi: 10.1093/bioinformatics/bts635

Fu, B. S., Chen, Y., Li, N., Ma, H. Q., Kong, Z. X., Zhang, L. X., et al. (2013). *PmX*: a recessive powdery mildew resistance gene at the *Pm4* locus identified in wheat landrace Xiaohongpi. *Theor. Appl. Genet.* 126, 913–921. doi: 10.1007/s00122-012-2025-1

Han, G. H., Liu, H., Zhu, S. Y., Gu, T. T., Cao, L. J., Yan, H. W., et al. (2024a). Two functional CC-NBS-LRR proteins from rye chromosome 6RS confer differential age-related powdery mildew resistance to wheat. *Plant Biotechnol. J.* 22, 66–81. doi: 10.1111/pbi.14165

Han, G. H., Liu, S. Y., Wang, J., Jin, Y., Zhou, Y. L., Luo, Q. L., et al. (2020). Identification of an elite wheat-rye T1RS·1BL translocation line conferring high resistance to powdery mildew and stripe rust. *Plant Dis.* 104, 2940–2948. doi: 10.1094/PDIS-02-20-0323-RE

Han, G. H., Wang, J., Yan, H. W., Cao, L. J., Liu, S. Y., Li, X. Q., et al. (2024b). Development and molecular cytogenetic identification of a new wheat-rye 6RL ditelosomic addition and 1R (1B) substitution line with powdery mildew resistance. *J. Integr. Agr.* doi: 10.1016/j.jia.2023.10.004

Han, G. H., Wang, J., Yan, H. W., Gu, T. T., Cao, L. J., Liu, S. Y., et al. (2024c). Development and identification of two novel wheat-rye 6R derivative lines with adult-plant resistance to powdery mildew and high-yielding potential. *Crop J.* 12, 308–313. doi: 10.1016/j.cj.2023.09.003

Hao, Z. M., Geng, M. M., Hao, Y. R., Zhang, Y., Zhang, L. J., Wen, S. M., et al. (2019). Screening for differential expression of genes for resistance to *Sitodiplosis mosellana* in bread wheat via BSR-seq analysis. *Theor. Appl. Genet.* 132, 3201–3221. doi: 10.1007/s00122-019-03419-9

He, H. G., Liu, R. K., Ma, P. T., Du, H. N., Zhang, H. H., Wu, Q. H., et al. (2021). Characterization of *Pm68*, a new powdery mildew resistance gene onchromosome 2BS of greek durum wheat TRI 1796. *Theor. Appl. Genet.* 134, 53–62. doi: 10.1007/s00122-020-03681-2

He, H. G., Zhu, S. Y., Zhao, R. H., Jiang, Z. N., Ji, Y. Y., Ji, J., et al. (2018). *Pm21*, encoding a typical CC-NBS-LRR protein, confers broad-spectrum resistance to wheat powdery mildew disease. *Mol. Plant* 11, 879–882. doi: 10.1016/j.molp.2018.03.004

Hikichi, Y. (2016). Interactions between plant pathogenic bacteria and host plants during the establishment of susceptibility. *J. Gen. Plant Pathol.* 82, 326–331. doi: 10.1007/s10327-016-0680-9

Huang, X. Q., Wang, L. X., Xu, M. X., and Röder, M. S. (2003). Microsatellite mapping of the powdery mildew resistance gene *Pm5e* in common wheat (*Triticum aestivum* L.). *Theor. Appl. Genet.* 106, 858–865. doi: 10.1007/s00122-002-1146-3

Krattinger, S. G., Lagudah, E. S., Spielmeyer, W., Singh, R. P., Huerta-Espino, J., McFadden, H., et al. (2009). A putative ABC transporter confers durable resistance to multiple fungal pathogens in wheat. *Science* 323, 1360–1363. doi: 10.1126/science.1166453

Li, H. J., Zhou, Y., Xin, W. L., Wei, Y. Q., Zhang, J. L., and Guo, L. L. (2019). Wheat breeding in northern China: achievements and technical advances. *Crop J.* 7, 718–729. doi: 10.1016/j.cj.2019.09.003

Li, Y., Wei, Z. Z., Sela, H., Govta, L., Klymiuk, V., Roychowdhury, R., et al. (2024). Dissection of a rapidly evolving wheat resistance gene cluster by long-read genome sequencing accelerated the cloning of *Pm69*. *Plant Commun.* 5, 100646. doi: 10.1016/j.xplc.2023.100646

Livak, K. J., and Schmittgen, T. D. (2001). Analysis of relative gene expression data using real-time quantitative PCR and the 2–CT method. *Methods* 25, 402–408. doi: 10.1006/meth.2001.1262

Ma, P. T., Xu, H. X., Xu, Y. F., Song, L. P., Liang, S. S., Sheng, Y., et al. (2018). Characterization of a powdery mildew resistance gene in wheat breeding line 10V-2 and its application in marker-assisted selection. *Plant Dis.* 102, 925–931. doi: 10.1094/PDIS-02-17-0199-RE

McIntosh, R. A., Dubcovsky, J., Rogers, W. J., Xia, X. C., and Raupp, W. J. (2020) *Catalogue of gene symbols for wheat 2020 supplement*. Available online at: https://wheat.pw.usda.gov/GG3/WGC.

McKenna, A., Hanna, M., Banks, E., Sivachenko, A., Cibulskis, K., Kernytsky, A., et al. (2010). The genome analysis toolkit: a MapReduce framework for analyzing next-generation DNA sequencing data. *Genome Res.* 20, 1297–1303. doi: 10.1101/gr.107524.110

Miedaner, T., Rapp, M., Flath, K., Longin, C. F. H., and Würschum, T. (2019). Genetic architecture of yellow and stem rust resistance in a durum wheat diversity panel. *Euphytica* 215, 71. doi: 10.1007/s10681-019-2394-5

Moore, J. W., Herrera-Foessel, S., Lan, C., Schnippenkoetter, W., Ayliffe, M., Huerta-Espino, J., et al. (2015). A recently evolved hexose transporter variant confers resistance to multiple pathogens in wheat. *Nat. Genet.* 47, 1494–1498. doi: 10.1038/ng.3439

Pankievicz, V. C. S., Camilios-Neto, D., Bonato, P., Balsanelli, E., Tadra-Sfeir, M. Z., Faoro, H., et al. (2016). RNA-seq transcriptional profiling of *Herbaspirillum seropedicae* colonizing wheat (*Triticum aestivum*) roots. *Plant Mol. Biol.* 90, 589–603. doi: 10.1007/s11103-016-0430-6

Pearce, S., Vazquez-Gross, H., Herin, S. Y., Hane, D., Wang, Y., Gu, Y. Q., et al. (2015). WheatExp: an RNA-seq expression database for polyploid wheat. *BMC Plant Biol.* 15, 299. doi: 10.1186/s12870-015-0692-1

Reiner, A., Yekutieli, D., and Benjamini, Y. (2003). Identifying differentially expressed genes using false discovery rate controlling procedures. *Bioinformatics* 19, 368–375. doi: 10.1093/bioinformatics/btf877

Sears, E. R., and Briggle, L. W. (1969). Mapping the gene *Pm1* for resistance to *erysiphe graminis* f. sp. *tritici* on chromosome 7A of wheat. *Crop Sci.* 9, 96–97. doi: 10.2135/cropsci1969.0011183X000900010033x

Sherman, B. T., Hao, M., Qiu, J., Jiao, X., Baseler, M. W., Lane, H. C., et al. (2022). DAVID: a web server for functional enrichment analysis and functional annotation of gene lists, (2021 update). *Nucleic Acids Res.* 50, W216–W221. doi: 10.1093/nar/gkac194

Si, Q. M., Zhang, X. X., Duan, X. Y., Sheng, B. Q., and Zhou, Y. L. (1992). On gene analysis and classification of powdery mildew (*Erysiphe graminis* f. sp. *tritici*) resistant wheat varieties. *Acta Phytopathol. Sin.* 22, 349–355. doi: 10.13926/j.cnki.apps.1992.04.021

Siddiqui, Z. A., Nesha, R., Singh, N., and Alam, S. (2012). ""Interactions of plantparasitic nematodes and plant-pathogenic bacteria,"," in *Bacteria in agrobiology : plant probiotics*. Ed. D. Maheshwari (Springer, Berlin).

Singh, R. P., Singh, P. K., Rutkoski, J., Hodson, D. P., He, X., Jørgensen, L. N., et al. (2016). Disease impact on wheat yield potential and prospects of genetic control. *Annu. Rev. Phytopathol.* 54, 303–322. doi: 10.1146/annurev-phyto-080615-095835

Soto, M. J., Nogales, J., Pérez-Mendoza, D., Gallegos, M. T., Olivares, J., and Sanjuán, J. (2011). Pathogenic and mutualistic plant-bacteria interactions: ever increasing similarities. *Cent. Eur. J. Biol.* 6, 911–917. doi: 10.2478/s11535-011-0069-x

Srichumpa, P., Brunner, S., Keller, B., and Yahiaoui, N. (2005). Allelic series of four powdery mildew resistance genes at the *Pm3* locus in hexaploid bread wheat. *Plant Physiol.* 139, 885–895. doi: 10.1104/pp.105.062406

Trapnell, C., Williams, B. A., Pertea, G., Mortazavi, A., Kwan, G., van Baren, M. J., et al. (2010). Transcript assembly and quantification by RNA-Seq reveals unannotated transcripts and isoform switching during cell differentiation. *Nat. Biotechnol.* 28, 511–515. doi: 10.1038/nbt.1621

Tsilo, T. J., Jin, Y., and Anderson, J. A. (2008). Diagnostic microsatellite markers for the detection of stem rust resistance gene *Sr36* in diverse genetic backgrounds of wheat. *Crop Sci.* 48, 253–261. doi: 10.2135/cropsci2007.04.0204

Tsujimoto, H., and Tsunewaki, K. (1988). Gametocidal genes in wheat and its relatives. iii. chromosome location and effects of two aegilops speltoides-derived gametocidal genes in common wheat. *Genome* 30, 239–244. doi: 10.1139/g88-041

Wang, Y., Cheng, X., Shan, Q., Zhang, Y., Liu, J. X., Gao, C. X., et al. (2014). Simultaneous editing of three homoeoalleles in hexaploid bread wheat confers heritable resistance to powdery mildew. *Nat. Biotechnol.* 32, 947–951. doi: 10.1038/nbt.2969

Wang, W. R., He, H. G., Gao, H. M., Xu, H. X., Song, W. Y., Zhang, X., et al. (2021). Characterization of the powdery mildew resistance gene in wheat breeding line KN0816 and its evaluation in marker-assisted selection. *Plant Dis.* 105, 4042–4050. doi: 10.1094/PDIS-05-21-0896-RE

Wang, B., Meng, T., Xiao, B., Yu, T. Y., Yue, T. Y., Jin, Y. L., et al. (2023). Fighting wheat powdery mildew: from genes to fields. *Theor. Appl. Genet.* 136, 196. doi: 10.1007/s00122-023-04445-4

Wang, Y., Xie, J. Z., Zhang, H. Z., Guo, B. M., Ning, S. Z., Chen, Y. X., et al. (2017). Mapping stripe rust resistance gene *YrZH22* in Chinese wheat cultivar Zhoumai 22 by bulked segregant RNA-Seq (BSR-Seq) and comparative genomics analyses. *Theor. Appl. Genet.* 130, 2191–2201. doi: 10.1007/s00122-017-2950-0

Wang, C. M., Zheng, Q., Li, L. H., Niu, Y. C., Wang, H. B., Li, B., et al. (2009). Molecular cytogenetic characterization of a new T2BL·1RS wheat-rye chromosome translocation line resistant to stripe rust and powdery mildew. *Plant Dis.* 21, 419–432. doi: 10.1094/PDIS-93-2-0124

Wu, S., Pumphrey, M. O., and Bai, G. (2009). Molecular mapping of stem-rust-resistance gene *Sr40* in wheat. *Crop Sci.* 49, 1681–1686. doi: 10.2135/cropsci2008.11.0666

Xue, F., Wang, C. Y., Li, C., Duan, X. Y., Zhou, Y. L., Zhao, N. J., et al. (2012). Molecular mapping of a powdery mildew resistance gene in common wheat landrace Baihulu and its allelism with *Pm24*. *Theor. Appl. Genet.* 125, 1425–1432. doi: 10.1007/s00122-012-1923-6

Yahiaoui, N., Brunner, S., and Keller, B. (2006). Rapid generation of new powdery mildew resistance genes after wheat domestication. *Plant J.* 47, 85–98. doi: 10.1111/j.1365-313X.2006.02772.x

Zhang, H. Z., Xie, J. Z., Cheng, Y. X., Liu, X., Wang, Y., Yan, S. H., et al. (2017). Mapping stripe rust resistance gene *YrZM103* in wheat cultivar Zhengmai 103 by BSR-seq. *Acta Agron. Sin.* 43, 1643–1649. doi: 10.3724/SP.J.1006.2017.01643

Zhou, R. H., Zhu, Z. D., Kong, X. Y., Huo, N. X., Tian, Q. Z., Li, P., et al. (2005). Development of wheat near-isogenic lines for powdery mildew resistance. *Theor. Appl. Genet.* 110, 640–648. doi: 10.1007/s00122-004-1889-0

Zhu, Z. D., Kong, X. Y., Zhou, R. H., and Jia, J. Z. (2004). Identification and microsatellite markers of a resistance gene to powdery mildew in common wheat introgressed from *Triticum durum*. *Acta Bot. Sin.* 46, 867–872. doi: 10.1016/j.molcel.2004.06.032

Zhu, S. Y., Liu, C., Gong, S. J., Chen, Z. Z., Chen, R., Liu, T. L., et al. (2023). Orthologous genes *Pm12* and *Pm21* from two wild relatives of wheat show evolutionary conservation but divergent powdery mildew resistance. *Plant Commun.* 4, 100472. doi: 10.1016/j.xplc.2022.100472

Zhu, T., Wang, L., Rimbert, H., Rodriguez, J. C., Deal, K. R., De Oliveira, R., et al. (2021). Optical maps refine the bread wheat *Triticum aestivum* cv Chinese Spring genome assembly. *Plant J.* 107, 303–314. doi: 10.1111/tpj.15289

frontiers | Frontiers in Plant Science

TYPE Original Research
PUBLISHED 12 June 2024
DOI 10.3389/fpls.2024.1395223

Check for updates

OPEN ACCESS

EDITED BY
Changlin Liu,
Chinese Academy of Agricultural Sciences (CAAS), China

REVIEWED BY
Francesca Desiderio,
Council for Agricultural and Economics Research, Italy
Jindong Liu,
Chinese Academy of Agricultural Sciences, China

*CORRESPONDENCE
Zhensheng Kang
kangzs@nwsuaf.edu.cn
Lin Cai
lincai@gzu.edu.cn

†These authors have contributed equally to this work

RECEIVED 03 March 2024
ACCEPTED 06 May 2024
PUBLISHED 12 June 2024

CITATION
Zhou X, Jia G, Luo Y, Li X, Cai L, Chen X and Kang Z (2024) Fine mapping of *QYrsv.swust*-1BL for resistance to stripe rust in durum wheat Svevo. *Front. Plant Sci.* 15:1395223. doi: 10.3389/fpls.2024.1395223

COPYRIGHT
© 2024 Zhou, Jia, Luo, Li, Cai, Chen and Kang. This is an open-access article distributed under the terms of the Creative Commons Attribution License (CC BY). The use, distribution or reproduction in other forums is permitted, provided the original author(s) and the copyright owner(s) are credited and that the original publication in this journal is cited, in accordance with accepted academic practice. No use, distribution or reproduction is permitted which does not comply with these terms.

Fine mapping of *QYrsv.swust*-1BL for resistance to stripe rust in durum wheat Svevo

Xinli Zhou[1†], Guoyun Jia[1†], Yuqi Luo[1], Xin Li[1], Lin Cai[2*], Xianming Chen[3] and Zhensheng Kang[4*]

[1]Wheat Research Institute, School of Life Sciences and Engineering, Southwest University of Science and Technology, Mianyang, Sichuan, China, [2]College of Tobacco Science of Guizhou University, Key Laboratory of Plant Resource Conservation and Germplasm Innovation in Mountainous Region (Ministry of Education), Guizhou Key Lab of Agro-Bioengineering, Guiyang, China, [3]US Department of Agriculture, Agricultural Research Service, Wheat Health, Genetics, and Quality Research Unit, and Department of Plant Pathology, Washington State University, Pullman, WA, United States, [4]State Key Laboratory of Crop Stress Biology in Arid Areas and College of Plant Protection, Northwest A&F University, Xianyang, Shaanxi, China

Stripe rust, caused by *Puccinia striiformis* f. sp. *tritici* (*Pst*), is a serious disease that affects wheat worldwide. There is a great need to develop cultivars with combinations of all-stage resistance (ASR) and adult-plant resistance (APR) genes for sustainable control of the disease. *QYrsv.swust-1BL* in the Italian durum wheat (*Triticum turgidum* ssp. *durum*) cultivar Svevo is effective against *Pst* races in China and Israel, and the gene has been previously mapped to the long arm of chromosome 1B. The gene is flanked by SNP (single nucleotide polymorphism) markers *IWB5732* and *IWB4839* (0.75 cM). In the present study, we used high-density 660K SNP array genotyping and the phenotypes of 137 recombinant inbred lines (RILs) to fine map the *QYrsv.swust-1BL* locus within a 1.066 Mb region in durum wheat Svevo (RefSeq Rel. 1.0) on chromosome arm 1BL. The identified 1.066 Mb region overlaps with a previously described map of *Yr29/QYr.ucw-1BL*, a stripe rust APR gene. Twenty-five candidate genes for *QYrsv.swut-1BL* were identified through comparing polymorphic genes within the 1.066 Mb region in the resistant cultivar. SNP markers were selected and converted to Kompetitive allele-specific polymerase chain reaction (KASP) markers. Five KASP markers based on SNP were validated in a F_2 and $F_{2:3}$ breeding population, providing further compelling evidence for the significant effects of *QYrsv.swut-1BL*. These markers should be useful in marker-assisted selection for incorporating *Yr29/QYrsv.swust-1BL* into new durum and common wheat cultivars for resistance to stripe rust.

KEYWORDS

stripe rust, resistance gene, durum wheat, fine mapping, quantitative trait locus

Introduction

Wheat is a widely cultivated grain crop and is critical for global food security. Thus, it is important to limit pathogen-caused losses in wheat yield. Stripe rust (Yellow rust, *Yr*), caused by the fungal pathogen *Puccinia striiformis* f. sp. *tritici* (*Pst*), is a growing threat to global wheat production (Chen, 2005, 2020). Although fungicides can control stripe rust, this approach can be costly and harmful to humans, animals, and the environment. The most economical, effective, and environmentally friendly approach to controlling stripe rust is to develop resistant cultivars. However, because of co-evolution pressures, race-specific resistance can be ultimately overcome by new races of the pathogen, often within just a few years (Beddow et al., 2015). There is an urgent need to identify effective stripe rust-resistant genes and develop new resistant cultivars.

At present, 86 formally named resistance genes, more than 70 temporarily named genes, and more than 380 quantitative trait loci (QTL) for resistance to stripe rust have been identified from common wheat, durum wheat, and wild relatives (Bansal et al., 2014; Wang and Chen, 2017; Feng et al., 2018; Nsabiyera et al., 2018; Gessese et al., 2019; Maccaferri et al., 2019; Pakeerathan et al., 2019; Li et al., 2020; Singh et al., 2021; Klymiuk et al., 2022; Yao et al., 2022; Feng et al., 2023; Zhu et al., 2023). However, most of the genes were overcome by the pathogen shortly after being introduced to commercial cultivars. Race-specific (mostly all-stage resistance genes) and non-race-specific [mostly adult-plant resistance (APR) genes] are two major classes of resistance to wheat stripe rust (Chen et al., 2013). Race-specific resistance genes typically encode nucleotide-binding site-leucine-rich repeat (NBS-LRR) resistance proteins. These proteins can detect the presence of pathogen effectors or modify the defense proteins they produce in the host, thereby triggering hypersensitive reactions and reducing the growth of pathogens (Periyannan et al., 2013; Zhang et al., 2017; Chen et al., 2018; Marchal et al., 2018). However, many race-specific resistance genes in commercial cultivars are no longer effective. This is because amino acid changes in the effectors can help the pathogen evade recognition by the nucleotide-binding leucine-rich repeat (NB-LRR) genes (Chen et al., 2017; Salcedo et al., 2017; Cobo et al., 2019). By contrast, APR genes typically show more durable but less strong resistance than all-stage race-specific genes (Krattinger et al., 2009; Singh et al., 2011; Chen et al., 2013). Three APR genes against wheat stripe rust have been cloned, encoding proteins that are more complex and diverse than NBS-LRR. *Yr18* encodes an ATP-binding cassette (ABC) transporter (Krattinger et al., 2009); *Yr36* encodes a kinase and a putative START lipid-binding domain (Fu et al., 2009; Gou et al., 2015); and *Yr46* encodes a hexose transporter (Moore et al., 2015). Using APR is a demonstrated approach to developing wheat cultivars with durable resistance to stripe rust (Chen et al., 2013; Liu et al., 2018, 2019).

Stripe rust resistance QTL *QYrsv.swust-1BL* was previously mapped between the linked SNP markers *IWB5732* and *IWB4839* in a 0.75 cM (1.74 Mb) region derived from durum wheat cultivar Svevo (Zhou et al., 2021), which overlaps the map of *Yr29*, a long-term utilized gene for APR to stripe rust (William et al., 2003; Kolmer, 2015). The known pleiotropic APR gene *Yr29/Lr46/Sr58/Pm39* has been reported in several studies (Ren et al., 2017; Cobo et al., 2018, 2019; Herrera-Foessel et al., 2011; Ponce-Molina et al., 2018; Li et al., 2020). *Yr29/Lr46* (Singh et al., 1998; William et al., 2003) provides partial APR to rust diseases (Herrera-Foessel et al., 2015) and powdery mildew (Lillemo et al., 2008, 2013) in wheat. *Yr29/Lr46* is also associated with the leaf tip necrosis (*Ltn*) gene *Ltn2* (William et al., 2003; Rosewarne et al., 2006). *QYrsv.swust-1BL* explained 11.0% to 34.4% of the phenotypic variation and was effective across all tested environments in China and Israel. The phenotypic variance explained by *QYrsv.swust-1BL* and *Yr29* was very similar (Zhou et al., 2021). However, it is not certain whether the two genes are the same gene, allelic genes, or closely linked genes. In addition, the flanking markers were not sufficiently close for efficient marker-assisted selection.

The objectives of this study were to genotype recombinant inbred lines (RILs) used in the previous study (Zhou et al., 2021) using the wheat 660K SNP iSelect array, produce a high-resolution map for the resistance gene *QYrsv.swust-1BL* in Svevo with more markers, identify candidates for this resistance gene, transfer *QYrsv.swust-1BL* into common wheat, and develop user-friendly markers for validation to hasten the use of this gene in breeding programs.

Materials and methods

Plant materials

To fine-map the locus of *QYrsv.swust-1BL* for stripe rust APR in Svevo, 137 RILs developed from Svevo/Zavitan (Avni et al., 2014; Zhou et al., 2021) were used as a mapping population. To transfer and validate stripe rust resistance from durum wheat Svevo to the Chinese common wheat (*T. aestivum*) background, Svevo was crossed with Mianmai 37 (MM 37), a widely grown common wheat cultivar developed by the Wheat Research Institute, Mianyang Academy of Agricultural Sciences, Sichuan, China. However, this cultivar has become susceptible to stripe rust in recent years. Twelve F_1 plants derived from MM 37/Svevo were selfed to generate 474 F_2 plants. Due to sterility, only 318 $F_{2:3}$ families were successfully harvested from 474 F_2 plants. F_2 plants correspond to 318 $F_{2:3}$ lines, which were phenotyped for stripe rust response and used to detect the availability of markers. Common wheat cultivars Jinmai 47 (JM 47) and Mingxian 169 (MX 169) were used in the phenotyping experiments as stripe rust-susceptible checks.

Field evaluation

In 2019 and 2020, the 137 RILs of Svevo/Zavitan were phenotyped for their responses to stripe rust in Yangling (YL, 34.292N, 108.077E), Shaanxi Province, and Mianyang (MY, 31.682N, 104.663E), Sichuan Province, China. A randomized complete block design was used, with two replicates in each year at each location. For each line in each replicate, 25 to 30 seeds were sown in a 1-m row, with 25 cm separating the rows. As susceptible checks, JM 47 was planted in every 20th row and MX 169 around the

nursery to increase the pathogen inoculum. The YL site was planted on 6 October 2019 and 10 October 2020, and the MY site on 12 November 2019 and 15 November 2020. In Yangling, when flag leaves emerged [Zadoks growth stage (GS) 40] (Zadoks et al., 1974) in late March, the plants were inoculated with a mixture of equal amounts of urediniospores of *Pst* races CYR32, CYR33, and CYR34, which were predominant races in China. The fields in Mianyang were tested for natural *Pst* infection in these two growing seasons, as this region is one of the major *Pst* inoculum sources in China (Chen et al., 2014). The parents, 12 F_1, and 474 F_2 plants of MM 37/Svevo were grown at the research farm of Southwest University of Science and Technology in Mianyang during the 2017–2018 and 2018–2019 growing seasons, respectively. Three hundred eighteen $F_{2:3}$ family seeds were harvested from 474 F_2 plants and were planted, together with the parental lines, at Mianyang on 12 November 2019 in a randomized complete block design with two replications. Infection type (IT) based on the 0–9 scale (Line and Qayoum, 1992) and disease severity (DS) as percentage of infected foliage were recorded for each parent and RIL when JM 47 and MX 169 had 80% or higher DS at Zadoks growth stages (GS) 65–69.

Phenotypic analysis

Relative to the phenotypic scores of the parents and susceptible checks, the RILs of Svevo/Zavitan and the $F_{2:3}$ families of MM 37/Svevo were classified into the groups of homozygous resistant (HR) and homozygous susceptible (HS). In addition, the segregating $F_{2:3}$ families were classified as segregating (Seg.). An analysis of variance (ANOVA) was conducted based on the IT and DS data of the populations in the tests of different years and fields (considered as different environments) using the "AOV" tool in QTL IciMapping V4.2 software (Wang, 2009; Meng et al., 2015).

DNA extraction, KASP marker development, and genotyping the RIL and F_2 populations

Total genomic DNA was extracted from the parents, 137 RILs of Svevo/Zavitan, and 318 F_2 plants from MM 37/Svevo using the cetyltrimethylammonium bromide (CTAB) method (Anderson et al., 1993). To identify closer SNP markers and saturate the targeted QTL region, the genetic maps of the RIL mapping population produced in the previous studies with the 90K SNP array (Avni et al., 2014; Zhou et al., 2021) and the sequences of closely linked polymorphic SNPs were used to BLAST search version 1.0 of the Chinese Spring and Svevo genome sequences from the International Wheat Genome Consortium (IWGSC) and at the GrainGenes Svevo Genome Browser (Durum Wheat Svevo RefSeq Rel. 1.0), respectively. Svevo, Zavitan, and MM 37 were first genotyped with the 660K SNP array by China Golden Marker Biotech Co., Ltd. (Beijing, China). The Kompetitive allele-specific polymerase chain reaction (KASP) markers were developed from the 660K SNP map (http://wheat.pw.usda.gov/ggpages/topics/Wheat660_SNP_array_developed_by_CAAS.pdf). Based on chromosome positions in the 660K SNP map, SNPs within a more conservative target region between *IWB8812* and *IWB4839* were selected for conversion to KASP markers (Figure 1). The KASP markers were used to screen the Svevo and Zavitan to confirm polymorphisms before genotyping the entire RIL population. Similarly, before screening the 318 F_2 plants, MM 37 and Svevo were tested with the KASP markers to confirm the polymorphisms before the markers were used to genotype the 318 F_2 plants from the MM 37/Svevo cross. The design of KASP primers, PCR amplification, and marker detection were conducted following the PolyMarker method (Ramirez-Gonzalez et al., 2015; Wu et al., 2018).

Construction of genetic maps and QTL mapping

Genome Studio Polyploid Clustering v1.0 (Illumina, New York, USA) was used for genotype calling and clustering. Markers with >20% of missing data were excluded from further analyses. Marker binning was done using pattern segregation methods (Wang, 2009; Meng et al., 2015). The linkage groups were ordered, and non-binned markers were placed in the groups based on their genome positions. The Chi-squared test was used to detect any segregation distortions. Markers with a p-value of < 0.01 in the Chi-squared test were removed prior to generating the genetic map.

Genetic linkage maps of the KASP markers were constructed using the previously described procedures (Zhou et al., 2019; 2021). The likelihood of an odd score of 2.5 was set as the threshold for linkages between loci, and QTL mapping was conducted based on the phenotyping and genotyping data using the software IciMapping V4.2 (Wang, 2009; Meng et al., 2015). Mapping was conducted first using the BIP (biparental population) module and the ICIM-ADD model in the years 2019–2020 and by combining the data from the previous years 2016–2018 from all environments. The MET (multi-environmental trials) module was also employed to identify the QTL loci in the years 2016–2020 in all environments. The methodology used for the BIP and MET analyses closely follows the approach described in Zhou et al. (2021). But the mapping parameters were step=0.1 cM and PIN=0.001 (probability of SNP to be included in the model).

Identification of candidate genes

The probes of the SNP identified in the QTL region were aligned to the newly released Chinese Spring sequences (IWGSC RefSeq V1.0, annotation V1.1, the International Wheat Genome Consortium (IWGSC), https://www.wheatgenome.org/about/iwgsc-2.0) through BLAST searching. This provided physical positions, reference sequences, annotations, and alignments of the polymorphic SNP markers. The SNP probes were also BLAST searched against the Svevo genome sequences at the GrainGenes Svevo Genome Browser (Durum Wheat Svevo RefSeq Rel. 1.0). Annotated genes in the target region were bioinformatically analyzed using the NCBI (https://bl-ast.ncbi.nlm.nih.gov/Blast.cgi)

10.3389/fpls.2024.1395223

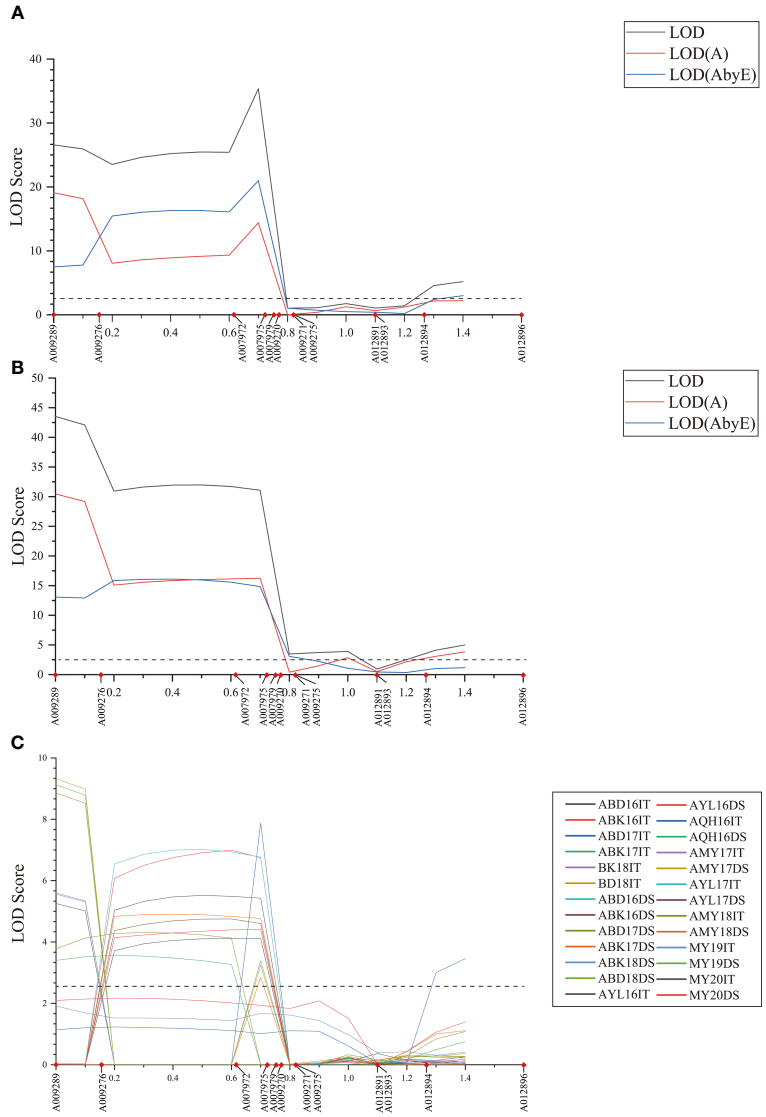

FIGURE 1
LOD scores of the MET **(A, B)** and BIP **(C)** analyses on infection type (IT) and disease severity (DS) values in stripe rust resistance *QYrsv.swust-1BL*. LOD, the total Lod score; LOD **(A)**, the additive effect component of the LOD; LOD (AbyE), the environmental by additive effect component of the LOD. The X-axis represents the genetic distance of the chromosomes. The Y-axis represents the threshold LOD score.

and Genoscope (https://www.cea.fr/drf/ifr-ancoisjacob/Pages/Departements/Genoscope.aspx) databases and the Web site-based software FGENSH (http://www.softberry.com/berry.phtml?topic=fgenesh&group=he-lp&subgroup=gfind) for their putative functions and possible involvement in plant disease resistance to identify candidates of the stripe rust resistance genes.

Results

Developing KASP markers

Using the initial markers *IWB8812* and *IWB4839* from the 90K wheat SNP array as the conservative flanking loci, *QYrsv.swust-1BL* from Svevo was mapped in the 1.855 Mb (physical position: 669,649,666 ~ 671,505,587 bp) region corresponding to the Chinese Spring IWGSC RefSeq v1.0 1BL chromosome, which includes the segments previously reported and considered as *QYr.ucw-1BL/Yr29* (Cobo et al., 2019; Zhou et al., 2021). By comparing the genome sequences of durum wheat Svevo RefSeq Rel. 1.0 (the GrainGenes Svevo Genome Browser) and Chinese Spring IWGSC RefSeq v1.0 (https://urgi.versailles.inra.fr/download/iwgsc/), a nucleic acid database was constructed with the genome sequences of Svevo. The sequences of 630,517 SNP probes from the 660K SNP array were compared to the genome sequences of Svevo by BLASTn. All SNP probes that matched the expected sequences of the 660,683,255 ~ 663,334,719 bp region of the Svevo chromosome 1BL were selected. Similarly, in the Chinese Spring genome, SNPs in the 669,649,666 ~ 671,505,587 bp region were identified. Based on both physical positions of the commonly polymorphic SNP loci on 1BL, a total of 42 SNP markers were selected from the wheat 660K SNP array in the 669,649,666 ~

10.3389/fpls.2024.1395223

671,505,587 bp region, from which 21 KASP markers were successfully developed. After confirming the polymorphisms between the parental lines (Svevo and Zavitan), thirteen KASP markers (*A009289*, *A009276*, *A009272*, *A007975*, *A007979*, *A009270*, *A009271*, *A007972*, *A009275*, *A012891*, *A012893*, *A012894*, and *A012896*) successfully distinguished Svevo and Zavitan (Table 1). A total of 47 wheat DNA samples, including the 2 parents and 23 resistant and 22 susceptible RILs from the Svevo/Zavitan cross, were selected to verify these markers, which were then tested on 137 RILs from the Svevo/Zavitan cross. The sequences of the 13 KASP markers are shown in Table 1. The SNP sequences associated with *QYrsv.swust-1BL* identified from the wheat 660K SNP array are shown in Table 2, which were used to design the KASP primer sequence. When these 13 KASP markers were used to genotype MM 37, Svevo, five markers—*A009289*, *A012891*, *A012893*, *A012894*, and *A012896*—were polymorphic between the parents (MM 37, Svevo) and among the tested F_2 plants from their cross. Indicating that the markers *A009289*, *A012891*, *A012893*, *A012894*, and *A012896* are useful in marker-assisted selection for introducing the resistance gene into common wheat.

Multi-environment analysis of *QYrsv.swust-1BL* stripe rust resistance loci

QTL for stripe rust resistance was scanned through all 13 KASP markers by the inclusive composite interval mapping (ICIM) method implemented in Ici-Mapping V4.2 software. *QYrsv.swust-1BL* was discovered using the BIP and MET methods (LOD > 2.5, P < 0.01). *QYrsv.swust-1BL* was significant for both IT and DS, with the highest peak in a 0.72 cM region. Figure 1 represents a summary of the analysis effects of *QYrsv.swust-1BL* using the BIP and MET models for IT and DS in multiple seasons from 2016–2020. On the BIP analysis, it has a PVE (percent of explained variation) of 10.43–24.12% in IT and a PVE of 9.32–27.34% in DS across 2016–2020 environments (Table 3). In the MET analysis, it has a high LOD score of 35.38 and a PVE of 11.68% in IT between markers *A007972* and *A007975*. Additionally, it has a high LOD score of 43.53 and a PVE of 24.20% in DS between markers *A009289* and *A009276* (Table 4).

Identification of recombination events

These 13 markers were used to genotype the 137 RILs, from which 4 RILs were found to have only one recombination event proximal to markers *A009289*, *A009276*, *A007972*, and *A007975*, respectively. Two markers (*A009289* and *A007975*) were most closely linked to the target gene on two sides and flanked the 1,065,719 bp region between the 660,683,255 bp and 661,748,974 bp positions on the durum wheat Svevo RefSeq Rel. 1.0 (Table 2) and the 568,518 bp region between the 669,955,772 and 670,524,290 bp positions in Chinese Spring IWGSC RefSeq v1.0 (Table 3) on chromosome 1BL. It is clear that *QYrsv.swust-1BL* overlaps with

TABLE 1 Marker name and primer sequences of polymorphic KASP markers developed from SNP markers in the genome region between the 669,955,772 and 672,333,864 bp positions on chromosome 1BL of the Chinese Spring reference genome (IWGSC Ref Seq v1.0).

Marker name	Primer sequences
A009289	Allele1 (Fam): GAAGGTGACCAAGTTCATGCTGAGCGGGAAGA GAGCAAGGGT
	Allele2 (Vic): GAAGGTCGGAGTCAACGGATTAGCGGG AAGAGAGCAAGGGG
	Com: CTTGTCCAACAGGCCCGCCAT
A009276	Allele1 (Fam): GAAGGTGACCAAGTTCATGCTCCAAAGCTG AGGGTGTCGTT
	Allele2 (Vic): GAAGGTCGGAGTCAACGGATTCCA AAGCTGAGGGTGTCGTC
	Com: AGAAGAACAAAGGCGTGATGGCGTA
A009275	Allele1 (Fam): GAAGGTGACCAAGTTCATGCTGCA AATCAATATAGCATGTTAAACAAAAAACA
	Allele2 (Vic): GAAGGTCGGAGTCAACGGATTCAAA TCAATATAGCATGTTAAACAAAAAACC
	Com: GGCTATTTCTGGTTTGGCACAGGTT
A009272	Allele1 (Fam): GAAGGTGACCAAGTT CATGCTGTCGTCTCTCCAGCACACCG
	Allele2 (Vic): GAAGGTCGGAGTCAACGGATT GGTCGTCTCTCCAGCACACCA
	Com: AAGTGGAGATCATATGCTTCCATCTGAAA
A009271	Allele1 (Fam): GAAGGTGACCAAGTTCATGCTAGAGAT CAAAACATACACGCAACGAAAA
	Allele2 (Vic): GAAGGTCGGAGTCAACGGATTAGAGATCAAAA CATACACGCAACGAAAT
	Com: CATCCATCGCTGTATCTATATATCGTGTT
A009270	Allele1 (Fam): GAAGGTGACCAAGTTCATGCTCAATGAAATTC TCGATTTTTTAGCCGTT
	Allele2 (Vic): GAAGGTCGGAGTCAACGGATTAATGAAA TTCTCGATTTTTTAGCCGTC
	Com: TAATGCACCGCAGCCATTCGACTTA
A007972	Allele1 (Fam): GAAGGTGACCAAGTTCATGCTTA AAGCCCACAACAGGCAGCG
	Allele2 (Vic): GAAGGTCGGAGTCAACGGATTAATA AAGCCCACAACAGGCAGCA

(Continued)

10.3389/fpls.2024.1395223

TABLE 1 Continued

Marker name	Primer sequences
	Com: GTGTTCGTTGTCTTGTAAGACTCTAAGTT
A007975	Allele1 (Fam): GAAGGTGACCAAGTTCATGCTCGTGCT TTGCGTTCACCATATGA
	Allele2 (Vic): GAAGGTCGGAGTCAACGGATTCGTGCTT TGCGTTCACCATATGC
	Com: GCATGGCCAGGAAGAACTGTGAAAT
A007979	Allele1 (Fam): GAAGGTGACCAAGTTCATGCTAGA AATCATTGCGGTAGCCGA
	Allele2 (Vic): GAAGGTCGGAGTCAACGGATTCTAGAAA TCATTGCGGTAGCCGG
	Com: GCAGTACTCCTAGCGTAACTGGTTT
A012891	Allele1 (Fam): ATAACCTAAGCTGCAGCATAACAGTA
	Allele2 (Vic): ACCTAAGCTGCAGCATAACAGTC
	Com: CAGTAAGTACTACATGCTCTGCCCTT
A012893	Allele1 (Fam): CAGGCACATGCTTAGGGATTGAG
	Allele2 (Vic): CAGGCACATGCTTAGGGATTGAC
	Com: GAACAGCGCATTTCCAGAATTTCCTAATT
A012894	Allele1 (Fam): AAGAAGTTCAAGGCATGGGCAGATA
	Allele2 (Vic): GAAGTTCAAGGCATGGGCAGATG
	Com: CTACTTCGGGAAGTACTTGTCCCAA
A012896	Allele1 (Fam): GTACGTCCACTCGCTCAAGGA
	Allele2 (Vic): GTACGTCCACTCGCTCAAGGT
	Com: CGTTATCTTTGGTGACCGCAGGATA

QYr.ucw-1BL/Yr29. Although the physical mapping region surpasses that of *QYr.ucw-1BL/Yr29* (669.902 ~ 670.234 Mp), it is noteworthy that only three candidate genes have been identified within the Chinese spring reference genome (Figure 2).

Candidates for *QYrsv.swust-1BL*

Based on the analysis of BIP and MET, as well as the examination of recombination events in RILs, *QYrsv.swust-1BL* was delimited by the linked markers *A009289* and *A007975* (0.72 cM) (Figure 2). The genetic distance between the two flanking markers in this candidate region was found to be conservative in the durum wheat Svevo genome and 1,065,719 bp in the Svevo RefSeq Rel. 1.0 (Figure 2). The 1.066 Mb region was found to contain 25 annotated genes (Figure 2; Table 5). These 25 high-confidence genes in Svevo were found to be related to disease resistance. The protein encoded by five of these genes (*TRITD1Bv1G220450*, *TRITD1Bv1G220460*, *TRITD1Bv1G220520*, *TRITD1Bv1G220540*, and *TRITD1Bv1G220550*) belongs to the disease resistance protein receptor-like protein kinase, which is involved in pathogen recognition and plays an important role in effector-induced protein status monitoring (Mchale et al., 2006). Four of these genes are S-type anion channels (*TRITD1Bv1G220620*, *TRITD1Bv1G220780*, *TRITD1Bv1G220800*, and *TRITD1Bv1G220810*). Two of these genes are glucan endo-1,3-beta-glucosidase (*TRITD1Bv1G220480* and *TRITD1Bv1G220530*). The other fourteen genes are: Acid beta-fructofuranosi-dase (*TRITD1Bv1G220430*), Sugar transporter (*TRITD1Bv1G220570*), WRKY family transcription factor (*TRITD1Bv1G220590*), Band 7 stomatin family protein (*TRITD1Bv1G220630*), FAD-binding Berberine family protein (*TRITD1Bv1G220650*), Calcium-dependent protein kinase (*TRITD1Bv1G220680*), Protein ABIL1 (*TRITD1Bv1G220690*), Divalention symporter (*TRITD1Bv1G220790*), Late embryogenesis abundant protein Lea14 (*TRITD1Bv1G220830*), F-box family protein (*TRITD1Bv1G220840*), Late embryogenesis

TABLE 2 Primer sequences were designed for the KASP markers derived from single nucleotide polymorphisms (SNPs) associated with *QYrsv.swust-1BL*, identified from the wheat 660K SNP array.

KASP ID	SNP ID	SNP physical position	SNP sequence
A009289	AX-111546688	669,955,772	GTGTTCGTTGTCTTGTAAGACTCTAAGTTTGTGTA[**G**[a]/T]GCTGCCTGTTGTGGGCTTTATTCAGTTAAAGCCGG
A009276	AX-94509279	670,180,628	ATCACTGTGGCCTCGTGCTTTGCGTTCACCATATG[**A**/C]ATTTCACAGTTCTTCCTGGCCATGCTATGCCAGAT
A009275	AX-109363092	670,373,377	TAGAATAATGCACCGCAGCCATTCGACTTAGATCC[A/**C**]ACGGCTAAAAAATCGAGAATTTCATTGTGTTTTTC
A009272	AX-109440891	670,379,326	TACTAGCAAGAGATCAAAACATACACGCAACGAAA[C/**T**]TATTAAAACAAACAAACACGATATATAGATACAGC
A009271	AX-109389405	670,382,321	AGTGGAGATCATATGCTTCCATCTGAAAAATAATA[A/**T**]GGTGTGCTGGAGAGACGACCTACAAACATGTAAAG
A009270	AX-110421026	670,475,930	AAAAGCAAATCAATATAGCATGTTAAACAAAAAAC[A/**G**]AACCTGTGCCAAACCAGAAATAGCCAAATTGGGCT

(Continued)

10.3389/fpls.2024.1395223

TABLE 2 Continued

KASP ID	SNP ID	SNP physical position	SNP sequence
A007979	AX-108800083	670,502,837	ATAACCAGAAGAACAAAGGCGTGATGGCGTACACT[**T**/C]ACGACACCCTCAGCTTTGGAGATGGGCGGAACCTC
A007975	AX-109391895	670,524,290	ACCTGCAGTACTCCTAGCGTAACTGGTTTAGCTTT[C/**A**]CGGCTACCGCAATGATTTCTAGCGTTCCATTGTGT
A007972	IWB5732 (90K)	670,783,618	ACCCCTTGGCCTTGTCCAACAGGCCCGCCATGGCCG[**T**/C]CCCTTGCTCTCTTCCCGCTCCTTCCCGCCTCTGAT
A012891	AX-86162829	671,740,550	ACTTCTGTGGTTATAGATAGCTAAATCTATATTGT[**G**/T]ACTGTTATGCTGCAGCTTAGGTTATGATCTGTTGT
A012893	AX-111736421	671,741,903	CCTAATTTCATTGTTTGTGAACAGTGTCTTCCCCA[C/**G**]TCAATCCCTAAGCATGTGCCTGCGCCGGGAAACCT
A012894	AX-94436701	671,742,114	AATCTTTGGCTGAGAAGTTCAAGGCATGGGCAGAT[A/**G**]ACACCTCCAGGGGGTTTACCTTCTATTCGATCGGG
A012896	AX-94735704	672,333,864	CGTCGACCGCATCGCGTACGTCCACTCGCTCAAGG[A/**T**]GAAGCCCATCCGCATCCCCAACTATCCTGCGGTCA

[a]Bold indicate the nucleotide in the resistant parent Svevo.

abundant hydroxyproline-rich glycoprotein family (*TRITD1Bv1G220860*), Thrombospondin type-1-domain-containing protein (*TRITD1Bv1G220890*), RING/FYVE/PHD zinc finger superfamily protein (*TRITD1Bv1G220900*), and the other is an unannotated gene (*TRITD1Bv1G220490*) (Table 5). There are a total of 13 candidate genes in the 568,518 bp region between positions 669,955,772 and 670,524,290 bp of the Chinese Spring IWGSC RefSeq v1.0 (Table 5) on chromosome 1BL. Five of the receptor-like protein kinases (*TraesCS1B02G454000*, *TraesCS1B02G454100*, *TraesCS1B02G454400*, *TraesCS1B02G454600*, and *TraesCS1B02G454700*), two of the glucan endo-1,3-beta-glucosidase (*TraesCS1B02G454200* and *TraesCS1B02G454500*), one of the sugar transporter (*TraesCS1B02G454800*), one of the WRKY family transcription factor (*TraesCS1B02G455000*), and one of the S-type anion channel (*TraesCS1B02G455100*) are

TABLE 3 Summary of stripe rust resistance gene *QYrsv.swust-1BL* identified using the biparental population model (BIP) based on mean disease severity (DS) and infection type (IT) of the Svevo/Zavitan recombinant inbred line (RIL) population tested in China and Israel from 2016 to 2020[a].

QTL, environment[b]	Marker	IT			DS		
		LOD	PVE	Add	LOD	PVE	Add
BD16	*A009276-A007972*	5.52	16.85	-0.82	7.02	20.91	-13.21
BK16	*A009276-A007972*	7.00	21.82	-1.01	4.75	14.92	-12.08
YL16	*A009289-A009276*	5.26	16.58	-1.09	/	/	/
QH16	*A012894-A012896* *A009276-A007972*	3.46	12.39	-0.74	3.57	12.95	-6.98
BD17	*A007972-A007975* *A009289-A009276*	7.88	24.12	-0.84	8.86	26.17	-16.93
BK17	*A007972-A007975*	3.39	10.97	-0.45	2.85	9.32	-5.99
MY17	*A009289-A009276*	5.60	17.55	-1.11	9.32	27.34	-17.39
YL17	*A009289-A009276*	5.56	17.42	-1.13	9.12	26.84	-17.85
BD18	*A007972-A007975*	3.24	10.43	-0.49	4.41	14.28	-7.50
BK18	*A009276-A007972*	4.11	13.18	-0.48	/	/	/
MY18	*A009276-A007972*	4.31	14.90	-0.81	4.91	16.97	-8.30
MY19	*A009289-A009276*	5.56	17.42	-1.13	9.12	26.84	-17.85
MY20	*A009276-A007972* *A009289-A009276*	4.11	13.18	-0.47	4.40	14.27	-7.49

[a]Marker, marker interval; LOD, logarithm of odds score; PVE, percentage of the phenotypic variance explained by individual QTL; Add, additive effect of resistance allele.[b]The Svevo/Zavitan RILs and their parents were evaluated for *QYrsv.swust-1BL* resistance to stripe rust in China fields in Yangling of Shaanxi Province in 2016 and 2017 (YL16 and YL17), Huzhu County, Qinghai Province in 2016 (QH16), and Mianyang, Sichuan Province in 2017, 2018, 2019, and 2020 (MY17, MY18, MY19, and MY20); and also in Israel fields in Bet Dagan (BD16, BD17, and BD18) and Barkai (BK16, BK17, and BK18) from 2016 to 2018.

10.3389/fpls.2024.1395223

TABLE 4 Summary of stripe rust resistance gene *QYrsv.swust-1BL* identified using the multi-environmental trials (MET) model based on the mean infection type (IT) and disease severity (DS) of the Svevo/Zavitan recombinant inbred line (RIL) population tested in China and Israel from 2016 to 2020[a].

QTL	Pos (cM)	Left Marker	Right Marker	IT							DS					
				LOD	LOD (A)	LOD (AbyE)	PVE	PVE (A)	PVE (AbyE)	Add	LOD	LOD (A)	LOD (AbyE)	PVE	PVE (A)	PVE (AbyE)	Add
QYrsv.swust-1BL	0.0	*A009289*	*A009276*	26.57	19.09	7.48	20.05	8.77	11.28	-0.43	43.53	30.46	13.06	24.20	11.69	12.51	-6.98
	0.7	*A007972*	*A007975*	35.38	14.40	20.98	11.68	6.54	5.15	-0.36	31.97	16.03	15.95	10.75	6.10	4.65	-5.00

[a]Pos = the scanning position in cM on the chromosome. LOD = likelihood of odds score for all effects. LOD (A) = LOD score for additive and dominance effects. LOD (AbyE) = LOD score for additive and dominance by environment effects. PVE = phenotypic variation explained by all effects at the current scanning position. PVE (A) = phenotypic variation explained by the additive and dominance effects at the current scanning position. PVE (AbyE) = phenotypic variation explained by additive and dominance by environment effects at the current scanning position, and Add = average additive effect at the current scanning position.

candidate genes that share common genes with the Svevo genome. The other three different genes are: protein kinase (*TraesCS1B02G454900*), ATP-dependent zinc metalloprotease FtsH (*TraesCS1B02G455200*), and carboxypeptidase (*TraesCS1B02G455300*). These four classes of genes are shared between the Chinese spring genome and the Svevo genome and will be used to verify candidate genes for *QYrsv.swust-1BL* in the future. A collinearity analysis of these genes was performed using the Zavitan (*WEWSeq v1.0*), *Triticum spelta* (*spelta PI190962 v1.0*), and other 5 *Triticum aestivum* genomes (http://wheat.cau.edu.cn/TGT/) data (Figure 3). The results of collinearity analysis indicate that there have been multiple chromosomal structural variations in this region. An intrachromosomal translocation exists within the range of approximately 673.1 MB to 673.8 MB, while there is a paracentric inversion within the range of 673.8 MB to 674.1 MB. Through candidate gene functional annotation. Most of the candidate genes in the Svevo reference genome have high match scores, which refer to high confidence.

QYrsv.swust-1BL KASP marker validation

To assess the applicability of the newly developed KASP marker in breeding programs, an F_2 breeding population derived from a cross between the Chinese hexaploid wheat variety Mianmai 37 and the durum wheat variety Svevo was utilized. The developed KASP markers *A009289*, *A012891*, *A012893*, *A012894*, and *A012896* effectively distinguished genotypes within the F_2 breeding population into three distinct clusters (Figure 4). The allele cluster nucleotide of homozygote associated with resistance for KASP markers *A009289*, *A012891*, *A012893*, *A012894*, and *A012896* were identified as 'G', 'G', 'G', 'G', 'T', respectively, while the alternative allele had a nucleotide cluster of 'T', 'T', 'C', 'A', 'A', respectively (Table 2; Figure 4). F_2 plants and corresponds to 318 $F_{2:3}$ lines, which were phenotyped for stripe rust response. Among homozygous alleles associated with resistance for marker *A009289*, F_2 plants carrying positive alleles from *QYrsv.swust-1BL* exhibited a reduction in IT and DS by 34.14% and 45.24% compared with those of the alternative allele 'T', respectively. Progenies of $F_{2:3}$ carrying positive alleles from *QYrsv.swust-1BL* exhibited a reduction in IT and DS by 54.29% and 41.63% compared with those of the alternative allele 'T', respectively. Progenies with heterozygous genotypes for marker *A009289* also demonstrated a decrease in IT and DS by 47.27 and 57.71 in F_2 plants and 53.80% and 46.92% in $F_{2:3}$ lines compared with those of the alternative allele 'T', respectively. Conversely, progenies carrying alternative alleles from Mianmai 37 showed an increase in IT and DS. The phenotypes of F_2 plants and $F_{2:3}$ families carrying positive alleles and heterozygous genotypes with *A012891*, *A012893*, and *A012894* markers were significantly different from those carrying alternative alleles, with a difference of 0.005 level, similar to the results of *the A009289* marker. The results of marker *A012896* in F_2 generation were not significant in IT and DS, while the IT differences in $F_{2:3}$ generation were significant at the levels of 0.05 and 0.01. These findings highlight the effective utilization of KASP markers *A009289*, *A012891*, *A012893*, *A012894*, and *A012896* for marker-assisted selection in breeding programs, confirming that

10.3389/fpls.2024.1395223

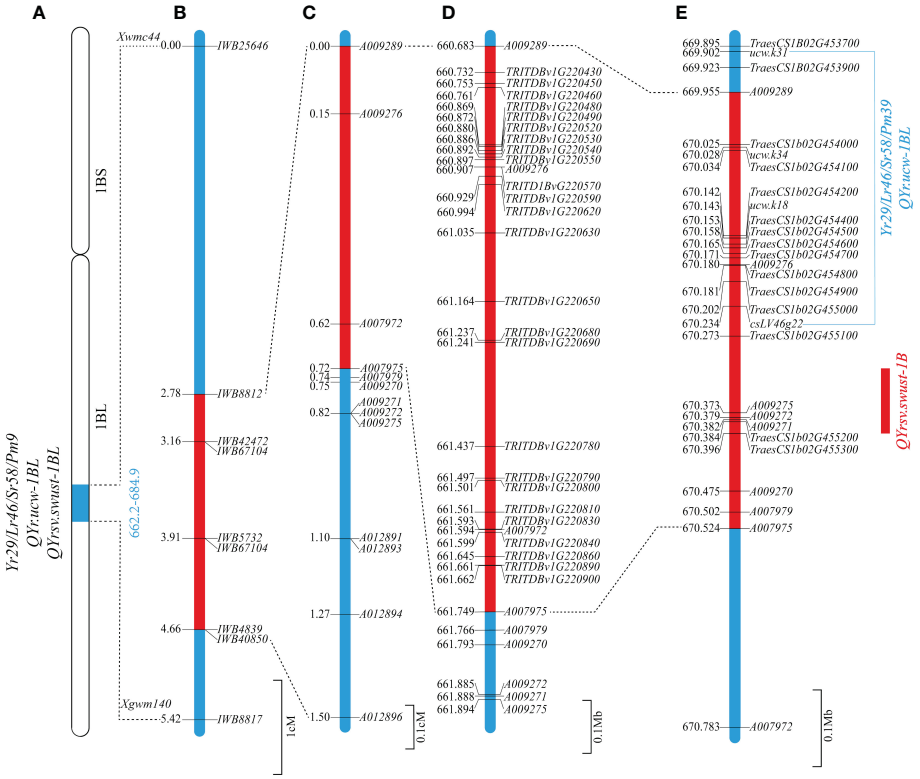

FIGURE 2
Genetic and comparative genomic linkage map of the stripe rust resistance QTL *QYrsv.swust-1BL*. **(A)** Stripe rust resistance gene/QTL: *Yr29/Lr46/Sr58/Pm38*, *QYr.ucw-1BL*, and *QYrsv.swust-1BL* share the same distal region in chromosome 1BL. **(B)** Genetic map constructed using a 90K SNP chip showing *QYrsv.swust-1BL* (red) within different flanked markers in comparison with *Yr29/Lr46/Sr58/Pm38* and *QYr.ucw-1BL* (blue). **(C)** A fine map of *QYrsv.swust-1BL* was constructed using newly developed KASP markers. **(D)** The Svevo genome region from the 660.372 Mb to 663.335 Mb position on chromosome 1B. **(E)** The Chinese Spring (RefSeq V1.0) genome region from the 669.956 Mb to 672.334 Mb position on chromosome 1B.

TABLE 5 The putative genes identified in the genomic regions of the durum wheat Svevo genome (Ref Seq Rel. 1.0.) and the Chinese Spring genome (IWGSC v1.0) covering *QYrsv.swust-1BL*.

Svevo Reference genome			Chinese Spring Reference genome		
Gene ID	Physical positions(bp)	Predicted gene function	Gene ID	Physical positions(bp)	Predicted gene function
TRITD1Bv1G220430	660,732,388	Acid beta-fructofuranosi-dase	*TraesCS1B02G454000*	670,025,361	Receptor-like protein kinase, putative, expressed
TRITD1Bv1G220450	660,752,810	Receptor-like protein kinase, putative, expressed	*TraesCS1B02G454100*	670,034,244	Receptor-like protein kinase, putative, expressed
TRITD1Bv1G220460	660,761,348	Receptor-like protein kinase, putative, expressed	*TraesCS1B02G454200*	670,142,373	Glucan endo-1,3-beta-glucosidase 3
TRITD1Bv1G220480	660,869,208	Glucan endo-1,3-beta-glucosidase 3	*TraesCS1B02G454400*	670,152,914	Receptor-like protein kinase, putative, expressed
TRITD1Bv1G220490	660,872,060	/	*TraesCS1B02G454500*	670,158,857	Glucan endo-1,3-beta-glucosidase 3
TRITD1Bv1G220520	660,879,885	Receptor-like kinase	*TraesCS1B02G454600*	670,164,776	Receptor-like protein kinase, putative, expressed
TRITD1Bv1G220530	660,885,534	Glucan endo-1,3-beta-glucosidase 3	*TraesCS1B02G454700*	670,170,577	Receptor-like protein kinase, putative, expressed

(Continued)

10.3389/fpls.2024.1395223

TABLE 5 Continued

Svevo Reference genome			Chinese Spring Reference genome		
Gene ID	Physical positions(bp)	Predicted gene function	Gene ID	Physical positions(bp)	Predicted gene function
TRITD1Bv1G220540	660,891,619	Receptor-like protein kinase, putative, expressed	*TraesCS1B02G454800*	670,180,417	Sugar transporter, putative
TRITD1Bv1G220550	660,897084	Receptor-like protein kinase, putative, expressed	*TraesCS1B02G454900*	670,181,368	Protein kinase
TRITD1Bv1G220570	660,906,924	Sugar transporter, putative	*TraesCS1B02G455000*	670,202,180	WRKY family transcription factor
TRITD1Bv1G220590	660,928,657	WRKY family transcription factor	*TraesCS1B02G455100*	670,272,504	S-type anion channel
TRITD1Bv1G220620	660,993,770	S-type anion channel	*TraesCS1B02G455200*	670,384,229	ATP-dependent zinc metalloprotease FtsH 1
TRITD1Bv1G220630	661,035,030	Band 7 stomatin family protein	*TraesCS1B02G455300*	670,395,913	Carboxypeptidase
TRITD1Bv1G220650	661,164,343	FAD-binding Berberine family protein			
TRITD1Bv1G220680	661,236,813	Calcium-dependent protein kinase			
TRITD1Bv1G220690	661,240,728	Protein ABIL1			
TRITD1Bv1G220780	661,436,635	S-type anion channel			
TRITD1Bv1G220790	661,497,106	Divalention symporter			
TRITD1Bv1G220800	661,501,096	S-type anion channel			
TRITD1Bv1G220810	661,560,685	S-type anion channel			
TRITD1Bv1G220830	661,593,365	Late embryogenesis abundant protein Lea14			
TRITD1Bv1G220840	661,598,766	F-box family protein			
TRITD1Bv1G220860	661,645,362	Late embryogenesis abundant hydroxyproline-rich glycoprotein family, putative			
TRITD1Bv1G220890	661,660,533	Thrombospondin type-1-domain-containing protein 7B			
TRITD1Bv1G220900	661,662,345	RING/FYVE/PHD zinc finger superfamily protein TE			

QYrsv.swust-1BL is indeed a significant and stable major gene locus controlling resistance to stripe rust disease.

Discussion

Conventional phenotypic screening approaches have been used to develop cultivars with long-lasting disease resistance, but the breeding process takes many years. Molecular markers associated with rust resistance can be used to speed up the process and stack different resistance genes into a single cultivar. In a previous study, a QTL, *QYrsv.swust-1BL*, for APR to stripe rust was identified and mapped in chromosome 1BL in durum wheat Svevo (Zhou et al., 2021). By comparing the genetic and physical positions of linked molecular markers, *QYrsv.swust-1BL* was found to be in the same position as *Yr29* on chromosome 1BL.

In the present study, we used the high-density wheat 660K SNP array to find more SNP markers in the *QYrsv.swust-1BL* region and successfully converted the SNP markers into KASP markers. By re-mapping *QYrsv.swust-1BL* using the same Svevo/Zavitan RIL population as used in the previous study (Zhou et al., 2021), we added 13 KASP markers to the target region with a much higher resolution. These KASP markers were validated using an F_2 population of 318 plants from a cross of Svevo with the common elite wheat cultivar MM 37. The genetic distance of the *QYrsv.swust-1BL* interval was reduced to 0.72 cM (Figure 2).

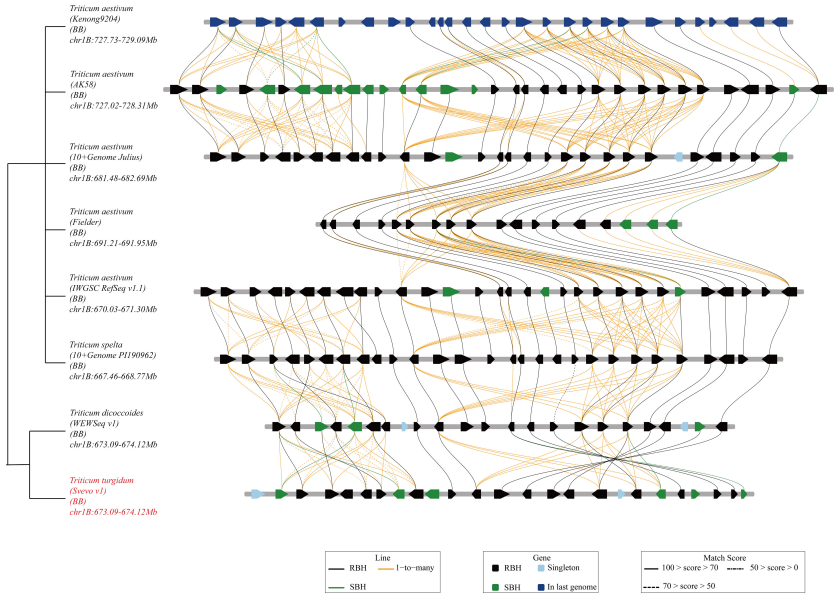

FIGURE 3
Collinearity analysis of predicted genes in *QYrsv.swust-1BL*.

Finally, we mapped this stripe rust resistance locus within a 1.066 Mb region of chromosome 1BL in durum wheat Svevo RefSeq Rel. 1.0, which overlaps with the previously reported genes, *Yr29/Lr46/Sr58/Pm39*, for resistance to stripe rust (yellow rust), leaf rust, stem rust, and powdery mildew, respectively (William et al., 2003; Lillemo et al., 2008; Singh et al., 2013). The genomic region between markers *A009289* and *A007975* in the Chinese Spring reference genome was found to be 0.569 Mb, comparable to the size of the region in the durum wheat genome.

Based on the results of high-resolution mapping using a large population, exome capture, and allelism analysis of a cross between common wheat RIL55 (with the Klein Chajá allele of *QYr.ucw-1BL*) and Lalbahadur (with the Pavon-1B allele of *Yr29*), Cobo et al. (2019) reported that *QYr.ucw-1BL* and *Yr29* represent the same gene. According to the comparative maps and annotated genes, we hypothesized that *QYrsv.swust-1BL* should be the same as *QYr.ucw-1BL/Yr29*. The genomic interval between KASP markers A009289 and A007975 in the Chinese Spring genome (IWGSC v1.0) spans a smaller region of 0.569 Mb and shares four complete classes of genes. However, the 1.066 Mb region between KASP markers *A009289* (at the 660,683,255 bp position) and *A007975* (at the 661,748,974 bp position) contains 25 high-confidence genes annotated in the Svevo reference genome, including the *QYr.ucw-1BL* region (Cobo et al., 2018, 2019). These 25 and 13 genes in Svevo RefSeq Rel. 1.0 and Chinese Spring IWGSC RefSeq v1.0 are listed in Table 5, respectively. Ten annotated genes were reported in the *QYr.ucw-1BL* region between markers *ucw.k31* and *csLV46G22* (Cobo et al., 2019). As *QYrsv.swust-1BL* and *QYr.ucw-1BL/Yr29* were mapped to the same regions of the Chinese Spring genome, we found four classes of identical genes in these genomic regions. Thus, *QYrsv.swust-1BL* and *QYr.ucw-1BL/Yr29* are likely the same gene. More conclusive evidence for these two QTL as the same gene needs future studies of direct comparison of both QTL in common wheat backgrounds through allelism testing, gene cloning, and expression. The $F_{2:3}$ lines or later generation lines with 42 chromosomes from the MM 37/Svevo cross can be used together with the *QYrsv.swust-1BL/QYr.ucw-1BL/Yr29* near-isogenic lines in the Avocet S background for such experiments.

In the present study, we showed that the common wheat Chinese Spring and durum wheat Svevo genome sequences can be used to hasten high-resolution mapping of traits of interest in wheat. We encountered difficulties, such as sterile plants caused by aneuploids from the common wheat and durum wheat crosses, when attempting to clone *QYrsv.swust-1BL* because of the ploid differences between the parental lines and the reference genomes. Therefore, regions like *QYrsv.swust-1BL* from durum wheat in this study should be assembled using the donor genome to enable the cloning of causal genes and to develop diagnostic markers that can be used in breeding programs.

For breeding wheat cultivars with stripe rust resistance, *QYrsv.swust-1BL* can be used together with other effective resistance genes. The progeny lines with 42 chromosomes and *QYrsv.swust-1BL* derived from cross MM 37/Svevo should be more efficient than the original donor of durum wheat for incorporating the APR QTL into other common wheat backgrounds. The KASP markers tightly linked to *QYrsv.swust-1BL* can be used in marker-assisted selection for speeding up its incorporation and pyramiding with other effective genes for developing wheat cultivars with high-level, durable resistance to stripe rust.

Conclusion

In this study, using high-density 660K SNP array genotyping, we fine-mapped the *QYrsv.swust-1BL* APR locus as a starting point to develop a diagnostic marker for use in breeding and to clone this gene. We mapped *QYrsv.swust-1BL* to within a 1.066 Mb region in

10.3389/fpls.2024.1395223

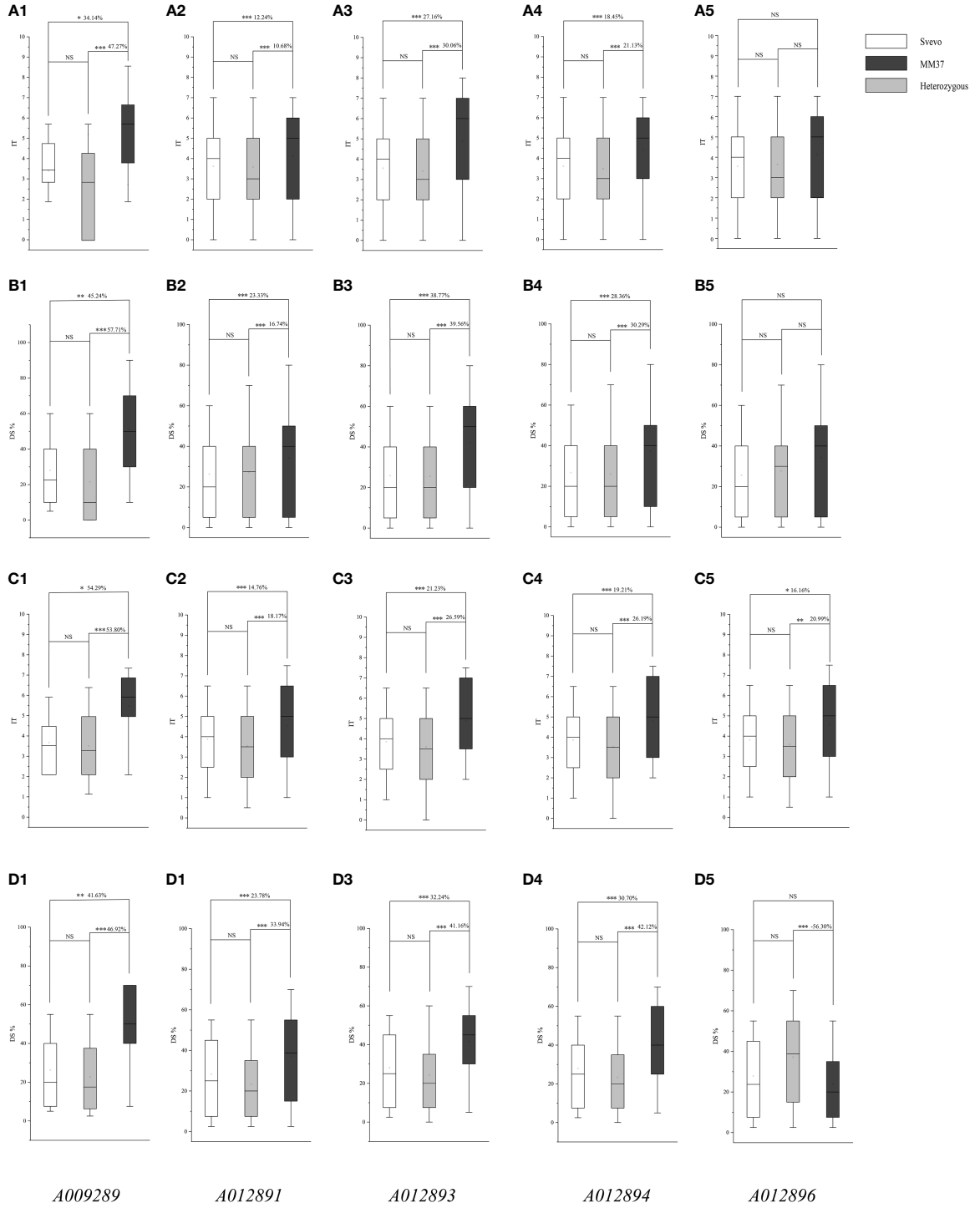

FIGURE 4
Effects of *QYrsv.swust-1BL* in the F_2 and $F_{2:3}$ validation populations. The lines with *QYrsv.swust-1BL* had lower IT and DS than the lines carrying the allele gene of MM37, and the difference between Svevo and heterozygous is not significant. **(A1-A5, B1-B5)** are based on the IT and DS data of the F2 population, and **(C1-C5, D1-D5)** are based on the IT and DS data of the $F_{2:3}$ lines. Numbers 1-5 refer to the validation by five KASP markers *A009289, A012891, A012893, A012894* and *A012896*. * Significance level at P < 0.05; ** Significance level at P <0.01; *** Significance level at P < 0.005. "ns" refers to the none significance.

Triticum turgidum durum wheat Svevo (RefSeq Rel. 1.0) on the chromosome arm 1BL, which overlaps with a previously described map of *QYr.ucw-1BL*/*Yr29*, a *Pst* resistance gene. The four gene families within the identified 1.066 Mb region, identical to the Chinese spring reference genome, have been implicated in disease resistance. SNP markers were then used to select high-throughput KASP markers that could be used in wheat breeding programs to hasten the deployment of these *Pst* resistance loci.

Data availability statement

The original contributions presented in the study are included in the article/supplementary material. Further inquiries can be directed to the corresponding authors.

Author contributions

XZ: Writing – review & editing, Writing – original draft, Visualization, Investigation, Formal analysis, Data curation. GJ: Writing – review & editing, Writing – original draft, Visualization, Investigation, Formal analysis, Data curation. YL: Writing – review & editing. XL: Writing – review & editing, Supervision. LC: Writing – review & editing, Visualization, Supervision, Data curation. XC: Writing – review & editing, Visualization, Supervision, Investigation, Data curation. ZK: Writing – review & editing, Visualization, Supervision.

Funding

The author(s) declare financial support was received for the research, authorship, and/or publication of this article. This study was financially supported by the International S&T Cooperation Program of China (2015DFG32340) and was partially funded by the Key Research and Development Program of International Science and Technology Innovation Cooperation of Science and Technology Department of Sichuan Province, China (No. 22YFH0032), the National Natural Science Foundation of China (32101707), the Longshan Academic Talent Research Support Program of SWUST (No. 17LZX5), and the PhD Foundation of Southwest University of Science and Technology (No. 16zx7162).

Conflict of interest

The authors declare that the research was conducted in the absence of any commercial or financial relationships that could be construed as a potential conflict of interest.

Publisher's note

All claims expressed in this article are solely those of the authors and do not necessarily represent those of their affiliated organizations, or those of the publisher, the editors and the reviewers. Any product that may be evaluated in this article, or claim that may be made by its manufacturer, is not guaranteed or endorsed by the publisher.

References

Anderson, J. A., Churchill, G. A., Autrique, J. E., Tanksley, S. D., and Sorrells, M. E. (1993). Optimizing parental selection for genetic-linkage maps. *Genome* 36, 181–186. doi: 10.1139/g93-024

Avni, R., Nave, M., Eilam, T., Sela, H., Alekperov, C., Peleg, Z., et al. (2014). Ultra-dense genetic map of durum wheat × wild emmer wheat developed using the 90K iSelect SNP genotyping assay. *Mol. Breed.* 34, 1549–1562. doi: 10.1007/s11032-014-0176-2

Bansal, U. K., Kazi, A. G., Singh, B., Hare, R. A., and Basiana, H. S. (2014). Mapping of durable stripe rust resistance in a durum wheat cultivar Wollaroi. *Mol. Breed.* 33, 51–59. doi: 10.1007/s11032-013-9933-x

Beddow, J. M., Pardey, P. G., Chai, Y., Hurley, T. M., Kriticos, D. J., Braun, H. J., et al. (2015). Research investment implications of shifts in the global geography of wheat stripe rust. *Nat. Plants* 1, 1–5. doi: 10.1038/nplants.2015.132

Chen, X. M. (2005). Epidemiology and control of stripe rust (*Puccinia striiformis* f. sp. *tritici*) on wheat. *Can. J. Plant Pathol.* 27, 314–337. doi: 10.1080/07060660509507230

Chen, X. M., Coram, T., Huang, X. L., Wang, M. N., and Dolezal, A. (2013). Understanding molecular mechanisms of durable and non-durable resistance to stripe rust in wheat using a transcriptomics approach. *Cur. Genomics* 14, 111–126. doi: 10.2174/1389202911314020004

Chen, W. Q., Wellings, C., Chen, X. M., Kang, Z. S., and Liu, T. G. (2014). Wheat stripe (yellow) rust caused by *Puccinia striiformis* f. sp. *tritici*. *Mol. Plant Pathol.* 15, 433–446. doi: 10.1111/mpp.12116

Chen, J., Upadhyaya, N. M., Ortiz, D., Sperschneider, J., Li, F., Bouton, C., et al. (2017). Loss of AvrSr50 by somatic exchange in stem rust leads to virulence for *Sr50* resistance in wheat. *Science* 358, 1607–1610. doi: 10.1126/science.aao4810

Chen, S., Zhang, W., Bolus, S., Rouse, M. N., and Dubcovsky, J. (2018). Identification and characterization of wheat stem rust resistance gene *Sr21* effective against the Ug99 race group at high temperature. *PloS Genet.* 14, e1007287. doi: 10.1371/journal.pgen.1007287

Chen, X. M. (2020). Pathogens which threaten food security: *Puccinia striiformis*, the wheat stripe rust pathogen. *Food Secur.* 12, 239–251. doi: 10.1007/s12571-020-01016-z

Cobo, N., Pflüger, L., Chen, X. M., and Dubcovsky, J. (2018). Mapping QTL for resistance to new virulent races of wheat stripe rust from two argentinean wheat cultivars. *Crop Sci.* 58, 2470–2483. doi: 10.2135/cropsci2018.04.0286

Cobo, N., Wanjugi, H., Lagudah, E., and Dubcovsky, J. (2019). A high-resolution map of wheat *QYr.ucw-1BL*, an adult plant stripe rust resistance locus in the same chromosomal region as *Yr29*. *Plant Genome* 12, 180055. doi: 10.3835/plantgenome2018.08.0055

Feng, J. Y., Wang, M. N., See, D. R., Chao, S. M., Zheng, Y. L., and Chen, X. M. (2018). Characterization of novel gene *Yr79* and four additional QTL for all-stage and high-temperature adult-plant resistance to stripe rust in spring wheat PI 182103. *Phytopathology* 108, 737–747. doi: 10.1094/PHYTO-11-17-0375-R

Feng, J., Yao, F., Wang, M., See, D. R., and Chen, X. (2023). Molecular mapping of *Yr85* and comparison with other genes for resistance to stripe rust on wheat chromosome 1B. *Plant Dis.* 0, null. doi: 10.1094/PDIS-11-22-2600-RE

Fu, D., Uauy, C., Distelfeld, A., Blechl, A., Epstein, L., Chen, X. M., et al. (2009). A kinase-START gene confers temperature-dependent resistance to wheat stripe rust. *Science* 323, 1357–1360. doi: 10.1126/science.1166289

Gessese, M., Bariana, H., Wong, D., Hayden, M., and Bansal, U. (2019). Molecular mapping of stripe rust resistance gene *Yr81* in a common wheat landrace Aus27430. *Plant Dis.* 103, 1166–1171. doi: 10.1094/PDIS-06-18-1055-RE

Gou, J. Y., Li, K., Wu, K., Wang, X., Lin, H., Cantu, D., et al. (2015). Wheat stripe rust resistance protein WKS1 reduces the ability of the thylakoid-associated ascorbate peroxidase to detoxify reactive oxygen species. *Plant Cell* 27, 1755–1770. doi: 10.1105/tpc.114.134296

Herrera-Foessel, S. A., Singh, R. P., Huerta-Espino, J., Salazar, V. C., and Lagudah, E. S. (2011). "First report of slow rusting gene *Lr46* in durum wheat," in *Poster Abstracts of the Borlaug Global Rust Initiative Technical Workshop*. Ed. M. McIntosh (Saint Paul, Minnesota, USA), 191.

Herrera-Foessel, S. A., Singh, R. P., Lan, C. X., Huerta-Espino, J., Calvo-Salazar, V., Bansal, U. K., et al. (2015). *Yr60*, a gene conferring moderate resistance to stripe rust in wheat. *Plant Dis.* 99, 508–511. doi: 10.1094/PDIS-08-14-0796-RE

Klymiuk, V., Chawla, H. S., Wiebe, K., Ens, J., Fatiukha, A., Govta, L., et al. (2022). Discovery of stripe rust resistance with incomplete dominance in wild emmer wheatusing bulked segregant analysis sequencing. *Commun. Biol.* 5, 826. doi: 10.1038/s42003–022–03773–3

Kolmer, J. A. (2015). A QTL on chromosome 5BL in wheat enhances leaf rust resistance of *Lr46*. *Mol. Breed.* 35, 74–81. doi: 10.1007/s11032-015-0274-9

Krattinger, S. G., Lagudah, E. S., Spielmeyer, W., Singh, R. P., Huerta-Espino, J., McFadden, H., et al. (2009). A putative ABC transporter confers durable resistance to multiple fungal pathogens in wheat. *Science* 323, 1360–1363. doi: 10.1126/science.1166453

Li, J., Dundas, I., Dong, C., Li, G., Trethowan, R., Yang, Z., et al. (2020). Identification and characterization of a new stripe rust resistance gene *Yr83* on rye chromosome 6R in wheat. *Theor. Appl. Genet.* 133, 1095–1107. doi: 10.1007/s00122-020-03534-y

Lillemo, M., Asalf, B., Singh, R. P., Huerta-Espino, J., Chen, X. M., He, Z. H., et al. (2008). The adult plant rust resistance loci *Lr34/Yr18* and *Lr46/Yr29* are important determinants of partial resistance to powdery mildew in bread wheat line Saar. *Theor. Appl. Genet.* 116, 1155–1166. doi: 10.1007/s00122-008-0743-1

Lillemo, M., Joshi, A. K., Prasad, R., Chand, R., and Singh, R. P. (2013). QTL for spot blotch resistance in bread wheat line Saar co-locateto the biotrophic disease resistance loci *Lr34* and *Lr46*. *Theor. Appl. Genet.* 126, 711–719. doi: 10.1007/s00122-012-2012-6

Line, R. F., and Qayoum, A. (1992). *Virulence, aggressiveness, evolution and distribution of races of* Puccinia striiformis *(the cause of stripe rust of wheat) in North America 1968–1987* (Washington, DC: US Department of Agriculture).

Liu, L., Wang, M. N., Feng, J. Y., See, D. R., Chao, S. M., and Chen, X. M. (2018). Combination of all-stage and high-temperature adult-plant resistance QTL confers high level, durable resistance to stripe rust in winter wheat cultivar Madsen. *Theor. Appl. Genet.* 131, 1835–1849. doi: 10.1007/s00122-018-3116-4

Liu, L., Yuan, C. Y., Wang, M. N., See, D. R., Zemetra, R. S., and Chen, X. M. (2019). QTL analysis of durable stripe rust resistance in the North American winter wheat cultivar Skiles. *Theor. Appl. Genet.* 132, 1677–1691. doi: 10.1007/s00122-019-03307-2

Maccaferri, M., Harris, N. S., Twardziok, S. O., Pasam, R. K., Gundlach, H., Spannagl, M., et al. (2019). Durum wheat genome highlights past domestication signatures and future improvement targets. *Nat. Genet.* 51, 885–895. doi: 10.1038/s41588-019-0381-3

Marchal, C., Zhang, J., Zhang, P., Fenwick, P., Steuernagel, B., Adamski, N. M., et al. (2018). BED-domain containing immune receptors confer diverse resistance spectra to yellow rust. *Nat. Plants* 4, 662–668. doi: 10.1038/s41477-018-0236-4

Mchale, L., Tan, X., Koehl, P., and Michelmore, R. W. (2006). Plant NBS-LRR proteins: adaptable guards. *Genome Biol.* 7, 212. doi: 10.1186/gb-2006-7-4-212

Meng, L., Li, H. H., Zhang, L. Y., and Wang, J. K. (2015). QTL IciMapping: integrated software for genetic linkage map construction and quantitative trait locus mapping in biparental populations. *Crop J.* 3, 269–283. doi: 10.1016/j.cj.2015.01.001

Moore, J. W., Herrera-Foessel, S., Lan, C., Schnippenkoetter, W., Ayliffe, M., Huerta-Espino, J., et al. (2015). A recently evolved hexose transporter variant confers resistance to multiple pathogens in wheat. *Nat. Genet.* 47, 1494–1498. doi: 10.1038/ng.3439

Nsabiyera, V., Bariana, H. S., Qureshi, N., Wong, D., Hayden, M. J., and Bansal, U. K. (2018). Characterization and mapping of adult plant stripe rust resistance in wheat accession Aus27284. *Theor. Appl. Genet.* 131, 1–9. doi: 10.1007/s00122-018-3090-x

Pakeerathan, K., Bariana, H., Qureshi, N., Wong, D., Hayden, M., and Bansal, U. (2019). Identification of a new source of stripe rust resistance *Yr82* in wheat. *Theor. Appl. Genet.* 132, 3169–3176. doi: 10.1007/s00122-019-03416-y

Periyannan, S., Moore, J., Ayliffe, M., Bansal, U., Wang, X., Huang, L., et al. (2013). The gene *Sr33*, an ortholog of barley *Mla* genes, encodes resistance to wheat stem rust race Ug99. *Science* 341, 786–788. doi: 10.1126/science.1239028

Ponce-Molina, L. J., Huerta-Espino, J., Singh, R., Basnet, B. R., Lagudah, E. S., Aguilar-Rincón, V. H., et al. (2018). Characterization of adult plant resistance to leaf rust and stripe rust in Indian wheat cultivar 'New Pusa 876'. *Crop Sci.* 58, 630–638. doi: 10.2135/cropsci2017.06.0396

Ramirez-Gonzalez, R. H., Uauy, C., and Caccamo, M. (2015). PolyMarker: a fast polyploid primer design pipeline. *Bioinformatics* 31, 2038–2039. doi: 10.1093/bioinformatics/btv069

Ren, Y., Singh, R. P., Basnet, B. R., Lan, C. X., Huerta-Espino, J., Lagudah, E. S., et al. (2017). Identification and mapping of adult plant resistance loci to leaf rust and stripe rust in common wheat cultivar Kundan. *Plant Dis.* 101, 456–463. doi: 10.1094/PDIS-06-16-0890-RE

Rosewarne, G. M., Singh, R. P., Huerta-Espino, J., William, H. M., Bouchet, S., Cloutier, S., et al. (2006). Leaf tip necrosis, molecular markers and β1-proteasome subunits associated with the slow rusting resistance genes *Lr46/Yr29*. *Theor. Appl. Genet.* 112, 500–508. doi: 10.1007/s00122-005-0153-6

Salcedo, A., Rutter, W., Wang, S., Akhunova, A., Bolus, S., Chao, S., et al. (2017). Variation in the *AvrSr35* gene determines *Sr35* resistance against wheat stem rust race Ug99. *Science* 358, 1604–1606. doi: 10.1126/science.aao7294

Singh, R. P., Herrera-Foessel, S. A., Huerta-Espino, J., Lan, C. X., Basnet, B. R., Bhavani, S., et al. (2013). "Pleiotropic gene *Lr46/Yr29/Pm39/Ltn2* confers slow rusting, adult plant resistance to wheat stem rust fungus," in *Proceedings of the Borlaug Global Rust Initiative Technical Workshop, 19–22 Aug* (Indian Council of Agricultural Research, New Delhi), 17.1.

Singh, R. P., Huerta-Espino, J., Bhavani, S., Herrera-Foessel, S. A., Singh, D., Singh, P. K., et al. (2011). Race non-specific resistance to rust diseases in CIMMYT spring wheats. *Euphytica* 179, 175–186. doi: 10.1007/s10681-010-0322-9

Singh, R. P., Mujeeb-Kazi, A., and Huerta-Espino, J. (1998). *Lr46*: A gene conferring slow-rusting resistance to leaf rust in wheat. *Phytopathology* 88, 890–894. doi: 10.1094/PHYTO.1998.88.9.890

Singh, A. K., Zhang, P., Dong, C., Li, J., Singh, S., Trethowan, R., et al. (2021). Generation and molecular marker and cytological characterization of wheat - Secale strictum subsp. anatolicum derivatives. *Genome* 64, 29–38. doi: 10.1139/gen-2020–0060

Wang, J. K. (2009). Inclusive composite interval mapping of quantitative trait genes. *Acta Phytopathol. Sin.* 35, 239–245. doi: 10.3724/SP.J.1006.2009.00239

Wang, M. N., and Chen, X. M. (2017). "Stripe rust resistance," in *Stripe Rust*. Eds. X. M. Chen and Z. S. Kang (Springer, Dordrecht), 353–558. doi: 10.1007/978–94-024–1111-9

William, H. M., Singh, R. P., Huerta-Espino, J., Islas, S. O., and Hoisington, D. (2003). Molecular marker mapping of leaf rust resistance gene *Lr46* and its association with stripe rust resistance gene *Yr29* in wheat. *Phytopathology* 93, 153–159. doi: 10.1094/PHYTO.2003.93.2.153

Wu, J. H., Zeng, Q. D., Wang, Q. L., Liu, S. J., Yu, S. Z., Mu, J. M., et al. (2018). SNP –based pool genotyping and haplotype analysis accelerate fine–mapping of the wheat genomic region containing stripe rust resistance gene *Yr26*. *Theor. Appl. Genet.* 131, 1481–1496. doi: 10.1007/s00122-018-3092-8

Yao, E., Blake, V. C., Cooper, L., Wight, C. P., Michel, S., and Cagirici, H. B. (2022). "Graingenes: a data-rich repository for small grains genetics and genomics". *Database*, 2022, baac034. doi: 10.1093/database/baac034

Zadoks, J. C., Chang, T. T., and Konzak, C. F. (1974). A decimal code for the growth stages of cereals. *Weed Res.* 14, 415–421. doi: 10.1111/j.1365-3180.1974.tb01084.x

Zhang, W., Chen, S., Abate, Z., Nirmala, J., Rouse, M. N., and Dubcovsky, J. (2017). Identification and characterization of *Sr13*, a tetraploid wheat gene that confers resistance to the Ug99 stem rust race group. *Proc. Natl. Acad. Sci. U.S.A.* 114, E9483–E9492. doi: 10.1073/pnas.1706277114

Zhou, X. L., Hu, T., Li, X., Yu, M., Li, Y., Yang, S., et al. (2019). Genome-wide mapping of adult plant stripe rust resistance in wheat cultivar Toni. *Theor. Appl. Genet.* 132, 1693–1704. doi: 10.1007/s00122-019-03308-1

Zhou, X. L., Zhong, X., Roter, J., Li, X., Yao, Q., Yan, J. H., et al. (2021). Genome-wide mapping of adult plant stripe rust resistance locus derived from durum wheat Svevo by 90K SNP array. *Plant Dis.* 105, 879–888. doi: 10.1094/PDIS-09–20-1933-RE

Zhu, Z., Cao, Q., Han, D., Wu, J., Wu, L., Tong, J., et al. (2023). Molecular characterization and validation of adult-plant stripe rust resistance gene *Yr86* in Chinese wheat cultivar Zhongmai 895. *Theor. Appl. Genet.* 136, 142. doi: 10.1007/s00122-023-04374-2

Frontiers in
Plant Science

Cultivates the science of plant biology and its applications

The most cited plant science journal, which advances our understanding of plant biology for sustainable food security, functional ecosystems and human health.

Discover the latest Research Topics

See more →

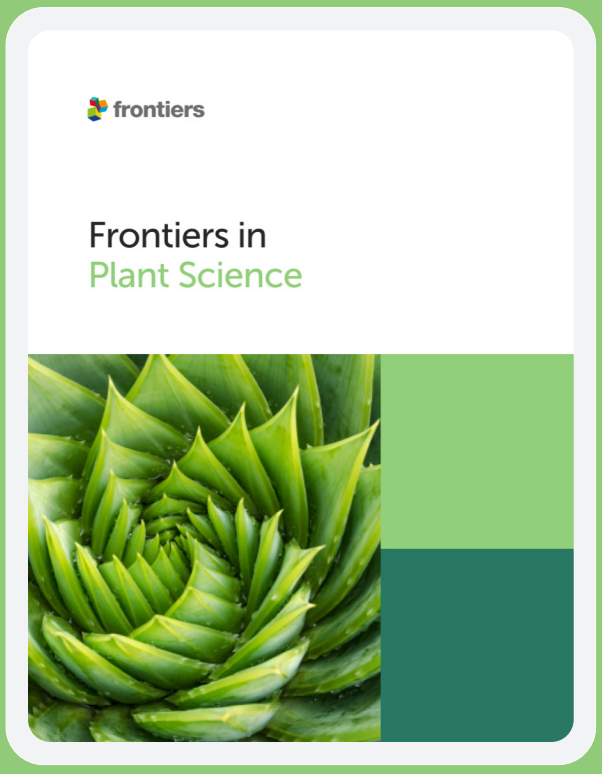

Frontiers

Avenue du Tribunal-Fédéral 34
1005 Lausanne, Switzerland
frontiersin.org

Contact us

+41 (0)21 510 17 00
frontiersin.org/about/contact